OCEANS and ATMOSPHERE

www.csiro.au

Port Phillip Bay Coastal Hazard Assessment

Final Report

Kathleen L. McInnes, Julian O'Grady, Mahesh Prakash, Peter Dahlhaus, Neville Rosengren, Ron Hoeke, Christine Lauchlan Arrowsmith, Vanessa Hernaman, Raymond Cohen, Blake Seers, Yang Chen, Derek Walters, Phellipe Couto, Claire Trenham, Nick Forbes-Smith, Rebecca Gregory, Mark Hemer, Robert Power

May 2022

CSIRO Oceans and Atmosphere

Citation:

McInnes, K.L., O'Grady, J.O., Prakash, M., Dahlhaus, P., Rosengren, N.J., Hoeke, R.K., Lauchlan Arrowsmith, C., Hernaman, V., Cohen, R., Seers, B., Chen, Y., Walters, D., Couto, P., Trenham, C., Forbes-Smith, N. Gregory, R., Hemer, M. and Power, R. (2022) Port Phillip Bay Coastal Hazard Assessment: Final Report. Report to Department of Environment, Land, Water and Planning. 236 pages + 11 Appendices.

Contents

Contents **3**

Abbreviations and Glossary **8**

Executive Summary **13**

1 Introduction **18**

1.1 Background ... 18

1.2 Overview of Report ... 18

2 Overview of Study Region **21**

2.1 Introduction ... 21

2.2 Geology and Structure of the Port Phillip Region ... 21

2.2.1 Geological and Landform Evolution ... 21

2.2.2 Tectonic Framework and Faulting ... 25

2.2.3 Geological Variations ... 26

2.2.4 Coastal Processes ... 27

2.2.5 Sea-level Changes ... 28

2.2.6 Engineering Modifications ... 29

2.3 Meteorology and Climatology ... 30

2.3.1 Meteorological Drivers of Coastal Hazards in Port Phillip Bay ... 30

2.3.2 Climatological Influences on Coastal Hazards along Victoria's Coast ... 31

2.4 Hydrodynamics and Tides ... 31

2.4.1 Tide and Hydrodynamic Processes in Port Phillip Bay ... 31

2.4.2 Regional Scale Hydrodynamic Model Studies ... 32

2.4.3 Hydrodynamic Modelling Studies of Port Phillip Bay ... 33

2.4.4 Summary ... 36

2.5 Waves 36

2.5.1 Overview of Wave Processes in Port Phillip Bay ... 36

2.5.2 Observational Studies ... 37

2.5.3 Regional Scale Wave Model Studies ... 37

2.5.4 Wave Modelling Studies in Port Phillip Bay ... 38

2.5.5 Summary ... 38

2.5.6 Overview of Inundation Methods ... 39
2.5.7 Inundation Studies of Port Phillip Bay ... 39
2.5.8 Hydrology Considerations ... 40
2.5.9 Summary ... 42
2.6 Shoreline Processes ... 42
2.6.1 Overview of Shoreline Processes in Port Phillip Bay ... 42
2.6.2 Frameworks for Understanding Shoreline Change ... 43
2.6.3 Factors Contributing to Erosion Hazards ... 44
2.6.4 Summary ... 45
2.7 Groundwater ... 46
2.7.1 Overview of Groundwater Processes ... 46
2.7.2 Groundwater Hazards ... 47
2.7.3 Groundwater Management in Victoria ... 48
2.7.4 Summary ... 52
3 Study Design 53
3.1 Gap Analysis Key Findings ... 53
3.2 Project Design ... 54
3.2.1 Decision Support Systems and Integration of Hazard Assessments ... 55
3.2.2 Inundation Hazard Assessment ... 56
3.2.3 Groundwater Hazard Assessment ... 58
3.2.4 Hydrodynamic Modelling and Climate Scenarios ... 58
4 Decision Support System 60
4.1.1 Introduction ... 60
4.1.2 Development Process for the DSS and Guiding Principles ... 60
4.1.3 Available Datasets ... 63
5 Inundation Hazard Assessment 65
5.1 Introduction ... 65
5.2 Model Setup ... 66
5.2.1 EurOtop Overtopping Algorithms ... 67
5.2.2 Regions ... 68
5.2.3 Simulation Scenarios ... 69
5.2.4 Inundation Hazard Zone Mapping ... 70

5.3 Input Data, Pre- and Post-Processing 71
5.3.1 Digital Elevation Models 71
5.3.2 Catchment Inputs 73
5.3.3 Drainage Networks 74
5.3.4 Wave Overtopping 75
5.3.5 Wave Setup and Wave Runup 78
5.3.6 Developing Inundation Hazard Layers 80
5.4 Sensitivity Experiments 82
5.4.1 Process Contributions 82
5.4.2 Comparison Between Results at 5 and 25 m 89
5.5 Inundation Hazard Results 92
5.5.1 Inundation by Depth 92
5.5.2 Inundation Areas 96
5.5.3 Integration of Wave Setup 96
5.5.4 Wave Runup Excursion Hazard 101
5.6 Summary of Inundation Hazard Assessment 106
5.6.1 Discussion of Findings 106
5.6.2 Summary 108

6 Groundwater Hazard Assessment 110

6.1 Introduction 110
6.2 Groundwater Hazard Assessment Methods 111
6.2.1 Data Availability 111
6.2.2 Constructing the Groundwater Hazard Visualisations 114
6.2.3 Challenges and Limitations 117
6.3 Groundwater Hazard Assessment – Results and Discussion 118
6.3.1 Whole-of-Bay Conceptual Model 118
6.3.2 Werribee Delta Region (focus area) 122
6.3.3 The Mentone to Frankston ‘sand belt’ (focus area) 128
6.3.4 The Nepean Peninsula (focus area) 134
6.4 Summary of Groundwater Hazard Assessment 139
6.4.1 Discussion of Findings 139
6.4.2 Summary 141

7 Shoreline Data and Information 143

OFFICIAL

7.1 Introduction 143
7.2 Shoreline Data 143
7.2.1 Coastal Compartment Analysis 143
7.2.2 Sediment Surveys, Sampling and Analysis 146
7.2.3 LiDAR Surveys 149
7.2.4 Beach Profile Surveys 150
7.2.5 Coastal Protection Structures 152
7.2.6 Aerial Photogrammetry and Shoreline Change Analysis 154
7.3 Geomorphic Shoreline Analysis 160
7.4 Summary 168

8 Hydrodynamic and Wave Modelling of Port Phillip Bay 169

8.1 Introduction 169
8.2 Model Setup and Processing 169
8.2.1 Model Grids 169
8.2.2 Mannings Roughness 170
8.2.3 Model Experiments 170
8.2.4 Computing Requirements 170
8.3 Input Data Requirements and Assessment 172
8.3.1 Bathymetry and Topography 172
8.3.2 Atmospheric Boundary Conditions 172
8.3.3 SCHISM-WWMIII Southern Boundary Conditions 173
8.3.4 Inflow Boundary Conditions 173
8.4 Model Calibration and Validation 175
8.4.1 Atmospheric Input Data 175
8.4.2 Tides and Water Levels 178
8.4.3 Waves 185
8.5 Baseline (Hindcast) Results 197
8.5.1 Extreme Water Level Analysis 198
8.5.2 Extreme Wave Analysis 201
8.6 Impact of Sea Level Rise 204
8.6.1 Tidal Harmonic Analysis 204
8.6.2 Sea Level Extremes 205
8.6.3 Waves Extremes 206

8.7 Summary 207

9 Summary and Study Recommendations **209**

9.1 Summary of Key Findings from this Study 209

9.2 Synthesis of Key Findings 211

9.3 Uncertainties and Recommendations for Future Work 219

Acknowledgements **222**

References **223**

Appendix A. Geology of Port Phillip Bay **233**

Appendix B. Additional Inputs for C-FAST **236**

Appendix C. Storm Duration and Design Storms **244**

Appendix D. Comparison with Melbourne Water Flood Extents **249**

Appendix E. Geomorphological Definitions **259**

Appendix F. Sediment Surveys and longshore transport **277**

Appendix G. Beach Profile Survey Digitisation **296**

Appendix H. Unsupervised Shoreline Detection **299**

Appendix J. SCHISM Model Comparisons **305**

Appendix K. Coastal Hazards by LGA **326**

Appendix L. Hazard Maps for Western, Northern and Southeastern PPB **347**

Abbreviations and Glossary

ADCP	Acoustic Doppler Current Profiler
AEP	Annual Exceedance Probability: The measure of the likelihood (expressed as a probability) of an event equalling or exceeding a given magnitude in any given year
AHD	Australian Height Datum. A common levelling plane in which mean sea level is approximately 0.0 m AHD
AR4	Fourth Assessment Report of the IPCC
AR5	Fifth Assessment Report of the IPCC
ARI	Average Recurrence Interval – the average or expected value of the periods between exceedances of an event over time
Astronomical tide	Tidal level variations due to gravitational effects of the earth, moon and sun
AWAC	Acoustic Wave and Current Profiler
Backshore	The area immediately landward of normal high-water mark (backshore proximal) and extending variable distances inland enclosing features previously formed by coastal processes (backshore distal).
Bruun factor	The Bruun Factor indicates the landward distance the shoreline will move per meter of SLR
Calibration	The process of adjustment of computer model parameters are brought to agreement with observed data
CCAM	CSIRO Conformal-Cubic Atmospheric Model – used to provide an atmospheric hindcast at 5 km resolution to provide boundary forcing for the SCHISM-WW
CDP	Port of Melbourne Channel Deepening Project
CERC equation	Coastal Engineering Research Center longshore transport equation
C-FAST	CSIRO City Flood Adaptation Solutions Tool
CFSR	Climate Forecast System Reanalysis produced by the National Centers for Environmental Prediction (NCEP)
CMIP5	Coupled Model Intercomparison Project – Phase 5. The suite of Global Climate Models used to support the IPCC Fifth Assessment Report (AR5)

Coastal hazard	Physical changes and impacts to the natural coastal environment which are significantly driven by coastal or oceanographic processes, which create a risk of damage to property, environment or people
CGC	Coastal Geomorphic Category – broad coastal landforms defined by backshore geology, elevation, slope and intertidal composition
CGS	Coastal Geomorphic Sector – discrete short length of coastline defined inside a CGU by considering further classification of the backshore and shore zone characteristics. Consistent with a tertiary scale assessment, also referred to as tertiary compartments
CGU	Coastal Geomorphic Unit – length of coastline containing a limited range of Coastal Geomorphic Categories
D50	D50 refers to the average particle size and is the median diameter of sediments
Diurnal	A daily variation
DEM	Digital Elevation Model
DSS	Decision Support System
Ebb tide	The outgoing tidal current of water leading to a low tide
ENSO	El Niño – Southern Oscillation
ERA5	A global atmospheric reanalysis at approximately 31 km resolution produced by the European Centre for Medium-Range Weather Forecasts (ECMWF)
ERA-Interim	A global atmospheric reanalysis at approximately 79 km resolution produced by the ECMWF
Flood tide	The incoming tidal current of water leading to a high tide
Foreshore	The area between normal low and high tide marks, also referred to as the intertidal zone, beach face and separated by lower beach face – the more seaward part of the beach – and upper beach face
GCM	Global Climate Model
GIS	Geographical Information System
HAT	Highest Astronomical Tide – The highest water level that can occur due to the effects of the astronomical tide
Hindcast	A hindcast is a historical simulation, in which a numerical model is integrated forward in time from a past date with forcing conditions provided by another model and/or reanalysis products

Hydrodynamic model	A numerical model that simulates water movement for a given area which uses boundary inputs including tides, winds and surface pressure
Intertidal	The area of land covered by water at high tide, but uncovered at low tide
Inundation	The area of land covered in water that would otherwise remain dry, from flooding by elevated coastal water levels
Inverse barometric pressure effect	The rise (or fall) in sea level that occurs when atmospheric pressure falls (or rises) relative to average atmospheric pressure (for every hectopascal (hPa) fall in pressure, sea level increases by 1 cm)
IPCC	Intergovernmental Panel on Climate Change
Levee	Constructed raised embankment along the edge of a coastal area at the backshore proximal to prevent overflow of water
LiDAR	Light Detection and Ranging – is a remote sensing method that is used to measure variable distances to Earth to generate highly accurate 3D maps of the Earth's surface
LGA	Local Government Area
LT	Long term change in shoreline
MHHW	Mean Higher High Water
MHWS	Mean High Water Springs
MLLW	Mean Lower Low Water
MSL	Mean Sea Level
Neap tides	Tides that occur twice a month when the sun and moon lie at right angles relative to the Earth resulting in the smallest difference between the high and low tides
NMB-LM	Semi-empirical Ninety Mile Beach Longshore Transport Model
Non tidal residual water level	The non-tidal residual water level is the total water level that remains once the astronomical tidal component has been removed
Overtopping	The process of water flowing over a structure, due to the wave action
PPB	Port Phillip Bay
PPBCHA	Port Phillip Bay Coastal Hazard Assessment
PMA	Port of Melbourne Authority

PoMC	Port of Melbourne Corporation
RCP	Representative Concentration Pathway. Refers to assumptions on future greenhouse gas emissions that lead to future warming. Four RCPs were considered in climate model simulations undertaken in CMIP5; RCP2.6 (low emissions), RCP4.5 (low-intermediate emissions), RCP6.0 (intermediate to high) and RCP8.5 (high)
Reanalysis	A scientific method for developing a comprehensive historic global gridded dataset that is temporally homogeneous. Observations and a numerical model that simulates aspects of the Earth system are combined objectively using data assimilation techniques to generate a synthesized estimate of the state of the system at each time step. Reanalysis datasets typically span several decades and can also provide many derived fields for which direct observations are sparse in time or space
RPM	Rate per metre of SLR (subscript m for model and o for observed)
RPY	Rate per year into the future (subscript m for model and o for observed)
SB	Modelled storm bite
SCHISM	Semi-implicit Cross-scale Hydroscience Integrated System Model
SCHISM-WWMIII	SCHISM coupled with the WWMIII spectral wave model to simulate water currents, depths and waves
Semi-diurnal	Twice per day
Significant wave height	The mean wave height of the highest third of the waves. The measurement consists of the height difference between the wave crest and trough of the preceding wave. Defined as Hs
SKM	Sinclair Knight Merz
SLR	Sea level rise
Spectral wave model	A numerical model used to simulate ocean conditions including wind-generated waves and swells in offshore and coastal regions
Spring tides	Spring tides occur twice a month during a new and full moon, when the sun, moon and earth are in alignment. The difference between the high and low tides is the largest at this time
SRW	Southern Rural Water
Storm surge	The unusual rise in coastal water levels during a storm due to the barometric and wind set-up effects. It is measured as the water height above the usual predicted astronomical tide

Storm tide	An extreme sea level event, which is the combination of astronomical tide, storm surge (caused by low atmospheric pressure and winds that elevate coastal sea levels). Wind waves can also influence the storm surge (and therefore storm tide) via ocean surface roughness and wave-current interactions. In the usage in this report, storm tide does not include surf zone breaking wave setup or beach face swash runup
SWL	Still Water Level, relative to a datum. In the context used here, this accounts for the storm tide plus SLR scenario, which is a time-mean water level on the time scale of a storm surge
Tidal constituents	The components that impact tidal changes over a period of time. These include semi-diurnal and diurnal constituents
Tidal prism	The volume of water in an estuary or inlet between mean high tide and mean low tide
Tidal range	The height difference between successive high and low tides
Tides	The alternating rise and fall in sea level due to the gravitational attraction of the sun, moon and earth
TWL	Total Water Level relative to a datum. In the context used here, it accounts for storm tide plus wave setup plus SLR scenario
$TWL_{2\%}$	2% exceedance Total Water Level, relative to a datum. In the context used here, it accounts for storm tide, wave setup, wave runup and SLR scenario
VCP19	Victorian Climate Projections 2019
Vulnerability	Vulnerability is a measure of exposure to climatic factors, and the extent of which communities, infrastructure or environment may be impacted
Wave runup	The height of uprush of water at the shoreline above the still water level
Wave setup	The elevation in the mean sea level at the shoreline due to wave action
Wind fetch	The distance over water which the onshore wind is blowing
Wind setup	The elevation in the mean sea level due to the impact of wind on the water surface
WWMIII	Wind Wave Model. Third generation Spectral wave model used with SCHISM

Executive Summary

This report presents a comprehensive assessment of inundation and groundwater hazards around Port Phillip Bay (PPB), delivered through a purpose-built Port Phillip Bay Coastal Hazards Assessment Decision Support System (PPBCHA DSS). The project was funded by the Department of Environment, Land, Water and Planning (DELWP) and carried out in partnership with the Association of Bayside Municipalities, the ten local governments around the Bay, Parks Victoria, Catchment Management Authorities, and Melbourne Water.

The area of the Bay covers around 1,930 km^2 and has approximately 310 km of shoreline at high tide. The landscape of PPB has been established by rock-forming and tectonic events and climate and sea level changes across southeastern Australia over the past 600 million years. The Bay is mostly protected from the high energy conditions of the open ocean by the rocky headlands and shore platforms at Point Nepean and Point Lonsdale, and the extensive accumulation of mobile sand shoals (Great Sands) inside the entrance that restricts the ocean swell and reduces the tide range progressively in the bay.

Since European occupation in the 1830's, much of the coast of PPB has been artificially modified. Parts of PPB and the lower Yarra River channel have been artificially deepened since the 1850's to facilitate shipping and to accommodate larger vessels. Breakwater-defended marinas and canal estates are widespread around the bay and beach renourishment, landfill, seawalls, revetments and groynes have been constructed to prevent or reduce coastal recession and secure built assets.

Beach renourishment has been applied to at least 30 sites around the bay since the mid-1970's and extensive areas of the immediate backshore are now fundamentally reshaped by industrial and service facilities including the former salt works at Altona and Moolap, Western Treatment Plant at Werribee, aerodromes at Point Cook and Laverton, and widespread residential subdivisions including bay-linked canal estates at Point Cook, Paterson Lakes, The Point (Point Lonsdale) and Martha Cove.

Climate change poses a threat to PPB and will continue to exacerbate coastal hazards in the future. Ongoing sea level rise (SLR) is the most pervasive threat for the coastal zone. Sea levels will continue to rise for centuries to come, with the future rate of rise determined by global emissions of greenhouse gases and their influence on atmospheric and ocean temperatures. Rising sea levels will amplify extreme sea levels within PPB. The narrow entrance to the bay serves to restrict tidal flows leading to a tidal range within the bay that is approximately half that of Bass Strait. However, under higher sea levels the effect of hydraulic friction through Port Phillip Heads will be reduced leading to an increase in the tidal range within PPB. This amplification effect means that coastlines will experience an increase in extreme sea levels over and above that due to SLR alone and this will have implications for coastal hazards such as inundation, erosion and groundwater. This assessment focusses on future SLR as the major climate driver of future changes to coastal hazards.

A comprehensive assessment of inundation and groundwater hazards around PPB has been undertaken, under the combination of tides, storm surges and waves (referred to collectively as storm tides). In developing the hazard layers five SLR scenarios were considered; 0.2, 0.5, 0.8, 1.1 and 1.4 m above current MSL. To underpin the physical data requirements of the study, a 35-year hydrodynamic and wave model simulation was undertaken over the period 1980 to 2014 to obtain spatially relevant data inputs for the hazard assessments. Additionally, simulations were carried out to assess the effects of selected future sea level increases on storm tides. The purpose-built Decision Support System (DSS) was designed to house the outputs of the hazard assessments together with other relevant coastal data including shoreline and geomorphic data to facilitate decision-making.

Hydrodynamic and Wave Modelling of Port Phillip Bay

The hydrodynamic and wave model (SCHISM-WWMIII) was set up over the whole-of-bay including significant portions of the surrounding ocean coasts and Bass Strait. It was used to simulate water levels due to astronomical tides, weather and waves and aspects of wave-flow interaction over multiple decades, allowing for full consideration of the dynamics of extreme sea levels and waves within the Bay. Simulations were also carried out to assess changes in dynamics associated with the various SLR scenarios used in this study.

The relative increases in extreme water levels and waves within PPB under the modelled SLR scenarios are predicated on the assumption that the seabed remains static under SLR. While this simplifying assumption is not unfounded, since evidence suggests many shallow areas of PPB consist of a relatively thin veneer of sediment over rocky bases of the Great Sands, it is an important caveat. In reality, some degree of morphological change under future SLR scenarios is almost certain, although how this may further affect the water level and wave dynamics remains unknown. This is a recommended area of future study.

The model simulations indicate that extreme water levels within PPB will increase with SLR beyond the value of SLR itself. For example, for many locations within PPB, under the 0.8 m SLR scenario, the 1% annual exceedance probability (AEP) (1 in 100-year ARI), extreme water level is not 0.8 m higher but up to 0.9 m higher. Overall, throughout much of the bay the increase in extreme water levels is approximately between 2 and 10% higher than the value of SLR itself, although there is considerable variation depending on location. These increases are due primarily to increases in tidal ranges within the bay associated with SLR, as a result of increases in the water exchange through the heads. Storm surge dynamics also exhibit small changes with SLR, but they do not result in any significant net increase or decrease in extreme water level probabilities relative to SLR increases.

The model simulations indicate that storm wave energy within PPB will also increase with SLR. For example, under the 0.8 m SLR scenario, the 1% AEP significant wave height increases by 5-10% in most areas of PPB. This is primarily due to increased water depths over the Great Sands and other relatively shallow areas in PPB, which effectively increases the fetch within the bay, allowing slightly larger waves to be generated for a given wind strength. Additionally, there is evidence that the increased water depths through the heads and over the Great Sands allows slightly more ocean wave energy (swell) to “leak” through the heads and penetrate into the bay.

Inundation Hazard Assessment

For the inundation hazard assessment, the hydrodynamic modelling was carried out at two levels of detail around the bay using the CSIRO City Flood Adaptation Solutions Tool (C-FAST) hydrodynamic model. A design storm approach was applied in which inundation was investigated for storm tides of 1, 2 and 5% AEPs under baseline and future SLR scenarios. The assessment of AEPs was based on the SCHISM-WWMIII model simulations. The highly urbanised and low-lying areas of Greater Geelong, Werribee, City of Port Phillip and Mordialloc to Frankston were deemed most at risk from hazards posed by SLR. Therefore, for these locations C-FAST was implemented at 5 m resolution and accounted for the dynamic overland inundation due to SLR combined with storm tides of 1, 2 and 5% AEPs, local wave overtopping where seawalls and barriers were present, catchment inputs due to rainfall over the model grid for a 10% AEP rainfall event and stormwater drainage. Outside these regions, which are generally less urbanised, C-FAST was implemented at 25 m resolution and accounted for dynamic overland inundation and catchment inputs for the same storm tides and SLR. The results from the various grids were combined with wave setup extents calculated around PPB to provide seamless inundation layers.

Much of the area associated with inundation hazard was focussed on the western side of PPB, including Queenscliff, Swan Bay, Portarlington, Point Henry, Avalon, Point Wilson, Werribee and Altona. On the eastern side of PPB, Southbank, Port Melbourne to Elwood and Patterson Lakes included areas of inundation hazard that were more pronounced under the 1.4 m SLR scenario.

The trend in inundation area between the different SLR scenarios was useful for determining; a) how soon protective structures may be required, b) how adaptable these protective structures need to be for future upgrades and c) the cost-benefits associated with building protective structures with consideration of staging further upgrades in the future when particular trigger points are reached. For the whole bay under a 1% AEP storm tide event the area of inundation increases almost linearly in relation to SLR between the baseline assessment and a SLR of 1.4 m, with the area of inundation increasing approximately three to fourfold. However, for specific Bayside local government areas (LGA's) the rates of change show significant differences. For the Borough of Queenscliffe and City of Bayside the area of inundation approximately doubles between present conditions and 1.4 m of SLR whereas for the Cities of Hobsons Bay, Greater Geelong, Frankston and Mornington Peninsula Shire the inundation area undergoes an approximate two to three-fold increase for a 1.4 m SLR. For the City of Melbourne, the City of Port Phillip, City of Wyndham and City of Kingston the area affected by inundation accelerates with SLR and inundated areas increase dramatically beyond a SLR of 0.5 m. For example, for City of Melbourne under present sea levels the inundation from a 1% AEP storm tide event is 0.17 km^2 and increases six-fold and 28-fold for 0.5 and 1.4 m SLR scenarios respectively.

Groundwater Hazard Assessment

While the hydrogeology of PPB is generally well understood under present climate conditions, there is limited understanding of the impacts of rising sea levels and other projected changes in climate on the current hydrogeology. In this study, conceptual models were developed at the whole-of-bay scale and for three local regions; the Werribee region, the Mentone to Frankston sand belt, and the Nepean Peninsula, to qualitatively assess the impacts of SLR, and other changes in climate over the PPB region such as the projected decrease in rainfall and increase in evapotranspiration.

Groundwater flows from recharge to discharge were based on hydraulic gradients and PPB is a groundwater sink. Local flow systems with short paths from recharge to discharge have shorter response times (less than a decade) compared to the regional flow systems with long flow paths, which may take five to ten decades to respond to changes in SLR, rainfall and evapotranspiration. Additionally, flatter gradients were more susceptible to the influence of SLR, since a small vertical rise can affect a greater lateral distance. The whole-of-bay conceptual model indicates that in the northeast of the bay and along the northern shoreline of the Bellarine Peninsula, the flow is short and the gradient steep. In contrast, in the Mentone-Frankston sand belt and the western shore of PPB (Point Wilson to Williamstown), flows are long, and gradients are much flatter.

Shallow groundwater can be both an asset (e.g. sustaining groundwater dependent ecosystems) and a threat (e.g. impacting on below ground engineering infrastructure such as foundations and service conduits). Areas where the watertable is shallow (<2 m) tend to occur close to the shoreline. Increases in sea level will affect unconfined aquifers through the inland migration of the seawater-groundwater interface.

Detailed conceptual models were developed for the Werribee delta region, the Mentone to Frankston sand belt region and the Nepean Peninsula where the watertable is relatively shallow, the hydraulic gradient is low, and the recharge of the unconfined aquifers is dependent on rainfall. At all three locations, the projected decrease in precipitation and increase in evaporation will lower the watertables by a small amount (order of centimetres) while SLR will cause an inland migration of the seawater-groundwater interface on the order of tens to hundreds of metres, although precise values are subject to a large degree of uncertainty. For Werribee, the lowering of the watertable was predicted to be approximately 0.01 m over the next century, while the seawater-groundwater interface migrated inland by approximately 250 m at 20 m depth under a scenario of a 1.4 m rise in sea level. This will mean that drawdown triggers for management of groundwater extraction for agriculture and horticulture, which are based on the depth to watertable in specified bores, will need to be reconsidered over time.

For the Mentone to Frankston sand belt and the Nepean Peninsula, the effect of reduced rainfall and increased evapotranspiration was estimated to lower the watertable by 0.04 m over the next century. At Patterson Lakes, the effect of SLR was estimated to lead to the inland migration of the seawater-groundwater interface by approximately 100 m at 20 m depth for a 1.4 m rise in sea level. At Blairgowrie, the seawater-groundwater interface was predicted to migrate approximately 50 m inland at 20 m depth for a 1.4 m rise in sea level.

Geomorphic Assessment

Shoreline data and information was also compiled to aid in the interpretation of the hazards presented in this study as well as provide foundational information for future erosion hazard assessments. A geomorphic survey identified 528 coastal geomorphic sectors (CGS - also referred to as tertiary compartments) around PPB. The sectors were determined on the basis of backshore and intertidal landform characteristics. More than half of these sectors (290 CGS) totalling around 200 km of coastline, are beach fronted. However, these beaches have a variety of backshore features ranging from engineered structures to cliffs and wetlands. Hard or soft rock cliffs occur extensively on the eastern side of PPB and the Bellarine Peninsula whereas low-lying wetland areas are most prevalent in the west, south-west and central-east parts of PPB.

Decision Support System

The PPBCHA DSS was built as an all-coastal hazards data visualisation and analysis tool that can be accessed via the web. The DSS uses the open source Terria JS (https://terria.io/) geospatial visualisation and analytics capability developed by CSIRO Data61. The key datasets available through the DSS are inundation and groundwater hazard layers for current day conditions and for future SLR scenarios up to 1.4 m. Additional data layers have been incorporated into the DSS including those that were produced as part of this project and/or used as input into the various hazard models such as the geomorphic classification data, bathymetry and Digital Elevation Models. Historical aerial imagery from the 1930's to current day supplied by the DELWP Coordinated Imagery Program have also been included in the DSS. These data consist of up to 7,000 frames of aerial images that were originally in various formats but have been synthesised into a high-resolution set of historical images for visualisation within the DSS. The DSS also provides a number simple of analysis tools.

Summary

The project scenarios present a range of future options in PPB that can be considered by various management agencies to consider the risks and impacts of SLR using a visual, probabilistic DSS. The DSS can support managers in decision making by bringing together a range of data sets, hazard variables under present day and future scenarios and simple analytical tools to assist in considering investment decisions (e.g. seawalls), water extraction and land planning and use into the future. The use of the DSS (or any other decision support tools) may be improved by incorporating new information on variables already considered (e.g. storm tide, groundwater and wave runup hazard), incorporating new sources of information (e.g. aerial images, erosion hazard). The value of the DSS will be realised through engagement with government and non-government stakeholders to explore scenarios and impacts of decisions over a range of time and spatial scales.

1 Introduction

1.1 Background

The Port Phillip Bay Coastal Hazard Assessment (PPBCHA) is being undertaken by the Department of Environment, Land, Water and Planning (DELWP) in partnership with the Association of Bayside Municipalities, the ten local governments around Bay, the Municipal Association of Victoria, Parks Victoria, Catchment Management Authorities, and Melbourne Water. The project funding was provided by the Sustainability Fund, a trust fund with legislated objectives focused on fostering best practice, innovation and systemic change to address waste and climate change. This coastal hazard assessment (PPBCHA) builds on experience gained in the delivery of four pilot coastal hazard assessments in Victoria, undertaken between 2013 and 2016 under the earlier Future Coasts initiative, and the Local Coastal Hazards Assessment Learnings Project. The PPBCHA supports implementation of Victoria's Marine and Coastal Reforms Final Transition Plan (released 1 August 2018), helps to address the findings of the Victorian Auditor-General's Office report *Protecting Victoria's Coastal Assets*, and aligns with the directions set out in the Marine and Coastal Policy 2020. This report presents a comprehensive assessment of inundation and groundwater hazards around Port Phillip Bay which account for:

- tidal and storm surge variability (including consideration of inter-annual and inter-decadal sea level variability for the region) and extreme events
- the wave climate of PPB and its variability, incorporating swell and fetch modelling as appropriate, together with impact modelling for extreme events
- near-shore processes of wave set-up/run-up and overtopping
- associated SLR and joint probability event scenarios (minimum of four) including:
    - 0.2 m and 0.8 m of SLR plus 1% AEP storm tide and wave height with 10% AEP catchment flows as consistent with state planning policy, and 0.5 m and 1.4 m of SLR plus 1% AEP storm tide and wave height with 10% AEP catchment flows, as well as consideration of future changes on storm tide and wave climate. In addition to the above SLR scenarios, a 1.1 m SLR scenario was also investigated.

A comprehensive coastal geomorphological survey and classification around the PPB coastline is also undertaken, which provides relevant information to inform further studies around erosion hazard. At the outset of the Coastal Hazard Assessment, a gap analysis was undertaken to synthesise the relevant existing data and information and identify any critical gaps in the existing baseline information and data that would be required to complete the PPBCHA. This was used to refine the project design to carry out the hazard assessments for inundation and groundwater. In parallel with the coastal hazard assessment was the development of a Decision Support System (DSS) to house key datasets and results from the assessment and enable stakeholder access to the relevant data layers.

1.2 Overview of Report

The remainder of this report is organised as follows:

- Chapter 2 provides a description of the study region. It reviews key topics relevant to the coastal hazard assessment such as the geological context of Port Phillip Bay, the meteorology and climatology, the hydrodynamics and waves, shoreline processes as well as inundation, erosion and groundwater. The overarching processes are discussed, and a review of relevant studies is provided.

- Chapter 3 summarises the key findings of the gap analysis. It also provides a high-level description of the various components of work undertaken, commencing with the purpose-built DSS that introduces the reader to the system in which the hazard assessments are delivered, followed by the approach taken for the hazards of inundation and groundwater. Finally, the design of the whole-of-bay hydrodynamic modelling, which provides various input parameters to the inundation hazard assessment is discussed.

- Chapter 4 describes the DSS that delivers the relevant outputs and features of the hazard assessments. It is introduced to orient the reader with the end products that were derived and described in detail in the following hazard chapters.

- Chapter 5 describes the methodology for the inundation hazard assessment. It begins with the relevant data inputs and how they relate to the inundation modelling. A hydrodynamic model is used to assess the inundation hazard around the entire bay on a total of seven different model grids, with the results combined to produce whole-of-bay inundation hazard information. The resolution of the model is either 5 m or 25 m with low-lying and developed areas prioritised for the 5 m resolution modelling. Simulations were undertaken for 1%, 2% and 5% AEP storm tide events with and without 10% AEP rainfall event. The model setup and data inputs are described and tested with sensitivity experiments that include varying the model mesh resolution and also comparing results to other inundation modelling studies. Inundation is presented as probabilistic areas of inundation as well as inundation depth. The hydrodynamic modelling of inundation extent, which accounts for tides, storm surge, SLR and wave overtopping is combined with separately modelled wave setup around the bay to provide storm tide extents. An additional inundation layer that represents runup of waves on a beach is also presented for the entire bay. This can be viewed in conjunction with or independently of the inundation hazard layers in the DSS.

- Chapter 6 describes the methodology for the groundwater hazard assessment. It begins by summarising data availability such as conceptual hydrogeological models of PPB including the depth to watertable and watertable salinity. The whole-of-bay conceptual model describes groundwater elevations and flow paths. Since most shallow groundwater is saline to some extent, the groundwater hazard is assessed as the change in area of shallow groundwater or groundwater that becomes surface water due to SLR. Conceptual cross-sections of the groundwater systems are also provided for three locations around PPB: Werribee, Mentone to Frankston and the Nepean Peninsula.

- Chapter 7 presents a coastal geomorphic analysis, which classifies the coastline in terms of its backshore and intertidal characteristics and other relevant data and analysis. This information is provided as relevant contextual information to aid in interpretation of the other hazards and also to provide foundational data for estimating erosion hazard in future studies.

- Chapter 8 describes the hydrodynamic and wave modelling undertaken to provide simulated wave and sea level data for use in the hazard assessments. A description of the model setup and required data inputs is given. The models are first calibrated over two selected time periods using tide gauge data at multiple locations within the model domain and wave data just outside PPB. Then, model simulations from a 35-year historical period are validated against available tide and wave data inside the bay over the longer simulation period to demonstrate that the model is fit-for-purpose. Simulations under assumed SLR of 0.2, 0.8 and 1.4 m are also undertaken to understand the nonlinear effect that SLR would be expected to have on tides, waves and storm surges across the bay. Statistical methods are applied to the historical and each of the SLR simulations to produce sea level and wave heights expected to occur on average every 20, 50 and 100 years across the bay. These are among the various products derived from the hydrodynamic modelling that are used in the inundation and erosion hazard modelling.

- Chapter 9 summarises the methodological approach and high-level findings from each hazard assessment. A synthesis of the combined results of the three hazard assessments is then provided from an LGA perspective. Key uncertainties arising from the study and recommendations for future work are also discussed.

2 Overview of Study Region

This chapter provides a description of the study region. It reviews key topics relevant to the coastal hazard assessment such as the geological context of Port Phillip Bay, the meteorology and climatology, the hydrodynamics and waves as well as inundation, shoreline processes and groundwater. The overarching processes are discussed, and a review of relevant studies is provided.

2.1 Introduction

The waters of PPB (the study region for the PPBCHA project) cover approximately 1,930 km^2 and extend an approximate 310 km of coastline between Point Lonsdale and Point Nepean (Figure 2.1). The suburbs of Greater Melbourne extend from the north along the eastern shores of PPB while Greater Geelong is located in the west of PPB includes the Bellarine Peninsula and extends northwest to Little River. The entrance to PPB, between Point Lonsdale and Point Nepean (The Rip), is just over 3 km wide at high spring tides (Bird, 2011) and features a narrow curving canyon – the Entrance Deep, which is in places over 90 m deep with near-vertical walls incised into limestone. The bay itself is relatively shallow with about half of the area less than 8 m in depth and the deepest regions only around 24 m – with the exception of a relict linear channel 30 m deep (The Portsea Hole) offshore from Portsea. The bay also features the Great Sands, Mud Island, and various natural and artificial channels. The remainder of this chapter provides a more detailed description of the physical and climatological features of the study region, together with a review of studies that are relevant to the PPBCHA.

2.2 Geology and Structure of the Port Phillip Region

2.2.1 Geological and Landform Evolution

The landscape context of Port Phillip has been established by rock-forming and tectonic events across southeastern Australia beginning in Neoproterozoic times, more than 541 million years ago (Ma). The basement rocks across Victoria are derived from marine and non-marine sedimentation extending from the Cambrian to Early Carboniferous (about 541 to 350 Ma), interspersed with episodes of volcanicity and emplacement of granitic plutons. Victoria is divided into ten north-south oriented structural zones across the state—the zone boundaries essentially defined by major faults (Figure 2.2; VandenBerg et al., 2000).

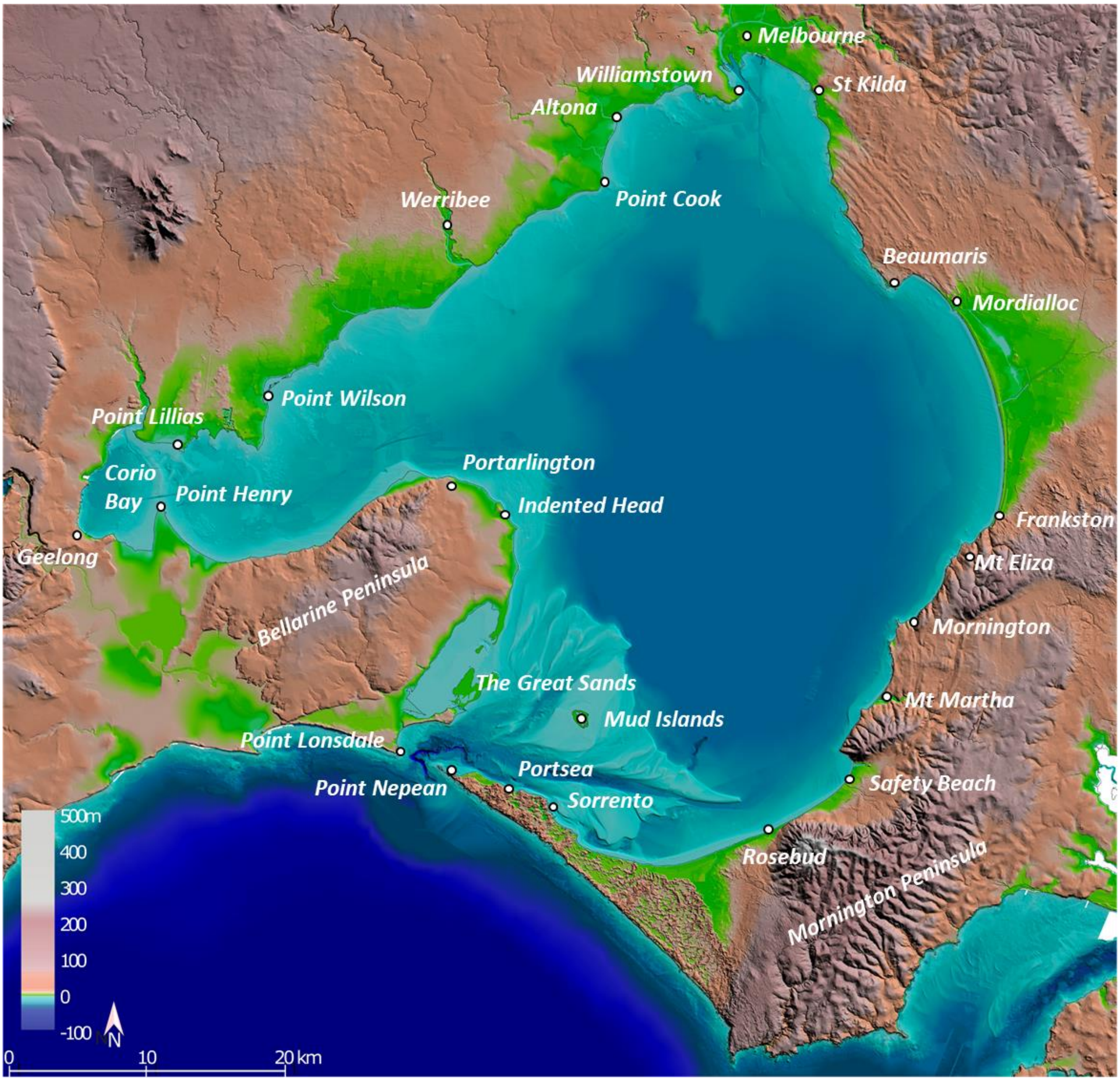

Figure 2.1: Map of the PPB Study region with locations commonly mentioned in following sections.

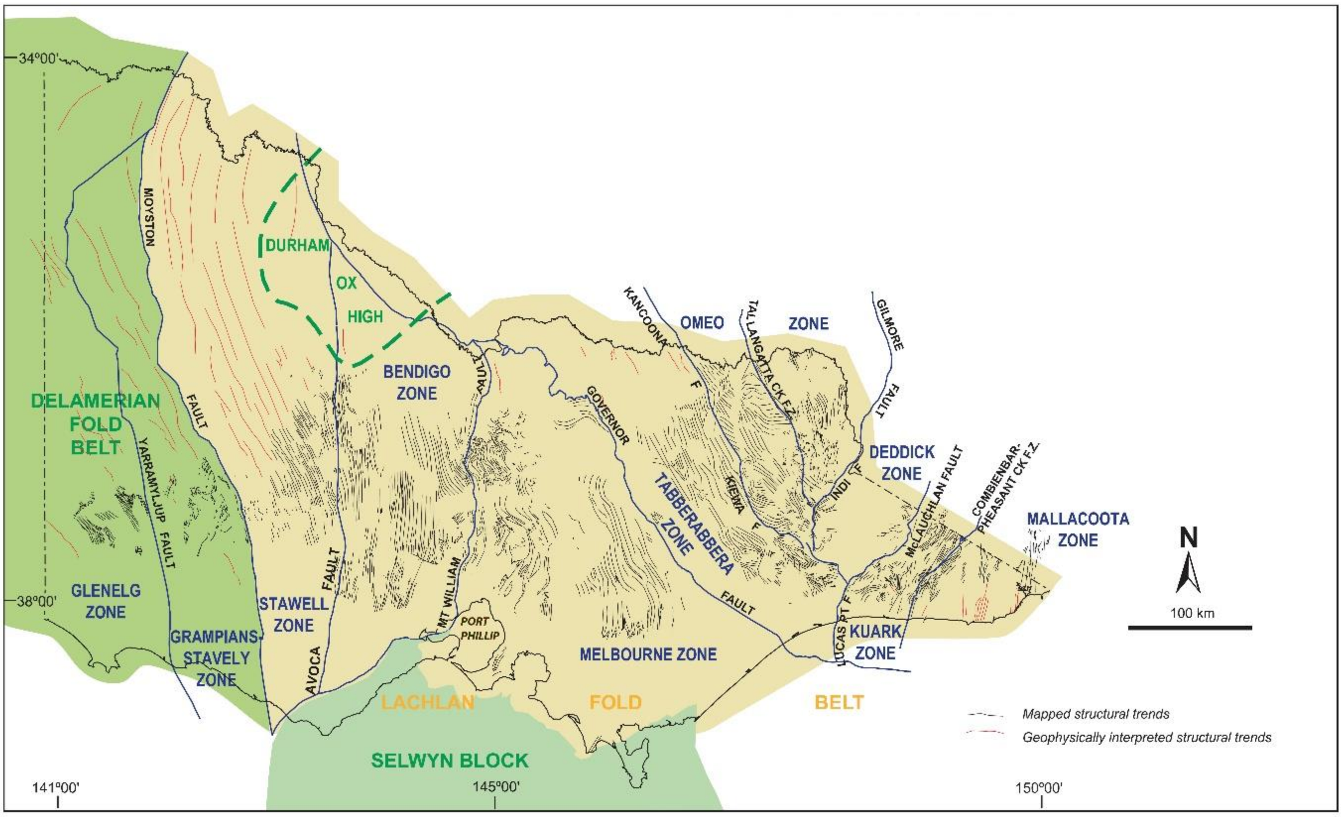

Figure 2.2: Structural zones, Victoria. (VandenBerg et al., 2000).

Cayley et al., (2002), Cayley (2011) and Moore (2016) showed that the basement under central Victoria is an extension of the Selwyn Block—a north-south zone of Neoproterozoic to Cambrian metasedimentary and metavolcanic continental crustal rock about 600 to 560 Ma —extending from northern Tasmania across Bass Strait to northern Victoria (Figure 2.3).

Although of limited outcrop in Victoria the Selwyn Block has played a major role in defining the structure of the Melbourne Zone and is a partial source of magmas that produced granitic and associated volcanic rocks in south-central Victoria during the Middle-Upper Devonian (390 – 360 Ma) (see Appendix A, Figure A1). Most of Port Phillip lies in the Melbourne Zone that has a basement of thick Ordovician to Middle Devonian (490 – 350 Ma) sequences of sand and mud rocks intruded by granitic bodies. Coastal Palaeozoic outcrops in Port Phillip are limited to a small area of now obscured Silurian sediments at St Kilda and smaller granitic bodies on the Mornington Peninsula between Mount Eliza and Martha Cove.

Tectonics is a major determinant of bedrock outcrop and faulting and rock structure has substantial influence on present landforms across southern Victoria. The broad configuration of Port Phillip and Western Port is determined by faulting and the Mornington Peninsula is an uplifted ridge of Palaeozoic sedimentary rocks and granites. The main characteristics of the geological and landform regions surrounding Port Phillip are summarised in Appendix A (Figure 2.3, see also Figure A2 and Table A1).

The main events in the geological and landform evolution of the south-central Victorian coastal region are:

- *Late Proterozoic -Cambrian:* (600 – 490 Ma) development of Selwyn Block as an exotic Proterozoic microcontinent
- *Ordovician - Middle-Late Devonian:* (490 – 350 Ma) continuous marine sedimentation

- *Late Devonian:* (380 – 350 Ma) deformation of earlier formed sedimentary rocks producing the structural overprint of folding and faulting that persists to the present time
- *Late Devonian*: (380 -350 Ma) igneous activity producing granitic batholiths
- *Permian:* (300 – 285 Ma) widespread continental glaciation and accumulation of glacial meltwater deposits
- *Mesozoic (Lower Cretaceous):* (150 – 100 Ma) pre-separation of Australia and Antarctica rifting and non-marine sedimentation in Bass, Otway and Gippsland Basins
- *Mesozoic (Upper Cretaceou*s): 100 Ma – 66 Ma) continental rifting and separation of Australia and Antarctica. Initial uplift of south-eastern Australian uplands
- *Palaeogene - Palaeocene to Oligocene:* (66 – 23 Ma) development of the central sedimentary basins along faulted-subsiding margins (Torquay, Port Phillip Western Port), initially non-marine clastic sedimentation followed by marine carbonate sedimentation. Episodes of volcanic activity (Older Volcanics) produced lava flows and local pyroclastic deposits on the Mornington Peninsula and Bellarine Peninsula
- *Neogene: Miocene to Pleistocene:* (23 – 2.7 Ma) alternating subsidence (transgression) and uplift (regression) with corresponding marine and terrestrial sedimentation in the Port Phillip Basin including coal deposits in Port Phillip Basin. Extensive volcanism in the west and north of PPB with basalt lava flows extending to (now) offshore western Port Phillip and down Yarra River valley
- *Pleistocene:* (2.7 Ma – 10 ka (thousands of years ago)) fluctuating sea levels corresponding to global glacial (low sea level) and inter-glacial (equal or higher sea levels). Continuing movement of Selwyn Fault and Rowsley Fault
- *Late Pleistocene:* (130 ka – 11.7 ka) emplacement and cementation of large coastal carbonate dune sands (Bridgewater Group) from Barwon Heads to Point Nepean and extending across the southern Mornington Peninsula—creating the Nepean Peninsula—and periodically closing the outflow of the Yarra River
- *Holocene:* (last 11.7 ka) establishment of present sea levels with short episodes of slightly higher and lower sea level, and
- Post 1788: European settlement, introduction of exotic plant and animal species influencing coastal and marine sedimentation and landforms. Intense engineering interaction with the coast and marine areas such as dredging to deepen the entrance and port channels, installing structures for commercial and recreational use and implementing a range of coastal defence measures.

The configuration and geomorphology of Port Phillip coastline is determined by tectonic processes, geological variations, coastal processes and sea level changes. These are discussed in the next sections.

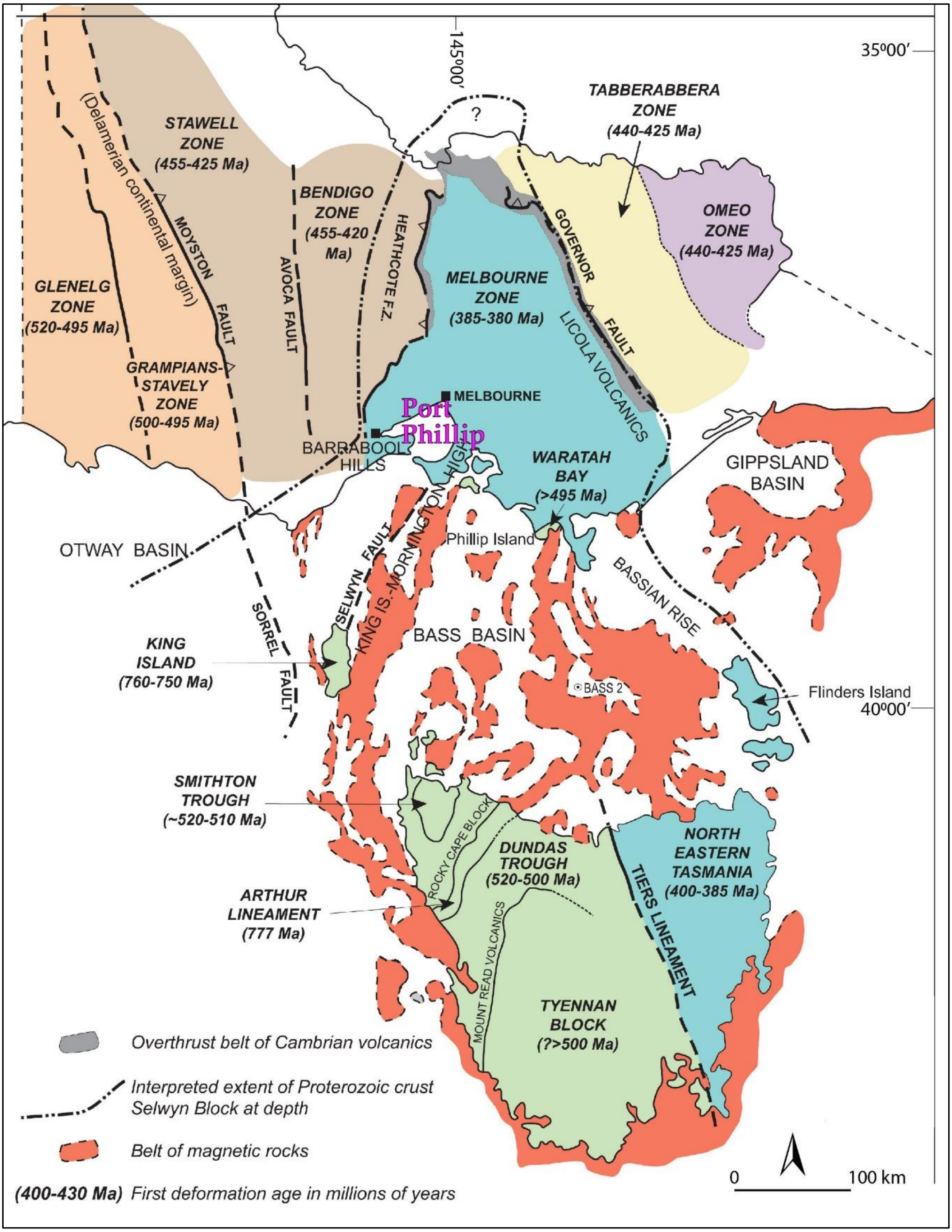

Figure 2.3. Structural zones, Victoria. (VandenBerg et al., 2000).

2.2.2 Tectonic Framework and Faulting

Faults have four clear expressions in Port Phillip.

- The dimension and broad outline of the bay is produced by tectonic structures – faults, folds and warps. Port Phillip Sunkland lies in the downthrown block between the Rowsley Fault and Selwyn Fault at the western edge of the Mornington Horst, a fault bounded geological and topographical high between the Port Phillip and Western Port Sunklands. The Rowsley Fault—the western margin of the Port Phillip Sunkland—is a rejuvenated older fault, the downthrow resulting in the basalt-covered plains and low coast from Point Cook to Point Lillias.
- Geomorphic consequence of tectonics along parts of the bay coastline is shown by: (a) coastal orientation and backshore elevation from Frankston to Dromana - defined by the strike and uplift of the Selwyn Fault), (b) the change in coastal direction at Table Rock Point from SSE to NNE along the Beaumaris Monocline, (c) the broad configuration, elevation and backshore geology of the Bellarine Peninsula northeast of Clifton Springs defined by the Curlewis Monocline.
- Faults develop fractures and shear zones in brittle rocks leaving them more vulnerable to weathering and erosion, e.g. Mount Eliza Granite north of Daveys Bay and Sunnyside and Mount Martha Granodiorite. The Mount Martha pluton is deeply weathered and lacks the boulders and bold slope outcrops commonly associated with this rock. A deep mantle of sandy regolith—a remnant of which occurs immediately north of Martha Cove canal entrance—has been stripped from the coast exposures exposing irregularly fractured granite in cliffs and (unusually in granite) a horizontal shore platform.
- Uplift exposes several geological formations with different properties of structure, cohesion and resistance or response to weathering and subaerial and coast/marine processes e.g. changes from basalt to Sandringham Sandstone at Mornington.

As well as being the main component of the present landform, the Port Phillip Sunkland has been a depositional basin (the Port Phillip Basin) over the Cainozoic (66 Ma to present), accruing marine and terrestrial sediment and interbedded lava flows. The thickest accumulation (>1,000 metres) including Sandringham Sandstone[1] is in the Sorrento Graben between the Bellarine Fault and Selwyn Fault (Holdgate et al., 2002).

2.2.3 Geological Variations

The high tide shore of Port Phillip is backed by geological materials mostly of low resistance to displacement or erosion. Long sectors of coast are topographically low and comprised of beach and dune sediments including barrier and dune ridges and alluvial and intertidal sands, silts and clays. Relatively resistant geology is limited to short sectors of granites at Mornington and Mount Martha, Newer Volcanics Group basalt at Williamstown and Point Lillias, outcrop of strongly ferruginous beds of Sandringham Sandstone at Black Rock, Beaumaris, Mt Eliza, Mornington and western Corio Bay, and short sectors of secondarily cemented calcarenite (calcrete) in Bridgewater Formation at Point Nepean and Point Lonsdale (see Figures 2.1, 2.4).

[1] Sandringham Sandstone replaces the several terms used to describe the Miocene-Pliocene sandy silt, fine sandstone, sandy conglomerate to pebbly sandstone, clayey sand, clayey gravel etc. beds previously known as Brighton Group, Black Rock Sandstone, Red Bluff Sands, Baxter Formation, Moorabool Viaduct Formation.

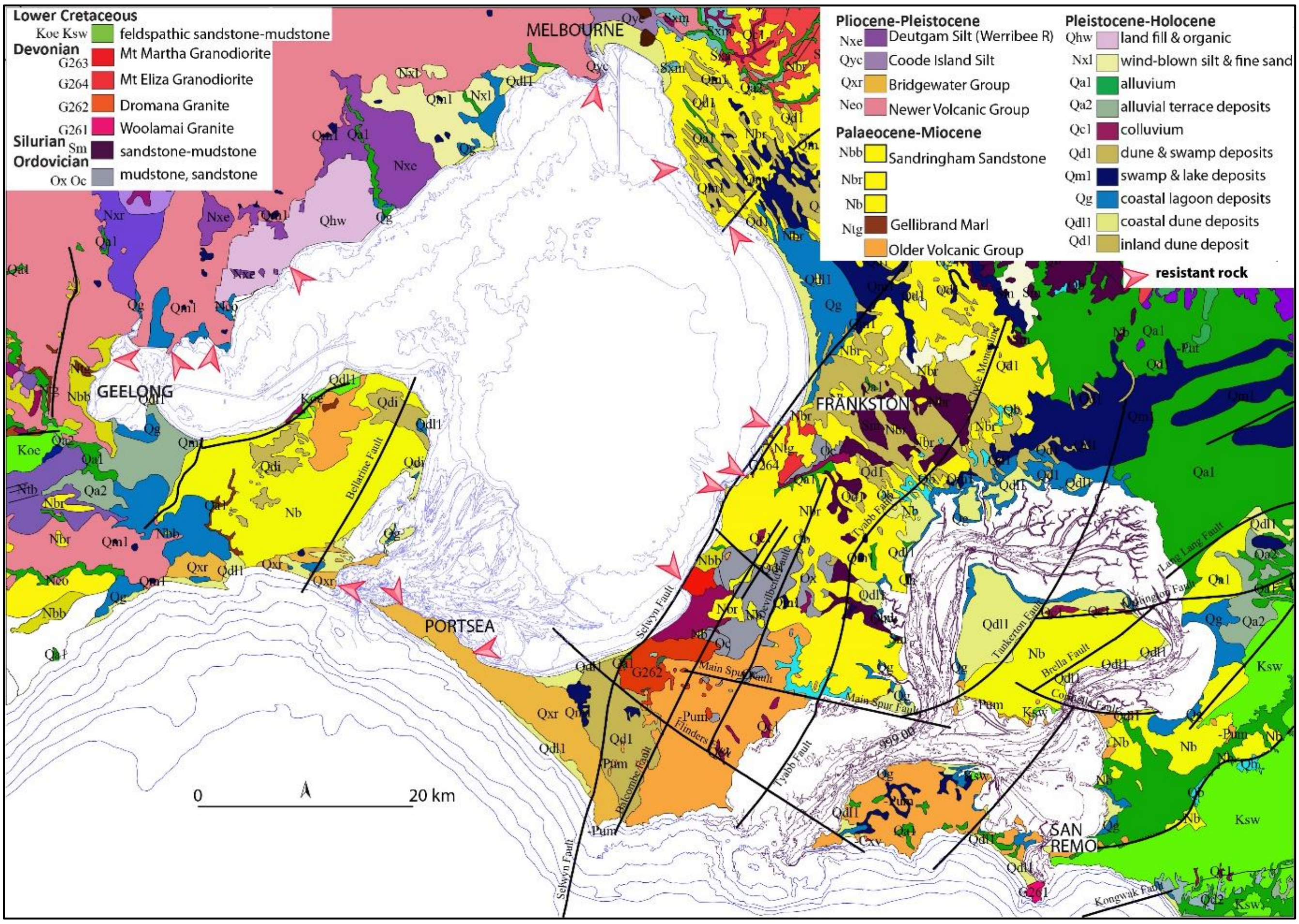

Figure 2.4: Coastal geology and structure, and sectors of resistant rock: Port Phillip and Western Port (after, Seamless Geology, Geoscience Victoria 2011 (Note that red arrows indicate resistant rock outcrops)

The basalt lavas of the Newer Volcanics that underlie much of the western shoreline are on the downthrow side of the Rowsley Fault and crop out below high-water level or are of low relief in the backshore. Many sectors of the steep coast of the Bellarine and Mornington Peninsulas—including the granitic and Older Volcanic geologies—are fault-elevated and the rocks are closely fractured, sheared and often deeply weathered and susceptible to erosion. Although marine Ordovician and Silurian sediments form the uplifted core of the Mornington Peninsula, they have no coastal outcrop in Port Phillip.

2.2.4 Coastal Processes

To the north of the entrance to PPB lies a flood tidal shoal and channel complex (collectively known as the Great Sands). Mud Islands is a low emerged sector of this sediment body that contains sand bars and barriers and also mud in parts of the lagoons. The Great Sands are an unconsolidated sand veneer between 1.5 m and 7 m thick comprised primarily of sand washed in through the entrance in Holocene times. They are underlain by Pleistocene Bridgwater Formation calcareous sandstone derived from transgressive sand dunes during lower and rising sea levels of the penultimate and last glacial stages (Keble 1946, 1968, Holdgate et al., 2001, Healy 2010). The Great Sands is covered by less than 5 m of water at most tides and exerts significant hydrodynamic and sedimentological controls on the bay.

The single narrow ocean connection defined by rocky headlands and shore platforms of Bridgewater Formation at Point Nepean and Point Lonsdale and the extensive accumulation of mobile sand shoals (Great Sands) inside the entrance underlain by Bridgewater Formation restricts the movement of ocean swell and reduces the tide range progressively in the bay. The high-water shoreline length of Port Phillip including Swan Island, Duck Island and Mud Islands is approximately 310 km (Marine Bathymetry data set: Dept. of Sustainability and Environment 2014). Low Water shoreline length measured from the same data set is 332 km, the increase due largely to low tide exposure of channels and pools in Swan Bay.

PPB is fetch-limited and waves and currents that determine onshore-offshore and long-shore sediment movement and backshore energy are determined by local winds. The east coast is subject to storm wave conditions with local occurrence of high wave energy conditions and subsequent impact on beaches and soft rock and low backshores. Sand around the northern, eastern and western shore and nearshore appears to be derived from earlier weathering of Cainozoic sedimentary rocks and Palaeozoic granite previously exposed as active cliffs. On a bay-wide scale, there is now minimal opportunity for beach sands to be derived from these cliffs due to the extent of coast protection structures where these beds crop out at the backshore. Fluvial input of beach sediment is minimal. Sand-sized shell debris is a variable component and locally significant on some west coast beaches. The wide and variable cover of seagrass/macroalgae along the western coast further limits onshore and alongshore sediment movement. There is a limited area of coastal wetland (mangrove and saltmarsh) associated with fine sediment substrate.

2.2.5 Sea-level Changes

A late-Pleistocene sea-level chronology for eastern Australia shows Port Phillip would have been emerged during lower sea level for most of the last 120,000 years before submergence by the post-glacial – Holocene SLR around 8,000 years ago (Figure 2.5). Holdgate et al., (2011 their Figure 3) shows sea level in Port Phillip did not reach present level until approximately 6,500 years BP or 1,000 years later than the open ocean sea level.

Holdgate and Norvick (2017) showed that estuarine and deltaic sediments were deposited along the submerging Yarra River channel by 8,000 years BP and built up to 1 m higher than present by 6,000 to 5,000 BP. They further propose (as did Holdgate et al., 2011) that a sea level fall in Port Phillip began 2,800 years ago as sand blocked the entrance channel. A combination of continuing blockage and lengthy droughts saw water-level in PPB continue to fall to ~20 m below present level and remain at that level until 1,000 years BP. Lengthy droughts and an excess of evaporation over precipitation saw the isolated lake shrinking to expose most of the bay floor. Breaching of the entrance sand blockage around 1,000 years BP, possibly due to storms or flood, allowed marine submergence to be re-established.

If the scenario of a late Holocene episode of a dry Port Phillip is accepted (and the evidence is robust), the shorelines of the present bay are geologically newly submergent. Effectively the 20 and 21st century sea level rises are a continuation of a very rapid rise over a few years or decades 1,000 years ago. Sediment transport and depositional regimes and beach and backshore dynamics are therefore relatively recently developed and were still adjusting when artificial modifications of PPB shoreline commenced, compared with a longer-term period of several thousand years of adjustment.

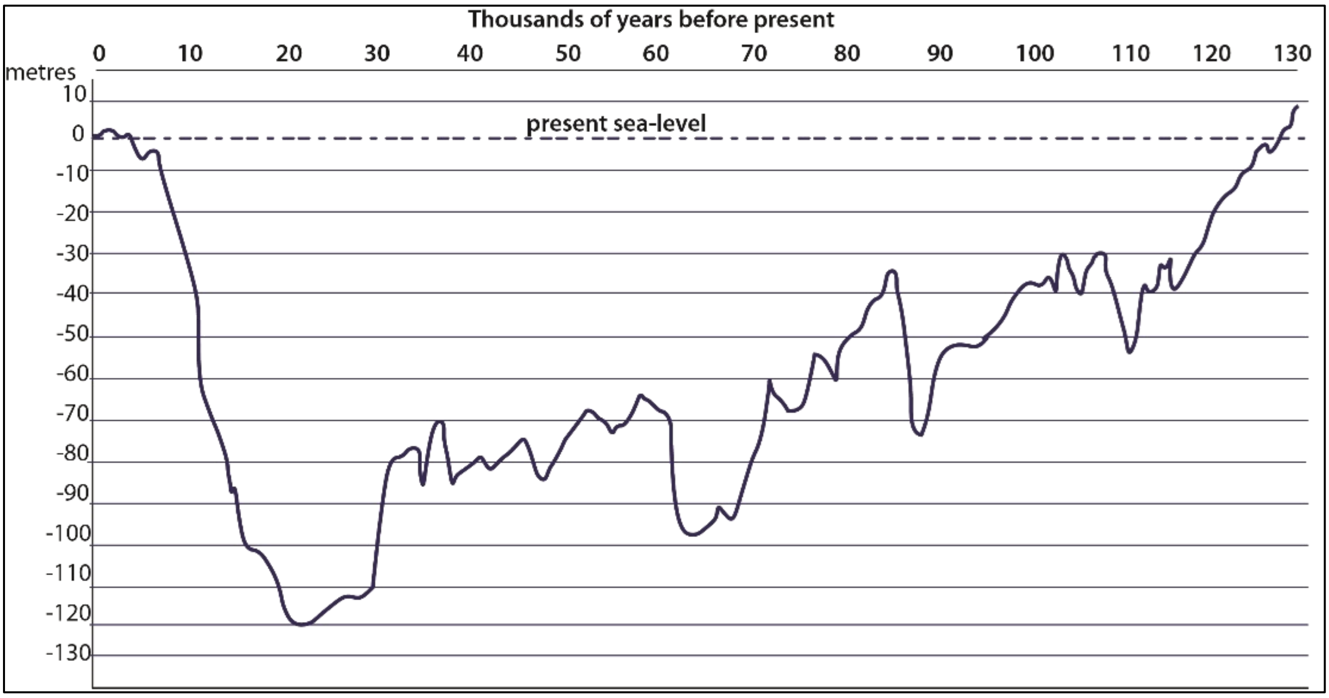

Figure 2.5: Graph of sea-level changes in eastern Australia over the last 130,000 years (after Brooke et al., 2017).

2.2.6 Engineering Modifications

Much of the pre-1840's shoreline of Port Phillip is now obscured or extensively modified by engineering works dating from the 1840's (Figure 2.6). Parts of PPB and the lower Yarra River channel have been artificially deepened since the 1850's to facilitate berthing and to accommodate larger vessels. Initial works focussed on the Yarra River and included steam dredging the river mouth, blasting basalt rock bars at Queen Street and Spencer Street, shortening the river by constructing the Coode Canal and excavations for Victoria Dock. Deepening the bay entrance by blasting limestone rock began in 1864 and continued until the 1950's. Subsequently, shipping channels in the south of the bay were established and maintained by regular dredging (South Channel, the Corio Bay and Yarra entrance channels) and dredge material grounds established.

The initial structures to service passenger and cargo trade were concentrated at Portsea, Port Melbourne and near Geelong, but to meet increasing requirements of recreational boating, mooring and launching facilities including large breakwater-defended marinas and canal estates are now widespread around Port Phillip. The building of seawalls, revetments and groynes, beach nourishment and landfill have been undertaken to prevent or reduce coastal recession and secure built assets. Since the mid 1970's beach re-nourishment using sand from land sources, nearshore dredging or low tide scraping has been applied to at least 30 sites around the bay. Extensive areas of the immediate backshore are now fundamentally reshaped by industrial and service facilities including the former salt works at Altona, Western Treatment Plant at Werribee, aerodromes at Point Cook and Laverton, and widespread residential subdivisions including bay-linked canal estates at Point Cook, Patterson Lakes and Martha Cove.

Figure 2.6: Picnic Point Sandringham in 1972 showing seawall isolating former active cliffs and in 2012 after construction of groynes and beach re-nourishment. (Photos N. Rosengren).

2.3 Meteorology and Climatology

2.3.1 Meteorological Drivers of Coastal Hazards in Port Phillip Bay

The weather and climate of PPB is affected by the seasonal movement of the sub-tropical ridge (STR), a region of high atmospheric pressure that moves between its winter location at around 30°S and its summer position at 40°S (Figure 2.7). To the south of the STR is a band of eastward-propagating low pressure and frontal systems (Kent et al., 2013), which are the major cause of storm surges along the Victorian coast including PPB (McInnes and Hubbert, 2003; McInnes et al., 2016). Storm surges occur most frequently during the winter months (McInnes and Hubbert, 2003) when the STR is at its northernmost extent.

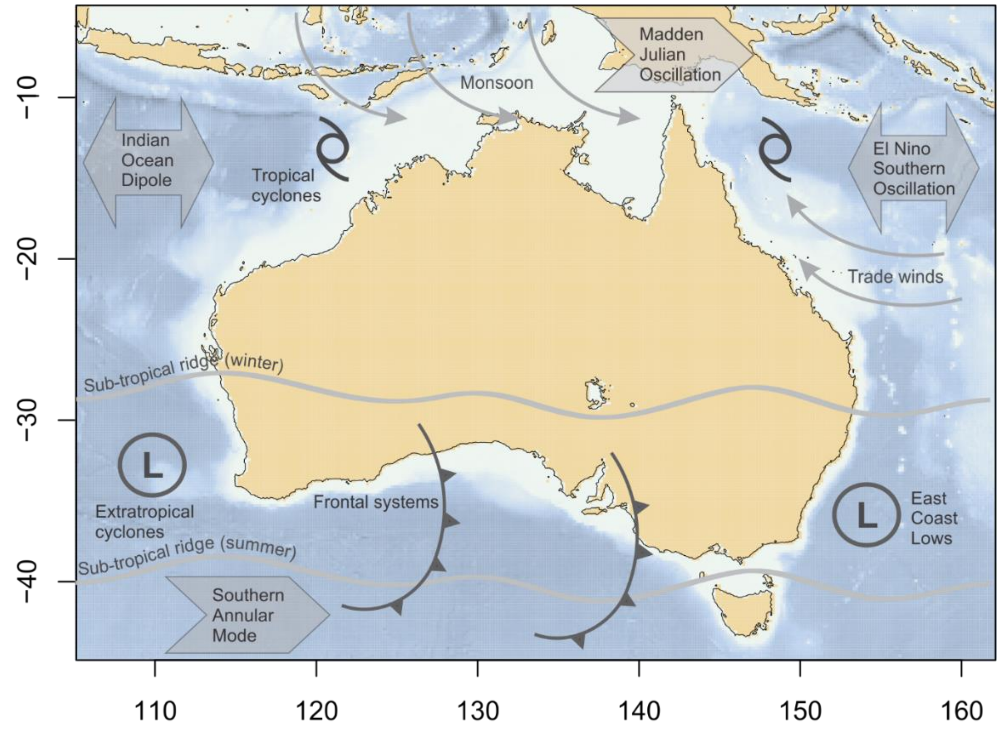

Figure 2.7: Weather and climate drivers that cause extreme coastal sea levels (from McInnes et al., 2016).

2.3.2 Climatological Influences on Coastal Hazards along Victoria's Coast

Natural climate variability affects the behaviour of weather patterns from year to year and this in turn influences the year-to-year frequency of extreme sea level events including those in PPB. Along Australia's south coast, a major cause of variability on multiyear time scales is due to the Southern Annular Mode (SAM) (Figure 2.6). In the positive phase of SAM, the mid-latitude westerly wind belt together with storm surge-producing frontal systems shifts poleward, while in the negative phase they shift equatorward.

El Niño Southern Oscillation (ENSO) is another mode of variability that affects sea surface temperature (SST) patterns across the Pacific and influences sea levels and weather conditions around Australia's coast. Along the southeastern coast of Australia, the effect of ENSO on sea levels is minor compared to its effect along the northern (west of Cape York Peninsula) and western coastline (McInnes et al., 2016; their Figure 2a). In addition to ENSO events, which typically last for 18 months, is the longer lasting Interdecadal Pacific Oscillation (IPO) that typically varies on decadal or longer time scales. The IPO positive (negative) phase has similar effects on weather and ocean levels and temperature as an El Niño (La Niña) event. The relationship between ENSO and coastal winds, waves and currents in eastern Victoria were studied in O'Grady et al., (2019b). They found that on seasonal to annual time scales there was a weak connection between the transport caused by waves and currents between *El Niño* and *La Niña* events. During *La Niña* (*El Niño*) events, the weather systems shift north (south) and cause in anomalous eastward (westward) transport along the east Victorian coast.

2.4 Hydrodynamics and Tides

2.4.1 Tide and Hydrodynamic Processes in Port Phillip Bay

PPB is a large coastal re-entrant (tidal embayment), largely sheltered from ocean swell, and dominated by wind and tidal currents. Therefore, understanding how SLR influences the hydrodynamics of the bay is a key element of the coastal hazard assessment.

Coastal sea levels vary on a range of time scales due to astronomical tides, and variations in weather and climate. Astronomical tides vary on multiple timescales from daily high and low tides to fortnightly spring and neap tides. Seasonal variations, related mainly to the movement of pressure patterns as discussed in the previous section and interannual variations in tides, also occur. Typically, the highest astronomical tide (referred to as HAT) occurs on an 18.6-year lunar tidal cycle, although small variations associated with the Earth's orbit around the sun cause additional variations on longer time scales. Tide types range from strongly diurnal (one high and one low tide per day), to mixed, through to semi-diurnal (two high and two low tides per day). Over much of Bass Strait (including PPB), tides are predominantly semi-diurnal (McInnes et al., 2016). Within PPB the tidal range is reduced to about half of the value in Bass Strait with HAT at Geelong 0.7 m AHD (Australian Height Datum) compared to HAT at Lorne of 1.3 m AHD (Cardno, 2015).

Storm surges, in comparison, are gravity waves (waves where the velocity of propagation is a function of gravity) arising from the inverse barometer effect and wind stress. The former elevates sea levels approximately 1 cm for every 1 hPa fall in atmospheric pressure relative to surrounding conditions, and wind stress induces currents over shallow water. Wind stress directed onshore leads to an increase in sea levels (i.e. 'wind setup'), particularly within semi-enclosed embayments or under severe wind forcing such as produced by tropical cyclones. In mid-latitudes, wind-induced coast-parallel currents, which persist for a day or more, undergo Coriolis deflection. In the southern hemisphere this increases coastal sea levels when the direction of current flow has the coast to the left and is referred to as 'current setup'. Conversely if the forward flow of coastal currents has the coast to the right in the southern hemisphere, sea levels fall and this is referred to as 'current setdown' (McInnes et al., 2016). Current setup is the dominant cause of storm surges along the Victorian coast due to the west to east passage of cold frontal systems embedded in the mid-latitude westerlies (Figure 2.6) during the winter months of the year (McInnes and Hubbert, 2003). Sea level residuals at Williamstown exhibit similar variations to those on the open coast during such events (Hubbert and McInnes, 1996) although local winds on the bay typically cause higher sea levels on the northern and eastern sides of the bay (McInnes et al., 2009a). This NE-SW gradient is reflected in the 1% AEP storm tides at Williamstown, St Kilda, Geelong and Queenscliff, which were estimated to be 1.12 ± 0.06 m, 1.19 ± 0.08 m, 1.10 ± 0.07 m and 1.04 ± 0.08 m AHD respectively (ABN, 2015).

The Victorian coast is microtidal. The tide range at Port Phillip Heads is around 1.6 m spring and 1.06 neap, reducing to 0.6 m and 0.4 m respectively at Williamstown. Tidal currents vary accordingly throughout the bay with the strongest currents exceeding 3.5 ms^{-1} at Port Phillip Heads, over 1 ms^{-1} in the channels in the south of PPB to below 0.2 ms^{-1} throughout much of the remainder of the bay (Cardno, 2007; 2015). Current measurements at the vicinity of the Sands indicate lower currents of around 0.1 ms^{-1} (Walker and Sherwood, 1997). During storms, current speeds of 0.3-0.6 ms^{-1} are found to occur in the vicinity of St Leonards (Cardno, 2011). Mobilisation of sediment by currents (however generated) is governed by a wide range of factors including current velocity and fluid properties, and the size, shape and compaction of the bottom sediment. Because of these variables, no single value of threshold velocity can be presented. However, the velocities of tidal currents across most of the bay are below the threshold for sand mobilisation. This process is therefore restricted to the entrance channels, parts of the Great Sands and limited areas of beach in the southern bay. Wind-derived currents greatly exceed tidal currents (temporally and spatially) as the mechanism for sediment transport onshore and alongshore of most (if not all) bay beaches.

2.4.2 Regional Scale Hydrodynamic Model Studies

Several hydrodynamic modelling studies have been undertaken from regional to national scale for the purposes of providing hydrodynamic outputs (mainly sea level heights) to be used to provide estimates of Average Recurrence Intervals (ARI) of extreme sea-level events consistently along the broader coastline. Haigh et al., (2014) developed an Australia-wide version of the MIKE21 model on an unstructured grid with a maximum coastal resolution of 10 m to simulate the water levels arising from weather and tides over the period 1949 to 2009 using 6-hourly gridded meteorological forcing obtained from the National Centers for Environmental Prediction (NCEP) reanalyses. Recently Pattiaratchi et al., (2018) updated this work using a 3D unstructured implementation of the Semi-implicit Cross-scale Hydroscience Integrated System Model (SCHISM) using tides and 3-hourly meteorological forcing from the Japanese Reanalysis (JRA) hindcast over 1959 to 2016 with coastal horizontal grid resolution up to 800 m. A depth-integrated implementation of the ROMs model at 5 km resolution over southeastern Australian (Colberg and McInnes, 2012) and the whole of Australia (Colberg et al., 2019) was developed to assess how projected future changes in weather conditions would affect coastal extreme sea levels. Both studies included a 'hindcast' simulation including tides and meteorological reanalysis with Colberg and McInnes, (2012) using NCEP reanalysis for meteorological forcing and Colberg et al., (2019) using hourly forcing provided by the higher spatial resolution (38 km) Climate Forecast System Reanalyses

(CFSR) data (Saha et al., 2010) over the period 1981-2012. None of these studies include the modelling of wave effects.

Colberg and McInnes (2012) and Colberg et al., (2019), studied the effect of future changes in atmospheric conditions on storm surges using atmospheric forcing from Coupled Model Intercomparison Project (Phases 3 and 5) (CMIP3 and CMIP5) global climate model simulations and higher resolution regional climate simulations. Both studies simulated the hydrodynamic response using twenty years of climate model wind and pressure forcing from the end of the twentieth century and the twenty-first century in eight different climate models. The differences in simulated annual maximum sea levels between the two time periods were then compared. Colberg and McInnes (2012) found the change in modelled average maximum sea levels between the latter and former periods was in the range of +1.0 to -6.0 cm. Similarly, Colberg et al., (2019) found changes in seasonal maximum sea levels that ranged from +2.0 to -5.0 cm. This tendency for declines in the magnitude of storm surges over this time period was found to be due to the projected southward movement of the subtropical ridge (STR), the mid-latitude storm track and the associated cold frontal systems that typically cause elevated sea levels along Australia's south coast. It is a considerably smaller effect than the projected mean SLR over the same time period which is in the range of +50 to +100 cm depending on emission scenario (McInnes et al., 2015) and highlights that mean SLR rather than changes in storm systems will be the dominant cause of changes in extreme sea levels in the future.

2.4.3 Hydrodynamic Modelling Studies of Port Phillip Bay

A large number of previous studies have addressed the hydrodynamics of PPB through the development of hydrodynamic models to address a range of applications. A subset of these studies is discussed here in more detail because of their relevance to the hydrodynamic modelling in the PPBCHA.

Hydrodynamic modelling studies of the bay have used 2D (depth-averaged) shallow water equation models on orthogonal Cartesian grids, where the priority to maximise model resolution and regional coverage of events while managing computational overheads was addressed by using multiple nested model grids (e.g. Black et al., 1990; McInnes and Hubbert, 1996, 2003; McInnes et al., 2009a, b, c; McInnes et al., 2013) where information simulated on the outer, lower-resolution grids provided boundary forcing for the inner grid. More recent modelling studies of PPB have generally used models with variable orthogonal grid resolutions (Cardno, 2007; Lawson and Treloar, 2004), or unstructured, triangular model grids of variable resolution that maximise the resolution in the region of interest (Water Technology, 2017c) and some of these have also included wave models.

Black et al., (1990) investigated the impact of sea level rises of 0.3 m and 1.0 m on tidal range in PPB and found an increase in tidal amplitude of 0.015 and 0.06 m (or 4% and 15%) respectively. From their results they derived an empirical relationship between SLR and tidal range increase of $\xi_p = \xi + A(\xi - \xi_{msl}) + R$ where R is mean SLR, ξ is original high tide level, ξ_{msl} is the original mean sea level and A varies in value of (0.010, 0.037, 0.070, 0.145) for SLR of (0.1, 0.3, 0.5 and 1.0) respectively. The sensitivity of changes in water depths at the Heads on tidal range increases within the bay was demonstrated by Cardno (2007) and Lawson and Treloar (2004) in simulations that included pre- and post-channel deepening at the entrance to PPB.

McInnes and Hubbert (1996, 2003) investigated the weather systems leading to extreme water levels on the bay, finding that transitory cold frontal weather systems that travelled from west to east along the southern Australian coast, most frequently during autumn to spring, were responsible in 83% of storm surges studied. The remaining causes of storm surges were due to low pressure systems that develop and intensify within Bass Strait. While the events they studied were not particularly severe, they noted that a particularly severe form of this type of weather event was responsible for the 1934 floods and the largest ever recorded sea level at Williamstown (1.33 m AHD at 2100 hours on 30 November 1934 local time). In that event, the low that developed in Bass Strait intensified to about 985 hPa (based on Bureau of Meteorology analyses), equivalent to a 25 cm increase in sea level due to the inverse barometer effect. The rainfall was significant (144 mm of rainfall recorded at Melbourne between 1900 hours on 30 November and 0230 on 1 December 1934) and widespread, causing major flooding across Victoria (McInnes et al., 1996).

McInnes and Hubbert (2003) also used a series of hydrodynamic model simulations forced with gridded Bureau of Meteorology wind and surface pressure analyses to show that when the western boundary of the hydrodynamic model was moved progressively eastwards from the western edge of South Australia to the western edge of Bass Strait, the modelled storm surge heights in Bass Strait became progressively underestimated. This demonstrated the need to model the broader southern Australian coast to correctly capture the storm surge amplitudes in Bass Strait and PPB.

Following a national ‘first pass’ assessment of inundation and erosion (Australian Government Dept. Climate Change, 2009), as part of the ‘Future Coasts Program’, storm tide return periods were developed for Victoria’s coast (McInnes et al., 2009a) and PPB (McInnes et al., 2009b) to provide data to underpin more detailed assessments of coastal hazards utilising a state-wide Light Detection and Ranging (LiDAR) data set. McInnes et al., (2009a, b) modelled the storm surge associated with extreme sea level events identified in tide gauges over a 38-year period. A joint probability method combined the modelled storm surge levels with tides to produce storm tides, and Average Recurrence Intervals (ARI) were estimated (Table 2.1). Projections of future wind speed change from Coupled Model Intercomparison Project 3 (CMIP3) ensemble of climate models ranged from decline to increase in future wind speeds in the vicinity of the Victorian coast, depending on the climate model. Adopting a worst-case approach, the upper end of the range of change (i.e. the highest projected wind speed increase) was applied to the storm surge calculations via a scaling relationship. The wind change together with SLR were applied to the assessed 1-in-100-year ARI storm tides and these formed the basis for future climate scenarios for application in inundation modelling and mapping. Using the Victorian terrestrial LiDAR dataset, inundation potential (using the bathtub approach) was investigated for a selection of low-lying locations in PPB by McInnes et al., (2009b, 2013) as well as for the entire state by Lacey and Mount (2011) to provide a digital dataset of spatial layers indicating the extent of land subject to coastal inundation due to projected SLR from 2009 to 2100.

A number of caveats with the storm tide return period modelling and inundation analysis discussed above have been noted (McInnes et al., 2013). For the storm tide assessment, these included the omission of the effects of SLR on tidal range within PPB and the absence of wave contributions to extreme sea levels. For the inundation assessment they noted that while the bathtub approach to inundation mapping was an economical method for a high-level assessment of inundation hazard, a number of additional factors were proposed to improve the inundation assessment. These included using dynamic inundation approaches that account for the time dependency of water level extremes in the storm tide component to more realistically model inundation extents, which are potentially more important in semi-enclosed bays like PPB compared to the open coast. They also noted that the catchment inflows, wave effects and drainage systems may also influence inundation extents.

Subsequent local scale coastal hazard assessments have been carried out for the Victorian coast including for Bellarine to Corio Bay (Cardno, 2015), Mordialloc (Water Technology, 2014a), Lakes Entrance (Water Technology, 2014b), Western Port (Water Technology, 2014c, d), and Port Fairy (Water Research Laboratory, 2013).

Table 2.1: The 1% AEP storm tide height levels for selected locations around PPB under current climate conditions and climate change scenarios from McInnes et al., (2009b).

Location	Current Climate	2030			2070			2100			
		1	2	3	1	2	3	1	2	3	4
Point Lonsdale	1.41	1.56	1.62	1.61	1.88	2.07	2.11	2.23	2.53	2.51	2.81
Queenscliff	1.23	1.38	1.46	1.43	1.70	1.90	1.93	2.05	2.34	2.33	2.63
Geelong	1.06	1.21	1.28	1.26	1.53	1.72	1.76	1.88	2.16	2.16	2.46
Werribee	1.09	1.24	1.32	1.29	1.56	1.77	1.79	1.91	2.22	2.19	2.49
Williamstown	1.12	1.27	1.36	1.32	1.59	1.81	1.82	1.94	2.26	2.22	2.52
St Kilda	1.15	1.30	1.39	1.35	1.62	1.83	1.85	1.97	2.28	2.25	2.55
Aspendale	1.14	1.29	1.39	1.34	1.61	1.83	1.84	1.96	2.29	2.24	2.54
Frankston	1.15	1.30	1.40	1.35	1.62	1.84	1.85	1.97	2.28	2.25	2.55
Mornington	1.14	1.29	1.39	1.34	1.61	1.82	1.84	1.96	2.28	2.24	2.54
Rosebud	1.09	1.24	1.34	1.29	1.56	1.77	1.79	1.91	2.22	2.19	2.49
Rye	1.04	1.19	1.29	1.24	1.51	1.71	1.74	1.86	2.16	2.14	2.44
Sorrento	1.00	1.15	1.25	1.20	1.47	1.66	1.70	1.82	2.10	2.10	2.40

Notes: Scenario 1 incorporates the Intergovernmental Panel on Climate Change (IPCC) AR4 high-end A1FI SLR scenario, Scenario 2 incorporates the IPCC AR4 high-end A1FI SLR scenario together with a high-end wind speed scenario, Scenario 3 considers sea level projections of the Netherlands Delta Committee (Vellinga, 2008) and Scenario 4 considers sea level estimates from Rahmstorf (2007). All values are in metres relative to late 20th century mean sea level.

A recent coastal inundation assessment undertaken by Water Technology (2017c) for Melbourne Water, used a Flexible Mesh hydrodynamic model of the bay coupled to a wave model to simulate 1% and 10% AEP events in PPB. The heights of the 1% and 10% events were defined through extreme value analysis of the Lorne and Williamstown tide gauge data and extreme events identified in the longer (undigitised) Williamstown record described in Adams (1987). They found that the inclusion of historical extreme events in the analysis (including the 1934 event) increased the 1% AEP water level estimates by 0.09 m compared to only considering tide gauge data from 1966-2015. The extreme events identified in the record were also used to inform the construction of design storms (the duration and height of the storms that could plausibly lead to the required AEP levels) for the purposes of providing inputs to the hydrodynamic modelling. The hydrodynamic modelling provided coastal water levels, consistent with the required AEPs that also included local hydrodynamic and wave effects. Differences in the 1% AEP levels were found across PPB between McInnes et al., (2009b) and Water Technology (2017c) where the levels in the latter study are higher by about 0.25 m. These differences are likely due to (methodological differences between the way that storm tides were modelled between the two studies. McInnes et al., (2009b) modelled actual events with meteorology, tidal and storm surge levels covarying temporally and spatially across the boundaries of the model and the simulated events were statistically analysed to produce AEPs. Water Technology (2017c) used a design storm approach where a single design storm time series for sea level height, adjusted to peak at the AEP level of interest, was applied to the entire southern boundary of the model and a design wind timeseries of constant direction was constructed from anemometer winds at South Channel Island during storm surge events and applied uniformly to the entire hydrodynamic model domain. The assumptions and simplifications made in the design storm approach for application to a large model domain such as PPB creates uncertainties in the spatial patterns and magnitudes.

2.4.4 Summary

In summary, the majority of storm surges in PPB are caused by transitory eastward moving frontal systems, and less frequently by low pressure systems that intensify in Bass Strait. Hydrodynamic modelling has demonstrated that to accurately simulate the amplitude of the storm surges in Bass Strait and PPB from frontal systems, the western boundary of the model needs to extend as far west as the western border of South Australia. Within PPB, the prevailing southwesterly winds also cause local wind setup so that the highest sea levels typically occur in the northeast of the bay. Hydrodynamic modelling with winds and pressure from climate models have been used to investigate how climate change may affect extreme sea levels along the southern coast of Australia in the future. They have shown that the general southward movement of the storm tracks, including the weather systems responsible for storm surges in this region, would lead to small changes (mainly reductions) in extreme sea levels of several cm, highlighting that mean SLR rather than changes in storm systems will be the dominant cause of changes in extreme sea levels in the future. Hydrodynamic modelling of PPB under SLR scenarios has also shown that the tidal range within the bay would become amplified due to reduced hydraulic friction through Port Phillip Heads, thereby potentially leading to higher extreme sea levels than due to SLR alone.

2.5 Waves

2.5.1 Overview of Wave Processes in Port Phillip Bay

The wave climate of the interior of PPB is predominantly a result of waves generated by local winds in a fetch-limited embayment. The limited fetch (maximum of approximately 50 km), and in places shallow waters, mean that wave heights and periods are limited, rarely exceeding 2 metres and 4 seconds respectively, with the wave direction aligned with the prevailing wind. The wave climate of the PPB is thus heavily dependent on the climatology of the local winds (see Section 4.1).

The Port Phillip Heads are exposed to the energetic Bass Strait wave climate, which receives long swell waves generated in the Southern Ocean. The swell propagates into the southern part of the bay, where its influence is largely limited to the area between Swan Island and Portsea (Advisian, 2016).

Locally generated wind waves and remotely generated swell waves dissipate as they approach the shoreline, primarily through wave breaking. This dissipation (momentum flux or radiation stress gradient) can elevate mean water levels shoreward of the region where wave breaking occurs—a process known as wave setup. Unbroken individual waves and variations in incoming wave heights (“surf beat”) lead to the uprush of water at the shoreline, a process known as wave runup. Wave energy (height and period) is defined by wind speed, duration and wind fetch (the distance over which the wind is blowing). Sheltered coastal areas such as harbours and lagoons—the typical location of tide gauges—generally do not experience significant wave runup or setup.

2.5.2 Observational Studies

Wave measurements have been made in Bass Strait since 2003 at the Port of Melbourne Corporation (PoMC) wave buoy located approximately 8 km southeast of Point Nepean. These indicate that the wave climate is swell dominated with about 92% of the waves coming from the south-south-west and south-west directions with the most frequent direction of origin around 213° (Cardno, 2015). The average significant wave height (Hs) and average peak wave period (Tp) from Cardno (2017a) are provided in Table 2.2. This limited swell direction variability is further limited and modified by refraction, wave-current interaction and diffraction through the narrow PPB entrance. Thus, within PPB the (attenuated) swell waves presumably have very limited local directional variability within the parts of PPB where they are of any significance, although more detailed wave frequency-directional (spectral) analysis would be required to quantify this. The locally generated wind-waves within PPB, however, are important over the whole bay, and more variable in direction (depending on wind direction variability).

Table 2.2: Measured average wave conditions 8 km south of Point Nepean (source; Cardno, 2015).

Season	Hs (m)	Tp (s)
Annual	1.7	12.8
Summer (DJF)	1.6	11.7
Winter (JJA)	1.7	13.6

Within PPB waves are mainly wind-generated and are generally much smaller compared to the larger Bass Strait swell waves, with Hs typically less than 1 m within the bay. However, depending on water depth, strong winds from certain directions are able to produce Hs up to 2 m. Analysis of wind directions and frequency show that winds rarely occur from the direction of the greatest fetch (northeast), therefore the occurrence of waves from that direction is similarly infrequent. The presence of Mud Islands and the surrounding Great Sands (Figure 1.1) limits the wave energy reaching the shoreline of the east coast of the Bellarine Peninsula. Similarly, in Swan Bay, the water depths are very shallow with large areas of seagrass. This results in a very low wave-energy environment. At Portsea, longer period waves appear to propagate further into the bay from Bass Strait, with more swell wave energy predicted at Portsea under long wave conditions (20 s waves) than shorter (10 s waves) (Advisian, 2016). Waves measurements inside PPB have been limited to short term deployment of instruments for specific studies. Therefore, developing physically consistent wave information across the bay has typically required the running of wave models (e.g. Cardno, 2007).

2.5.3 Regional Scale Wave Model Studies

Modelling studies that cover the broader Victorian coastline potentially provide relevant information at the Heads. A global wave hindcast was developed by Durrant et al., (2014) covering the period 1979 to 2010 using the WaveWatch III spectral wave model at a spatial resolution of 0.4° (~50 km resolution) as well as two higher resolution nested grids around Australia and the South Pacific of 10' (~18 km) down to 4' (~7 km). Efforts continue to update this hindcast to the present. Gridded outputs include commonly used variables such as H_s, T_p, mean wave period, T_m, as well as many other wave-related parameters.

An increase in Southern Ocean wave heights is projected to continue through the twenty-first century, with the southern and western coasts of Australia exposed to this projected increase (Hemer et al., 2013). A recent study has found that the 1% AEP event increases by 5 to 15% over the Southern Ocean by the end of the 21st century (2081-2100), compared to the 1979‑2005 period (Meucci et al., 2020). Associated with wave height increase in the Southern Ocean is a projected increase in wave period along the Australian south coast. This is associated with an increase in wave swell by the end of the 21st century compared to the late 20th Century (e.g. Fan et al., 2014, Morim et al., 2018, 2019). Changes in wave period, together with projected changes in wave direction (Hemer et al., 2013; Morim et al., 2019) have the potential to influence coastal stability as much (or more) than the changes in wave height.

2.5.4 Wave Modelling Studies in Port Phillip Bay

Inside PPB, several wave modelling studies were undertaken to support the Channel Deepening Project (CDP) (e.g. Cardno, 2007; 2010). The increased erosion at Portsea Beach was also investigated by using wave models which were shown to simulate the refraction of incoming swell waves onto the Portsea Beach by the edges of the shipping channel (Water Technology, 2010).

Cardno (2007) developed a wave climatology for two locations in the bay based on two 50 m resolution SWAN grids in the southeast of the bay (Safety Beach to Rye) and north of the Bay (Hobson's Bay to Black Rock) and nested in a 500 m wave model of the bay with no open boundaries to Bass Strait and hence no swell input. The model was used to simulate the waves arising from six representative wind speeds and 16 directions (22.5° intervals). The results from these 96 runs were combined using the frequency of occurrence of the different wind speeds and directions in the bay. A third 50 m grid was setup over the entrance to PPB and used boundary forcing on the southern boundary from 10 representative wave conditions derived from offshore wave buoy observations. Each case was run with different tidal conditions (peak tide, ebb tide and slack water) with the currents simulated by a hydrodynamic model of the bay, to ensure the influences of tidal currents on the waves were captured. This third set of simulations, which included wave refraction, was used to study the impact of channel dredging on wave conditions inside the entrance. The models were calibrated against limited available wave data and found to perform satisfactorily in most locations considered. However, some disagreement between the model and observations was found around the Entrance and limited data availability and data quality were flagged as possible causes. The wave patterns in the Entrance are complex due to the interaction of the waves with the bathymetry and the strong tidal currents which cause marked changes in the wave conditions.

Changes to wave climate within the bay have not been assessed. However, recent changes in wind climate over Victoria were assessed as part of the "Climate Projections for Victoria 2019" (VCP19; Clarke et al., 2019) project. This study found that projected changes in 10 m wind speed were consistent with previous climate model simulations, with projected changes of less than 10% (mostly less than 5%) even under Representative Concentration Pathway 8.5 (RCP8.5) by the end of the century, and low agreement on the magnitude or even sign of change in all VCP19 regions. Mean wind direction changes have not been specifically analysed from the VCP19 simulations. No studies to date have investigated how the range in projected changes in 10 m wind speeds and directions could affect the wave climate of PPB.

2.5.5 Summary

Waves over most of PPB are wind-generated except in the southern part of the bay where there is some influence of swell that enters through Port Phillip Heads. Wave measurements have been collected at wave buoys southeast of Point Nepean since 2003, however inside PPB wave data is limited to short periods of observations for specific studies. Numerical wave models at global scale have been undertaken to provide wave hindcasts from 1979 to the present and these sources provide relevant wave information outside PPB. These include future wave climate simulations for the period 2081-2100 that indicate a future increase in wave height and swell reaching the Victorian coastline as well as associated rotation in mean wave direction to more southerly. Future changes to local wind generated waves have not been assessed for PPB but projected 10 m wind climate changes over this region are generally small and mostly within ±5% of present climate by the end of the century. Within the bay, previous studies have used short observational data to calibrate wave models for use in a range of applications. Inundation

2.5.6 Overview of Inundation Methods

Overland inundation is typically caused by factors such as storm tides, rainfall over coastal zones, fluvial input and backwater effects in drainage system networks. Large scale assessments of inundation typically involve the static bathtub or bucket-fill approach, which assumes that a rise in sea level will inundate all locations of elevation up to the magnitude of the sea-level rise. Such methods, while efficient, ignore transient effects such as wave breaking, which causes wave setup and runup. Furthermore, because the temporal variation in storm surge flooding is not accounted for, other relevant aspects of inundation such as duration of inundation and the maximum flow speeds of water are not able to be calculated.

Hydrodynamic models on the other hand, can simulate overland flow and account for frictional influences exerted on the flow within the landscape (e.g. ground roughness) that influences flow speeds. Hydrodynamic models therefore capture temporal variations in inundation events and hence the duration of flooding, the strength of the associated currents as well as the water depths. They can also account for other processes such as fluvial and pluvial inputs if required and coupling hydrodynamic models to wave models enables the modelling of coastal wave setup. Connectivity in the urban landscape via underground drainage networks can also be incorporated (e.g. Cohen et al., 2016a, Prakash et al., 2019). The disadvantages of using hydrodynamic models are the much higher computational overheads that often limit the spatial extent of the studies (McInnes et al., 2013). Furthermore, even high-resolution hydrodynamic models tend to be of lower resolution than the available LiDAR elevation datasets meaning that features in the landscape that may influence overland flow may not be correctly resolved.

2.5.7 Inundation Studies of Port Phillip Bay

Since the Future Coasts Program, which saw the development of storm tide AEP's and analysis of inundation over specific low-lying areas within PPB and the Victorian Coastline using a bathtub infill approach (McInnes et al., 2009a, b), several inundation hazard assessments have been undertaken using a variety of static and dynamic inundation approaches. Lacey and Mount (2011) developed inundation layers along the state coastline using the bathtub infill approach and the coastal ARI information from McInnes et al., (2009a, b). Cardno (2015) undertook an inundation hazard assessment for Corio Bay in which bathtub approaches were used for most locations within Corio Bay except in southern Geelong, which used dynamic inundation modelling based on the model Sobek combined with calculations of wave overtopping using EurOtop (Van der Meer, 2016).

Dynamic inundation modelling of PPB was undertaken to assess the 1% and 10% AEP storm tide events on PPB inundation levels and extents (Water Technology, 2017b). This study incorporated the effects of wave setup and used a design storm approach to develop maps of ARIs across the bay (see 2.4.3).

A number of other studies have focussed on inundation mapping and modelling of specific locations or assets in PPB. For example, inundation mapping was undertaken for the Western Treatment Plant (Water Technology, 2017a). Dynamic inundation modelling for the City of Greater Geelong and Borough of Queenscliffe using the C-FAST model was undertaken by Cohen et al., (2016a) (see also Prakash et al., 2015), which incorporates not only overland inundation but also hydraulic modelling to account for the stormwater drainage system thereby also modelling backwater effects. This model was also applied to the modelling of inundation around the City of Port Phillip (Cohen et al., 2015).

2.5.8 Hydrology Considerations

Australian Rainfall & Runoff (Ball et al., 2016) (Book 6, chapter 5) discusses with practical examples the procedure for calculating the probability of a particular flood height in the coastal zone that considers the combination of rainfall and storm tide under different levels of dependence between the two. Based on Zheng et al., (2013), a multivariate threshold-excess model is used to calculate the dependence parameter[2] α (Coles, 2001) assuming rainfall bursts of less than 12 hours, 12-48 hours, and 48-168 hours. They note that when extremes are completely dependent, the probability of the flood height is the same as the probability of the storm surge event and the runoff event. For events that are completely independent, then the probability of the two coinciding is the product of their individual probabilities of occurring in a particular day. When there are intermediate levels of dependence, then the joint probability must be considered, to account for the probability of floods arising from different combinations of smaller rainfall and storm tide events. Strictly speaking, even if the two events are statistically independent, it is still necessary to calculate the joint probability because combinations of smaller values of the two can lead to flood levels exceeding the threshold. Australian Rainfall & Runoff (Ball et al., 2016) describes a method to calculate the joint probability of the two events.

The same approach as Zheng et al., (2013) was used by Wu et al., (2018) to investigate dependence between storm surges and rainfall totals above the 99th percentile using both tide gauge data and hydrodynamically-modelled storm surge around Australia based on a 32-year, 5 km gridded hydrodynamic model hindcast (Colberg et al., 2019). For both observations and model, they found that the value of α for the Victorian coast in general was greater than 0.99 indicating a tendency for the rainfall and storm surge events to be independent of each other. This is attributed to the highest storm surge events tending to occur in the colder months due to frontal systems, which although typically rain-bearing, do not usually produce extreme rainfall totals (see Figure 2.8). On the other hand, the heaviest rainfall events tend to be convective rainfall events that occur during the warmer months with weather conditions that are not conducive to causing storm surges. Although Wu et al., (2018) did not study the effect of climate change on this dependence relationship, it is notable that for southern Australia, the Colberg et al., (2019) study found a robust (small) decline in storm surge values along the southern

[2] The dependence parameter is an exponent in the bivariate distribution function used to model the two random variables, rainfall and storm surge. It has a value of 1 when the two random variables are independent and typically a value less than 0.9 indicates strong dependence between the two variables.

.

Australian coast due to the southward migration of storm systems. This implies the rainfall associated with these storm systems will also migrate south. In the recent VCP19 project, rainfall for Victoria was projected to undergo declines, consistent with this southward migration of rain-bearing systems, although extreme rainfall events (5% AEP) were generally projected to increase by the end of the century in general due to the increased moisture holding capacity of a warmer climate but the range of possible change across a multi-model ensemble was large, ranging from a decline of 20% to an increase of 40%.

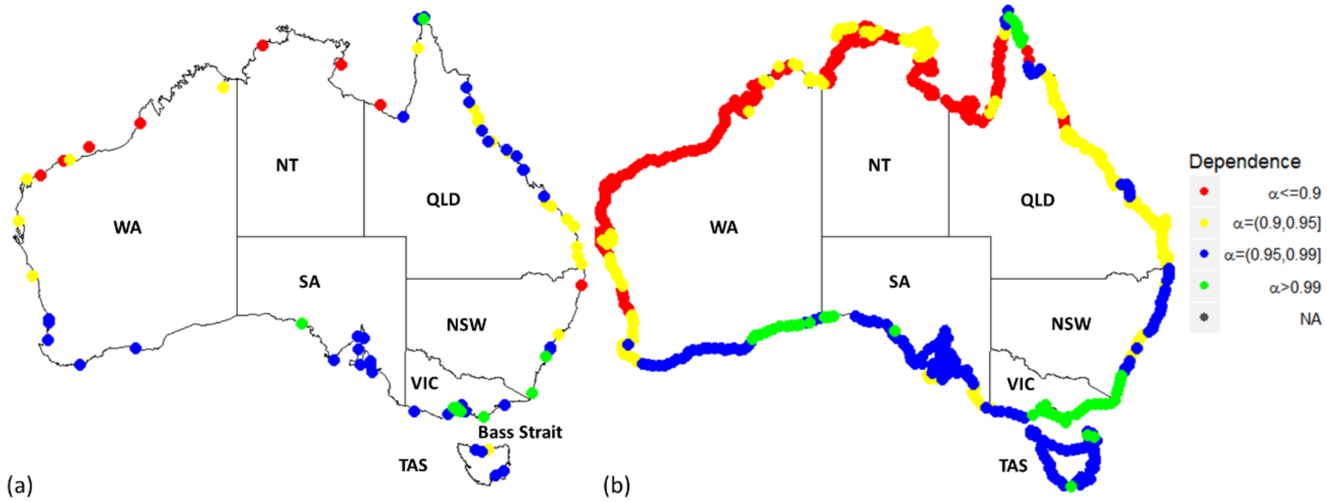

Figure 2.8: Australian wide dependence mapping between extreme rainfall and storm surge using (a) observed storm surge and (b) ROMS modelled surge. (Note. The dependence parameter α, = 1 when there is complete independence and α< 0.9 indicates relatively strong dependence in the Australian context). (Source: Wu et al., 2018).

BMT WBM (2015) developed flood maps for Southbank based on different ARIs of Yarra floods to consider future flood hazard. Under future climate conditions, they modelled flood height changes for 2100 including SLR and storm surge estimates based on McInnes et al., (2009a) together with higher tidal range under SLR based on Black et al., (1990) and storm tides. For rainfall runoff, future temperature change based on an RCP6.0 greenhouse gas emissions scenario that assumes an average temperature increase of 3°C by 2090 was used to derive an increase in rainfall intensity of 15%. In addition, an increase in rainfall intensity of 32% was modelled because this is a climate scenario adopted by Melbourne Water for 2100. Joint probability of flooding due to rainfall and storm tides was not undertaken, but rather a design storm approach was adopted. Model simulations were undertaken for rainfall runoffs representing 5, 10, 20, 50 and 100-year ARI catchment flow events, which were represented by peak discharges at three locations within the Southbank precinct. These catchment flows were combined with tailwater conditions at the Yarra River comprising highest astronomical tide under present day (0.52 m AHD) and 0.8 m SLR and an assumed change to tidal range under 0.8 m SLR to make it 1.36 m AHD. Additionally, a 1% AEP storm surge under present day (0.9 m) and 0.8 m SLR including an assumed change to windspeed and hence storm surge change (2.04 m) and a 1% AEP Yarra River Flood level (1.6 m).

Cardno (2015) in their inundation hazard assessment for Geelong combined a 99th percentile daily flow rate for the Barwon River with their current and future storm tide scenarios and also considered a scenario of 10% AEP catchment flow but noted that extreme catchment flows coinciding with the peak 1% AEP storm tide level was extremely rare and was only simulated to investigate sensitivity.

2.5.9 Summary

Although early mapping of inundation hazard was based on bathtub infill approaches, coupled hydrodynamic and wave models offer an efficient means to simulate the temporal evolution of overland flooding from storm tides (including wave setup) and rainfall in the coastal zone, although these models do not simulate the transient effects of wave breaking (i.e. wave runup) and overtopping at the coast that can contribute to inundation. Recent high-resolution hydrodynamic modelling studies within PPB have simulated the flooding that occurs due to 'design storms', as opposed to bathtub approaches. Design storms consist of simulating overland inundation from transient water levels whose peak coincides with an AEP of interest.

Extreme storm surge and rainfall events along the Victorian coast tend to occur independently of each other. Future climate conditions will likely change the joint probability of coastal flood events through changes in sea level, storm surge, tidal range and rainfall runoff. A practical method (The Design Variable Method) for calculating the joint probability of flood events in the coastal zone due to the coincidence of storm tides and rainfall is provided by AR&R (Ball et al., 2016) although no studies within PPB were found that had undertaken such an assessment, instead adopting a design storm approach to assessing flood risk. Consistent with this approach, and in view of the time constraints on this project and the fact that previous studies have found that storm surge and rainfall events tend to occur independently, this study will also adopt a scenario approach in the inundation hazard assessment.

2.6 Shoreline Processes

2.6.1 Overview of Shoreline Processes in Port Phillip Bay

Shoreline change is influenced by four main factors; the sediment budget, the composition of coastal landforms, the wave climate and the frequency and intensity of extreme events (Thom et al., 2018). Along sandy ocean coastlines, sediment may be supplied through onshore transport from the shelf, alongshore transport, river input or cliff erosion. Similarly, sediment may be lost through offshore transport to the shelf, transport onshore to dune systems, longshore transport or transport into estuaries and deltas.

Sediment supply to Port Phillip from oceanic (shelf and alongshore) sources is limited by the narrow tidal entrance between Point Lonsdale and Point Nepean. The configuration of the entrance determines that the bulk of sand entering the bay is carried between Point Lonsdale and Queenscliff – Swan Island. Cardno (2011) estimated approximately 50% of the sediment entering Port Phillip is carried offshore by the ebb tide or into the Entrance Deep. The residual is distributed onto the Great Sands and across the sands northward into deeper water, with minimal contributions to beach accretion inside the bay (see Section 2.2.4). The morphology, composition and coherence of material of a coastal landform determines its erodibility as well as its capacity to recover from erosion events. Erosional processes are driven by the wave climate, which includes both remotely generated swell and locally generated wind waves. Extreme events – when high waves combine with a storm surge – can initiate severe, short term, episodic erosion of a beach often referred to as a storm bite.

2.6.2 Frameworks for Understanding Shoreline Change

Understanding the role of the different physical factors on coastal change is often considered using the framework of coastal sediment compartments. These are coastal spatial units that describe coastal geology and behaviour at a hierarchy of spatial and temporal scales and are commonly used in the context of facilitating coastal management. The approach for delineating coastal compartments in Australia is three-tiered, where each tier supports different types of decision making, as summarised in Figure 2.9 (Eliot et al., 2016; Thom, 2018).

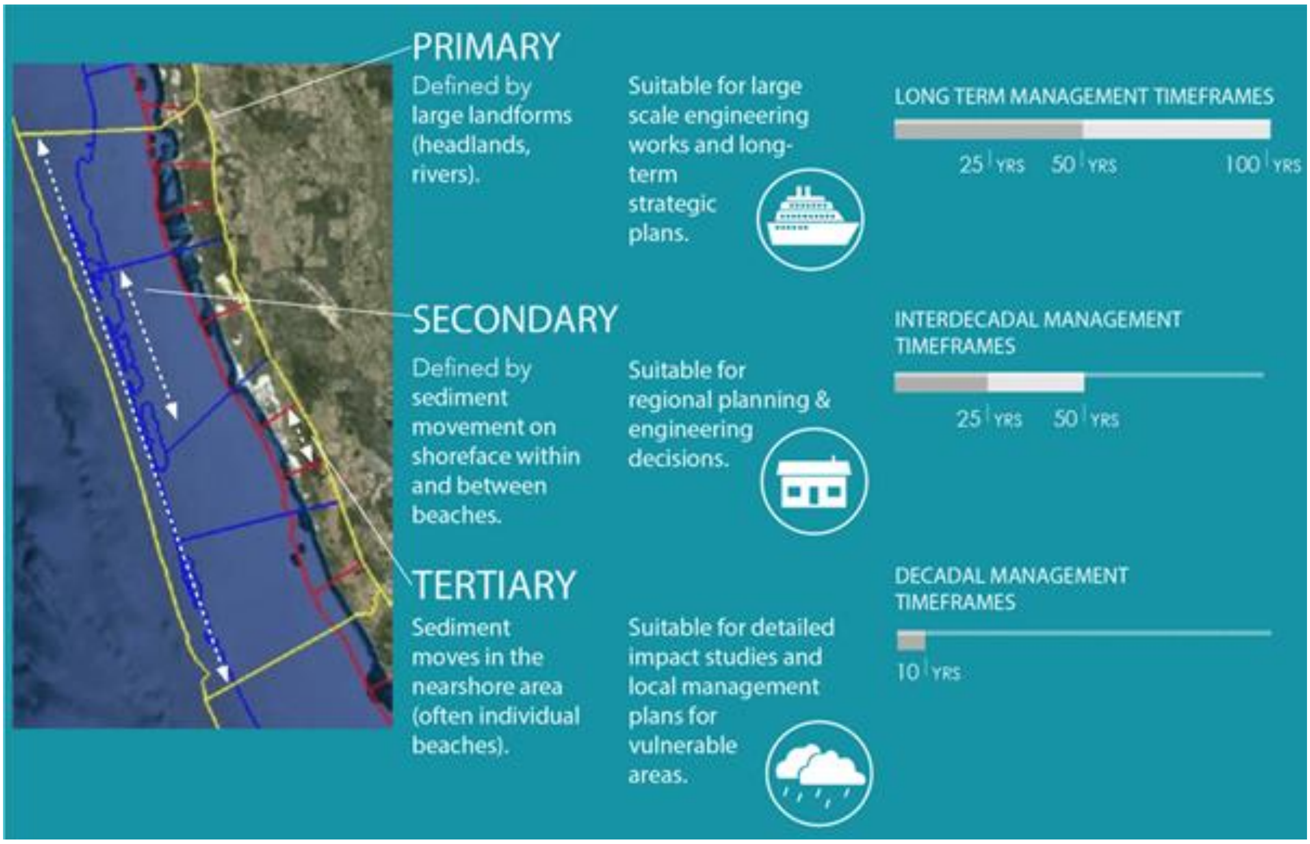

Figure 2.9: Coastal compartment scales, use and timeframes (Thom, 2015).

Similar to the national scale Coastal Sediment Compartment project, which defined each compartment as an area of the coast based on sediment flows and landform (Figure 2.9; Thom et al, 2018) the Victorian Marine and Coastal Policy (2020) defines primary, secondary and tertiary coastal compartments as “sections of coastline defined by landform and the sediment transportation processes that occur within the compartment:

- **Primary compartments** are defined by large landforms (such as headlands and rivers) and are suitable for long-term strategic planning.
- **Secondary compartments** are defined by sediment movement on the shoreface within and between beaches. They are suitable for regional planning and engineering decisions.
- **Tertiary compartments** are defined by sediment movement in the nearshore areas (often individual beaches). They are suitable for detailed impact studies and local management plans for vulnerable areas.”

The Australian Coastal Sediment Compartments Project (McPherson et al., 2015; Thom, 2018) generated a national coastal sediment compartment dataset for Australia. The compartment data sets were generated through the combined experience of an expert panel of coastal scientists. The compartment boundary points along the coastline are typically defined by prominent geological or geomorphic features and these were identified by the expert panel as being potentially significant for sediment movement processes in the coastal zone. Coastal compartments were generated at a regional (primary) and sub-regional (secondary) level. The two secondary coastal compartments defined for PPB, as detailed in the CoastAdapt Shoreline Explorer (http://coastadapt.com.au/coastadapt-interactive-map), are summarised in Table 2.3. In the context of the present study, this earlier work constitutes a secondary (coarse scale) assessment relevant to the national scale.

Table 2.3: Secondary coastal compartments defined for PPB.

Sediment Compartment Name	Port Phillip Bay West	Port Phillip Bay East
Included Area	**From Williamstown to Point Lonsdale**	**From Point Nepean to Williamstown**
Geomorphology	Mostly swell-sheltered shores with narrow low-energy beaches backed & interspersed by Cainozoic soft-rock sediments from Queenscliff to Geelong, and by interspersed hard basalt and soft sediment shores and backshores from Avalon to Williamstown.	Swell-sheltered tidal embayment shore with numerous narrow sandy beaches, backed by & interspersed with generally soft-rock materials, including Cainozoic sediments, volcanics and calcarenite, and deeply weathered Palaeozoic granites.
Sensitivity	Later response to SLR for Bellarine Peninsula beaches with ongoing sand supply. However, NW shore beaches from Avalon NE-wards may be medium term responders with limited sand supply. Geelong shores mainly artificial and resilient.	With little sand supply & limited capacity for recovery, most beaches will be early or medium-term responders to SLR, unless artificially protected.

The term compartment in the context above therefore refers to a section of coastline defined at various scales, by the specific composition of the landform (offshore, nearshore, beach/intertidal and backshore morphology components), wind and wave climate, and sediment dynamics. The scale adopted for an assessment then depends on the aim of the assessment being undertaken.

2.6.3 Factors Contributing to Erosion Hazards

Shoreline change depends on processes that operate on different time and space scales. These include short-term processes associated with single extreme events or clusters of events such as successive cold fronts that cause episodic erosion events with subsequent recovery, and longer-term processes that cause shoreline recession (or accretion) over several years to decades. The longer-term assessment may be based on observed historical shoreline change and modelled future recession that will occur due to SLR over several years to decades (e.g. DSE, 2012; Water Research Laboratory, 2013; Water Technology, 2014e).

For shorelines comprised primarily of beaches (either with backshore dunes or rock slopes), the short-term component is referred to as storm erosion or storm bite and is caused by the extreme waves, high water levels and currents that accompany a coastal storm. In the aftermath of storm erosion, where sand has been moved offshore, calm-weather swells move sand back onshore. It may also be transported along the coast by longshore currents in a persistent or variable manner. Eroded finer sediments, including sand may, in some cases, be permanently lost from the system by being taken offshore into deeper water by currents and turbulence.

In the absence of significant swell or exposure to swell, such as in an estuary or harbour setting, there may be little or no recovery between short term erosion events, compared to episodic recovery that occurs on open sandy coasts. PPB is an unusual environment intermediate between these extremes, with a range of sandy shore behaviours. The underlying and backshore geology often provides a natural limit to recession of sandy shorelines if harder more resistant material is present. This means that there will be potentially different types of shoreline response and future variation in evolution of the shoreline around PPB.

Longer-term shoreline erosion is often due to a combination of factors, such as changes to net longshore transport and sediment supply (for beaches) and sea level rise (SLR). In the case of coastal cliffs, long term recession is often associated with cliff lithology and structural features promoting instability such as the angle of repose of the material and height of the cliff, as well as wave energy at the toe.

Since most accepted future SLR scenarios represent a significant acceleration or addition to historical sea level rise, this is often considered a separate additional erosion hazard component. On sandy coasts under higher sea levels waves run further landwards over deepened water to erode the beach face, transporting sediment offshore.
Sand transported offshore may be lost from the active system or transported elsewhere. With sufficient foredune erosion, some sand may also be lost inland via wash-overs (where wave action washes over the dune crest transporting sediment with it). Over time these processes (offshore sand movement and wash-overs, acting independently or in combination) translate the shoreline profile shoreward and upward in response to the relative higher sea level.

In this scenario, currently eroding beaches may recede faster, while currently accreting (growing) beaches may continue to accrete more slowly, or switch to receding. The long-term trend of a shoreline in response to sea level change may be delayed or masked by swell-driven or local wind-wave driven beach recovery between storm events.

Methods for estimating the contribution of short-term and long-term erosion depend on local geomorphology, chiefly width, composition and thickness of intertidal sediment (i.e. beaches and mudflats) height, geology and structure of backshore materials (hard rock, soft rock, earth cliffs, beach ridges, dunes, wetlands), orientation of the coastline, and other factors. In PPB, this is further complicated by the number and diversity of engineering structures, beach nourishment activities and other historical interventions. Therefore, any detailed, locally relevant assessment of erosion hazard requires the identification of tertiary scale geomorphic sectors (the specific composition of the landform) and shoreline types (Thom, et al., 2018) along with local wind and wave climate information. A detailed geomorphic assessment carried out in the present study is discussed in detail in Chapter 7.

2.6.4 Summary

Sediment budget, morphology and composition of coastal landforms, the wave climate and the frequency and intensity of extreme events are the main factors that influence shoreline change. Coastal erosion hazards are generally assessed in terms of short-term processes, associated with single extreme events or clusters of events, and longer-term processes resulting in shoreline recession (or accretion) over several years to decades. Sediment supply into PPB is limited by the narrow tidal entrance and much of the sediment that does enter is mainly distributed onto the Great Sands and across the sands northward into deeper water or settles in the deeper channels with minimal contributions to beach accretion. The PPB coastline includes sections featuring sandy beaches, hard and soft rock cliffs and muddy shorelines, each of which will vary in terms of their response to SLR. Sandy shores respond to both short term storm events as well as long term SLR. Muddy shorelines are susceptible to wave-induced erosion. Rocky cliffs offer some resistance to rising sea levels and storm events although the level and longevity of protection depends on the hardness of the cliff material.

2.7 Groundwater

2.7.1 Overview of Groundwater Processes

Groundwater refers to water within the saturated zone in the weathered rocks below ground surface with the groundwater host materials referred to as an aquifer. The upper boundary of the saturated zone is defined as the watertable and above the watertable lies the unsaturated zone. Groundwater recharge occurs below water bodies such as rivers and streams and via infiltration of precipitation through the unsaturated surface zone to the watertable. The amount of precipitation reaching the watertable is offset by evaporation and evapotranspiration by vegetation cover. Like rivers, gravity influences the movement of groundwater from high to low elevation areas and coastal sea level defines the discharge boundary for regional groundwater systems.

The interfaces between surface water, groundwater and seawater are particularly complex along coastlines because of density differences between freshwater and saltwater (Figure 2.10). Discharging fresh groundwater tends to form a wedge with seawater along the coastline. This is significant both for how the watertable could respond to climate change through changing precipitation, temperature and evaporation and for the risk of salinization of water supplies. In general, when sea level rises or the rate of groundwater discharge decreases, a saline wedge will move further inland. These processes are further complicated by the changed (and changing) hydrology due to urbanisation, such as hard paving of surfaces, removal and planting of vegetation, garden and park irrigation, installation of infrastructure conduits, construction of stormwater retention ponds and so on.

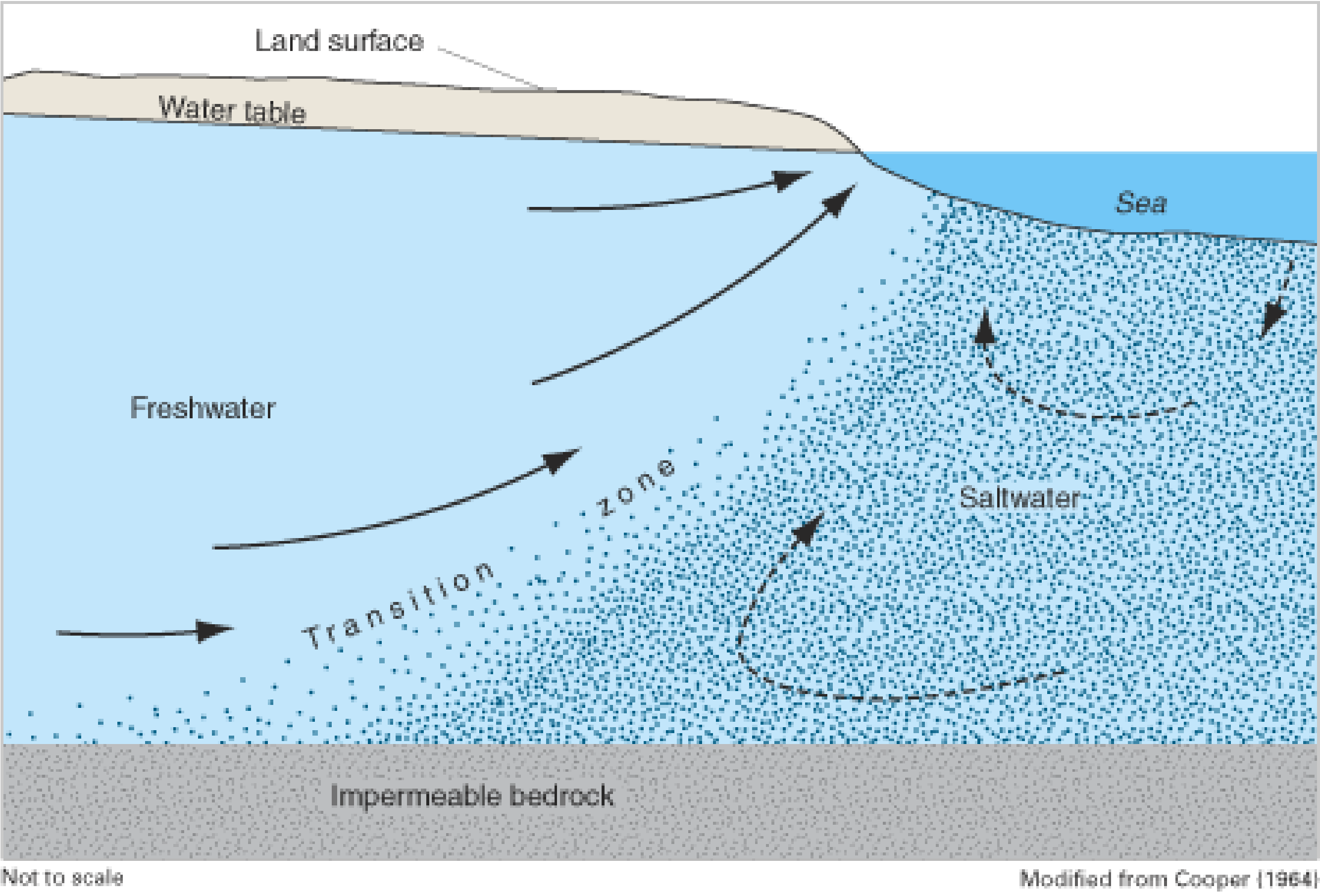

Figure 2.10: Saltwater-freshwater interface (from Fetter, 2001).

2.7.2 Groundwater Hazards

The groundwater hazard related to SLR and changing climates is mainly reflected in the changing depth to watertable and the migration of the seawater – groundwater interface. The potential impacts of changes in groundwater hydrology in response to SLR has two components: one in which the changes to groundwater levels and quality pose a threat to assets, and the other where the changes threaten groundwater as an asset. Examples on the natural and built environment include:

- changing watertable levels that may impact on natural and built assets (e.g., flooding due to groundwater tables rising to the surface)
- changing the groundwater quality (salinity, chemistry, biology) of shallow watertables that underlie natural and built assets (e.g., increasing penetration of saline groundwater and potential corrosion of built assets)
- changing the quantity and quality of groundwater that services natural assets, social amenity and cultural heritage values, and
- changing the quantity and quality of the groundwater resources currently exploited for human consumption, stock watering, irrigation, industrial or commercial uses, including wastewater treatment plants/ponds.

The distribution of groundwater bores around PPB clearly shows the importance of groundwater extraction in the Werribee Delta for market garden irrigation, and the extraction of groundwater for domestic garden irrigation in the southeastern bayside suburbs and Nepean Peninsula (Figure 2.11). The depth to the watertable in these areas is generally less than 5 metres below the surface and the quality is relatively fresh. The groundwater in the Bellarine Peninsula, is quite shallow and relatively saline under the urban area of the City of Greater Geelong. Hence changes to groundwater levels may pose a threat to urban infrastructure, parks, waterways, and wetlands, including Ramsar-listed wetlands.

Figure 2.11: Bore distribution around PPB (from the databases accessed in the study).

Sea-level rise will cause changes in groundwater levels and quality. These changes may contribute to coastal erosion risk (mainly due to changes to groundwater discharge) and inundation risk (due to shallower watertables). However, such changes are anticipated to be minimal and comparable to the present-day impacts.

It is noted that coastal groundwater tables are not acidic unless their flow path passes through an active acid sulphate soil area. Acid sulphate soils are triggered by falling water-tables (i.e. oxidation of sulphides in the sediments) and not rising water-tables (which stop the acid-generation processes), therefore this report does not address groundwater acidity.

2.7.3 Groundwater Management in Victoria

The contemporary conceptual hydrogeological model for the PPB region is the Victorian Aquifer Framework (VAF), developed by the Department of Sustainability and Environment, now DELWP, for the Securing Allocation Future Entitlement (SAFE) project (SKM, 2012a). The SAFE project, funded by the National Water Commission, aims at ensuring that Victoria's groundwater is consistently managed across the State.

The VAF is intended to be an overarching unifying aquifer classification presented as a tiered system of 14 layers that still allows local scale studies to focus on the detail within a tier, but ties into the regional scale. The VAF components present in the PPB region are listed (Table 2.4) and illustrated (Figure 2.12).

A simplified version of the VAF was used in the most recent conceptual model of the groundwater systems of the PPB region, illustrated in the Port Phillip and Western Port Groundwater Atlas (Southern Rural Water, 2014) for the larger part of the study area, and for the Corio Bay region, the South West Victoria Groundwater Atlas (Southern Rural Water, 2011).

Table 2.4: Victorian Aquifer Framework (VAF) components in the PPB region.

Victorian Aquifer Framework component	In Port Phillip Bay region
Quaternary Aquifer	✓
Upper Tertiary/Quaternary Basalt Aquifer	✓
Upper Tertiary/Quaternary Aquifer	
Upper Tertiary/Quaternary Aquitard	
Upper Tertiary Aquifer (marine)	✓
Upper Tertiary Aquifer (fluvial)	✓
Upper Tertiary Aquitard	
Upper Mid-Tertiary Aquifer	✓
Upper Mid-Tertiary Aquitard	✓
Lower Mid-Tertiary Aquifer	
Lower Mid-Tertiary Aquitard	✓
Lower Tertiary Aquifer	✓
(Lower) Tertiary Basalts	✓
Cretaceous and Permian Sediments	
Mesozoic and Palaeozoic Bedrock	✓

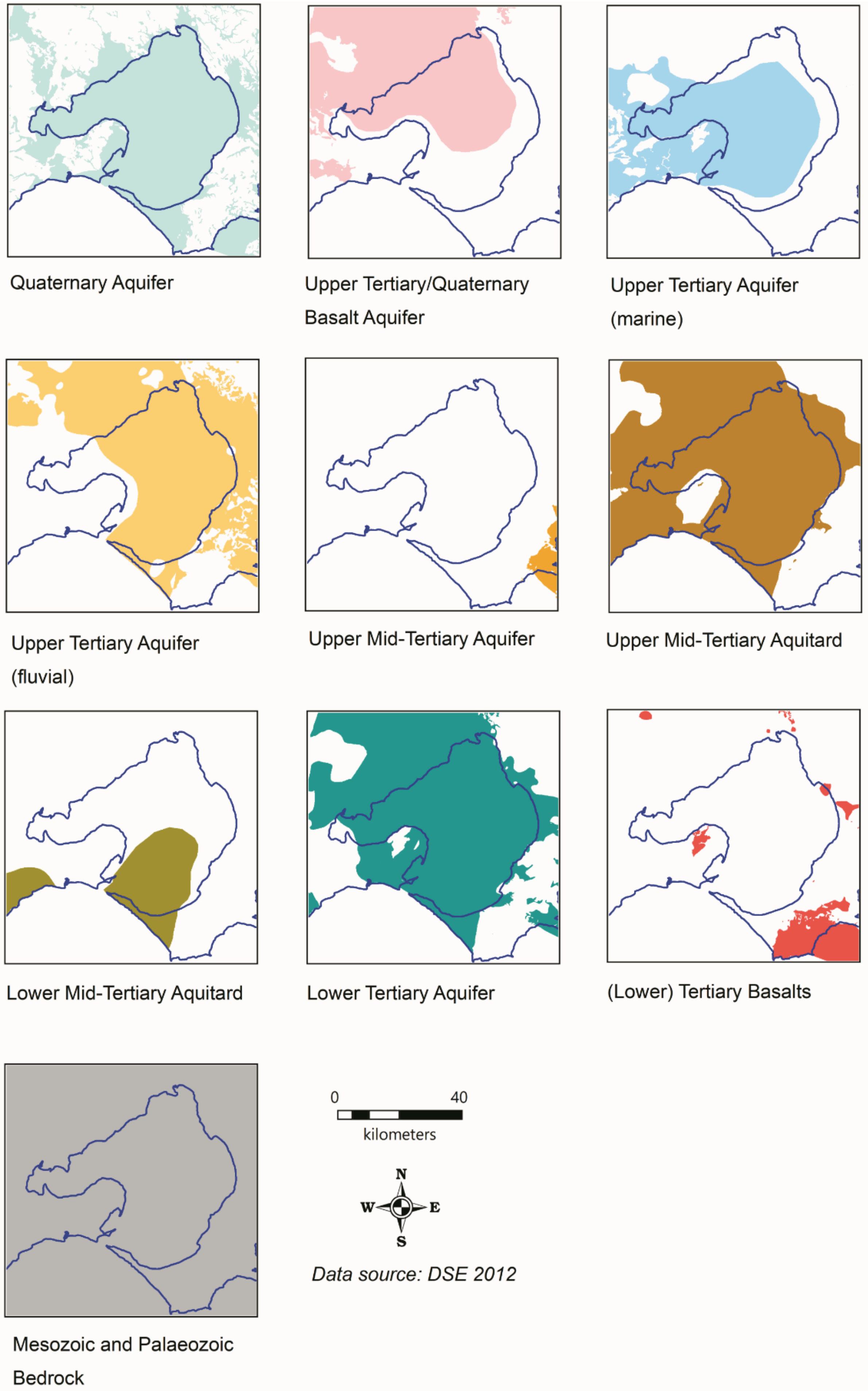

Figure 2.12: Victorian Aquifer Framework (VAF) for the PPB region, showing the distribution of the aquifers and aquitards from the uppermost (Quaternary) to the basement.

Within the PPB region a number of groundwater management areas are legislated (Figure 2.13). These are the:

- Deutgam Water Supply Protection Area – often referred to as Werribbee
- Cut Paw Paw Groundwater Management Area
- Moorabbin Groundwater Management Area
- Frankston Groundwater Management Area, and
- Nepean Groundwater Management Area.

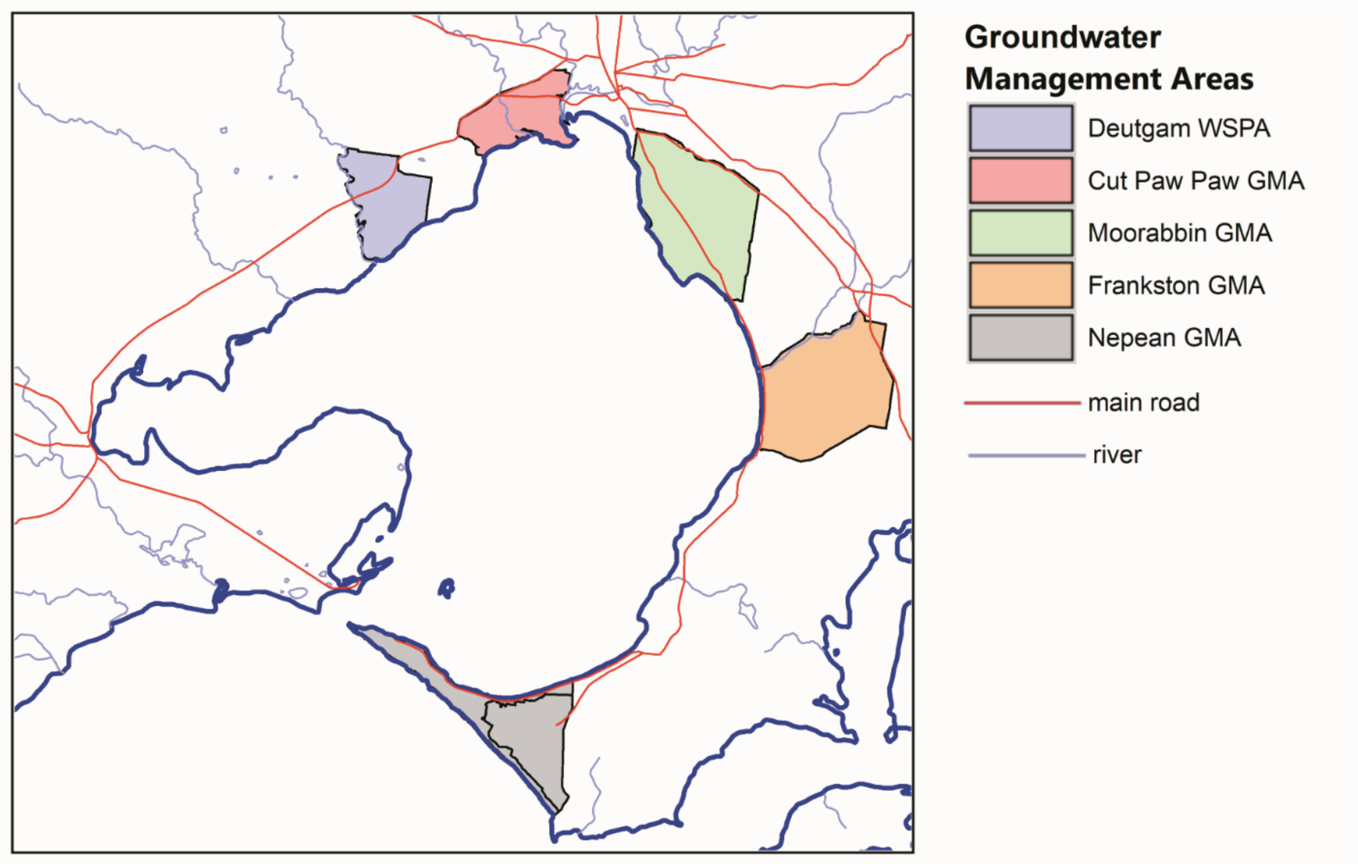

Figure 2.13: Groundwater management areas (source: CeRDI, 2020).

The contamination of groundwater has occurred where pollutants have found their way to the watertable, either from point sources or diffuse sources. The EPA data records a number of contaminated and previously contaminated sites around the fringes of PPB (Figure 2.14), including areas where the use of the groundwater is restricted in some manner (i.e. the Groundwater Quality Restricted Use Zones). Some of these sites are within one to five kilometres of the shoreline and therefore pose a potential hazard under changing groundwater levels in response to SLR.

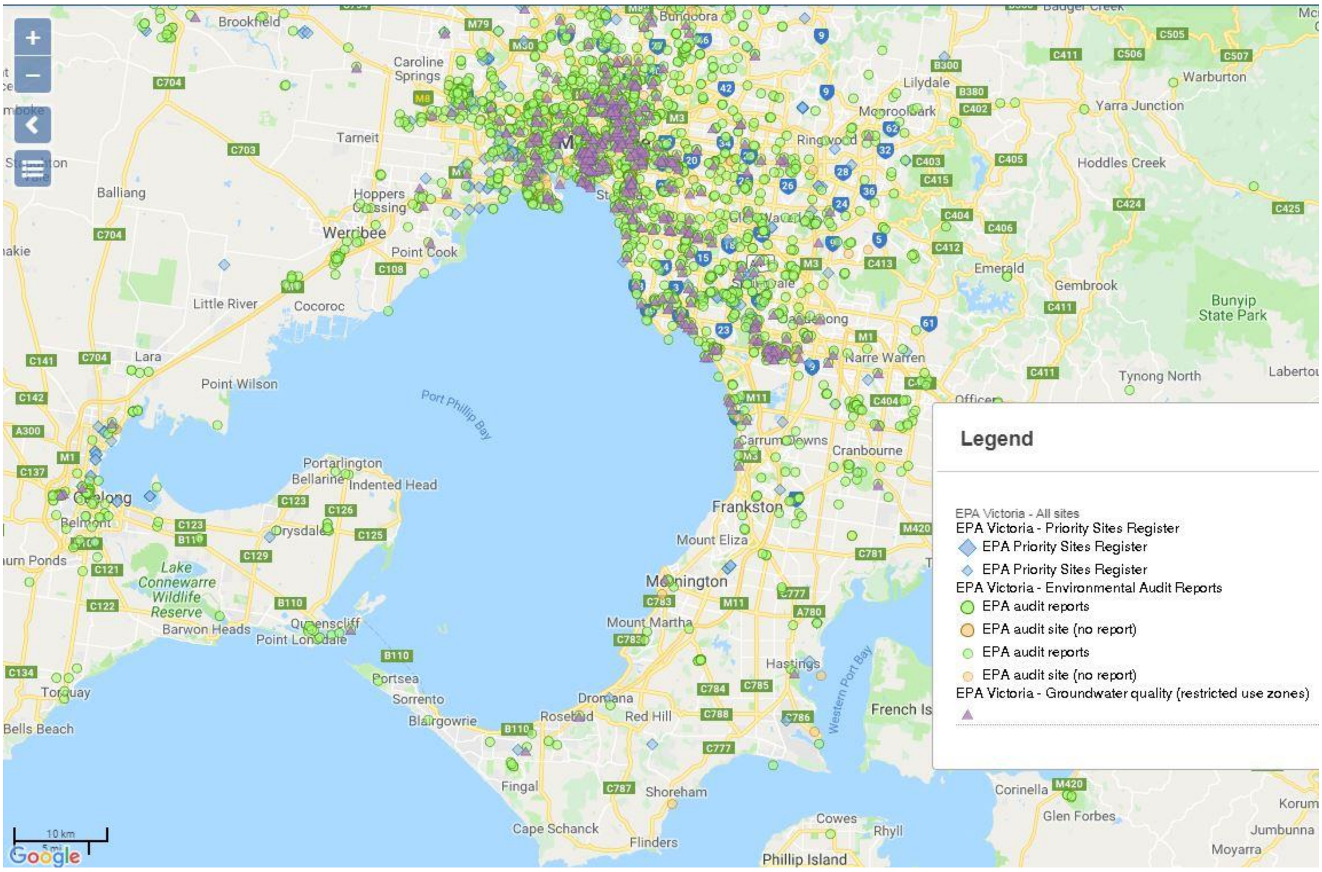

Figure 2.14: EPA sites in the PPB region (Source: CeRDI, 2018).

2.7.4 Summary

The interfaces between surface water, groundwater and seawater are particularly complex along coastlines because of density differences between freshwater and saltwater. In general, when sea level rises or the rate of groundwater discharge decreases and the saline wedge will move farther inland. The impacts of changes to groundwater levels and quality may manifest as a threat to assets such as built infrastructure, and also threaten groundwater as an asset. Contaminated groundwater may also pose a potential hazard under changing groundwater levels in response to SLR. The Victorian Aquifer Framework (VAF) provides a conceptual hydrogeological model for the PPB region. Within PPB there are five legislated groundwater management areas and the Securing Allocation Future Entitlement (SAFE) project ensures consistent management of Victoria's groundwater.

3 Study Design

This chapter summarises the key findings of a gap analysis undertaken to identify relevant data and information for this study. It also provides a high-level description of the various components of work undertaken. A purpose-built DSS in which the hazard assessments are delivered is also described. This is followed by the method for the inundation and groundwater hazard assessments. Finally, the design of the whole-of-bay hydrodynamic modelling, which provides various input parameters to the hazard assessments, is discussed.

3.1 Gap Analysis Key Findings

The quantification of the hazards of coastal inundation and groundwater, and associated uncertainties, depends heavily on the availability and quality of morpho/geo/hydrology and physical datasets to inform and calibrate the models to be used for the assessment. In the first stage of the project a gap analysis was undertaken to identify relevant reports and articles as well as the availability and quality of the required data (see McInnes et al., 2019). In the following sections, a high-level summary of the findings of the gap analysis is provided together with the detailed project design. The details of available datasets are discussed in the relevant chapters that describe the methodologies and the hazard assessments.

A comprehensive review of over 600 items of literature, numerous datasets and data repositories and tools was undertaken in planning for the PPBCHA project. Several data and knowledge gaps were identified but none were found to be critical to the original project brief and design, although revisions were incorporated into the project design to account for these gaps. Many of the gaps identified in the analysis reinforced the need to undertake the PPBCHA to provide a suite of data products and information on the hazards in PPB using up-to-date climate information to inform ongoing management.

Key findings of the gap analysis were:

- Coupled hydrodynamic and wave modelling of PPB under current and future conditions was identified as a fundamental requirement for the assessment of coastal hazards. Sufficient wave and tide data existed to allow the calibration of such a model from which a multi-decadal hindcast can be performed. Data from this simulation together with simulations under SLR scenarios then provided for a range of data needs for the hazard assessments.
- Hydrodynamic models were available that can resolve detailed features of the urban environment including structures, stormwater drainage systems, riverine and rainfall inputs. These dynamic modelling approaches provide a more comprehensive assessment of inundation hazard. However, wave-related overtopping was not accounted for in such models which represented a gap that was addressed in this project for the parts of the coast where most coastal protection structures were located.
- While joint probability methods were available for estimating inundation from the combination of ocean processes and rainfall runoff, the review findings highlighted that extreme storm surge and

rainfall events in PPB tend to occur independently of one another. This suggested that a design storm approach rather than a joint probability approach for assessing the inundation hazard was appropriate in this project.

- The groundwater review identified a number of gaps including a lack of a whole-of-bay groundwater conceptual model. Three additional locations were identified as priority areas of focus for the development of more detailed conceptual groundwater models, the Werribee Delta, the Mentone to Frankston 'sand belt' and the Nepean Peninsula.
- A detailed geomorphic survey based on intertidal and backshore morphology was required to provide consistent, locally relevant data to inform a shoreline hazard assessment, although it is noted that an erosion hazard assessment is not presented in this study.
- A review of decision support tools identified a range of tools that could incorporate the outputs of the hazard assessments. However, no single tool could accommodate all forms of data being generated in the PPBCHA and so it was recommended that a purpose-built tool be developed that allowed users to visualise and analyse outputs from the hazard assessments together with a range of other relevant datasets.

3.2 Project Design

The various components of the PPBCHA are described in the following sections and the relationship between each of the components is summarised in Figure 3.1. The delivery of the hazard assessments through a purpose-built DSS is an important output of the project in allowing end-users to engage with the hazard layers and relevant ancillary data. The design of the DSS and an introduction to the hazard layers it contains is provided in Chapter 4. Following this, a detailed description of the data inputs and methodology used to develop the layers for the inundation and groundwater hazards as well as a geomorphological survey of the bay follow in Chapters 5 to 7. Chapters 5 and 6 also include an overall discussion and interpretation of the hazards at the bay level as well as specific examples of the hazards at key locations.

To support the physical data requirements in the hazard assessments, including tides, storm surges and waves on the bay under historical climate conditions, as well as under scenarios of SLR, a coupled hydrodynamic/wave model of PPB was developed, run and analysed. Chapter 8 describes this model, its performance and the model-derived information required for the hazard assessments. A large amount of supporting information is also provided in a series of Appendices. A brief overview of the project design and key aspects follows in this chapter.

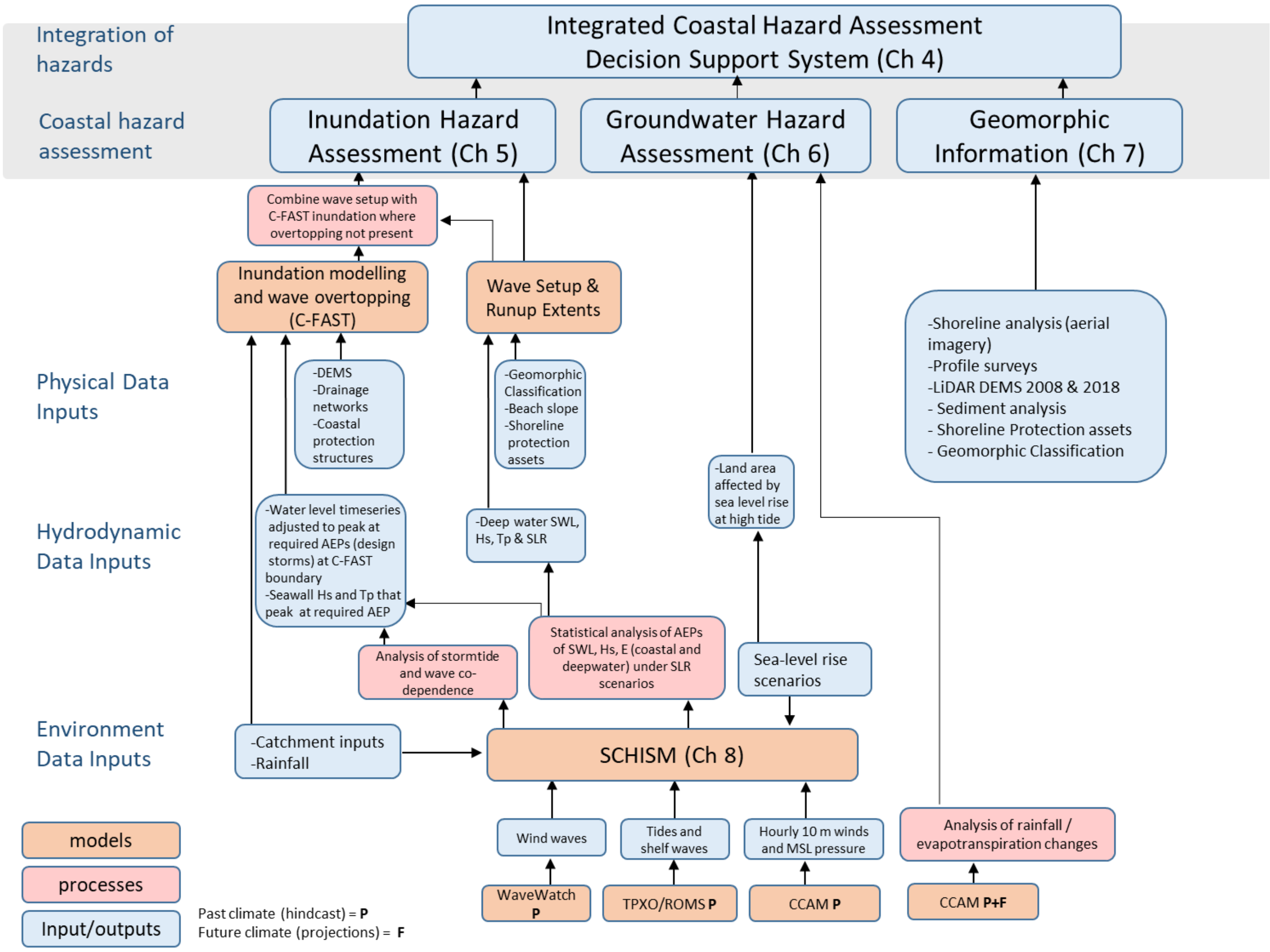

Figure 3.1: Data flows and analysis processes between the various models used in the PPBCHA. The report chapters in which the main components are discussed in detail are indicated.

3.2.1 Decision Support Systems and Integration of Hazard Assessments

The Gap Analysis reviewed various tools that were considered relevant for the integration of the data products from the PPBCHA. A subset of the most relevant tools (Table 3.1) identified national scale and Victorian-specific tools. These tools also tended to focus on providing information on a single hazard. It was recognised that interactions between the hazards can occur. For example, increases in groundwater levels may also exacerbate inundation. A key finding of the review was that no tool was currently available that allowed the integration of all hazards in a single location, leading to the decision to develop a tool that would allow users to visualise and analyse outputs from the three hazard assessments together. This tool also accommodated a range of other relevant datasets developed or used as part of PPBCHA. The DSS developed for the PPBCHA is described in Chapter 4.

A key assumption in the development of the hazard layers was that existing coastal protection structures or coastal protection measures undertaken, such as periodic beach renourishment, would be maintained into the future, but would not be adapted for future sea levels. The datasets from the PPBCHA have been mapped in a Geographical Information System (GIS) and are also available for integration into other tools that are being used by end-users, where the tool has an existing and ongoing mechanism for support and maintenance. For example, FloodZoom is used by a range of agencies and catchment management authorities, and outputs can be directly incorporated into the FloodZoom software.

Table 3.1: A summary of existing flood/emergency management related tools and databases

Name	Custodian	Relevant hazard	Comments and URL
CoastAdapt	National Climate Change Adaptation Research Facility	Inundation, Erosion	Contains shoreline and inundation mapping tools for Australia and offers a framework for the inclusion of inundation and erosion data. Lack of ongoing funding leads to uncertainty about the long-term maintenance and legacy of the platform. https://coastadapt.com.au/
Smartline	Geoscience Australia	Erosion	Nationally consistent coastal 'Smartline" geomorphic and stability map for Australia, last revised in 2016, provides geomorphic information about the coastline and an initial "first pass" assessment of coastal erosion-related hazards, i.e. it does not address erosive processes (wave climate, storm climate) to which various coastal locations are exposed. https://ozcoasts.org.au/external-link/smartline-data/ and also https://coastadapt.com.au/tools/coastadapt-datasets
Australian Coastal Sediment Compartment Dataset	Geoscience Australia	Erosion	Information on landforms and sediment (sand and other beach material) at compartment scale to support coastal erosion assessments.
FloodZoom	DELWP	Inundation	Current flood risk information platform encompassing data from a range of sources for the operational management of emergency events https://www.floodzoom.vic.gov.au/FIP.Site/Identity/Login
EM-COP	Emergency Management Victoria	Inundation	Common operating platform for management of emergency events https://cop.em.vic.gov.au/sadisplay/nicslogin.seam
Victorian Aquifer Framework	DELWP	Groundwater	Aquifer classification system as a tiered 14-layer system allowing local scale studies to focus on the detail within a tier, but with links to the regional scale https://www.water.vic.gov.au/groundwater/victorias-groundwater-resources/victorian-aquifer-framework

3.2.2 Inundation Hazard Assessment

For the PPBCHA, inundation assessments by the C-FAST (CSIRO Data61 Flooding Adaptation Solutions Tool) model at a spatial resolution of 5 m were carried out for four low-lying regions around PPB covering respectively,

- Greater Geelong
- Werribee
- City of Port Phillip
- Mordialloc to Frankston

To complete the whole-of-bay assessment, inundation modelling was also carried out at 25 m resolution within C-FAST over three additional regions that covered the southeastern bay, the western bay and northern bay regions. The results from the different grids were combined to provide seamless inundation maps around the PPB coast for the DSS.

C-FAST is a GPU-based coupled hydrodynamic/hydraulic model built specifically for understanding water flows in the urban environment from extreme sea levels, river flows or rainfall (Cohen et al., 2015). C-FAST includes a dynamic wetting and drying algorithm to account for overland flow of water, can incorporate hydrological inputs from rivers and streams as well as direct rainfall over the model domain. It can also simulate flows through underground storm water drainage networks using a pressure head-based pipe network.

C-FAST was further developed for use in the PPBCHA to allow for wave setup and overtopping in the presence of seawalls and coastal barriers. This development allows water volumes arising from wave setup and runup that exceeds the height of coastal barriers to be discharged across the coastal defences into the urban landscape. The C-FAST model was run using 'design storms' which are constructed water levels and waves that replicate storm tide conditions and are designed to attain peak levels that align with the AEPs (Table 3.2). Further details of C-FAST, its configuration, and inundation hazard layers developed for the DSS are provided in Chapter 5.

As C-FAST does not simulate ocean wave processes, wave setup was represented in the simulations in locations that did not contain seawalls. (Note that wave setup would not be properly resolved on the 25 m resolution C-FAST meshes even if it was coupled to a wave model because features such as seawalls that trigger overtopping would not be resolved by the model). The contribution to inundation extents from wave setup were therefore calculated using an empirical relationship for the entire bay and this layer was combined with the dynamically modelled inundation. The empirical model also provided wave runup hazards for the whole of PPB as a separate data layer in the DSS (see Chapter 5). Peak sea levels heights and wave heights that match the AEPs were calculated from a whole-of-bay hydrodynamic model, SCHISM (Figure 3.1, see Chapter 8).

Table 3.2: Scenarios used for C-FAST modelling. Simulations are performed for 1%, 2% and 5% storm tide AEPs, and for each AEP, three simulations are carried out using the 5th , 50th and 95th percentile estimate of the AEP level to account for the uncertainty in the estimate.

Climate Scenarios	Storm Tide AEP (no rainfall)	Storm Tide AEP (10% AEP rainfall included)
Present climate (baseline)	5%, 2%, 1%	5%, 2%, 1%
0.2 m	5%, 2%, 1%	5%, 2%, 1%
0.5 m	5%, 2%, 1%	5%, 2%, 1%
0.8 m	5%, 2%, 1%	5%, 2%, 1%
1.1 m	5%, 2%, 1%	5%, 2%, 1%
1.4 m	5%, 2%, 1%	5%, 2%, 1%

3.2.3 Groundwater Hazard Assessment

The approach for assessing groundwater hazard in PPB was to develop conceptual models based on the available data and existing conceptual and numerical models. Conceptual models are regularly used in hydrogeology and are based on a series of hypotheses that logically describe the observations of groundwater across the landscape. Like geological models, they are developed through inductive reasoning or inference (McLean and Gribble, 1985). The general principles are inferred from recognising the pattern in a set of observations (such as borehole logs, chemical analyses or hydraulic test properties), and hypotheses are then made and tested.

The whole-of-bay conceptual model together with three more detailed conceptual models in areas where finer resolution data exists are presented in Chapter 6. The three locations selected are (1) the southeastern suburbs between Mentone and Frankston, (2) the Nepean Peninsula, where the groundwater asset is threatened by change, and (3) the Werribee region to assess the potential hazards for market gardens and the wastewater treatment plant, which treats most of Melbourne's sewage.

The outputs comprise a series of models that includes the geological and hydrogeological components and their geometry, groundwater flow, movement and quality. The models also consider SLR and future changes to rainfall and evaporation. These were obtained from the VCP19 project in which the CCAM model was run over Victoria with a resolution of 5 km as part of the DELWP-funded VCP19 to downscale six IPCC CMIP5 models to simulate future climate change at high spatial resolution.

The conceptualisations form the basis for the development of numerical models in later research and investigations (see Chapter 6). Numerical models are typically developed using continuum mechanics models such as Modflow (modular finite-difference) or Feflow (finite element) that can also include fluid density effects and chemical kinetics.

3.2.4 Hydrodynamic Modelling and Climate Scenarios

The simulation of several decades of climate information was required to ensure that the hazard assessments were predicated on credible meteorological, hydrodynamic and climate information, at a scale capable of resolving most local coastal defences and associated infrastructure. The Semi-implicit

Cross-scale Hydroscience Integrated System Model (SCHISM, http://ccrm.vims.edu/schismweb/, see Chapter 8) was setup over the entire PPB and run over a 35-year period (1980-2014) to provide marine hazard information for the inundation and groundwater components of the project.

Atmospheric forcing for the SCHISM model was obtained from a simulation of the CSIRO Conformal Cubic Atmospheric Model (CCAM), a stretched grid global model (McGregor and Dix, 2008). CCAM allows for high-resolution “downscaling” of Global Climate Models (GCMs) without lateral boundaries by initialising and then constraining CCAM at larger scales to match the GCMs, through application of spectral nudging (Thatcher and McGregor, 2009), while resolving smaller-scale features such as orographic wind and rainfall and land/sea breezes. The CCAM model was also run over Victoria over the 1980-2014 period with a resolution of 5 km as part of the DELWP-funded VCP19 project. The surface pressure and 10 m winds from this simulation provided atmospheric forcing for the SCHISM model. Note that future changes to pressure and wind patterns were not considered in this study due to the large computational overhead that would have been required to perform the required simulations.

A summary of the model experiments using SCHISM is given in Table 3.3 with the focus on assessing how future changes in mean sea level affect the hydrodynamics of PPB. The procedure adopted to undertake this assessment is:

- The wave and hydrodynamics model simulations are calibrated and verified against available tide and wave observations identified in the Gap Analysis.
- A 35-year hindcast (1980-2014) is created with the calibrated and verified model.
- A series of simulations is undertaken under different SLR scenarios and the results analysed to determine the changes in tidal and wave behaviour. Scaling relationships are developed to allow other SLR scenarios to be considered.
- The outputs of the model simulations from SCHISM are processed to produce a range of information relevant to the three hazard assessments. This includes the estimation of revised AEP statistics for PPB, inclusive of the effects of tides, storm surge and wave setup using extreme value analysis for present and future SLR scenarios.
- The various outputs were processed and made available as a resource within the DSS (see Chapter 8 for more details).

Table 3.3: Hydrodynamic/wave simulations to support PPBCHA. Note that for computational efficiencies, the SLR scenarios were run only for 20 years to capture a complete 18.6-year tidal cycle.

	Atmospheric Forcing	Sea Level Rise (m)
Baseline (Past Climate)	ERA-Interim Hindcast/CCAM (1980-2014)	0.0
SLR scenarios	ERA-Interim Hindcast/CCAM 1980-1999	0.2
		0.8
		1.4

4 Decision Support System

This chapter describes the DSS that was developed to deliver the relevant outputs of the three hazard assessments. It is introduced before the hazard assessments chapters to orient the reader with the available outputs that are described in detail in the following chapters.

4.1.1 Introduction

The PPBCHA DSS was built as an 'all coastal hazards' data visualisation and analysis tool that can be accessed via the web by anyone who has appropriate access permissions to the site. The DSS uses the open source Terria JS (https://terria.io/) geospatial visualisation and analytics capability developed by CSIRO Data61. The decision to use Terria JS followed an evaluation of existing tools and platforms currently being used to serve up coastal hazard and related datasets such as CoastAdapt (https://coastadapt.com.au/), CoastalRisk (http://coastalrisk.com.au/) and FloodZoom (https://www.floodzoom.vic.gov.au/). It was found that while each of these tools were useful and relevant for their designed purposes, there was no tool that allowed planners, engineers, scientists and the wider community an ability to understand and analyse all relevant coastal hazards in a unified and integrated manner.

4.1.2 Development Process for the DSS and Guiding Principles

The DSS outputs were designed and developed with end user requirements in mind. A User Testing Group with membership from EPA, DELWP, Parks Victoria, Melbourne Water, Local Government and Catchment Management Authorities has been consulted regularly throughout the project to ensure that the representation of hazards and the accompanying analytical capabilities within the DSS are being implemented with end-user outcomes in mind.

The DSS has the following key features and functions:

- Web-based and therefore does not require specific software installation
- Secure user login ability
- Coastal hazards datasets are integrated, including climate change components
- Ability to carry out analytics such as "distance of hazard from a specific point of interest", "extent and area of hazard calculation for a relevant region", "hazard uncertainty considerations" for specific parcels of coastal land
- Ability to extract relevant hazard layers for further analysis with other layers if necessary
- Additional relevant information from a coastal management perspective including beach profile calculations as well as historic aerial imagery for the region (Figure 4.1)
- Ability to carry out visual "side-by-side" comparisons of data layers such as inundation to understand the relative impact of a given SLR scenario or the historical imagery (Figure 4.2)
- Ability to view the outputs in a "3D" environment. This feature provides the user a perspective of the local impact of the hazard (Figure 4.3), and

- Ability to record a ‘story’ to provide a digital record of hazard interpretation and analysis that can be used for communication, decision making and visualisation.

In order to remain consistent around “data usage” the aim of the DSS is to provide information on the hazards in a “policy relevant” context. For example, currently Victorian Government coastal and planning policy stipulates the consideration of SLR planning guidelines for all planning and management considerations using a baseline and a 0.8 m SLR as the key scenarios. The analytics in the DSS have been developed to ensure that the end user can investigate the hazards in the context of these planning guidelines. For example, coastal planners can use the DSS to evaluate, “What are the impacts from inundation and groundwater hazards for a 0.8 m SLR”. It is noted that although the DSS has been developed initially for this project it is intended to be used for several other coastal hazards-related projects. This means that the development of the DSS will extend beyond the duration of this project.

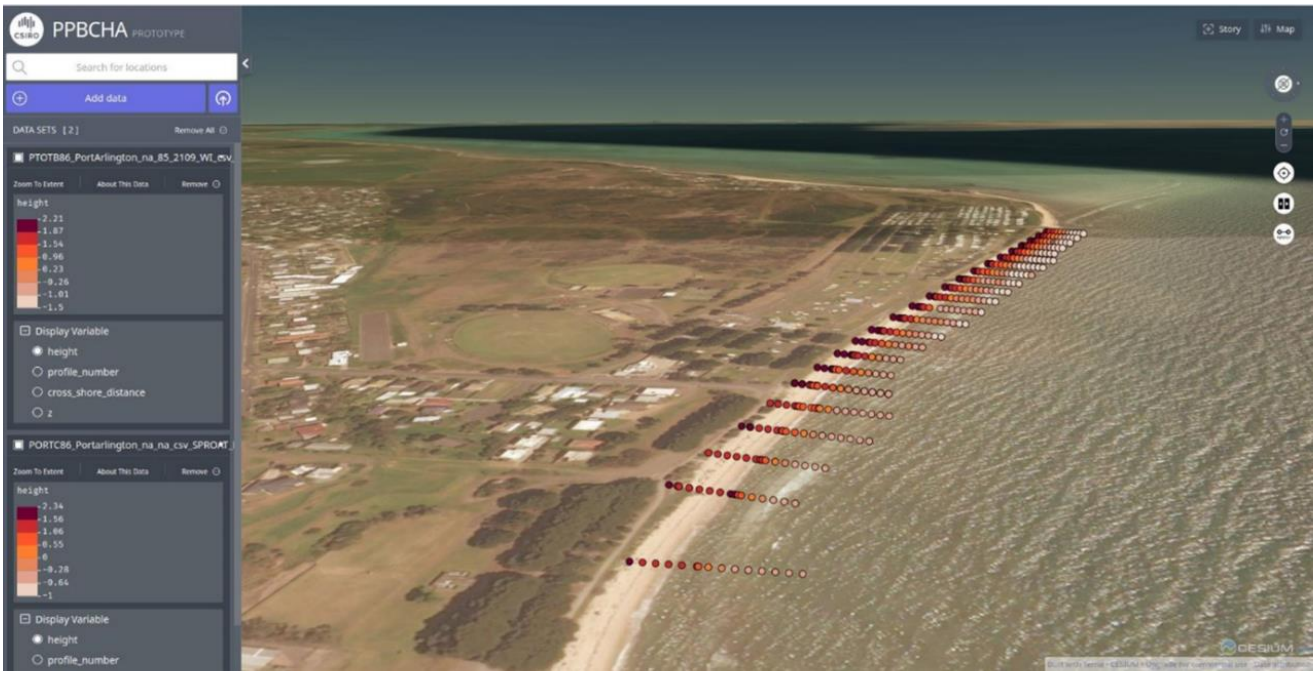

Figure 4.1: Beach profiles for a representative beach in the PPB (Portarlington to Point Richards).

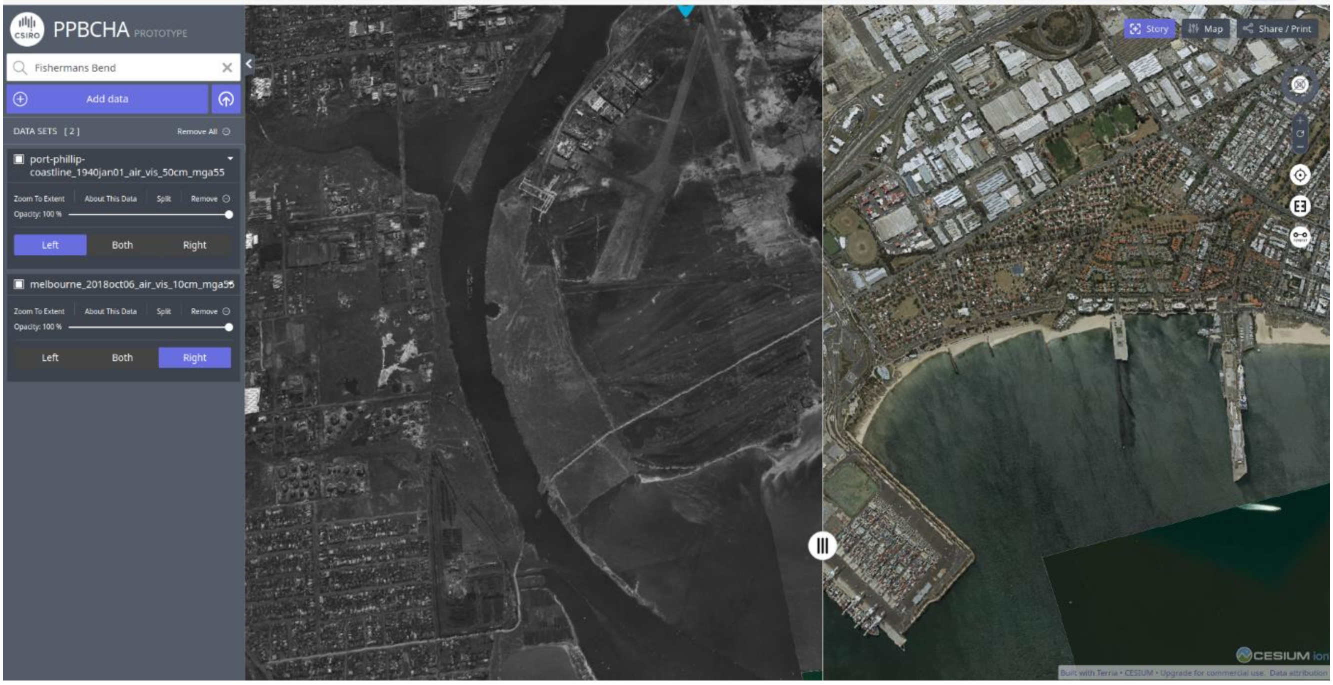

Figure 4.2: Comparison of historical aerial imagery (1940, left) with more recent day imagery (2018, right) in the DSS for the Fisherman's Bend region.

Figure 4.3: Three-dimensional perspective showing coastal protection structures within the DSS at Point Nepean.

4.1.3 Available Datasets

The key datasets available through the DSS include inundation and groundwater hazard layers for current day conditions and for future SLR scenarios up to 1.4 m, as well as datasets pertaining to coastal geomorphology. These include datasets that were either produced as part of this project and/or used as input into the various hazards modelling such as Geomorphic Assessment, Bathymetry and Digital Elevation Models. These are referred to as secondary data layers. For example, historical Aerial Imagery from the 1930's to current day have been included in the DSS supplied by the DELWP Coordinated Imagery Program. The data consists of approximately 7,000 frames of aerial images. These were originally in various formats but have been synthesised into a high-resolution set of historical images for the region and presented within the DSS (Figure 4.2). These images along with the outputs of the hazard assessments provide a valuable set of data that can be used by various stakeholders for a range of applications.

In addition to the above datasets the DSS includes data from the Victorian Government Open Data Portal: www.data.vic.gov.au, the Federal Government Open Data Portal www.data.gov.au and the freely available Melbourne City 3D Model from http://aero3dpro.com.au/ so as to provide users a "one-stop-shop" for visualising and analysing relevant geospatial data for the PPB region. Table 4.1 provides a detailed list of datasets that are available in the DSS for the three hazards.

Table 4.1: Summary of hazard data presented in the DSS. For each SLR scenario (0.0, 0.2, 0.5, 0.8, 1.1, 1.4 m) the hazard layers described below will be replicated.

<table>
<tr><th colspan="2">Hazard Type</th><th>Type of Data</th><th>Number of Outputs</th></tr>
<tr><td rowspan="2">Inundation</td><td>Flooding</td><td>Raster</td><td>
<table>
<tr><td>Storm tide (% AEP)</td><td>Catchment (% AEP)</td><td>Inundation Depth (>10 cm**) for 5% probability layer*</td><td>Layer showing combined probabilistic estimates for 5, 50 and 95% (zones 3, 2, and 1) inundation extents</td></tr>
<tr><td>1</td><td>0</td><td>1</td><td>1</td></tr>
<tr><td>1</td><td>10</td><td>1</td><td>1</td></tr>
<tr><td>2</td><td>0</td><td>1</td><td>1</td></tr>
<tr><td>2</td><td>10</td><td>1</td><td>1</td></tr>
<tr><td>5</td><td>0</td><td>1</td><td>1</td></tr>
<tr><td>5</td><td>10</td><td>1</td><td>1</td></tr>
</table>
*Note that the inundation depth layer is based on the 5% probability of occurring to provide a conservative estimate as suggested by Melbourne Water.
**Inundation > 10 cm is based on a definition of nuisance flooding for urban environments (coastal and catchment) described in Moftakhari et al., (2018). Further details can be found in Chapter 5.
</td></tr>
<tr><td>Wave runup excursion on beaches</td><td>Shape file</td><td>
<table>
<tr><td>Storm tide (%)</td><td>Catchment (%)</td><td>Layer showing combined probabilistic estimates for 5, 50 and 95% (zones 3, 2 and 1) wave runup extents</td></tr>
<tr><td>1</td><td>n/a</td><td>1</td></tr>
<tr><td>2</td><td>n/a</td><td>1</td></tr>
<tr><td>5</td><td>n/a</td><td>1</td></tr>
</table>
</td></tr>
<tr><td colspan="2" rowspan="2">Ground Water</td><td>Shape file</td><td>
<table>
<tr><td>Storm tide (%)</td><td>Catchment (%)</td><td>Watertable depth colour coded as shallow, intermediate and deep</td><td>Groundwater salinity</td></tr>
<tr><td>n/a</td><td>n/a</td><td>1</td><td>1</td></tr>
</table>
</td></tr>
<tr><td>pdf</td><td>2D vertical sections in three “hotspot” locations around the bay (Werribee, Mentone to Frankston and Nepean Peninsula) illustrate how the ground watertable will change with SLR. Further details can be found in chapter 6.</td></tr>
</table>

5 Inundation Hazard Assessment

This chapter describes the methodology for the inundation hazard assessment. It begins with the relevant data inputs and how they relate to the inundation modelling. A hydrodynamic model is used to assess the inundation hazard around the entire bay on a total of seven different model meshes, with the results combined to produce whole-of-bay inundation hazard information. The resolution of the model was either 5 m or 25 m depending on the physical processes that are incorporated in the modelling. Low-lying and developed areas are prioritised for the 5 m resolution modelling. Simulations were undertaken for 1%, 2% and 5% AEP events without rainfall and including a 10% AEP rainfall event. The model setup and data inputs are described and tested through sensitivity experiments by varying the model mesh resolution and comparing results from other inundation modelling studies. Inundation is presented as probabilistic areas of inundation as well as inundation depth. In addition to the hydrodynamic modelling that accounts for tides, storm surge, SLR and wave overtopping, additional inundation layers that represent setup and runup of waves on a beach are also calculated for the entire bay. Wave setup is integrated into the inundation hazard extents for the relevant AEP and wave runup is available as a separate layer that can be viewed in conjunction with or independently of the inundation hazard layers in the DSS.

5.1 Introduction

The inundation hazards in the PPBCHA were assessed at two levels of detail around the bay. For highly urbanised low-lying areas, the CSIRO City Flood Adaptation Solutions Tool (C-FAST) was used at a 5 m resolution to account for seawall and drainage infrastructure. For the rest of the bay, overland inundation was assessed with the same model at 25 m resolution accounting for SLR, storm tide and catchment inputs. Except where overtopping of seawalls is implemented in C-FAST using wave overtopping algorithms, wave setup is not simulated in C-FAST on either the 5 m grids or the 25 m grids. Instead, wave setup is calculated using an empirical model for the entire bay and the inundation extents are combined with the C-FAST simulated inundation to provide seamless inundation maps around the PPB coast for the DSS. Wave runup hazard, is also simulated by an empirical model for the entire bay and provided as a separate layer in the DSS.

The inundation hazard assessment considers ocean inputs from SCHISM (as illustrated in Figure 3.1 and detailed in Chapter 8), catchment inputs, geomorphic inputs from vertical surveys (LiDAR and beach surveys) and compartment (Coastal Geomorphic Sectors) landform analysis. The specific inputs and the way they were used in the inundation hazard assessment are provided in more detail in Table 5.1. Results were analysed for each design storm AEP and its associated uncertainties to inform probabilistic zones of inundation.

Table 5.1: Summary of information and data usage in hazard assessments. Input variables which are shapefile attributes are within quotation marks. Note that these inputs are additional to the time varying design storm boundary conditions applied to the offshore C-FAST model grid for each AEP event considered and that C-FAST at 25 m resolution does not include overtopping (see section 5.2).

Input Variable	C-FAST (5 km grids)	C-FAST (25 m grids)	WAVE SETUP and RUNUP EXCURSION (all of bay)
GEOMORPHOLOGY	**Defines the local geomorphology (e.g. beach, cliff), see section 7.2.1**		
"INTERT_TYP"			-identify compartments with a beach
HEIGHT SURVEYS	**Beach profile slope, LiDAR, see 7.2.3, 1980's beach surveys, see 7.2.4**		
Slope Beta [-]			-Stockdon et al., 2006.
Digital elevation model (DEM) [m AHD]	-bathymetry and topography	--bathymetry and topography	-Mask the runup hazard behind steep slopes > 30 deg.
STRUCTURES	**Seawall, Groyne, Revetment etc, see 7.2.5**		
"Asset_Type"	-Define EurOtop equation -modify DEM.		-Mask the runup hazard behind structure
"Face_Slope" [deg]	Average slope of seawall revetment face -EurOtop-C-FAST discharge (m3/s) AEP		
"Ave_Height" [m]	Front Average height of front of seawall -EurOtop-C-FAST discharge (m3/s) AEP		
"Mid_RL"[m AHD] "Start_RL" "End_RL"	-Survey height of wall at approximate central and end points.		
SCHISM	**Various local hydrodynamic inputs, see Chapter 8 and Appendix C**		
Significant Wave Height Hs [m]	-EurOtop input (AEP)		-Stockdon et al., 2006. (AEP)
Peak Wave Period TP [s]	-EurOtop input (AEP)		-Stockdon et al., 2006. (AEP)
Still Water Level SWL [m]	-EurOtop input (AEP and time series)		-Stockdon et al., 2006. (AEP)
Event duration D [hrs]	-HS triangular timeseries design storm for EurOtop calculation. Duration in Hours.		
CATCHMENT	**Input from rainfall**		
R [mm/hr]	Rain on grid		

5.2 Model Setup

The core component of C-FAST is a finite volume shallow water solver written for GPU hardware (Cohen et al., 2015). This is coupled with five processor modules relevant for this project including storm tide boundary conditions, overtopping, rain-on-grid modelling of rainfall, river inflows and drainage network modelling. Further details of the C-FAST model are available in Cohen et al., (2016b) and a description of its use for assessing adaptation measures is available in Cohen et al., (2019). Specifically, for this project, a new module was developed for C-FAST to include the simulation of wave overtopping for the 5 m spatial resolution regions as described below.

5.2.1 EurOtop Overtopping Algorithms

Seawall overtopping was identified as an important flooding mechanism to be considered in this coastal inundation hazard assessment. Time-varying overtopping discharge processes were modelled as a subgrid-scale process, akin to river discharge, which was accounted for with model parameterisation. The discharge parameterisations were sourced from the EurOtop formulations (Van der Meer, 2018, see 5.3.7).

A schematic of the model implementation for the overflow and overtopping conditions is shown in Figure 5.1 for the simple test case provided in O'Grady et al., (2019a). Within the C-FAST hydrodynamic model, overtopping discharge takes place at the neighbouring-landward grid point of a prescribed coastal structure (seawall) in the model domain. It is assumed that overtopping (using EurOtop) only occurs at the time the Still Water Level (SWL comprising the storm tide and any applied SLR scenario) height is between the height of the toe and crest of the prescribed coastal structure. When the SWL was greater than the seawall crest height EurOtop overtopping was turned off, and dynamic inundation (using SWASH or C-FAST) occurred due to long-wave overflow. Further details of this model implementation, integration and its comparison with the wave-resolved overtopping model SWASH are available in O'Grady et al., (2019a).

The EurOtop equations (Van der Meer et al., 2018) were used with the C-FAST inundation modelling. In the absence of field observations of wave overtopping in PPB, a preliminary benchmark test was undertaken with C-FAST for simple slope tank experiments (O'Grady et al., 2019a) using an earlier version of the EurOtop equations (Pullen et al., 2007). The results showed sensible and comparable results to a phase-resolved wave model (Zijlema et al., 2011). Similar to the approach used here, other studies have successfully applied pre-2018 EurOtop equations in numerical inundation models to model the contribution of overtopping to inundation in engineering applications. These include studies using TELEMAC (Dugor et al., 2014) and ADCIRC (Suh and Kim, 2018).

A selection of the equations from the latest version of EurOtop (Van der Meer et al., 2018) were used in C-FAST according to the defence structure characteristics, (e.g. vertical seawalls or revetments with a simple sloping face). The EurOtop guidelines (Van der Meer et al., 2018) provided two sets of equations for estimating overtopping discharge:

1. The "mean value approach" equations, which are the more likely estimates of discharge that would occur, i.e. would be used for validation studies
2. The "design approach" equations, in which the "mean value" discharge is increased by one standard deviation to include some safety in the design and assessment of coastal structures.

In this hazard assessment study of PPB, the design approach equations were used

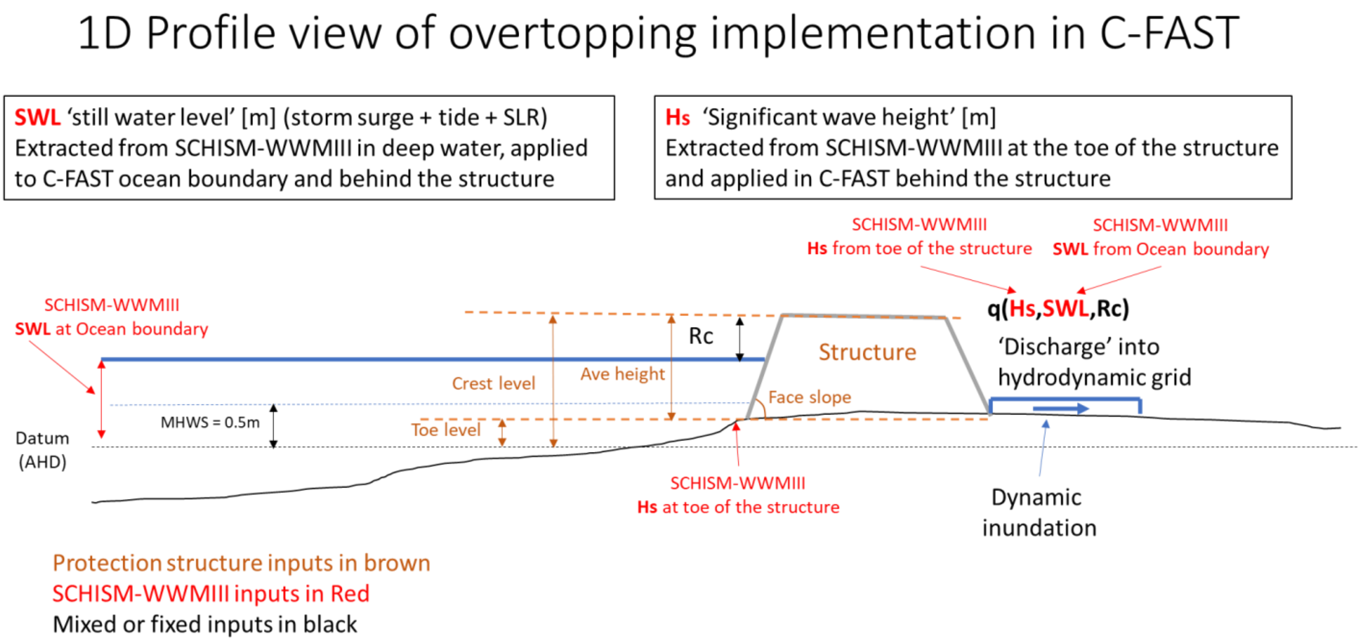

Figure 5.1 Idealised diagram of C-FAST overtopping implementation. Ocean boundary to the left, blue thick line is the SWL, black thick line is the ground elevation (topography/bathymetry), grey line is the seawall, and black dashed line is the datum.

5.2.2 Regions

Four high-resolution (5 m) inundation modelling regions were considered in this study and three additional larger extent, lower resolution (25 m) model regions considered to ensure seamless, whole-of-Bay results are generated (Figure 5,2). The regions are:

- Region A – City of Greater Geelong (5 m)
- Region B – Wyndham City Council (5 m)
- Region C – Hobsons Bay City Council to City of Port Phillip (5 m)
- Region D – Kingston City Council (5 m)
- Region W – Western (25 m)
- Region E – Eastern (25 m), and
- Region S – Southern (25 m).

The simulations performed on the 5 m grids include the effects of wave overtopping and drainage. However, over the larger scale regions (W, E and S) at 25 m resolution, which are less urbanised and coastally armoured, the effects of seawalls and drainage networks were not modelled since these are of sub-grid scale and therefore would not be adequately resolved by C-FAST at 25 m resolution. In addition, wave setup was not modelled by C-FAST except in locations on the 5 m grid containing seawalls where overtopping algorithms were invoked. Instead, wave setup was calculated for the entire bay using an empirical model based on Stockdon et al., (2006). The wave setup results for the whole of PPB were combined with C-FAST results to provide seamless inundation extent layers around PPB for inclusion in the DSS. A description on the approach to creating the seamless whole-of-bay outputs is provided in Section 5.5.

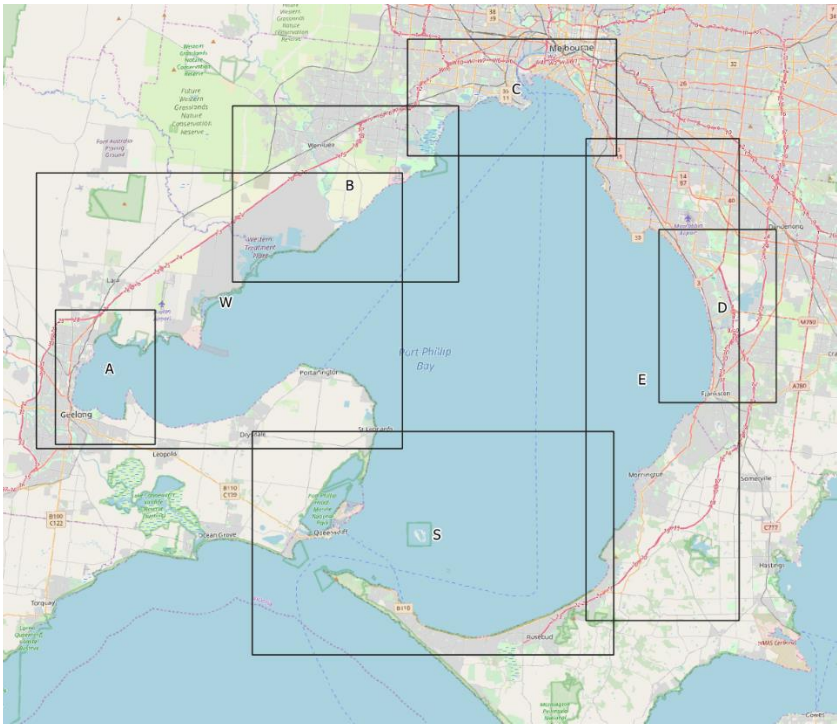

Figure 5.2: Inundation simulation regions. For the 5 m resolution simulations the regions are A, B, C and D. For the 25 m resolution simulations the regions are W, E and S.

5.2.3 Simulation Scenarios

For the inundation assessment, six scenarios were modelled including the baseline and five SLR values (see Table 3.2). The storm tide AEP levels are derived from the SCHISM model output at a central offshore location for each of the regions; A, B, C, D, W, E and S, in Figure 5.2 and include a central value (i.e. 50th percentile) per AEP event together with the 5th and 95th percentile values associated with the statistical uncertainty of the extreme value analysis that determined the AEP levels. The underlying wave input was also derived from SCHISM model output in a similar manner at a location offshore from each seawall for regions A, B, C and D. In addition, wave heights during storm tide events were analysed in the SCHISM simulations to determine the most appropriate way to phase the wave height timeseries with design storm tide time series (Appendix C). For simulations that included rainfall, a 10% AEP value was used for all AEP storm tides considered. Overall, there were a total of 108 simulations per study region.

A design storm tide timeseries of 48-hour duration was used as a boundary condition for the C-FAST model. The 48-hour event duration was consistent with the study conducted by Water Technology (2018) for Melbourne Water. The shape of the design storm tide event together with the associated wave conditions (required to calculate the overtopping) was defined based on the analysis described in Appendix C. The levels associated with the AEP events were determined from the analysis of sea levels in PPB simulated by the SCHISM model (see Chapter 8) and the design storm time series was adjusted to peak at the specified AEP levels associated with the 1%, 2% and 5% AEP events (Table 3.2).

Scenarios without catchment input are also important to consider. This is to ensure that there is a clear understanding of the coastal inundation component. It is also clear that a 1% catchment AEP input along with the storm tide AEP events would lead to scenarios that are highly unlikely for the region. As discussed in Chapter 2, extreme rainfall and storm tide events tend to be independent along the southern coastline meaning that their combined probability is the product of the probabilities of the individual events (e.g. Wu et al., 2018). Therefore, only a single catchment input (a 10% AEP catchment input) was considered together with a no catchment input set of simulations. Catchment inputs consist of local rainfall (local catchment flooding). According to Melbourne Water the response time of the Yarra River is around 3 days whereas it is around 24 hours for the other rivers. This means introducing rain-on-grid (local catchment flooding) as well as river inflow-based flooding could potentially result in double counting the amount of introduced flood waters. Additionally, the appropriate timing of the flood waters in rivers in relation to the storm tide in a design storm context is not well defined. A similar issue exists with "rain-on-grid" flood inputs. In the simulations undertaken here, the phasing of the rainfall with the storm tide was addressed as follows:

- Catchment flooding was introduced only via local catchment flooding, i.e. through rain-on-grid inputs. This was to ensure that the catchment flood response time had a meaningful impact on the coastal area of interest. Excluding streamflow inputs ensures that there is no double counting of flood water, and
- The rain-on-grid flooding was applied in a spatially uniform manner across each model grid. The rainfall duration included 2, 12 and 24 hrs for a 10% AEP, based on the Intensity-Frequency-Duration (IFD) charts from the Bureau of Meteorology (BoM), (see Appendix B, Figure B1). The rainfall was introduced so that it would peak in the middle of the storm tide event. For example, a 2-hr rainfall event was commenced at 23 hrs into the 48-hr simulation and ended at 25 hrs. In Section 5.4, sensitivity simulations apply the rainfall over the 2, 12 and 24-hour intervals to assess the most suitable rainfall duration to be used in the inundation hazard layers for the DSS.

5.2.4 Inundation Hazard Zone Mapping

In presenting the results of the inundation modelling, the inundation extents that occurred for each storm tide AEP (i.e. the central estimate of which is the median, or 50th percentile value) were modelled as well as the extents for the 5th and 95th percentile AEP values to capture the uncertainty in the AEP estimates. The three extents were combined in a single inundation map with zones coloured according to the likelihood of the inundation extent occurring (Figure 5.3).

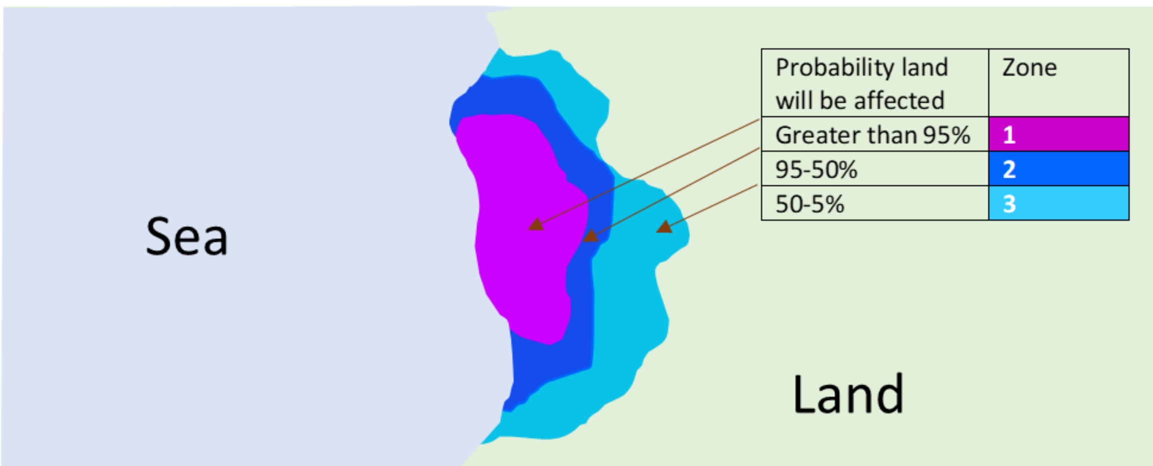

Figure 5.3: Schematic map of probability of inundation used in the presentation of inundation layers in the DSS.

5.3 Input Data, Pre- and Post-Processing

5.3.1 Digital Elevation Models

Table 5.2 lists the 5 digital elevation models (DEMs) that were available for use in the PPB study. The VicCoasts 2007 survey data (A and B) were superseded by the 2017 reanalysis (C and D) and were used in preference. The 2017 coastal survey (E) was for the near shore region only and did not contain bathymetry data. It also did not contain data for the Bellarine Peninsula. For inundation modelling it is critical to use elevation data that has seamless connectivity between bathymetry and terrain. This connectivity could not be established with the 2017 coastal survey and therefore, although it is of a high spatial resolution, it was not used for the inundation modelling. Instead, to ensure smooth transition between the underwater and overland DEM data, only data sets C and D were used to define the elevations in the C-FAST grids. Furthermore, in processing these datasets for use in the model, data set D was composited on top of data set C, meaning the best available data is used for each grid cell (Figure 5.4).

Table 5.2: Simulation cases for each study region.

Data Set	Description	Topography	Bathymetry	Resolution	Notes
A	VicCoasts 2007 survey [REF]		Yes	2.5 m	
B	Same as A	Yes		1 m	
C	2017 reanalysis of VicCoasts 2007 survey (2017)	Yes	Yes	10 m	Continuous and seamless
D	Same as C	Yes	Yes	2.5 m	Contains gaps
E	2017 coastal survey	Yes		1 m	Very near shore coastal terrain only. No Bellarine Peninsula data.

In general, the composition of the digital elevation model (DEM) for the inundation simulations was achieved by selecting a rectangular simulation region of the required grid resolution. The ground height at each grid cell was obtained from the best available data at that location (see Figure 5.5). Any grid cells that still had missing data were filled in using a Laplacian-based interpolation method. Since seawalls are smaller than the grid resolution, the DEM were manually adjusted along each seawall polyline. The bathymetry of rivers, that are poorly reflected in the input DEMs, were corrected using supplementary vector-based data.

C-FAST uses spatially varying values for the Manning's roughness coefficient across each simulation region. The Manning's roughness coefficients used in the C-FAST grids for the underwater bay regions were obtained from the same source data as used in the SCHISM simulations (see Section 8.4.1) whilst for the land areas, variable Manning's coefficients were used based on recommendations provided in the Australian Rainfall and Run-off guidelines (ARR, 2012). The Manning's roughness coefficients range from 0.35 for high density residential areas to 0.04 for minimally vegetated areas. The average of suggested values by Engineers Australia were used for the study (Babister and Barton, 2012).

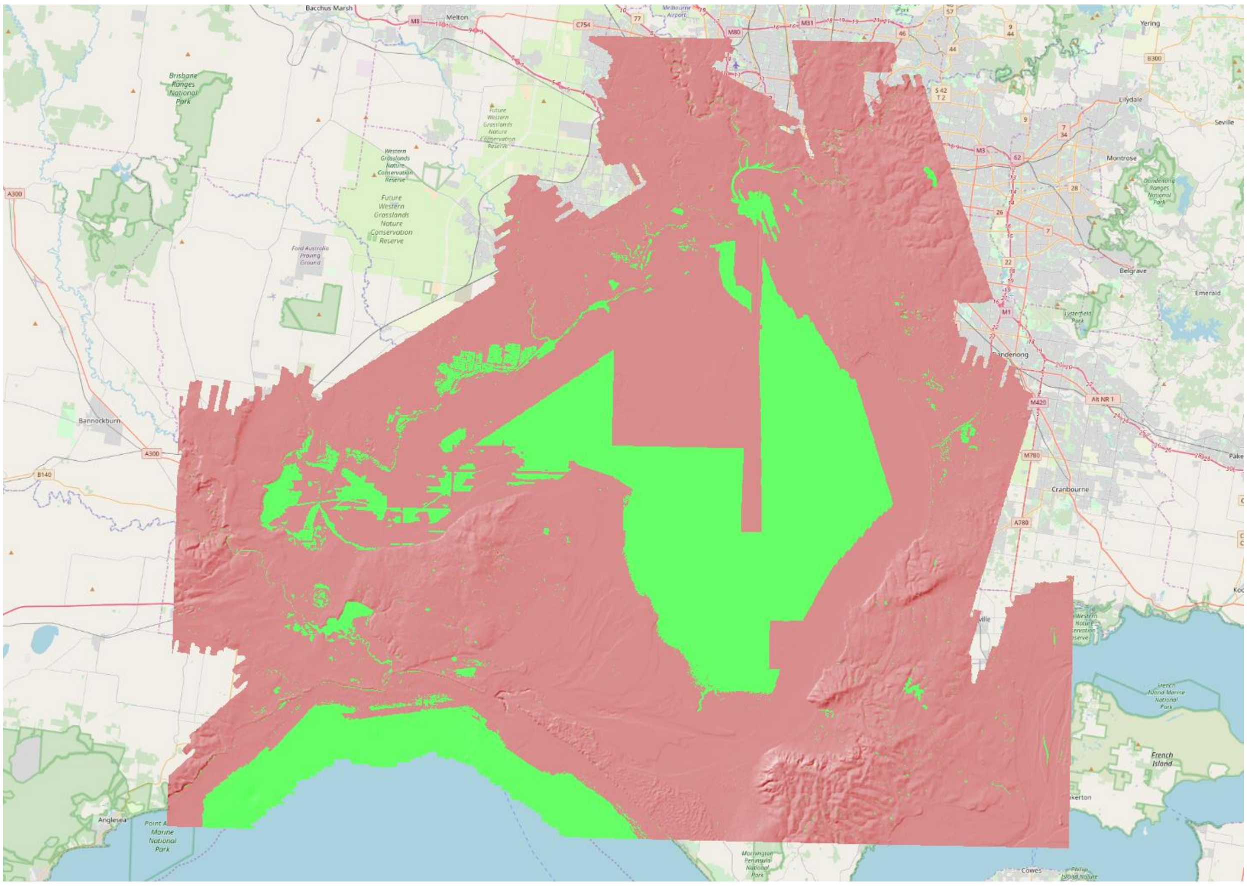

Figure 5.4: Sources of DEM data used in the flooding simulations. Red is from the finer data set D and green is from coarser data set C.

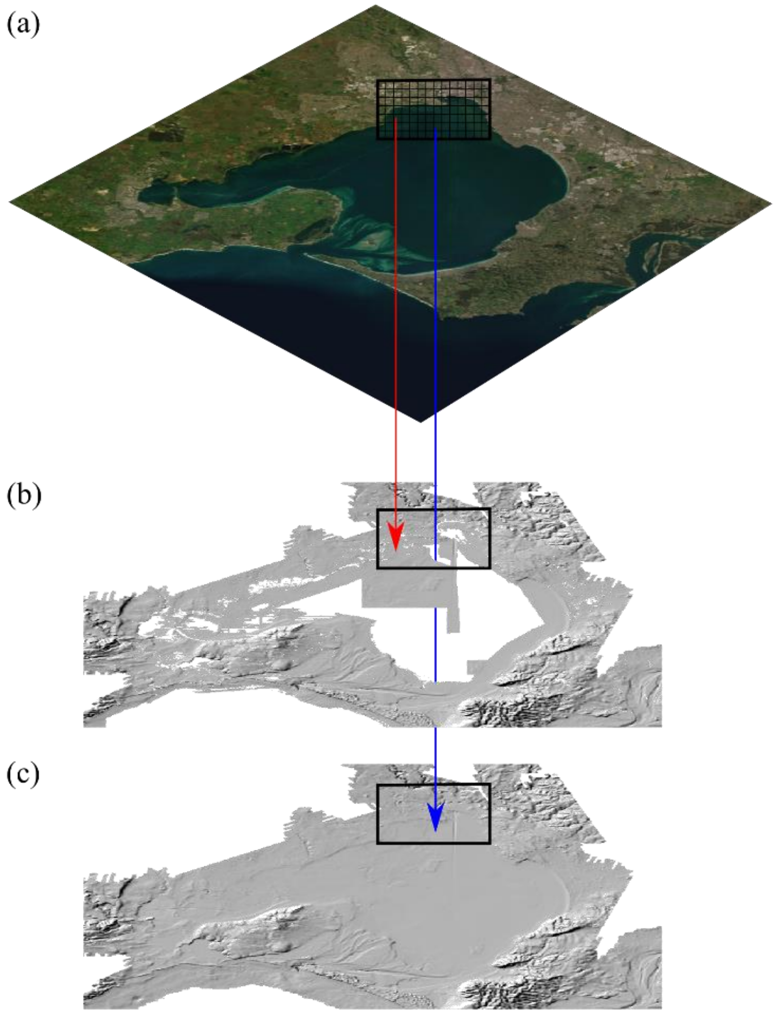

Figure 5.5: The composition of the simulation digital elevation model (DEM) takes the best available data from the input DEM data sets. (a) The simulation region and grid. (b) The high-resolution DEM data was able to be sampled successfully for certain grid cells (red arrow). (c) The low-resolution DEM was sampled (blue arrow) for grid cells when the high-resolution DEM was missing the corresponding data.

5.3.2 Catchment Inputs

Catchment inflows were restricted to local catchment rain-on-grid inputs for all regions and all scenarios. A 10% AEP rainfall total was simulated as a short burst of uniform rainfall over a 2-hour period at around the time of the peak storm tide level in the middle of the 48-hr design storm simulation. This choice of scenario was based on consultation with Melbourne Water. For the purposes of understanding the sensitivity of this assumption, two additional simulations were performed on grid C: the first in which the rainfall was distributed to fall uniformly over a 12-hour period and the second over a 24-hour period in the middle of the 48-hour simulation. The rainfall totals associated with the 10% AEP were derived from IFD data from the Bureau of Meteorology website

(http://www.bom.gov.au/water/designRainfalls/revised-ifd/) (see Table 5.3 and relevant tables in Appendix B; Figure B1).

Table 5.3: Rainfall IFD summary

Annual Exceedance Probability (AEP)	Duration (Hours)	Rainfall Rate (mm/hour)			
		Region A	Region B	Region C	Region D
10%	24	2.83	3.05	3.38	3.17
10%	12	4.27	4.86	5.31	5.04
10%	2	13.5	16.3	17.8	17.3

5.3.3 Drainage Networks

Stormwater drainage pipe network data was sourced from each individual council within the study regions (Figure 5.6). This data included pipes as polylines (with cross-sectional information) and pits as point data. A substantial effort was made to pre-process this data to make it suitable for flow modelling. The steps included:

- merging together data sets from adjacent councils within a single region
- resolving broken and disconnected pipes, junctions and pits
- removing orphaned elements
- resolving missing pipe property data, and
- removing network sections that cross over the simulation boundaries.

The resultant drainage networks were used in the pressure-head based pipe network solver of C-FAST. In most cases only drainage pipes that were larger than 1 m were used in the study as these are the ones that have a significant impact on the flood outcomes. This approach also ensures that the simulation run times are sustainable.

Figure 5.6: Locations of stormwater drainage pipes within each simulation region.

5.3.4 Wave Overtopping

Input required for the overtopping calculations is summarised in Table 5.1. The characteristics and attributes of the seawalls and revetments were sourced from the 2013 "VIC Protection Structures Condition Attributes" shapefile. In this, the height of the crest was calculated as the minimum of the three surveyed structure heights relative to AHD (shapefile attributes: Start_RL, Mid_RL and End_RL). The toe level was calculated as the crest level less the average height of the wall (shapefile attribute: Ave Height) (see Appendix B, Table B2). The face slope was sourced to identify if a simple slope or vertical wall equation was used (shapefile attribute: Face_Slope). The EurOtop equations for composite walls were not considered as there were no attributes available detailing the height of any mound in front of vertical walls. If the exposed toe of a vertical wall was above Mean High Water Springs (MHWS) (0.5 m) the equations that considered a foreshore were used (Table B2). A summary of the equations to be used are in Table 5.4 and the locations of the seawalls and revetments in relation to the C-FAST grids are shown in Figure 5.7.

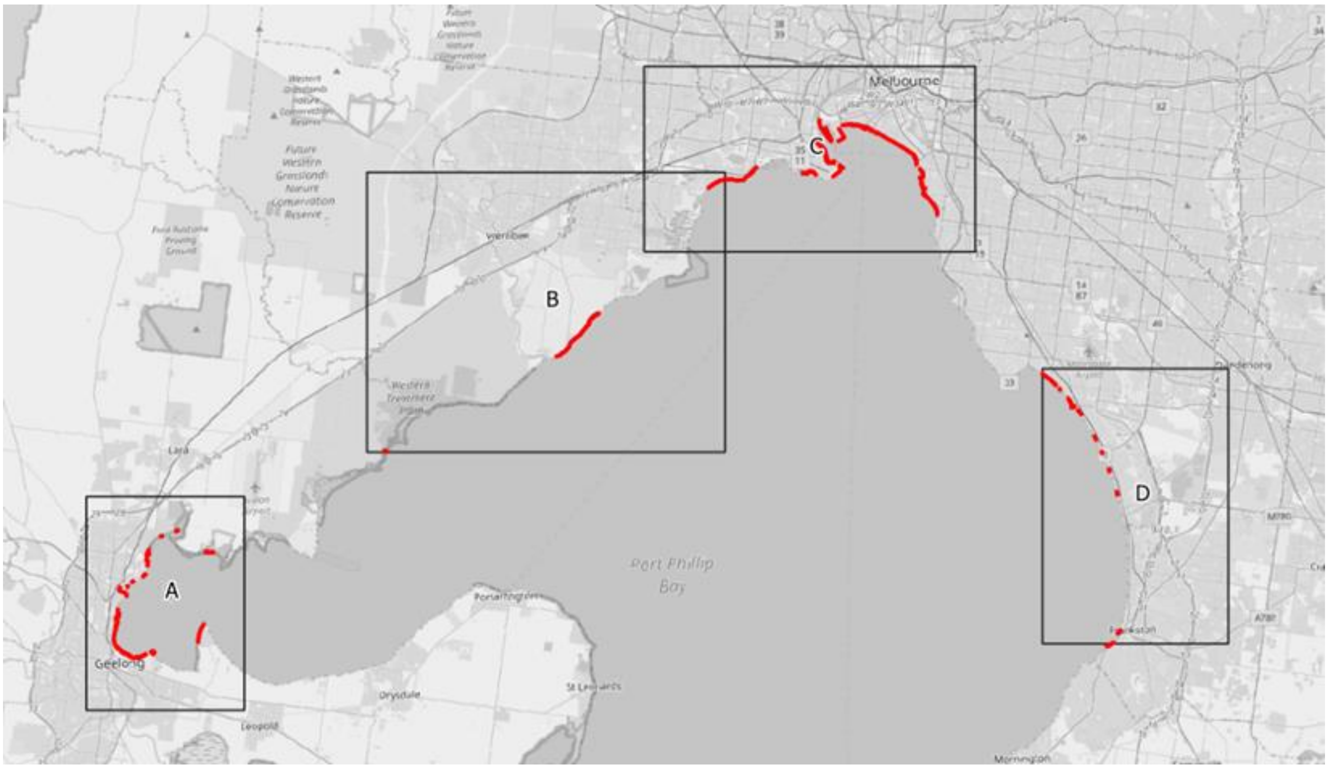

Figure 5.7: Locations of the seawalls modelled in Regions A-D.

For the Werribee grid, a section of low vertical cliff on Campbells Cove Rd was identified as a natural overtopping location, and therefore heights were surveyed from the DEM so that it could be treated as a vertical wall in the overtopping equations. Each structure was provided as a polyline, representing the spatial extent of each structure. Corresponding properties for each seawall polyline were also extracted, those relevant to the overtopping modelling being:

- Structure type (seawall or revetment)
- Toe level (m AHD)
- Crest level (m AHD)
- Seawall type (vertical or sloped), and
- Slope angle (degrees).

Additional data required from the SCHISM model results for the seawall overtopping included local values for each structure of:

- Deep water still water level time series - the same as used for the C-FAST tidal boundary conditions.
- AEP short-wave height at the toe of each wall segment. From SCHISM model output, a constant maximum local wave height was obtained for each seawall. Common practice is to use a "triangular" time series as an input where the peak value is scaled to match the relevant AEP value considered in the simulation (see Appendix C).

Table 5.4: The criteria for the EurOtop Equations used in C-FAST. See Van der Meer et al., (2018) for equations.

Face_Slope	Foreshore Toe height	Impulsive conditions $H^2/(H_{m0}\ L_{m}\text{-}1{,}0)$	Low freeboard R_c/H_{m0}	EurOtop 2018 equation
< 90 Deg (simple slope)				5.12
= 90 Deg (vertical wall)	< 0.5m			7.2
= 90 Deg (vertical wall)	>= 0.5m	>= 0.23		7.6
= 90 Deg (vertical wall)	>= 0.5m	< 0.23	< 1.35	7.9
= 90 Deg (vertical wall)	>= 0.5m	< 0.23	>= 1.35	7.10

An extreme value statistical distribution is fitted to hourly SCHISM time series of Hs at the grid node corresponding to the level of the toe near the centre point of each coastal defence structure (seawall or revetment). These are used to evaluate the design AEP significant wave heights for input into the EurOtop equations in C-FAST. If a neighbouring deeper SCHISM grid node was required to line up with the toe, a depth-induced breaking wave height limiter was used to transform the wave to shallower water,

$$\gamma = 0.7 = \frac{H_{s,max}}{(SWL - h)}$$
$$H_{s*} = \text{minimum}(0.7(SWL - h), H_{s,n})$$

where $H_{s,max}$ is the maximum significant wave height in a given depth h corresponding to the surveyed toe level. Investigation of the SCHISM model ratio of Hs to SWL-h indicated a value of 0.7 was the apparent limiter of H_{s*} in shallow water in the SCHISM land output points, which is within the range reported in other modelling studies (SWAN_Team, 2016). Figure 5.8 shows the AEP significant wave height at the toe of each structure for the baseline climate, which varies between 0.8 m - 1.6 m for a 1% AEP. Under 0.8 m of SLR increase the significant wave heights increase to 1.2 - 1.8 m (Figure 5.9), where the deep-water wave height is around 2.2 - 2.4 m for both simulations.

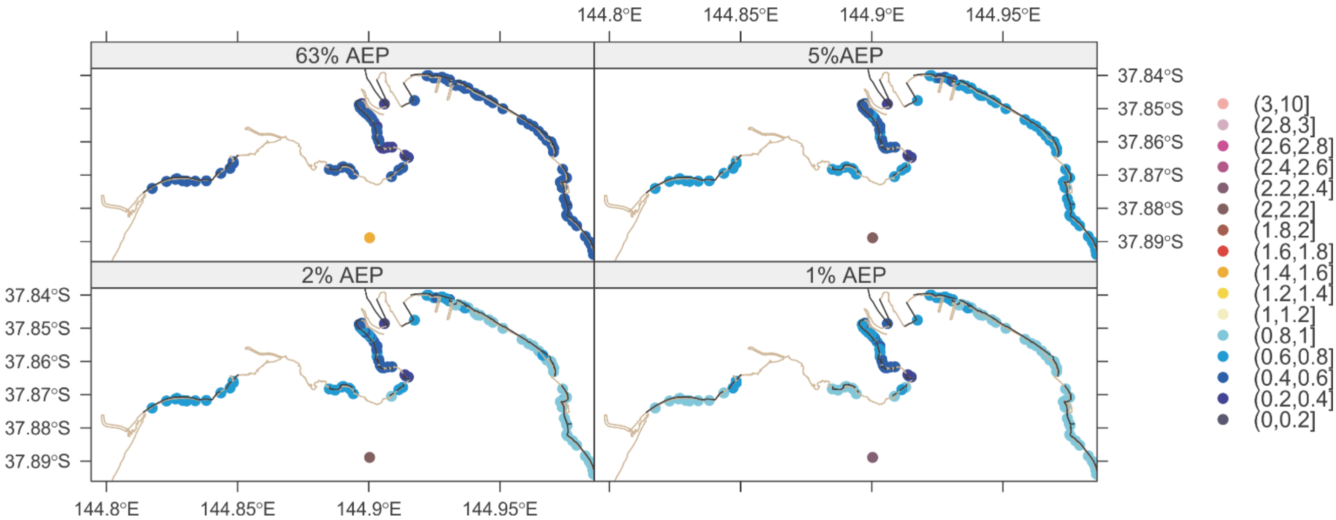

Figure 5.8: Values of Hs (m) at the toe of the coastal defence structures for Grid C for the baseline simulation for the AEPs indicated. Colour legend indicates values of Hs in m.

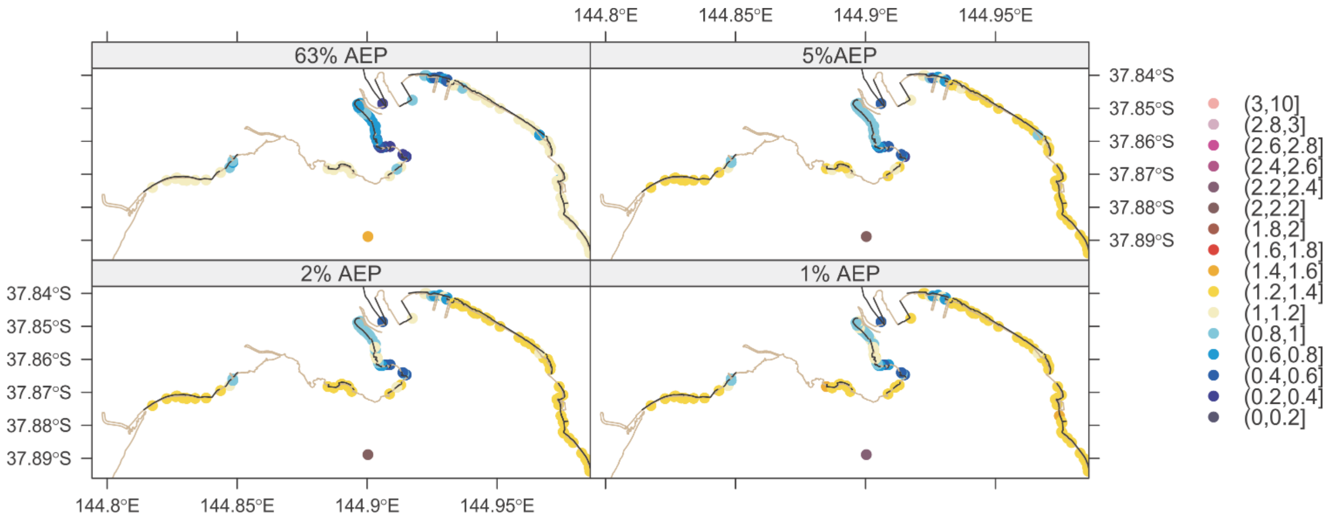

Figure 5.9: Values of Hs at the toe of the coastal defence structures for Grid C for the 0.8 m of SLR simulation for the AEPs indicated. Colour legend indicates values of Hs in m.

Time series of SWL at deep-water SCHISM locations that coincided with the offshore boundaries of each C-FAST model domain were used to derive design time series to use as boundary conditions for each C-FAST simulation under AEP peak SWL (Appendix C). The water-level values at these deep-water points were also used as the time series input of SWL for EurOtop in C-FAST at each structure to avoid double-counting of wave setup, which is included in both the SCHISM modelled water levels at the structure, and also calculated in the EurOtop formulation. Estimates of the TWL (the combination of SWL and wave setup) at the defence structures from SCHISM are provided in Figure 5.10.

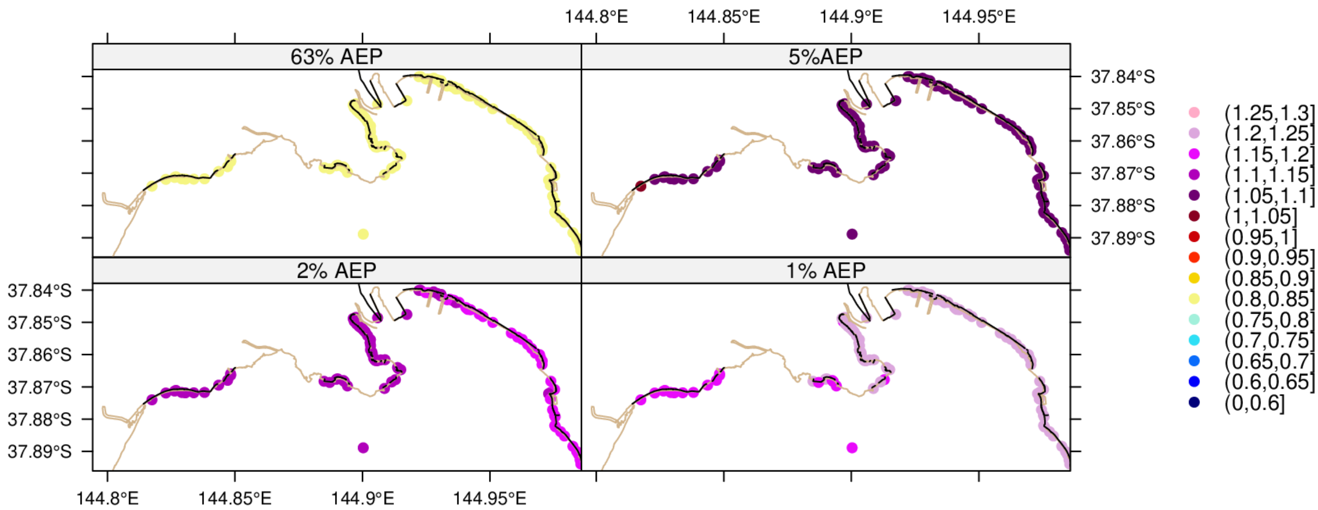

Figure 5.10: AEP of TWL at the toe of the coastal defence structures for the baseline simulation. Colour legend indicates values of TWL in m.

5.3.5 Wave Setup and Wave Runup

Both wave setup (the time averaged contribution of waves to extreme water level) and wave runup (the 2 percent exceedance contribution) were calculated using empirical equations derived from both global and Australian observational datasets (Stockdon et al., 2006, Atkinson et al., 2017). Input from the SCHISM-WWMIII model and beach slope surveys were used to predict both the wave setup and runup height for beaches around PPB. How high waves swash up the beach, whether it be the mean height (wave setup) or the 2% exceedance height (wave runup), is estimated using the input of deep-water significant wave height (H_{s0}), wavelength (L) as well as the beach slope (β) using a relationship based on the Iribarren (surf similarity) formulation:

$$\boldsymbol{\eta = \alpha H_{s0} \beta \left(\frac{H_{s0}}{L}\right)^{-1/2}},$$

where α is a constant. The wavelength L is defined by:

$$\boldsymbol{L = \frac{g T_{p0}{}^{2}}{2\pi}},$$

which is a function of the deep-water spectral wave peak period T_{p0}. Values of H_{s0} at the coast were calculated by reverse-shoaling values of H_{s0} from the 8 m contour using the method of (Vitousek et al., 2008).

No observations of wave setup or runup exist for PPB to calibrate this model. Therefore, wave setup ($\eta = \bar{\eta}$) estimates were made using the scaling parameter α = 0.35 derived from the global dataset (Stockdon et al., 2006, O'Grady et. al., 2019a, Gomes da Silva et al., 2020). Wave runup ($\eta = R$) estimates are made using both the scaling parameter of α = 0.73 for international and 0.99 for Australian sandy beaches studies (Stockdon et al., 2006; Atkinson et al., 2017). Here, a random sampling (bootstrapping) method was used to compute the probabilistic estimates from these two studies, where α was sampled from a normal distribution centred on the two values (α = 0.86) with a standard deviation of 0.05.

The horizontal wave setup/runup excursion χ of both the SWL and wave setup ($\bar{\eta}$) or runup (R) are calculated trigonometrically, by projecting the vertical height (($SWL + \bar{\eta},\ or\ SWL + R$) onto an infinite slope where $\tan(\beta) \approx \beta$. The equations for the wave setup/runup excursion are the same differing only in the value of the α parameter. A graphical representation for wave runup is shown in Figure 5.11 and the equations are formulated as,

$$\boldsymbol{\chi = \frac{SWL}{\beta} + \alpha H_{s0} \left(\frac{H_{s0}}{L}\right)^{-1/2}}$$

where the wave setup/runup excursion extends inland from the 2009 LiDAR zero AHD contour line (which is also used as the Geomorphic Smartline). Most of the uncertainty with wave setup/runup lies in the measurement of beach slope. To encapsulate this uncertainty, for each geomorphic compartment identified as a beach or platform, the hourly SWL, Hs and Tp time series were sourced from the 8 m depth contour in SCHISM within that compartment. Intertidal beach slopes were sampled from the LiDAR DEM and the 1980s PMA beach surveys along transects within that compartment to develop a frequency distribution of beach slopes. For each compartment, a 35-year time series of waves and water levels was obtained from the SCHISM model at the 8 m depth contour. In calculating the wave runup excursion χ, values of beach slope from the LiDAR DEM and 1980s beach profiles were randomly sampled to provide 100 instances of wave runup time series. In the random sampling (bootstrapping) method, α was sampled from a normal distribution centred on the two values (alpha mean = 0.86) with a standard deviation of 0.05. For each of these time series a Gumbel distribution was fitted to the values of runup and an average of these fits was calculated. The 5th, 50th and 95th percentile values of this distribution where then used to define the runup excursion extents for zones 1 to 3 respectively.

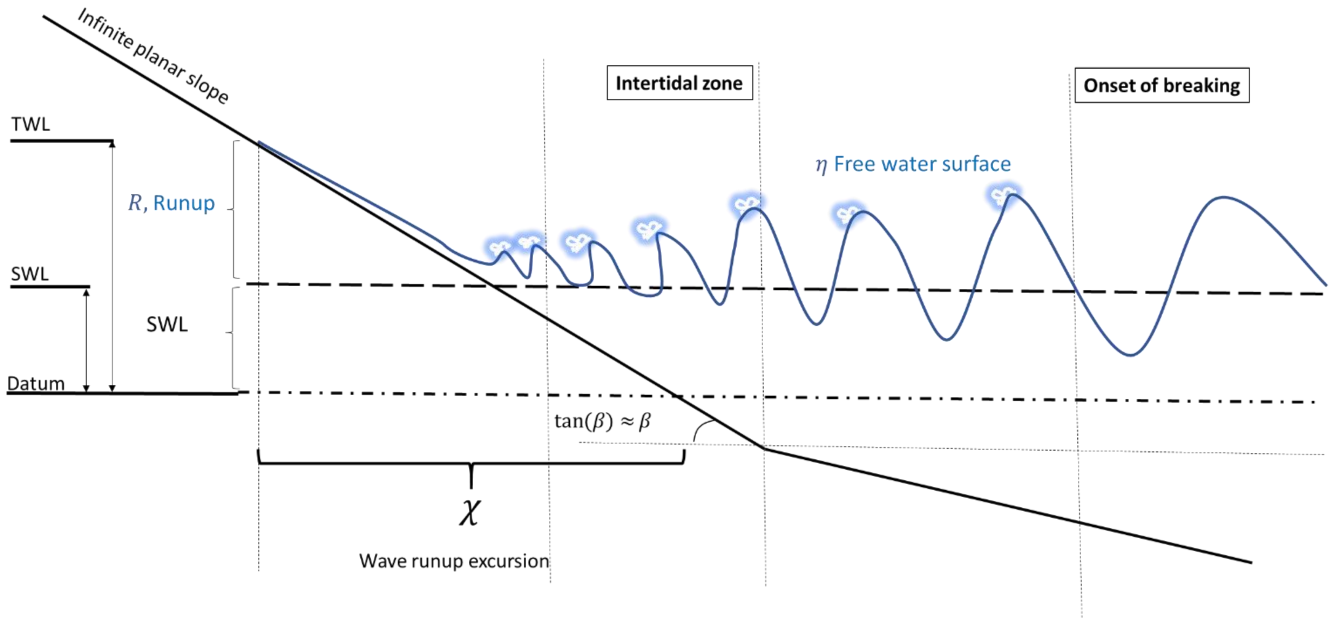

Figure 5.11: Cross-shore profile depicting wave runup excursion on an infinite planar beach slope (wave setup excursion is calculated in the same way).

5.3.6 Developing Inundation Hazard Layers

For the development of whole-of-bay inundation hazard layers, the following procedure was adopted for combining the 25 m resolution results on grids (W, E and S) with the 5 m resolution results modelled on grids A, B, C and D:

- Interpolate the 25 m resolution outputs (regions W, E and S) to 5 m resolution
- Generate rasters of the bay portion of the model grids for the purpose of masking them out of the modelled results. The rasters were generated by using a bathtub fill to 0.0 m AHD on each computational grid. Manually generated polygons were used to mask out additional low-lying coastal regions. Also, a small buffer region was masked out around the boundaries of each simulation region to remove simulation boundary condition edge effects and reduce overlap between adjacent grids
- A whole-of-bay raster was created to encompass all simulation regions at 5 m to match the finest resolution of the simulation grids, and
- For each grid cell in the whole-of-bay raster, the result was obtained by sampling the best available result grid at the grid cell location. The best available result is either the highest resolution or if the resolution is the same (as occurs with a small region of overlap between grids B and C) then the order of preference for sampling results was region A, C, B, D, W, E and then S.

Based on the methodology discussed above the whole-of-bay inundation outputs focus on two key output types:

- Inundation with water coloured by depth as a 'heat map' and
- Inundation showing likely probabilities as per Figure 5.3, showing 95%, (zone 1), 50% (zone 2) and 5% levels (zone 3)

The final processing step involves incorporating wave setup into the inundation extents. Wave setup polygons, produced using the empirical method of Stockdon et al., (2006), are combined with the C-FAST modelled inundation, which accounts for rainfall, drainage, coastal inundation and catchment flooding further inland. This is to addresses the lack of wave setup being modelled in C-FAST in areas not fronted by a sea wall and it also provides a more consistent visualisation of inundation near the coast at the boundaries of the 5 and 25 m C-FAST grids where the changes in model resolution affect the visualisation of inundation.

Following the combining of the C-FAST inundation layers from the high-resolution focus regions (A, B, C and D) and also coarse (25 m) resolution regions (W, E and S), the wave setup polygons are combined with the C-FAST inundation polygons. For much of the bay on both the 5 or 25 m grids, the procedure amounted to taking the maximum inundation extent from the C-FAST-modelled inundation or the wave setup layer. However, on the eastern side of the bay, which is characterised in places by steep cliffs and narrow beaches, the 25 m C-FAST model, due to its low resolution and inability to resolve steep cliffs, simulated inundation further inland than the confines of the narrow beaches whereas the wave setup algorithm resolved the sharp changes in elevation and produced a narrower, more realistic region of inundation. In these locations wave setup replaced the C-FAST inundation in the coastal zone. For the simulation that included rainfall, the wave setup in the coastal zone was combined with the C-FAST simulated rainfall over the interior of the grid. The procedure for combining the C-FAST and wave setup at each raster cell was undertaken using the algorithm shown in Figure 5.12.

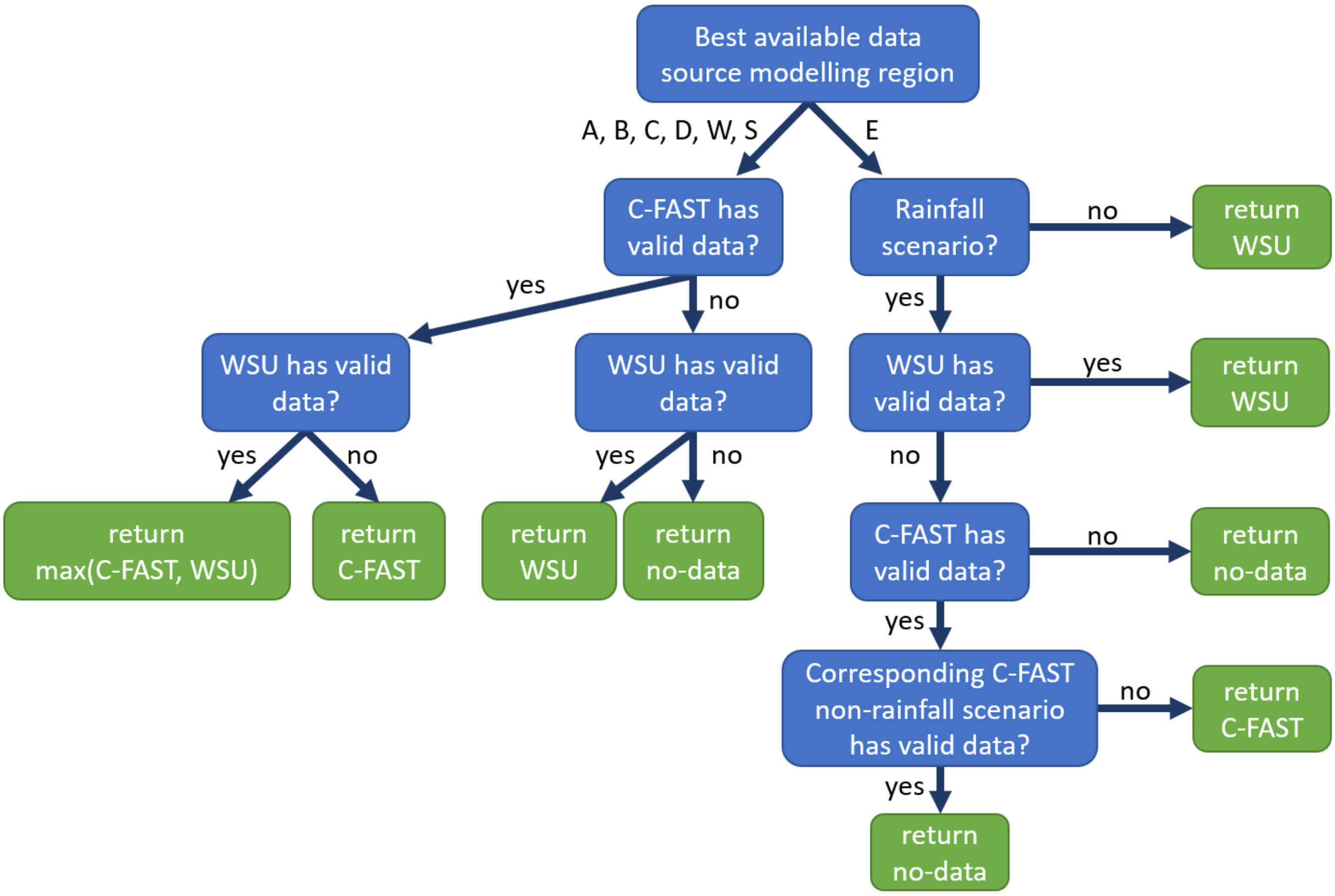

Figure 5.12: Flow chart detailing how the combined inundation hazard rasters were generated from the empirical wave setup (WSU) based on Stockdon et al., (2006) and the C-FAST probabilistic flood extents. The procedure in this flow chart was performed for every raster cell.

This process was able to improve coastal inundation results for the 25 m C-FAST simulations, for cases with and without rainfall as shown in the following section. The whole-of-bay inundation hazard outputs were presented in the DSS-based visualisation tool described in Chapter 4.

5.4 Sensitivity Experiments

This section provides an examination of the relative contribution of different model components in the C-FAST inundation model. In the first section, the sensitivity of C-FAST to different model components is examined, to provide insights into the relative contribution of storm tides, overtopping, rainfall and drainage under 0 and 0.8 m SLR. The second section compares the inundation results from the 5 km and 25 km grids at selected locations where the two sets of simulations overlap to understand the impact of the lower resolution on the inundation results. The third section demonstrates the combination of C-FAST modelled inundation extents with wave setup derived from empirical modelling. Additional comparisons were undertaken between modelling conducted here and flood maps used by Melbourne Water for planning purposes (see Appendix D).

5.4.1 Process Contributions

This section presents a set of sensitivity runs, conducted for grid C (summarised in Table 5.5: that include two sea level values (0.0 m and 0.8 m AHD), each combined with design storm tides that peak at 3 different AEPs. The different model elements of drainage, overtopping and discharge are progressively activated to understand the relative role these processes have on inundation. Note that overtopping applies only where seawalls are present (e.g. Figure 5.8). To measure the effect and display these effects, the following quantities were calculated across the model grids for the different experiments:

- Area of land (m^2) where the maximum flood height exceeds 0.1 m, which exceeds nuisance flooding as defined by Moftakhari et al., (2009), (see Figure 5.13)
- Area of land (m^2) where the flood height exceeds 0.1 m for more than 3 hours (Figure 5.14)

Figure 5.13 provides a comparison of the modelled flood extents as different model components are applied for a baseline 0 m SLR and a 0.8 m SLR simulation. Figure 5.14 summarises the total area inundated for each SLR scenario and each process included in C-FAST for the 5%, 50% and 95% likelihoods. Results indicated that the introduction of additional processes increased the extent of the flooded area. For example, the inclusion of overtopping under 0 m SLR led to a small change to inundation extent (from 3.7 km^2 to 4.0 km^2 for the 50th percentile likelihood case, representing a 7% increase). In the 0.8 m SLR case, the inundated area was greater as expected (10.4 km^2 with storm tide only for the 50th percentile likelihood case) and this increased to 13.2 km^2 with overtopping, representing a 25% increase. This increased inundation was particularly evident on the eastern side of the bay. The addition of 24-hour rainfall increases the inland extent of inundation tenfold for the 0 m SLR case with a marginally lower inundation extent for rainfall applied over 12 hours. The 2-hour rainfall scenario produced about 2.5 km^2 less area of inundation than the 12-hour rainfall case. When drainage was switched on, the likelihood of becoming inundated reduced. For example, in the 0 m SLR case the 50th % likelihood inundation extent decreased 1 km^2 from 29.1 km^2 to 28.1 km^2 due to drainage being on. Under 0.8 m SLR, the effect of drainage reduced the area inundated by 1.5 km^2 from 35.4 km^2 to 33.9 km^2.

Table 5.5: List of simulation cases considered for the sensitivity study.

Case	SLR (m)	Storm tide	Storm tide height (m)	Overtopping modelling	Rainfall modelling 10% AEP Duration (hours)	Intensity (mm/hr)	Drainage Modelling
1	0.0	1% AEP 95th	1.06				
2	0.0	1% AEP 95th	1.06	On			
3	0.0	1% AEP 95th	1.06	On	24	3.38	
4	0.0	1% AEP 95th	1.06	On	12	5.31	
5	0.0	1% AEP 95th	1.06	On	2	17.8	
6	0.0	1% AEP 95th	1.06	On	2	17.8	On
7	0.0	1% AEP 50th	1.20				
8	0.0	1% AEP 50th	1.20	On			
9	0.0	1% AEP 50th	1.20	On	24	3.38	
10	0.0	1% AEP 50th	1.20	On	12	5.31	
11	0.0	1% AEP 50th	1.20	On	2	17.8	
12	0.0	1% AEP 50th	1.20	On	2	17.8	On
13	0.0	1% AEP 5th	1.34				
14	0.0	1% AEP 5th	1.34	On			
15	0.0	1% AEP 5th	1.34	On	24	3.38	
16	0.0	1% AEP 5th	1.34	On	12	5.31	
17	0.0	1% AEP 5th	1.34	On	2	17.8	
18	0.0	1% AEP 5th	1.34	On	2	17.8	On
19	0.8	1% AEP 95th	1.80				
20	0.8	1% AEP 95th	1.80	On			
21	0.8	1% AEP 95th	1.80	On	24	3.38	
22	0.8	1% AEP 95th	1.80	On	12	5.31	
23	0.8	1% AEP 95th	1.80	On	2	17.8	
24	0.8	1% AEP 95th	1.80	On	2	17.8	On
25	0.8	1% AEP 50th	1.95				
26	0.8	1% AEP 50th	1.95	On			
27	0.8	1% AEP 50th	1.95	On	24	3.38	
28	0.8	1% AEP 50th	1.95	On	12	5.31	
29	0.8	1% AEP 50th	1.95	On	2	17.8	
30	0.8	1% AEP 50th	1.95	On	2	17.8	On
31	0.8	1% AEP 5th	2.10				
32	0.8	1% AEP 5th	2.10	On			
33	0.8	1% AEP 5th	2.10	On	24	3.38	
34	0.8	1% AEP 5th	2.10	On	12	5.31	
35	0.8	1% AEP 5th	2.10	On	2	17.8	
36	0.8	1% AEP 5th	2.10	On	2	17.8	On

SLR = 0.0 m	SLR = 0.8 m
Storm tide	
	
Storm tide + overtopping	
	
Storm tide + overtopping + rainfall 24 hr	
	

Figure 5.13: Sensitivity study simulations (5 m resolution) flood extent maps (maximum height exceeding 0.1 m) with each map showing three different 1% AEP storm tide likelihood results (pink is 95% likely, dark blue is 50% likely and light blue is 5% likely).

<table>
<tr><th>SLR = 0.0 m</th><th>SLR = 0.8 m</th></tr>
<tr><td colspan="2">Storm tide + overtopping + rainfall 12 hr</td></tr>
<tr><td></td><td></td></tr>
<tr><td colspan="2">Storm tide + overtopping + rainfall 2 hr</td></tr>
<tr><td></td><td></td></tr>
<tr><td colspan="2">Storm tide + overtopping + rainfall 2 hr + drainage</td></tr>
<tr><td></td><td></td></tr>
</table>

Figure 5.13: Continued.

(a)

SLR = 0.0 m

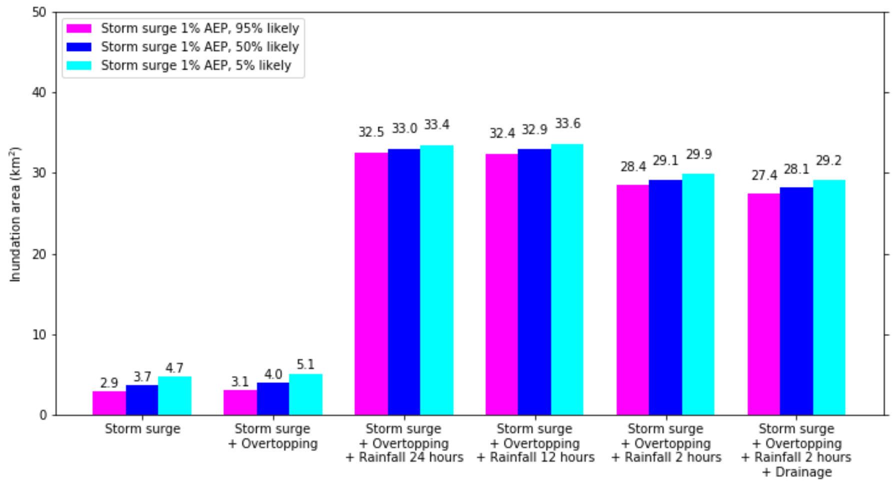

(b)

SLR = 0.8 m

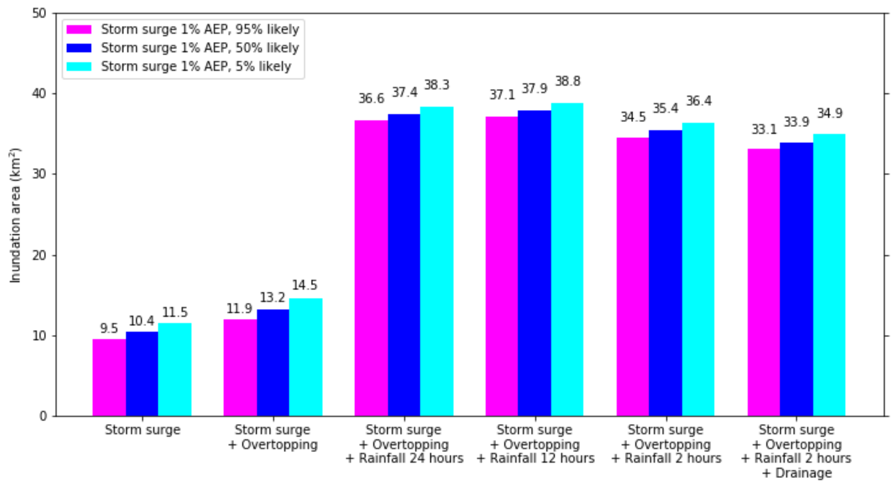

Figure 5.14: Sensitivity study simulations (5 m resolution) flood extent areas (maximum height exceeding 0.1 m).

Figure 5.15 compares flood extents for water that exceeds a height of 0.1 m and a duration in excess of 3 hr. Figure 5.16 summarises the total area inundated for each SLR scenario and each process included in C-FAST for the 5%, 50% and 95% likelihoods. These results provided an indication of flooding where the water is deep (>30 cm) and long lived (>3h) and as such poses a heightened risk for people and infrastructure. The progression of floods extended as more processes were added and followed a similar pattern to Figure 5.13. However, the flood extent covered a smaller area for the metric shown in Figure 5.13 because of the additional requirement that the flood water remains present for at least 3 hrs.

SLR = 0.0 m	SLR = 0.8 m
Storm tide	
	
Storm tide + overtopping	
	
Storm tide + overtopping + rainfall 24 hr	
	

Figure 5.15: Sensitivity study simulations (10 m resolution) flood extent maps (maximum height exceeding 0.1 m for at least 3 hours) with each map showing three different 1% AEP storm tide likelihood results (pink is 95% likely, dark blue is 50% likely and light blue is 5% likely).

SLR = 0.0 m	SLR = 0.8 m
Storm tide + overtopping + rainfall 12 hr	
	
Storm tide + overtopping + rainfall 2 hr	
	
Storm tide + overtopping + rainfall 24 hr + drainage	
	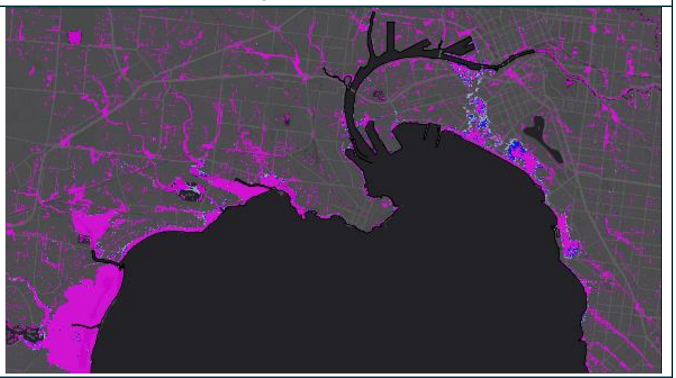

Figure 5.15: Continued.

(a) **SLR = 0.0 m**	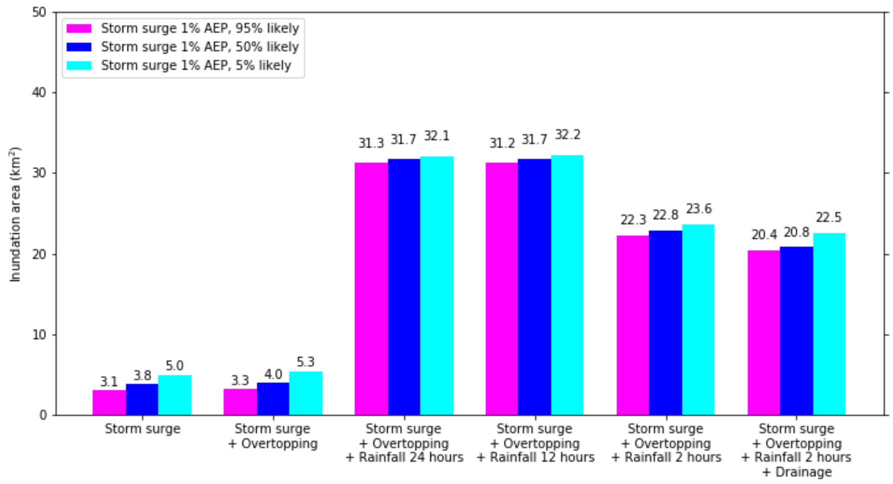
(b) **SLR = 0.8 m**	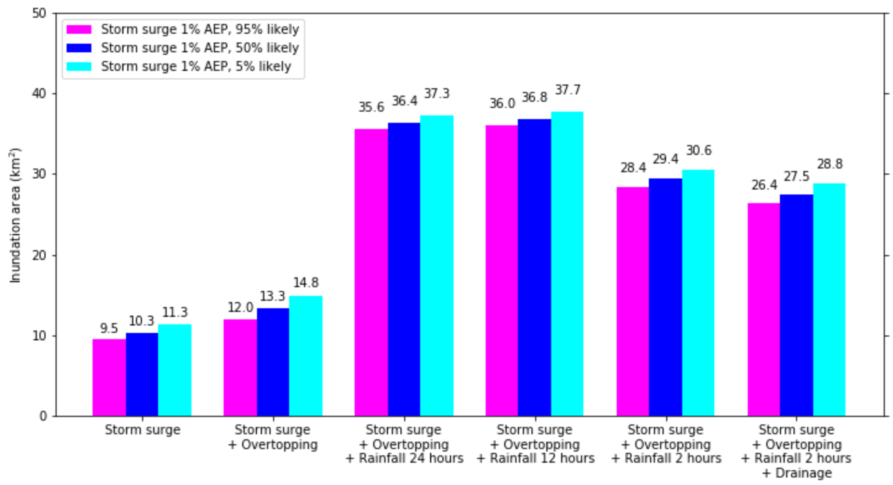

Figure 5.16: Sensitivity study simulations (10 m resolution) flood extent areas (maximum height exceeding 0.1 m for at least 3 hours).

5.4.2 Comparison Between Results at 5 and 25 m

Since outputs were generated at two different resolutions and all the outputs are then seamlessly integrated into a 5 m resolution whole-of-bay inundation map. The difference between the 5 m and 25 m results for the 0.8 and 1.4 m SLR scenarios are compared for two locations where simulations were run at both resolutions (i.e. regions A (5 m) and W (25 m) around Geelong and regions D (5 m) and E (25 m) around Mordialloc, Figures 5.17 and 5.18). These comparisons show that the 25 m results lead to higher levels of inundation with this more evident at Mordialloc compared to Geelong. Despite this, projected inundation from 5 m and 25 m resolutions produced broadly consistent outcomes. With the exception of the Swan Bay region, the 25 m simulations generally encompass the regions outside the 5 m grids where the inundation hazard is less significant.

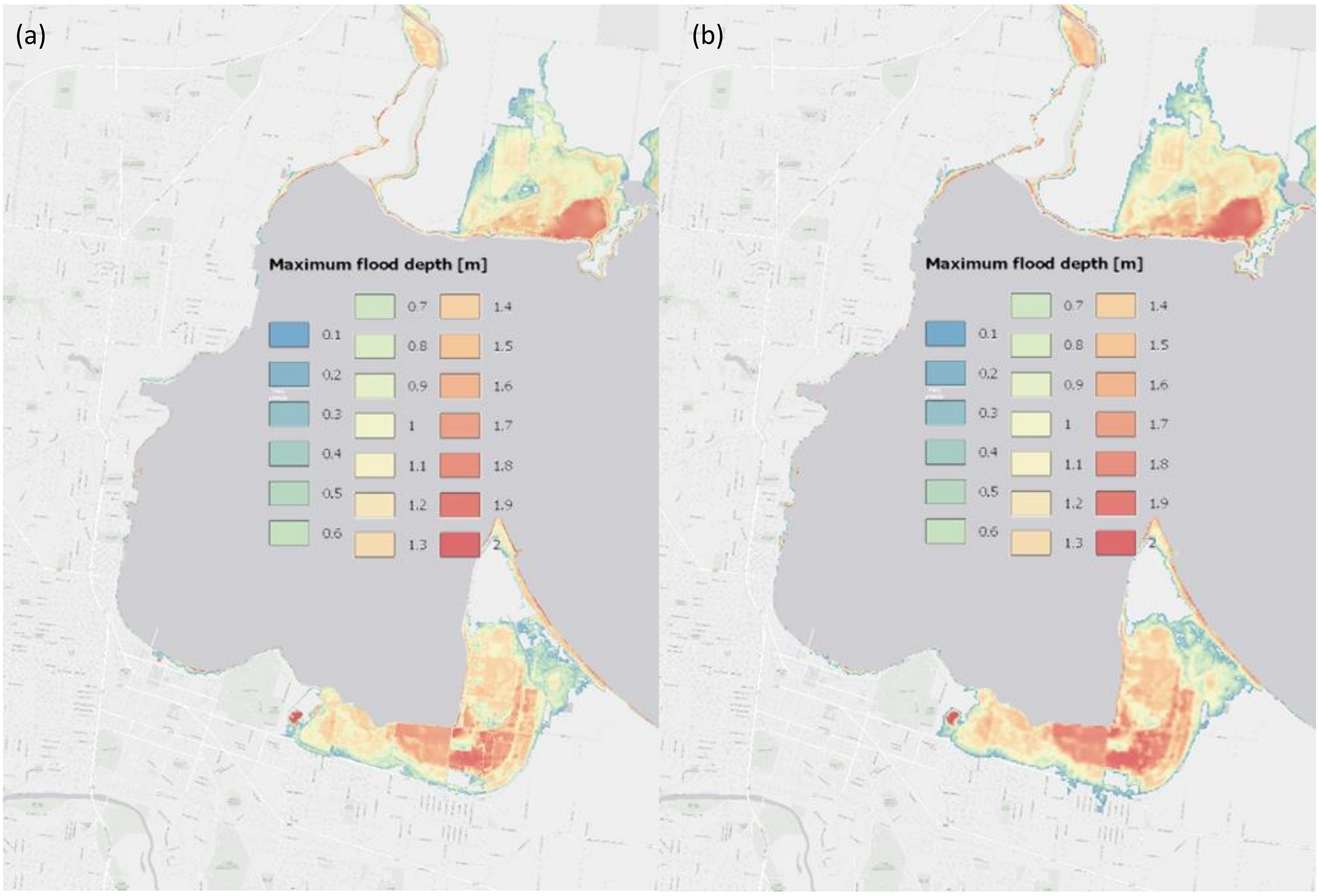

Figure 5.17: Comparison between flood extents for a region around Geelong at (a) 5 m resolution 0.8 m SLR and (b) 25 m resolution 0.8 m SLR and, (c) 5 m resolution 1.4 m SLR (d) 25 m resolution 1.4 m SLR.

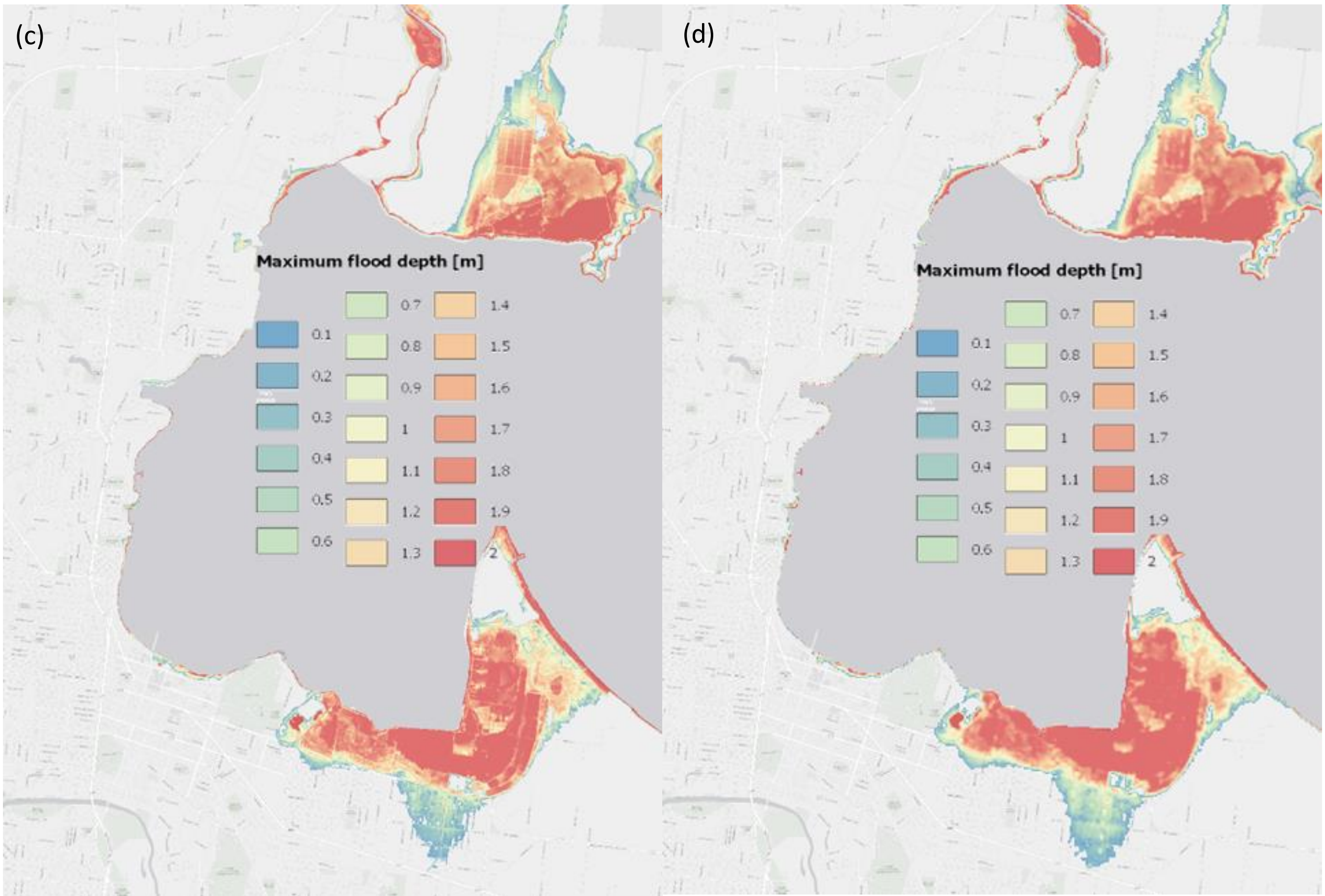

Figure 5.17: Continued.

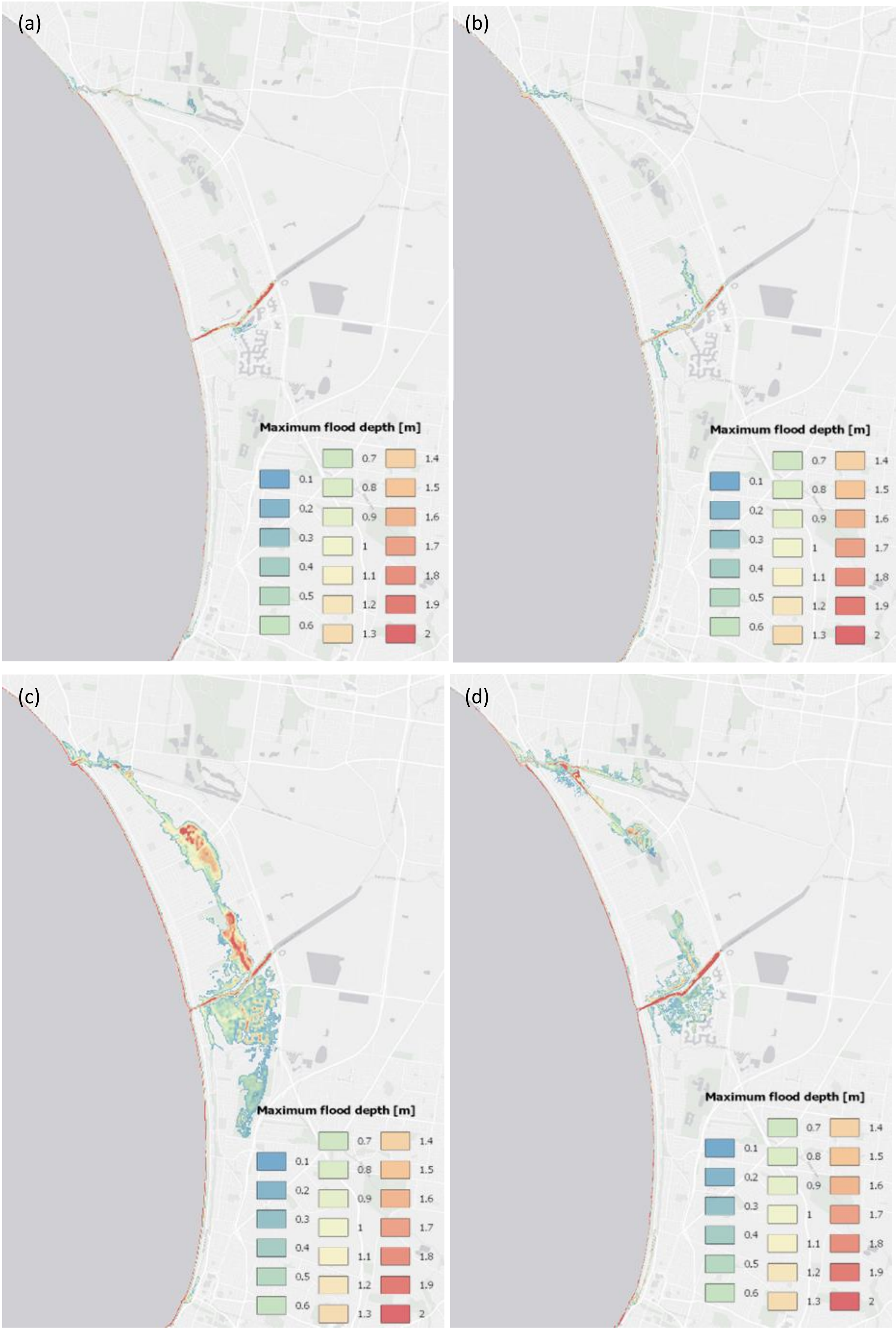

Figure 5.18: Comparison between flood extents for a region around Mordialloc at (a) 5 m resolution 0.8 m SLR, (b) 25 m resolution 0.8 m SLR, (c) 5 m resolution 1.4 m SLR and (d) 25 m resolution 1.4 m SLR.

5.5 Inundation Hazard Results

5.5.1 Inundation by Depth

Results are presented for inundation by water depths for the baseline and five SLR scenarios for a storm tide with an intensity of 1% AEP (Figure 5.19). Flood extents included all three likelihood zones where the 5% zone represents a lower likelihood but more extensive flooding scenario (see Figure 5.3). Regions coloured light blue (Figure 19) have a water depth of 0.1 m and red have a water depth of 2.0 m or higher. The results are presented with a flood depth cut-off of 0.1 m as any flood water below a depth of 0.1 m is assumed to be nuisance flooding (Moftakhari et al., 2018). Previously identified low-lying sections of the coast presented as regions A (encompassing the Geelong area from Point Henry to Point Lillias), B (encompassing the Wyndham Council region), C (encompassing the Hobsons Bay, Melbourne City and City of Port Phillip regions) and D (encompassing the City of Kingston and City of Frankston) are all regions that experience inundation levels above 1.5 m especially for SLR above 0.8 m.

In order to understand the differences for the whole of the bay, outputs from the current hydrodynamic study are compared with an equivalent bathtub fill approach developed as part of the Victorian Government's Future Coasts Project (Figure 5.20) (note that the results from Melbourne Water discussed in Appendix D were provided only for the north of the Bay). A fundamental difference in the two approaches being compared is that bathtub infill assumes that the water levels from the combination of storm tide AEP and SLR scenario are constant in time. This is not the case for the storm tide component, which typically peaks around high tide and is therefore associated with temporary flooding and draining, which limits the amount of inundation that occurs. In other words, for equivalent inputs, bathtub fill approaches can lead to more extensive inundation than hydrodynamic modelling that takes account of the temporal evolution of flooding and draining.

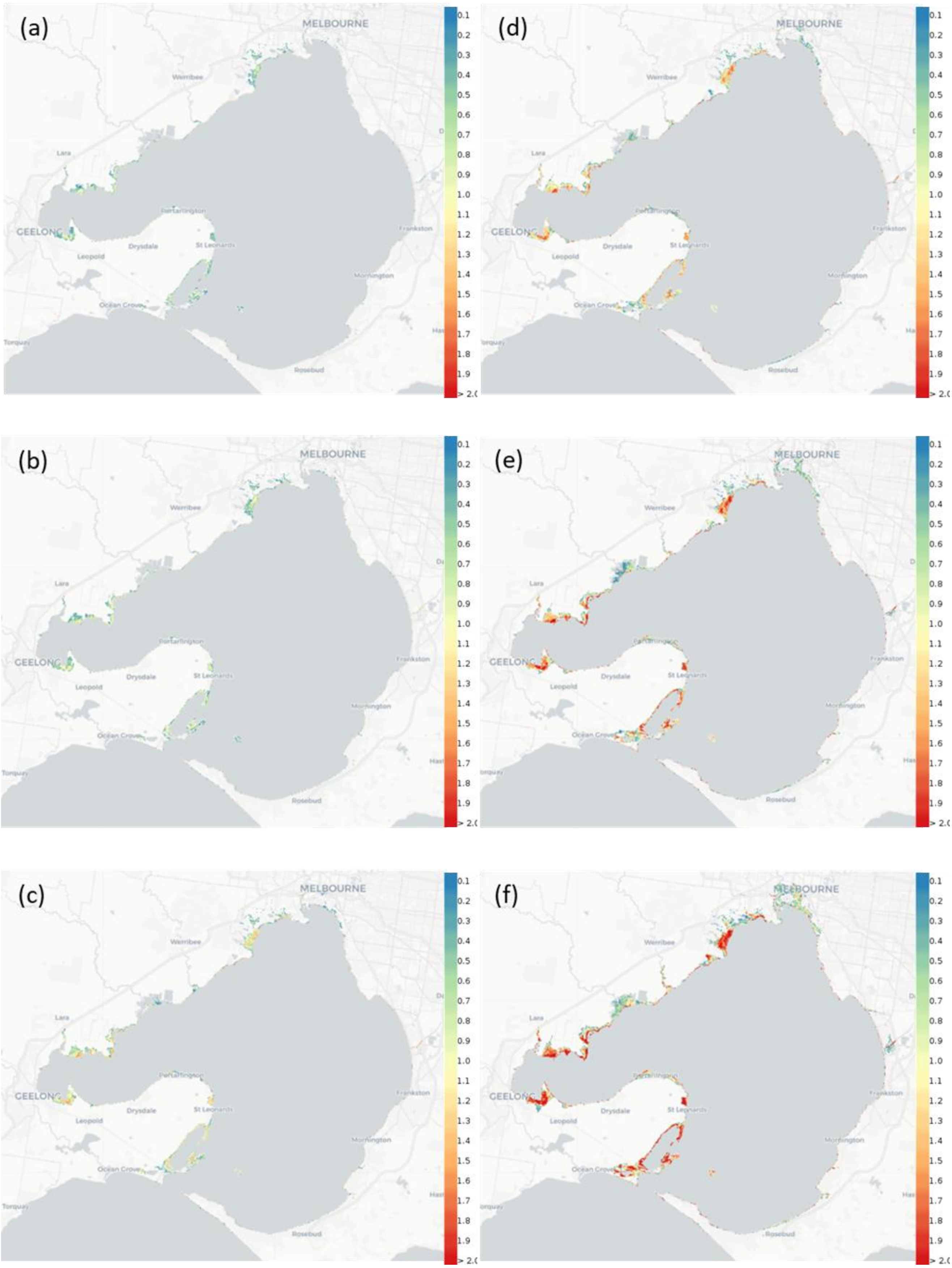

Figure 5.19: Whole-of-bay Inundation Hazard Maps at SLR of (baseline), 0.2, 0.5, 0.8, 1.1 and 1.4 m. This scenario has no rainfall and has a 1% AEP storm tide. Water is coloured by inundation depth with light blue representing 0.1 m and red representing 2.0 m and above.

In the comparison of the results of the present hydrodynamic study with the Future Coasts Project, the scenario selected for comparison from the present study was the 0.8 m SLR scenario with a 1% AEP storm tide, no rainfall and the 5% likelihood estimate (zone 3). The Future Coast Data available at data.vic.gov.au uses a 0.82 m SLR, a 1% AEP storm tide and enhanced wind forcing (scenario 2 in Table 2.1). It should be noted that the enhanced wind forcing was applied as a scaling factor to the storm surge component of the storm tide as discussed in McInnes et al., (2009a, b) and leads to 1% AEP storm tide values that are approximately 30 cm higher than the 1% AEP with SLR only. The water level input scenario is therefore somewhat higher in the Future Coast Data than the input considered in the present study, although this is partially offset by the use of the 5% likelihood estimate (i.e. the upper end of the uncertainty range of storm tide estimates for the given AEP) here rather than the central estimate of the storm tide that is used in the Future Coast Data.

As seen in Figure 5.20, inundation between the two data sets varies along different sections of coastline. For the Geelong City, Hobsons Bay and Wyndham City regions the two approaches lead to comparable areas of inundation, despite the differences in inputs and methodologies. A possible reason for this is that these areas are not as built up as others with engineered structures and therefore the bathtub fill approach, which does not take into account the presence of these structures, is closer to the hydrodynamic output. Another possible reason is that in these regions the coastal flooding is mainly due to overland inundation rather than the flood waters being carried inland via river systems or creeks. This means that as soon as a certain sea level is reached inundation occurs, which is consistent with the bathtub fill methodology.

For the City of Melbourne and City of Port Phillip (Figure 5.20c and h) the bathtub approach tends to overpredict the flooded area but there is some agreement between the results in the western part of the model grid. In these areas the differences arise mainly because these are fairly built up with coastal protective structures and the effect of these may not have been included in the bathtub model.

Finally, for the region around Kingston and Frankston, there are quite significant differences between the two outputs. There are likely several reasons for these differences: a) a bathtub fill approach tends to overpredict flood inundation especially in instances where the coastal flooding is caused via a creek or river system such as Mordialloc Creek and Patterson River because it does not account for the temporal evolution of the flooding. In such instances as soon as the banks are breached the bathtub model floods the entire low lying region around the river/creek instantaneously whereas a hydrodynamic model only floods regions where the water is able to flow within the time constraints of the storm tide event and other factors such as frictional drag on the flow that dynamic modelling accounts for, b) the previous bathtub fill studies may not have taken into account the presence of coastal protective structures and this may have resulted in more extensive inundation, c) river/creek levels at Patterson River and Mordialloc Creek may not be well resolved as leading to potential uncertainty in predicted flood levels in these regions. This last issue could affect all hydrodynamic model estimates.

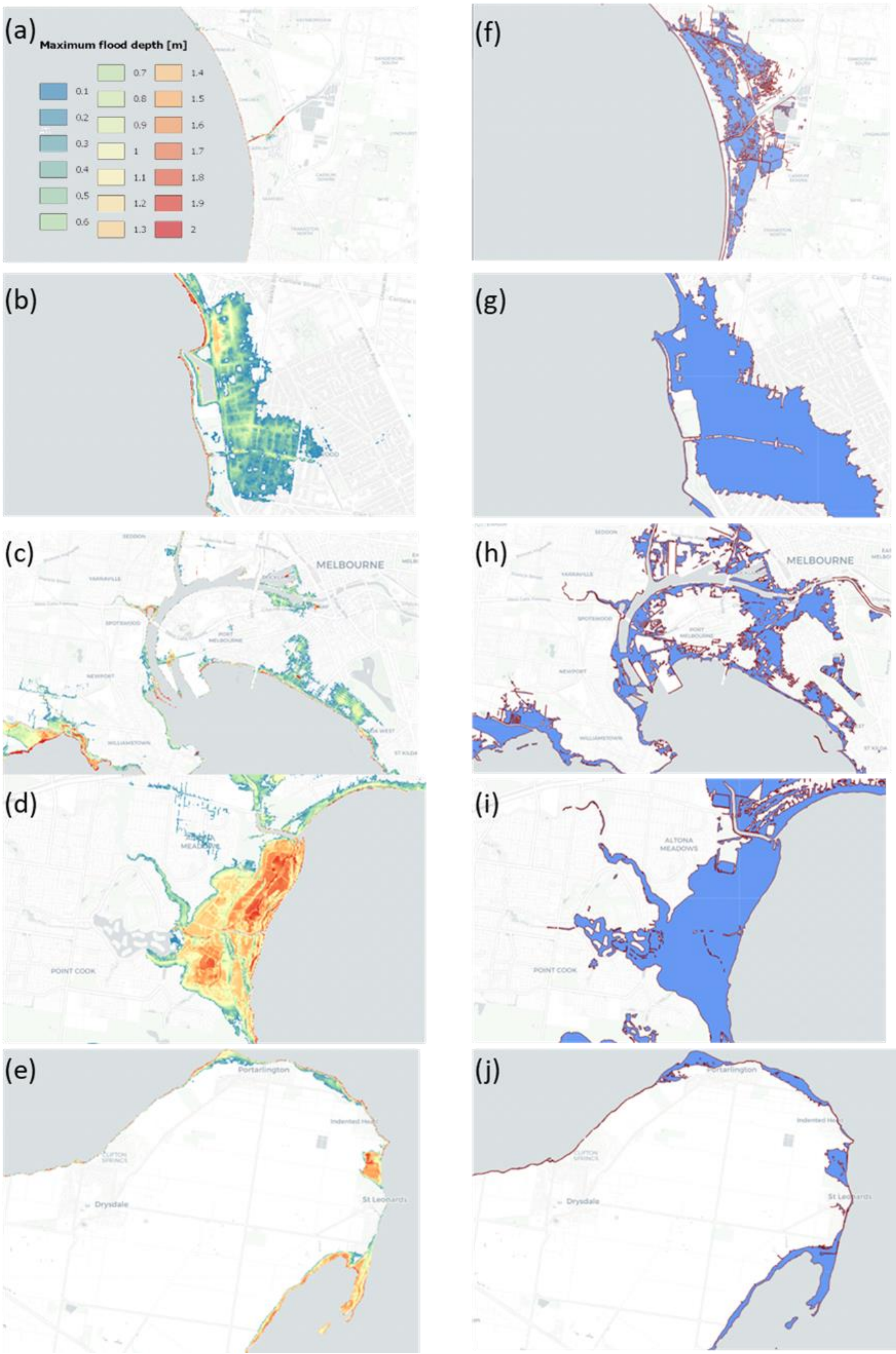

Figure 5.20: Comparison of areas subject to inundation modelled in the present study for a 1% AEP storm tide, including zone 3 extents and 0.8 m SLR (left) compared to the Victorian Governments Future Coasts Project for a 0.82 m SLR for a 1% AEP storm tide and wind speed increase scenario (right) for (a) and (f) Mordialloc to Frankston, (b) and (g) Brighton, (c) and (h) Hobsons Bay, (d) and (i) Point Cook and (e) and (j) Portarlington.

5.5.2 Inundation Areas

As well as producing inundation outputs for each scenario coloured by inundation depth with a cut-off of 0.1 m, probabilistic flood extent outputs at levels 95% likelihood (zone 1), 50% likelihood (zone 2), and 5% likelihood (zone 3) were produced. These outputs are relevant for considering the likelihoods of areas subject to inundation and are predicated on the uncertainty range of the AEP's so that the 5% inundation estimate is aligned with the 95th percentile (upper bound) of the AEP estimate while the 95% inundation estimate is associated with the 5th percentile (lower bound) of the AEP estimate. An example output of the inundation extent is shown in Figure 5.21 for a 1% AEP storm tide, no rainfall and 1.4 m SLR. In the context of decision making, the risk appetite of the decision maker will determine which inundation extent (likelihood level) to consider. For example, for a low-risk appetite in the case of critical infrastructure, decision makers may elect to use the zone 3 flood extent (5% likelihood level), flood depth and flood duration, whereas for a high-risk appetite in the case of temporary structures and where overall cost is not a consideration, a decision maker may use the zone 1 flood extents (95% likelihood levels).

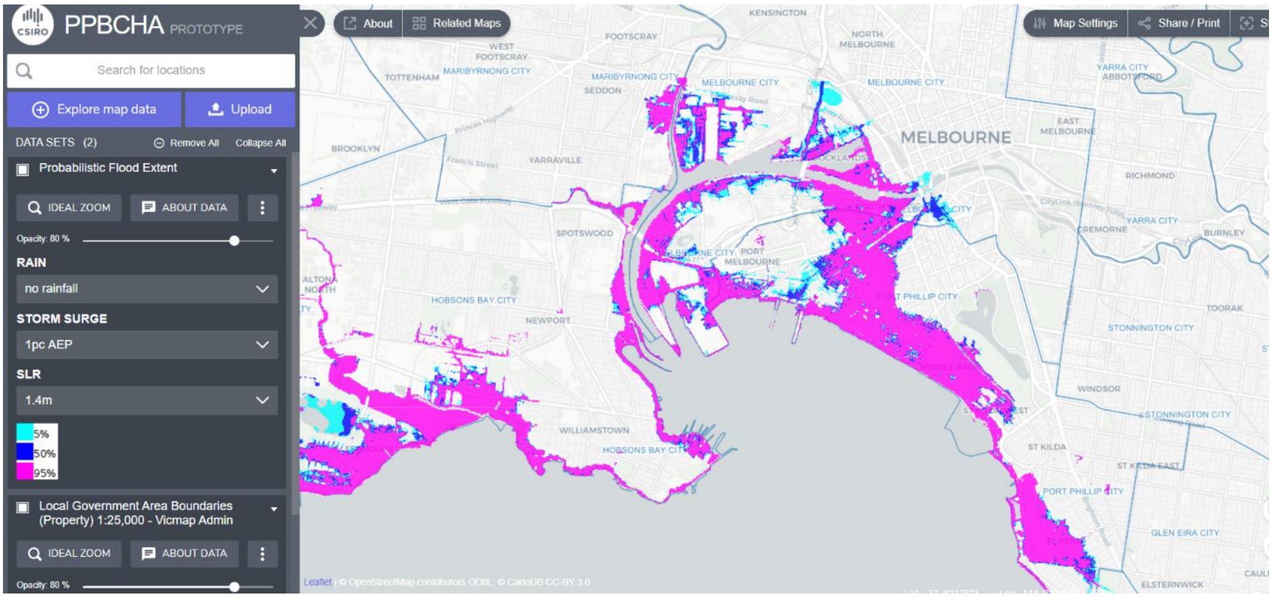

Figure 5.21: Sample output showing probability-based inundation zones centred around region C (Melbourne City) for a 1% AEP storm tide, no rainfall and a 1.4 m SLR. Magenta indicates 95% likelihood (zone 1), dark blue indicates 50% likelihood (zone 2) and light blue indicates 5% likelihood (zone 3).

5.5.3 Integration of Wave Setup

Section 5.3.5 introduced the method of generating combined inundation hazard rasters from the C-FAST probabilistic flood extent results and the wave setup hazard results. In this section, the combined results, which comprise the inundation extent layers in the DSS, are presented for Aspendale, Ricketts Point, Port Melbourne, Elwood, Altona and Geelong respectively (Figures 5.22 to 5.27). These results show that combining the wave runup with modelled inundation hazard provides greater consistency for inundation in the immediate coastal zone, for coastal sectors that do not contain a seawall on the 5 m grid or for the 25 m grid results where wave setup was not implicitly modelled.

Figure 5.22 compares the separately modelled wave setup, the C-FAST modelled inundation (modelled at 5 m resolution) and the combined inundation extent for a section of eastern PPB at Aspendale for the 0.8 m SLR scenario. This shows that the C-FAST modelled inundation at the coast was less extensive than the separately modelled wave setup.

Wave Setup	Rainfall	C-FAST Probabilistic Flood Extent	Combined Inundation Hazard
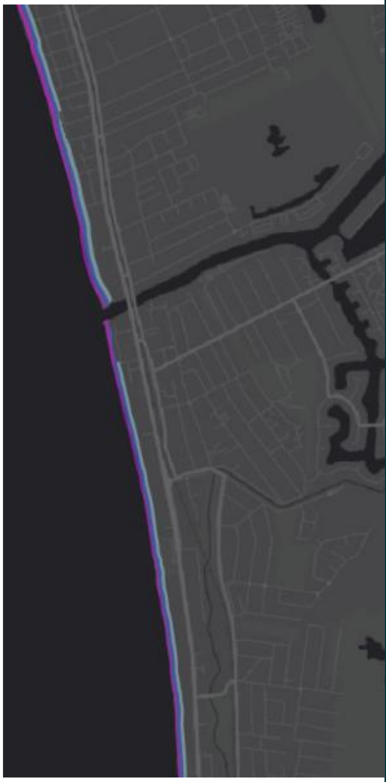	None	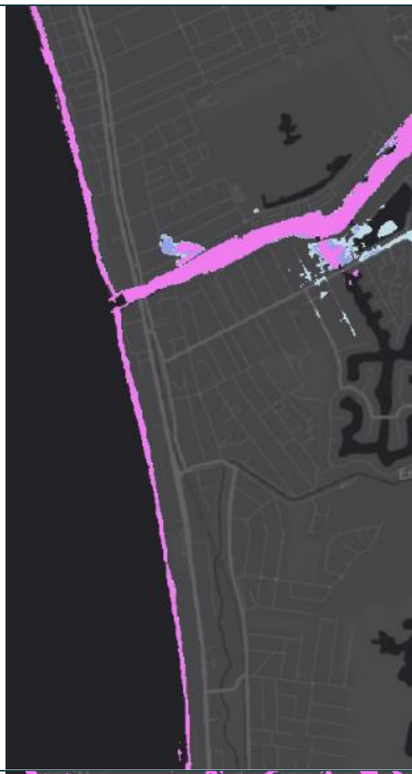	
	10% AEP	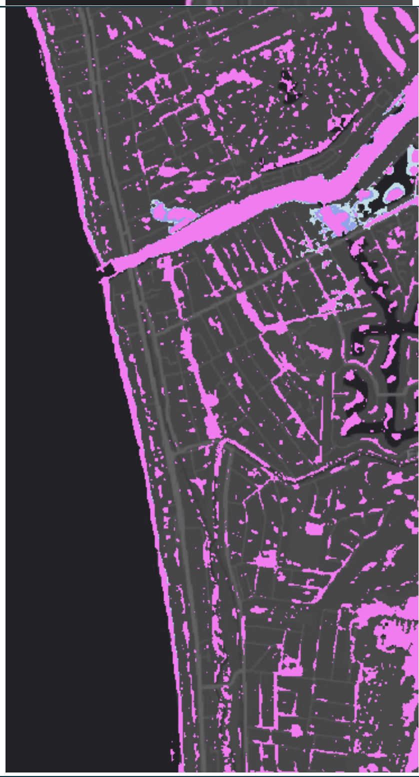	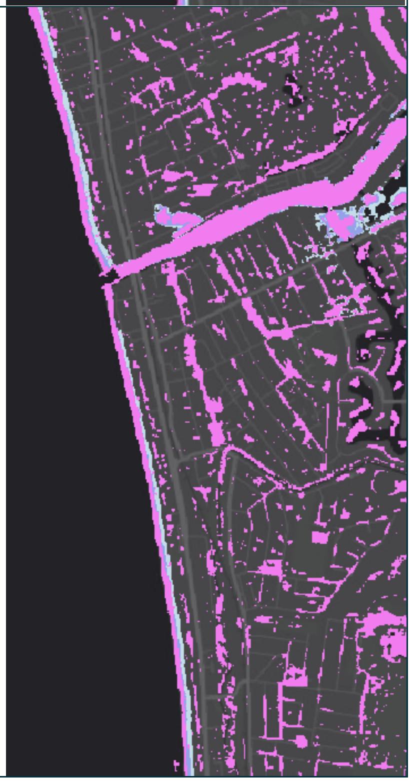

Figure 5.22: Flood extents in the Aspendale region for the 0.8 m SLR scenarios with 1% AEP storm tide. Magenta indicates 95% likelihood (zone 1), dark blue indicates 50% likelihood (zone 2) and light blue indicates 5% likelihood (zone 3).

For Ricketts Point, it can be seen that the C-FAST model simulated more extensive inundation at the coast than indicated the by the wave setup calculation (Figure 5.23). This is related to inadequate resolution of the shore at the lower resolution. Elwood, (Figure 5.24), contains extensive seawalls and so wave setup and overtopping have been calculated by C-FAST. This example shows the combined inundation layer is largely unchanged from the C-FAST inundation, demonstrating that the method for combining the results preserves the C-FAST results when they yield more extensive coastal inundation.

For the western side of the Bay, including Altona, Geelong and the Bellarine Peninsula (Figures 5.26 to 5.28), where there is considerable extent of low-lying back shore areas, the inclusion of wave setup does not influence the already extensive areas of inundation modelled by C-FAST. On the southern side of the Bay, the inclusion of wave setup leads to some small increases in inundation extent for the lower SLR scenarios but with higher SLR scenarios C-FAST inundation is more extensive (Figure 5.29).

Wave Setup	Rainfall	C-FAST Probabilistic Flood Extent	Combined Inundation Hazard
	None		
	10% AEP		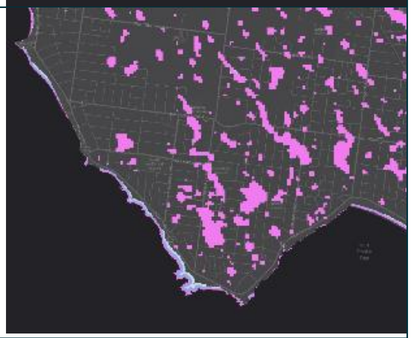

Figure 5.23: Flood extents in the Ricketts Point region for the 0.8 m SLR scenarios with 1% AEP storm tide. Magenta indicates 95% likelihood (zone 1), dark blue indicates 50% likelihood (zone 2) and light blue indicates 5% likelihood (zone 3).

Wave Setup	Rainfall	C-FAST Probabilistic Flood Extent	Combined Inundation Hazard
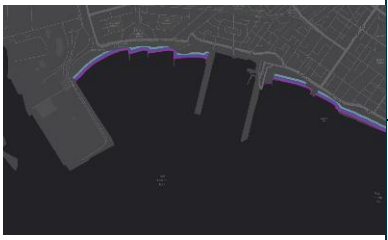	None		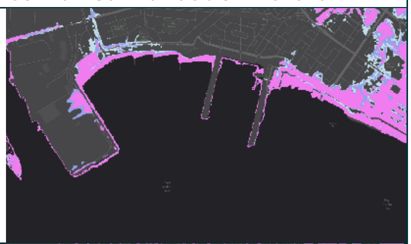
	10% AEP	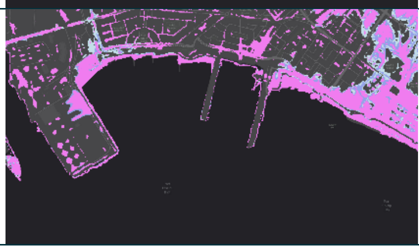	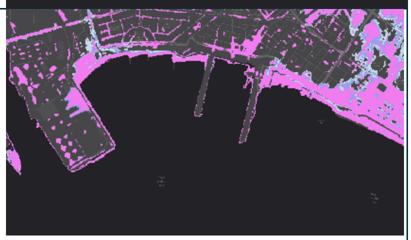

Figure 5.24 Flood extents in the Port Melbourne region for the 0.8 m SLR scenarios with 1% AEP storm tide. Magenta indicates 95% likelihood (zone 1), dark blue indicates 50% likelihood (zone 2) and light blue indicates 5% likelihood (zone 3).

Wave Setup	Rainfall	C-FAST Probabilistic Flood Extent	Combined Inundation Hazard
	None		
	10% AEP		

Figure 5.25: Flood extents in the Elwood region for the 0.8 m SLR scenarios with 1% AEP storm tide. Magenta indicates 95% likelihood (zone 1), dark blue indicates 50% likelihood (zone 2) and light blue indicates 5% likelihood (zone 3).

Wave Setup	Rainfall	CFAST Probabilistic Flood Extent	Combined Inundation Hazard
	None		
	10% AEP		

Figure 5.26: Flood extents in the Altona region for the 0.8 m SLR scenarios with 1% AEP storm tide. Magenta indicates 95% likelihood (zone 1), dark blue indicates 50% likelihood (zone 2) and light blue indicates 5% likelihood (zone 3).

Wave Setup	Rainfall	C-FAST Probabilistic Flood Extent	Combined Inundation Hazard
	None		
	10% AEP	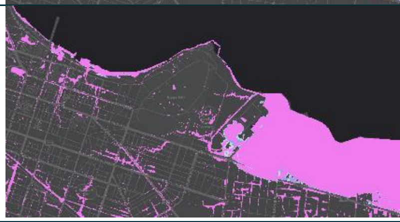	

Figure 5.27: Flood extents in the Geelong region for the 0.8 m SLR scenarios with 1% AEP storm tide.

Wave Setup	Rainfall	C-FAST Probabilistic Flood Extent	Combined Inundation Hazard
	None	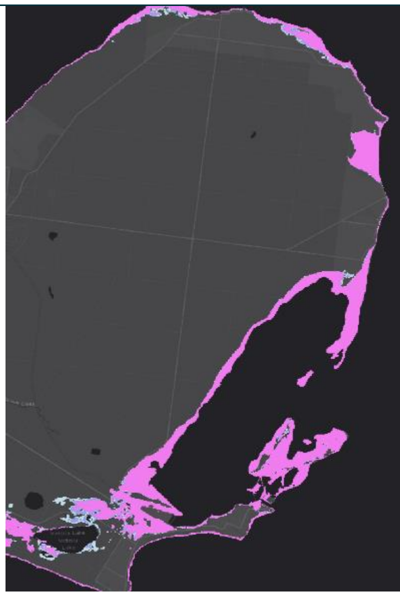	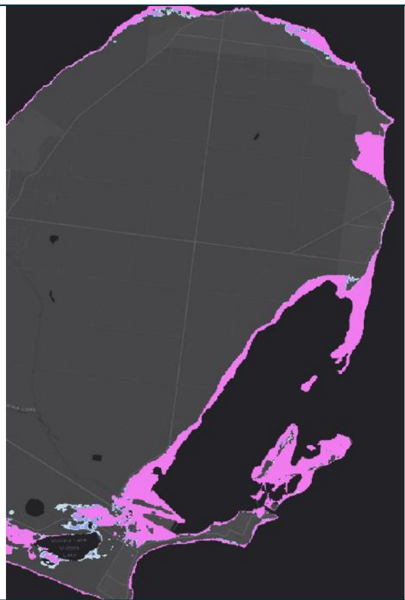
	10% AEP	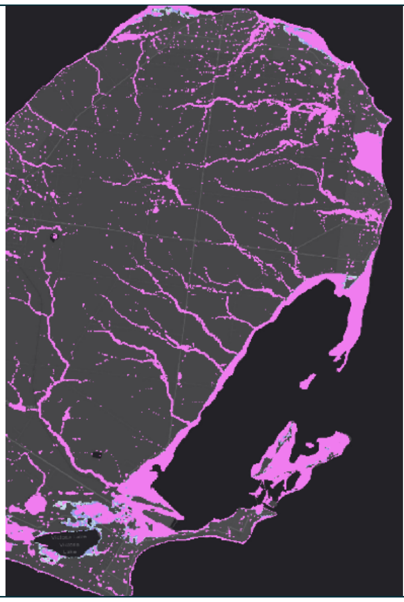	

Figure 5.28: Flood extents in the east Bellarine region for the 0.8 m SLR scenarios with 1% AEP storm tide.

Wave Setup	Rainfall	C-FAST Probabilistic Flood Extent	Combined Inundation Hazard
	None		
	10% AEP	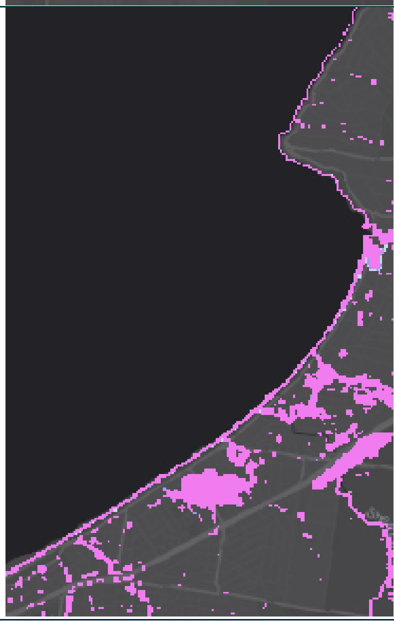	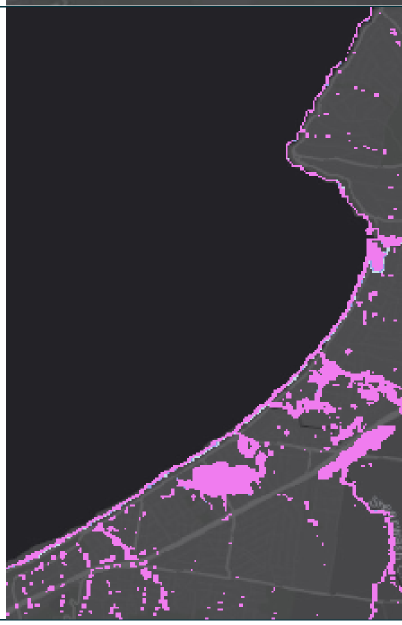

Figure 5.29: Flood extents in the Mornington region for the 0.8 m SLR scenarios with 1% AEP storm tide.

5.5.4 Wave Runup Excursion Hazard

Wave runup excursion provides an additional hazard layer arising from the transitory effects of wave breaking that is not captured in C-FAST, which only simulates water flows due to storm tides (SWL), and in the case of the 5 m grids, also the wave overtopping discharge via the EurOtop model where there are protection structures. The wave runup excursion hazard is useful for understanding the potential for wave impacts on foreshore land and assets and hence can be used to map the exposure of coastal infrastructure (e.g. bathing boxes and fences) and coastal vegetation that are located seaward (or in the absence) of protection structures or cliffs.

The wave runup excursion hazard layers were calculated separately from C-FAST using an empirical model based on observational studies of wave excursion up sandy beaches. Estimates of how far waves will runup and inundate all beaches around PPB were developed based on input from the SCHISM simulations (see Chapter 8) and surveys of beach slope steepness for each local compartment (LiDAR DEMs and 1980s PMA beach surveys). These inundation hazard layers are referred to as the “probabilistic wave runup excursion hazard”. The estimates are for 18 scenarios comprising the 1% 2% and 5% AEP design storms, each for the baseline climate, 0.2, 0.5, 0.8, 1.1 and 1.4 m SLR simulations.

The probabilistic estimates, which account for uncertainty and variability in the surveyed beach slope and the hydrodynamic inputs (i.e. Hs, Tp, and SWL derived from SCHISM simulations) and the statistical estimation of AEPs, are divided into three zones in Figures 5.28a, 5.29a and 5.30a):

- Zone 1 (**purple**) represents where the beach/land is covered in 100-95% of model estimates
- Zone 2 (**blue**) represents where the beach/land is covered in 95%-50% of model estimates. The inland extent of this zone represents the most likely model estimate, based on calculations using the empirical method
- Zone 3 (**light blue**) represents where the beach/land is only covered in 50%-5% of model estimates.

Excursion of waves landward of zone 3 is possible due to the limitation of the modelling and randomness of extreme events but have a low likelihood (less than 5%). The zones of inland extent are truncated at the base of steep slopes (i.e. a DEM terrain slope greater than 30 degrees) representing a cliff, bluff, or a documented coastal protection structure, defining the horizontal inland limit of the wave excursions.

Figure 5.30 shows 1% AEP runup excursion hazard zones together with the inundation during the 24 June 2014 event for Port Melbourne. During this event, it is shown that the water levels extended to the dunes at the back of the beach. Other comparisons of the 24 June 2014 event are shown for Daveys Bay (Figure 5.31) where the hazard zones are truncated at the cliff toe, Mount Martha bathing boxes (Figure 5.32) and the Brighton Beach bathing boxes (Figure 5.33). The 24 June 2014 event had widespread impact, however the north-westerly winds resulted in differing AEP wave runup extents around the bay.

The estimates do not consider coastline change (erosion), but instead use an infinite beach slope, so for more extreme scenarios of SLR, the zone overlays can extend well inland in the absence of steep slopes (in the DEM) or coastal protection datasets. An example of the extra excursion from 0.8 m of SLR is presented for the Brighton Bathing Boxes (Figure 5.33c).

The results of the 1% AEP wave runup are from a statistical extrapolation of an extreme value distribution fitted to the nonlinear combination of the storm tide, wave height and period overlapping hourly timeseries and the randomly sampled beach slope. Therefore, the exact combination of inputs (SWL, Hs, Tp or Beta) resulting in the 1% AEP TWL cannot be extracted or easily summarised in tabular format from this statistical analysis. The wave runup excursion, $TWL_{2\%}$ values are detailed in Table 5.6 for the locations shown in Figures 5.30 to 5. 33.

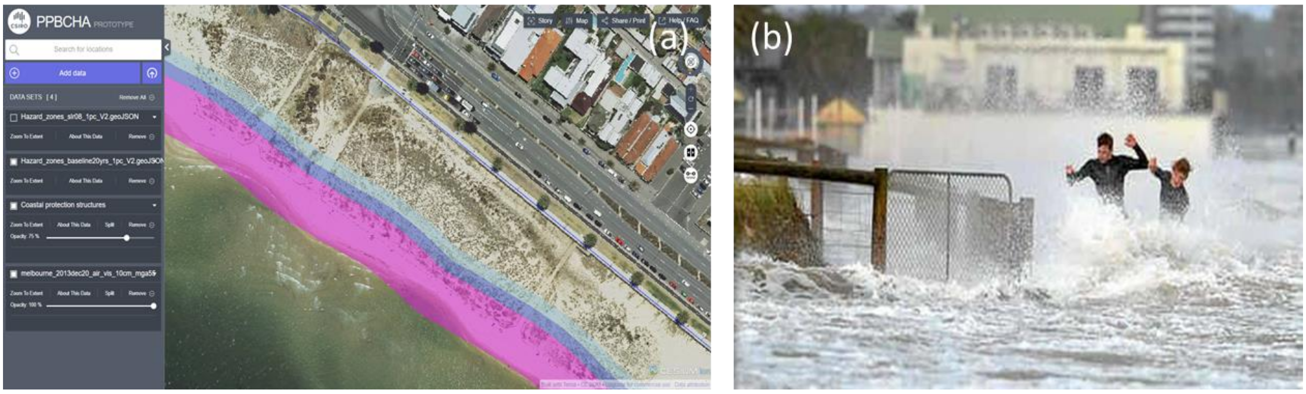

Figure 5.30: (a) Top: 1% AEP wave runup excursion hazard for the baseline climate (b) Photo from The Age 24/6/2014 Storm hits Port Melbourne beach near the intersection of Pickles St and Beaconsfield Parade. Photo by Joe Armao https://www.bendigoadvertiser.com.au/story/2372401/melbourne-weather-june-24-2014/.

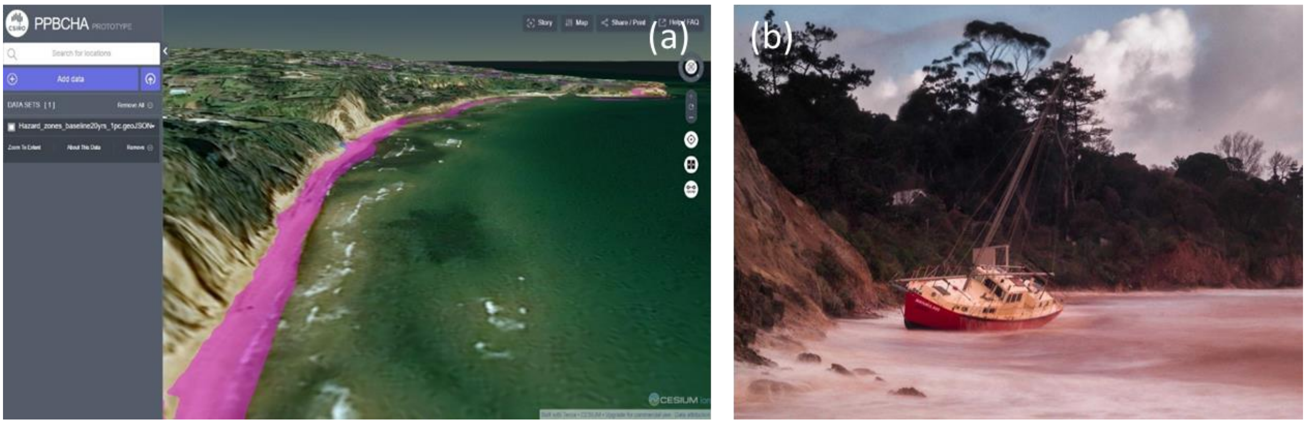

Figure 5.31: (a) 1% AEP wave runup hazard for baseline, showing the truncation of the hazard zones at the base of the cliff, indicating 95% of model estimates predict the beach will be covered during a 1% AEP storm, (b) A yacht sits high and dry at Daveys Bay, south of Frankston on PPB in Victoria, after being blown onto the beach during wild weather on June 24, 2014. By Ben Taylor https://www.abc.net.au/news/2014-06-25/a-yacht-sits-on-the-beach-at-daveys-bay/5548042.

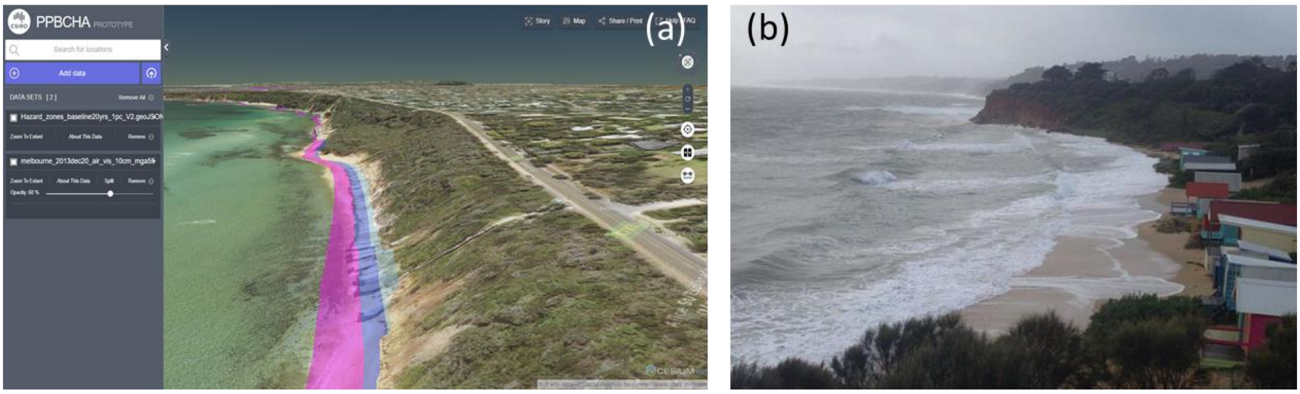

Figure 5.32: (a) 1% AEP wave runup hazard for the baseline climate, showing the truncation of the hazard zones at the base of the cliff. (b) Photo of Mount Martha bathing boxes during wild weather on June 24, 2014 by Wayne Shields @penfreshorganic https://twitter.com/penfreshorganic/status/481276938514735104.

Table 5.6: 1% AEP baseline TWL and wave runup excursion estimates for the 50th percentile, along with the 5th and 95th percentile estimates in square brackets, for the examples provided in Figures 5.27 to 5.30. The mean slopes Beta are from the LiDAR DEMs and 1980s PMA beach surveys (Table I1), the slopes resulting ratio of TWL to X are shown in the final column.

Sector Number	Location	TWL (storm tide+runup) [m]	X (runup excursion) [m]	Input Beta (Mean Slope) [-]	TWL/X [-]
269	Port Melbourne	2.98 [1.28, 4.68]	36.51 [31.52, 41.5]	0.08	0.082 [0.041, 0.031]
339	Brighton Beach Bathing boxes	2.88 [1.71, 4.05]	29.70 [24.53, 34.87]	0.10	0.097 [0.070, 0.049]
405	Kackeraboite Creek, Daveys Bay	3.14 [1.47, 4.81]	37.31 [30.10, 44.52]	0.08	0.084 [0.049, 0.033]
284	Hawker Beach, Mount Martha	1.86 [1.56, 2.16]	18.65 [10.54, 26.76]	0.11	0.100 [0.148, 0.058]

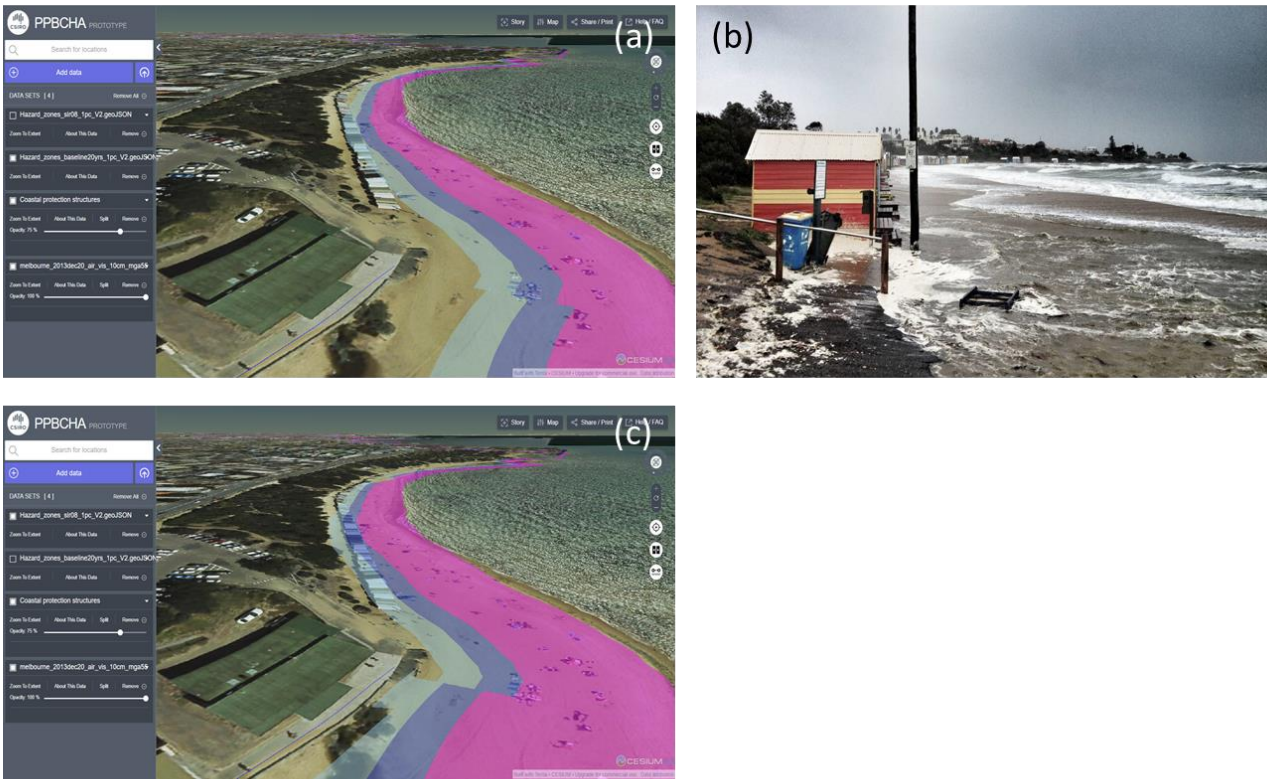

Figure 5.33 (a) 1% AEP wave runup hazard for the baseline 5% AEP event, (b) Wild scenes at Brighton Beach during wild weather on June 24, 2014 - photo by Nichola Clark https://www.bendigoadvertiser.com.au/story/2372401/melbourne-weather-june-24-2014/ Bottom 1% AEP wave runup hazard for the baseline climate and (c) Impact of 0.8 m SLR on the 1% AEP event.

5.6 Summary of Inundation Hazard Assessment

5.6.1 Discussion of Findings

To summarise the effect of SLR on inundation hazard, the total areas of inundation hazard (i.e. the combination of zones 1, 2 and 3) for a 1% AEP for each SLR scenario are provided in Figure 5.34. This indicates that much of the inundation hazard is focussed on the western side of the bay with notable areas including Queenscliff, Swan Bay, Portarlington, Point Henry, Avalon, Point Wilson, Werribee and Altona. On the eastern side of the bay, Southbank, Port Melbourne to Elwood and Patterson Lakes show areas of inundation hazard that are more pronounced under the 1.4 m SLR scenario. Focussed views of the inundation zones for the different SLR scenarios for the western, northern and southeastern parts of the bay are also available in Appendix L.

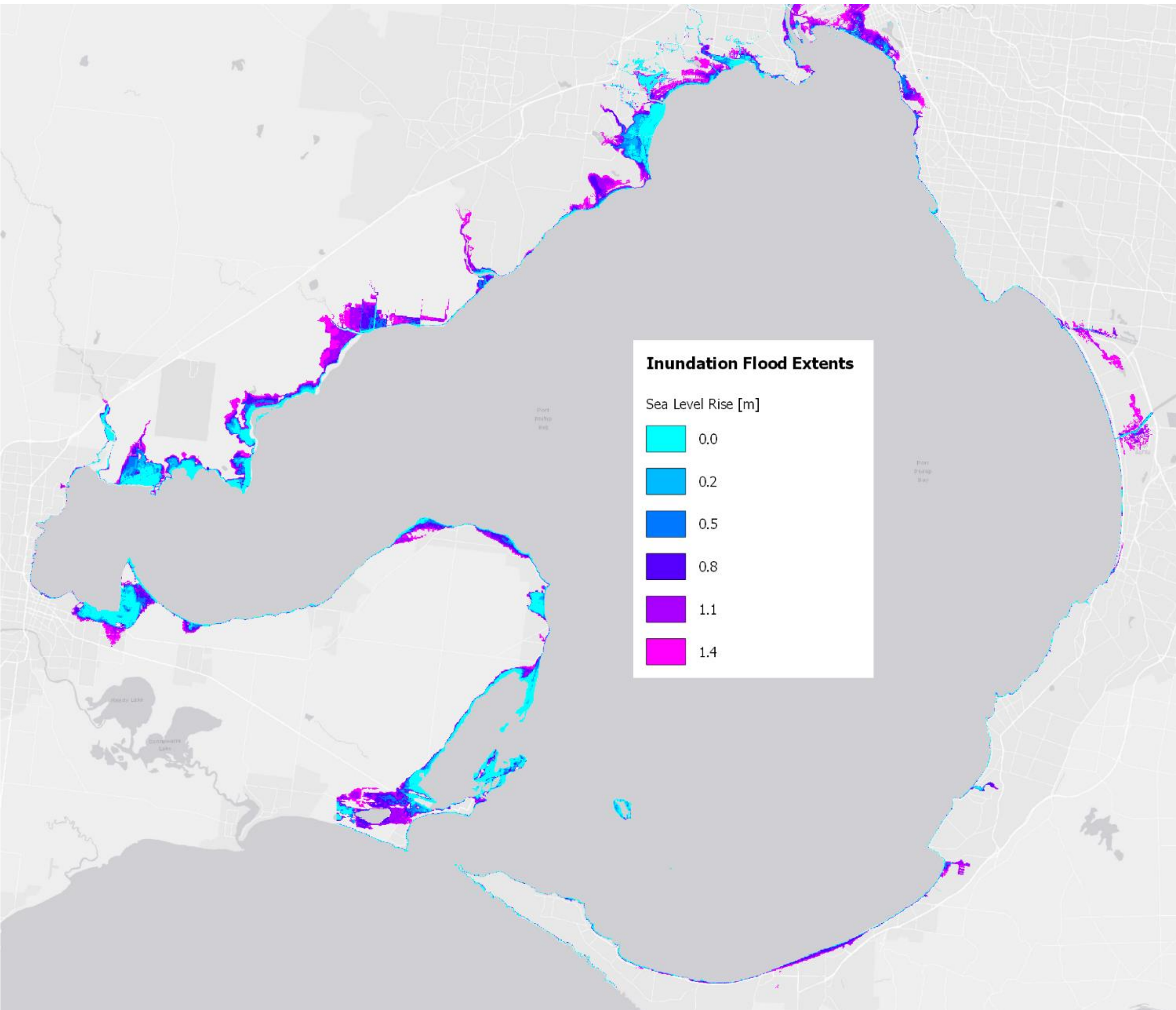

Figure 5.34: Whole-of-bay assessment of inundation hazard for the 1% AEP storm tide (zone 3) and no rainfall for the different SLR scenarios.

The analysis of the trend in area of inundation between the different SLR scenarios is useful because the rate at which inundation increases between different scenarios can have implications for determining: a) how soon protective structures may be required, b) how adaptable these protective structures need to be in terms of being upgraded in future years and c) the cost benefit associated with building protective structures with consideration of staging further upgrades in the future as particular trigger points are reached.

Figure 5.35 provides a quantitative estimate of the inundated area for PPB under the different SLR scenarios for the 1% AEP storm tide with no rainfall, illustrating the differences in area for the three likelihood zones. These estimates are based on C-FAST modelled inundation and include areas where water depths are above 0.1 m (the definition used for nuisance flooding). They are provided to give a broadscale estimate of how inundation will change across urban areas under different SLR scenarios. Note that here zones 2 and 3 represent cumulative totals. In other words, zone 3 includes the area inundated for zones 1, 2 and 3 and zone 2 includes the area for zone 1. A breakdown of these results for individual LGAs is provided in Appendix K (Figures K2a-K17a). For the whole bay there is an almost linear increase in inundated area in going from the baseline assessment to a SLR of 1.4 m with the area of inundation in each of the likelihood zones increasing approximately three to fourfold.

However, for specific Bayside LGA's the rates of change show significant differences. For example, the City of Melbourne, the City of Port Phillip, City of Wyndham and City of Kingston the area affected by inundation accelerates with SLR and inundated areas begin to increase significantly beyond a SLR of 0.5 m. For example, for City of Melbourne under present sea levels, the zone 3 area of inundation is 0.17 km^2 whereas for 0.5 m SLR this area increases to 0.95 km^2 and for 1.4 m SLR increases to 4.74 km^2, six-fold and 28-fold increases respectively. This suggests these regions may require earlier adaptation measures in order to reduce the hazard associated with inundation and these measures will require more frequent monitoring and updating compared to other locations. The adaptation approaches used may need to be more flexible from a design as well as material of construction perspective, noting that Melbourne will have more exposed infrastructure than many other parts of the Bay.

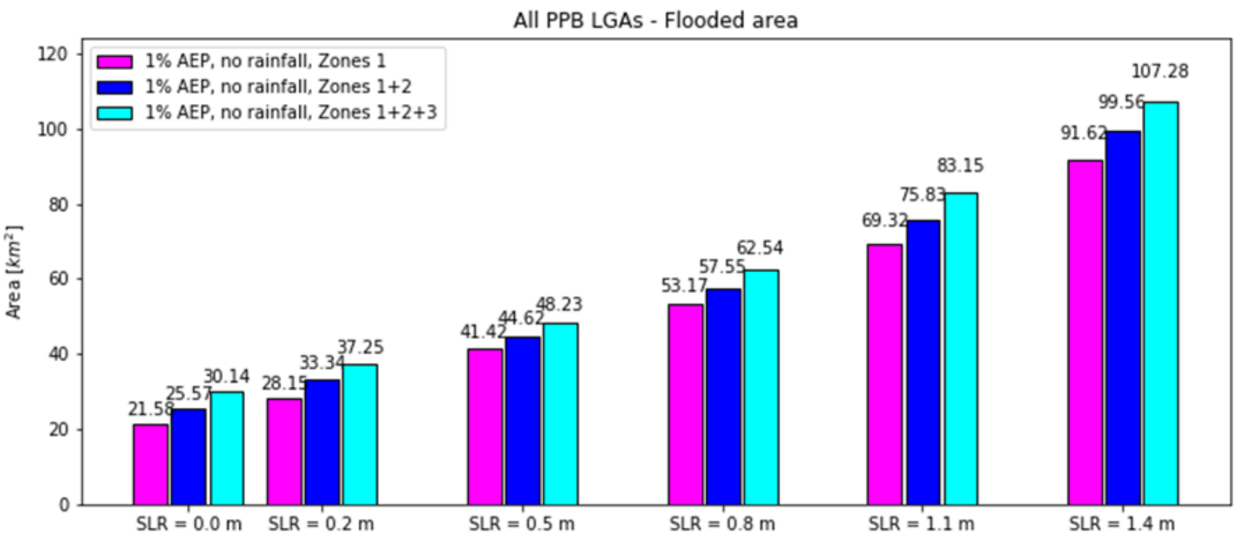

Figure 5.35: Change in inundation area with SLR for the whole of PPB under a 1% AEP storm tide and no rainfall. Note that the totals are cumulative i.e. magenta indicates 95% likelihood (zone 1), dark blue indicates zones 1+2 and light blue indicates zones 1+2+3 and areas are based on C-FAST modelled inundation.

In contrast, for the Borough of Queenscliffe and City of Bayside the change in area with SLR is approximately linear although the Borough of Queenscliffe shows a slightly less steep trend beyond 0.5 m SLR. This suggests that inundation will have only a gradually increasing impact in this region providing more time for planners to adapt. Also applying adaptation measures in this region could have a longer-term positive impact if designed carefully. For Bayside, the zone 3 area inundated under present conditions is 0.34 km^2 and increases to 0.74 km^2 for the highest SLR of 1.4 m.

The Cities of Hobsons Bay, Greater Geelong, Frankston and Mornington Peninsula Shire show relatively linear increases in area subject to inundation under the different SLR scenarios. The inundation area under today's conditions undergoes approximately two to three-fold increases for a 1.4 m SLR. While the increase is more moderate than other LGAs such as City of Melbourne, they nevertheless contain sections of coastline that will require significant management.

Figure 5.36 provides similar information to Figure 5.35 but here only the zone 3 inundation area is shown for the 5% and 2% AEP events as well as the 1% AEP event. Similar to Figure 5.33, the whole-of-bay area of inundation shows approximately a linear increase in area inundated. The breakdown of these results for individual LGAs (Appendix K, Figures K2b-K17b) indicates similar patterns of change for the different LGAs as described above.

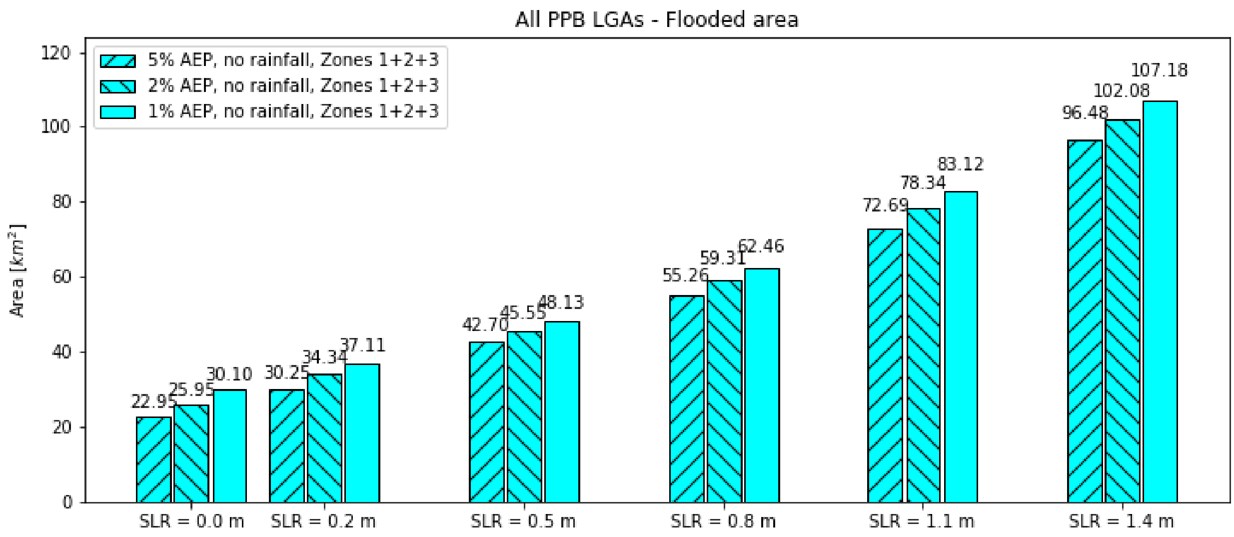

Figure 5.36: Change in inundation area for whole of PPB and for the relevant LGA's with SLR for a 1%, 2% and 5% AEP storm tide, no rainfall and for Zone 3 (i.e. 5% likelihood) scenario. Areas are calculated from the C-FAST modelled inundation.

5.6.2 Summary

The inundation hazards in the PPBCHA were assessed for different values of SLR based on storm tides, wave overtopping and other catchment inputs using the hydrodynamic model, C-FAST. In addition, wave setup and runup were calculated using an empirical wave runup model, to provide additional for the hazard assessment. The hydrodynamic modelling was carried out at two levels of detail around the bay. For selected, highly urbanised and low-lying areas where inundation hazard under SLR was deemed to be high, the dynamic overland inundation due to SLR in combination with storm tide, local wave overtopping where seawalls and barriers are present, catchment inputs and stormwater drainage was modelled with a hydrodynamic model at 5 m resolution. For the rest of the bay, less-urbanised and containing less low-elevation land, overland inundation is assessed with the same model at 25 m resolution accounting for SLR, storm tide and catchment inputs. The 5 m and 25 m results of the simulations were combined to provide seamless inundation maps around the PPB coast for the DSS. Wave setup at the coast was also combined with the inundation maps at locations around the bay where overtopping was not calculated. In addition to the C-FAST-derived inundation, the wave runup excursion hazard layers were separately calculated. Wave runup is useful for understanding the potential for wave impacts on foreshore land and assets.

To demonstrate the performance and model developments of the C-FAST model, this chapter demonstrated how the different physical variables and processes contribute to overland inundation. This gives the user confidence that the model can replicate these processes. The inputs were also compared to existing inundation mapping based on static infill methods to understand the differences in the results that arise from the methods presented here. While the inundation results necessarily show different extents of inundation due to the different underlying methods (e.g. dynamic versus bathtub infill) the differences appear sensible based on the expected effects of the different physical processes.

A methodology for developing probabilistic wave runup hazard zones was described. Wave runup hazard was calculated as an additional hazard layer to provide information about the transitory behaviour of wave breaking on foreshore land and assets. The wave runup hazard layers as they are represented in the DSS, together with photographs of observed wave run-up examples during severe weather conditions were given to aid interpretation of the wave runup hazard layers around PPB.

6 Groundwater Hazard Assessment

This chapter describes the methodology for the groundwater hazard assessment. It begins by summarising data availability such as conceptual hydrogeological models of the bay including the depth to watertable and watertable salinity. The whole-of-bay conceptual model describes groundwater elevations and flow paths. Since most shallow groundwater is saline to some extent, the groundwater hazard is assessed as the change in area of shallow groundwater or groundwater that becomes surface water due to SLR. Conceptual cross-sections of the groundwater systems are provided for three locations around PPB: Werribee, Mentone to Frankston and the Nepean Peninsula.

6.1 Introduction

Although an unseen resource, the groundwater of the PPB region provides many critical services and functions such as baseflow to rivers, streams and swamps, environmental water flows to ecological systems, water sources to support commercial industries and agricultural production, irrigation for gardens, parks and golf courses, and cultural and heritage features such as mineral springs. These beneficial uses are recognised in the *Water Act 1989* that ensures groundwater is conserved and properly managed, and in the *State Environment Protection Policy (Waters)* in the *Environment Protection Act 1970,* which protects water quality.

Climate change, changing land uses and ground water management result in changes to the groundwater systems around PPB that impact on the services that groundwaters provide. The VCP19 projects reduced rainfall and higher evapotranspiration (Clarke et al., 2019) and this will result in lower meteoric recharge, which is the main input for the groundwater systems (Leonard, 2003; Dong, 2005). Increasing urbanisation results in a greater area of impervious surfaces, more domestic bores, particularly along the east coast of PPB and the Nepean Peninsula (Southern Rural Water, 2014), and greater use of recycled water for garden irrigation, all of which impact on groundwater inputs and outputs. The net result of these changes is that less water enters the groundwater system and groundwatertables drop, lowering the hydraulic gradient and diminishing the rate of groundwater discharge to rivers, lakes, springs and the bay.

At the coast, the interface between groundwater table and seawater is complex due to the densities of the two water bodies. In most locations, groundwater in the watertable aquifer is less saline than seawater and forms a lower density wedge above the marine water of greater density (Figure 6.1). Both rising sea levels and lowering watertables will alter the geometry of the interface, potentially impacting on the assets that groundwater services, such as irrigation supplies or ecological health. The changes to the groundwater-seawater interface may also bring saline watertables into contact with built assets such as subsurface pipes, conduits, basements and footings.

There may be potential for offshore groundwater discharge from deeper aquifers semi-confined or confined at the coast, where they occur close to the seafloor. Such groundwater discharge could support unique marine ecosystems. While this has been postulated for Port Phillip Bay (e.g. Leonard 1979), there is no definitive evidence in the published literature that offshore groundwater discharge occurs.

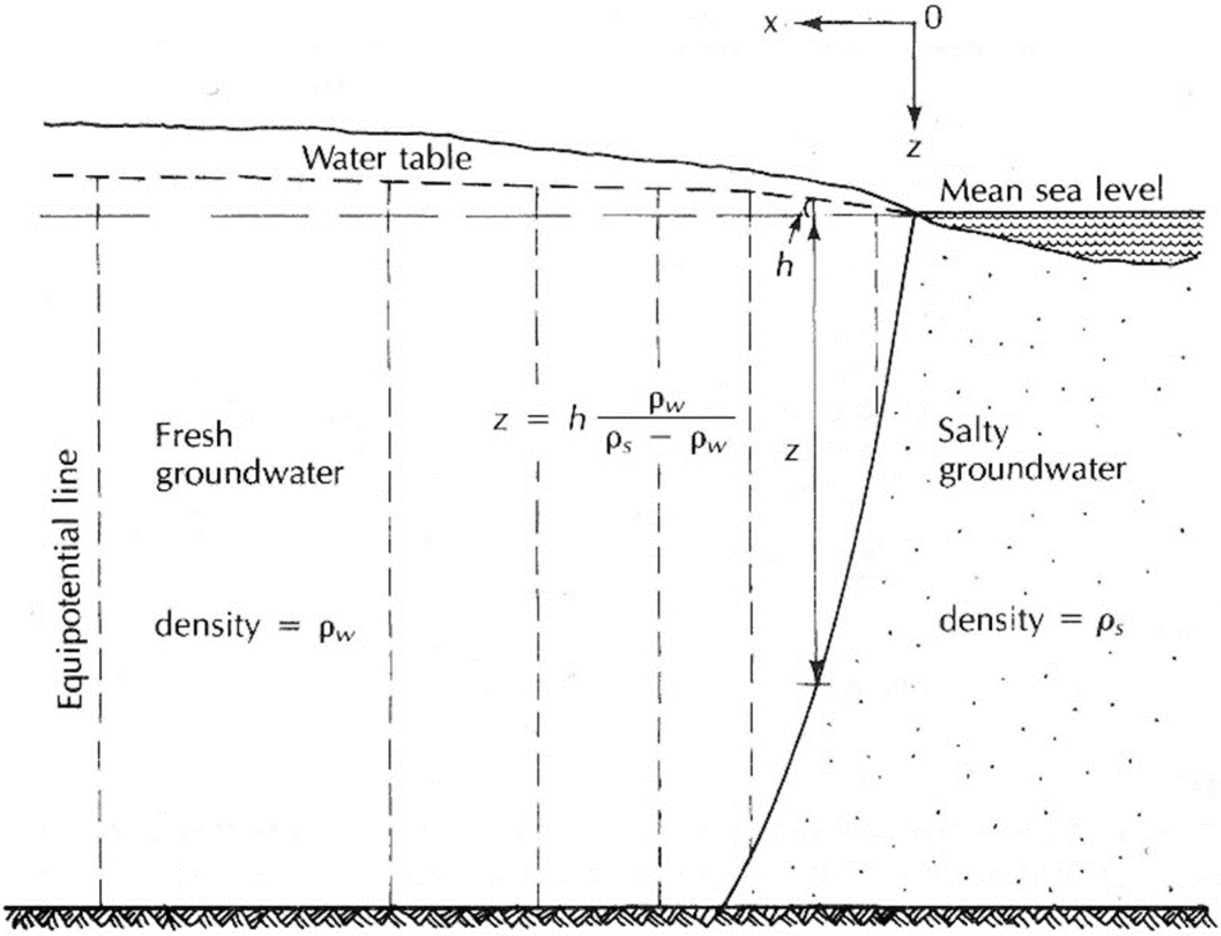

Figure 6.1: Generalised relationship between fresh groundwater and seawater at a coastline. (source: Fetter 2001).

6.2 Groundwater Hazard Assessment Methods

The groundwater components of the PPB CHA project align with a Stage 2 assessment since the modelling is conceptual rather than numerical. A hazard assessment requires an analysis of what can happen, where in the landscape it is likely, and when it could occur (Standards Australia, 2002).

6.2.1 Data Availability

Groundwater data typically comprises measurements, tests and analyses taken from groundwater bores and groundwater discharge such as springs and seeps. Data sources include Federation University's Visualising Victoria's Groundwater (VVG) portal, DELWP's Water Measurement Information System (WMIS), the Geological Survey of Victoria's borehole database (GSV-BD), The Victorian EPA's Victoria Unearthed portal (EPA-VU), the Westgate Tunnel Project website, the Level Crossing Removal Project (LXRP) website, Port of Melbourne GIS system, Melbourne Water GIS system, Southern Rural Water's (SRW) database, the Victorian Government's DataVic platform and the Australian Research Data Commons Research Data Australia metadata catalogue. In addition, there are dozens of databases and thousands of reports in the private sector and research sector that hold good groundwater data for the PPB region but have restricted access.

While extensive effort has been made to source data, some data gaps remain. This is particularly obvious in rural areas where the groundwater resources have not been exploited and there are few bores. Even in areas with many groundwater bores the available data is limited in its accuracy and range and dates of measurements. At this stage there are insufficient volumes of suitable quality groundwater data readily available to construct and calibrate a numerical groundwater model for the entire PPB region, that has a resolution to confidently determine watertable movements in response to SLR.

Borehole data was collated from VVG, WMIS, GSV-BD, EPA-UV, LXRA, and miscellaneous past investigations undertaken by consultants, universities and research organisations (Figure 6.2). Not all bores are groundwater bores or have groundwater data, but most provide some information of the subsurface geology (boring record), and around a quarter of the bores have some useful groundwater information (usually a water level at the time of drilling). There are some monitoring bores with longer time-series of groundwater levels and the most recent bores constructed for the LXRP along the Frankston railway line provide high quality data.

Figure 6.2: Bore distribution (green dots) around PPB (from the databases accessed in the study).

The bore data were used to validate the Victorian Aquifer Framework (VAF; see Section 2.8.3), the depth to watertable modelling, and watertable salinity modelling undertaken for the Securing Allocation Future Entitlement (SAFE) project (SKM, 2012a, 2012b). The modelled tops of formation layers of the aquifer framework were imported into a GIS system and used to create cross sections at various places around PPB (Figure 6.3). These sections were then used as the primary base for a whole-of-bay conceptual groundwater systems model.

Based on the availability of data and the modelled surfaces, three areas were chosen for more detailed analysis of the impacts. These are the Werribee Delta, where groundwater is used for irrigation of horticultural crops and the value of the groundwater is high and potential assets would be at risk; the ‘eastern sand belt’ from Mentone to Frankston where groundwater gradients are flat and the assets potentially at risk are numerous; and the Nepean Peninsula, where groundwater extraction is high and the freshwater groundwater system is a relatively narrow lens along the peninsula.

Figure 6.3: Areas selected for more detailed conceptualisations (focus areas).

In each focus area, conceptual cross-section models have been derived through merging and harmonising cross-sections derived from previous investigative work and calibrating the harmonised sections against the available borehole logs. In this part of the project, there are three significant previous investigations that we have used:

- The DELWP SAFE models: the VAF, depth to watertable and watertable salinity (SKM 2011, 2012a, 2012b).
- Parsons Brinckerhoff (2010), *Groundwater Resource Appraisal for Southeast Melbourne*. This was a significant investigation undertaken by Parsons Brinckerhoff for Southern Rural Water Authority, Victoria.
- GHD (2011) *Report for Lower Tertiary Aquifer (Port Phillip) - Groundwater Resource Appraisal*. This was a significant investigation undertaken by GHD for Southern Rural Water and DELWP.

The outputs of the above reports were digitised and overlaid in a GIS. Cross-sections constructed in the previous investigations were then compared to the VAF geometry and the data was harmonised into credible and defendable representative cross-sections for each of the focus areas. These new cross-sections were updated using the latest borehole information and are based on the VAF as the groundwater system framework (as opposed to the previous ones, which were not).

6.2.2 Constructing the Groundwater Hazard Visualisations

The groundwater hazard related to SLR and changing climates is mainly reflected in the changing depth to watertable and the migration of the seawater – groundwater interface, both of which can impact on natural, built and cultural assets (refer to Section 2.7.2). Since shallow groundwater can be both an asset (e.g. sustaining groundwater dependent ecosystems) and a threat (e.g. impacting on below ground engineering infrastructure such foundations and service conduits), it is the change in depth to watertable that poses a potential hazard.

A watertable of less than two metres below the natural surface in urban areas is usually considered a hazard (Dahlhaus 2010). This is due to the accumulation of salts from capillary rise and evaporation from watertables (where the groundwater contains some salts), the saturation of below ground infrastructure which may require waterproofing and reducing the bearing capacity of foundation materials. Similarly, in groundwater dependent ecosystems, rising watertables can change the vegetation mosaic, especially of phreatophytes and halophytes.

The generalised situation within the Port Phillip region is that changing climate is decreasing rainfall and increasing evapotranspiration (Clarke et al., 2019), which results in decreased groundwater recharge, which in turn, lowers the watertables in the unconfined aquifers. As sea levels rise, the watertables in the discharge zones at the coast rise. The overall result is a lowering of the hydraulic gradient, resulting in a lower rate of groundwater discharge (Figure 6.4). To add more complexity, watertables are continuously fluctuating in response to landscape changes (e.g. urbanisation), seasonal and annual climate variations, tidal and barometric responses, and groundwater response lag times.

Ideally, quantifying the changes in the depth to watertable would require considerable effort in transforming the conceptual models to numeric models, but that may require significant research to reach a credible result at the site-scale. As an alternative, a method was developed to approximate the changes to watertable depth based on estimates of predicted changes to the recharge and discharge rates of the various unconfined aquifers around PPB. The results of this method can be stated qualitatively as groundwater hazard depicted spatially as shallow watertables (high hazard) to deeper watertables (low hazard).

The starting point was the current depth to watertable model prepared by consultants for Southern Rural Water (Wiltshire 2009) and later incorporated into the Statewide Watertable Mapping (SKM 2011). The model does not timestamp a particular year or season, nor show the range of watertable fluctuation. In consideration of the inherent uncertainties, the model is usually shown (e.g. in the VVG portal) as a classified raster map showing typical depths to watertable as less than 5 metres, 5 to 10 metres, 10 to 20 metres, 20 to 50 metres and more than 50 metres below the ground surface (Figure 6.5).

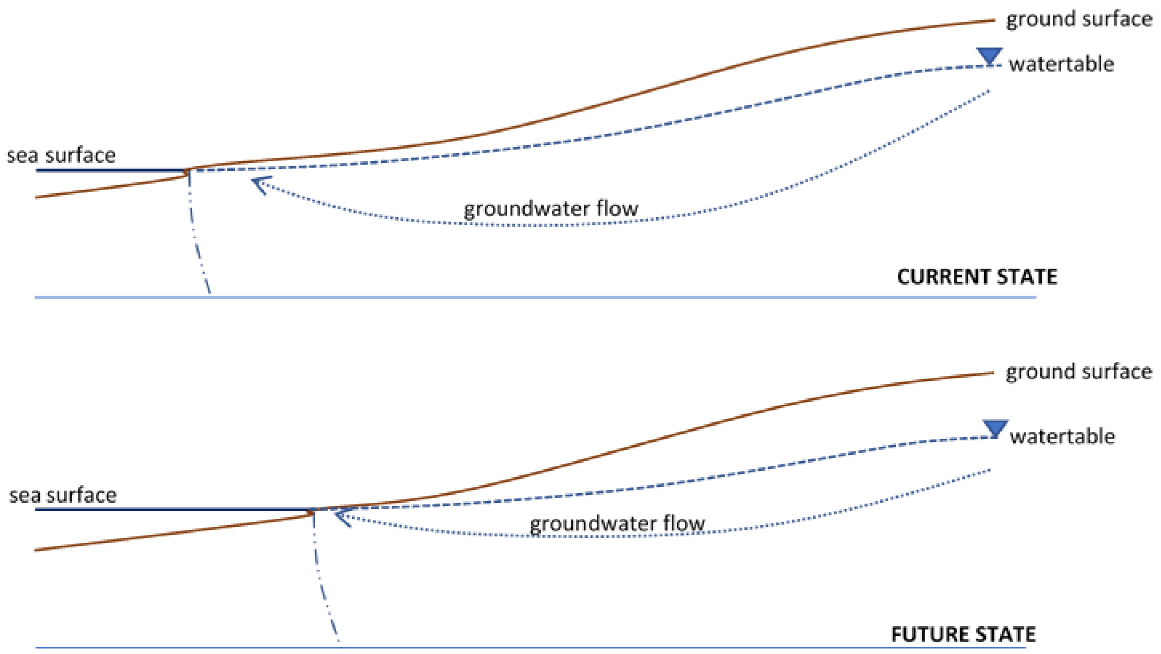

Figure 6.4: Hypothetical changes to the coastal watertable due to changed climates.

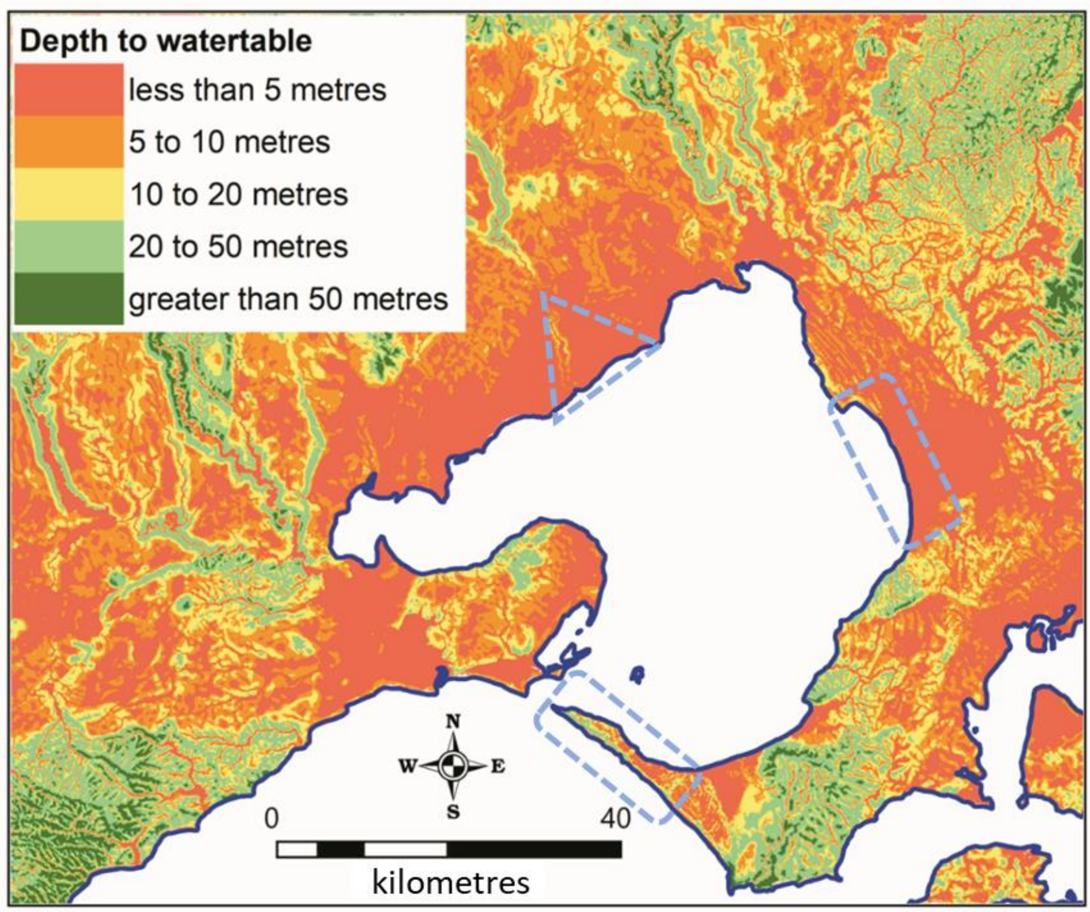

Figure 6.5: Depth to watertable in the PPB region (source: CeRDI, 2020). The locations of the detailed conceptualisations are also indicated.

To understand the impact of the projected decreased rainfall on the depth to watertable, grids (i.e. modelled raster maps) were sourced from the CSIRO CCAM climate projections from the VCP19 that represent the projected average seasonal rainfall for the PPB region for RCP 4.5 and RCP 8.5 scenarios. This type of projections dataset is termed "application-ready" and is produced by modifying a high-quality 5 x 5 km observational dataset by the projected percentile change from the high-resolution climate modelling using a quantile-quantile scaling approach[3]. The projected climate change factor is obtained for each of four 20-year future periods (centred on 2030, 2050, 2070 and 2090) relative to a 20-year baseline period of 1986-2005 and is applied to a 30-year (1981-2010) observational dataset (Table 6.2). This produces internally consistent datasets that preserve the spatial and temporal relationships in the observations while also capturing any projected changes in climate variability from the climate model. In VCP19, application-ready datasets are available for six CCAM downscaled GCMs, although only one model was used here (ACCESS1-0). These modelled values were used to estimate the percentage decrease in recharge for each of the groundwater flow systems (Dahlhaus et al., 2002; Dahlhaus et al., 2004) representing the unconfined aquifers in the selected focus areas (Figure 6.3, Table 6.2).

Table 6.2: Projected average annual rainfall and evaporation values in the focus areas. Note that period 1981-2010 is the baseline and so there is no difference between RCP 4.5 and 8.5

Location	Range	Annual Rainfall (mm)		Annual Evaporation (mm)	
		RCP 4.5	RCP 8.5	RCP 4.5	RCP 8.5
Werribee delta (at Werribee South)	1981 -2010	505	505	1245	1245
	2015-2044	524	491	1325	1340
	2035-2064	518	511	1357	1399
	2055-2084	489	493	1396	1472
	2075-2104	511	423	1437	1554
Mentone to Frankston ‘sand belt’ (at Patterson Lakes)	1981 -2010	692	692	1183	1183
	2015-2044	670	635	1165	1165
	2035-2064	669	628	1185	1168
	2055-2084	625	623	1189	1187
	2075-2104	665	542	1209	1218
Nepean Peninsula (at Blairgowrie)	1981 -2010	683	683	1204	1204
	2015-2044	648	614	1194	1198
	2035-2064	670	627	1221	1209
	2055-2084	655	630	1226	1231
	2075-2104	647	525	1247	1272

For example, in the Blairgowrie area on Nepean Peninsula, the watertable occurs in the unconfined aquifers of the local groundwater flow system of the Nepean Barrier Dunes with an estimated recharge of 20% to 30% of rainfall (Dahlhaus et al., 2004). The modelled depth to watertable is generally <2 m (Wiltshire, 2009). The estimated base-case recharge is 25% of 683 mm = 170.75 mm per annum. The projected worst-case scenario by 2100 is 25% of 525 mm = 131.25 mm. That is, a 39.5 mm per annum decrease in recharge. Assuming no other changes to the spatial and temporal[4] recharge and that hydrological equilibrium is achieved, the average depth to watertable under the worst-case scenario

[3] https://www.climatechangeinaustralia.gov.au/en/climate-projections/future-climate/victorian-climate-projections-2019/vcp19-accessing-datasets/

[4] It is acknowledged that in a drying climate, the soil profile would probably be drier for longer periods of the year, thus reducing the average annual volume of water available for recharge. In this calculation, the percentage of precipitation committed to recharge groundwater would slowly decrease in comparison to the current day. However, there are no reliable predictions to quantify that change, which would be different for each soil type; and influenced by changes to groundcover; and changes in the spatial intensity, frequency and duration of precipitation events.

would be 0.04 m (39.5 mm) lower by 2100 than the current situation. At Werribee South, the equivalent calculation results in a 0.01 m (8 mm) drop in watertable and at Patterson Lakes a 0.04 (37 mm) drop.

From these calculations it was concluded that the projected drop in watertables was a fraction of the normal range of seasonal and annual watertable fluctuations for the unconfined aquifers and therefore not a sensitive component in the coarse scale of this projection. Hence, the overall decrease in recharge was not considered in the approximated models for the whole-of-bay region.

To model the impact of SLR at the coastal discharge zones, grids were sourced from CSIRO which represented a 10 m DEM with flood fills in 10 cm increments from 0.0 m AHD to 1.5 m AHD, with thresholds for where the flood water depth was incremented in 10 cm intervals from >10 cm to >50 cm deep. For the modelled approximations in change to depth to watertable, sea level rises of 0.0 m, 0.2 m, 0.5 m, 0.8 m, 1.1 m and 1.4 m were used to fit with the modelled inundation levels used in the project. The changes in depth to watertable were approximated for each step with areas permanently inundated by >10 cm water depth being set to zero. This assumes that the rising seawater displaces the groundwater and the watertable discharges at the shoreline (see Figure 6.1). To maintain a similar hydraulic gradient for the unconfined coastal aquifers, the depth to watertables within a buffer zone of 0.2 km from the coastal groundwater discharge were halved and in the buffer zone from 0.2 km to 0.5 km depths were calculated as 0.8 (i.e. 80%) of initial depth. The resulting hazard maps (refer to next section) are presented as classified depth to groundwater maps in traffic light colours with red representing <2 m depth, orange 2 m to 5 m depth and green >5 m depth.

The changes to groundwater quality are expected to follow the seawater-groundwater density interface (Figure 6.1) as sea levels rise. That is, the interface will move inland, but remain a sharp delineation in water quality. This assumption is based on the Uniformitarian Principle[5] that the same natural processes that operate today will continue in the future. In other words, even though the groundwater-seawater interface will move landwards, there is no evidence to suggest that the nature or form of interface will change from that observed at the present time. Speculating otherwise would require the rate of change (due to sea level rise) to be faster than the pace of hydrologic equilibrium for the unconfined aquifer at the coast (Currell et al. 2016), which is unlikely.

6.2.3 Challenges and Limitations

The limitations and challenges in the estimation of groundwater hazards related to SLR and climate change around all of PPB are substantial. Apart from the limitations associated with lack of FAIR data (findable, accessible, interoperable, and reusable), this component of the project substantially relies on previous models, each with their own uncertainties that are poorly documented or described by the model custodians.

It is acknowledged that the whole-of-bay groundwater hazard maps (refer to next section) constitute a coarse estimation based on previous depth-to-watertable models, consideration of the terrain slopes, groundwater flow systems and time taken to reach a new equilibrium. The depths to watertables are never static, since they temporally vary with changes in recharge, discharge, land-use, barometric

[5] The assumption that the same natural laws and processes that operate in our present-day scientific observations have always operated in the universe in the past and apply everywhere in the universe.

pressure, transpiration by phreatic plants[6], and tides. The maps are presented as qualitative hazard maps, intended to inform rather than use for definitive input to decisions.

The focus areas selected for a more detailed conceptualisation (Figure 6.3) have more available data and the conceptual models, presented as a series of cross-sections, have been harmonised from the various legacy investigations, considering past and present observation data. Nevertheless, the uncertainties are still significant due to the biased distribution of data towards the groundwater management areas or infrastructure development areas. The predicted groundwater responses in the face of changing climate and land management remain somewhat speculative.

6.3 Groundwater Hazard Assessment – Results and Discussion

The groundwater systems of the PPB region have been conceptualised at two scales: the whole-of-bay, and the more detailed models for the Werribee Delta, Mentone to Frankston sand belt, and the Nepean Peninsula (i.e. the focus areas).

6.3.1 Whole-of-Bay Conceptual Model

Comprehensive reports on the hydrogeology of the entire PPB region are those by Leonard (1992, 2006) who conceptualised the groundwater systems and resources, GHD (2011) who undertook a resource appraisal of the Lower Tertiary Aquifer, and the Port Phillip and Western Port Groundwater Atlas (Southern Rural Water 2014). Despite these excellent reports, it was recognized in the literature review and gap analysis that a whole-of-bay conceptual model remains an obvious gap. Although it is recognized that the regional groundwater gradient is towards the bay, the contribution of groundwater discharge to the bay has yet to be quantified in the published literature (McInnes et al., 2019).

The constructed watertable elevation model, relative to the Geodetic Datum of Australia 1994, is illustrated in Figure 6.6. The model is calculated from the depth to watertable model (Wiltshire, 2009; SKM, 2011) and the DEM sourced from Data61. The image is coloured to show the height of the watertable above datum (which closely approximates sea level), with red as high and blue as low. The model contours indicate the watertable equipotential lines, which in turn indicates the hydraulic gradient and direction of movement of the groundwater in the uppermost unconfined aquifers, illustrated by the black arrows.

Apart from confirming that the bay acts as a groundwater sink, the model also indicates the lengths of groundwater flows from recharge to discharge, and the hydraulic gradients, of the unconfined (watertable) aquifers. In the northeast corner of the bay, the groundwater flows are short with steep gradients, whereas in the Mentone to Frankston sand belt, the groundwater gradients are relatively flat. Similarly, along the northern shoreline of the Bellarine Peninsula, the flow is short and gradient steep, whereas along the western shore of PPB (Point Wilson to Williamstown), the flows are long, and gradients are much flatter.

[6] Phreatic plants are those that are supplied with surface water.

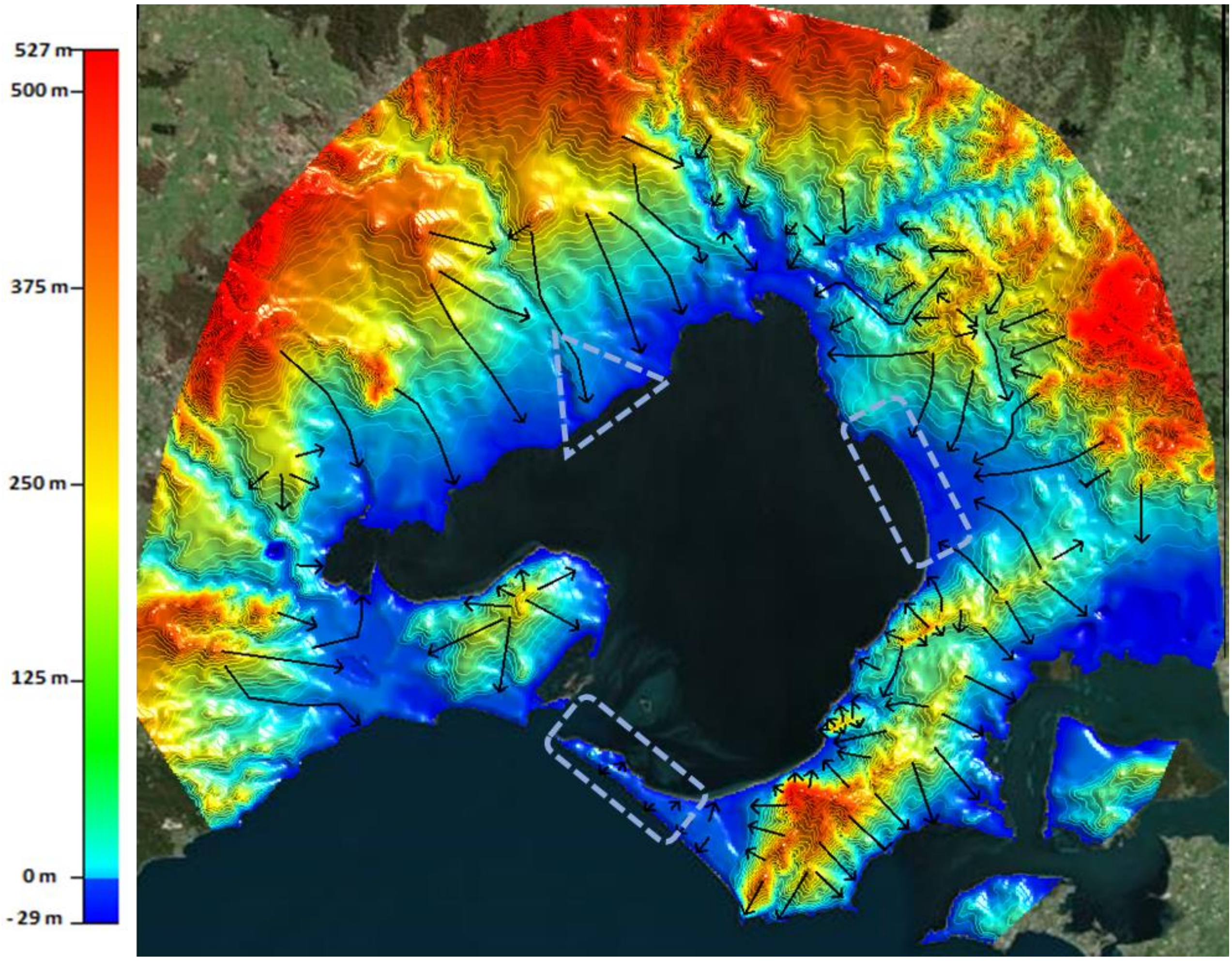

Figure 6.6: Elevations of watertable in m (AHD) and generalised flow paths. Source: based on Wiltshire (2009), SKM (2011) and Data61 supplied DEM.

The implications are that the local flow systems with short paths from recharge to discharge have shorter response times than the regional flow systems with long flow paths. Local systems may respond in less than a decade, whereas regional systems may take five to ten decades to respond. Similarly, the flatter gradients are more susceptible to be influenced by SLR, since a small vertical rise can affect a longer lateral distance. The elevation of the watertable also confirms that close to the shoreline the watertables are very shallow (<2 metres below ground surface) and therefore more responsive to changes in discharge through rising sea levels than changes to recharge through diminished rainfall.

This groundwater hazard assessment provides an analysis of where the depth to watertable is likely to change according to the SLR scenarios. It does not analyse the risk (likelihood and consequence) associated with the watertable rise. The hazards associated with shallow groundwater tables have been stated previously in Section 2.8.

The resulting model of depth to watertable under baseline and SLR scenarios for the whole-of-bay area are illustrated in Figure 6.7a. In keeping with the convention for groundwater hazard maps, the classification is set as red being watertables up to 2m depth, orange as watertables between 2 m and 5 m below ground, and green as deeper than 5m below ground.

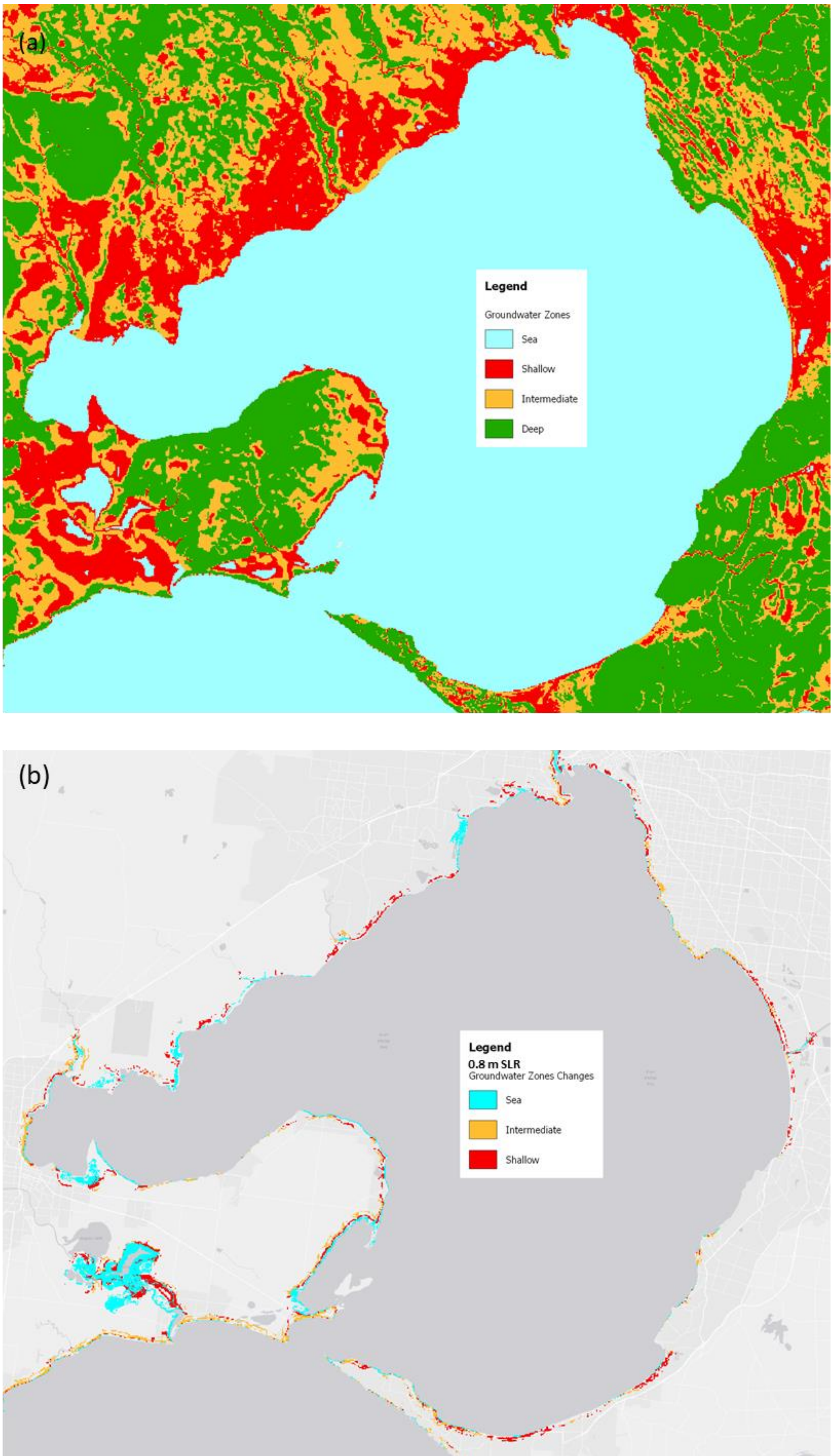

Figure 6.7: (a) Modelled approximate depths to watertable hazard under 0 m SLR (maps for SLR for 0.2-1.4 m SLR not shown). (b) to (c), areas where gains have occurred in shallow and intermediate groundwater hazard (red and yellow) and where ground water has become surface water (blue) between the 0 SLR scenario and the present SLR scenario.

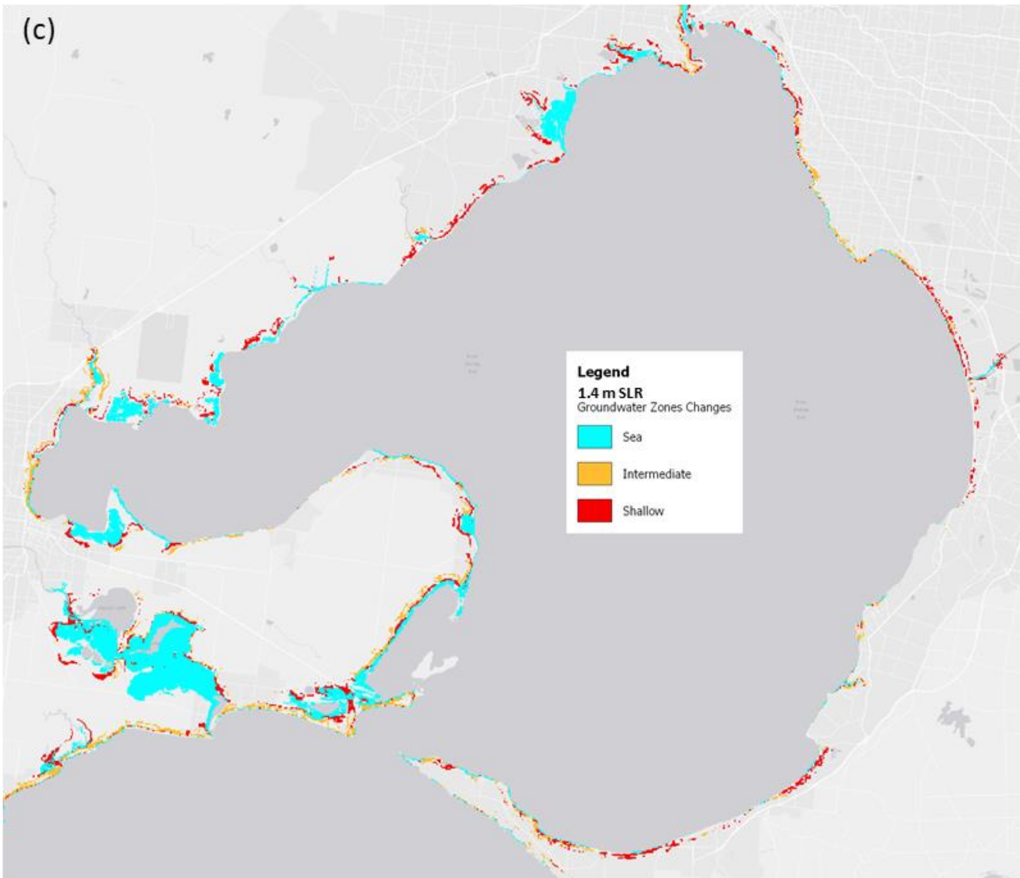

Figure 6.7: Continued.

Maps showing where surface water, and shallow and intermediate groundwater has been gained for 0.8 and 1.4 m SLR scenario are presented (see Figure 6.7b and c). These show that the models produce relatively small differences in the areal extents of the changes in depth to watertable due to SLR. However, it is apparent that the main impact of the groundwater response to SLR will be on the terrestrial groundwater dependent ecosystems (see Figure 2.13), especially the Ramsar wetlands of the Lower Barwon River, and groundwater dependent ecosystems along the western shore of PPB.

Since most of the shallow groundwater is saline to some extent (see Figure 6.8), salt attack on building and construction materials, through chemical corrosion and erosion of materials by prolonged wetting and drying cycles (Bucea and Sirivivatnanon, 2003) may be significant.

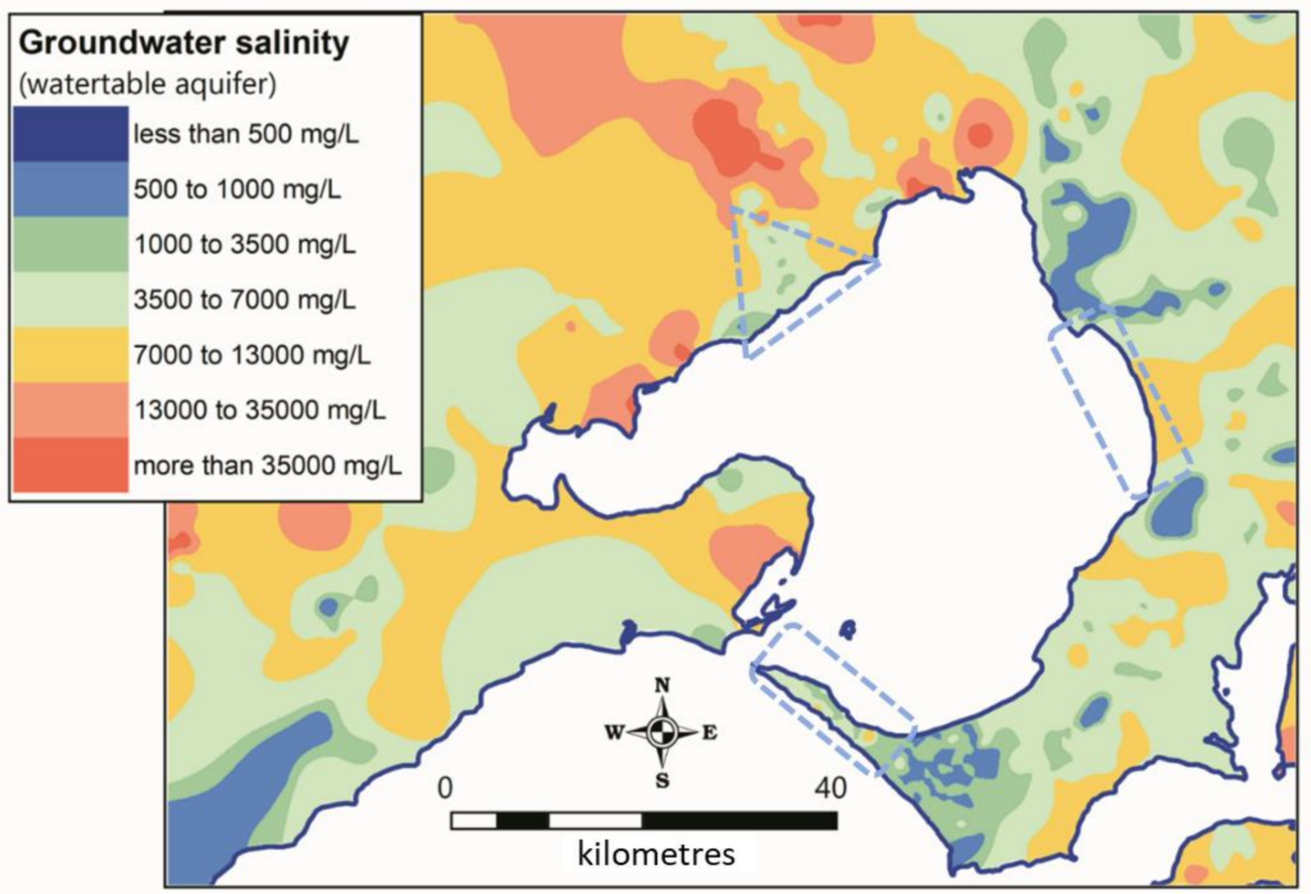

Figure 6.8: Watertable salinity in the PPB region (source: CeRDI, 2020).

6.3.2 Werribee Delta Region (focus area)

The Werribee Delta is an area where considerable research and investigation has been completed in the past and relatively detailed conceptual and numerical models have been developed for groundwater management. Groundwater has been used in the Werribee area for horticultural irrigation for many decades and is extracted from the Deutgam Water Supply Protection Area (WSPA), in which groundwater is managed under the Deutgam Local Management Plan (Southern Rural Water, 2015). The Deutgam WSPA currently has a Permissible Consumptive Volume of 5,100 ML/yr for all formations from the surface to a depth of 30 metres. There are 145 groundwater licences for 4,898.6 ML, 95% of which is licensed for irrigation and the remainder for industrial or commercial purposes. No new licences will be allocated. Stock and domestic use does not require a licence to take and use water. Within the Deutgam WSPA the estimated production value from the groundwater is $1,991,860 for agribusiness users and $311,645 for domestic and stock users (Southern Rural Water, 2014).

The groundwater is extracted from aquifers that mostly comprise sediments of the delta of the Werribee River (Southern Rural Water, 2016), which comprise sand and gravel lenses, surrounded by clay and silt deposited in a terrestrial deltaic environment (Leonard, 1992; SKM, 1997). These sediments create a small coastal aquifer approximately 8.5 m to 19 m thick (Williams 1992) and around 117 km^2, that is unconfined to semi-unconfined and provides reasonable quality water for the Werribee Irrigation District (WID) (Leonard, 1992; Salzman, 2010).

At depth, the Werribee Delta is underlain by the Werribee Formation, an aquifer consisting of sand, gravel, clay and some coal (Leonard, 1992). It drops to approximately 150 m below ground level towards the coast and is confined to semi-confined by the overlying Brighton Group and Fyansford Formation (SKM, 2005), which on the western side of the bay have higher clay content and lower hydraulic conductivities (Leonard, 1992). Above these is the Newer Volcanic aquifer, in which groundwater is contained and moves through an extensive and unpredictable network of fractures and joints in basalt and scoria.

In recent times, issues with over extraction have resulted in increased salinity (Southern Rural Water, 2003) such that salinities ranging from 1,500 mg/L to 4,000 mg/L in 1992 (Leonard, 1992) increased to over 11,000 mg/L (SKM 2005) during the Millennial Drought.

The Deutgam Local Management Plan was declared in May 2015 by Southern Rural Water to manage seawater intrusion into the aquifer (Southern Rural Water, 2015). The plan was founded on extensive investigations (SKM, 1997; Southern Rural Water, 2003; SKM, 2005) which resulted in detailed conceptual and numerical models. Under the plan, groundwater levels must remain well above sea level at the coast and at the tidal extent of the river. Groundwater recharge is supplemented during summer with surface water sourced from recycled wastewater from the Melbourne Water Treatment Plant and river water. Groundwater levels are monitored in 25 observation bores, with salinity samples taken from up to 9 bores each month (Figure 6.9). Trigger levels are set according to Table 6.3. The trigger levels do not consider SLR or climate change predictions.

Table 6.3: Groundwater allocation triggers in the Deutgam WSPA (source: Southern Rural Water, 2015).

Bore ID	50% Allocation Trigger	25% Allocation Trigger	0% Allocation Trigger
	Head (mAHD)	Head (mAHD)	Head (mAHD)
145273 (coast)	3.9	3.6	3.2
145272 (river)	2	1.5	1
145271 (river)	1.25	1	0.75
145270 (inland)	9	8.25	7.5
113018 (coast)	1.2	0.9	0.75

(Note: Bore locations are shown in Figure 6.9).

Three conceptual cross-sections were developed in this study for the Werribee groundwater hazard assessment, a regional cross-section, local cross-section and smaller scale coastal model. The first, which illustrates the regional groundwater systems (Figure 6.10) was compiled from a number of previous investigations, including SKM (2012a), Nolan ITU (2001), GHD (2010, 2011), Leonard (1992) and Holdgate et al., (2002).

The conceptualisation includes three main aquifer groups: the upper aquifer group of the Werribee Delta sediments, overlying the Newer Volcanic Formation basalts, which overlie the Brighton Group sediments. These are separated from the confined aquifers comprising the Maddingly Coal, Werribee Formation and Older Volcanics by the confining bed of the Fyansford Formation. This lower confined aquifer group overlies the basement aquifer.

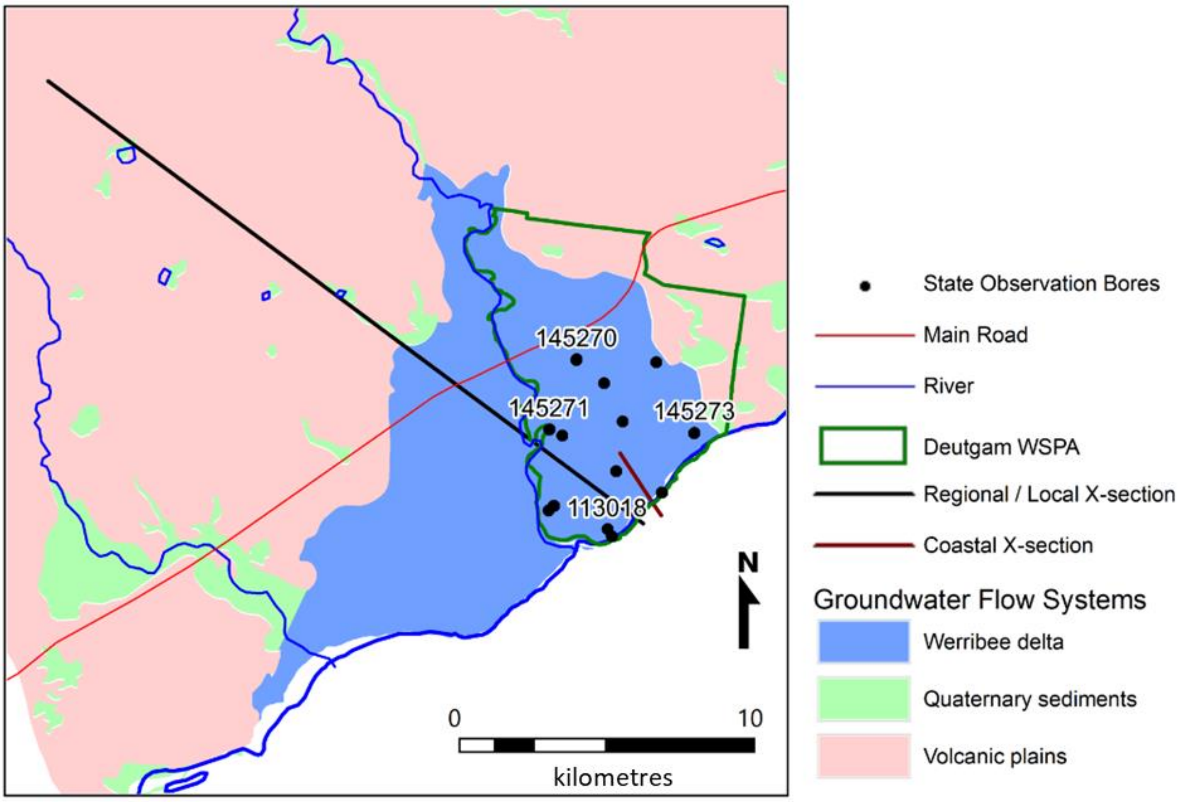

Figure 6.9: Location of bores, cross-section lines and groundwater flow systems in the Werribee region.

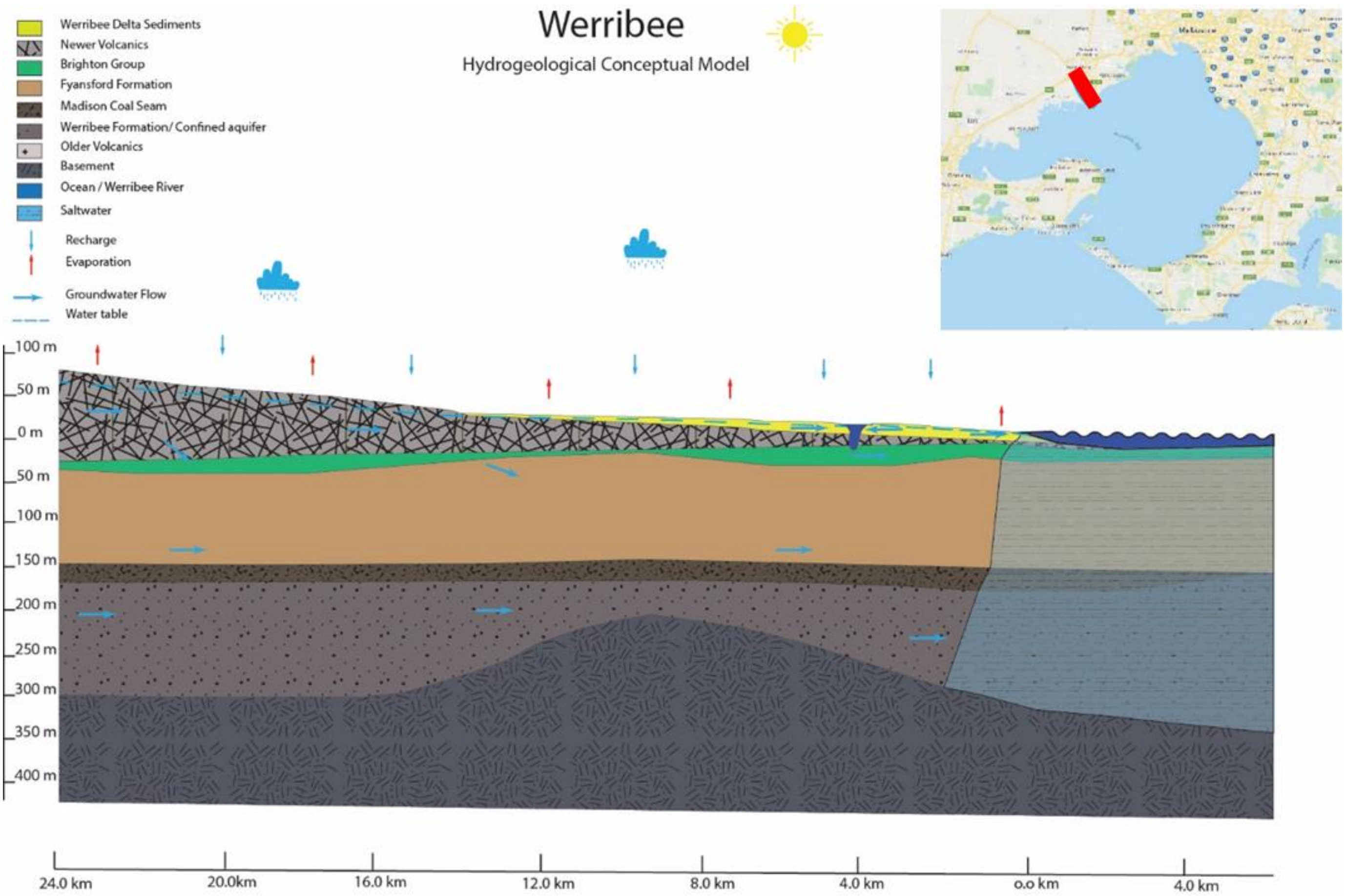

Figure 6.10: Regional-scale conceptual cross-sectional model for the Werribee groundwater systems. The legend for the cross-section is shown (top left) and its location is shown in red (top right).

In conceptualising the Werribee region groundwater processes and responses to SLR and climate drivers, the report by Leonard (1992) provides the following useful metrics. Direct discharge from the principal Cainozoic aquifers (of the Werribee delta) into PPB is of the order of 30,000 ML/year. Average discharge to the Werribee River is estimated at 1,400 ML/yr, with 910 ML/yr east of the river and 510 ML/yr west of the river. Total annual average streamflow is 104,000 ML. Bore yields can be up to 15 L/s but average <5 L/s. For the unconfined aquifer system, the regional hydraulic gradient is around 0.001 (1 in 1000) and the regional hydraulic conductivity is in the order of 1 to 15 m/d with an estimated average of 5 m/d. Specific yield varies from 0.05 to 0.25 and the estimated average is 0.10 (10%).

Direct annual recharge (based on the area of 117 km^2) for 3%, 5% and 10% of the average annual rainfall (510 mm) is estimated as 1,800 ML/yr, 3,000 ML/yr and 6,000 ML/yr. The saturated volume of the upper unconfined aquifer system is estimated as 160,000 ML, and the sustainable yield of the deltaic sediments is estimated at 3,000 ML/year.

In 1998, the Permissible Annual Volume was calculated based on 10% of the average annual rainfall (i.e. 52 mm/yr) as 2,394 ML (SKM, 1997). In addition, 258 ML/yr were required to prevent seawater intrusion. This Permissible Annual Volume calculation allows for the freshwater - saltwater interface to migrate 500 metres onshore (Nolan ITU 2001). These calculations did not consider projected sea level rises.

In considering the rainfall – recharge relationship for the Werribee Delta region the (more complete) rainfall record at the Laverton weather station was compared to the bore monitoring records sourced mainly from Southern Rural Water and the VVG portal (Figure 6.11). The rainfall data was graphically compared to four bore hydrographs: bore 59522 - an inland bore, bore 59534 - east of the Werribee River and bores 112804 and 145273 - both coastal bores. All four bores are screened in the Quaternary Werribee Delta sediments as representative of the watertable in the unconfined aquifer.

The rapid response of the watertable to the rainfall, especially to the 2010 recharge rain that ended the Millennium Drought (1996 – 2010), testifies to the permeable nature of the unconsolidated sediments that comprise the deltaic sediments. Nolan ITU (2001) attributed the watertable decline prior to 2001 to increasing groundwater extraction.

The local scale conceptual cross-section has been constructed based on the bore information and geological interpretation closer to the shoreline (Figure 6.12). It should be noted that the sea water – groundwater interface is interpretative, and not based on observed data, since none could be found. The variation in the shape of the interface is based on the relative hydraulic conductivities of the materials that make up the groundwater system.

Based on the previous reports and conceptualised groundwater system, it is apparent that the groundwater levels in the Werribee Delta respond rapidly to rainfall recharge and to discharge from abstractions. Therefore, it can be assumed that the migration of the seawater – groundwater interface will quickly equilibrate with the SLR.

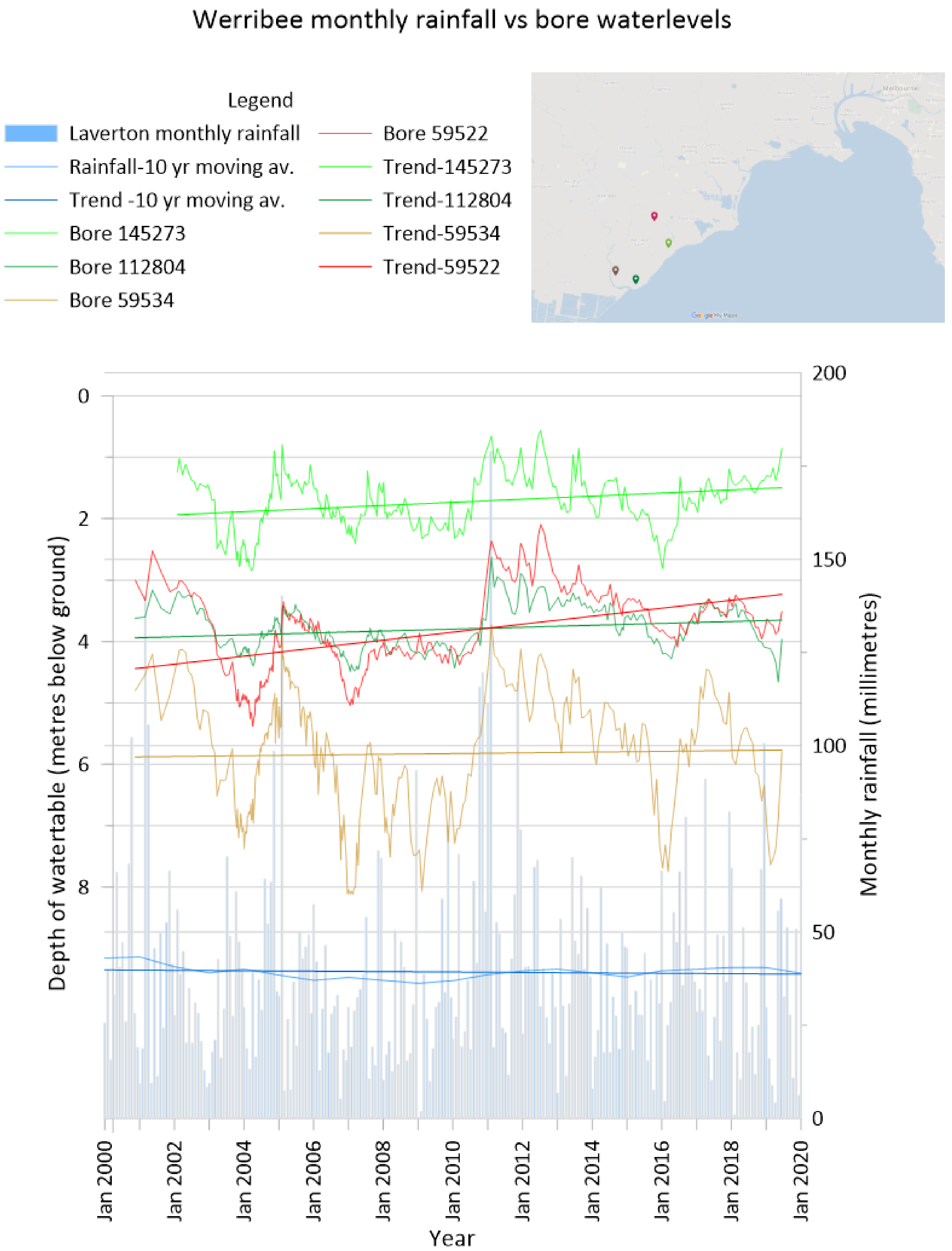

Figure 6.11: Correlation of rainfall with bore hydrographs 2000 – 2019, Werribee area. The locations of the colour-coded bore holes in the legend are shown in the map (top left) and the corresponding watertable depths are shown in the lower figure as colour-coded curves and trend lines with values indicated on the left axis, together with bars representing monthly rainfall totals with values indicated on the right axis.

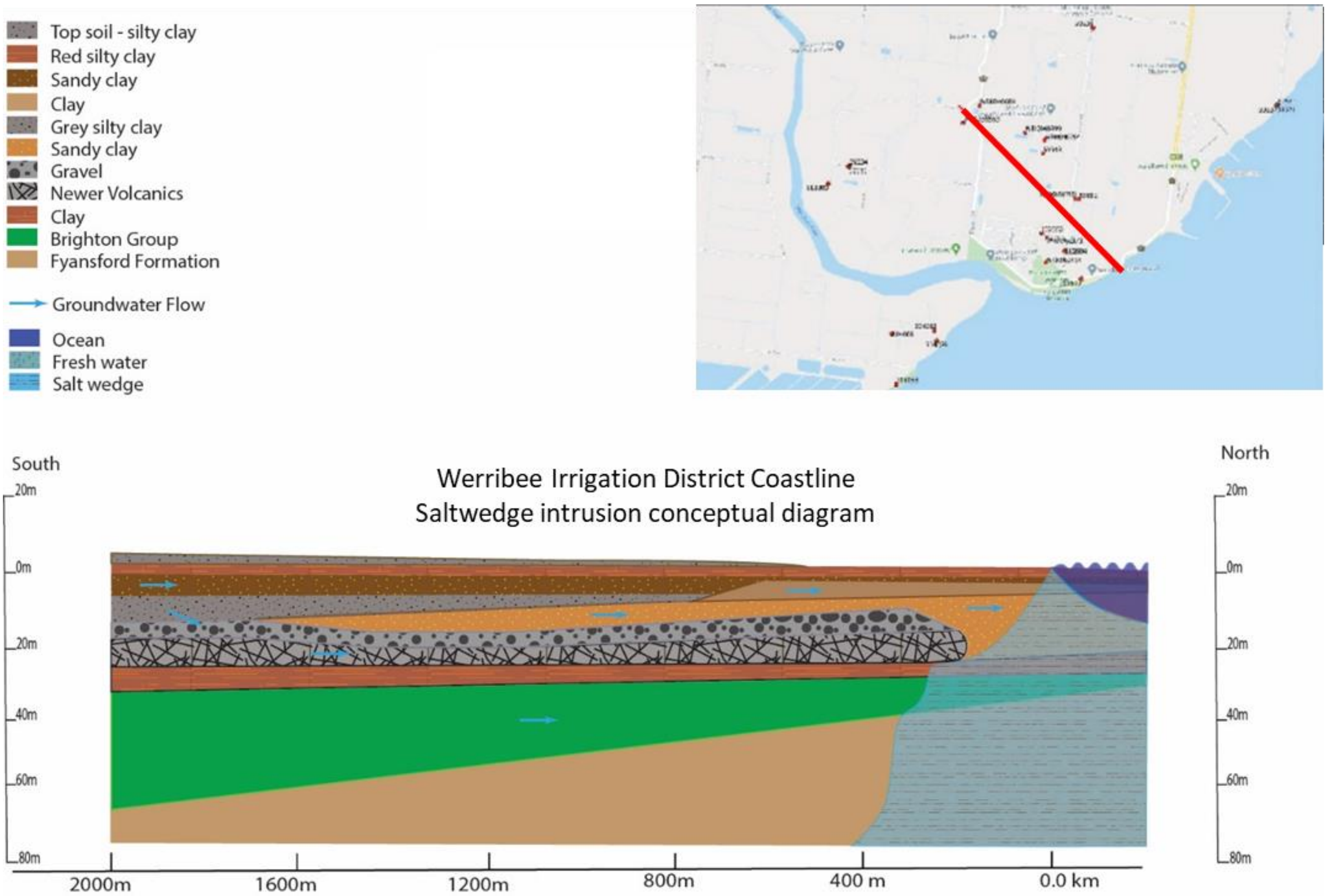

Figure 6.12: Local-scale conceptual cross-sectional model for the Werribee groundwater system showing saltwedge intrusion. The legend for the cross-section is shown (top left) and its location is shown (red line) and bores used (top right).

A coastal-scale calculation of the groundwater-seawater interface is graphically illustrated in Figure 6.13, which has been constructed using the DEM for the ground surface and the modelled depth to groundwater grids (as illustrated in Figure 6.7a). The graph represents the line shown as ‘coastal x-section’ in Figure 6.9. Simplifying the Ghyben-Herzberg relation[7], assuming isotropic and homogeneous aquifer materials for the unconfined aquifer (or watertable aquifer) system and taking the hydrographic responses in the adjacent bores 122804 and 113018 as examples, a 1.4 metre rise in sea level would move the current interface approximately 250 metres inland at 20 metres depth.

The main implications of groundwater response to SLR and changing climate in the Werribee region will be from the slowly migrating seawater-groundwater interface. Groundwater resource management will require revision as the potential for upconing of seawater (i.e. the drawing of migrated seawater interface upwards) into irrigation bores will increase.

[7] In reference to Figure 6.1, this means $z = 40h$.

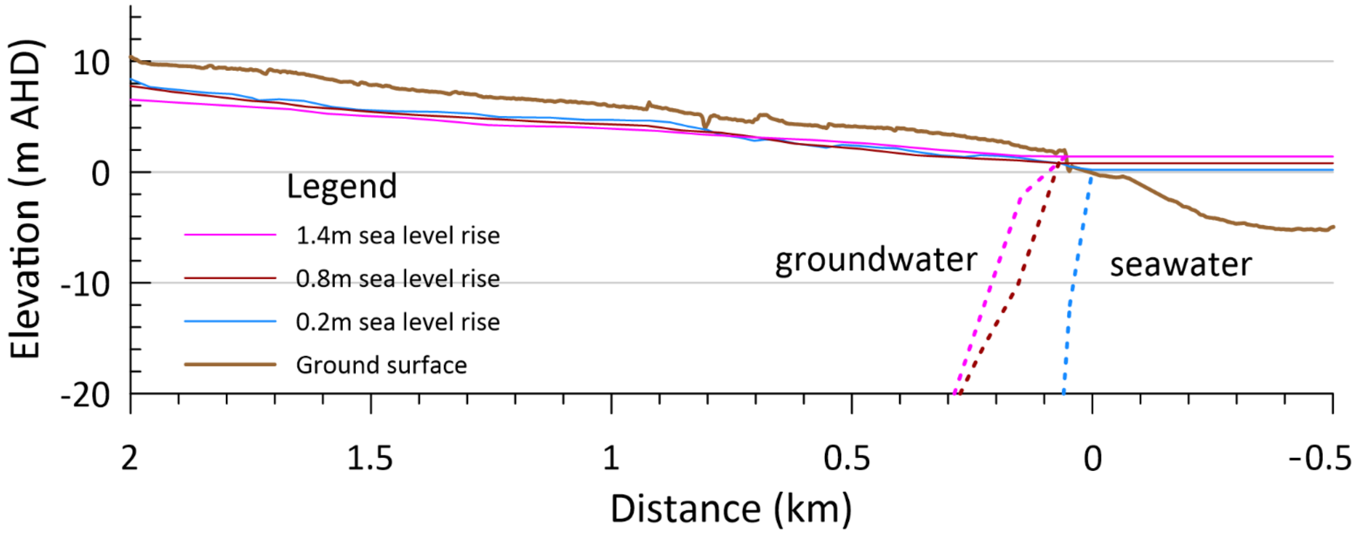

Figure 6.13: A graphical illustration of the calculated watertable[8] and migration of the seawater – groundwater interface in relation to SLR at the Werribee coast.

Groundwater hazard due to SLR in the Werribee delta region can be summarised as:

- The depth to watertable across the Werribee Delta is relatively shallow and the recharge to the unconfined aquifers[9] is dependent on rainfall.
- Groundwater sustains the agricultural (horticultural) industry, and its extraction is currently limited to prevent seawater intrusion into the aquifer. The triggers are based on the depth to watertable in specified bores.
- The predicted decreased precipitation and increased evaporation will have a small effect on the watertables, potentially lowering them by around 0.01 m over the next century.
- The rising sea levels are predicted to have a greater impact through the landward migration of the seawater-groundwater interface. Using today as a base case, this is predicted as approximately 250 m inland at 20 metres depth for a 1.4 m rise in sea level.
- Over time, the drawdown triggers for management of groundwater extraction will need to be reconsidered.

6.3.3 The Mentone to Frankston 'sand belt' (focus area)

The Mentone to Frankston sand belt is an area where watertables are being affected by SLR because of the low-elevation planar topography and correspondingly flat gradient of the shallow watertable (as shown in Figure 6.6) in permeable the aquifer materials. The sand belt includes the Frankston Groundwater Management Area (GMA), which extends along the coastline from Carrum to Frankston. The Permissible Consumptive Volume of the Frankston GMA is 3,200 ML/yr, for all formations below surface. There are currently 30 groundwater licences authorised to take and use a total of 1,671.4 ML/yr for irrigation, industrial and commercial purposes (excluding stock and domestic usage). Within the Frankston GMA the estimated annual production value from the groundwater in 2014 was $445,097 for urban and industrial users, $30,862 for agribusiness users and $311,645 for domestic and stock users (Southern Rural Water, 2014).

[8] Note that the watertable is not static and varies with seasons and climate. The graph does not illustrate the range of temporal fluctuation.

[9] The unconfined aquifers are the system that host the watertable (phreatic groundwater surface).

Because of the historic groundwater extraction in the Frankston GMA and the more recent infrastructure development by the Level Crossing Removal Authority, there are relatively good geological and hydrogeological conceptualisations in the existing literature supported by good data. The main aquifer includes surface sediments comprising dune sands, swamp deposits and young marine and non-marine sediments, of varying lithologies (gravels, sand, silts and clays) up to 20 metres thick (SKM, 1998; GHD, 2011). The sediments overlie the Brighton Group, sub-divided into the upper Red Bluff Formation, which is up to 15 m thick and fossiliferous, and the lower Black Rock Formation that is 24 m thick, poorly fossiliferous and iron stained sands (Holdgate and Gallagher, 2003). These combined strata are considered as the main aquifer (Leonard, 2006).

The Brighton Group overlies the Fyansford Formation, consisting mainly of sands, gravel, iron stained (glauconitic) carbonaceous and shelly marls, with some clay content (Holdgate and Gallagher, 2003). The Fyansford Formation is generally considered as a confining bed, overlying the Werribee Formation, a saline semi-confined to confined aquifer, which was deposited in the Middle Tertiary and is composed of silty sand, coal and basalt (SKM, 1998). The Werribee Formation is intercalated with Older Volcanics comprising fractured basalt rocks that have their recharge zone mainly within the Silvan area where they can be up to 90 metres thick (SKM, 1998) but become thinner (5 – 10 metres thick) to the west, resting on the Werribee Formation or basement rocks (Leonard, 1992). Significant anthropogenic changes include the draining of the Carrum Swamp to create the Patterson River and Patterson Lakes, altering the surface and groundwater of the area (GHD, 2011).

Two conceptual cross-sections were developed in this study for the groundwater hazard assessment: a regional scale cross-section and a coastal scale section. A local scale cross-section was recently constructed by consultants for the Level Crossing Removal Authority and adopted for this study. The regional-scale conceptual cross-sectional model for the Mentone to Frankston sand belt groundwater systems (Figures 6.14 and 6.15) was compiled from a number of previous investigations, including SKM (2012a), Victorian Government (2017b, 2018), GHD (2011), Parsons Brinckerhoff (2010) and Leonard (1992). The cross-section is based along a common line used in these reports. It illustrates the two-dimensional geometry of the strata along the slice, with the groundwater flow directions, watertable and estimated seawater interface.

Parameters relating to the unconfined aquifer (which hosts the watertable) were sourced from the available literature to inform the predicted response of the watertable to SLR and climate drivers. These include hydraulic conductivity values ranging from 0.01 m/d to more than 33 m/d, with most being below 3 m/d. The highest values are recorded closest to the coast, reflecting the unconsolidated sands and gravels. The correlation of watertable levels to rainfall (Figure 6.16) in the upper unconfined aquifers (Quaternary sediments and Brighton Group) testifies to the overall higher response of the shallow groundwater system largely due to permeability of the aquifer materials.

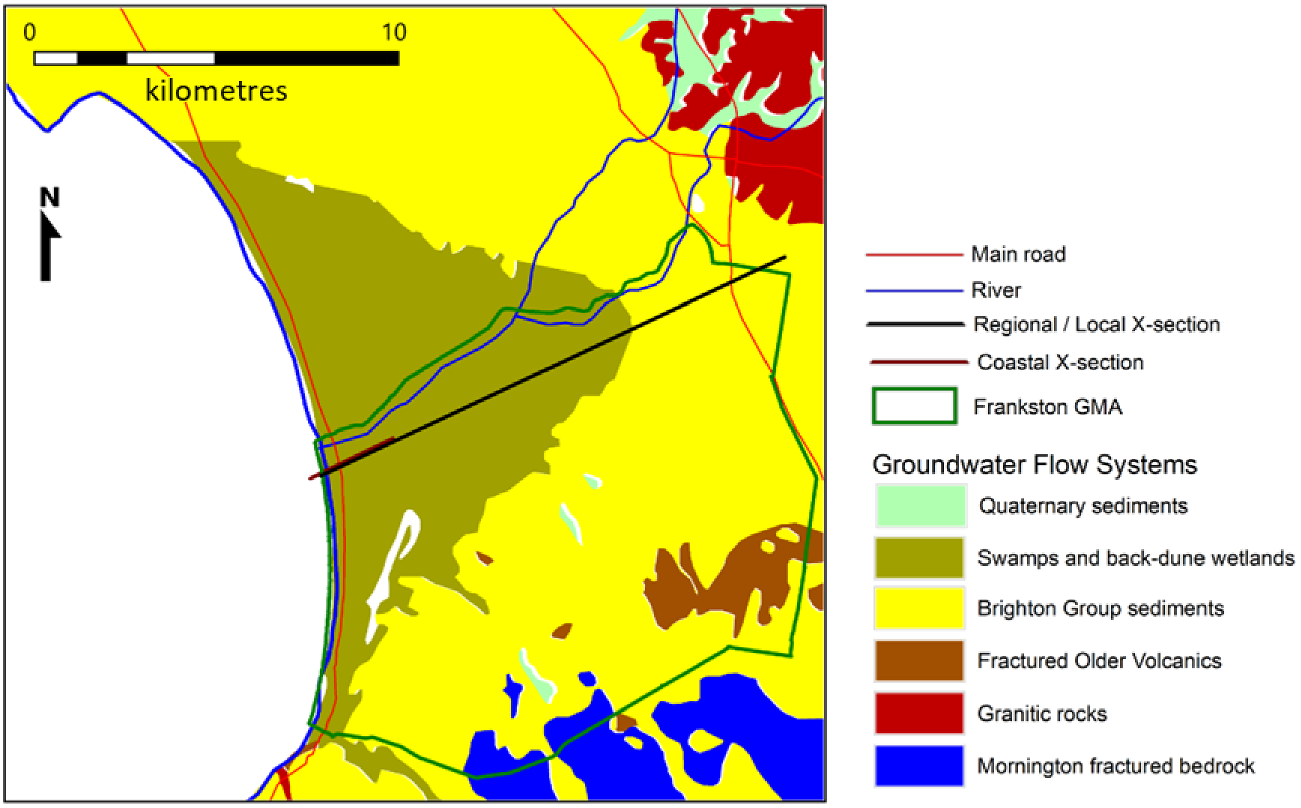

Figure 6.14: Mentone to Frankston cross-section lines and groundwater flow systems.

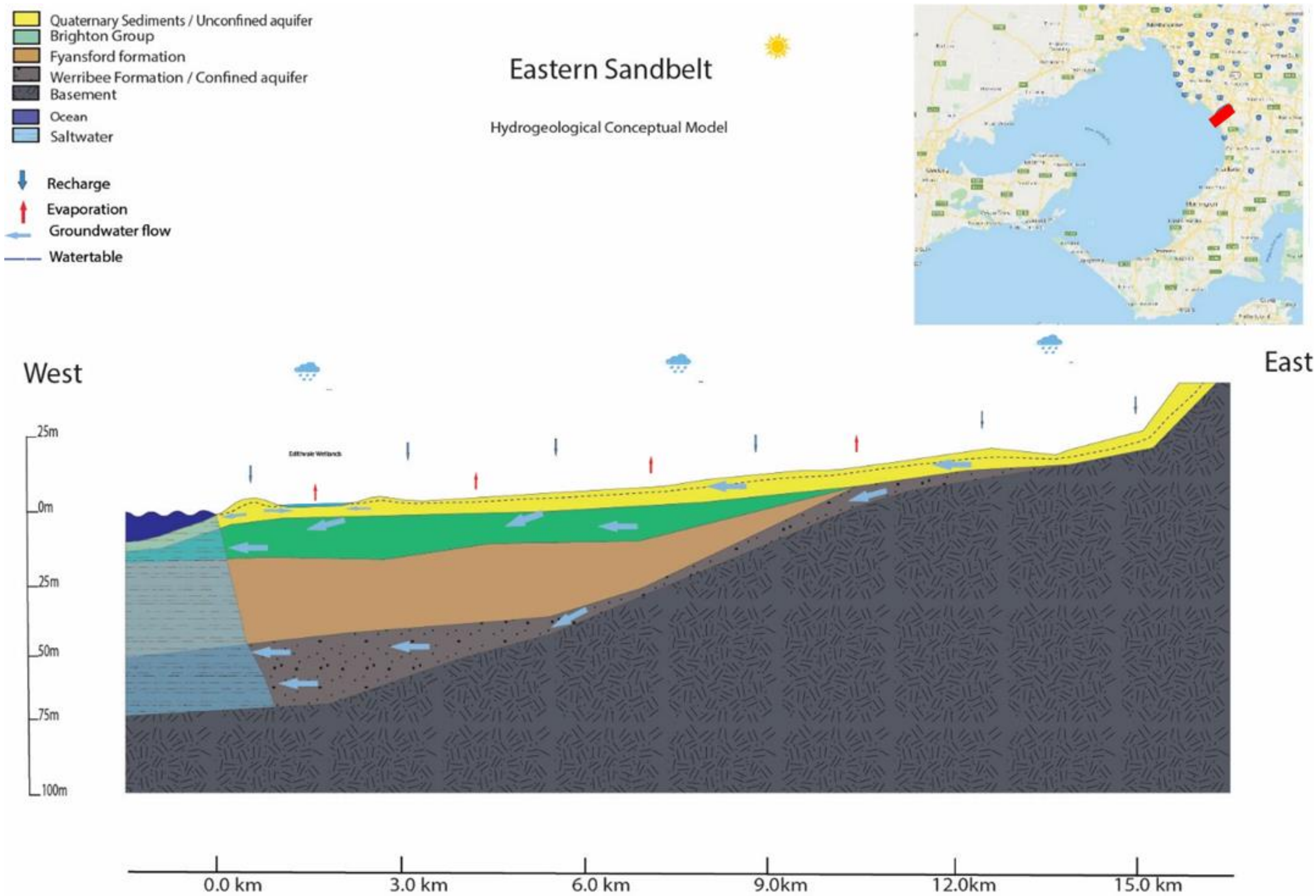

Figure 6.15: Regional-scale conceptual cross-sectional model for the Mentone to Frankston sand belt groundwater systems. The legend for the cross-section is shown (top left) and its location is shown in red (top right).

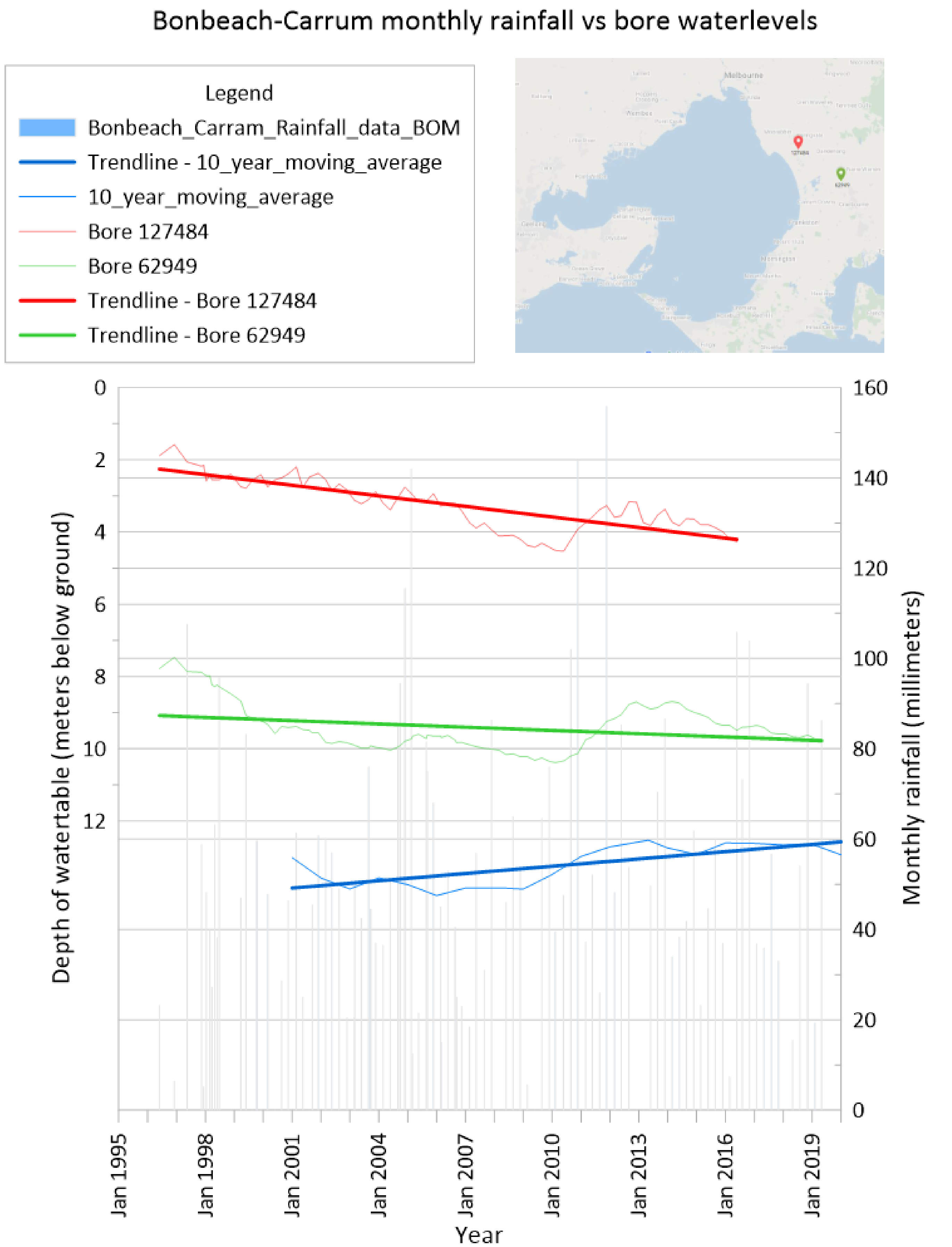

Figure 6.16: Correlation of rainfall with bore hydrographs 1992 – 2020, Mentone to Frankston. The locations of the colour-coded bore holes in the legend are shown in the map (top left) and the corresponding watertable depths are shown in the lower figure as colour-coded curves and trend lines with values indicated on the left axis, together with bars representing monthly rainfall totals with values indicated on the right axis.

Leonard (1992) reports that while surface water runoff contributed to the wetlands, groundwater discharge is equally, if not more important. His investigation estimates that approximately two-thirds of the groundwater flow in the upper unconfined aquifer is towards the original Carrum Swamp area. These act as groundwater sinks, in which the saline water is partly attributable to the concentrating effects of evapotranspiration from the shallow watertable in the vicinity of the swamps. More recent investigations in the Edithvale and Bonbeach level crossing removal projects environment effects statement (Victorian Government, 2018) confirms that the groundwater flow discharging to the wetland cells is sourced from localised flows around these topographically low lying areas (as opposed to intermediate or regional groundwater flow fields recharged from further away). Focussing on the regional section near the coast, the local-scale conceptual model of the groundwater flows closer to the coastline is best represented in the most recent investigations (Figure 6.17) (Victorian Government, 2018).

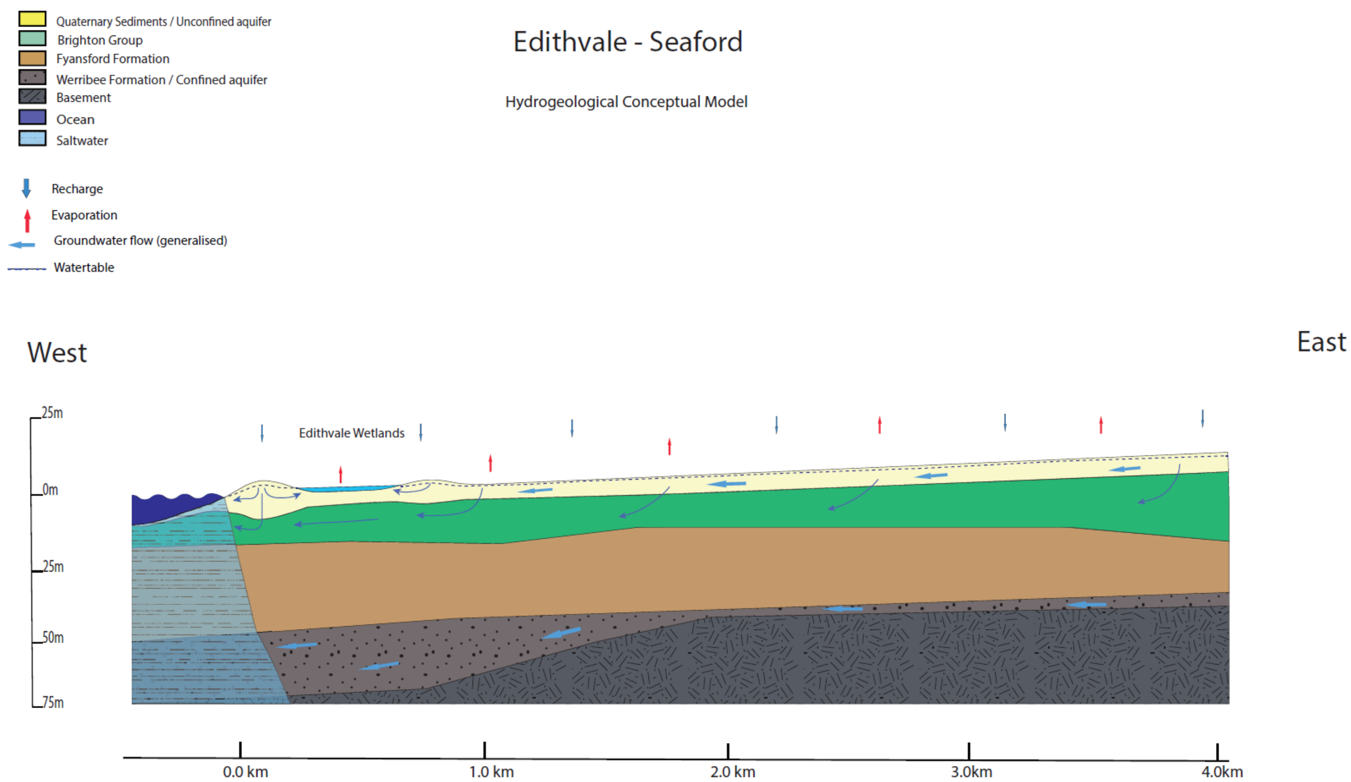

Figure 6.17: Local-scale conceptualisation of coastal watertables, Edithvale-Seaford wetlands (source: Victorian Government 2018).

The groundwater hazard resulting from SLR is related to the low hydraulic gradient (Figure 6.6) and the permeable Quaternary Aquifer sediments (Figure 6.17). While there appears to be potential for the seawater-groundwater interface to migrate at the same pace as rising sea levels, the most recent numerical modelling undertaken by consultants for the Level Crossing Removal Authority indicates the opposite. Their report states: *"…the model was run for a 100-year period, to predict potential changes to salinity concentrations. The model calibration indicated that it takes more than 10,000 years for the saltwater wedge to migrate inland from the coastal boundary and reach a steady state condition. This implies that the current location of the saltwater wedge and associated mixing zone would have developed over thousands of years."* (Victorian Government 2017a, p.46).

Furthermore, the report states: "*Irreversible impacts are predicted to occur at Edithvale over a period of 100 years, with model predictions indicating a similar predicted increase in the salinity of shallow* *groundwater, with and without the effect of climate change (a 0.8 metre increase in sea level and a 53 per cent reduction in recharge[10]).”*

The report concludes that with the risk mitigation measures undertaken in the infrastructure project, the saltwater intrusion impacts represent a moderate risk at Edithvale and minor risk at Bonbeach. All other risks (e.g. to foundations, groundwater users, etc.) are also mitigated to acceptable levels (Victorian Government 2017a, p.62).

A coastal-scale calculation of the groundwater-seawater (Figure 6.18) has been constructed using the DEM for the ground surface and the modelled depth to groundwater grids (as illustrated in Figure 6.7a for 0.0 SLR). The graph represents the line shown as ‘coastal x-section’ in Figure 6.11. The construction of the graph assumes a simplified Ghyben-Herzberg relation for the seawater-groundwater interface, isotropic and homogeneous properties for the unconfined (watertable) aquifer system, and hydraulic equilibrium. More importantly, the calculation assumes that the current groundwater flow towards the wetlands is maintained, as reported by Leonard (1992) and shown in Figure 6.17. If this assumption is correct, the migration of the seawater-groundwater interface is calculated as approximately 100 m landwards at 20 m depth for a 1.4 m SLR. However, if the assumption is incorrect and the watertables in the foredunes fall below sea level, then the seawater interface could migrate inland to the wetlands (up to 1,500 m).

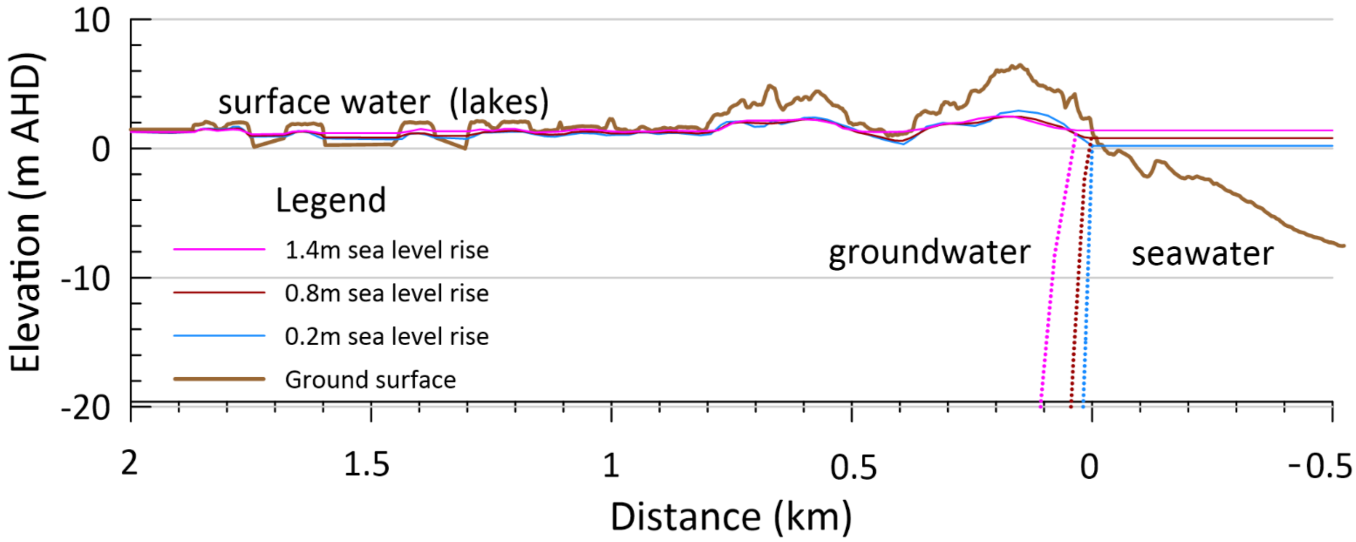

Figure 6.18: A graphical illustration of the calculated watertable[11] and migration of the seawater – groundwater interface in relation to SLR at Patterson Lakes.

Groundwater hazard due to SLR in the Mentone to Frankston sand belt region can be summarised as:

- The depth to watertable across the Mentone to Frankston sand belt is relatively shallow, the hydraulic gradient is low, and the recharge to the unconfined aquifers is dependent on rainfall.
- The predicted decreased precipitation and increased evaporation will have a small effect on the watertables, potentially lowering them by around 0.04 m over the next century.

[10] It is noted that the data sources for calculating their reduction in recharge are uncertain, but this mismatches those used in this study (Table 6.2), which predicts half that amount.

[11] Note that the watertable is not static and varies with seasons and climate. The graph does not illustrate the range of temporal fluctuation.

- The rising sea levels are predicted to have a greater impact through the landward migration of the seawater-groundwater interface. At Patterson Lakes, this is predicted as approximately 100 m inland at 20 metres depth for a 1.4 m rise in sea level. The prediction has a high degree of uncertainty.

6.3.4 The Nepean Peninsula (focus area)

Groundwater use on the Nepean Peninsula is by far the highest in the PPB region, with the area renowned for having a high density of bores, most of which are for domestic use. The area is covered by the Nepean GMA with a Permissible Consumptive Volume of 6,110 ML/yr. The Permissible Consumptive Volume applies to:

- the natural surface to 200 metres below the natural surface, or
- the natural surface to 50 metres below the base of the Quaternary Aquifer (QA), Upper Tertiary Fluvial Aquifer (UTAF) or the Lower Tertiary Basalt (LTB); whichever is the deeper.

There are currently 74 groundwater licences authorised to take and use a total of 6,109.5 ML/yr most of which is for irrigation, with only six (6) bores licensed for industrial and commercial purposes. Stock and domestic usage is not included in the licensing requirements but may be considerable during drier years. Within the Nepean GMA the estimated production value from the groundwater is $6,131,764 for urban and industrial users, $3,462,085 for agribusiness users and $3,072,313 for domestic and stock users (Southern Rural Water 2014). If the volume of water extracted from the Nepean Peninsula exceeds recharge, infiltration by sea water will occur (Harris 1976).

The groundwater system (see Figure 6.19 for location) comprises four components (Figure 6.20), which are (from uppermost to lowermost):

1. The Bridgewater Formation (barrier dunes) which is approximately 80 metres thick, loosely cemented aeolianites (reworked calcareous fossil fragments, quartz sand grains and shell fragments) interlayered with paleosols (thinner sandy layers with higher clay content) and calcrete layers (Holdgate, 1976; Leonard, 1992; Zhou et al., 1994). It provides limited quantities of groundwater for stock watering and domestic use (Shugg, 1985)
2. the Wannaeue Formation is approximately 100 metres thick (Holdgate et al., 2002; SKM, 2007), formed in a shallow marine environment and consists of sandy calcarenites, shelly sands and shelly muds and clays
3. the Brighton Group which is approximately 30 metres thick (Holdgate, 1976; SKM, 2007), and
4. the Fyansford Formation, which is around 400 metres thick (Holdgate, 1976) and acts as the basal confining bed to the groundwater system.

Three conceptual cross-sections were developed in this study for the Nepean Peninsula groundwater hazard assessment (regional, local and coastal). The regional-scale conceptual cross-section for the Nepean Peninsula groundwater systems (Figure 6.20) was built up from information in the VAF (SKM, 2012a), and modified using GHD (2011), Parsons Brinckerhoff (2010), Leonard (1992) and Holdgate et al., (2002).

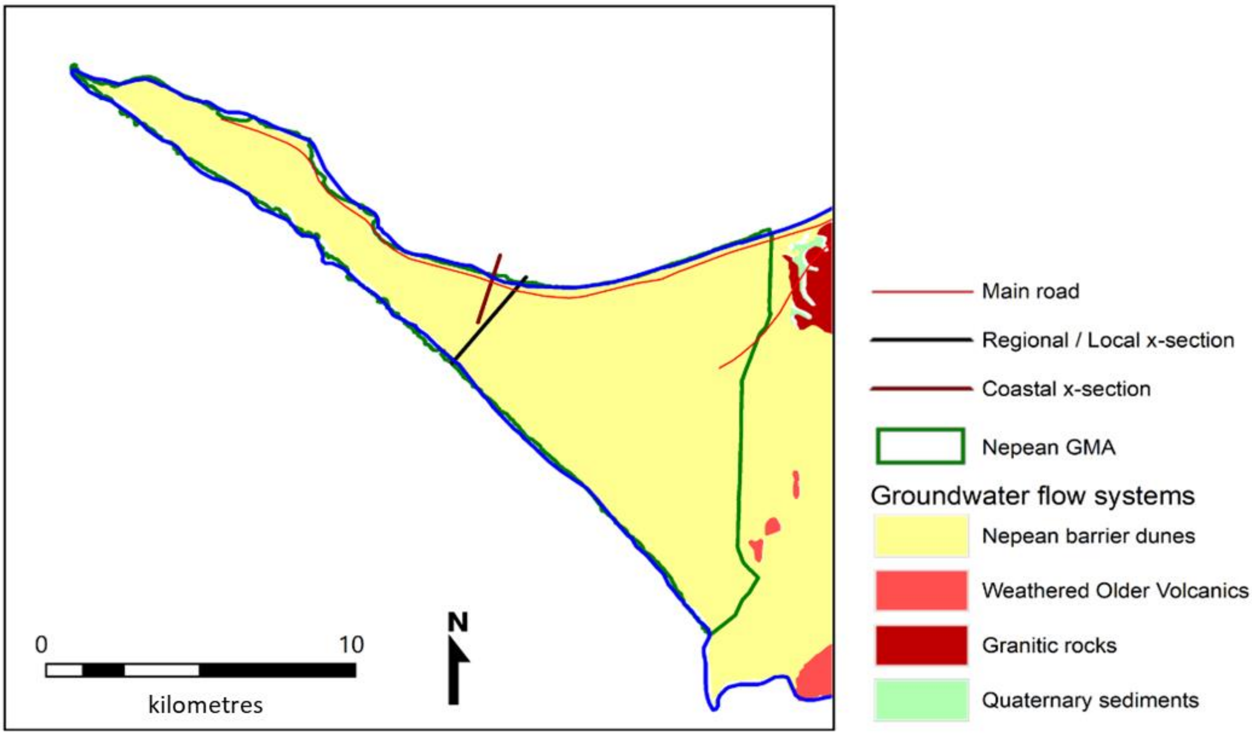

Figure 6.19: Nepean Peninsula cross-section lines and groundwater flow systems.

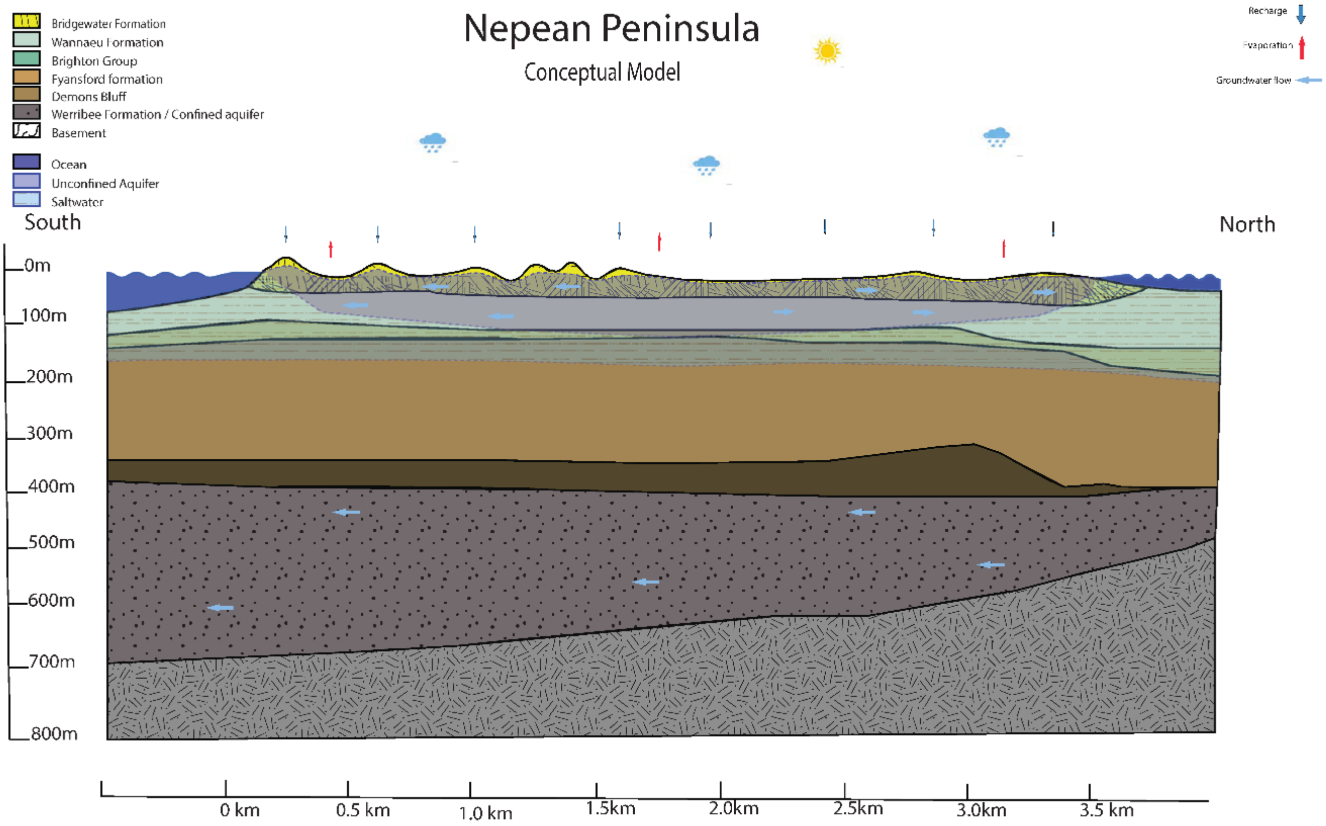

Figure 6.20: Conceptual cross-sectional model for the Nepean Peninsula groundwater systems.

A groundwater divide runs east–west along the centre of the peninsula resulting in groundwater flowing north into the bay or south into the ocean, with the Selwyn Fault to the east acting as a flow boundary (SKM 2007).

The groundwater parameters used to estimate the response of the watertable on the Nepean Peninsula to SLR and changing climates are mostly sourced from Leonard (1992). The aquifers extend across approximately 100 km^2 and holds around 2,350,000 ML, of which approximately 820,000 ML is in the top 100 metres. The specific yield in the unconfined aquifer varied from 0.15 – 0.35, with an average of 0.2 (20%). Regional hydraulic conductivities range from 5 m/d to 30 m/d, with an average of 10 m/d and hydraulic gradients are generally around 0.001 (1 in 1,000). Bore yields are commonly less than 10 L/s, but can be up to 15 L/s.

The responsiveness of the unconfined aquifer system to rainfall was investigated using the forty-year monitoring records of four bores and the rainfall records for Point Nepean (Figure 6.21). Despite a slight decline in rainfall, the long-term water levels in the bores are remarkably steady suggesting that the long-term hydrologic response is weakly correlated. This observation fits with the relatively high hydraulic conductivity and low gradient in the watertable aquifer, suggesting that rainfall recharge is efficient. The general lack of well-formed surface drainage features (such as significant streams and rivers) also fits with these observations.

Focussing on the regional section closer to the coastline, the local-scale conceptual cross-section through the unconfined aquifer on the northern side of the Peninsula is illustrated in Figure 6.22. This cross-section is based on the available bore logs that have been re-interpreted in the context of the depositional environments of the geological materials. The seawater-groundwater interface is schematic as there are no bores that provide useful data to indicate its exact position.

The groundwater response to the rising sea levels on the Nepean Peninsula is less predictable than for the other two focus areas (i.e. Werribee Delta and the Mentone – Frankston sand belt), since less data is available. However, it is logical the impact will be seen in groundwater bores close to the coast, where the inland migration of the seawater-groundwater interface will increase the likelihood of pumping saltwater to the surface.

The coastal-scale calculation of the groundwater-seawater interface is graphically illustrated in Figure 6.23). The graph represents the line shown as ‘coastal x-section’ in Figure 6.19. The construction of the cross-section assumes a simplified Ghyben-Herzberg relation for the seawater-groundwater interface, isotropic and homogeneous properties for the unconfined (watertable) aquifer system, and hydraulic equilibrium. The dune morphology makes the prediction less accurate due to the sparse data density, and it is assumed that the watertable is a subdued reflection of the topography, as would be the case with efficient recharge (Heath, 1983).

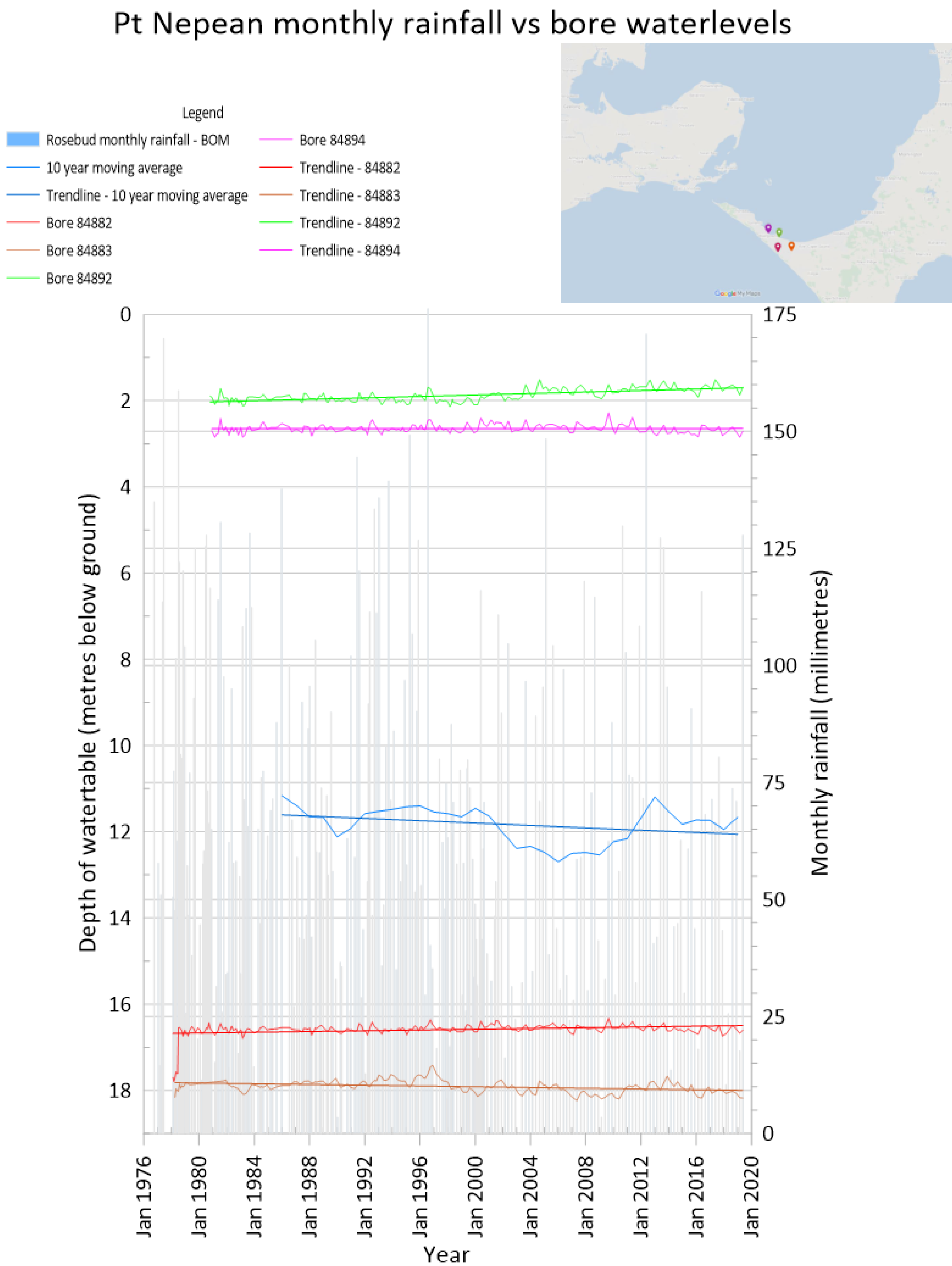

Figure 6.21: Correlation of rainfall with bore hydrographs over the past four decades, Nepean Peninsula. The locations of the colour-coded bore holes in the legend are shown in the map (top left) and the corresponding watertable depths are shown in the lower figure as colour-coded curves and trend lines with values indicated on the left axis, together with bars representing monthly rainfall totals with values indicated on the right axis.

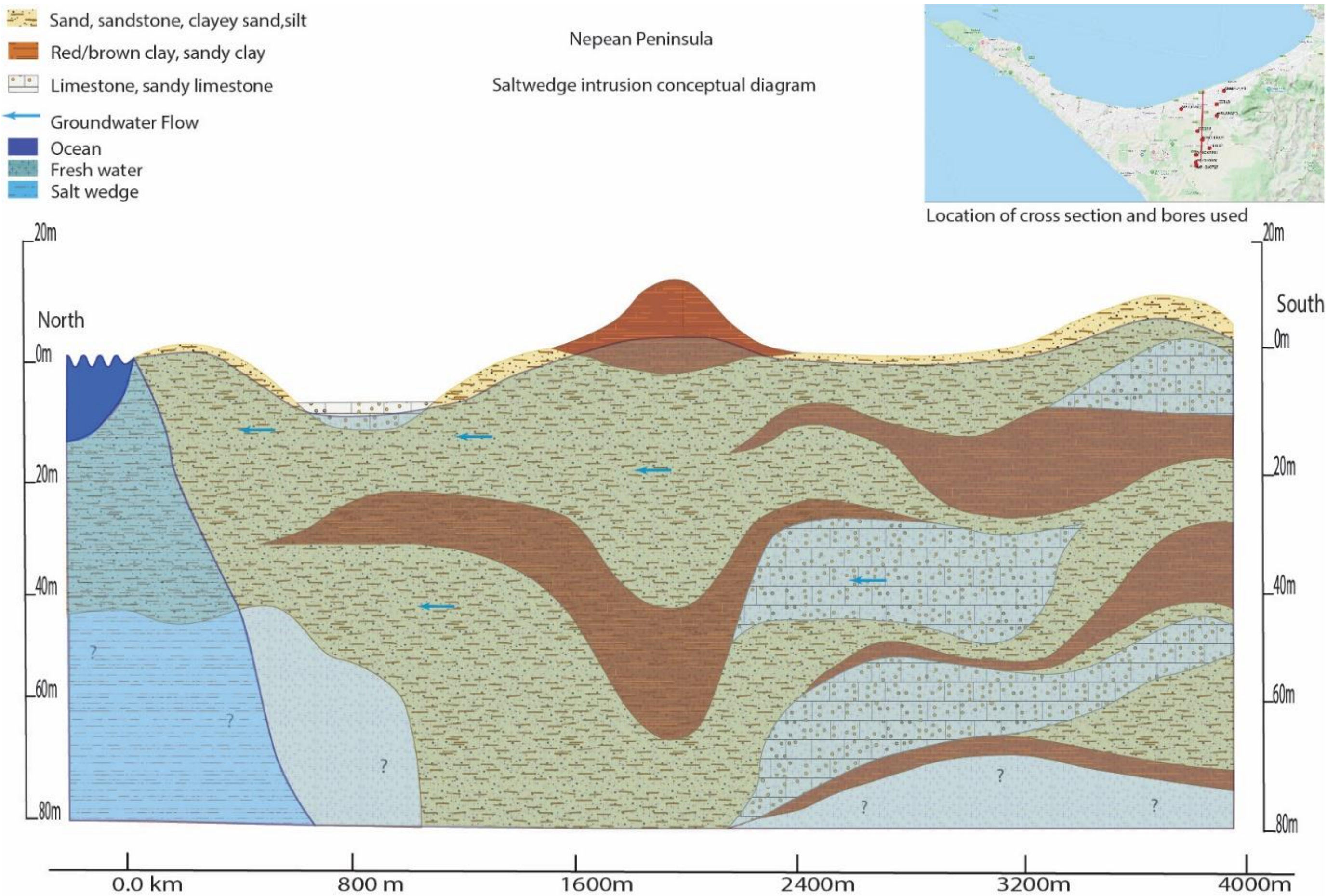

Figure 6.22: Local-scale conceptual cross-sectional model for the Nepean Peninsula unconfined groundwater systems.

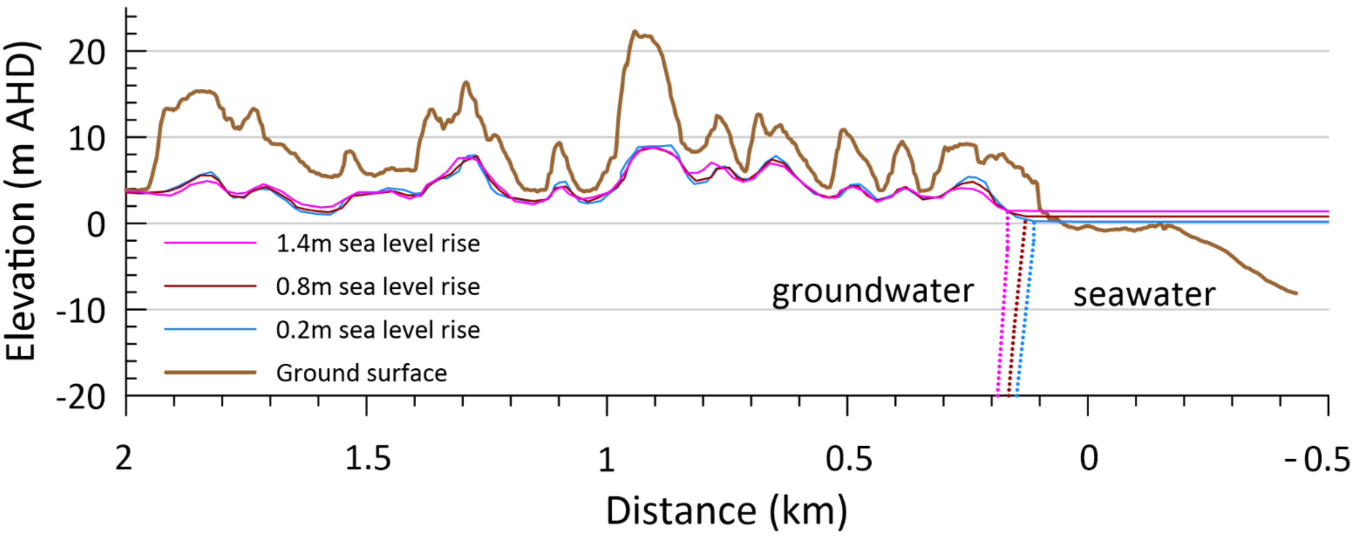

Figure 6.23: graphical illustration of the calculated watertable[12] and migration of the seawater – groundwater interface in relation to SLR at Blairgowrie.

The calculated migration of the seawater-groundwater interface for a 1.4 m SLR is around 50 m inland at 20 m depth. This can be partly attributed to the steeper shorelines and steepening hydraulic gradient of the watertable as it approaches the coastline.

Groundwater hazard due to SLR on the Nepean peninsula region can be summarised as:

---

[12] Note that the watertable is not static and varies with seasons and climate. The graph does not illustrate the range of temporal fluctuation.

- The depth to watertable across the Nepean Peninsula is relatively shallow, the hydraulic gradient is low, and the recharge to the unconfined aquifers is a significant proportion of the rainfall.
- Groundwater extraction is close to the annual permissible volume, in addition to a high density of domestic bores (that are not counted in the permissible volume).
- The predicted decreased precipitation and increased evaporation is calculated to have a relatively small effect on the watertables, potentially lowering them by around 0.04 m over the next century.
- The rising sea levels are predicted to have a greater impact especially on bores close to the coast. At Blairgowrie, the seawater-groundwater interface is predicted to migrate approximately 50 m inland at 20 metres depth for a 1.4 m rise in sea level. The prediction has a high degree of uncertainty.
- The mitigation of this hazard may eventually require a revision of the management plan for the Nepean Groundwater Management Area.

6.4 Summary of Groundwater Hazard Assessment

6.4.1 Discussion of Findings

Changes in groundwater pose several types of potential hazard. When the depth to watertable decreases due to SLR and the saline/freshwater wedge migrates further inland, this both increases the area containing shallow groundwater as well as increasing the salinity of that groundwater. The hazards therefore relate to the quality of the groundwater for domestic and commercial use as well as the hazard posed to build infrastructure that becomes more frequently exposed to the groundwater. In particular, in low-lying coastal areas such as wetlands, the rise in the watertable can lead to groundwater becoming surface water and this becomes a potential hazard for the natural environment that wetland areas support. The groundwater hazard is therefore summarised and mapped as the combination of the changes to shallow groundwater and surface water due to the applied SLR scenarios and these changes are provided in Figure 6.24. For 0.2 m SLR, the changes to shallow groundwater are mainly confined to the coastal rim of PPB, particularly the northern half of the bay, Geelong, the Bellarine Peninsula and in the south from Safety Beach to Point Nepean. Under larger scenarios of SLR such as 1.1 and 1.4 m SLR, more extensive inland migration of groundwater hazard occurs in Queenscliff, Salt Lake near St Leonards, Moolap, Avalon, the Cheetham Wetlands and Altona coastal park. In most locations, these increases in hazard area are due to the increase in surface water (see Figure 6.7).

The areas occupied by surface water and shallow, intermediate and deep groundwater shown in Figure 6.7 together with equivalent figures for the SLR scenarios that fall within the boundaries of the ten LGA's around PPB are summarised in Figure 6.25. Equivalent bar charts for individual LGA's are provided in Appendix L. At a whole-of-bay level, Figure 6.25 shows that as sea level rises the largest changes are due to the increase in area covered by surface water. The area occupied by shallow groundwater increases by between 18 and 19 km^2 for SLR scenarios of 0.2 and 0.5 m but then levels off for a SLR of 0.8 m and decreases for SLR scenarios of 1.1 and 1.4 m. This reflects that SLR is causing more shallow groundwater to become surface water than intermediate depth groundwater is becoming shallow groundwater. The area where groundwater is classified as intermediate declines incrementally with each SLR scenario with a reduction in area of 37.3 km^2 under a 1.4 m SLR as the watertable rises, leading to a larger reclassification of intermediate ground water as shallow.

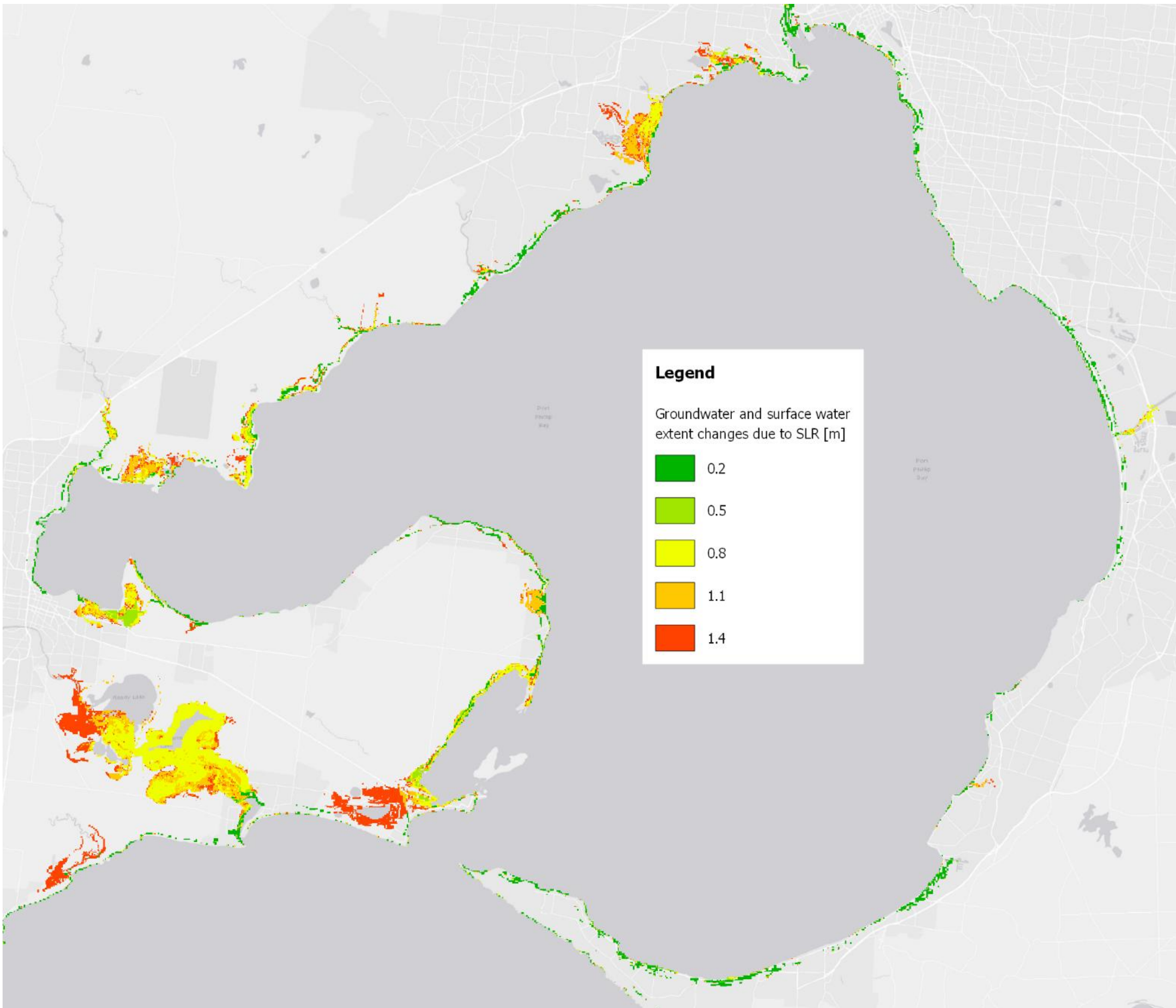

Figure 6.24: Change in groundwater hazard under the different SLR scenarios where hazard is the combination of the shallow groundwater and surface water changes.

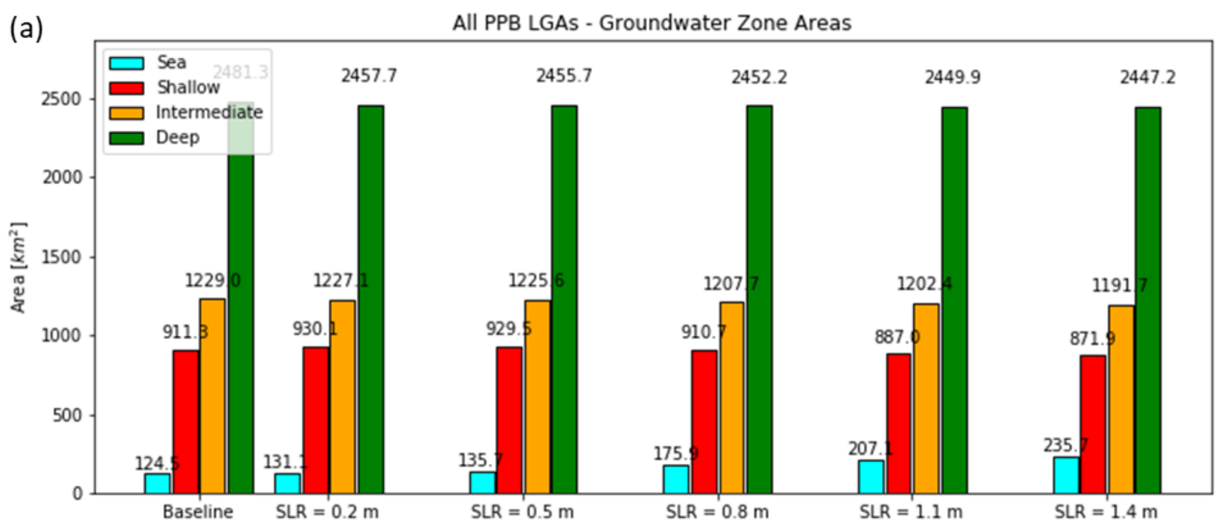

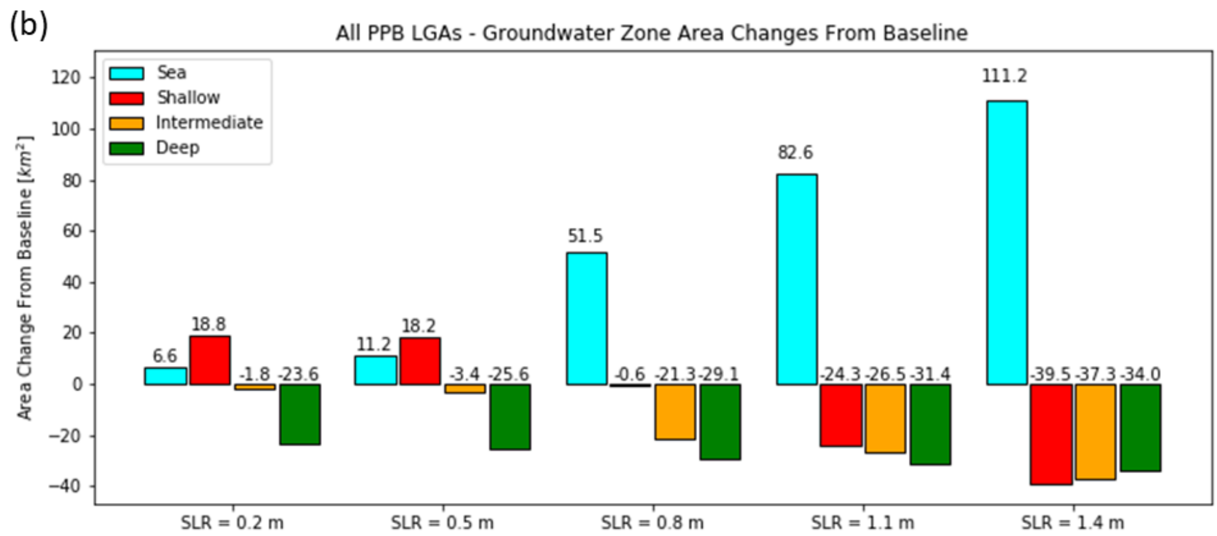

Figure 6.25: (a) Total area of surface water, shallow, intermediate and deep ground water for all PPB LGAs and (b) change to the total area of the layers under the different SLR scenarios.

6.4.2 Summary

This groundwater hazard assessment has qualitatively analysed what can happen, where in the landscape it is likely, and when it could occur (ISO 2002). While it is clear that the conceptual framework of the hydrogeology of PPB is well understood, and detailed numerical models exist at the local scale, very little quantitative research and investigation has been published on the impacts of rising sea levels on the current hydrogeology. In the absence of such investigations, the groundwater hazards associated with climate change and rising sea levels remains unable to be accurately quantified, resulting in more qualitative statements of hazard.

The evidence gathered and the conceptualisations produced for this study provide qualitative predictions that there will be permanent changes to spatial and temporal behaviour of watertables. These changes will occur in the unconfined aquifers through the inland migration of the seawater-groundwater interface. By comparison, the impact on watertable depths through decreased rainfall and increased evaporation will be less important to consider.

The rate of change to the groundwater systems varies with the hydraulic parameters of the aquifer materials and the physics of the hydrogeological systems. Where hydraulic gradients are low (flat) and the hydraulic conductivity of the materials is high (permeable), the system will take less time to reach equilibrium with the rising sea levels, reduced rainfall, and increased evapotranspiration. Evidence from some areas, such as the Ocean Grove Spit, shows an almost instant response to daily tidal fluctuations in the monitored groundwater levels (FedUniSpatial 2020a, 2020b). Yet in one case where the rate of change has been quantified (Edithvale – Bonbeach), the changes in salinity are predicted to be less than 500 mg/l over a century and the seawater-groundwater interface migration to be over millennia (Victorian Government, 2017a). With such slow and incremental changes, the risk could be easily managed in a timely fashion.

The resulting hazards will impact many of the groundwater dependent ecosystems close to the coast. The greatest impact will be on the PPB (Western Shoreline) and Bellarine Peninsula Ramsar Site (DELWP, 2018). Other wetlands along the western shoreline, including Cheetham Wetlands, Altona Coastal Park, and Jawbone Flora and Fauna Reserve will also be impacted. The changing groundwater levels and salinity will slowly impact on the wetland ecologies as illustrated by the modelled rise in coastal watertables (Figure 6.7).

It is likely that the rising watertable hazard will also impact on built assets, mainly those within a kilometre of the coast, but the rate of change will be relatively slow and perceived as similar to an urban salinity hazard associated with rising watertables (e.g. Buckland and McGhie, 2005; Nicholson et al., 2008). By comparison, the impact on groundwater used for domestic, stock watering, irrigation, commercial and industrial purposes will manifest more quickly, as the pumping may draw the migrated seawater interface upwards to the bore (known as upconing). Although the migration of the interface will likely take decades (as illustrated by the coastal cross-sections in the three focus areas), Groundwater Management Plans will require ongoing revision to mitigate the potential hazard.

7 Shoreline Data and Information

Although a shoreline hazard assessment is not presented in this study, Chapter 7 describes additional data and analysis that provides relevant foundational information for the consideration of future shoreline hazards. These are: (1) a coastal geomorphic analysis to classify the coastline in terms of its backshore and intertidal characteristics to inform the appropriate method for estimating erosion hazard and; (2) the identification of the coastal vegetation lines in historical photogrammetry from which long term historical shoreline movement is assessed; (3) sediment samples of PPB beaches; and (4) digitised shoreline surveys.

7.1 Introduction

Shoreline change depends on processes that operate on different time and space scales. These include short-term processes associated with the erosion and recovery from extreme events, and longer-term processes that cause shoreline recession (or accretion) over several years to decades. The longer-term can be based on observed historical shoreline change and modelled future recession that will occur due to SLR.

As discussed in Chapter 2, historical shoreline change is likely to have occurred due to a combination of factors, which include local geomorphology, natural climate variability, severe storms, and long-term trends due to natural processes that affect sediment supply. For the densely populated PPB coast, historic shoreline change is also influenced by human factors such as development pressure, coastal management interventions (e.g. building seawalls, beach renourishment) and SLR due to global warming. In this chapter data sets that provide relevant information on the shoreline in PPB are presented.

7.2 Shoreline Data

7.2.1 Coastal Compartment Analysis

Coastal compartment analysis was undertaken to quantify the coastal landforms for all of PPB, which provides a foundation for future efforts to calculate the likely coastal erosion hazard extents under current and future SLR, for which information is required on:

- The composition of the landform: defined by the coastal geomorphic sectors, CGS (similar to the approach adopted in *Smartline* (Sharples et al, 2009)
- Wave climate & extreme events: (see Chapter 8)
- Knowledge of the sediment budget: (assessed through analysis of the sediment transport processes, aerial imagery analysis and storm erosion calculations)

The identification of discrete landform components inside Port Phillip is based on intertidal and backshore morphology—defined as Coastal Geomorphic Sectors (CGS).

A previous study (Rosengren 2017) showed that 14 broad coastal landforms (Coastal Geomorphic Categories - CGC - see Figure 7.1) re-occur in Port Phillip. Each CGC has a limited range of backshore geology, elevation, slope and intertidal composition. A key difference between each category is the response to changed water levels and wave energy. Spatial grouping of the 14 CGCs allowed 48 Coastal Geomorphic Units (CGU) to be recognised around the bay. Here, using terrestrial and bathymetric LiDAR, high resolution aerial photography (Nearmap 2018-2019), experience from prior field-based studies, and ground and aerial inspection of the entire coastline in May - June 2019, Port Phillip was divided into 528 CGS (Figure 7.2). Table 7.1 summarises the backshore, nearshore and intertidal landform characteristics that are used to define the CGS and Appendix D describes and illustrates the key geomorphological terms used in this report. Although the majority of the coastline (290 CGS's) contain a beach, these beaches have a variety of backshore features ranging from engineered structures to cliffs. Cliffs are the next most common shoreline type accounting for 92 CGS's. The CGS's are discussed in more detail in Section 7.2.2.

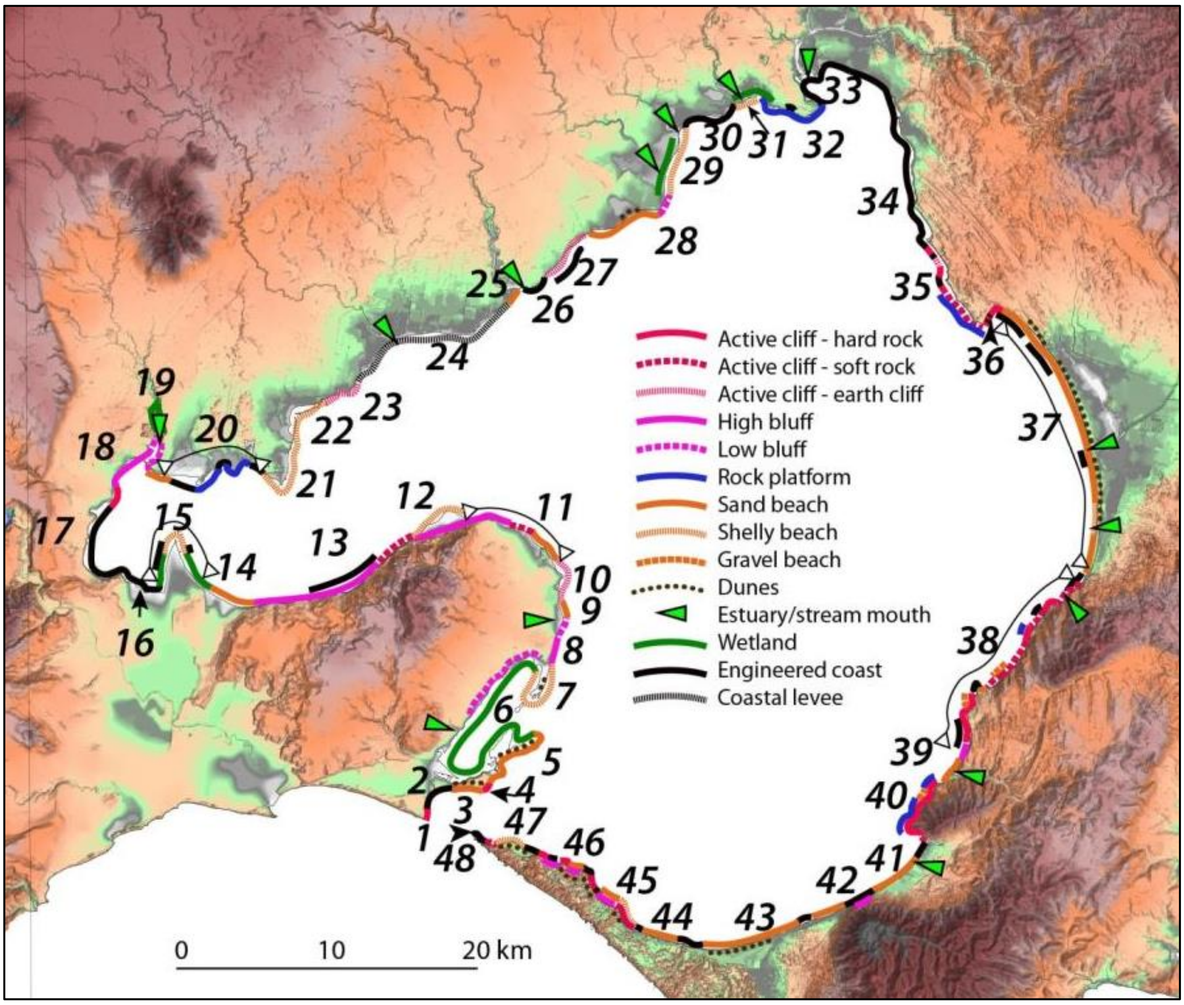

Figure 7.1: The 14 CGC's used to define the 48 CGU's for Port Phillip (Rosengren 2017).

Table 7.1: The variants of the 14 coastal geomorphic categories of Port Phillip Bay (Figure 6.1) used to define the 528 coastal geomorphic sectors.

BACKSHORE	Variants	SHORE ZONE (Intertidal)	Variants
Coastal Cliffs	Hard Rock Soft Rock Regolith	Beach, shore platform	Gravel, sand, shell, mud
Bluffs	High Low	Beach, shore platform	Gravel, sand, shell, mud
Sand Ridges	Foredunes Wave aligned Aeolian	Beach	Sand, shell
Estuaries	Open Intermittently closed	Beach	Sand, mud
Coastal Wetlands (not associated with estuary)	Saline Brackish Fresh	Beach	Sand, mud
Engineered	Effective/Professional Ineffective (informal)	Beach, shore platform	Gravel, sand, shell, mud

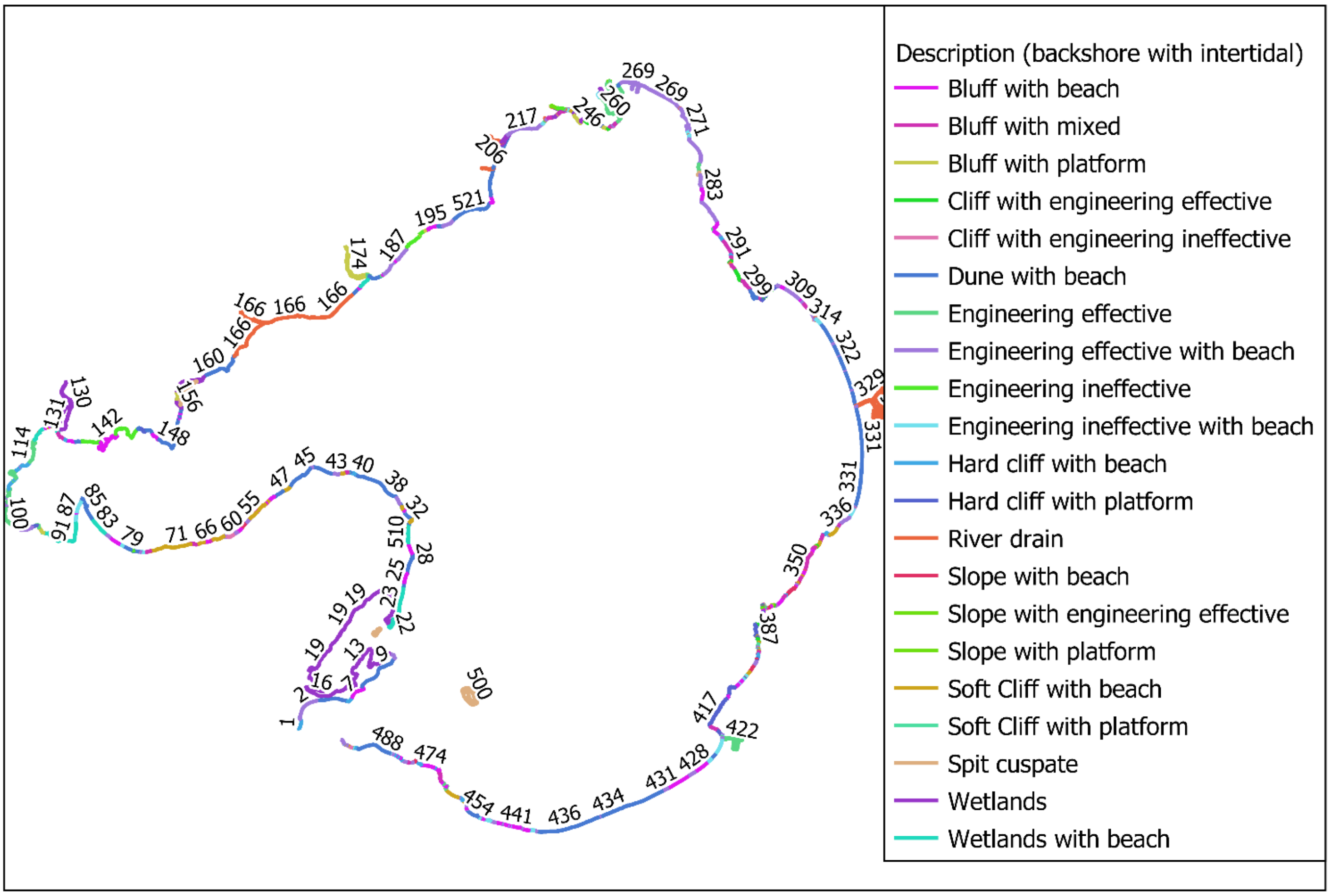

Figure 7.2: Geomorphic sectors for the PPB coast coloured by backshore resistance including the numbers of some coastal sectors indicated (note that while sector numbering generally proceeds clockwise around the bay, values above 500 were derived when a CGS was subsequently split on the basis of the historical shoreline analysis indicating both erosion and accretion within a CGS).

7.2.2 Sediment Surveys, Sampling and Analysis

Beaches occur in a variety of coastal settings around Port Phillip (Figure 7.3) and were sub-divided into types according to grain size and composition (gravel, sand, mudflat, shell), thickness and mode of occurrence (e.g. beach to below low water mark, platform beach and so on. Sediment size and composition varies cross-shore, alongshore and vertically along a beach as well as seasonally, annually or over the longer term. The sweep zone—the area between the highest and lowest beach elevation along a given profile between the backshore and the point of closure offshore—is relatively narrow in PPB compared with ocean or high energy beaches, hence the potential for vertical sediment variation is reduced.

Analysis of sediment and beach nourishment data were used with the longshore sediment transport modelling to help understand sediment movements and particularly sediment deficits along sections of the PPB coastline. In this project sediment data was collated from ten reports on beach nourishment projects around PPB and their associated data combined into a database which includes the sample location and D50. In total, 175 sample locations were identified (Appendix F). Appendix F also summarises the various beach nourishment projects as detailed in Cardno (2017), which provides the sand grain size details for renourishment.

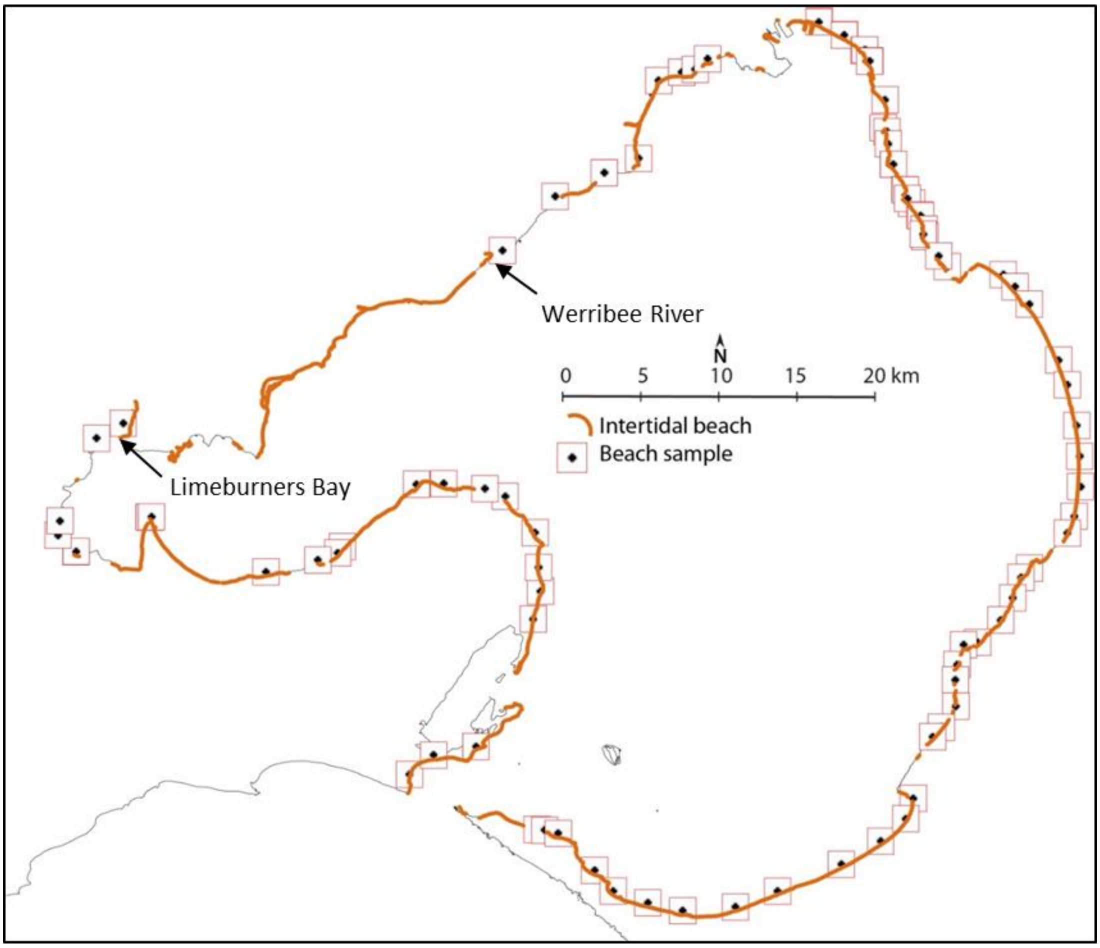

Figure 7.3: Occurrence of beaches (all types) and sand sample locations June 2019.

To supplement the sediment data from these previous studies, 94 beach sites around PPB (Figure 7.3) were visited over seven days from 24 - 30 June 2019 to collect beach sand samples. Sites were selected to be representative of a CGU or a group of CGUs with similar geomorphic characteristics. A total of 107 points were sampled at the 94 beaches. Constraints on site access due to management or ownership restricted the sample points between Limeburners Bay and the mouth of the Werribee River. This is a region of low-lying land with limited intertidal beach material and much of the backshore has a variety of engineered and informal defensive structures. Details of the sediment sampling methodology and analysis can be found in Appendix F.

An overview of the sediment size distribution (based on D50) across PPB is provided in Figure 7.4. Since these categorizations are broad, Figure 7.4, provides a more detailed breakdown of the D50 particle size categorizations, while Appendix E (Figures F3-F10) provide cumulative distributions of the particle sizes and additional figures of the sediment grain size are presented in Appendix F (see Figures F12 and F13). A shapefile of the dataset has been incorporated in the DSS.

On the Bellarine coast, the samples taken from Point Lonsdale to Queenscliff sites are much finer than the rest of the Bellarine samples collected for this study, with a typical D50 of around 0.21 mm (fine/medium sand), compared to 0.5 to 0.9 mm (medium/coarse sand) for locations further north (see also Figure F3). However, these finer sediments are similar in size to those samples collected previously across the Great Sands and for sites along the Nepean Peninsula, from Macrae towards Sorrento.

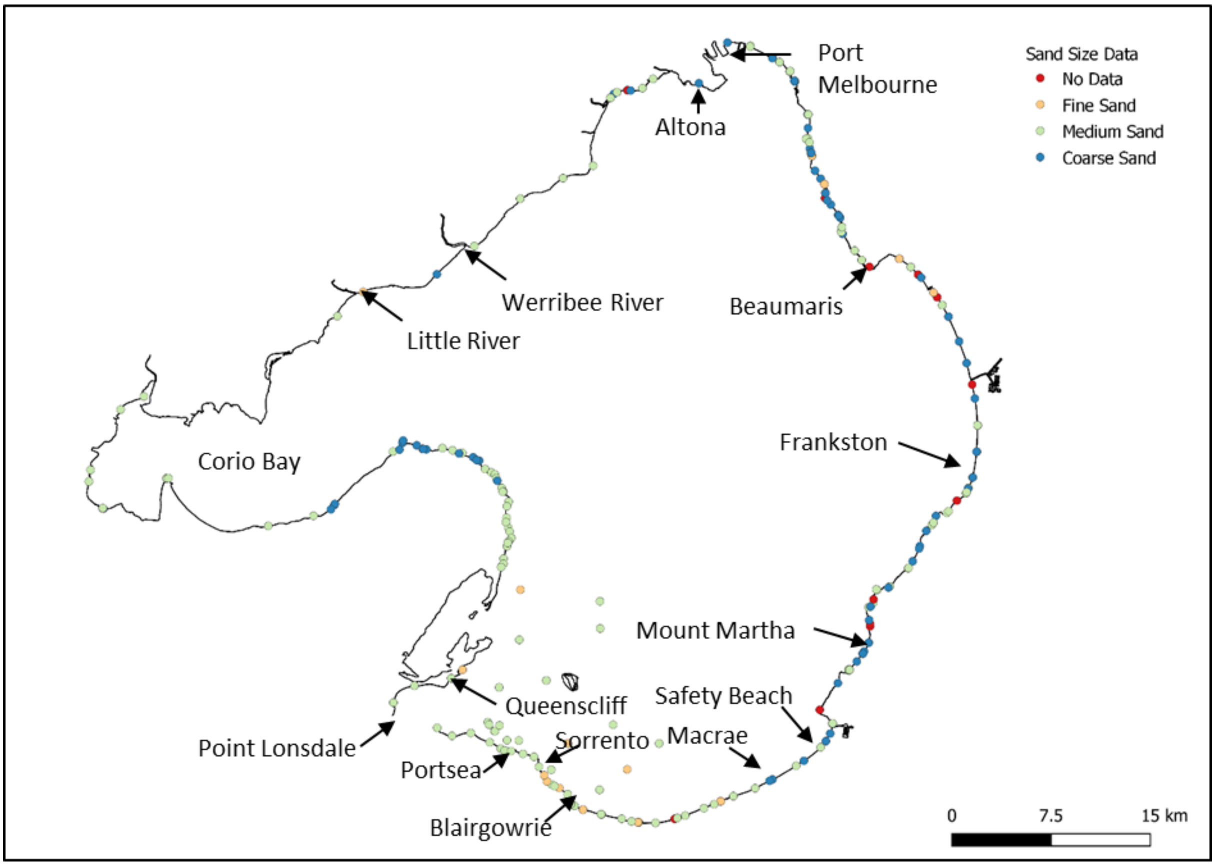

Figure 7.4: Sediment size distribution across PPB.

Within Corio Bay samples exhibited a wider range of sediment size distributions, particularly in the silt size range (< 0.06 mm). This likely reflects the low wave and current energy environment in Corio Bay. Although the D50 typically falls within the medium sand range the distribution in D50 values were much broader than elsewhere within PPB (Figure F4). There is increasingly limited sediment supply to form beaches alongshore from south of the Werribee River indicating that Little River and the Werribee River are not sources of sediment to build wide beaches on the western side of the bay. The distribution of sediments in areas south of Altona beach tended to be finer, while the beaches at Altona are coarser due to renourishment (Appendix Figure F5, Table F1).

The coastline from Port Melbourne to Beaumaris (Figure 7.4 and Appendix Figure F6) is complex in terms of sediment sizes, as many of the beaches along this section have been renourished (Appendix Table F1). Within sheltered areas such as the Sandringham Boat Harbour, finer sediments are present however most of the sand falls within the medium to coarse range.

As with the coastline to the north of the bay, sediments from Mentone to Frankston (Figure 7.5 and Appendix Figure F7) are typically in the medium to coarse sand range with many of the beaches being renourished at various times since the 1970's (Appendix Table E1).

Further south, from Frankston to Mt Martha (Figure 7.5 and Appendix Figure F8), the sediments tended to be coarser with many beaches having a D50 within the coarse sand range. The beaches tended to be short and bounded by headlands, with sediment movement contained within their individual compartments. There is only limited, if any, net sediment movement to the north or south.

Beach sediments between Safety Beach and Blairgowrie (Figure 7.5 and Appendix Figure F9) show a decreasing D50 from north to south. The coarser sediments are present from around Martha Cove while finer materials are found south towards Sorrento. The finer materials are similar in size to the sands found in the Great Sands. This would indicate some potential transport of sand from the Great Sands into this southern section. This limit to northward sediment transport coincides with the closest point of the main shipping channel to the eastern shoreline of PPB.

From Sorrento to Portsea the beach sediments collected for this study are generally medium sand size, with a D50 around 0.4-0.6 mm (Figure 7.5 and Appendix Figure F10). Data from previous sampling, has shown similar sized sand although with finer material generally offshore and for locations west of Portsea.

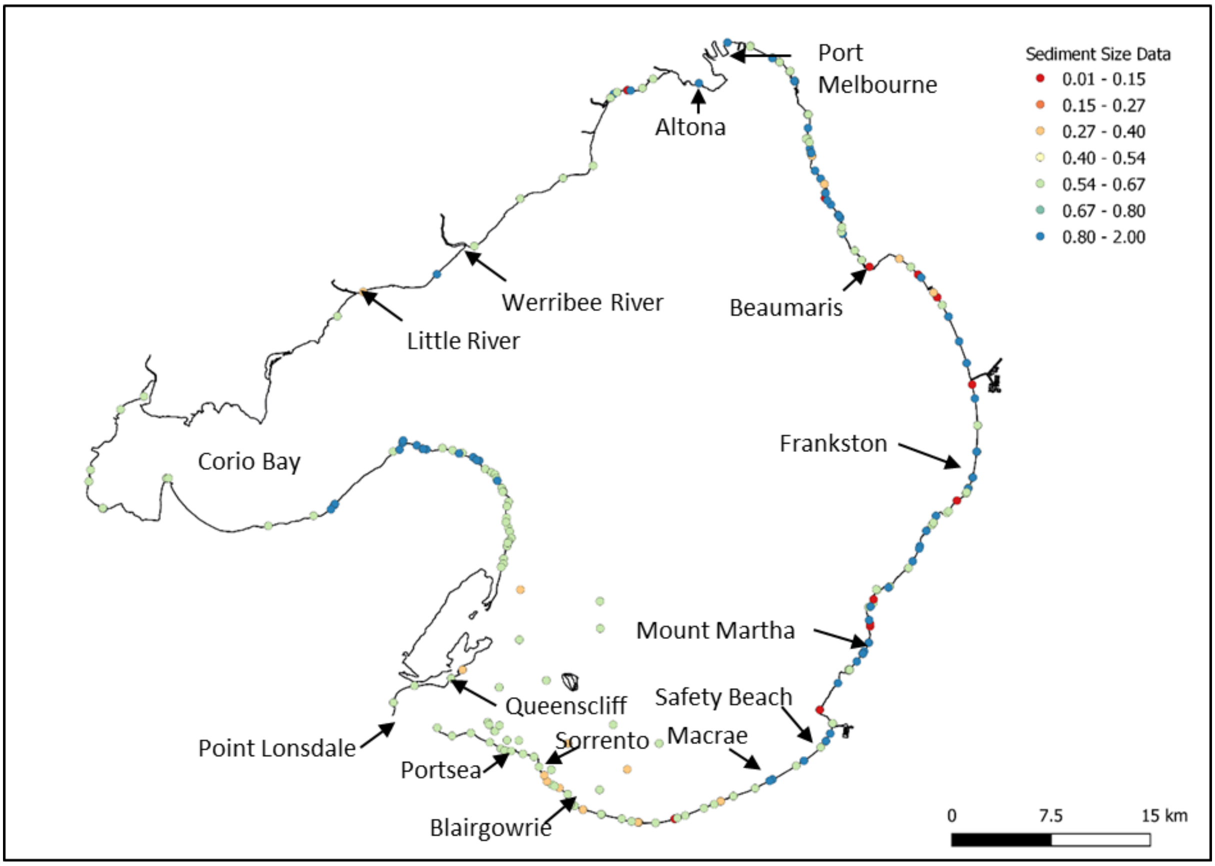

Figure 7.5: Sediment size distribution across PPB.

7.2.3 LiDAR Surveys

LiDAR surveys were conducted from November 2008 to April 2009 (Sinclair and Quadros, 2010) (Figure 7.6a) and between November 2017 and October 2018 (Figure 7.6b). These data were used to estimate shoreline profiles and the location of the toe and crest of bluffs and cliffs, the cliff slope and assess if and how the locations of these features have altered over the 10-year time span in locations where the datasets overlapped. Note that the LiDAR data collected in 2018 was not available for Geelong and the Bellarine coast.

(a) (b)

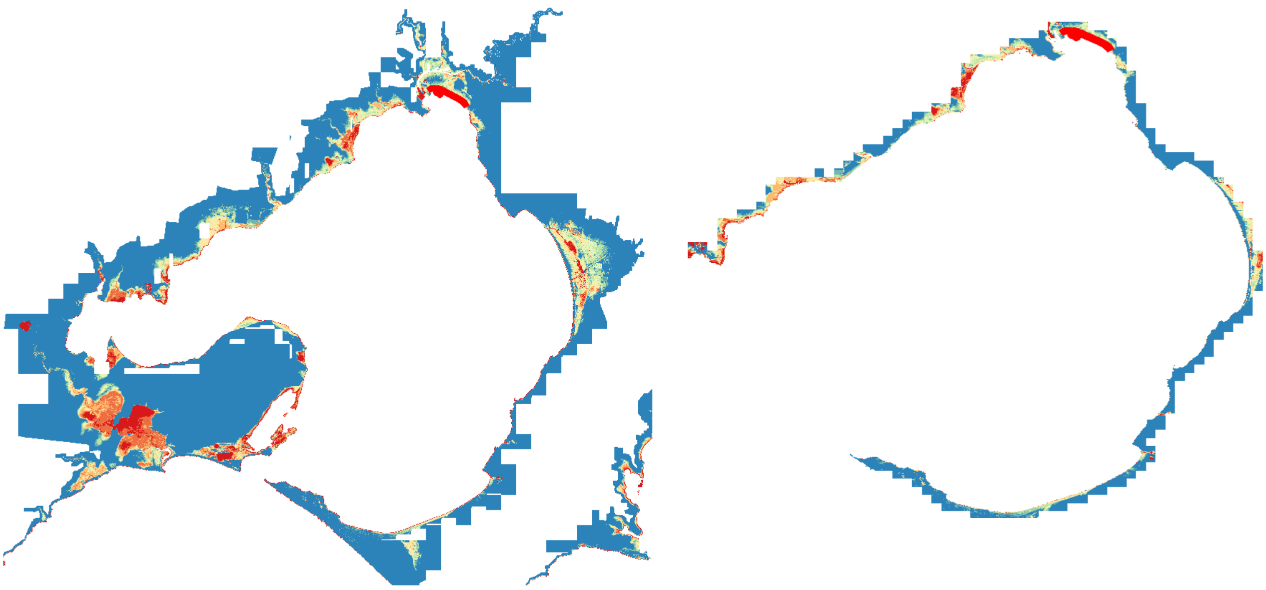

Figure 7.6: LiDAR survey coverage for (a) 2009 and (b) 2018. Elevations vary from 0 m (red) up to 3 m (blue). Elevations above 3 m are shaded in blue to indicate the landward extent of the survey.

7.2.4 Beach Profile Surveys

A series of shoreline surveys was carried out by Port of Melbourne Authority during the 1980's at 27 locations in PPB. The surveyed locations, described in MAFRI (1996), are presented in Table 7.2. Although the survey data were available in digital form, the locations where the surveys were undertaken were provided as maps in pdf documents. A procedure for digitising these maps using student volunteers was developed as described in Appendix G. The digitised survey locations around the bay are shown in Figure 7.7 and these data were used for estimating beach slope in the shoreline hazard assessment.

Table 7.2: Summary of beach profile data for which detailed survey maps were available.

Site	Location	No. of surveys	Period of data collection			Comments
			Start	End	Years	
Altona	Sargood St to Mount St	7	19/12/83	07/12/86	3	
Altona	Pier St to Webb St	2	15/09/88	09/12/88	0.24	Short record
Aspendale	Mordialloc Creek to the Esplanade	7	22/02/82	07/07/87	5	
Blairgowrie	Hughes Rd	7	04/07/83	24/02/88	5	2 profile locations
Black Rock	Balcombe Rd to Surf Ave	6	24/07/84	07/03/85	0.62	Short record
Brighton	Green Point to Holyrood St	2	15/05/87	19/06/87	0.1	Short record
Brighton	Park St to Were St	10	18/02/83	21/05/90	7	
Chelsea	The Esplanade to Williams Grove	3	11/08/86	22/09/87	1	
Elwood	Glenhuntly Rd to Cole St	9	25/05/82	13/11/90	8	
Frankston	Jetty Rd to Somme Ave	3	15/05/86	16/06/87	1	
Mentone	Charman Rd to Warrigal Rd	5	09/11/81	02/02/84	2	
Mentone	Charman Rd to Monaco St	3	02/02/87	08/08/90	4	
Middle Park	Mills St to Langridge St	6	26/04/82	26/10/84	3	
Mornington	Mothers Beach	8	24/08/83	03/06/87	4	2 profile locations
Mornington	Fishermans Beach	8	08/09/83	23/10/87	4	
Parkdale	Monaco St to Owen St	10	19/11/81	18/09/90	9	
Portarlington	Sailing Club	2	26/02/86	20/11/86	0.73	Short record
Portarlington	Sproat St to Boat Ramp	3	07/10/86	06/11/87	1	
Portarlington	West of Pier to Caravan Park	2	07/10/86	21/11/86	0.13	Short record
Portarlington	Western Park	3	07/10/86	29/10/87	1	
Portsea	Shelly Beach	3	04/03/87	24/02/88	1	
Rosebud	Chinamans Creek to Third Ave	5	20/06/85	05/11/87	2	
Rye East	Jetty to Daly Ave	5	09/06/82	07/11/84	2	
Seaford	Patterson River to Seaford Jetty	4	15/10/84	14/10/87	3	
Sorrento	Between Jetty and SC	5	28/04/82	11/10/84	2	
Watkins Bay, Beaumaris	Reserve Rd to Dalgetty Rd	9	17/07/84	15/06/88	4	
Williamstown	Victoria St to Giffard St	8	21/04/82	16/06/88	6	

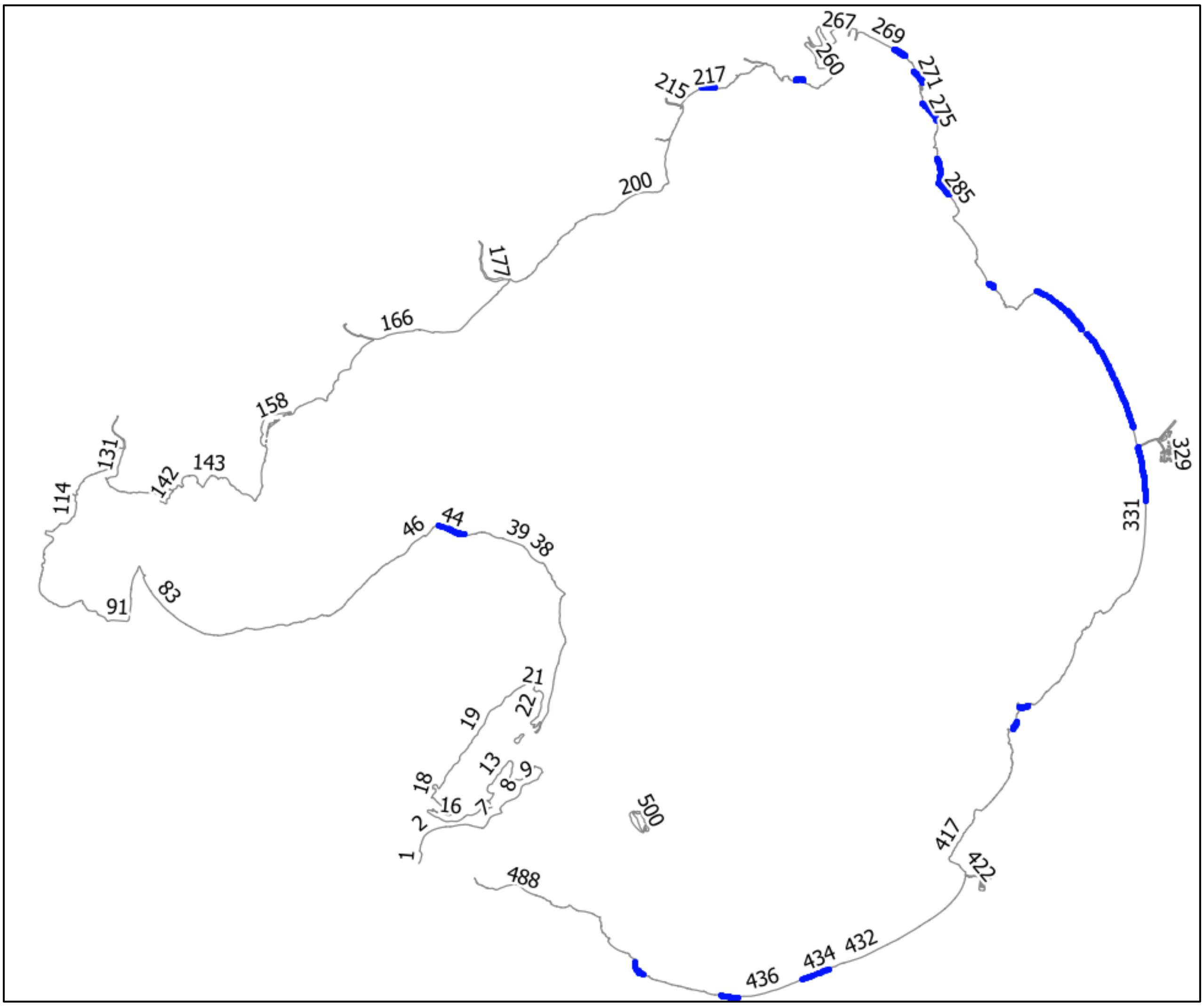

Figure 7.7: Blue lines indicate sections of coast where the 1980's shoreline profiles were collected. These have been digitised for estimating beach slope in the shoreline hazard assessment. Numbers are examples of Coastal Geomorphic Sectors.

7.2.5 Coastal Protection Structures

The coastal protective structures dataset derived from aerial photography as part of the Coordination Image Program (CIP) provides information on 873 coastal protection structures in a GIS shapefile database for PPB (Figure 7.8). Each structure's polylines were traced from aerial images and identified for asset type, e.g. seawall, groyne or breakwater (Figure 7.8). The database has attributes determined by site inspections that include details of height (i.e. reduced levels or RL in AHD), length, material, face slope. The structure attributes inform the landward limit of the coastline change hazard zones when the structure is deemed effective (Appendix E). Site inspection was conducted to identify if engineered structures including breakwaters, revetments, seawalls, and renourished beaches, were considered professionally designed and built to engineering standards appropriate for conditions at the site. If so, they were deemed as engineered effective. Structures that appear not to be built to professional engineering standards and/or were inadequate for the present conditions or in poor physical condition, were deemed engineering ineffective (See Appendix E).

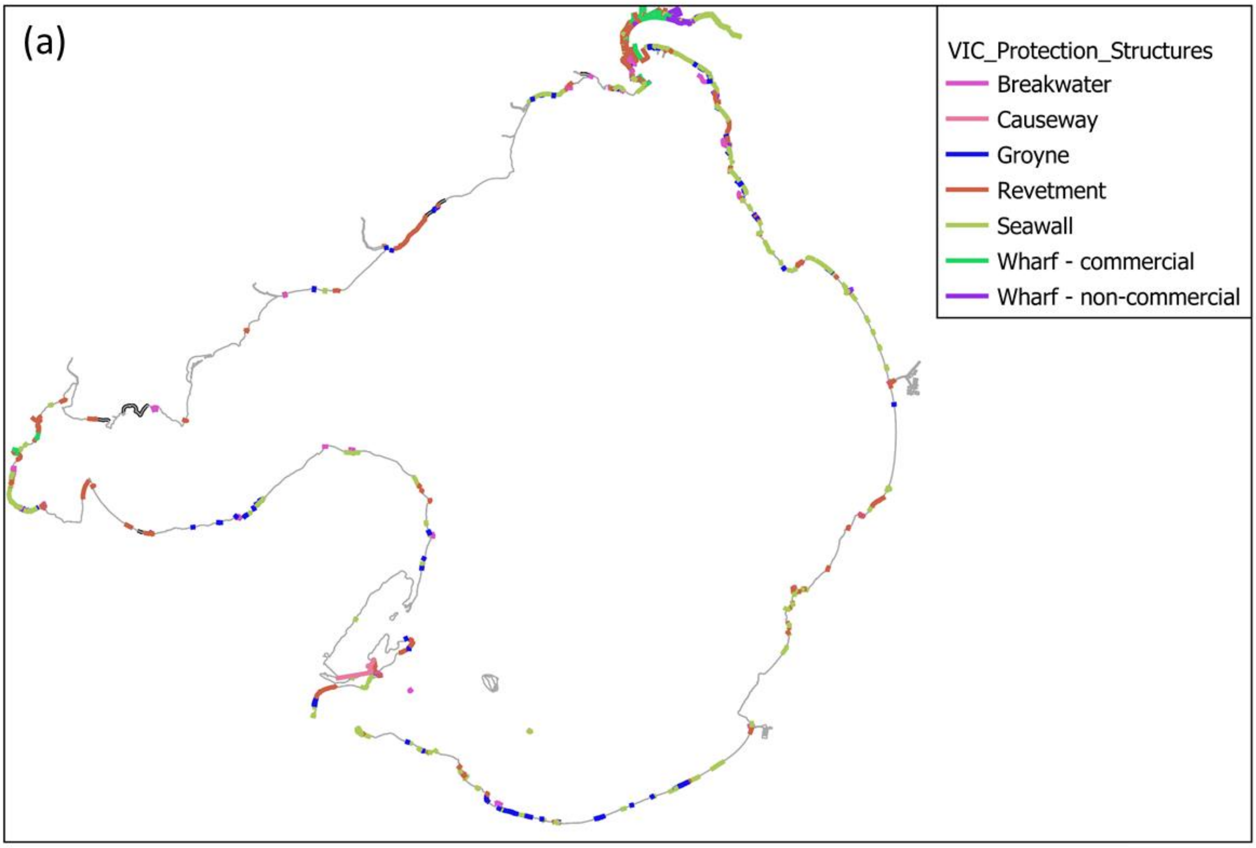

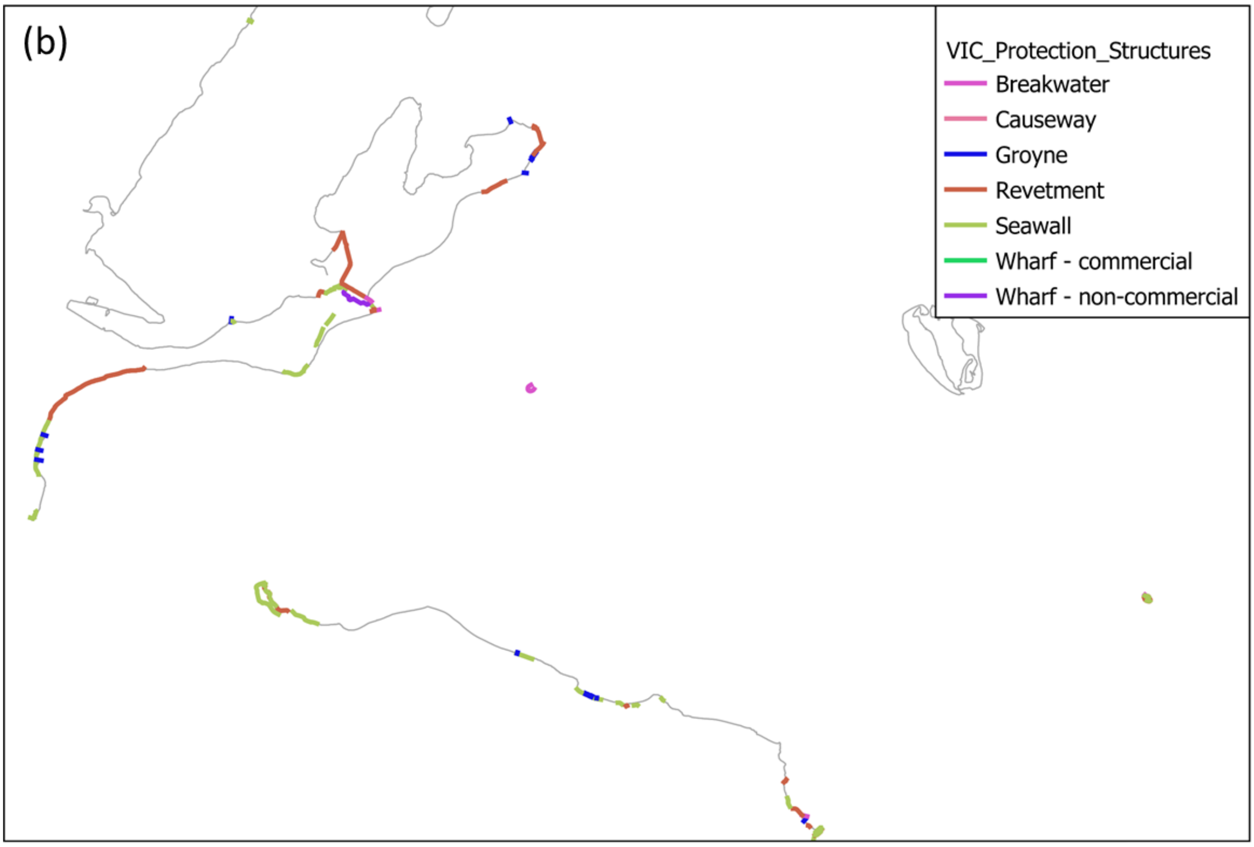

Figure 7.8: Coastal protection database. (a) all of bay, (b) zoomed into Queenscliff and Pt Lonsdale. From file "VIC_Protection_Structures_Condition_Attributes_13Jan2013_Port_Phillip_Bay_GDA94.shp".

7.2.6 Aerial Photogrammetry and Shoreline Change Analysis

As shorelines erode and accrete from storm and seasonal influences, the vegetation line gradually responds and migrates landwards and seawards, therefore the position of the vegetation line provides a useful measure of the long-term shoreline erosion and accretion over time. Here the assumption is that the long-term beach width (measured from the shoreline to the vegetation line) remains constant, because it is unknown if beaches will flatten and become wider or will steepen and become narrow.

As part of DELWP's Coordinated Imagery Program project, scanned historical aerial photographs that dated back to the 1930's along the coastline of PPB were orthorectified to create photo mosaics over seven decadal epochs from the 1930's to the 1990's inclusive. These were combined with more recent orthorectified imagery from 2000 onwards. The images were provided on 344 tiles around PPB as shown in Figure 7.9. The vegetation line is usually readily visible on the photos and so these images were used to identify how the coastline has changed over the decades. The type of imagery varied over different intervals with red, green, blue (RGB) and near-infrared bands (NIR) available for the 2018 images, RGB for the 1968 to 2017 images and black and white raster images for 1930 to 1966. The image resolution also varied depending on the optical sensors, the system of acquisition and the adopted platforms. The various spatial resolutions included 6, 8, 10, 15, 16, 20, 24, 35, 52, 100 and 125 cm. A total of 11,809 images were available across all times and tiles. The imagery was used to undertake an analysis of the vegetation line movement for input into the shoreline erosion hazard assessment.

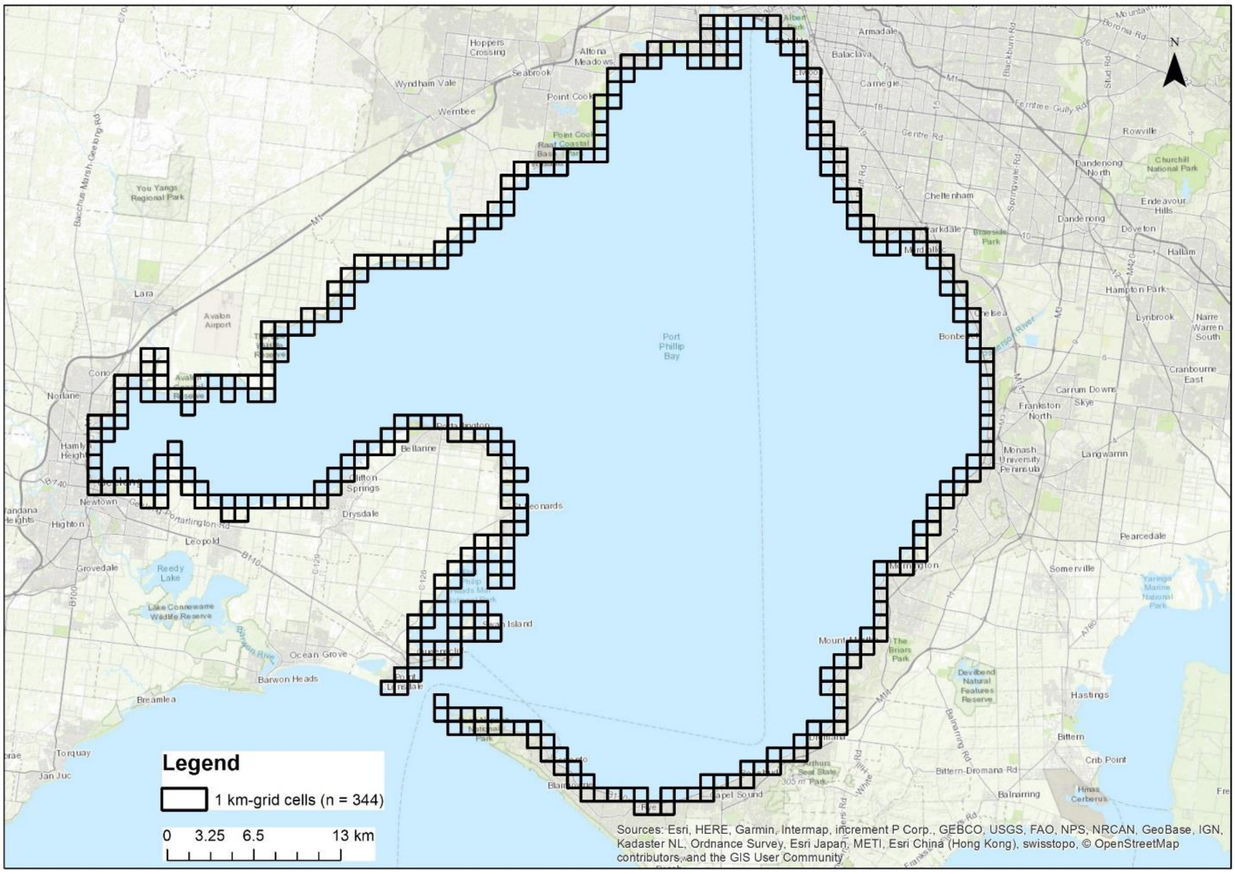

Figure 7.9: The 344 1-km image tiles around PPB.

An investigation of the efficacy of undertaking unsupervised classifications with the mixed imagery was undertaken (Appendix H). It was found that to have a consistent analysis across the 70 or so years, all tiled images needed to be converted from multiband to match the 1940s single band greyscale images and resolution. Colour balancing and matching between frames was undertaken where possible to ensure seamless variation across photo frames. Resampling of the images was undertaken (e.g., upscaling and downscaling) onto a grid with 50 cm resolution using the nearest neighbour interpolation (Sibson, 1981) to keep the pixel size consistent. Following that, the total-variation denoising algorithm (Chambolle, 2004) was applied to minimize the total variation of the image. Due to the limitation in ground truth data for training and validation, an unsupervised classification using the K Means clustering was performed (Pelleg and Moore, 1999). K was defined using 6 clusters to distinguish objects that have different intensity at given bands. These classes are listed from lowest to highest reflection as follows:

- deepwater/shadows
- shrubs/trees
- shallow water
- sealed road/darker colour built-up area
- lighter colour built-up area/lawn/low grass, and
- sandy beach/bare soil/unsealed road/bright colour rooftops

For each coastal compartment, the classified tiles were mosaicked into a single year raster image and for each of these rasters, a contour that surrounded the classifications was extracted to create a vector polyline. The next step involved extracting the vector line associated with the vegetation line. At 20 m intervals along the 2009 shoreline, a rectangular buffer zone extending inland from the shoreline was created (Figure 7.10) and the area seaward of its intersection with the classification vector polyline was divided by the width of the rectangle (20 m) to determine the average distance from the 2009 shoreline to the classification polyline over the 20 m interval.

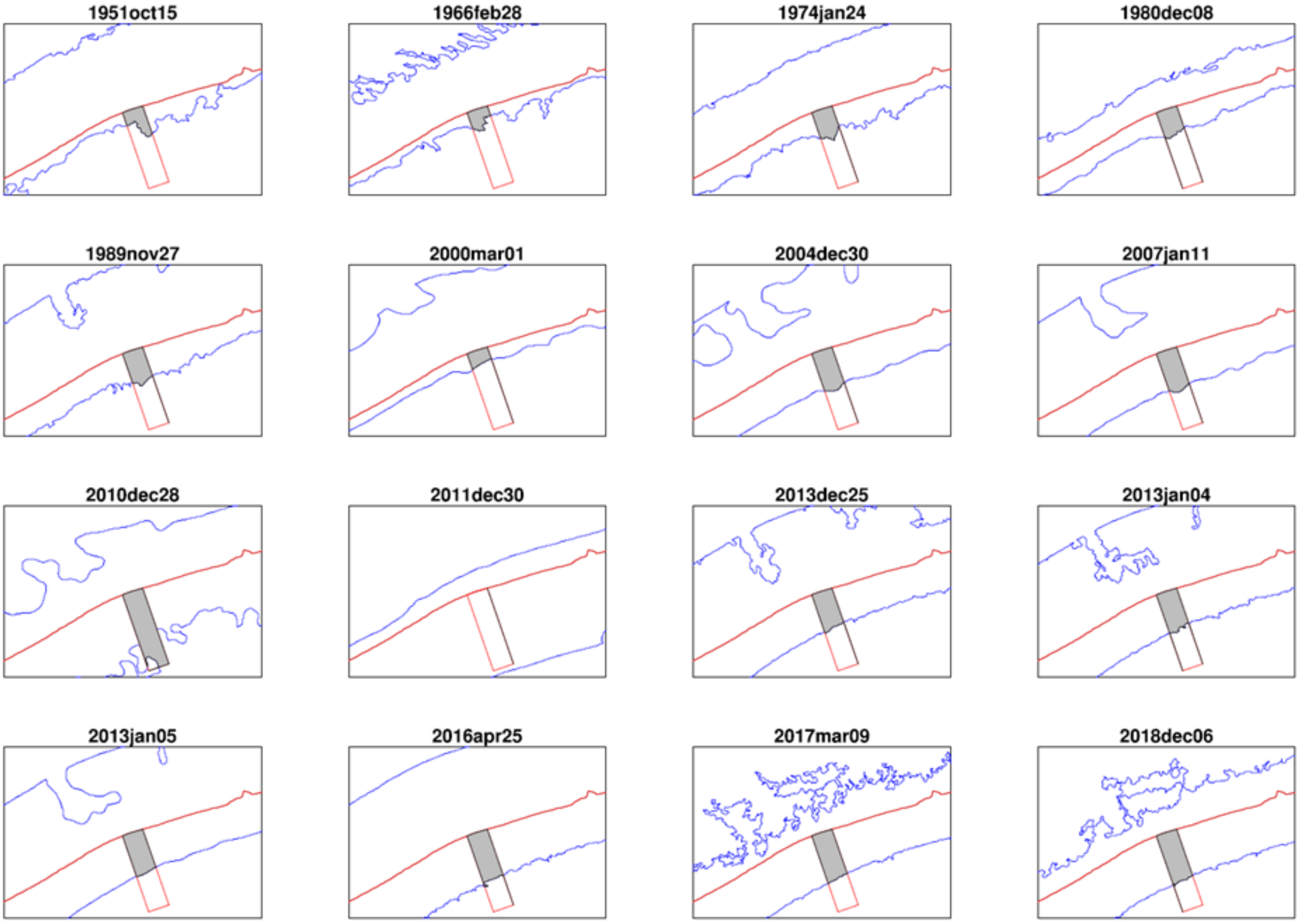

Figure 7.10: Vegetation line detection method for all available years for Point Nepean. The thin red line is the 2009 shoreline, blue line is the classification vector polyline surrounding the beach with the seaward limit in the top left and landward limit (vegetation line) bottom right of each tile, the red box is the rectangular buffer zone and the grey area is used to calculate the average distance from the shoreline to the classification polyline over the 20 m interval. The blue line on the landward side of the grey shaded area was stored as the vegetation line. Labels are the date for each image used from the available files.

These distances were then used to calculate the vegetation line movement over time to approximate the long-term change in the shoreline over the entire aerial survey period. The requirement for clear cloudless skies for the aerial surveys meant that the majority of the aerial image surveys were conducted in the summer months. Therefore, the surveys were too sparse to resolve a seasonal signal of variability. To estimate the vegetation line trend, the date of each image was regressed against the average distance from the 2009 shoreline to the classification polyline, to determine the offset to the shoreline in 2009 and the rate of change of the coastline per year from 2009. Outlier values, which were less than or greater than twice the standard deviation of the residual model fit, were removed and a second regression was made. Therefore, the linear model for the observed coastline position (CP_i) for a 20 m section of the compartment was modelled as,

$$CP_i(t) = BW_{i,2009} + RPY_i(t - 2009)$$

where $BW_{i,2009}$ is the beach width in 2009 (i.e. distance between the 2009 vegetation line and shoreline in the LiDAR DEM, which is the surveyed mean water line or 0 m AHD depth contour, RPY_i is the long-term trend and t is the model year and the subscript i indicates the i^{th} 20 m section in the geomorphic compartment. An example trend line for Point Nepean is shown in Figure 7.11 where positive values indicate the vegetation is moving landward (i.e. eroding) to align with the inland expanding hazard mapping.

Using the extracted coastlines at 20 m intervals for each year (Figure 7.12a), rectangular polygons were then created at the same 20 m intervals to display the linear model estimates of the location and change from an earlier time (1959) to the baseline shoreline datum time (2009) and colour coded red for landward movement and green for seaward movement (Figure 7.12b and Figure 7.13).

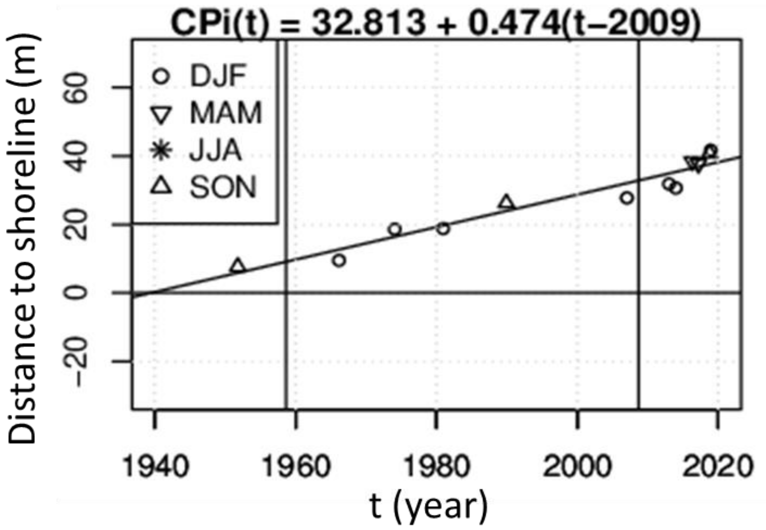

Figure 7.11: Coastline positions determined from vegetation line analysis (symbols) at Point Nepean and linear regression indicating the average distance of movement from the vegetation lines shown in Figure 7.12b. Positive values indicate landward movement of the vegetation line (long-term erosion of the coastline).

The observed trend of either erosion or accretion from 1959-2009 for all analysis locations around the bay is shown in Figure 7.14. In total 72% of detected vegetation lines have a seaward moving trend (accretion) while 28% have a landward moving trend (erosion). The map shows many locations where land has accreted and hotspots where land has eroded. The sectors that were dominated by erosion are listed in Table 7.3, the remaining sectors where changes in the vegetation line were detected are listed in Appendix G. The analysis tends to show accretion along sections of coast where beach nourishment has been undertaken and therefore may underestimate the natural erosion or accretion processes. For example, management actions such as extensive dune vegetation that has occurred along the Kingston City Council foreshore appears to have stabilised the vegetation extent, and in some cases, this has enabled the vegetation to colonise further seaward. The results of the historical analysis indicate that loss and gain of land are often in neighbouring 20 m segments, suggesting non-uniform longshore transport and exchange of sediments due to the undulating terrain.

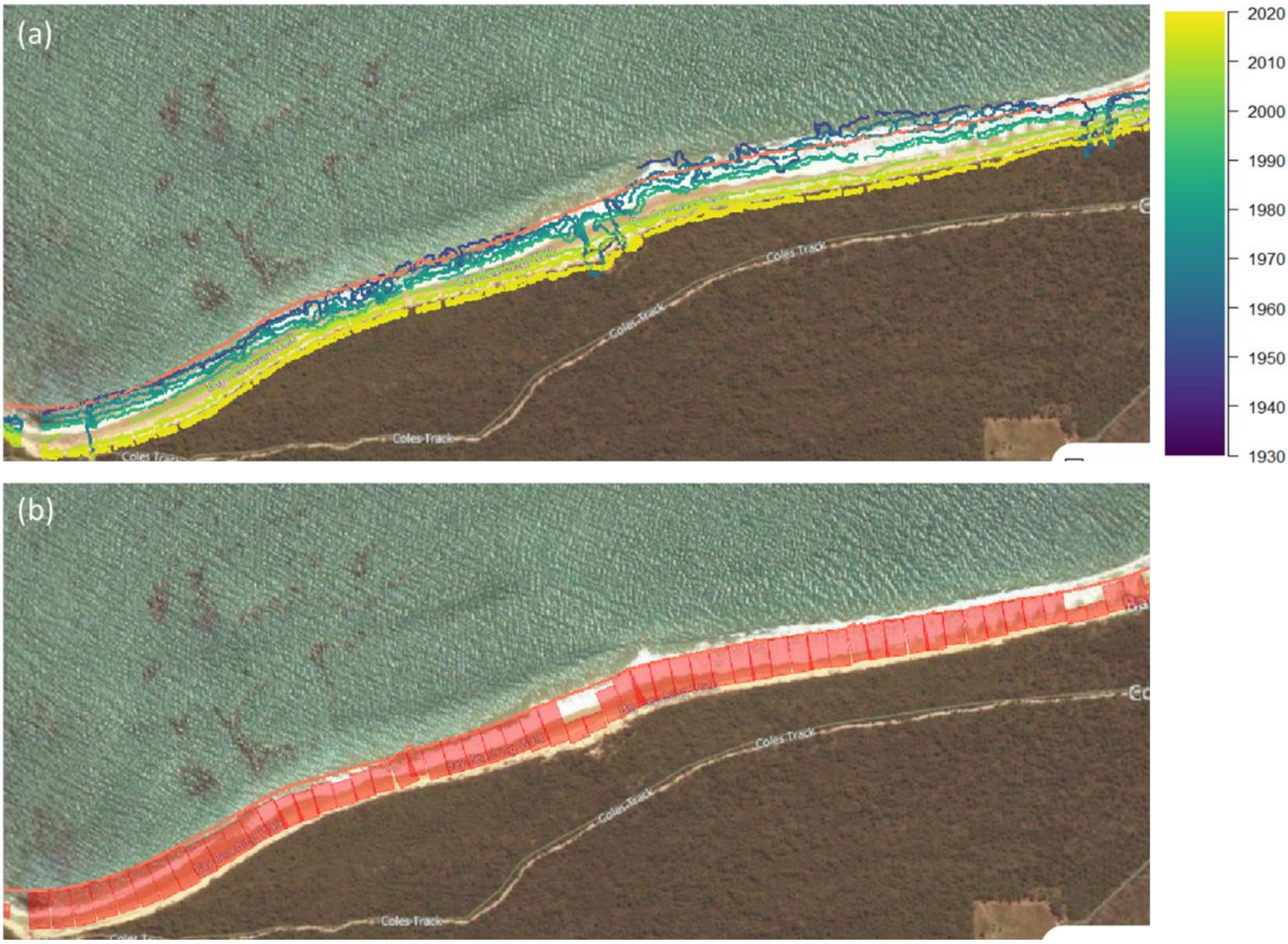

Figure 7.12: Point Nepean vegetation line detection. (a) extracted vegetation lines corresponding to year in colour key (right). The 2009 LiDAR shoreline (zero AHD) is shown in orange. (b) The linear model prediction of the vegetation line movement from all coastlines detected (1951 to 2018). The red polygons indicate the landward movement of vegetated land over the period 1959 to 2009.

The incomplete datasets on coastal management means that it is not possible to attribute the changes seen in the aerial imagery to natural changes, SLR or other causes such as coastal management. The limitations on the datasets include:

- Incomplete nourishment activity datasets (trucks and diggers either adding new sand or moving sand from one end of a beach to another. Sand raking burying fine windblown sediments below the surface)
- Unknown revegetation dataset (planting), and
- Incomplete engineering structure datasets (fences, sandbags, buried structures).

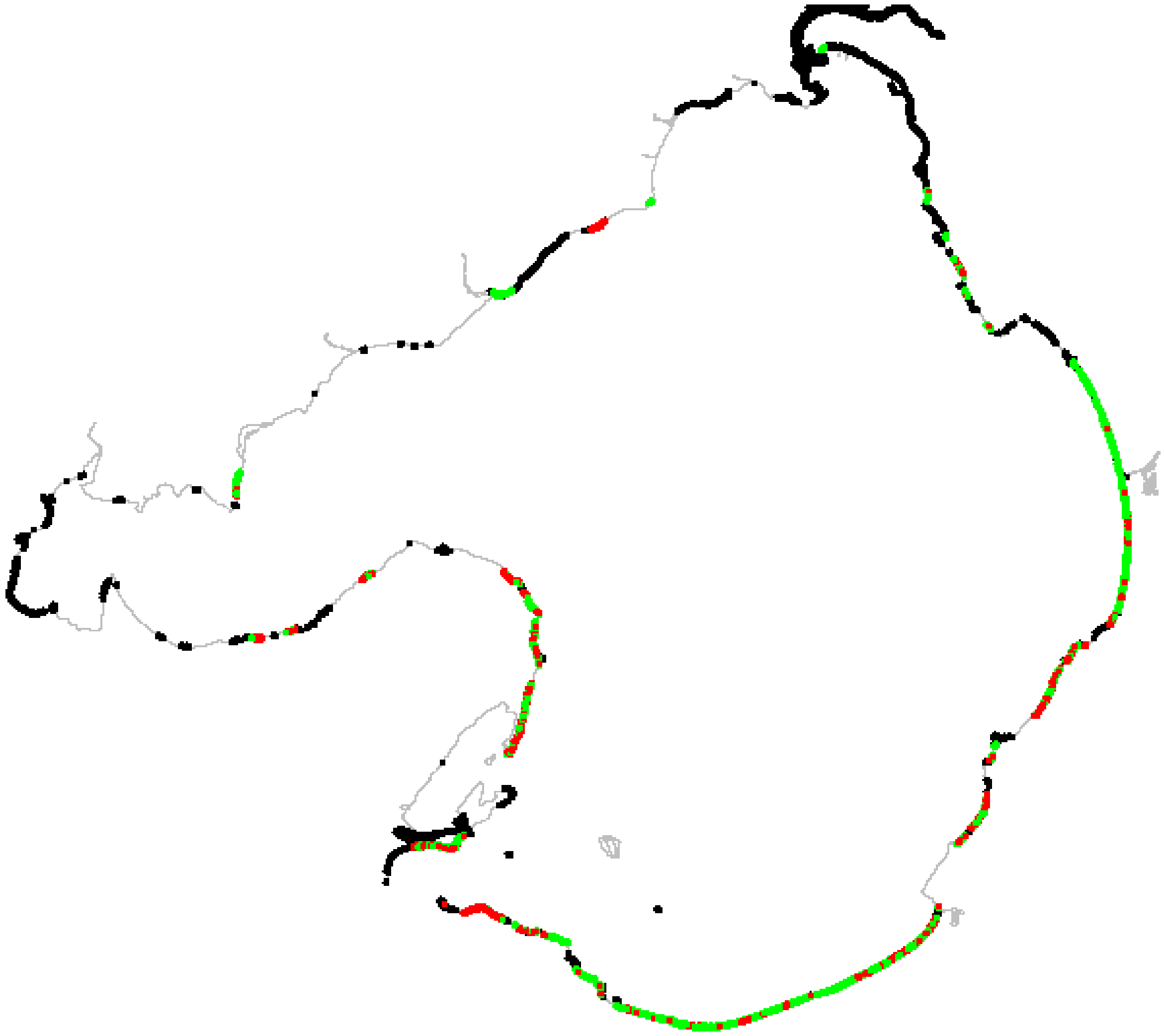

Figure 7.13: Long-term trends of erosion/accretion over the entire aerial photography period (1940 to 2018). The 2009 shoreline is shown in grey, coastal structures in black, erosion trend is shown in red, accretion trend is shown in green based on the coastline unsupervised vegetation line analysis on 20 m segments along the shoreline.

Table 7.3: Summary of coastal sectors exhibiting coastal erosion around the bay (defined as where the mean rate in the CGS was greater than zero). Rate per year values give the mean, and 5th and 95th percentile value in square brackets for each CGS (the 5 and 95% range is estimated from the distribution of results for the 20 m segments of coastline analysed within each CGS). Values are positive for landward moving vegetation lines (erosion) and negative for seaward moving vegetation lines (accretion). Locations are categorised on the basis of the CGS's in Figure 7.2. Details of the vegetation line rate of change detection for the remaining CGS's are provided in Table H1.

Location	Rate [m/yr]	Sector No.	Sector length [m]
Dune with Beach			
Observatory Point west	0.715 [0.275, 0.961]	516	1256
Dog Beach 1	0.600 [0.176, 0.814]	3	264
Point George	0.160 [0.002, 0.408]	44	240
Coach Road	0.098 [0.005, 0.302]	45	1280
Spray Farm	0.056 [-0.094, 0.184]	61	832
Observatory Point east	0.045 [-0.048, 0.103]	515	1402
Bluff with Mixed			
Scarborough Rd	0.211 [0.026, 0.522]	89	751
Collins Bay	0.198 [0.052, 0.262]	502	164
Sunnyside Beach	0.079 [0.075, 0.132]	383	118
Lower Bluff Road	0.075 [-0.171, 0.220]	25	693
Sandringham Beach Rd	0.033 [-0.052, 0.164]	314	1281
Sunnyside North	0.018 [-0.042, 0.041]	379	441
Engineering effective with beach			
Point Cook runway 35	0.546 [0.185, 0.966]	218	1132
Portsea Pier	0.060 [-0.050, 0.124]	505	314
Engineering ineffective with beach			
Taylor Reserve	0.091 [0.068, 0.152]	41	90
Safety Beach central	0.063 [-0.024, 0.149]	450	1044
Slope with Beach			
Hawker Beach	0.037 [-0.009, 0.107]	430	374
Mount Martha North	0.026 [-0.006, 0.056]	431	144
Sunnyside rocks	0.019 [-0.119, 0.039]	380	105
Soft Cliff with Beach			
Fossil Beach south	0.150 [0.071, 0.177]	421	59
Daveys Bay north point	0.132 [0.067, 0.305]	364	188
Manyung Rocks	0.042 [-0.040, 0.105]	378	150
Half Moon Bay north	0.012 [-0.057, 0.049]	40	137
Wetlands with beach			
Salt Lagoon	0.094 [-0.083, 0.205]	32	340
Edwards Point spit PP Bay	0.073 [-0.919, 0.892]	23	4606

7.3 Geomorphic Shoreline Analysis

The specific geomorphic characteristics of the coastal sector under consideration inform the approaches needed to assess shoreline response to SLR. This section provides an analysis of the coastal compartment information to inform approaches to calculating shoreline hazards. Key geomorphological categories of relevance in PPB are provided in Table 7.4 and their intertidal or backshore locations are illustrated in Figures 7.14a and b respectively.

Many sections of coastline are complex and would require multiple approaches to estimate the hazard zone. For example, short term erosion and recovery is relevant in the case of sandy shorelines but not cliffed shorelines. Table 7.5 describes 21 geomorphic typologies considered relevant for PPB based on analysis of the 528 CGS identified in the detailed geomorphic survey which are mapped in Figure 7.14. The most frequently used intertidal classification is sandy beach accounting for 290 CGS and around 200 km of coastline (Figure 7.14a). The backshore classification shown in Figure 7.14b shows extensive parts of the eastern side of PPB as well as the Bellarine Peninsula contain either hard or soft rock cliffs. It is noted that SLR may change the classification of a sector. For example, a backshore feature such as a bluff may not be relevant when assessing erosion under present-day sea-level conditions but may become an activated cliff because SLR has removed the sandy beach in front of the bluff, or the height of extreme water levels exceeds a protection structure and reaches the toe height of the bluff. Future high tide flooding can also activate wetlands behind sectors that are not classified as wetlands in the baseline climate geomorphic assessment. Table 7.5 also provides notes on the relevance of past erosional trends (LTHIST), short term erosion due to storms (ST) and future erosional trends due to SLR (LTFUT) to the various geomorphological classifications around PPB and approaches to assessing their contribution.

Table 7.4: Summary of the coastal types assigned.

Geomorphology	Located	Figure 6.17 Colours
Sandy shores (beaches dunes and ridges)	Intertidal and backshore	Yellow
Soft rock (bluffs, slopes and soft cliffs)	Backshore	Brown
Hard rock cliffs	Backshore	Grey
Engineered structure (effective or ineffective)	Structure line	Black
High tide hazard (salt marsh, wetland, low lying lands)	Intertidal and Backshore	Purple
Geomorphic hazard (cuspate spit, river drain)	Intertidal and Backshore	Pink

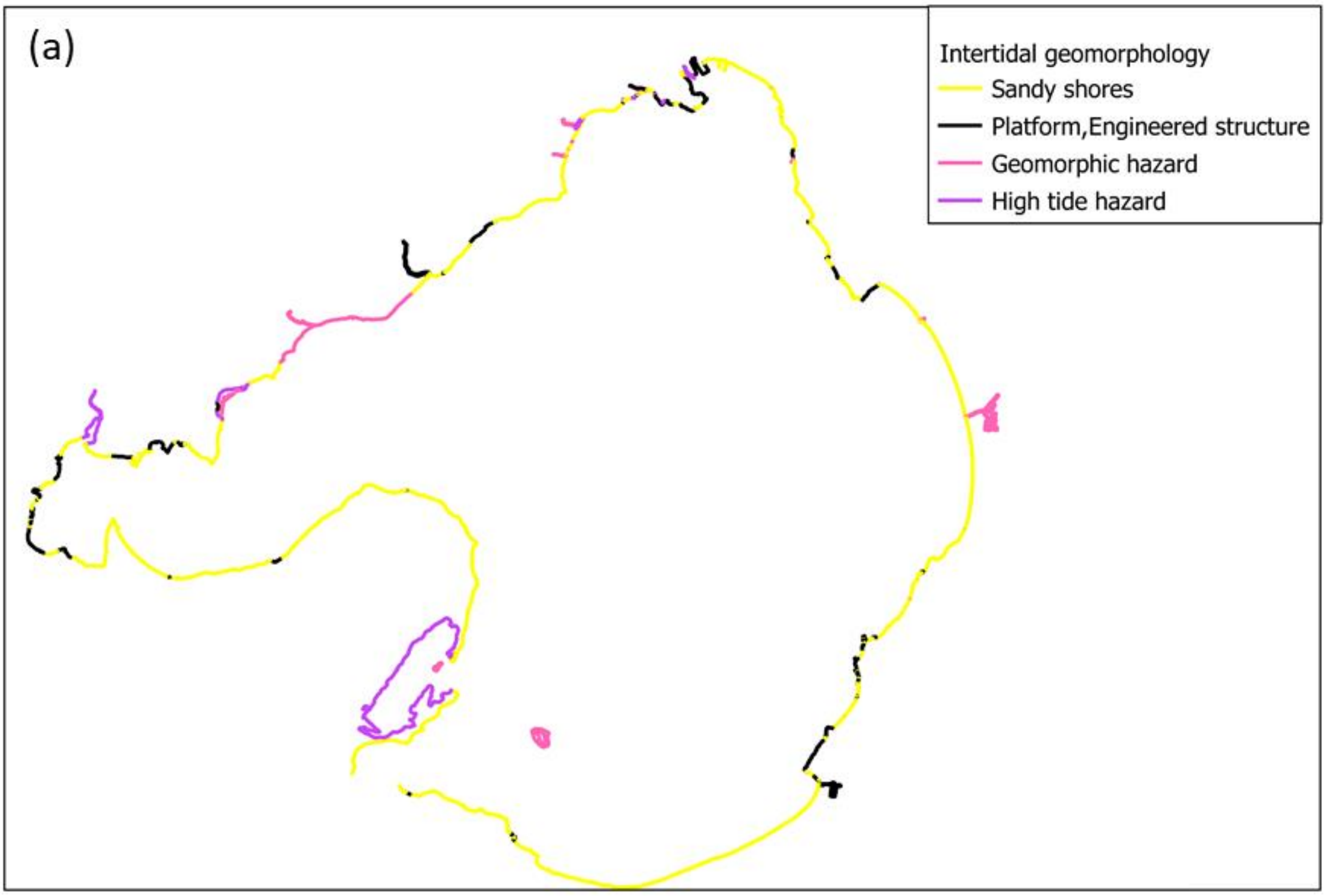

Figure 7.14: Shoreline classification delineating (a) intertidal and (b) backshore types that determine the method employed for evaluating the hazard zone. The colour-coded classification identifies sandy and mixed beaches (yellow), platforms and engineered structures (black), wetlands (purple) and geomorphically-complex coastlines (pink). Colours in the two legends link the intertidal and backshore method classification in Table 7.4 and the 21 methods in Table 7.5.

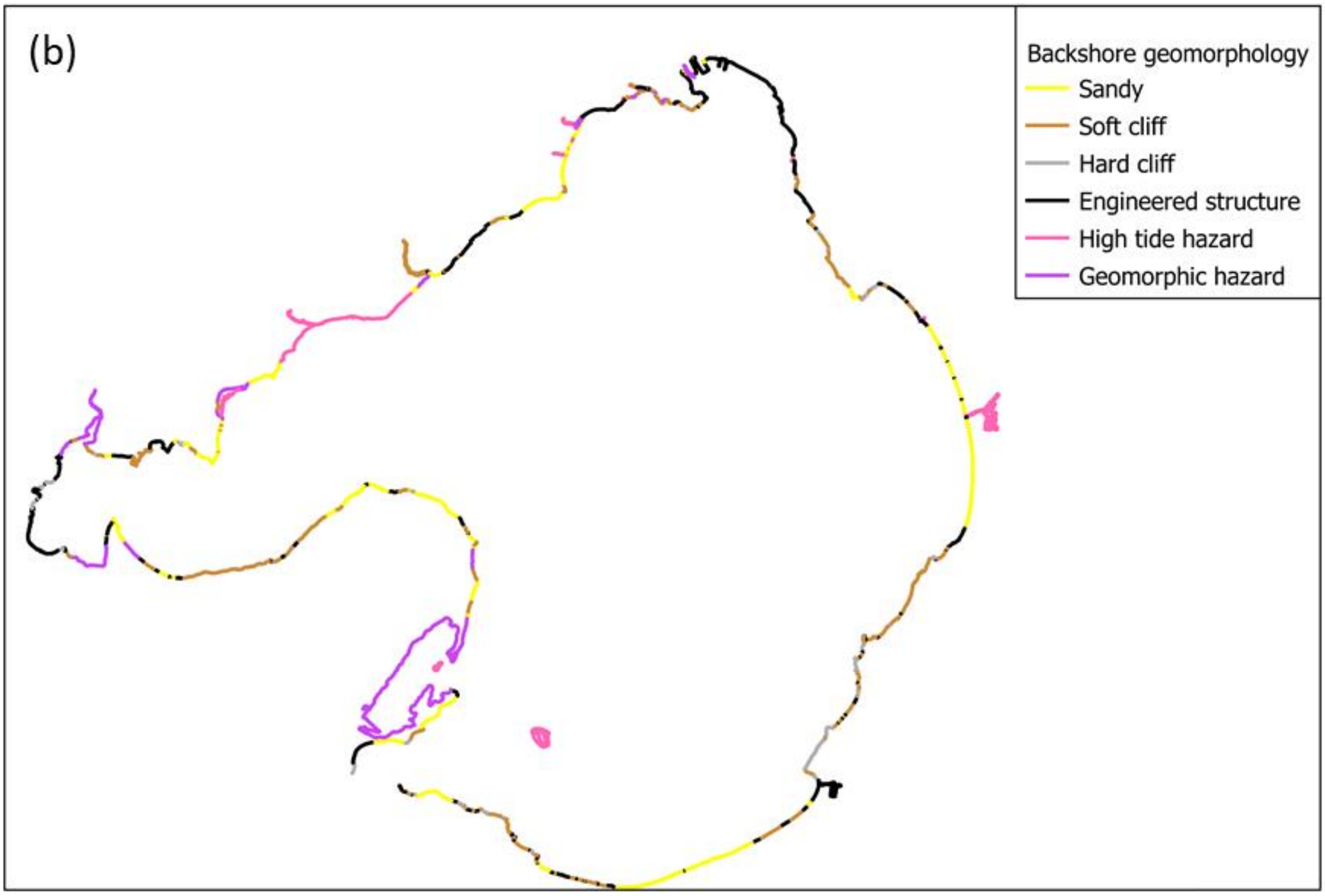

Figure 7.14: Continued.

Table 7.5: Summary of the coastal types assigned to the 528 Coastal Geomorphic Sectors around PPB, the number of sectors falling into each type, the length of coastline represented by each type.

Type	Description (backshore with intertidal	No. of Sectors	Length (km)	Type	Description (backshore with intertidal	No. of Sectors	Length (km)
1	Hard Cliff with Platform 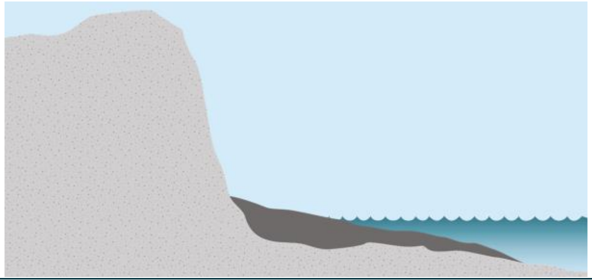	18	11.26	2	Hard Cliff with Beach 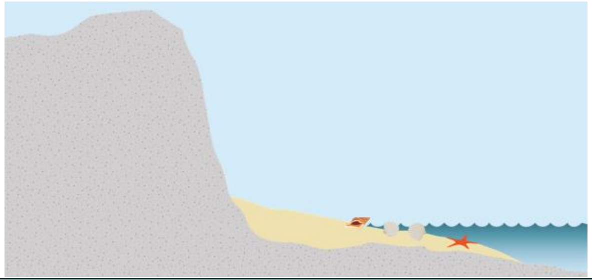	24	8.64
3	Soft Cliff with Platform 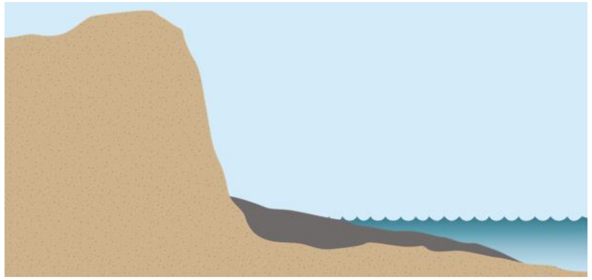	2	0.34	4	Soft Cliff with Beach 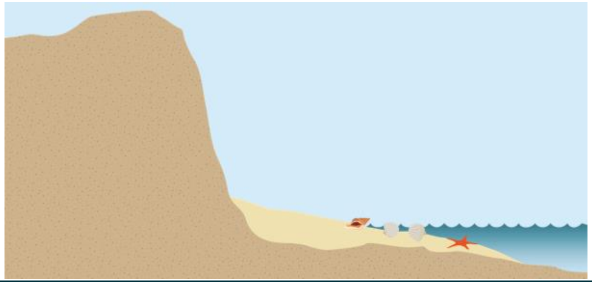	40	12.51
5	Bluff with Beach 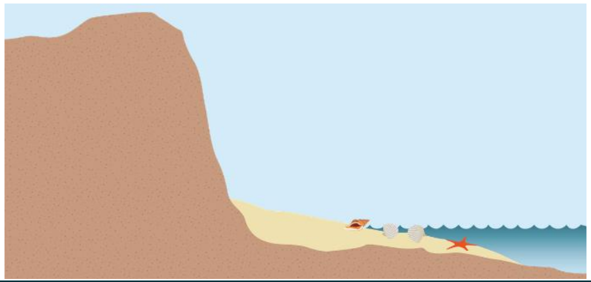	67	28.23	6	Bluff with Mixed 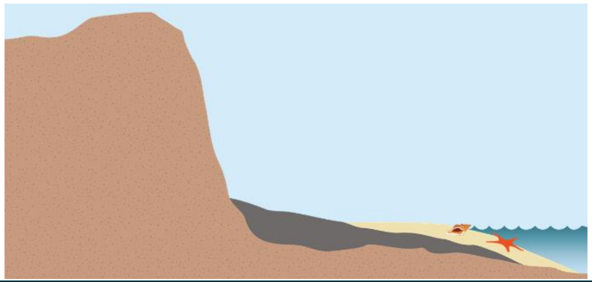	33	16.67

Type	Description (backshore with intertidal	No. of Sectors	Length (km)	Type	Description (backshore with intertidal	No. of Sectors	Length (km)
7	Slope with Beach 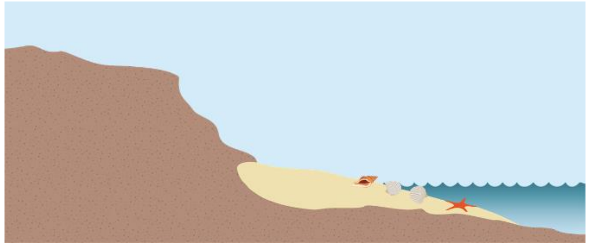	9	2.47	8	Dune with Beach 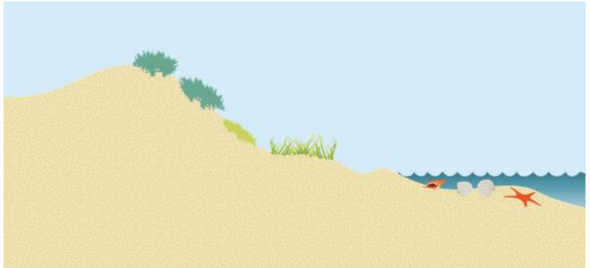	80	95.00
9	Cuspate Spit 	4	17.98	10	River drain 	19	46.83
11	Wetlands 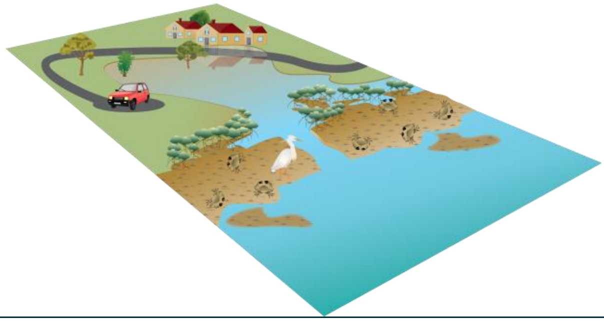	35	55.61	12	Engineering effective 	22	28.09

Type	Description (backshore with intertidal	No. of Sectors	Length (km)	Type	Description (backshore with intertidal	No. of Sectors	Length (km)
13	Engineering ineffective 	9	7.86	14	Slope with Platform 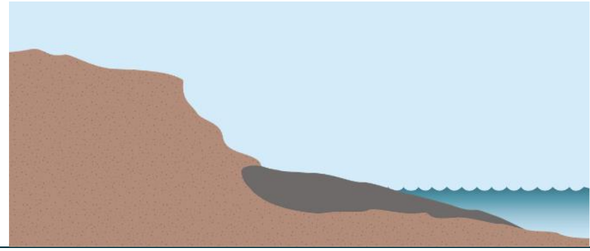	1	0.58
15	Engineering effective with Beach 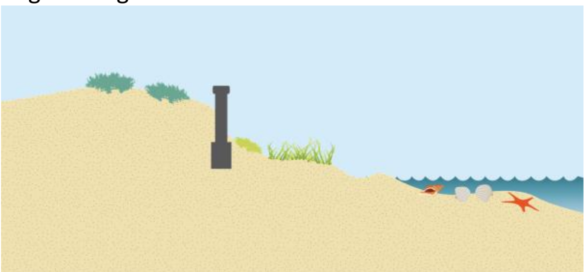	35	9.40	16	Engineering ineffective with Beach 	35	9.40
17	Slope with Engineering effective 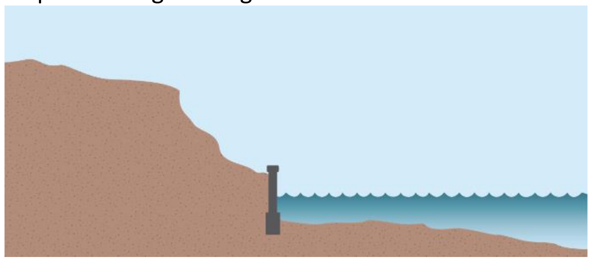	1	0.58	18	Cliff with Engineering effective 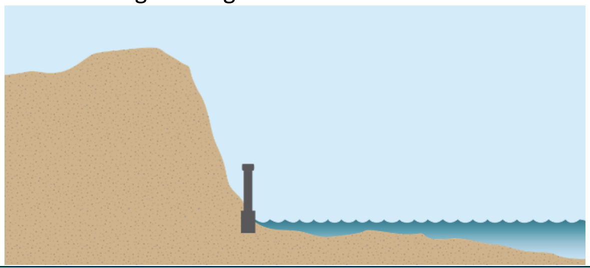	5	1.03

Type	Description (backshore with intertidal	No. of Sectors	Length (km)	Type	Description (backshore with intertidal	No. of Sectors	Length (km)
19	Cliff with Engineering ineffective 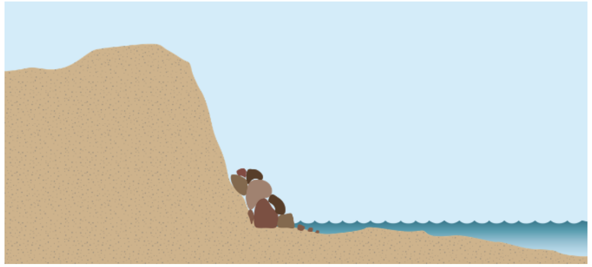	5	1.03	20	Bluff with Platform 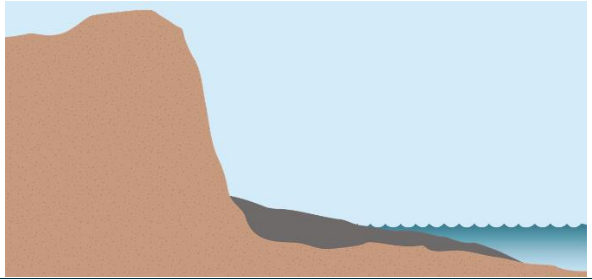	18	11.05
21	Wetlands with beach 	11	15.29				

7.4 Summary

This chapter has presented foundational information on the shoreline of Port Phillip Bay. The coastal geomorphic analysis is based on tertiary-scale data, which allows a sector-by-sector analysis for the 528 compartments that have been identified for PPB based on backshore, nearshore and intertidal characteristics. Twenty-one different combinations of these geomorphic characteristics have been identified around PPB. An analysis of coastal vegetation lines in historical photogrammetry provides an indication of historical shoreline movement. Results of an analysis of sediment samples of PPB beaches and digitised shoreline surveys have been presented. The information provided in this chapter provides contextual information to aid in the interpretation of results for the inundation and groundwater hazard assessments in the present study. It will also provide foundational information for future shoreline erosion hazard assessments.

8 Hydrodynamic and Wave Modelling of Port Phillip Bay

This chapter describes the hydrodynamic and wave modelling undertaken to provide simulated wave and sea level data for use in the hazard assessments. A description of the model setup and required data inputs is given. The models are first calibrated over selected time periods using tide gauge data at multiple locations within the model domain and wave data just outside PPB. Then model simulations from a 35-year historical period (year range 1980-2014) were validated against available tide and wave data inside the bay over the longer simulation period to demonstrate that the model is fit-for-purpose. Simulations under assumed SLR of 0.2, 0.8 and 1.1 m are also undertaken to understand the nonlinear effect that SLR would be expected to have on tides, waves and storm surges across the bay. Statistical methods were applied to the historical and each of the SLR simulations to produce 1%, 2% and 5% AEP sea level and wave heights as inputs for the inundation and erosion hazard modelling.

8.1 Introduction

The hazard assessment discussed in Chapter 5 required a range of inputs relating to waves and sea levels. To provide inputs to the assessment that cover the entire PPB region in a dynamically consistent way, a bay-wide coupled hydrodynamic and wave model (that also extended past the Heads and included Western Port) was run to provide the relevant parameters that were subsequently processed to feed into the hazard assessments. This chapter describes the model setup and presents model validation and the relevant outputs derived for the hazard assessment.

8.2 Model Setup and Processing

8.2.1 Model Grids

The coupled wave and hydrodynamics of PPB and adjacent areas were modelled using the SCHISM and the Wind Wave Model III (WWMIII), a state-of-the-art ocean modelling system widely used by the scientific community and industry for a range of regional and coastal scale applications. The southern boundary extends well into Bass Strait, approximately between Cape Otway and Cape Liptrap, necessary to accurately represent the tidal harmonics and storm surge dynamics of the region. The hydrodynamics for the southern boundary were provided by a broader, coarse-resolution Regional Ocean Modelling System (ROMS) hydrodynamic model at ~4 km resolution covering the entire Bass Strait and extending to the western border of South Australia to ensure accurate representation of coastally trapped waves that are associated with storm surge events within PPB (McInnes and Hubbert, 2003). Figure 8.1a shows the larger ROMS model grid while Figure 8.1b shows the SCHISM model grid. The wave forcing for the SCHISM-WWMIII southern boundary was provided by an implementation of the Simulating WAves Nearshore (SWAN, version 40.91) encompassing the Bass Strait region (Figure 8.1a) with a spatial resolution of approximately 4 km (0.035° by 0.035°).

SCHISM is a primitive-equation ocean model that solves the Navier-stokes equations over an unstructured hybrid triangular-quadrangular grid and adopts a semi-implicit finite-element and finite-volume framework. The SCHISM model was setup in 2D barotropic mode using an unstructured mesh

(Figure 8.1b). The mesh horizontal resolution varies from approximately 2 to 4 km at the offshore boundary to generally between 50 m and 30 m in the shallow coastal areas (defined as between 5 m water depth to the current mean shoreline), although in certain areas of complex bathymetry and/or shoreline horizontal resolution drops to approximately 20 m. The mesh also extends from the shoreline to the 3 m AHD land elevation contour. The 3 m elevation contour was a priori defined as the maximum extent of the computation grid by assuming 1.4 m (maximum SLR scenario) + 1.4 m (approximate 1% AEP maximum storm tide within bay from a variety of sources) + rounding up. Grid resolution coarsens with distance from the shoreline; in areas greater than 1 km from the current shoreline, grid resolution may be as large as 200 m. This was done for two reasons: (1) the 2017 DEM used to inform the model topography (see Section 8.3.1) was a "bare earth" DEM, so would not represent hydrodynamics appropriately where buildings, roads or other infrastructure are present (which is most of the mesh area within PPB); and (2) high resolution in the extensive low-lying areas of model domain would incur an exceptionally high computational cost. The resulting mesh has 300,953 elements, with the highest resolution concentrated in the nearshore region to capture the greatest detail in the shallow coastal waters (as previously discussed) as well as the narrow entrance to PPB.

The wave model (WWMIII) is an internal module of SCHISM, which operates on the same model grid to simplify exchange of information between the two models. It is two-way coupled to the hydrodynamic model to provide an accurate representation of wave-current interactions, crucial to the wave and circulation regime in PPB. WWMIII was configured to run in non-stationary mode with all third-generation physics included. The spectra were discretised with 36 directional bins (10° directional resolution) and 23 logarithmic frequencies between 0.04 and 0.6666 Hz.

8.2.2 Mannings Roughness

A spatially variable roughness field was configured using different Manning's coefficients for the different region/bottom characteristics across the model domain. Manning's coefficients (N) were defined following several model iterations where sensitivity to different combinations of N values were evaluated. The range of coefficients tested were based on existing literature and previous studies (Passeri et al., 2012; Garzon and Ferreira, 2016), and the Victorian Benthic Habitats - Biotope Classification Scheme[13] (CBiCS; Flynn et al., 2016) was consulted to define N values for rocky reefs habitats. Results from the model sensitivity tests and assessment of tidal responses across the domain led to the definition of the roughness field as shown in Figure 8.1c.

8.2.3 Model Experiments

The model experiments carried out with SCHISM-WWMIII comprised a baseline hindcast experiment spanning 35 years from 1980 to 2014 and three 20-year experiments that simulated the effects of a 0.2, 0.8 and 1.4 m of SLR, run with atmospheric pressure forcing from the 1980 to 1999 time period (Section 8.3.2; Table 8.1). Parameters for two additional SLR scenarios of 0.5 and 1.1 m were derived through interpolation of the results obtained from the 0.2, 0.8 and 1.4 m simulations.

8.2.4 Computing Requirements

The SCHISM-WWMIII model was run in the coupled wave-flow configuration on the Australian National Computational Infrastructure (NCI) high-performance computers, utilising around 200 cores. The real

[13] http://metadata.imas.utas.edu.au/geonetwork/srv/eng/metadata.show?uuid=9737f03b-8e6b-4a93-b530-d7687d1a8a01

time duration of the 35-year and three 20-year simulations was around 4,000 hours (167 days) requiring 1.1 million NCI core hours. The total data generated by the SCHISM-WWMIII simulations was in excess of 20 Terabytes.

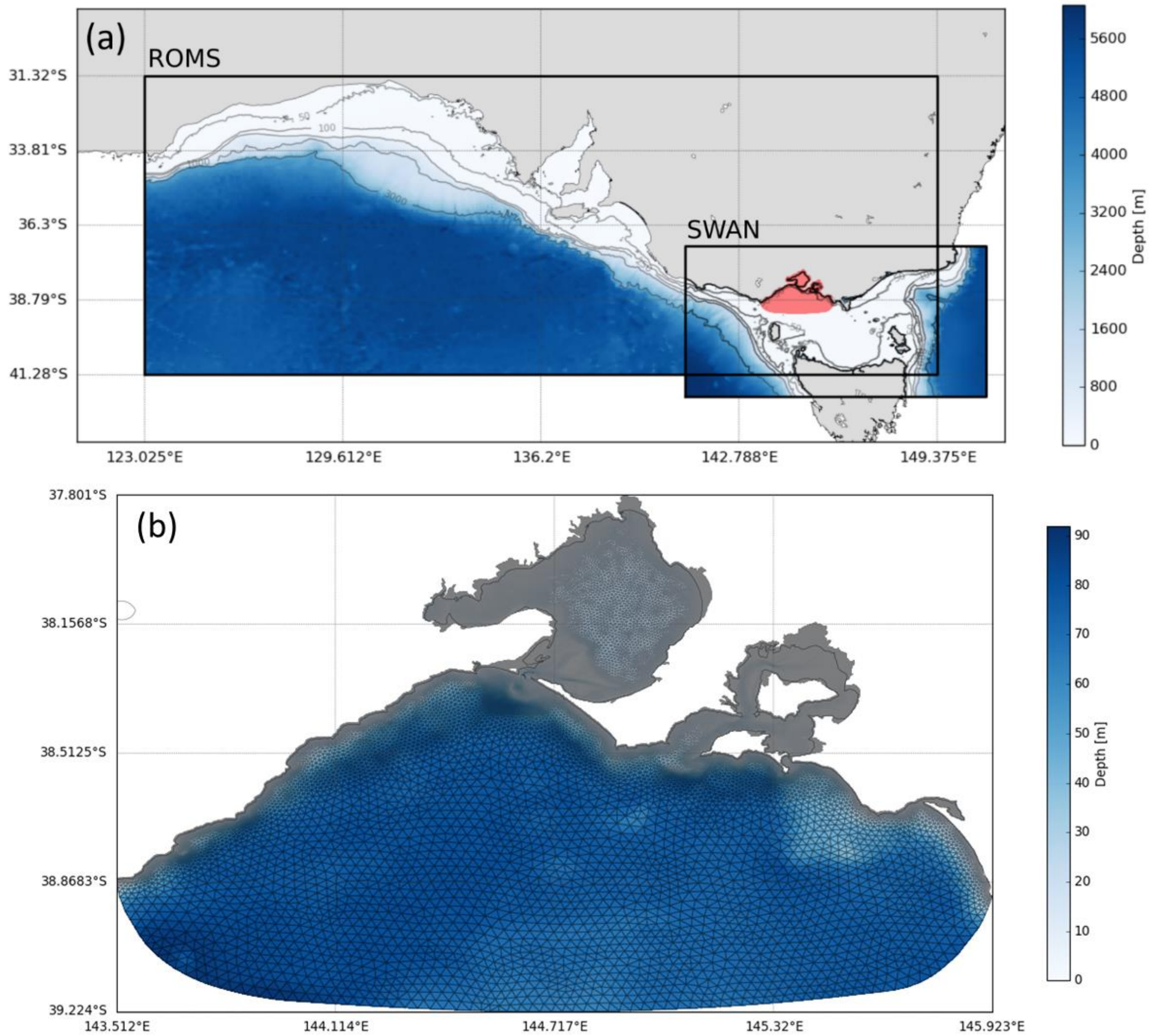

Figure 8.1: (a) the ~4 km resolution ROMS model and SWAN model used to supply hydrodynamic and wave boundary conditions respectively to the offshore boundary of SCHISM-WWMIII (red shaded area), (b) the domain of the PPB SCHISM-WWMIII model showing the grid mesh (note that the density of cells in shallower regions obscures the depth shading), and (c) the Manning's coefficients used in the bottom friction formulation of SCHISM.

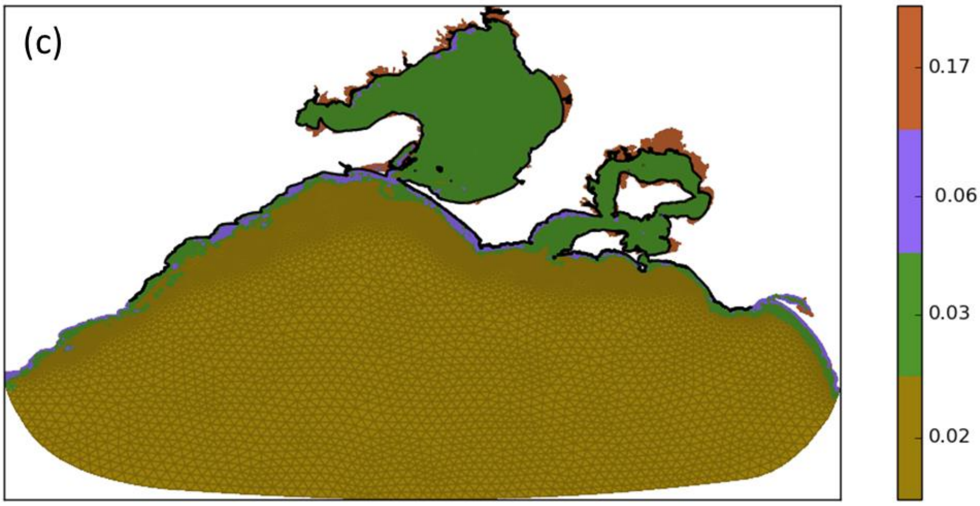

Figure 8.1: Continued.

8.3 Input Data Requirements and Assessment

8.3.1 Bathymetry and Topography

Bathymetric LiDAR surveys, conducted contemporaneously with topographic LiDAR surveys, cover the entire study region. The low-energy environment of PPB means that areas of missing or potentially inaccurate bathymetric LiDAR data due to breaking waves or suspended sediments are minimal. Furthermore, the 2017 reprocessed/merged DEMs used in this study specifically sought to minimise discontinuities. The overall error analysis published in the 2017 DEMs report (Allemand et al., 2017; and also summarised in the revised Gap Analysis) states that across Victoria, most mean differences between the input data and the high-resolution DEM were less than 10 cm (range: -0.15 cm to +0.15 cm), with an overall mean difference of 0.00 cm (standard deviation: ±4.0 cm).

The bathymetry and topography of the SCHISM model is primarily based on the 2017 VCDEMs identified in the gap analysis, which were optimally interpolated from multiple datasets. However, for historical simulations before 2008, bathymetry in the southern portion of the bay (e.g. the region encompassing the Great Sands, South Channel and the Entrance) is defined by the 2007-2008 Future Coasts LiDAR survey. For simulations after 2008, the bathymetry in this region is defined by the Port of Melbourne 2012 LADS (LiDAR) surveys. This is so that the changes to South Channel associated with the 2008 Channel Deepening Project, which has been shown to have an effect of the hydrodynamics of the bay, are reflected in the SCHISM model.

8.3.2 Atmospheric Boundary Conditions

The wind and pressure data required to force the SCHISM model were provided by a dedicated 35-year (1980-2014) simulation of the Conformal Cubic Atmospheric Model (CCAM) at 5 km resolution, which was nested within a 50 km version of CCAM. The 50 km version of CCAM also requires atmospheric boundary conditions, and these were obtained from the ERA-Interim global atmospheric reanalysis. ERA-Interim provides atmospheric variables every six hours from 1979 onwards at 79 km horizontal resolution. The two-step process of running CCAM at 50 km and using its simulation as boundary conditions for the 5 km CCAM model was necessary to avoid the large spatial difference in the resolutions of ERA-Interim and CCAM at 5 km, which can cause numerical instability issues. Mean Sea Level Pressure (MSLP) and 10 m winds for SCHISM-WWMIII were obtained from the 5 km CCAM simulation at an hourly time interval, while the 50 km CCAM version at 3-hourly intervals was used for the 4 km ROMS and SWAN models (Figure 8.1a). For the future climate runs, the objective was to investigate the effect of SLR on the hydrodynamics within PPB, therefore the same present day CCAM wind and pressure forcing was applied.

Since CCAM is a global model with no lateral boundaries, spectral nudging was used to apply the large-scale atmospheric forcing from ERA-Interim to CCAM at 50 km resolution and then from CCAM at 50 km to CCAM at 5 km resolution. This form of nudging constrains CCAM to follow large scale atmospheric weather patterns while at the same time allowing it to respond to local forcing such as land/sea temperature and frictional contrasts and topographic effects when simulating local meteorological events, which is important in coastal applications. A scale-selective filter with length scale cut-offs for atmospheric waves of 3000 km and 475 km is used for the 50 km and 5 km simulations respectively (Thatcher and McGregor, 2009).

8.3.3 SCHISM-WWMIII Southern Boundary Conditions

Tidal constituents along the SCHISM southern boundary were obtained from the TPXO7.2 Global Tidal Model (Egbert et al., 2002). Hourly tidal elevation and barotropic velocities were calculated from the constituents and linearly added to the ROMS non-tidal sea surface height and depth-averaged velocities respectively to comprise the SCHISM southern boundary forcing. Wave forcing for the SCHISM-WWMIII southern boundary was provided by the SWAN configuration, which provided 3-hourly wave characteristics including significant wave height (Hs), discrete peak period (Tp), mean direction of spectral peak (Dpm), mean wave period (Tm02), and directional spreading. The SWAN grid was nested into a global implementation of WAVEWATCH III (WW3) spectral wave model (Tolman, 1991) using the source term parametrisation of Ardhuin et al., (2010). This downscale nesting approach was used to resolve wave propagation in the shelf region around Bass Strait, where full spectral boundaries were prescribed from the global model. The relatively large domain of the SCHISM model (well beyond the proposed PPBCHA study boundaries) provides potential additional benefit for future coastal hazard assessments for the open coast and Westernport.

8.3.4 Inflow Boundary Conditions

River flow data from Melbourne Water was used as volume flux river input into the SCHISM model for two rivers: the Yarra River and the Maribyrnong River. Additional river inputs were not used because not all river gauges record volume flow, some only record water elevation, plus other available river gauges with flow measurements were reviewed and found to be at least an order of magnitude less than the Yarra and Maribyrnong. It was assumed these other catchments would have minimal impact on storm-surge levels and were not included as inputs to the SCHISM model. The farthest-downstream flow gauges for the Yarra and Maribyrnong catchments are not located at the SCHISM boundary river inflow locations, and so an approach was taken whereby a time lag was applied to the river flow data from the nearest upstream water flow gauge to produce river flow data at the SCHISM boundary. The approach comprised measuring the along-stream distance (D) between the upstream water flow gauge and the SCHISM river inflow boundary point, and applying a time lag estimated by assuming a mean stream flow velocity of ~4 m/s, which was based on the shallow water wave speed for water depths of 1-2 m (i.e. assuming a Froud number of 1, $u = \sqrt{gh}$). The calculated time lags (calculated as D/u) were then added to the upstream gauge flow times for input to SCHISM as described below.

For the Maribyrnong River, gauged water flow data was obtained for station 230105A (Figure 8.2) and time-lagged flow input at the water-elevation only gauge 230117a, whereas data from two stations (Merri Creek and Yarra River, 229149A and 229143A, respectively) were required for the Yarra River. Both these gauge flows were separately time-lagged and added together for input into the SCHISM model at the water-elevation only gauge 229663A (Figure 8.2). The time-lagged data can be seen in Figure 8.3 (the two water flow plots).

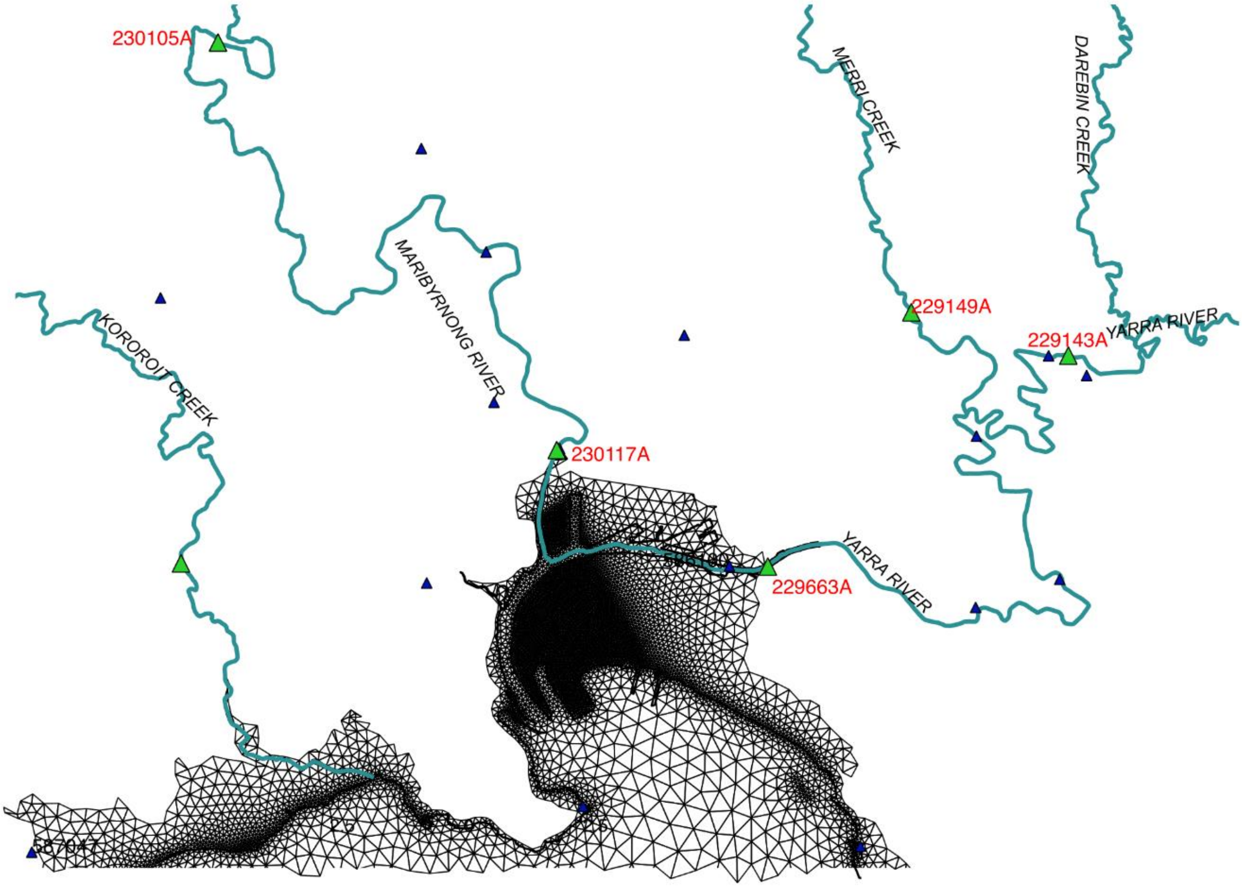

Figure 8.2: Map showing the location of the Melbourne Water gauges (230105A, 229149A, and 229143A) that record river flow (as opposed to just river height), and the locations at which the time lagged river flow data was applied to the SCHISM mesh as boundary river flow inputs (denoted by 230117A and 229663A).

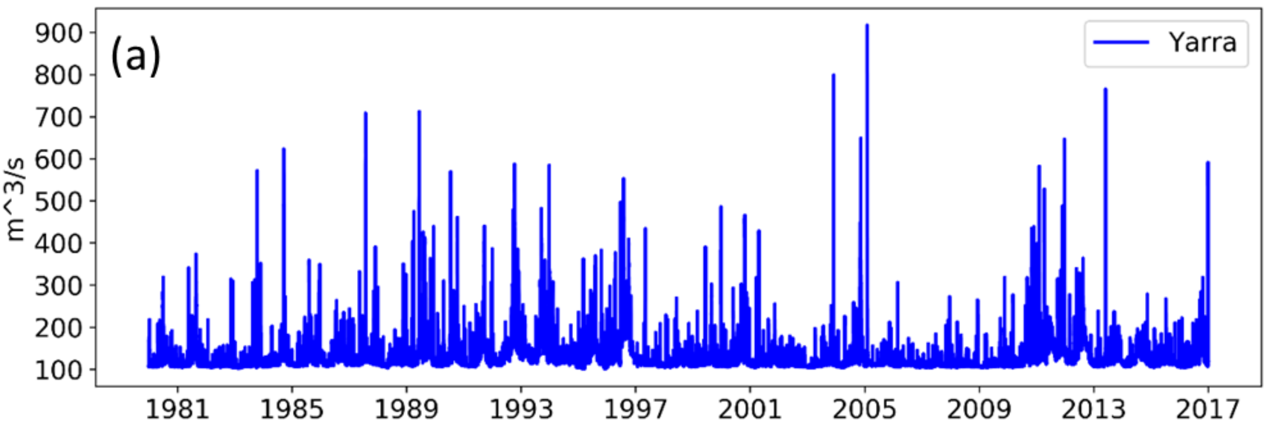

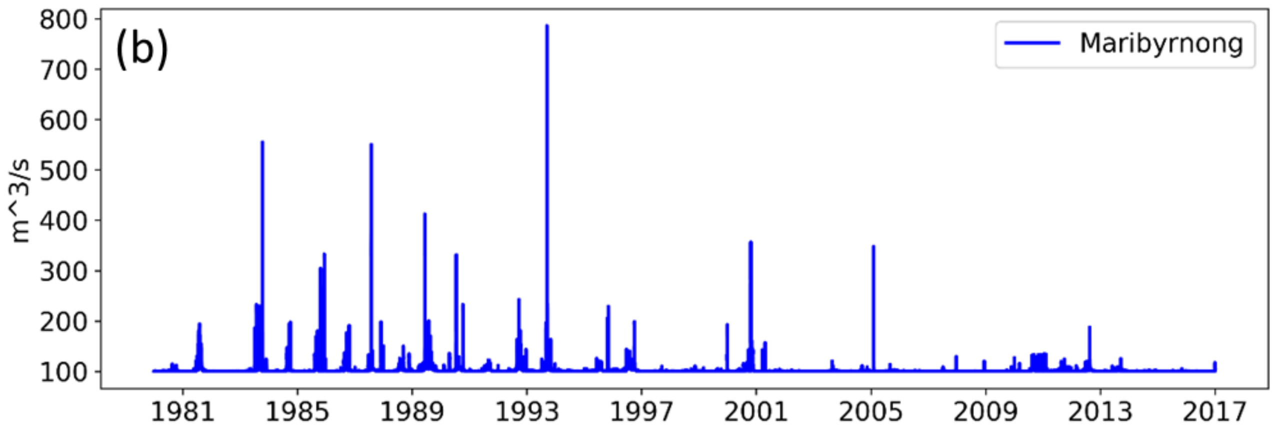

Figure 8.3: Processed hourly river flow data (Melbourne Water) for the (a) Yarra River and (b) Maribyrnong River, used as SCHISM boundary river flow inputs.

8.4 Model Calibration and Validation

This section is divided into three sub-sections on validation (verification) of the following aspects of the SCHISM model performance:

- atmospheric data used to force the SCHISM model
- modelled water levels (including tides), and
- modelled waves.

As previously discussed, the atmospheric input data was developed as part of the VCP19 project, and no additional calibration of the CCAM model was undertaken for this project. However, additional validation of CCAM's winds within PPB (described in Section 8.4.1) was undertaken for this project to better assess their fitness for purpose. The SCHISM model itself was calibrated using two time periods: between October 2011 and April 2012, and between June 2014 and August 2014, chosen because of data availability and also because the intervals contained extreme events. A combination of long-term tide gauge observations and primarily short-term wave, water level and current observations were available during the time periods of model calibration. In Section 8.4.2, a summary of validation of the baseline SCHISM simulation against water levels and tides from long-term tide gauge observations, as well as a historical event outside the calibration period, is given. In Section 8.4.3, a summary is provided of comparisons between the baseline SCHISM simulation against short-term wave observations during the calibration period, as well as further validations of the model against other short-term wave observations during other time periods in different locations around the bay. Additional information on SCHISM model validation, including comparison with short-term current observations, is given in Appendix J.

8.4.1 Atmospheric Input Data

Hourly 10 m winds and mean sea level pressure (MSLP) from CCAM at 5 km resolution were used as forcing and boundary conditions for the SCHISM-WWMIII simulations over PPB. CCAM's performance was assessed in relation to two other available reanalysis products, ECMWF's ERA5 and the National Centers for Environmental Prediction (NCEP) Climate Forecast System Reanalysis (CFSR) product (see Table 8.1 for model resolutions). Winds and MSLP from each product were compared to data from four Bureau of Meteorology stations: Melbourne Airport, Fawkner Beacon, Point Wilson, and South Channel Island (Figure 8.4).

Table 8.1: Atmospheric model products and their horizontal resolution.

Model Product	Horizontal Resolution
ERA-Interim (reanalysis)	79 km
CCAM	50 km & 5 km
ERA5	31 km
CFSR	38 km

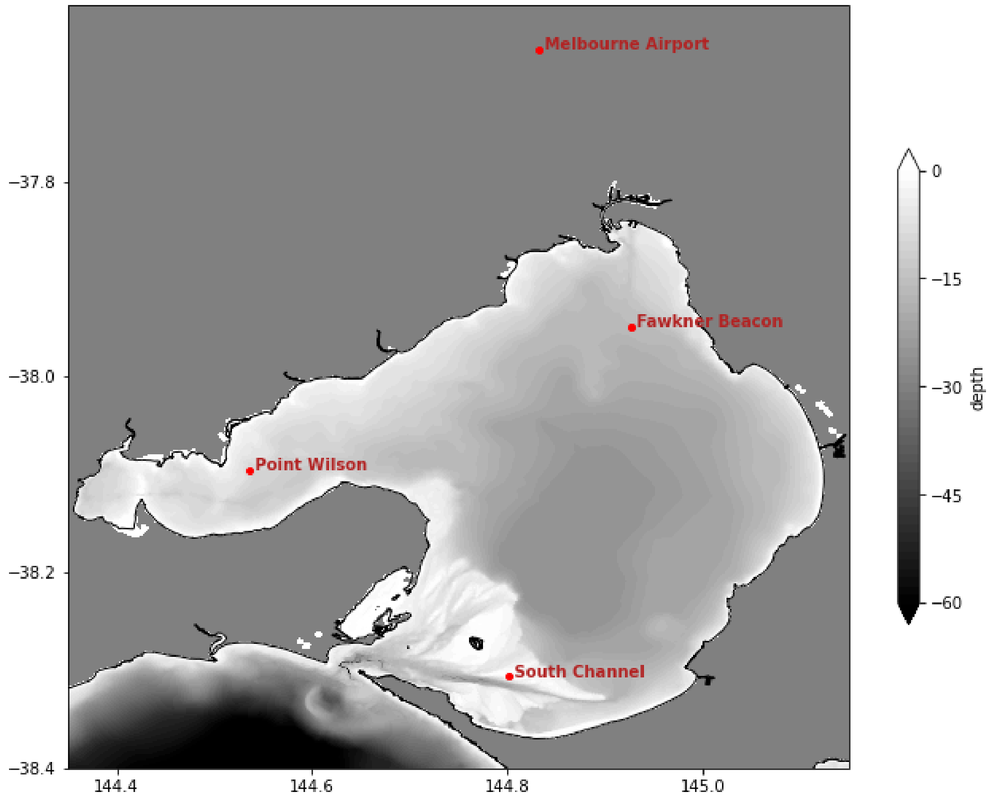

Figure 8.4: Location of wind validation analyses for PPB.

For clarity, Figure 8.5 shows the comparisons for one year, 2014, selected because it contained a particularly severe storm surge event. The comparisons indicate that while CCAM may under- or over-estimate the winds compared to observations for some events, there is generally good agreement between the two time-series. However, the time series of the lower resolution CSFR and ERA5 reanalyses systematically underestimate wind magnitudes compared with observed winds. This is also evident in wind speed histograms, shown in Figure 8.6, which again shows that CCAM winds are most closely aligned with wind observations. The quantile-quantile (Q-Q) plots using the entire timeseries of available data for each site (Figure 8.7) highlight the under-representation of the stronger wind speed classes in the lower resolution CSFR and ERA5 product relative to CCAM.

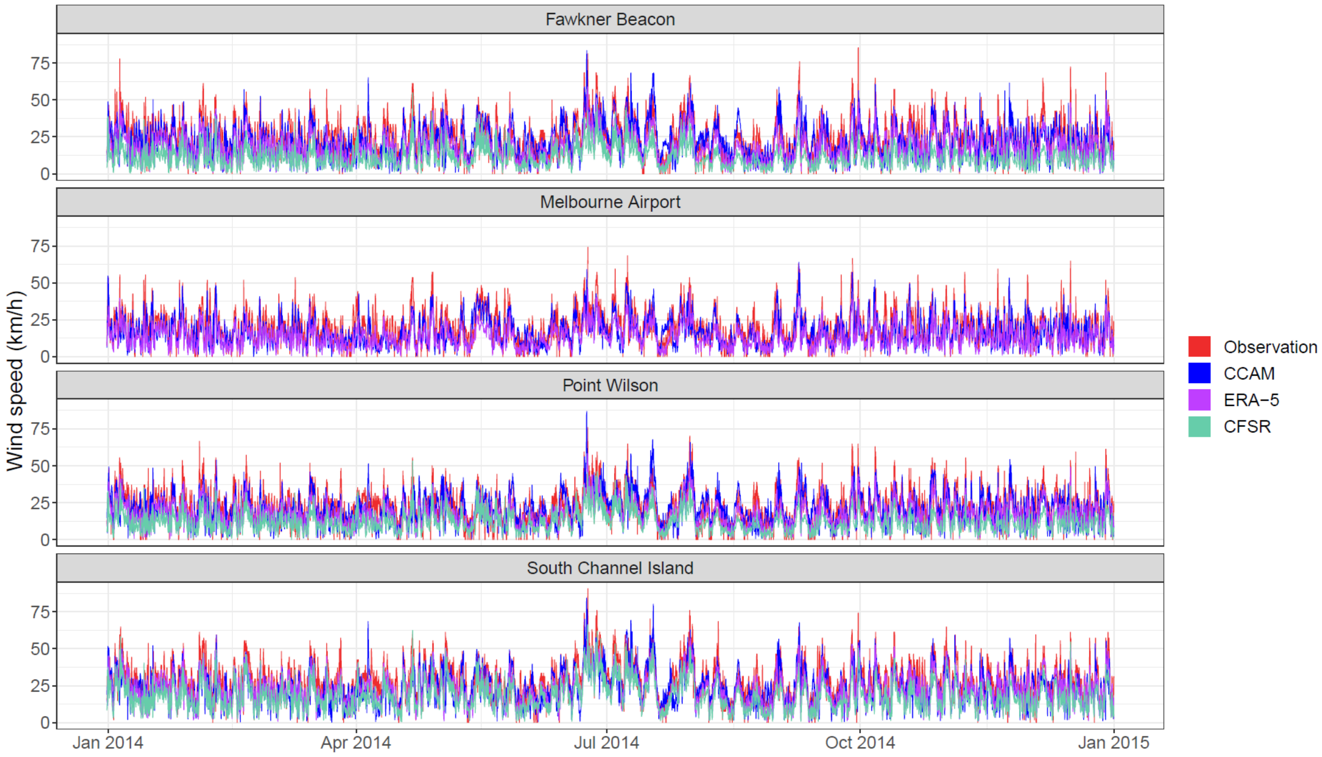

Figure 8.5: Comparison between observed 10 m wind speeds (red) and CCAM (blue), ERA5 (purple), and CFSR (green) for (a) Fawkner Beacon, (b) Melbourne Airport, (c) Point Wilson, and (d) South Channel Island at hourly intervals for 2014. (Note that CFSR data was not available for Melbourne Airport).

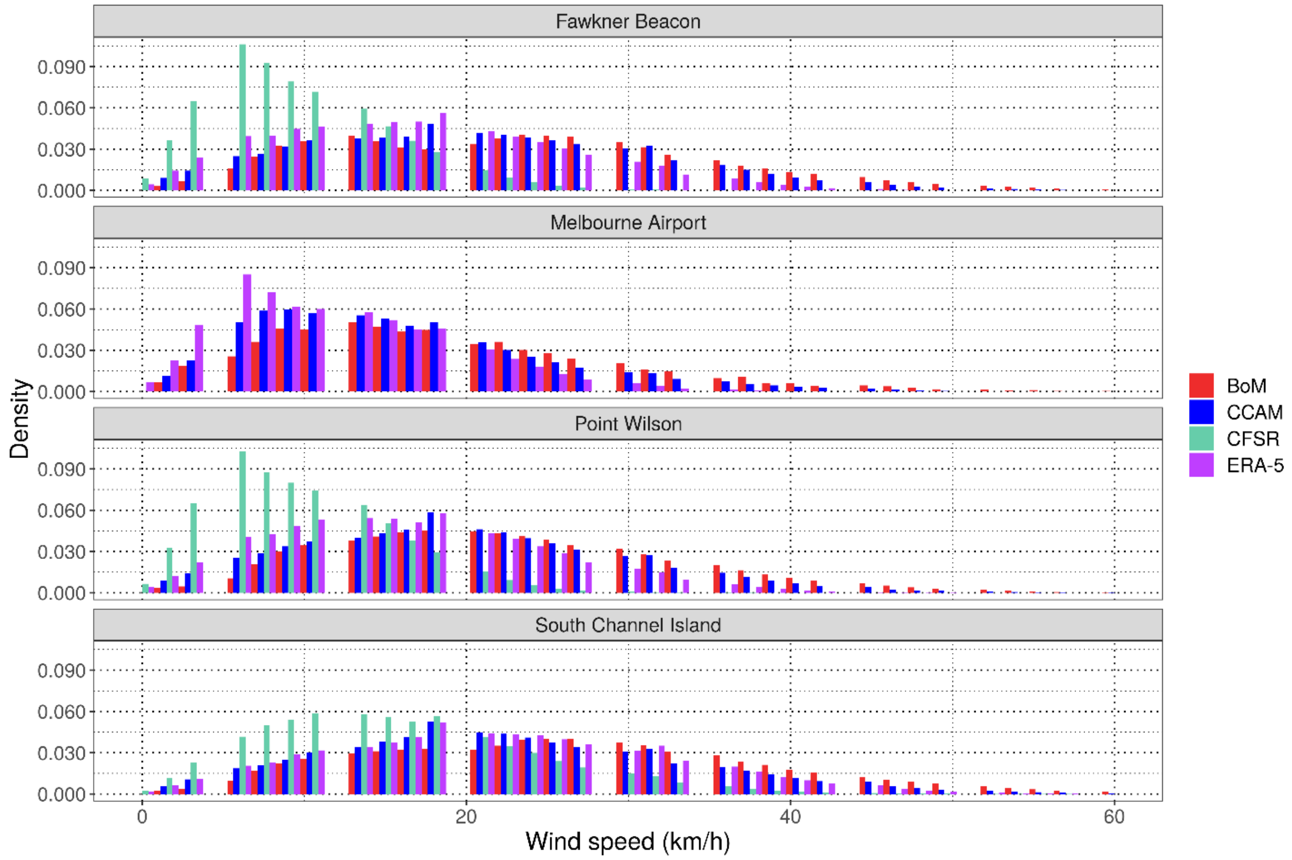

Figure 8.6: Histograms comparing Bureau of Meteorology (BoM) observed 10 m wind speeds (red) with modelled 10 m wind speeds for CCAM (blue), CFSR (green), and ERA5 (purple) for the indicated overlapping periods at Fawkner Beacon (1992-2015), Melbourne Airport (1980-2015), Point Wilson (1991-2015), and South Channel Island (1991-2015). (Note that CFSR data was not available for Melbourne Airport).

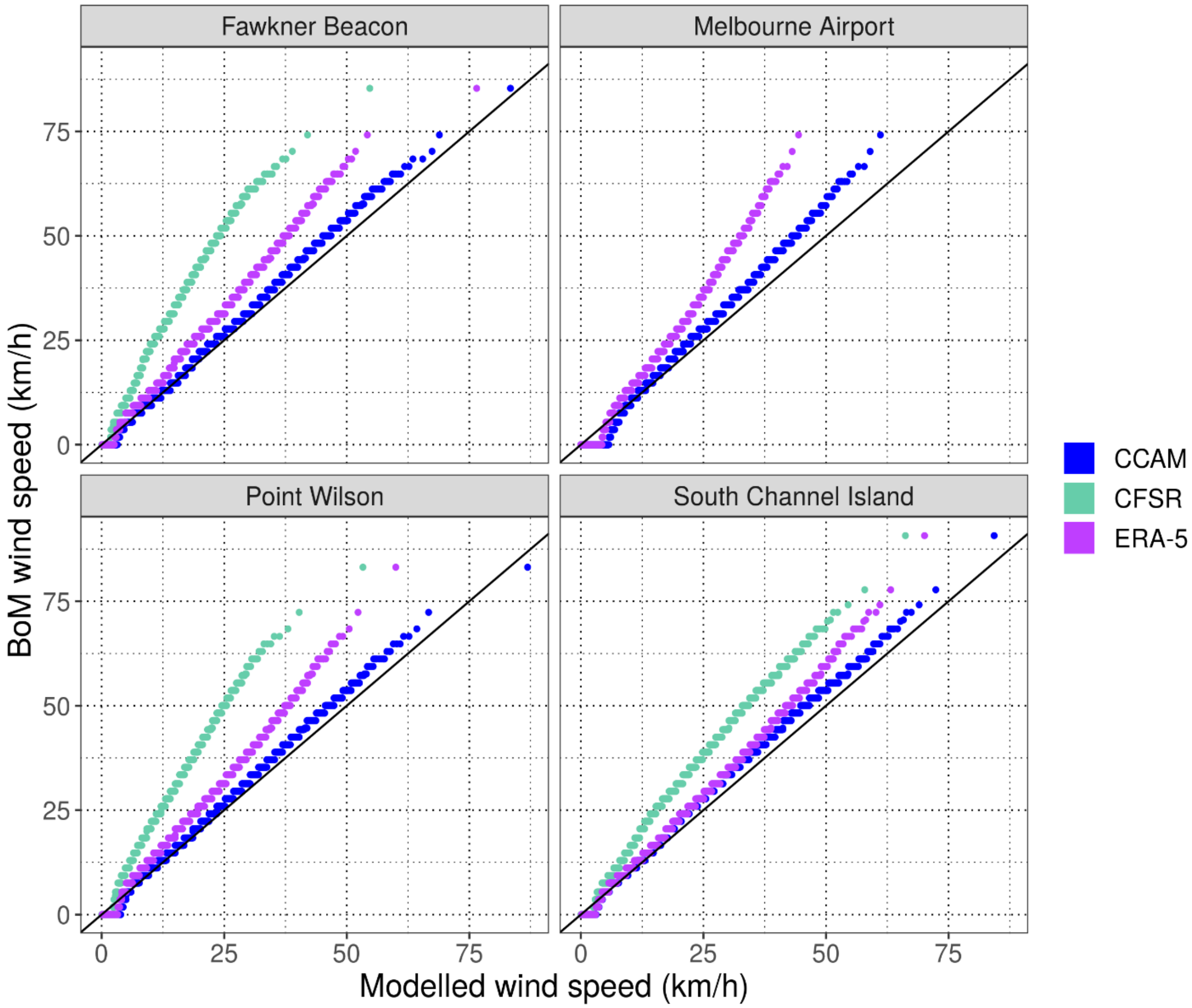

Figure 8.7: Quantile-quantile plots comparing Bureau of Meteorology (BoM) observed 10 m wind speeds (vertical axis) with modelled 10 m wind speeds (horizontal axis) for CCAM (blue), CFSR (green), and ERA5 (purple) for Fawkner Beacon, Melbourne Airport, Point Wilson, and South Channel Island. (Note that CFSR data was not available for Melbourne Airport).

8.4.2 Tides and Water Levels

This section provides comparisons from the SCHISM model with observations of total water levels, tides, and residuals (total water levels minus tides). Tide gauge locations and data sourced for analysis and subsequent validation of tides and non-tidal water levels are shown in Figure 8.8 and listed in Table 8.2.

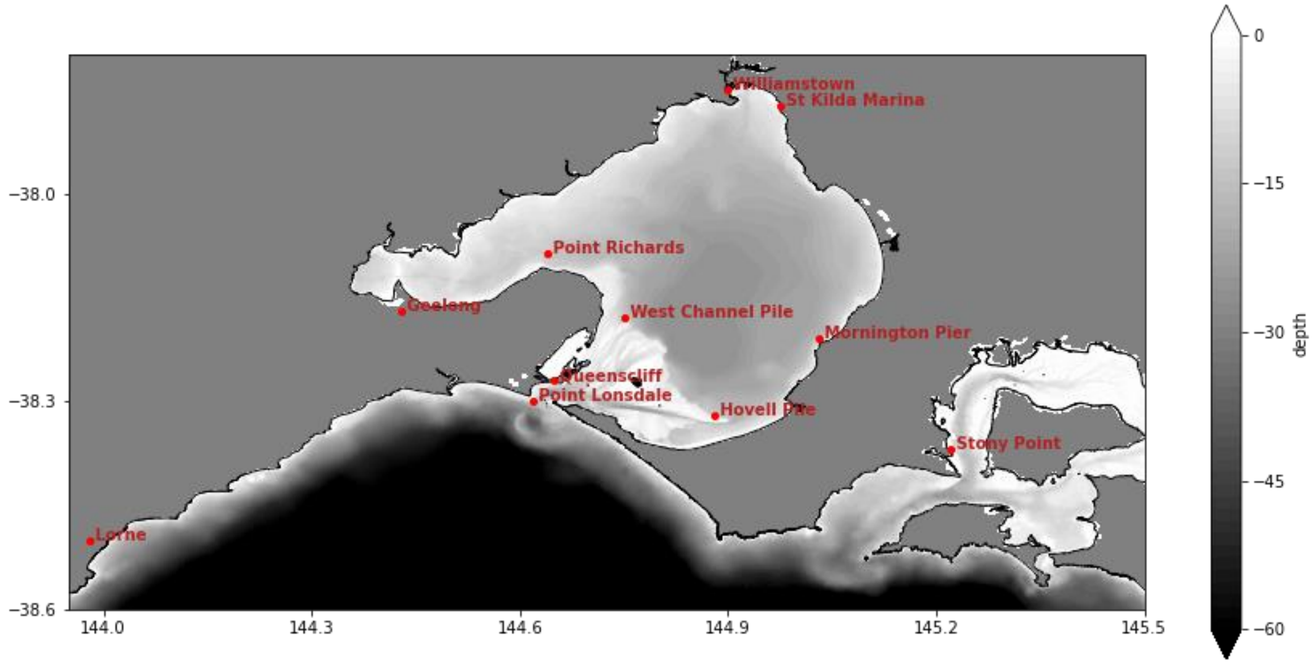

Figure 8.8: The location of tide gauges used for hydrodynamic validation.

Table 8.2: Tide gauge data obtained for use in the PPBCHA. NTC, PoMC, VRCA, and MW indicate data from gauges operated by the National Tidal Centre, the Port of Melbourne Corporation, the Victorian Regional Channels Authority, or Melbourne Water respectively.

Location	Longitude (E)	Latitude (S)	Period of record
Lorne (NTC)	143.98	38.5	1993–2017
Geelong (VRCA)	144.43	38.17	1965–2017
Point Lonsdale (PoMC)	144.62	38.3	1962–2017
Point Richards (VRCA)	144.641	38.086	1999-2017
Queenscliff (PoMC)	144.65	38.27	1991–2017
West Channel Pile (PoMC)	144.75	38.18	1991–2017
Hovell Pile (PoMC)	144.88	38.32	1991–2017
Williamstown (PoMC)	144.9	37.85	1966–2017
St Kilda Marina (MW)	144.975	-37.873	1977-present
Mornington Pier (MW)	145.03	-38.21	2010-present
Stony Point (NTC)	145.22	38.37	1993–2017

A primary use for the hydrodynamic model simulations is to provide total water level simulations to evaluate extreme water level statistics to define the design water levels for the inundation modelling around PPB. The focus in this section is therefore on total water level validation around PPB. Figure 8.9 provides a time-series comparison of model simulation with observations over a three-month period from May-July 1994 during which time a severe storm surge occurred. Additional time-series comparisons of other periods are shown in Appendix J.

A decrease in MSLP can be seen on May 26, 1994, associated with the passage of an easterly moving cold front along the Australian south coast (Figure 8.9a). In the preceding weeks, several weaker fronts occurred on the 18th and 21st, also indicated by pressure minima. The winds preceding the front are typically northwesterly and shift to southwesterly following the passage of the front. CCAM captured the pressure troughs and wind changes associated with these weather conditions extremely well during

May although it is noted that CCAM underestimated (by ~ 40%) the strength of another cold front that occurred late June. Figures 8.9(b-f) compares the SCHISM-simulated water levels with five tide gauges in PPB. Point Lonsdale, at the entrance to PPB, is a challenging location for models to replicate due to the strong gradients in flow and water level height on flood and ebb tide. At this and other locations, SCHISM captures the tidal range and phase well, although at some locations there is a tendency of SCHISM to slightly overestimate the tidal range. This is somewhat compensated by a tendency to underestimate the sea level residuals. Additional timeseries comparisons are provided in Appendix J for extreme events that occurred in 1999 and 2009.

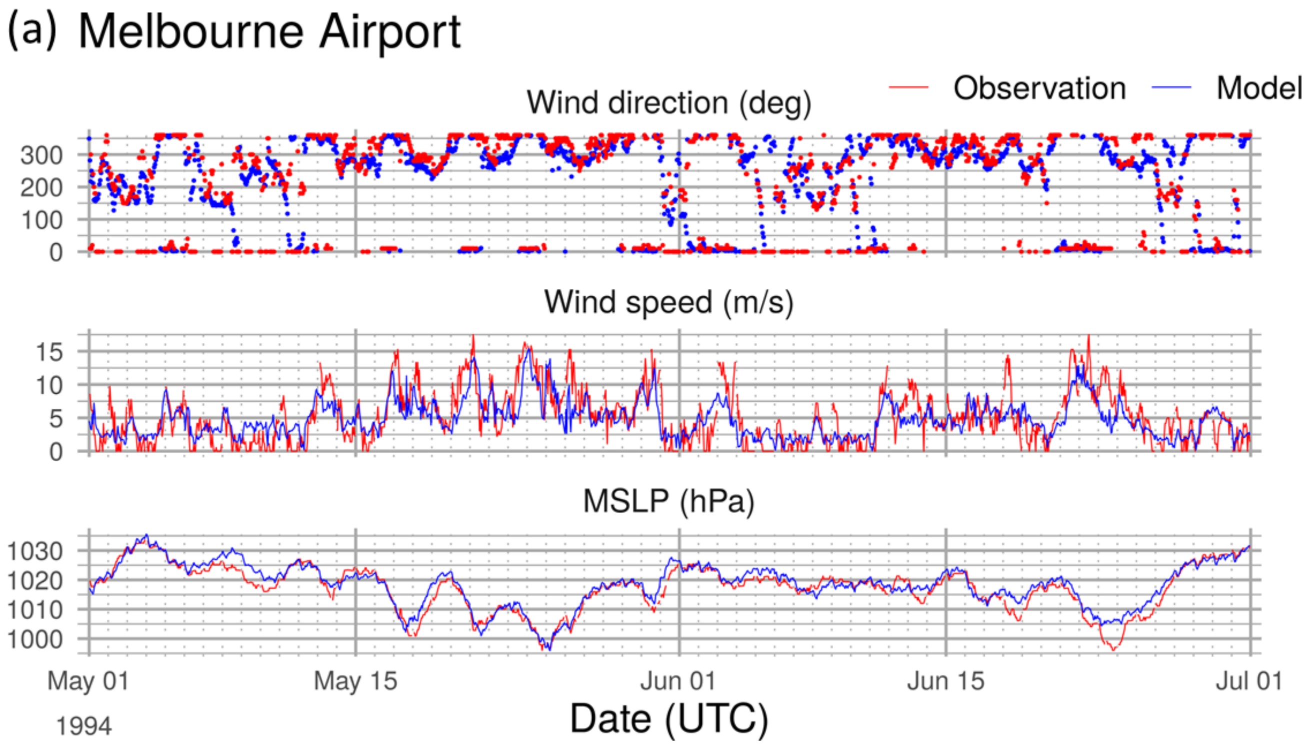

Figure 8.9: (a) Comparison of CCAM-simulated wind direction (degrees), 10 m wind speed (m/s), and mean sea level pressure (MSLP; hPa) with meteorological data at the location of Melbourne Airport over May and June 1994. (b-f) Comparison of SCHISM-simulated total water level, tidal and residual water levels with tide gauge measurements at Point Lonsdale, Queenscliff, Geelong, Williamstown and Hovell Pile.

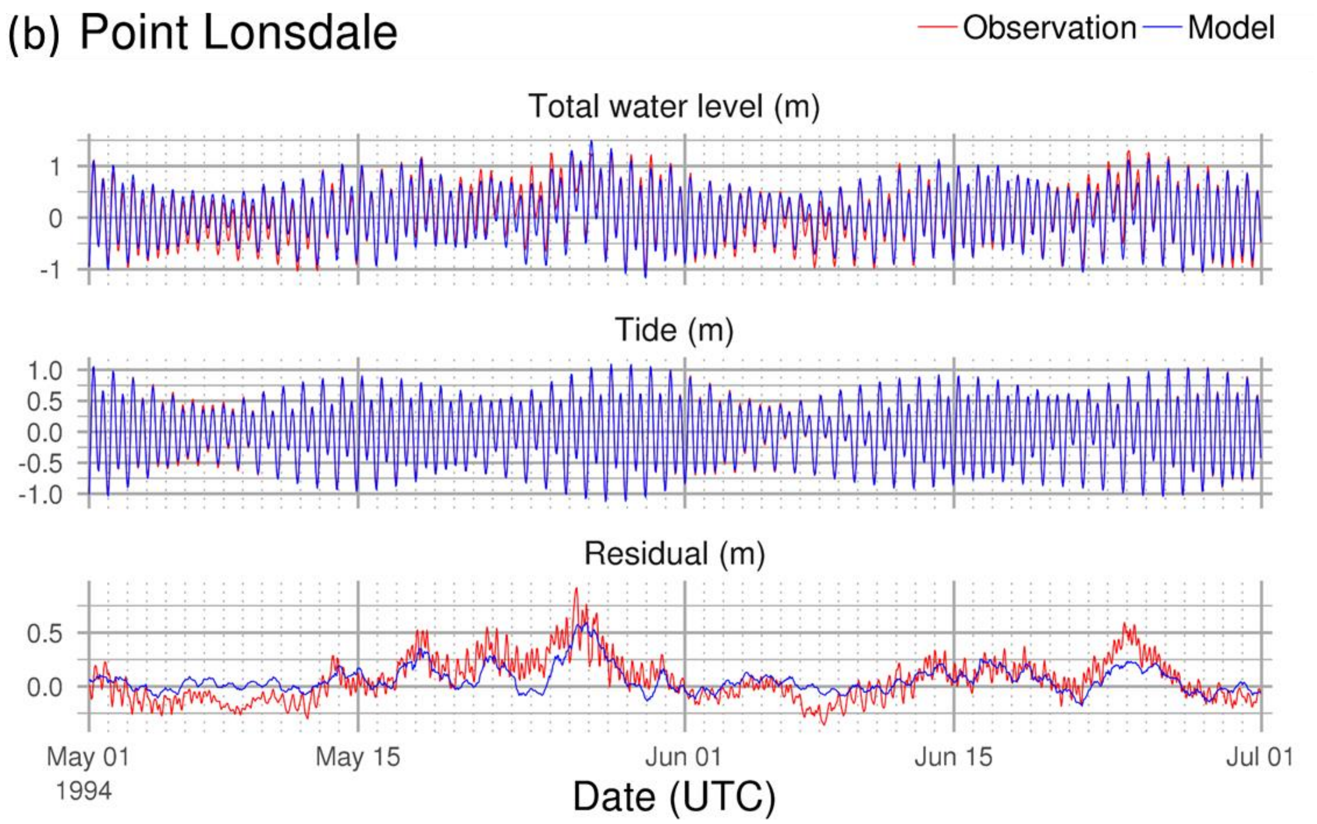

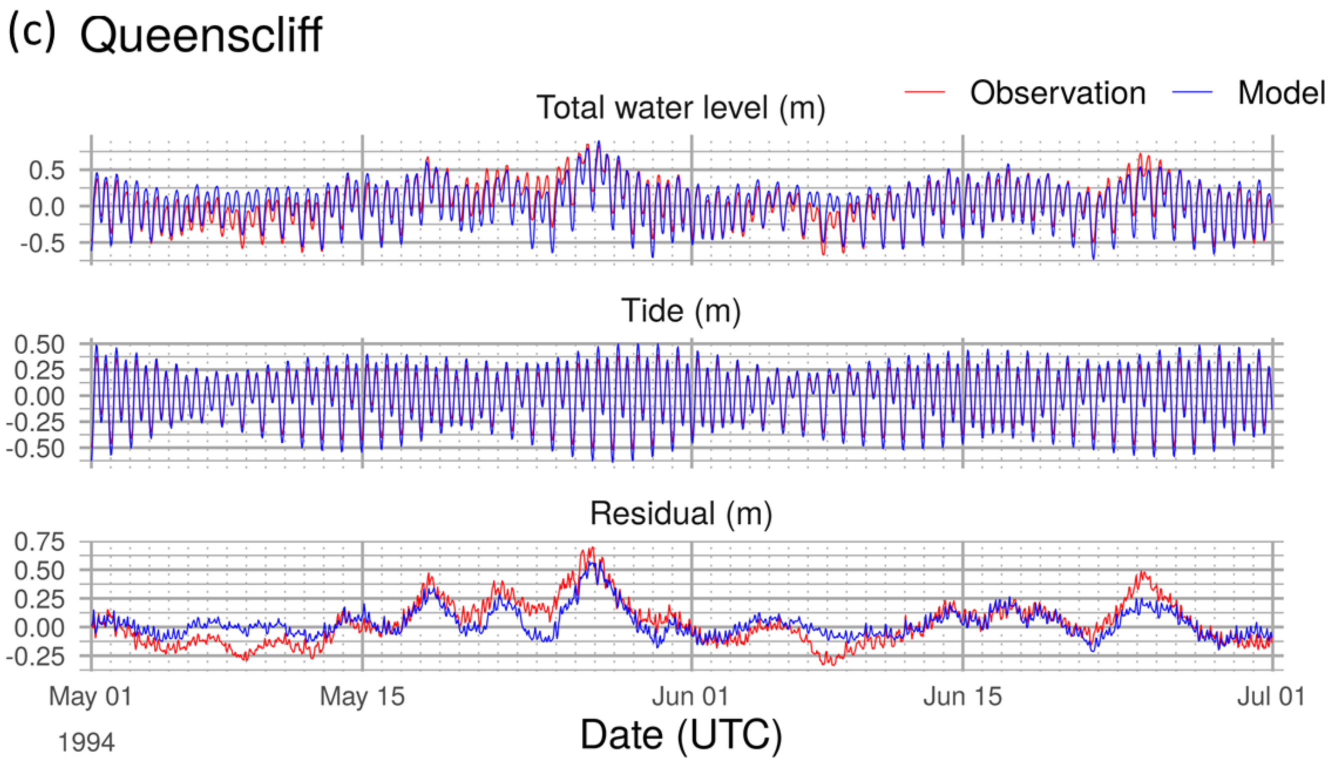

Figure 8.9: Continued.

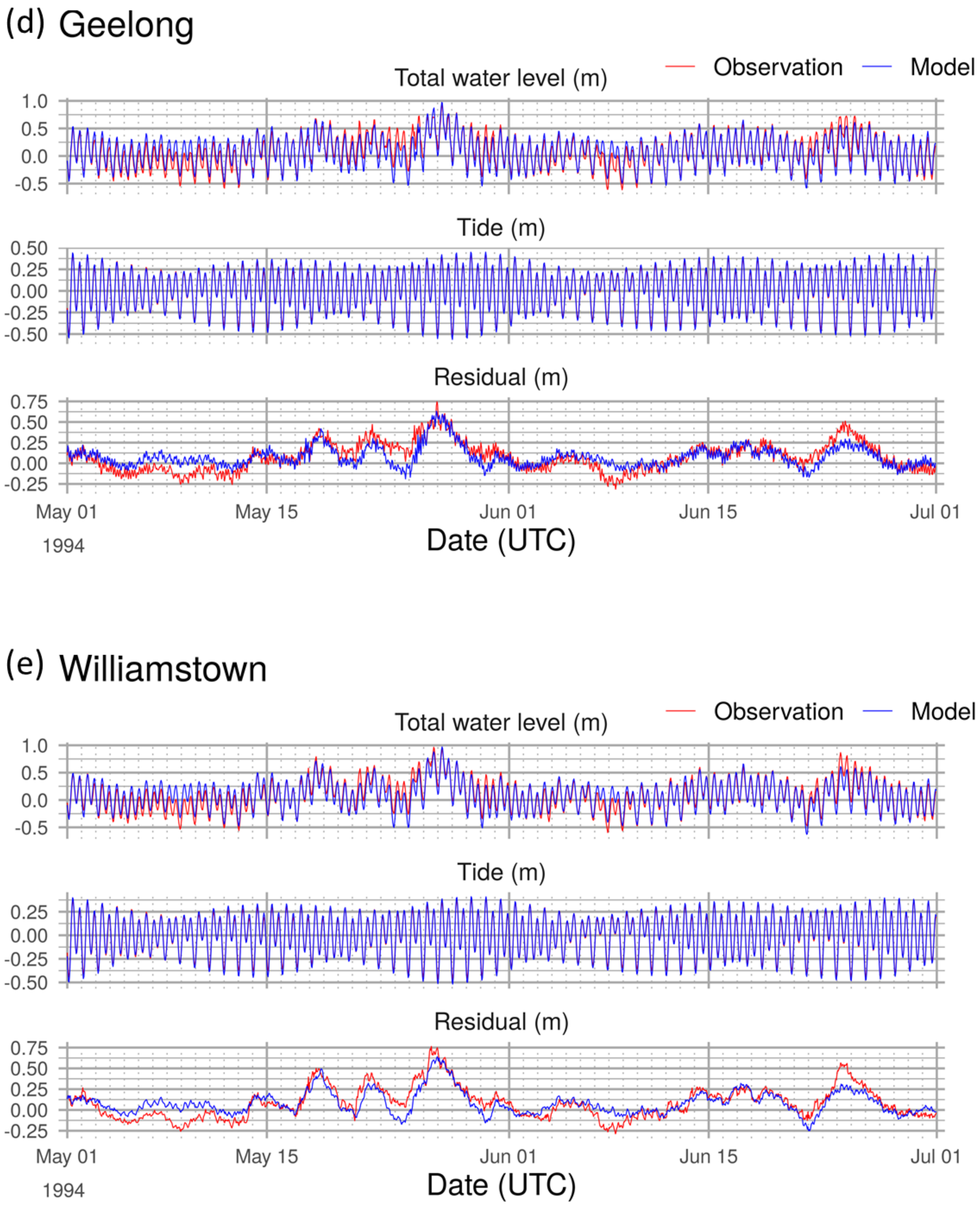

Figure 8.9: Continued.

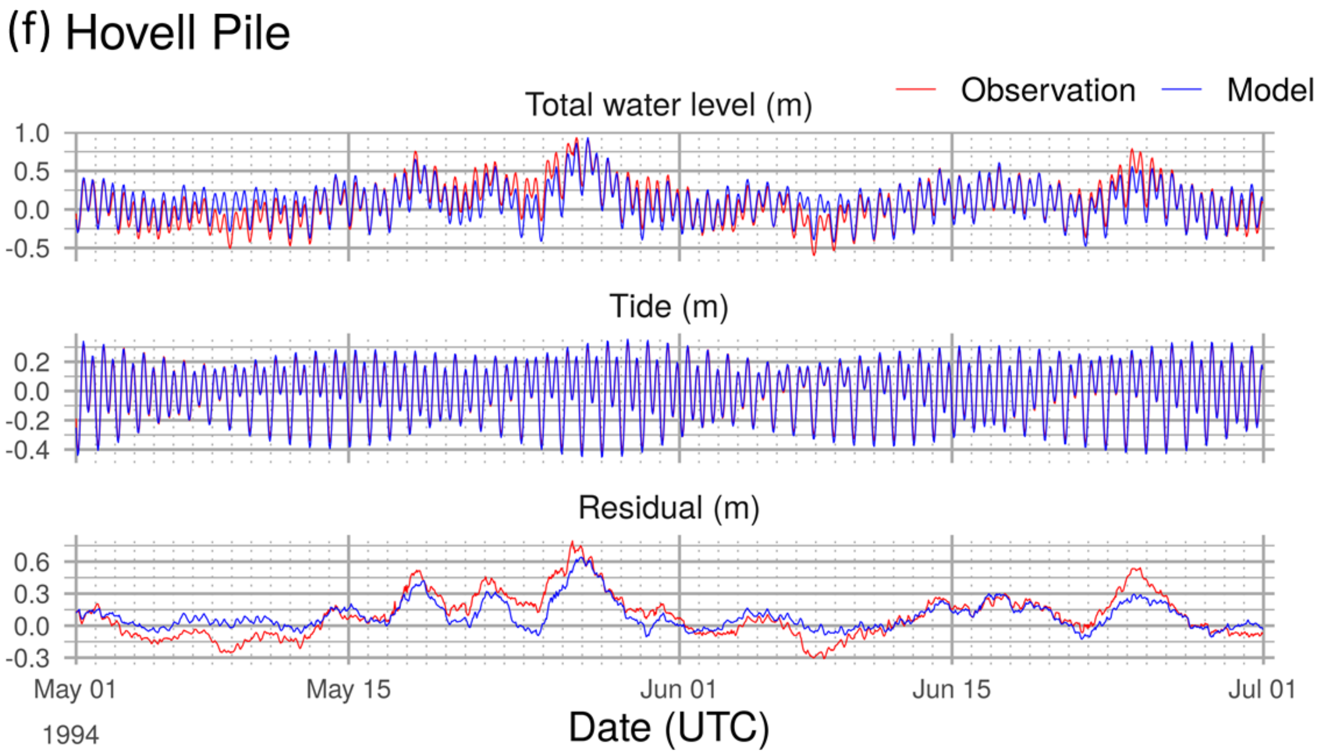

Figure 8.9 Continued.

A more systematic representation of model performance is given by quantile-quantile (Q-Q) plots, in which long-term, climatological differences (rather than individual events) between observed and modelled values can be more easily identified. This is particularly important for understanding the model's representation of extreme events, and subsequent calculation of total water level AEPs for the whole bay for use in the erosion and inundation hazard assessments, since observations are available at only discrete locations. The Q-Q plots for nine tide gauges distributed around PPB are shown in Figure 8.10 for the overlapping periods between the available observations and model simulations (see Table 8.2) with the top percentile values shown in red. These indicate that SCHISM has a tendency to underestimate extreme water levels at some gauges, particularly Point Richards, West Channel Pile, St Kilda Marina and Hovell Pile, while at the other locations, the agreement between modelled and observed extremes shows generally close agreement with only small biases in model simulations that are generally within ±0.1 m.

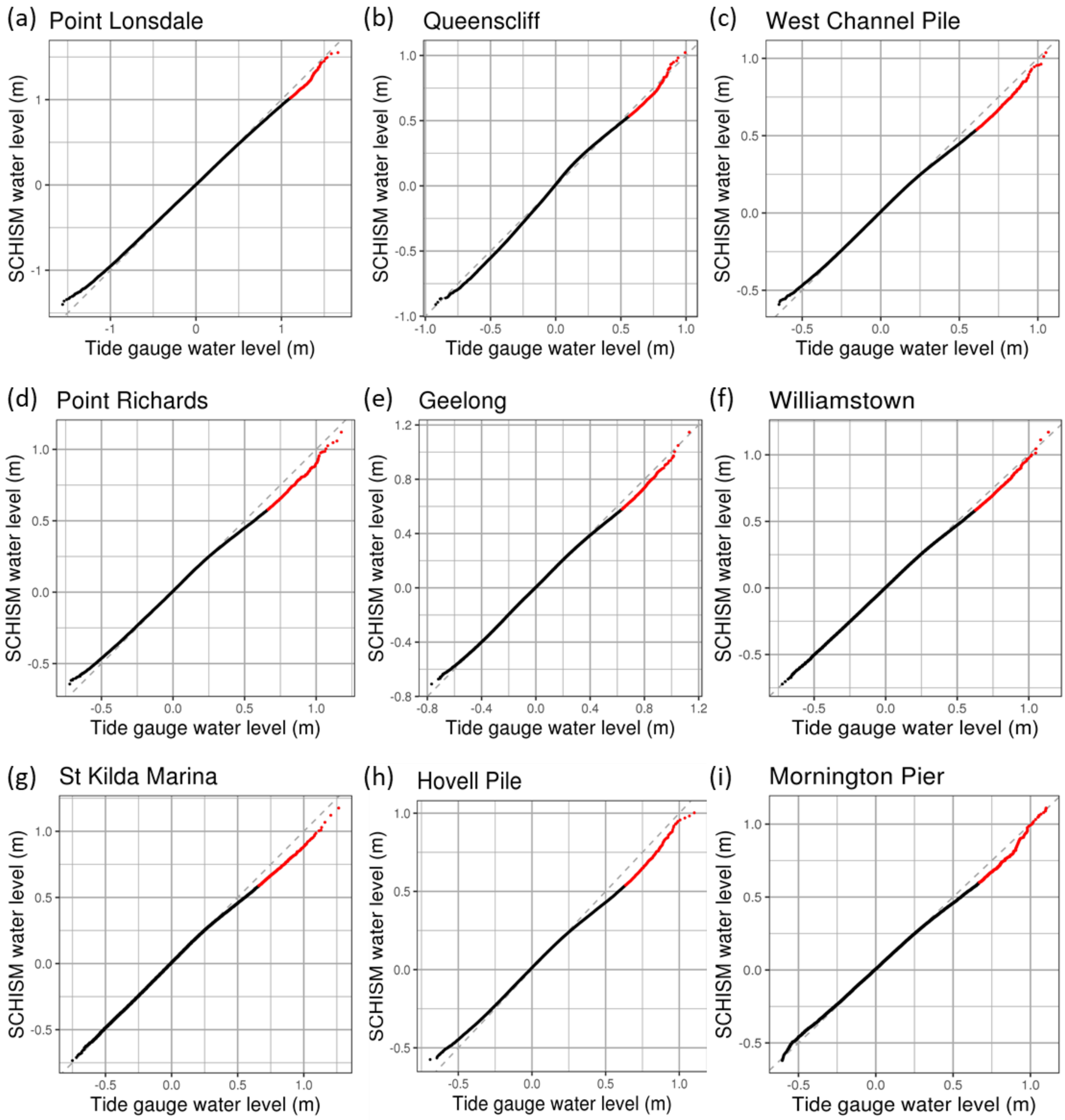

Figure 8.10: Quantile-quantile plots of total water levels at gauges within PPB for the overlapping time-periods for the data and model simulation as indicated in Table 8.2 (i.e. 35 years for Point Lonsdale, Geelong, Williamstown, St Kilda, and Hovell Pile). Values in red are the top 1 percentile values.

Summary statistics of root-mean-square error (RMSE) and correlation coefficient for the model performance against observations over the full calibration periods are presented in Table 8.3. Outside PPB at Lorne and Stony Point, RMSE errors are 0.12 and 0.17 m respectively. The largest RMSE error of 0.21 m occurs at Point Lonsdale at the entrance to PPB, owing to the aforementioned large gradients in sea levels and currents from tidal variations that occur over small distances in this region. However, further into PPB, the errors drop markedly to values ranging from 0.10 to 0.13 m across the six locations considered. Aside from Point Lonsdale, the RMSE errors in the tides are small in PPB ranging from 0.04 to 0.06 m whereas they range from 0.09 to 0.11 m for the non-tidal residuals (Table 8.3). The correlations between modelled and measured total water levels range from 0.87 to 0.97 arising from the extremely high correlations in the tides, which are all in the range of 0.97 to 0.99. The occurrence of timing errors in the meteorological forcing contributes to lower correlations for the non-tidal residuals, which range from 0.66 to 0.73. The meteorological forcing has a proportionately higher contribution to the overall correlation errors for locations inside PPB due to the smaller tidal range compared to Lorne and Stony Point. As discussed in relation to the observational periods, the errors in the meteorological forcing have been shown to lead to both over- and under-estimation of particular extreme sea level events. As a result, and because of the very good agreement shown by the Q-Q plots (Figure 8.10), these errors are considered unlikely to contribute to significant biases in the estimation of AEPs discussed in Section 8.5.1 for use in the hazard assessments.

Table 8.3: Root mean square errors (RMSE) and correlations calculated over the calibration periods

Location	RMSE (m)			Correlation		
	Total	Tidal	Non-tidal	Total	Tidal	Non-tidal
Lorne	0.12	0.07	0.10	0.97	0.99	0.71
Geelong	0.11	0.04	0.10	0.91	0.98	0.66
Point Lonsdale	0.21	0.17	0.11	0.95	0.99	0.68
Point Richards	0.11	0.04	0.10	0.90	0.98	0.71
Queenscliff	0.11	0.06	0.09	0.92	0.98	0.73
West Channel Pile	0.10	0.04	0.10	0.89	0.98	0.73
Hovell Pile	0.11	0.05	0.10	0.88	0.97	0.73
Williamstown	0.11	0.04	0.10	0.90	0.98	0.73
St Kilda Marina	0.13	0.05	0.11	0.87	0.97	0.70
Mornington Pier	0.11	0.04	0.10	0.90	0.98	0.72
Stony Point	0.17	0.12	0.12	0.97	0.99	0.68

8.4.3 Waves

Waves simulated by the SCHISM-WWMIII model were calibrated against wave observations from the Portsea wave buoy and two bottom-mounted acoustic wave and current profilers (AWACs) near the entrance to PPB (Figure 8.11) during two simulation time periods between 1 October 2011 and 1 April 2012, and between June 2014 and August 2014 (when the AWACs were deployed). Example time-series comparisons between measured and modelled wave heights (Hs) over two durations during the first (2011) time period are provided in Appendix J (Figure J13), and for brevity only the Q-Q plots are shown here (Figures 8.12 and 8.13).

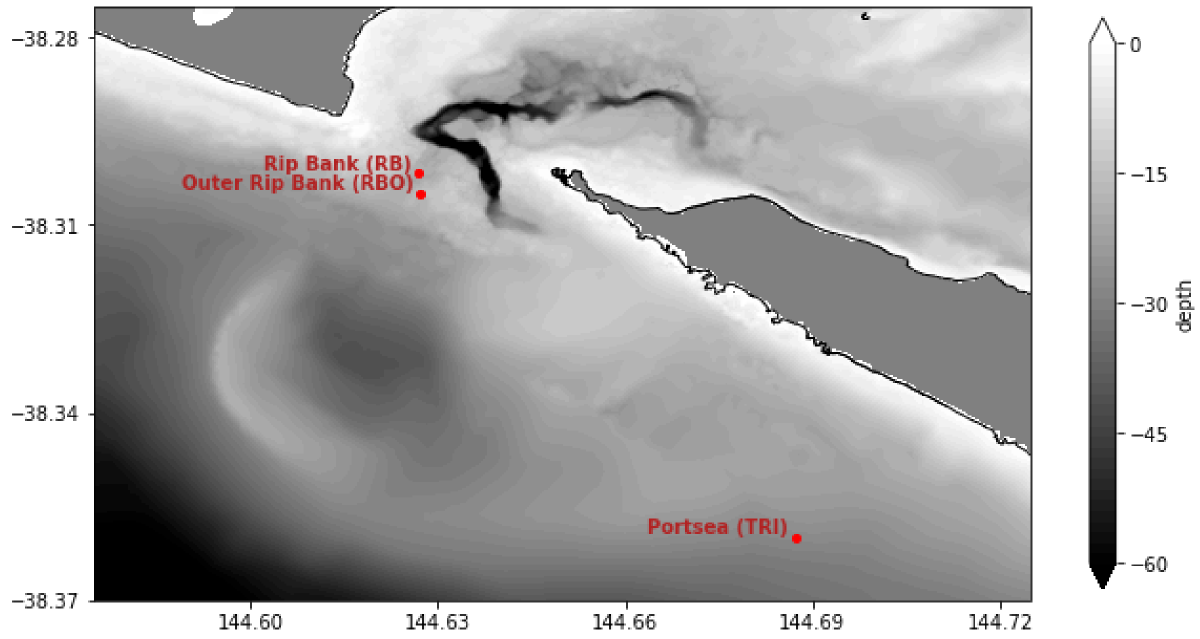

Figure 8.11: Locations of the Portsea wave buoy and AWAC moorings used for wave validation. The water depths at the wave buoy locations are: Rip Bank: 18.69 m, Outer Rip Bank: 21.08 m, Portsea: 27.94 m.

Figure 8.12 presents the Hs results over the 2011 period as a scatter-QQ plot. The ranked values are shown by the red points and indicate that there is overall close agreement between the modelled and observed wave heights over the period shown. These results indicate RMS difference errors of around 0.419 m for the AWACs at the entrance to PPB and 0.346 m at the Portsea buoy. There is a small positive bias of Hs at Rip Bank of 0.051 m and a small negative bias of -0.027 m at Outer Rip Bank. At Portsea the modelled Hs has a small positive bias of 0.029 m.

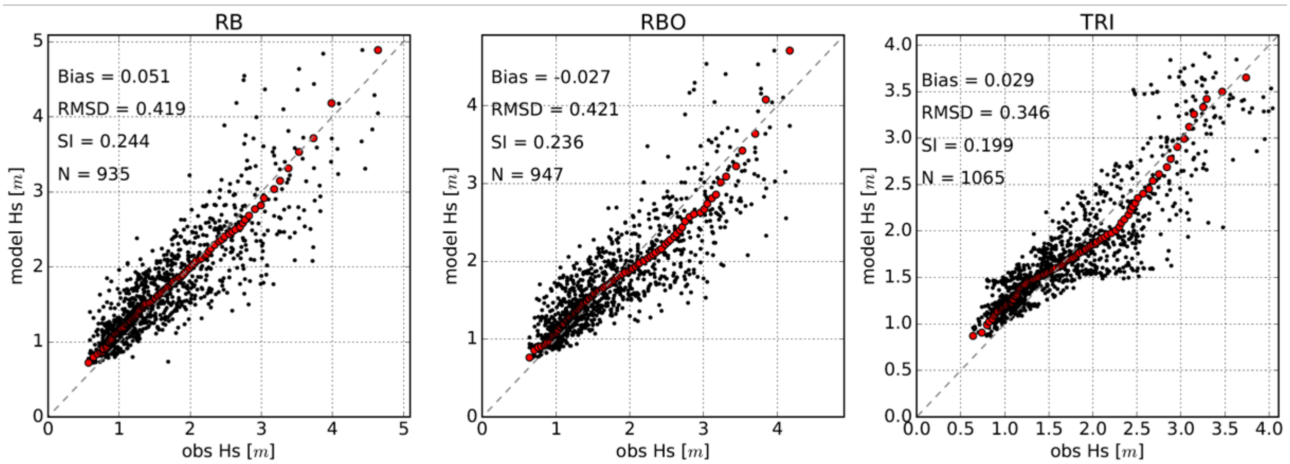

Figure 8.12: Scatter Q-Q plots of observed and modelled significant wave height (Hs) at the three wave observation locations shown in Figure 8.11.

In Figure 8.13, the observation points have been coloured by wave period and show that the highest density of modelled wave heights occur for values between 0.5 and 1.5 m and that there is close one-to-one agreement with the observed values. The wave periods for the most densely occurring values are mainly in the range of 10-13 seconds. Long period waves of 15 s or more (orange to red points) are distributed throughout the range of Hs values with no overall bias evident at Rip Bank (RB) or Outer Rip Bank (RBO). At Portsea (TRI), there appears to be a slight bias towards longer period waves in the model and at all three locations a slight negative bias in wave periods below 10 s in the model (blue points).

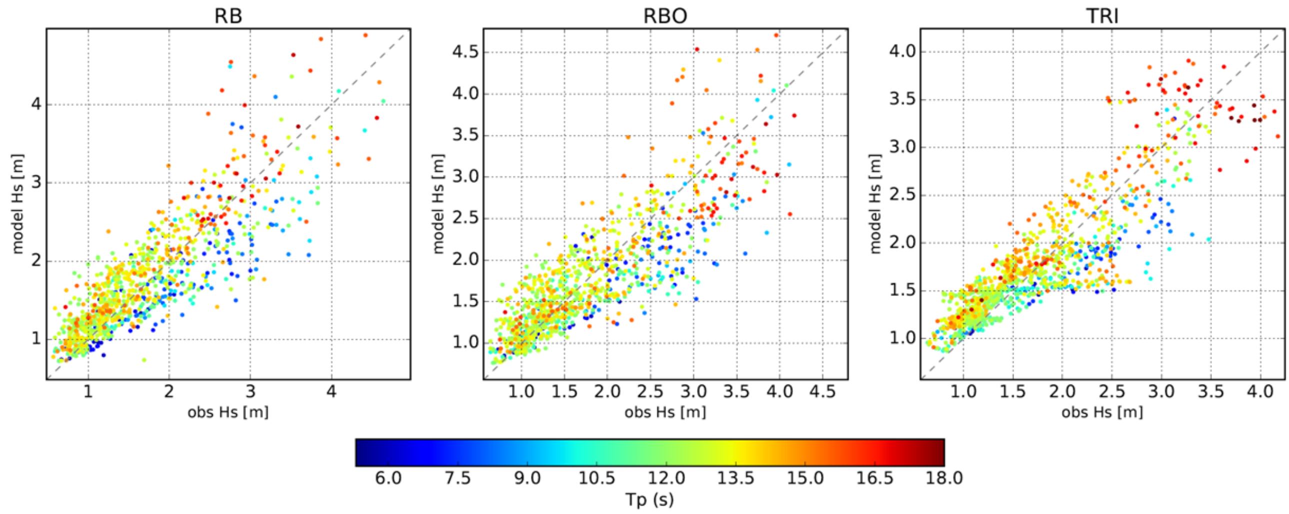

Figure 8.13: Significant wave height (Hs) scatter plot coloured by observed peak period (Tp) at the three wave observation locations shown in Figure 8.11.

The wave observations at the three locations (Rip Bank, Outer Rip Bank, and Portsea) for October and December 2011 were also used to validate the baseline SCHISM-WWMIII outputs of Hs and Tp (Figure 8.14). The influence of the semi-diurnal tides on significant wave height (Hs) at the two AWACs at the Entrance to PPB (Rip Bank and Outer Rip Bank) is well captured in the model, with the higher waves occurring during ebb tidal flow and lower waves occurring during the flood tide phase. The magnitudes of Hs are also well captured at these two AWACs for both time periods. The Portsea wave buoy data (in deeper water and away from the entrance channel) does not exhibit the semi-diurnal influence on wave height, which is also captured by the model. Observed and modelled Hs were well correlated at all three locations, with correlation coefficients of ≥0.87 (Table 8.4).

It is acknowledged that the SCHISM wave model calibration has been limited to the three locations outside PPB and that additional in-situ wave observations, particularly inside PPB, would be preferable for calibration. However, the three locations (shown in Figure 8.11) were the only wave data available for model calibration prior to this project's Gap Analysis (McInnes et al., 2019). Project timelines did not allow for wave data inside PPB, identified during the Gap Analysis and discussed in the following paragraphs, to be used for further calibration. However, it is noted that the entrance to PPB is an important location to correctly capture the swell waves entering the bay, which experiences complex wave-current interaction that is challenging for wave models, particularly those that do not account for currents (Rapizo et al., 2017). Furthermore, the "ST4" source terms physics package used in WWMIII (the wave model component of SCHISM) have been extensively tested and verified as highly accurate, particularly in enclosed, fetch-limited situations such as PPB (Liu, et al., 2019). Tuneable parameters in such physics packages in coastal wave models are primarily limited to shallow water physics (e.g. depth-induced wave breaking and bed roughness). Since all of the wave observations within PPB that were made available to the project team were in relatively deep water, there was little further calibration that could be performed. The data discussed in the following paragraphs is therefore used strictly for validation of the performance of the simulations and was not used to further tune (calibrate) the WWMIII model.

The Gap Analysis (McInnes et al., 2019) identified a programme of wave buoy deployments within PPB during the mid-1970s and 1980s by the Port Melbourne Corporation (PMC), known as the Port of

Melbourne Authority (PMA) at the time. Additionally, a small amount of wave data collected off Rosebud in 2003 was also obtained from a PMC report (Cardno, 2019). Figure 8.15 shows the locations and time periods of these various data sets. The wave buoy data were available from PMA from eight locations for various durations within a 2.5-year period (1974-1977; Figure 8.15). The data consist of 4-hourly wave parameters (bulk statistics) recorded by non-directional Datawell Waverider buoys. The bulk wave statistics included are maximum wave height (Hmax), significant wave height (Hs), significant wave period (Ts), and zero-crossing-wave period (Tz). However, the years of operation (1974-1977) mean that the data cannot be used directly for validation of the PPBCHA modelling, which runs from 1980-2014. This is due to the constraint of the availability of high-resolution wind and MSLP forcing data from CCAM that relies on ERA-Interim forcing, which is only available from 1979. Instead, the seasonal variability of Hs simulated by SCHISM is compared to short periods of observations from these early wave buoy deployments for three selected locations: St. Leonards, Altona and Aspendale, shown as boxplots in Figures 8.16, 8.17 and 8.18 respectively.

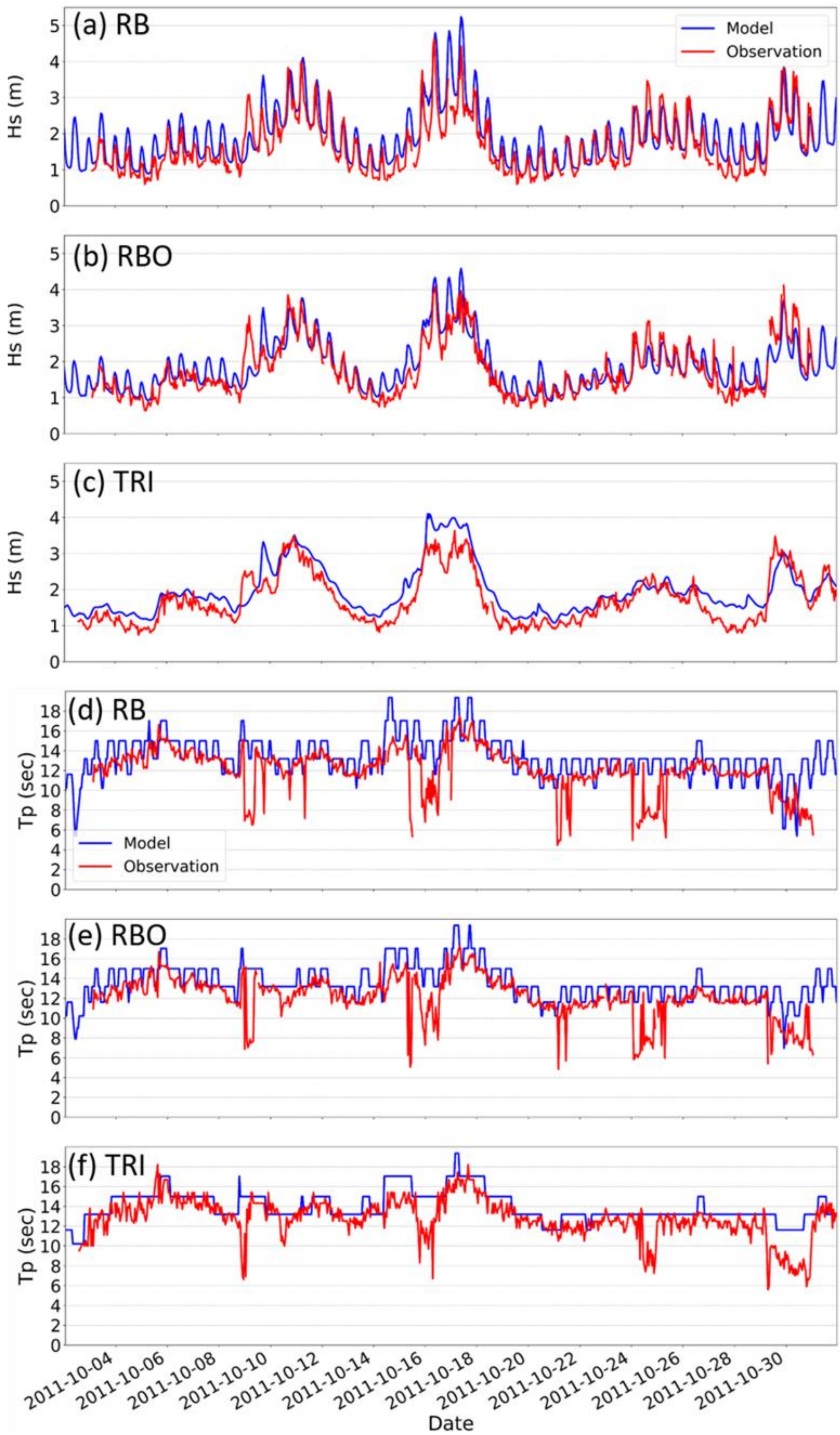

Figure 8.14: Measured (red line) and modelled (blue line) timeseries of significant wave height (Hs) (a-c; g-i) and wave peak period (Tp) (d-f; j-l) at the three observation locations shown in Figure 8.11 during October 2011 (a-f) and December 2011 (g-l).

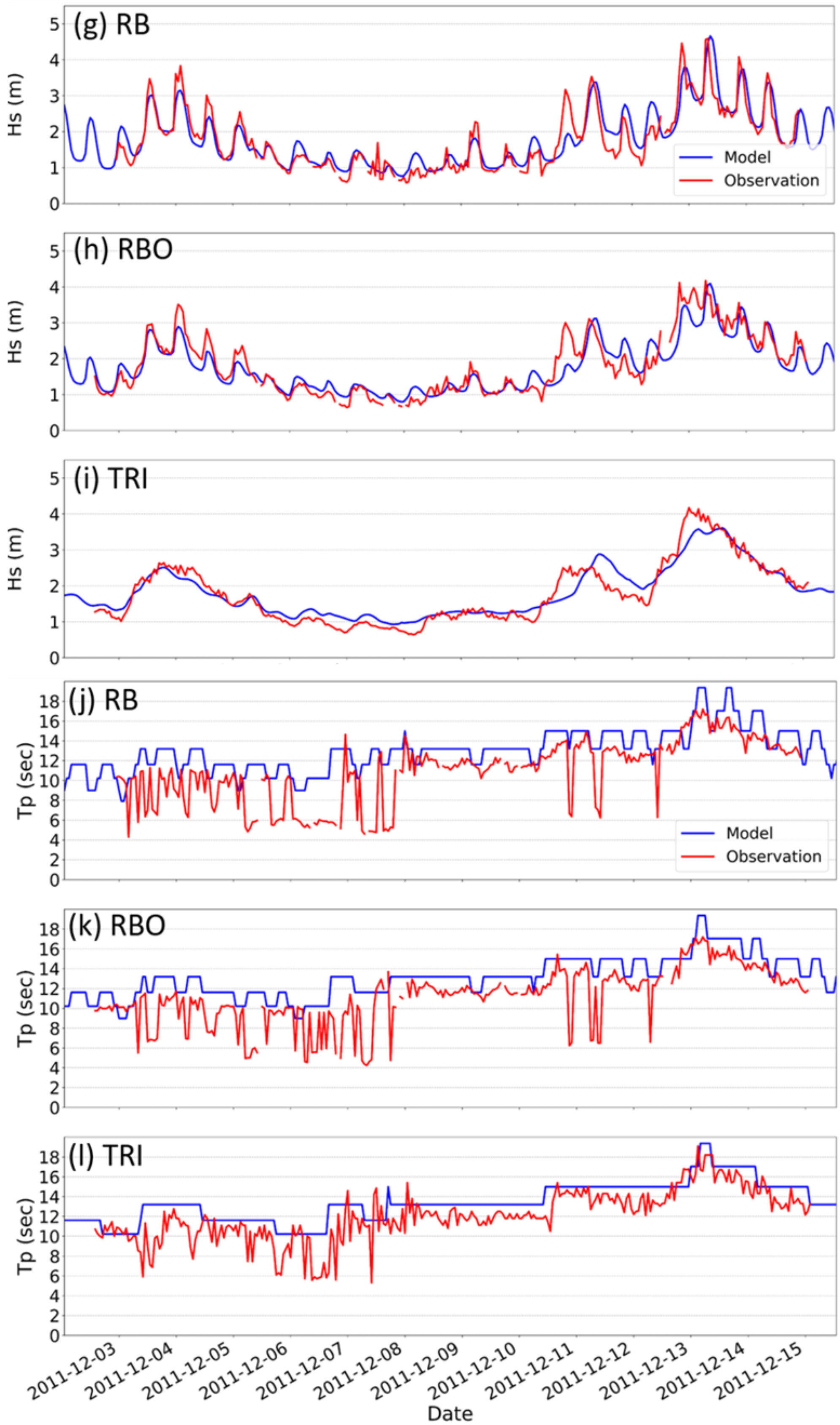

Figure 8.14: Continued.

Table 8.4: Root mean square errors (RMSE) and correlations between observations and modelled significant wave heights (Hs) for locations shown in Figures 8.11 and 8.15

Location	Observation period	RMSE (m)	Correlation	Number of observations (N)
Rip Bank	Oct & Dec 2011	0.449	0.87	937
Outer Rip Bank	Oct & Dec 2011	0.392	0.87	948
Portsea	Oct & Dec 2011	0.375	0.90	1065
Rosebud 1 & 2	Aug-Sep 2003	0.301	0.61	643
Hobsons Bay A & B	Oct 1983-Jan 1984	0.168	0.34	1297
Safety Beach A & B	Mar 1984-May 1985	0.248	0.56	2882

At the St Leonards wave buoy location, approximately 18 months of wave data was available from January 1976 to mid-1977, although due to gaps in the record, the seasonal averages for 1977 are less reliable (Figure 8.16). In summer, Hs from the model shows small interannual variability with mean values in the range of 0.3 to 0.4 m and the 75th percentile value typically around 0.5 m. Extreme values exceeding 1.5 m in the model simulation for this season occurred in 1990 and 1994 but for other years tend to be below 1.5 m. The available observations are generally consistent with these results. The model results for autumn are similar to summer in terms of the range of wave heights and their interannual variability, and these are also consistent with the observations for this season. In winter the modelled values of Hs typically show a higher mean of up to 0.5 m and more year-to-year variability. The less energetic modelled winter seasons (e.g. 1982 and 1987) exhibit a similar mean and quartile range to the 1976 observations. Waves in autumn exhibit similar characteristics to those in spring although the interannual variability is slightly more pronounced.

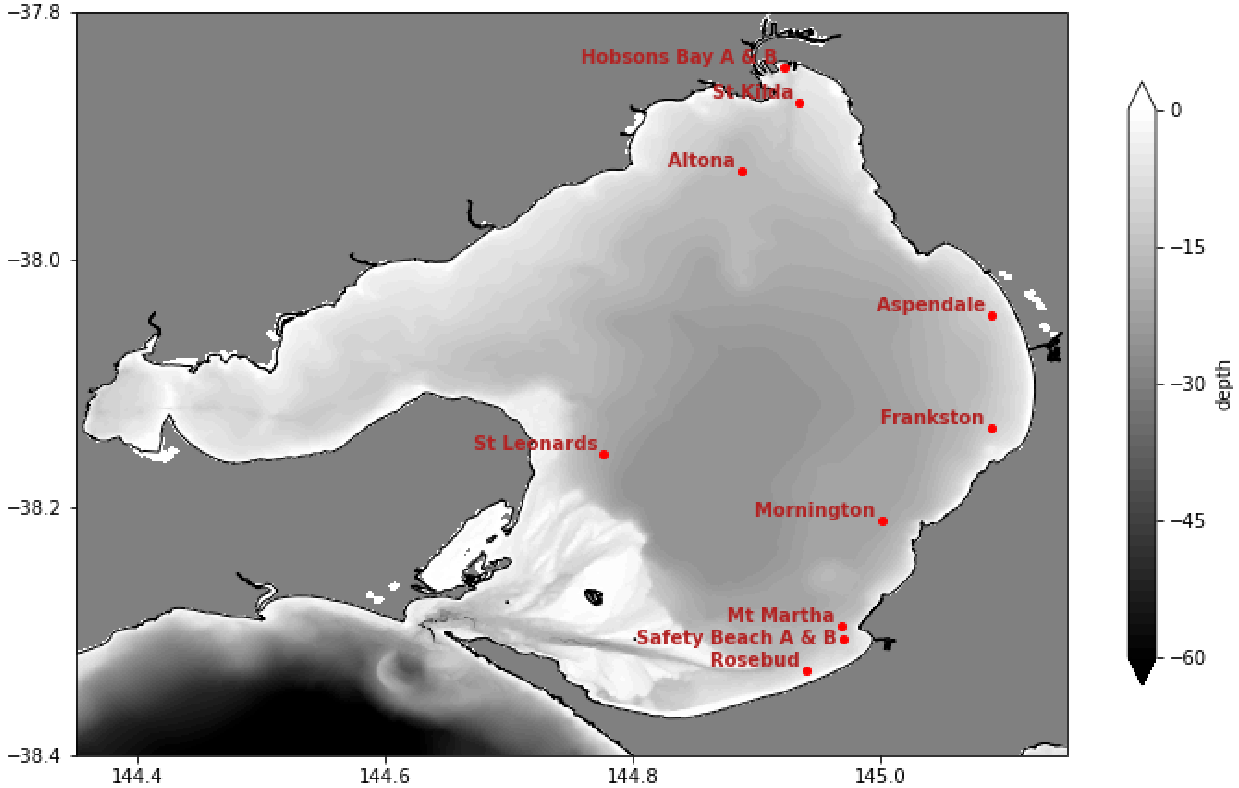

Figure 8.15: (a) Location and (b) time periods for which Waverider buoys (or other in-situ wave observations), used for validation in this report, were deployed in PPB within the period 1974-1977, 1984-1985, and 2003.

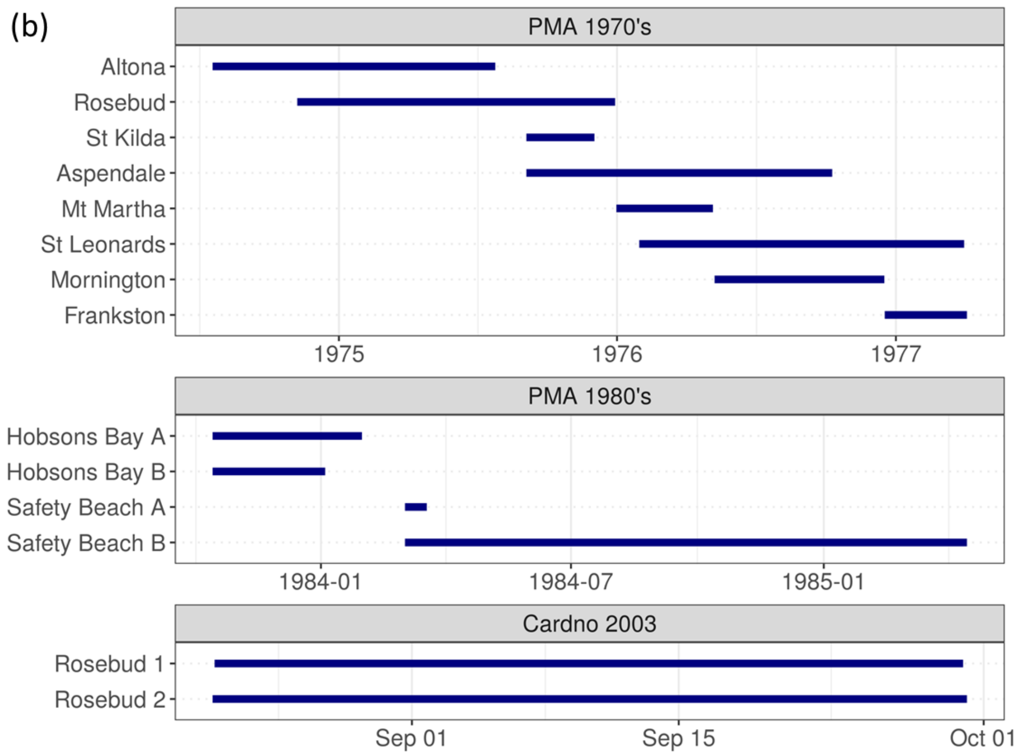

Figure 8.15: Continued.

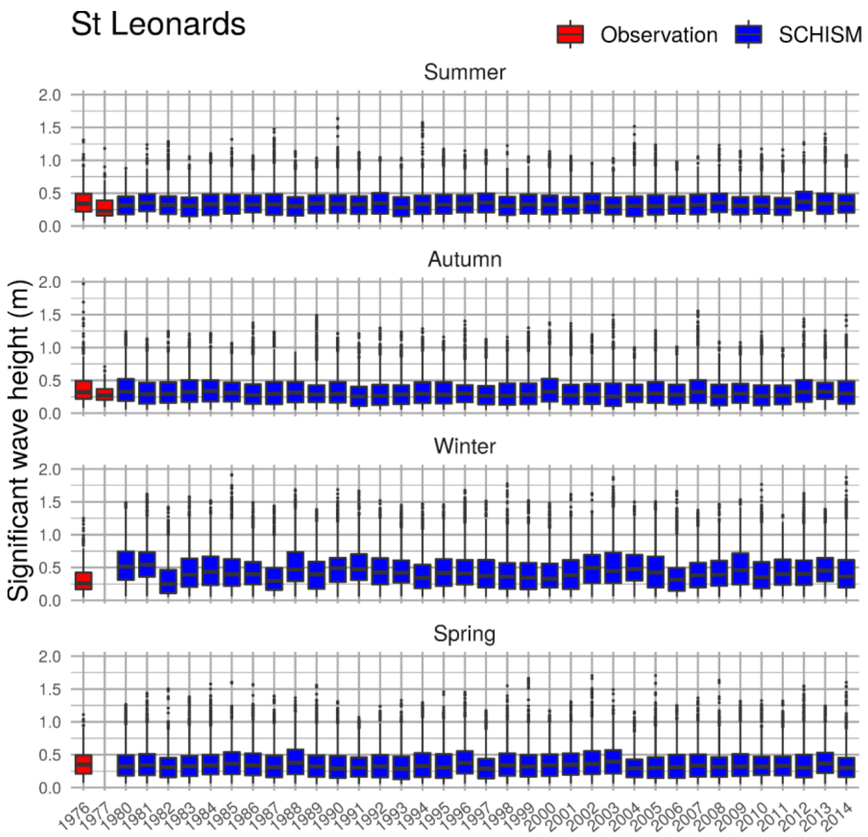

Figure 8.16: Boxplots showing seasonal mean significant wave height (Hs) (horizonal black bar), quartiles of Hs (coloured boxes) and full range of data (black dots) from SCHISM-WWMIII (blue boxes) over the hindcast period at St Leonards. Available PMA observations from the 1970s are shown in red.

Significant wave heights for Altona, in the north of the bay, are shown in Figure 8.17. In summer, the modelled means and 75th percentile values are typically slightly higher with slightly more interannual variability than St Leonards. The mean and range of the model results is consistent with available observations. In autumn the mean and range of the model results are both lower than the summer results and also the available autumn observations. Results for winter and to a lesser extent spring exhibit more interannual variability than the other seasons and are consistent with the observations for this location.

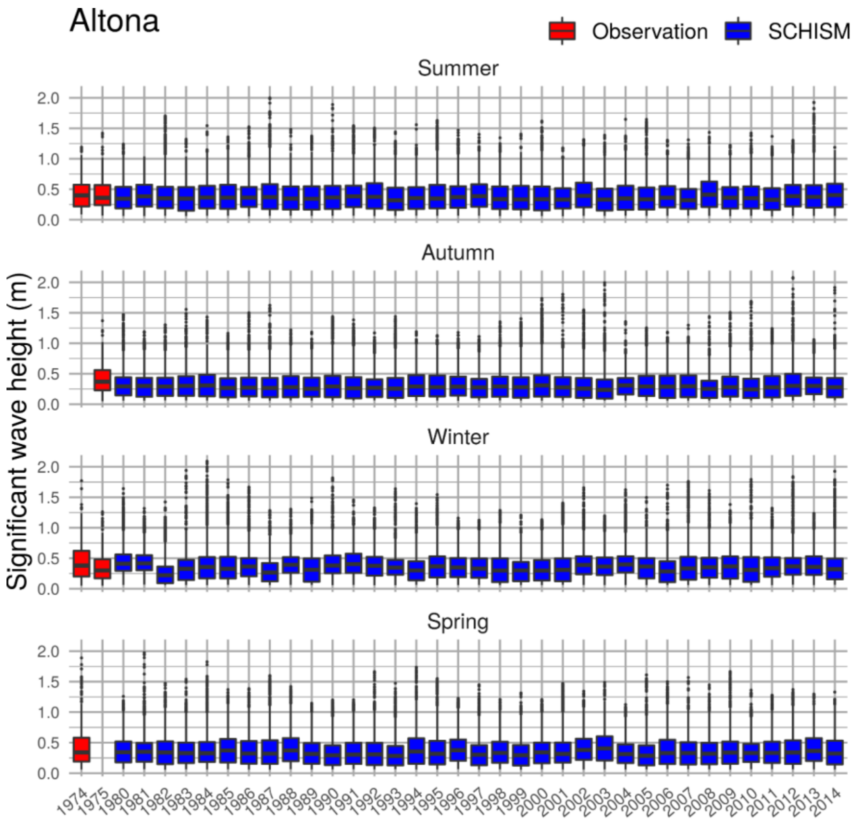

Figure 8.17: Boxplots showing seasonal mean significant wave height (Hs) (horizonal black bar), quartiles of Hs (coloured boxes) and full range of data (black dots) from SCHISM-WWMIII (blue boxes) over the hindcast period at Altona. Available PMC observations from the 1970s are shown in red.

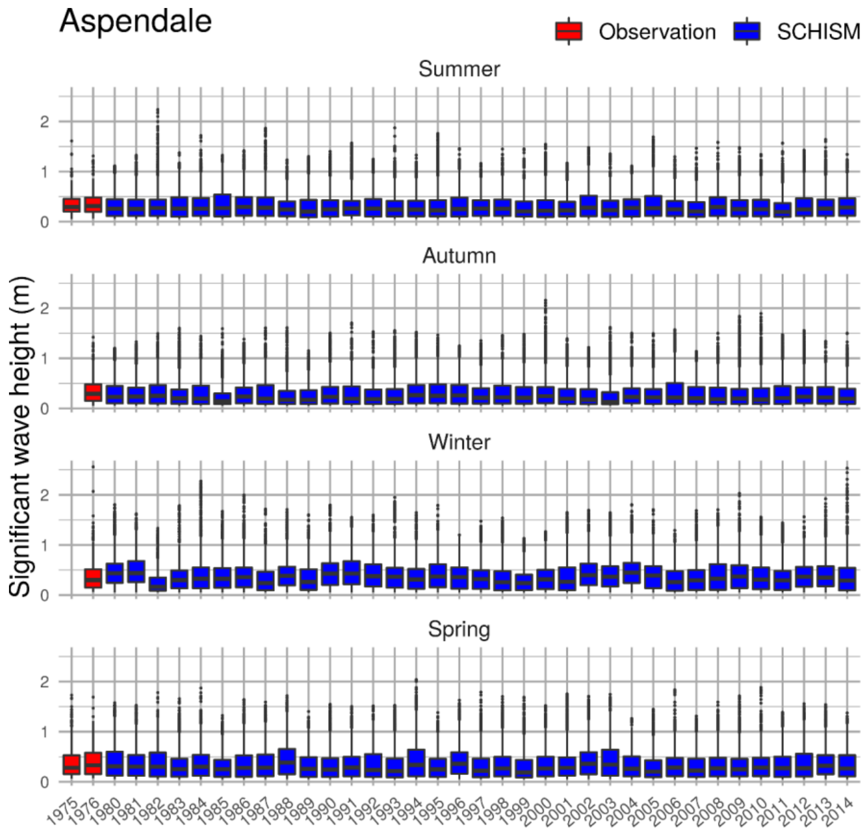

Figure 8.18: Boxplots showing seasonal mean significant wave height (Hs) (horizonal black bar), quartiles of Hs (coloured boxes) and full range of data (black dots) from SCHISM-WWMIII (blue boxes) over the hindcast period for Aspendale. Available PMC measurements at Aspendale and nearby sites of Frankston and Mornington from the 1970s are shown in red.

The PMA wave buoy data from the 1980s and the PMC data from 2003-2004 indicated in Figure 8.15 does overlap directly with the SCHISM-WWMIII hindcast, allowing for direct comparison of timeseries. Figures 8.19 and 8.20 compare observed and modelled significant wave height (Hs) and zero-crossing period (Tz) during the 1980s PMA buoy deployments at Hobsons Bay and Safety Beach, respectively. Figure 8.21 compares Hs and wave peak period (Tp) during the 1980s Rosebud deployments. These plots all show that the SCHISM-WWMIII hindcast simulates Hs in the same range, with a close correspondence between the timing and maxima of peaks in Hs. Tz comparisons are not as good, however it is noted that Tz is not a directly simulated quantity of spectral (phase-averaged) wave models (such as SCHISM-WWMIII), rather it is estimated from the frequency distribution. Spectral analysis-derived frequency statistics, e.g. peak period (Tp), generally provide much more meaningful comparisons between wave buoy data and spectral wave models. The comparison of Tp at Rosebud in Figure 8.21 is thus better than of Tz in the previous plots (the larger spikes in the buoy Tp tend to occur during periods of very low Hs and may thus be outliers).

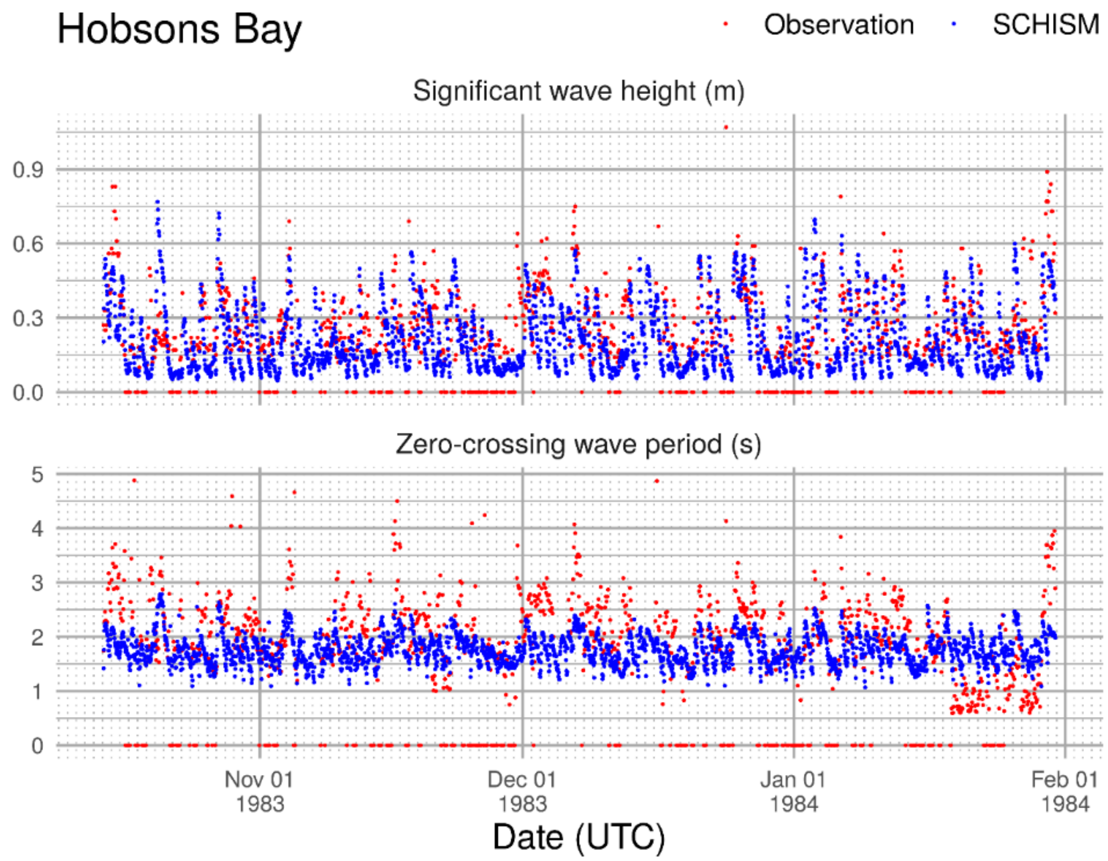

Figure 8.19 Significant wave height (Hs; m) and zero-crossing period (Tz; seconds) at Hobsons Bay A from observations (red dots) and SCHISM-WWMIII simulations (blue dots).

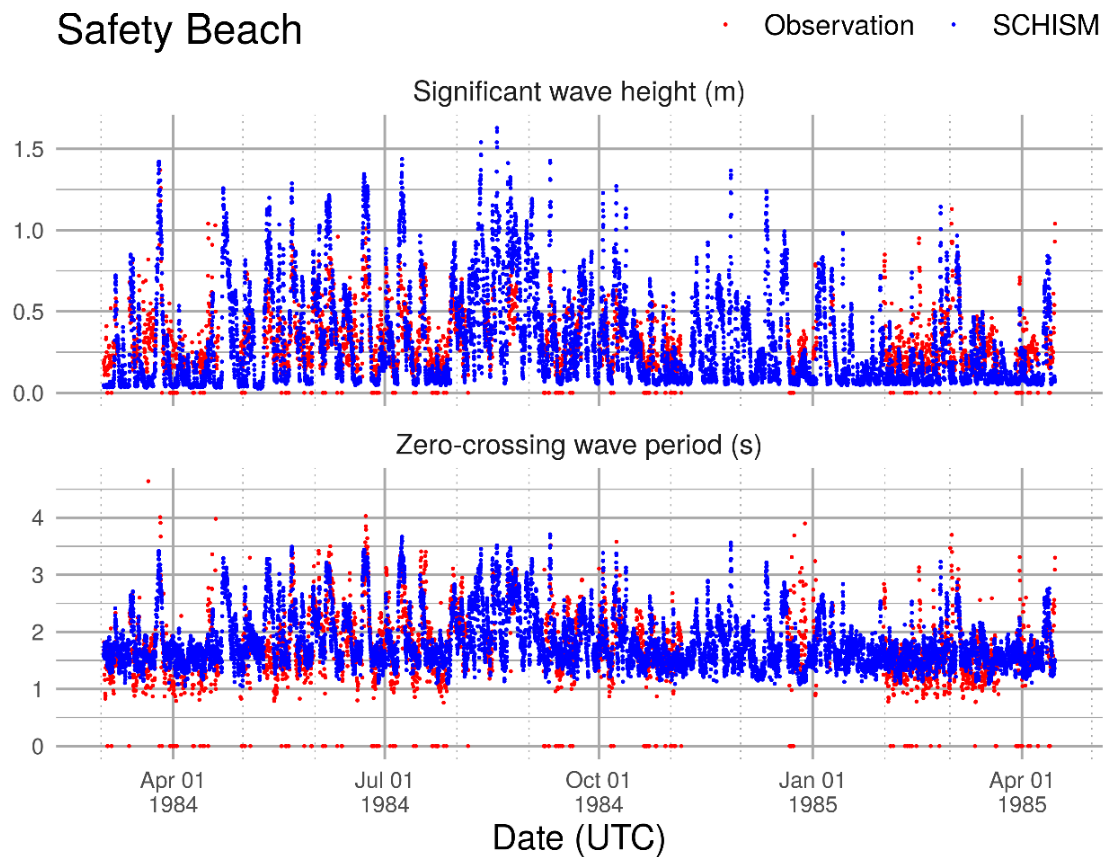

Figure 8.20: Significant wave height (Hs; m) and zero-crossing period (Tz; seconds) at Safety Beach from observations (red dots) and SCHISM-WWMIII simulations (blue dots).

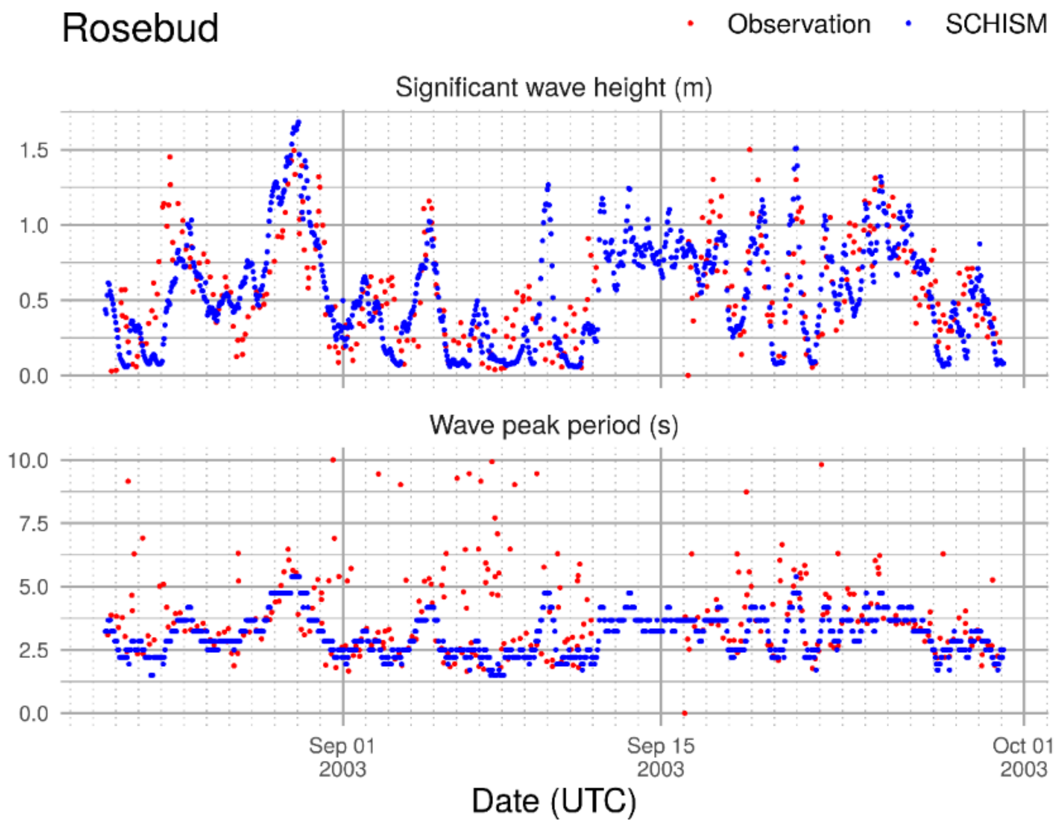

Figure 8.21: Significant wave height (Hs; m) and wave peak period (Tp; seconds) at Rosebud from observations (red dots) and SCHISM-WWMIII simulations (blue dots).

The Gap Analysis (McInnes et al., 2019) further identified other sea level (water level), wave and/or water current observations, all relatively short-term to support a particular area or process study within PPB. Probably the most relevant and relatively recent studies relate to the CDP. Instruments deployed were mainly the bottom-mounted acoustic doppler type (AWAC or ADCP) capable of recording wave information, current profiles, surface elevation and water temperature, as well as a number of pressure sensors (capable of recording water levels and waves, depending on configuration) and current meters. All were primarily located within the Entrance, along South Channel or near Portsea beach. Data were available from February 2005 to April 2008 (before the CDP) as well as measurements after the completion of CDP dredging in 2009-2011. This data is currently owned by the PoMC however and was not obtained for this project. These are potentially valuable datasets, and it is the authors' recommendation that efforts be made to make it available for future projects of this nature.

Overall, based on comparisons of available data (both that used for the model calibration and for the validation), the SCHISM-WWMIII model performs well at reproducing water levels (including tides), waves and aspects of wave-flow interaction, on par with (and in many cases significantly better) than that of other estuarine modelling studies of similar spatial and temporal scope (e.g. Clunies et al., 2017; Kumbier et al., 2018; Mulligan et al., 2019). Greater availability of long-term wave observations within the bay and neighbouring ocean waters (e.g. similar to the availability of tide gauge data) would allow a more complete validation of the SCHISM-WWMIII model. The relative paucity of coastal wave observations has been identified as an issue and a priority for further investment Australia-wide (Greenslade, et al., 2020). It is noted that DELWP has received funding in 2020-21 for the deployment of six Wave Spotter wave monitoring instruments in Port Phillip for a period of up to 12 months from October 2020 to September 2021. This project titled 'Port Phillip Wave Buoy Network' is presently being implemented. Despite this, due in part to the good validation of the wave model where data is available, as well as the overall maturity third-generation wave models such as WWMIII, the authors are confident in the veracity of SCHISM hindcast's estimation of PPB's wave climate, particularly in relatively deep water (i.e. before wave breaking) and its suitability to supply wave-related boundary conditions to the inundation hazard assessment. A limitation of all practical applications of hydrodynamically coupled wave models in multidecadal hindcast simulations is the accurate representation of waves after breaking in very shallow water. This limitation has been considered for the wave height values extracted at the toe of the defence structures, which were used in the overtopping estimates (Section 5.3.4).

8.5 Baseline (Hindcast) Results

This section presents statistical (extreme value) analysis of the sea level and wave fields to develop information on average recurrence intervals for inputs to the inundation and erosion hazard assessments. The panels of Figure 8.22 provide a "zoomed" view of water levels and waves for a single timestep near the peak of the storm tide event plotted in Figure 8.9, for two selected areas of PPB. Examination of such spatial output of the SCHISM model during storm events aids interpretation of these AEPs and changes associated with SLR, discussed in Section 8.6. For example, in Figure 8.22a, a combination of wind and wave setup leads to local increases in water levels along the eastern shoreline of the bay; in Figure 8.22b, the sheltering effects of Sandringham, Brighton and St. Kilda yacht harbours' breakwaters, as well as local wave shoaling along the bay's eastern shoreline, can be seen. In Figure 8.22c, water is surging through the heads and additional wind setup farther in the interior of the bay is visible; Figure 8.22d illustrates the complex propagation of ocean waves through the heads and interacting with local wind-generated waves within the PPB.

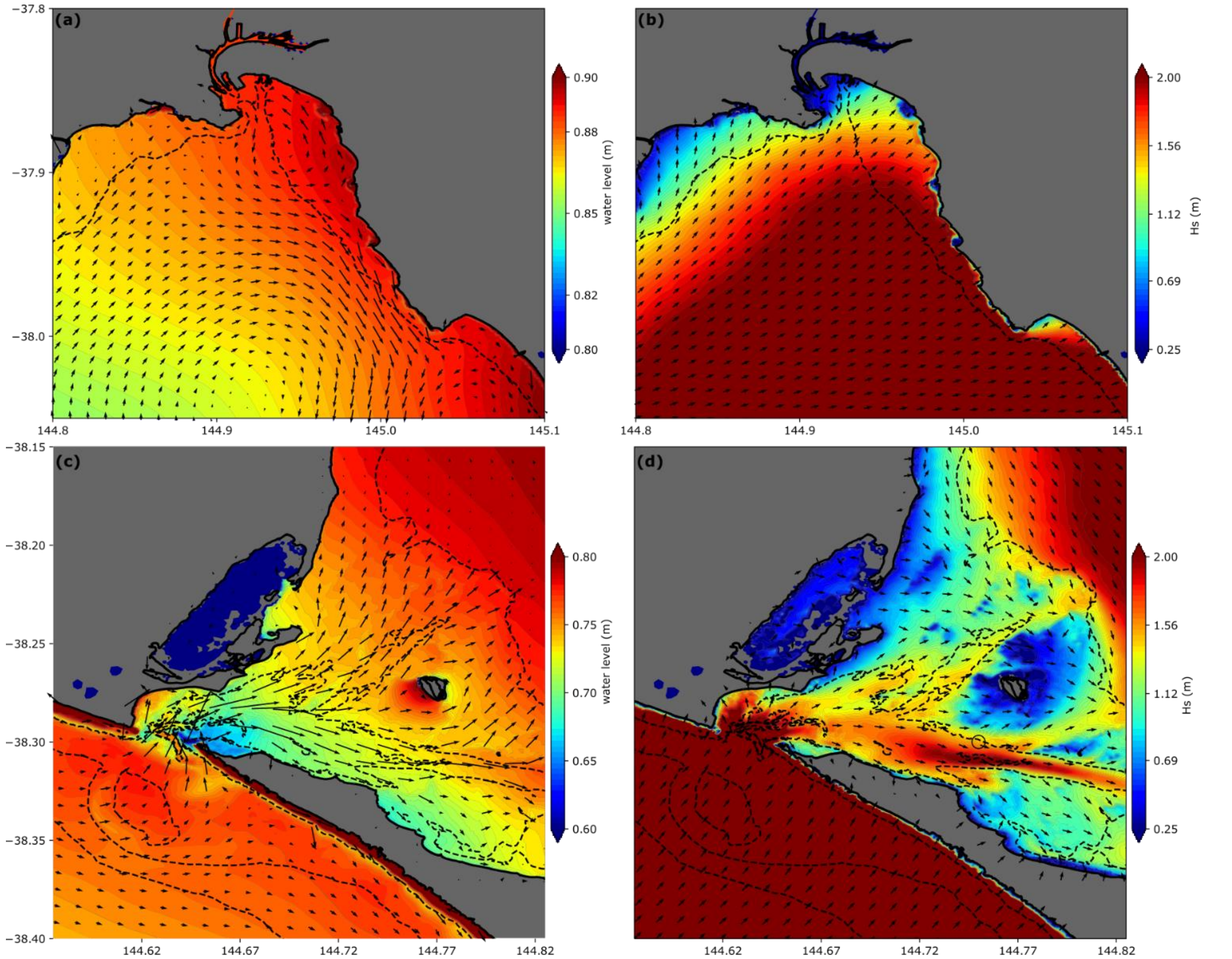

Figure 8.22: Single time-step output from the SCHISM baseline simulation on May 27, 1994, near the peak of the storm surge event shown in Figure 8.9; panels (a) and (b) indicate water level and significant wave height (Hs) for NW PPB; panels (c) and (d) indicate water level and Hs near PPB heads. In the water level panels, arrows indicate current direction and relative strength; in the Hs Panels, arrows indicate wave direction. In all plots, dashed lines indicated the 5, 10 and 15 m depth contours.

8.5.1 Extreme Water Level Analysis

Extreme value analysis was applied to water levels from the 35-year SCHISM hindcast, and results compared to the same analysis applied to tide gauge records of sufficient length. For the analysis, tide gauge data at Williamstown and Geelong and SCHISM sea levels at these locations were extracted and annual maximum values (for overlapping time periods) fitted to a Gumbel distribution, allowing calculation and subsequent comparison of annual exceedance probabilities (AEPs). Figure 8.23 shows an example comparison of the AEP fits of SCHISM and tide gauge water levels for Williamstown. Additionally, the results are compared to two previous studies: Water Technology (2017a); and the hydrodynamic modelling undertaken in McInnes et al., (2009). Note that the Water Technology study (WT17 here after) includes estimates from the Williamstown tide gauge starting in 1966 as well as historical extreme events (such as the 1934 flood event) reported on in Adams (1987).

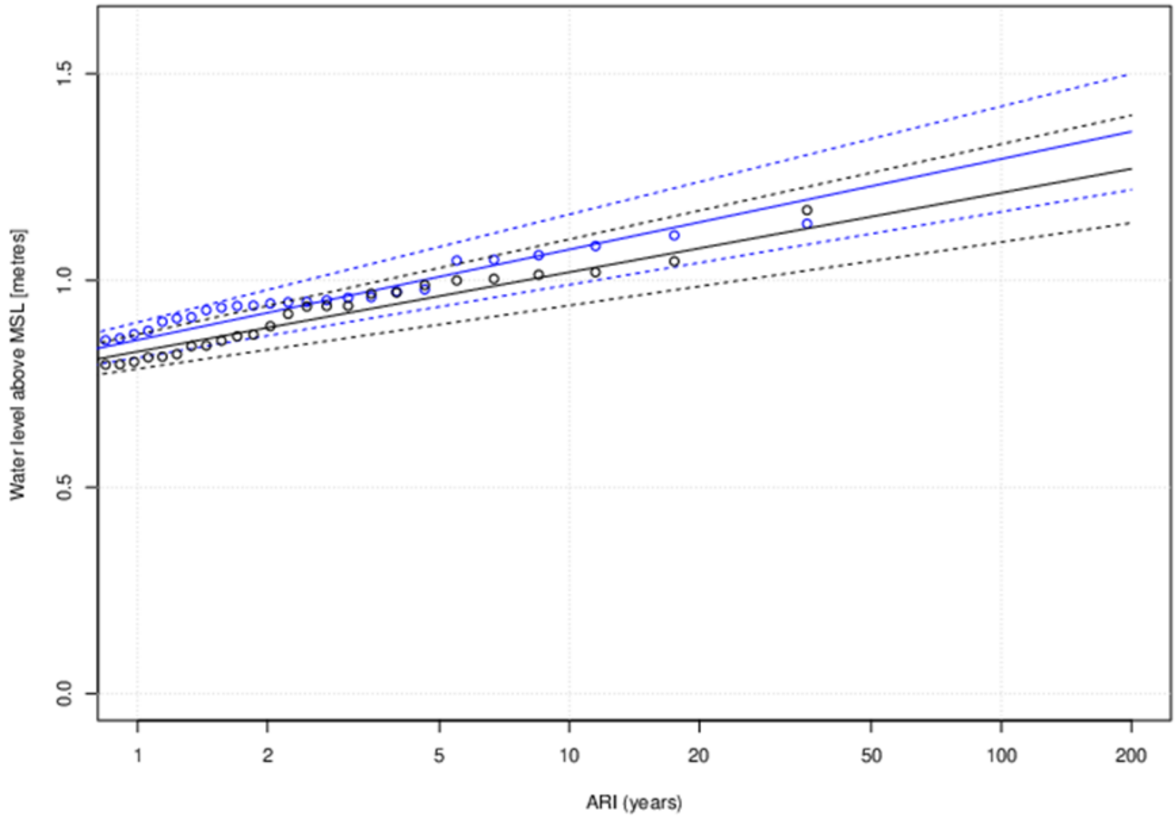

Figure 8.23: Extreme sea level AEPs (expressed as years) from Williamstown tide gauge data (blue curve) and SCHISM model data (black curve). Empirical AEPs of annual events are indicated with circles; Gumbel fits are indicated with solid lines (dotted lines the 95th percentile range).

To investigate the effect of utilising longer records on derived AEPs, recently digitised tide registers for Williamstown that include the 1934 event were also analysed. It was found that compared to the Gumbel fit to the 35 years of data, the fit for the 1934-2014 period produced heights for the 1% AEP that was 4 cm higher (see Table 8.5). However, the longer record meant that the uncertainty estimates were narrower as expected. There was therefore not a statistical difference between the longer and the shorter time periods. Furthermore, it would be inconsistent to use AEPs derived from the longer time period at only Williamstown as this is not proven to be representative of the entire bay and could result in erroneous estimates at other locations which did not respond in a similar way in 1934.

Water level AEPs at the 5, 2 and 1% level (corresponding to the 10, 50 and 100-year likelihoods, respectively) for Williamstown based on the 35-years of overlapping data are also shown in Table 8.5. These are about 9 cm higher than those based on SCHISM. This is consistent with the quantile-quantile water level plots (Figure 8.10), which shows top 1 percentile values tend to be slightly underestimated by SCHISM; despite this, the tide gauge AEP values fall within the 95th percentile confidence range of the SCHISM AEPs (and vice-versa). Similarly, the estimates of McInnes et al., (2009) and WT17 (both with and without the additional historical extreme reported by Adams (1987) fall within the 95th percentile confidence limits (Table 8.4).

Table 8.6 presents similar data, but for the location of the Geelong tide gauge (a similar analysis as for Williamstown was not available from WT17). Here the correspondence between AEPs derived from the 35-years of overlapping data is similar; differences for all three AEP water levels are 1 cm or less. The estimates of McInnes et al., (2009), while slightly higher, are still well within the 95th percentile confidence limits of the SCHISM modelled AEP confidence limits.

In both Table 8.5 and Table 8.6, AEPs based on 20-years (1980-1999) of SCHISM modelled water levels are also included. This is to establish differences with the 35-year AEPs, for extrapolation to the SLR scenarios, since these contain only 20-years of simulation (owing to the computational overheads of running longer simulations and because 18.6 years captures an entire lunar cycle). It also allows the implications of comparisons with other tide gauges within the study region, which might only be available for shorter periods to be assessed. The longer (35-year) period results in several centimetres higher AEPs compared to the shorter hindcast period; equating to an approximately 5% increase between the 20-year and 35-year based SCHISM AEP calculations.

To account for the difference in the 35-year hindcast and the 20-year SLR climate simulations, the differences between the co-located future and baseline 20-year AEP return levels (RLs) were calculated and the differences added to the baseline 35-year AEP RLs to derive the AEP RLs for the SLR scenarios. This method is analogous to the 'change factor' downscaling method (Ekström et al., 2015).

In summary, there is significant overlap in the two sets of uncertainty estimates of the extreme value fits from observed tide gauge and SCHISM-simulated water levels, based on relatively long (35-year) tide gauge data at Williamstown and Geelong. These uncertainty estimates also incorporate the central estimate of previous studies, indicating good agreement. This gives high confidence in the extreme sea level values estimated from the SCHISM hindcast, which provides the underlying sea levels around the bay in a consistent, dynamically coherent way. Therefore, AEP estimates from the SCHISM modelling are considered appropriate to define design storm tides as forcing for the C-FAST inundation modelling. Since, the uncertainty estimates of the SCHISM fits encompass the central estimate from the tide gauge analysis, consideration of the median and the upper and lower uncertainty estimates of the extreme value fits in the inundation hazard assessment will ensure that the uncertainties in inundation hazard are fully accounted for.

Table 8.5: Estimates of Annual Exceedance Probabilities (AEP) water levels (in metres) for Williamstown. Values in brackets represent the 95th percentile confidence limits.

Williamstown	5%	2%	1%
Tide Gauge 1934-2014	1.17[1.11, 1.23]	1.27[1.19, 1.35]	1.34[1.25, 1.43]
Tide Gauge 35 yrs	1.14 [1.05, 1.23]	1.23 [1.12, 1.34]	1.3 [1.17, 1.43]
SCHISM 35 yrs	1.07 [0.99, 1.15]	1.15 [1.05, 1.25]	1.21 [1.09, 1.33]
SCHISM 20 yrs	1.03 [0.94, 1.12]	1.09 [0.98, 1.2]	1.14 [1.01, 1.27]
WT17 (BoM only)	1.12	1.15	1.18
WT17 (BoM + Adams)	1.16	1.23	1.27
McInnes et al., (2009)	1.03 [0.94,1.12]	1.09 [1.00, 1.18]	1.12 [1.02, 1.22]

Table 8.6: Estimates of Annual Exceedance Probabilities (AEP) water levels (in metres) for Geelong. Values in brackets represent the 95th percentile confidence limits.

Geelong	5%	2%	1%
Tide Gauge 35 yrs	0.94 [0.87, 1.01]	1.00 [0.91, 1.09]	1.06 [0.96, 1.16]
SCHISM 35 yrs	0.95 [0.89, 1.01]	1.00 [0.92, 1.08]	1.05 [0.96, 1.14]
SCHISM 20 yrs	0.91 [0.85, 0.97]	0.95 [0.87, 1.03]	0.98 [0.89, 1.07]
McInnes et al., (2009)	0.98 [0.89, 1.07]	1.03 [0.94, 1.12]	1.09 [0.99, 1.19]

Extreme water level AEPs at the 8 m depth contour are shown in Figure 8.24. As with previous studies such as McInnes et al., (2009) and Water Tech (2017a) these show a strong northeast to southwest gradient in extreme sea levels across PPB with the highest sea level extremes extending from Hobsons Bay to Frankston. High values also occur around the Geelong coast whereas values are lowest in the southwest of the bay inside the entrance and across the Great Sands.

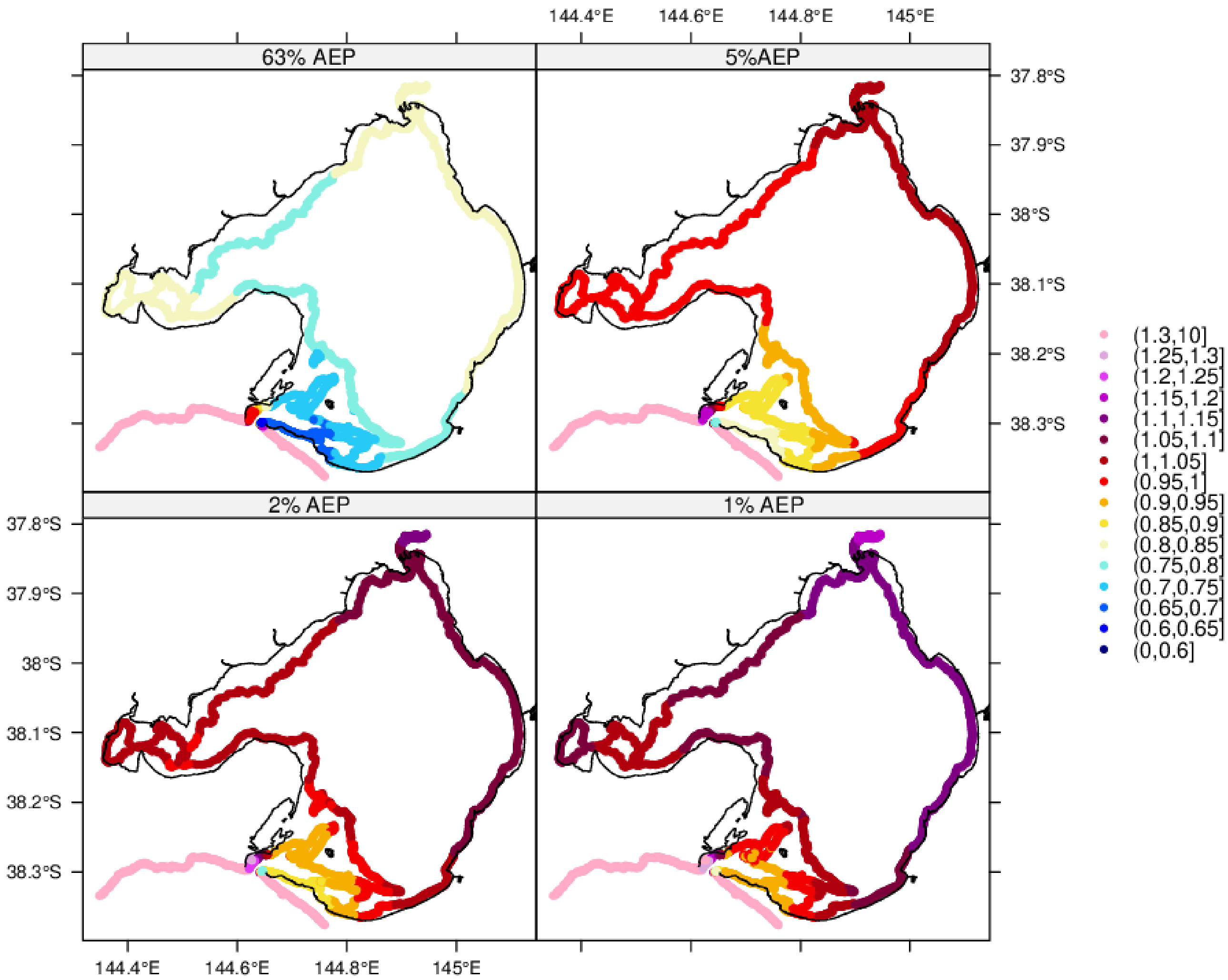

Figure 8.24: Extreme water level AEPs (m) for the 63% (1-year), 5% (20-year), 2% (50-year) and 1% (100-year) levels, based on the central (maximum likelihood estimate) Gumbel fit of the SCHISM baseline (hindcast) simulation.

8.5.2 Extreme Wave Analysis

For the fetch-limited PPB, several SCHISM simulation depth contours were used as input into the hazard assessments. These included:

- a nearshore location representing the local beach wave and water level climate
- a depth comparable to other modelling studies (e.g. 4 m depth contour for the Cardno (2018) study)
- at the toe of protection structures for input in the EurOtop overtopping equations in C-FAST (Chapter 5), and
- a deeper-water value where there are reduced shallow water effects from wave shoaling and depth-induced breaking (i.e. the 8 m depth for input into wave runup equations) (Chapter 5).

Significant wave heights (Hs) were extracted from the 35-year hindcast at the 4 m depth contour and analysed to produce wave height AEPs using the same approach as for the analysis of extreme water levels and results for selected AEP values (Figure 8.25). These show that extreme Hs is highest on the eastern side of the bay where the fetch is greatest under southerly to westerly wind directions, which are common during extreme weather events such as cold fronts. Values are lowest around the Geelong coast and are relatively low in the southwestern part of the bay where shallow water causes wave shoaling over the Great Sands.

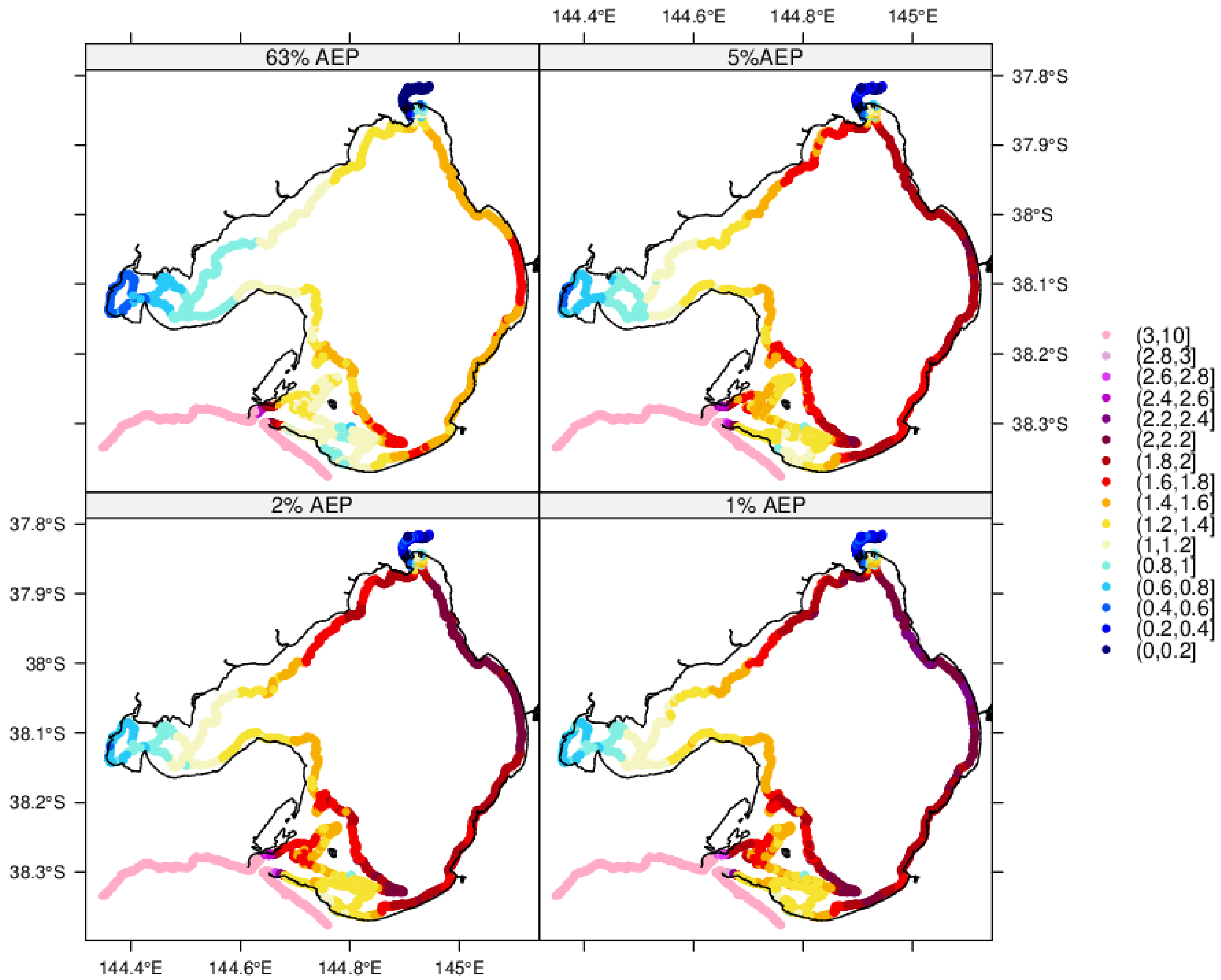

Figure 8.25: Extreme significant wave height (Hs) (m) AEPs for the 63% (1-year), 5% (20-year), 2% (50-year) and 1% (100-year) levels, based on the central (maximum likelihood estimate) Gumbel fit of the SCHISM baseline (hindcast) simulation.

Figure 8.26 compares the 1% AEP Hs from this study to results produced by Cardno (2018). The Cardno values were developed by running a wave model for thirteen representative wind speeds and 36 directions (10° intervals) and then combining the results from the total of 468 wave model simulations using the frequency of occurrence of wind speed and direction from a point in the bay. The Cardno results generally show a similar pattern of higher waves in the eastern side of the bay but differ in the magnitudes of the wave height for the 1% AEP in the order of 0.4 m. In the west, around Corio Bay Cardno values are up to 0.6 m higher than those derived from the SCHISM simulations and are higher by up to 0.5 m along the southern coastline from Geelong to Pt Arlington. On the eastern side of the bay SCHISM waves are up to 0.6 m higher.

There are a number of likely contributing reasons for the differences between the Cardno (2018) study and the results presented here. The key difference is that the Cardno study did not utilise a dynamically coupled wave-flow simulation (like the SCHISM hindcast), rather (as already mentioned) it was based on a series of discrete stationary wave model simulations, which did not include the influence of currents, varying background sea levels, tides or surge, nor could it account for the duration of wind strength and fetch around the bay. Varying water levels affect the wave heights such that in deeper water level conditions, higher waves can propagate closer to shore; changes in wind direction and strength that occur during the progression of storm events also have a significant impact on the wave field, e.g. the Cardno (2018) study assumed a fully developed wind-sea for all of its discrete simulations, which may not always be the case. Further reasons for the differences between the two studies include that the Cardno study was based on a much shorter time period (1991-2011) and a wind measurement from a single weather station (Point Wilson); reconstruction of wave climate from a single wind location will not be representative of the wind climate for the entire PPB. Also, the Cardno study does not include ocean swell penetrating into PPB through the heads, although the SCHISM results of this study indicate these effects are largely restricted to a relatively small area of PPB in the vicinity of the heads.

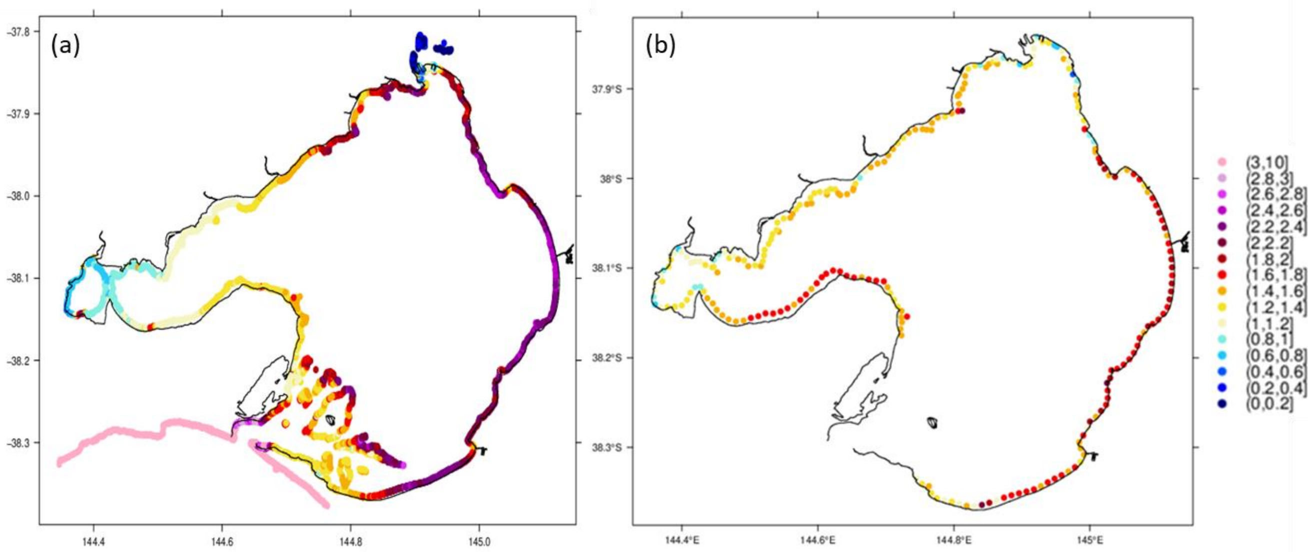

Figure 8.26: 1% AEP levels of significant wave height (Hs) based on (a) the SCHISM hindcast and (b) values derived from Cardno (2018).

8.6 Impact of Sea Level Rise

In this section, the effects of SLR on astronomical tides, extreme water level events (storm tides) and storm waves, as simulated by the SCHISM model, are discussed. It is noted that in the model simulations of future SLR the seabed remains static. As discussed in Section 2.1, there is some basis for this approach since evidence suggests many shallow areas of bay consist of relatively thin veneers of unconsolidated sediment over consolidated substrates. Nevertheless, it is noted as an uncertainty in the results.

8.6.1 Tidal Harmonic Analysis

First principles and earlier studies suggested that SLR would lead to amplification of the tidal range in PPB by reducing hydraulic resistance through Port Phillip Heads (the average tidal range is approximately 0.75 m greater outside the heads than inside the bay). For example, Black et al., (1990), using an empirical relation derived from hydrodynamic modelling, found an increase in sea level of 1.0 m would increase tidal amplitude by 0.06 m (15%). These potential changes in tidal amplitude have been investigated by comparing water levels from the SCHISM baseline simulation with those of the SLR scenarios. Predicted tide levels (assuming a zero-mean water level) at selected points for a typical neap-spring tidal cycle under both the baseline and 1.4 m SLR scenario (Figure 8.27). The tidal maximum and minimum (as well as total range) for each day is clearly larger for points inside PPB than at Lorne (outside the bay), where little if any detectable change has occurred.

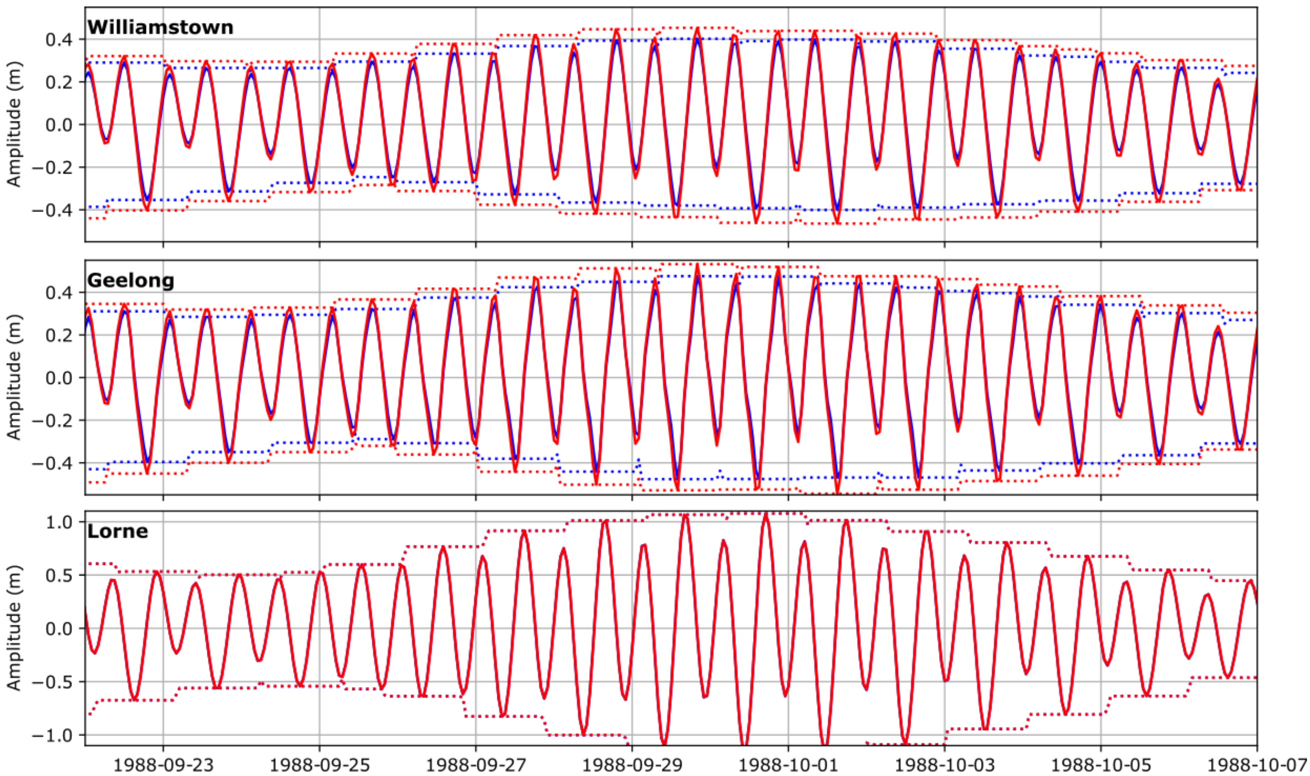

Figure 8.27: Astronomic tides based for an example neap-spring cycle for selected locations inside PPB (Williamstown and Geelong) and one outside (Lorne); blue is from the SCHISM baseline simulation, red from the 1.4 m SLR scenario; dotted lines indicate the daily higher high water (HHW) and lower low water (LLW) envelopes. The predictions are based on harmonic analyses of 20-year time slices of SCHISM water level output at locations coinciding with tide gauge names.

Table 8.7 provides values of astronomic tidal statistics, e.g. mean higher high water (MHHW) and highest astronomical tide (HAT) for hourly predictions. These constituents and predictions are based on all inferred constituents (68) under both the baseline and the 0.2 m, 0.8 m and 1.4 m SLR scenario between 1980 and 1999 (chosen as a full tidal epoch and for consistency in comparison). Note that while tidal amplitudes are significantly different (within PPB) between the baseline and 1.4 m SLR scenarios, tidal phases (or timing) were not significantly different (see Appendix J). Table 8.7 shows that, within PPB, tidal amplitude increases by 0.045 m for MHHW and 0.055 m for HAT with a 1.4 m SLR. These increases are somewhat more pronounced within Corio Bay, but not significantly. These values are slightly less, but consistent with the earlier study of Black et al., (1990). Note also that mean total daily tidal range within PPB increases by close to 0.1 m, indicating that intertidal zones will increase and suggesting that tidal currents may increase in some areas, which may lead to local erosion or other changes in sediment dynamics.

Table 8.7: Modelled changes in tidal characteristics for Williamstown, Geelong and Lorne between baseline sea level and the 0.2 m, 0.8 m and 1.4 m SLR scenarios. Characteristics include highest astronomical tide (HAT), lowest astronomical tide (HAT), mean higher high water (MHHW), mean lower low water (MLLW) and total tide range. The tidal heights are referenced to zero for all scenarios below, i.e. they do not include the respective 0.2 m, 0.8 m and 1.4 m mean SLR. All tidal harmonic predictions are based on 20-year time slices. Changes in different individual tidal constituents including a greater number of stations, are available in Appendix J.

	Williamstown				Geelong				Lorne			
	Base-line	SLR 0.2	SLR 0.8	SLR 1.4	Base-line	SLR 0.2	SLR 0.8	SLR 1.4	Base-line	SLR 0.2	SLR 0.8	SLR 1.4
HAT	0.435	0.444	0.465	0.484	0.511	0.520	0.540	0.563	1.144	1.146	1.144	1.143
LAT	-0.516	-0.527	-0.557	-0.584	-0.566	-0.576	-0.607	-0.637	-1.270	-1.270	-1.272	-1.271
MHHW	0.310	0.317	0.336	0.354	0.357	0.364	0.384	0.402	0.739	0.740	0.739	0.738
MLLW	-0.374	-0.382	-0.404	-0.424	-0.422	-0.430	-0.453	-0.473	-0.822	-0.822	-0.822	-0.822
Total range	0.902	0.924	0.980	1.029	1.038	1.056	1.111	1.160	2.396	2.399	2.398	2.396

8.6.2 Sea Level Extremes

Since extreme sea levels result from the combination of tides, storm surge, wave effects and background sea level, the predicted increase in tidal amplitudes associated with the SLR scenarios discussed in the previous section will lead an increase in sea level extremes above that of just the mean SLR. For example, although the same atmospheric forcing was used for the baseline (hindcast) simulation as for the 1.4 m SLR simulations, the difference between the baseline 1% AEP (100-year) water level and that of the 1.4 m SLR is consistently greater than 1.4 m, by up to approximately 7 cm, within PPB (Figure 8.28). While (non-tidal) storm surges could possibly also become larger within PPB through the same mechanism as the increased tidal range, i.e. reduced hydraulic resistance through Port Phillip Heads with SLR, the SCHISM simulations show little evidence of it. Quantile-quantile (not shown) comparisons of residual (non-tidal) water levels between baseline and SLR simulations do show minimal differences from each other, even at the highest quantiles, beyond that of the SLR signal. This is presumably due to the lower frequency of storm surge compared to semi-diurnal tidal constituents; it is changes in the semi-diurnal tidal constituents that give rise to the SLR-related changes in tidal range shown in Table 8.6, whereas the seasonal tidal components (SA and SAA) show no change with SLR. The apparent reduction (relative to SLR) in AEP water levels near and outside PPB heads may be partially due to reduced hydrodynamic restriction through the heads, and partially due to reduced wave setup at the location of the 8 m depth contour.

To account for the difference in the 35-year hindcast and the 20-year SLR climate simulations, the differences between the co-located future and baseline 20-year AEP return levels (RLs) were added to the baseline 35-year AEP RLs. This method is analogous to the 'change factor' downscaling method (Ekström et al., 2015).

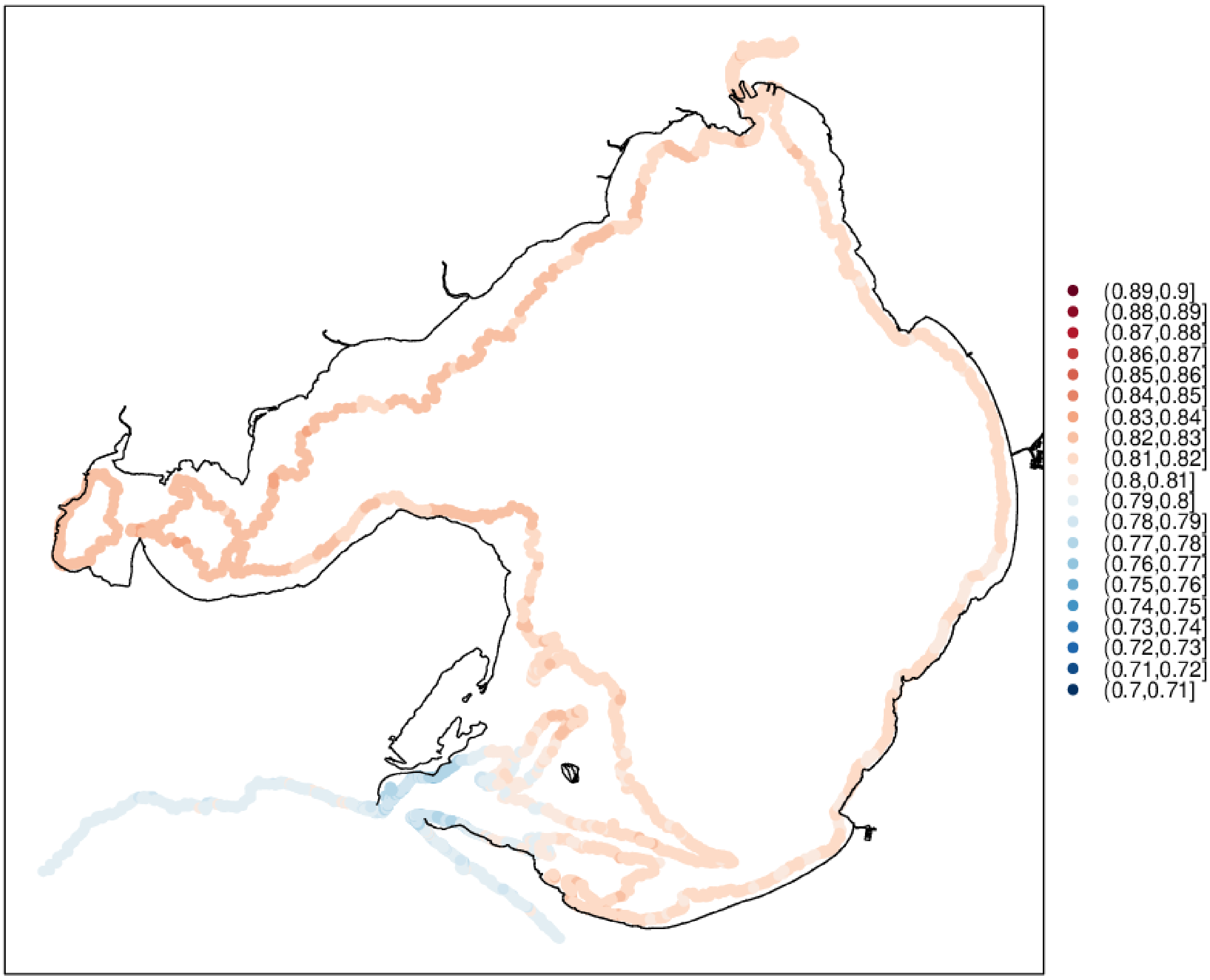

Figure 8.28: Change in 1% AEP (100-year ARI) 50th percentile (maximum likelihood estimate) water levels between the baseline and the 0.8 m SLR simulations, based on the central (maximum likelihood estimate) Gumbel fit values. Values are shown at the 8 m depth contour.

8.6.3 Waves Extremes

Generally speaking, wave heights (Hs) moderately increase with SLR for given storm conditions. For instance, the 1% AEP (100-year) Hs value for the 0.8 m SLR simulation is 0.1 - 0.2 m (5-10%) larger than the that of the baseline simulation along much of the coastline of PPB (Figure 8.29). The cause appears to be primarily due to increased water depths over the Great Sands and other relatively shallow-water areas in PPB. This is somewhat conceptually similar to that of the increase in tidal range within PPB: the greater water depths through the heads and over the Great Sands both effectively increase the fetch within the bay, allowing slightly larger waves to be generated for a given wind strength, and also allows slightly more ocean wave energy (swell) to “leak” through the heads and penetrate into PPB (due to reduced ocean swell dissipation in these areas). Quantifying the extent that these two processes contribute to the increase in wave energy throughout the bay would require a more extensive analysis (possibly including additional SCHISM simulations at refined grid resolution) and is beyond the scope of this report.

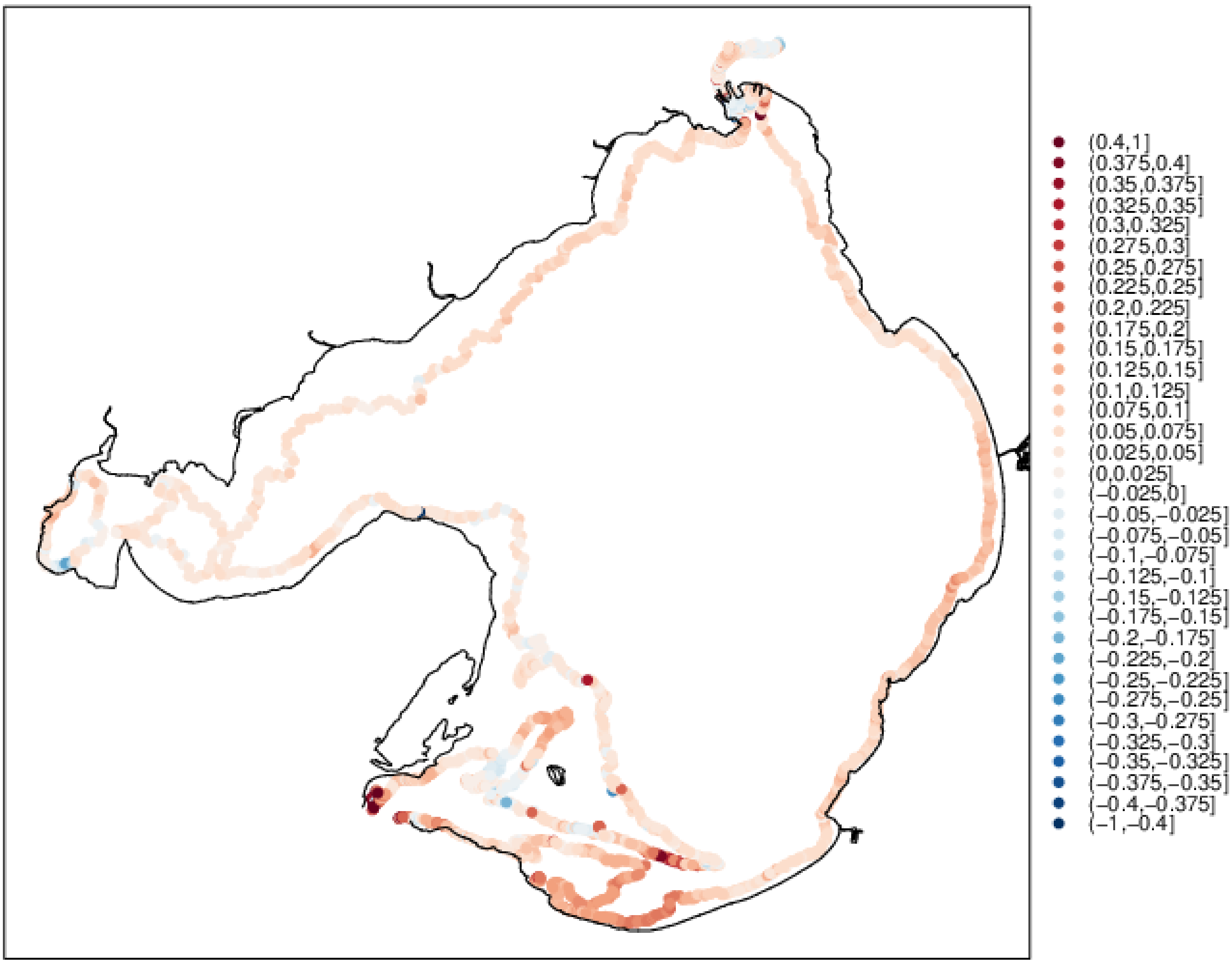

Figure 8.29: Change in 1% AEP (100-year ARI) 50th percentile (maximum likelihood estimate) Hs with 0.8 m SLR. Values are shown at the 8 m depth contour.

8.7 Summary

The hydrodynamic and wave model results presented in this chapter provided underpinning data for the hazard assessments and also enabled an analysis of the effect of SLR on tides, extreme sea levels and waves in the bay. A number of key conclusions arising from this modelling are discussed below.

The validation of the SCHISM-WWMIII model using available in-situ observations indicates it performs exceptionally well at reproducing water levels (including tides). The representation of waves and aspects of wave-flow interaction are on par with (and in many cases significantly better) than that of other estuarine modelling studies of similar spatial and temporal scope (e.g. Clunies et al., 2017; Kumbier et al., 2018; Mulligan et al., 2019).

This study would benefit from a greater availability of long-term wave observations within PPB and neighbouring ocean waters (e.g. similar to the availability of tide gauge data), particularly in shallow waters. This would allow more complete validation of the SCHISM-WWMIII model; it is noted that the relative paucity of coastal wave observations has been identified as an issue and a priority for further investment Australia-wide (Greenslade et al., 2020).

The whole-of-estuary (including significant portions of the surrounding ocean coasts and Bass Strait) approach of the SCHISM-WWMIII model, combined with its full dynamical simulation of multiple decades, allowed for full consideration of the dynamics of extreme sea levels and waves within the bay, including changes in dynamics associated with the various SLR scenarios used in this study. This is unique among the PPB modelling studies identified during the Gap Analysis and makes it well suited to generating the boundary conditions for probabilistic event-based scenario modelling used in the inundation hazard component of the study.

The model simulations indicated that extreme water levels within PPB will increase with SLR beyond the value of SLR itself. For example, for many locations within PPB, under the 0.8 m SLR scenario, the 1% (100-year) AEP extreme water level is not 0.8 m higher, but up to approximately 0.87 m higher. Overall, throughout much of the bay, the increase in extreme water levels is approximately between 2 and 10% higher than the value of SLR itself, although there is considerable variation depending on location. These increases are due primarily to increases in tidal ranges within the bay associated with SLR, which effectively increases the tidal prism and the related increase in water exchange through the heads. Although storm surge dynamics also exhibit small changes with SLR, they do not result in any significant net increase or decrease in extreme water level probabilities relative to SLR increases.

The model simulations indicate that storm wave energy within PPB will also increase with SLR. For example, under the 0.8 m SLR scenario, the 1% (100-year) significant wave height increases by 5-10% in most areas of the bay. This is due primarily to increased water depths over the Great Sands and other relatively shallow-water areas in the bay, which effectively increases the fetch within the bay, allowing slightly larger waves to be generated for a given wind strength. Additionally, there is evidence that the increased water depths through the heads and over the Great Sands allows slightly more ocean wave energy (swell) to “leak” through the heads and penetrate into the bay.

The relative increases in extreme water levels and waves within PPB under the modelled SLR scenarios are predicated on the assumption that the seabed remains static under SLR. While this simplifying assumption is not unfounded, since evidence suggest many shallow areas of bay consist of relatively thin veneers of unconsolidated sediment over consolidated (lithified or partially lithified) substrates, particularly the Great Sands (see Section 2.1), it is an important caveat. In reality, some degree of morphological change under future SLR scenarios is almost certain, although how this may further affect the water level and wave dynamics remains unknown. This is a recommended area of future study.

9 Summary and Study Recommendations

This chapter summarises the methodological approach and high-level findings from the hazard assessments. A synthesis of the combined results of the hazard assessments is provided from an LGA perspective. Key uncertainties arising from the study and recommendations for future work are also discussed.

9.1 Summary of Key Findings from this Study

This study has undertaken a comprehensive assessment of coastal hazards relating to inundation and groundwater around PPB. This was underpinned by a substantial review and assessment of the geomorphology of the bay as well as modelling of the wave and hydrodynamic characteristics of the bay. The construction of a dedicated DSS for the storage, analysis and display of the findings of the study ensures that the key outputs and associated datasets arising from the study are available to relevant coastal practitioners and decision makers.

PPB is a tectonic (fault-defined) embayment with a basement of Palaeozoic hard rocks overlaid by Cainozoic sedimentary and volcanic rocks, generally of low resistance to erosion. Long sectors of coast are topographically low and comprised of beach and dune sediments and alluvial and intertidal sands, silts and clays. The western coast (Williamstown to Corio Bay) is characterised by limited sand supply and low backshore elevation. The eastern side of the bay is geologically and topographically more diverse with headlands, and embayments from St Kilda to Beaumaris and Mt Martha to Frankston, separated by the tectonic Carrum depression. Landslides are generated in places by backshore slope failure and slope base undercutting by wave action. The geological complexity of the region is described in detailed mapping of geomorphic types (section 7.2.1).

Beaches comprise about 60% of the PPB coastline and are highly variable in texture, typically with complex stratigraphy, in part due to artificial beach nourishment. West coast beaches contain a higher proportion of whole and broken shell than east coast beaches. Longshore beach transport is seasonally determined on the central to north-east coast of PPB whereas seasonal influence is much less pronounced on the western coast (Appendix F). An analysis of historical orthorectified photogrammetry of the coast identified that 72% of detected vegetation lines have a seaward moving trend while 28% have a landward moving trend. Using the vegetation line detection as an indicator of long-term beach change indicates more beaches have grown and stabilised than eroded over the period 1940-2018. Further work is required to expand the coastline detection to other parts of the bay, which have challenging landform classifications (e.g. platforms and cliffs), to make a more complete estimate.

A geomorphic survey identified 528 coastal geomorphic sectors (CGS) around PPB. The sectors were determined on the basis of backshore and intertidal landform characteristics. More than half of these sectors (290 CGS) totalling around 200 km of coastline, are beach fronted. However, these beaches have a variety of backshore features ranging from engineered structures to cliffs and wetlands, which together can together influence erosion. Hard or soft rock cliffs occur extensively on the eastern side of PPB and the Bellarine peninsula whereas low-lying wetland areas are most prevalent in the southern and western parts of PPB.

PPB is a large coastal tidal embayment, largely sheltered from ocean swell, and dominated by wind and tidal currents. The bay itself is relatively shallow with about half of the area less than 8 m in depth and the deepest regions (apart from the entrance channel) are only around 24 m. The east coast is subject to storm wave conditions with local occurrence of high wave energy conditions resulting in the subsequent impact on beaches, soft rock cliffs and low backshores. The coupled hydrodynamic and wave model, SCHISM-WWMIII, was used to assess storm tide and wave 1, 2 and 5% AEPs for the inundation and erosion assessments over recent decades and under SLR scenarios of 0.2, 0.5, 0.8, 1.1 and 1.4 m. Comparisons between the AEPs for waves and storm tides, which were calculated in this study were found to be broadly consistent with previous modelling studies, with differences attributed to alternative methodological approaches. The model simulations indicated that for a SLR of 0.8 m, extreme water levels (storm tide plus wave effects) within PPB increased beyond the value of SLR itself by between 2 and 10% depending on location. The increases were mainly due to increases in tidal ranges within the bay due to SLR, which allows a larger exchange of water through the heads. For example, the total tide range at Williamstown increased from 0.90 under baseline conditions by 0.08 cm for 0.8 m SLR and by 0.13 m for 1.4 m SLR. In addition, wave heights associated with the 1% AEP Hs event (100-year) were found to increase by 5-10% in most areas of the bay under a 0.8 m SLR representing an increase of 0.1 – 0.2 m along much of the coastline.

The assessment of inundation was carried out using the CSIRO C-FAST model at up to 5 m spatial resolution over low-lying and urbanised parts of PPB. Over these locations, the model accounted for the overland flow of water from storm tides, wave overtopping and storm water flows through the underground storm water drainage system. Away from the most urbanised or low-lying parts of PPB C-FAST was run at 25 m resolution to capture inundation due to overland flow. Simulations with and without 10% AEP rainfall were carried out over all model grids. Since C-FAST does not account for wave setup (except on the 5 m resolution simulations where a seawall is present), wave setup calculated for the whole bay using an empirical model was combined with the modelled inundation extents. Sensitivity experiments demonstrated the relative contribution of the different physical processes. Simulations were also compared to similar studies and again provided results that were generally similar, but for which the differences could be understood in terms of the different physical processes that were accounted for between studies. The whole-of-bay inundation results showed that the area affected by inundation would increase approximately linearly with SLR but the sea level responses along some parts of the coast were highly non-linear. For the whole-of-bay under a 1% AEP storm tide event, 1.4 m of SLR is shown to increase the area of inundation by approximately three to fourfold. Results were also provided for the different LGA's around the bay. To complement the hydrodynamic modelling of inundation due to storm tides, wave setup and overtopping, wave runup excursion hazard was also separately estimated for PPB to indicate the assets at risk (e.g. bathing boxes, fences and coastal vegetation) from transient wave runup processes for 1,2 and 5% AEP wave events around the coast.

For groundwater, a whole-of-bay conceptual model of PPB was developed along with more detailed conceptual models for three regions; the Werribee delta region, the Mentone to Frankston sand belt region and the Nepean Peninsula, where the watertable is relatively shallow, the hydraulic gradient is low, and the recharge of the unconfined aquifers is dependent on rainfall. It was found that in all three locations, the projected decrease in precipitation and increase in evaporation will lower the watertables by a small amount (order centimetres) while SLR will cause an inland migration of the seawater-groundwater interface on the order of tens to hundreds of metres, although precise values are subject to a large degree of uncertainty.

9.2 Synthesis of Key Findings

This section discusses the collective findings of the three hazard assessments focussing on LGAs. For inundation and erosion all mapped hazard zones are considered for the 1% AEP event. Since groundwater hazard was defined as the area that underwent an increase in shallow groundwater or surface water from current conditions, the discussion is focussed on specific SLR scenarios (0.2, 0.8 and 1.4 m). While some figures are presented in this section, a complete selection of figures for each LGA can be found in Appendix K and maps can be found in Appendix L.

Figure 9.1 presents the footprint of the inundation and groundwater hazards around PPB under 1.4 m of SLR (equivalent figures for 0.2 and 0.8 m SLR are in Appendix L, Figures L7 and L8). Generally, the most extensive hazard zones are found on the very low-lying parts of the western side of the bay. In addition, for many low-lying regions, there is a convergence of both hazards.

The City of Greater Geelong contains a number of coastal hazard hotspots owing to the extensive low-lying land across the western side of the bay. Areas affected by both hazards include the former solar salt ponds at Stingaree Bay, Swan Bay, Portarlington (Ramblers Road to Indented Head), south of Point Henry (the Moolap region) and Point Lillias to Point Wilson, under SLR of 0.8 m or more (Figure 9.2b, c). Generally, the inundation hazard increases linearly with SLR from 17 km^2 under 0.0 m SLR up to 47 km^2 for SLR of 1.4 m (Appendix K, Figure K3a). Additionally, groundwater hazard affects the low-lying areas around Lake Connewarre due to increases in shallow groundwater and surface water under SLR of 0.5 m and higher (Appendix K, Figure K3d).

As much of the City of Greater Geelong coastline is rural, there is limited coastal protection such as seawalls and revetments and these are mainly found in small coastal settlements, (Figure 7.8). A number of rural and suburban areas have freehold title to high water mark, some with poorly constructed and ineffective engineered structures. Coastal protection along the Portarlington section of coast is particularly sparse. On the other hand, seawalls and revetments that are present along coastline adjacent to urban Geelong appear to be effective under all SLR scenarios.

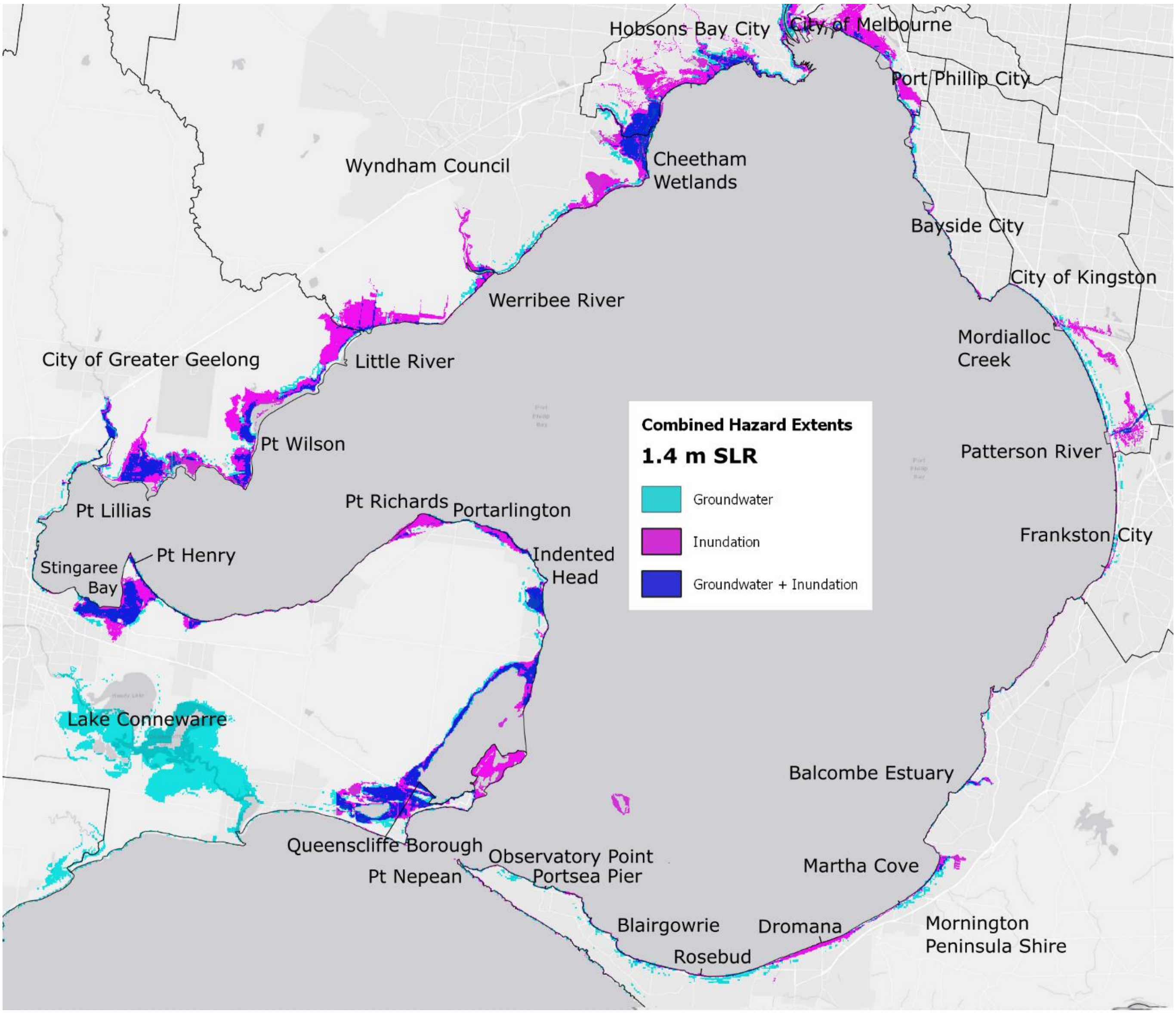

Figure 9.1: Overlay of hazard zones for inundation and groundwater under 1.4 m SLR where the inundation zone is based on a 1% AEP storm tide with no rainfall.

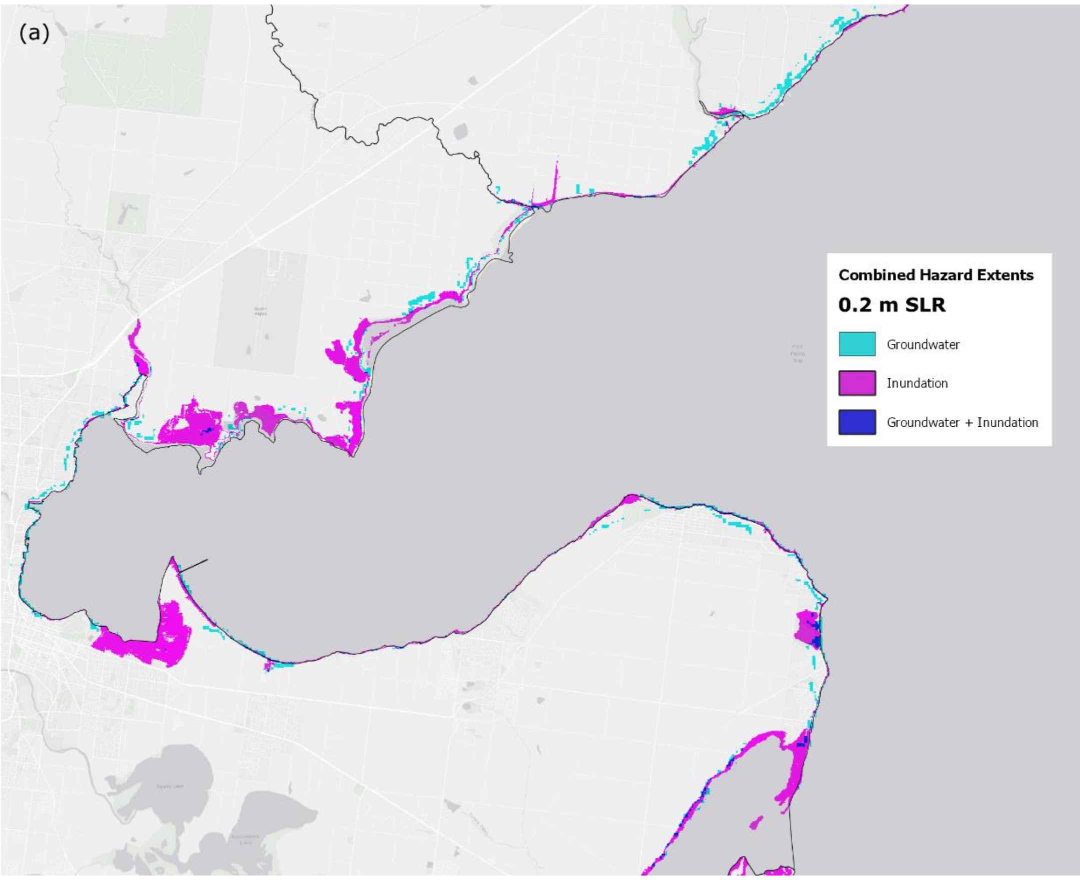

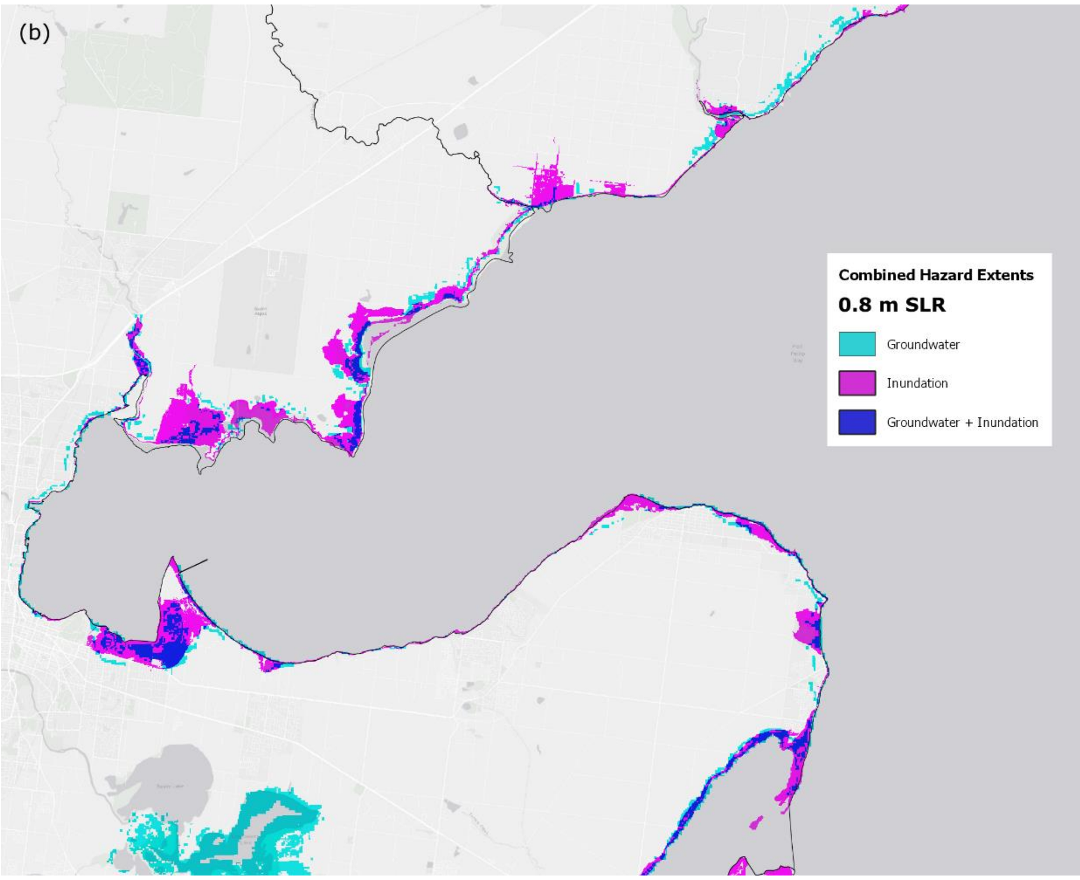

Figure 9.2: Overlay of hazard zones for inundation and groundwater for the west of the bay under (a) 0.2, (b) 0.8 and (c) 1.4 m SLR. The inundation zone is based on a 1% AEP storm tide.

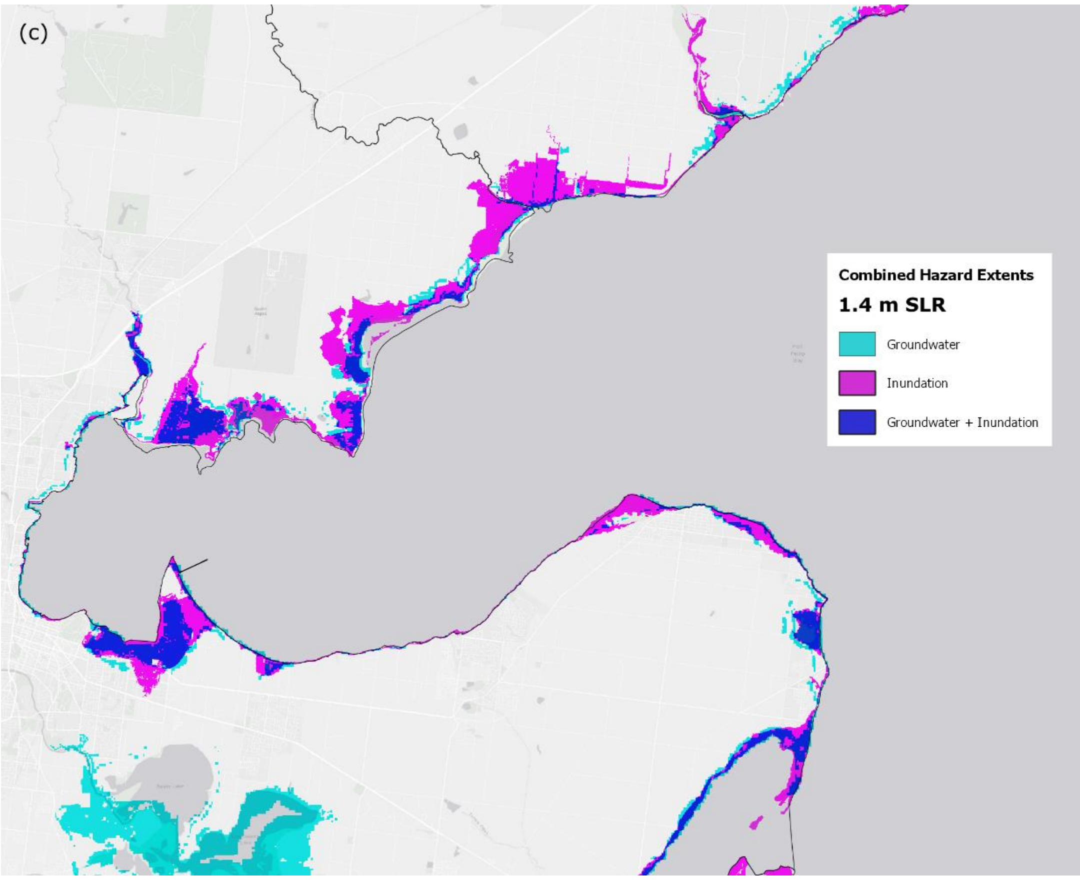

Figure 9.2: Continued.

Along the Wyndham coast, the hazards are most extensive between Little River and the Werribee River. Inundation hazard shows an accelerating trend with SLR increasing from 2 km^2 under 0.0 m SLR to 15.4 km^2 under 1.4 m of SLR (Appendix K, Figure K4). Although inundation and erosion hazards extend along the Werribee River coastline, particularly under SLR of 1.4 m, the low cliff coastline that the Werribee plain slopes down to is protected by an extensive revetment extending northeast along the coast from the Werribee River (Figure 7.8), indicating that this part of the Werribee plain appears to be at an effective height to avoid inundation under all SLR scenarios. The inland migration of the seawater-groundwater interface is predicted to be approximately 250 m at 20 m depth for a 1.4 m rise in sea level (Figure 6.13, Figure 9.2c). In this region, which supports agriculture and horticulture, drawdown triggers for management of groundwater extraction, which are based on the depth to watertable in specified bores, will need to be reconsidered over time.

Further northeast along the coast, inundation affects the Cheetham Wetlands in the Hobsons Bay City LGA under 0.2 m SLR (Figure 9.3a). The geomorphology is complex with elongate, overlapping spits rapidly extending north in front of Skeleton Creek, changing the position and dimensions of the intertidal and beach area on an annual to decadal scale. Under 0.8 and 1.4 m SLR, groundwater hazards also affect the area as well as further along the coast to the foreshores of Altona and Williamstown (Figures 9.3b and c). Inundation increases approximately linearly from 5.6 km^2 under 0.0 m SLR to 13.6 km^2 under 1.4 m of SLR (Appendix K, Figure K5a). The changing groundwater levels and salinity along this coastline will increasingly impact wetland ecology.

The City of Melbourne has limited coastline with significant coastal protection structures and extensive city infrastructure. Despite the relatively heavily armoured coastline, inundation hazard was found to increase in area dramatically beyond 0.5 m SLR. The area of inundation for a 1% AEP event increases from 0.45 km^2 to 0.95 km^2 under 0.8 m SLR to 4.7 km^2 under 1.4 m SLR, representing a tenfold increase (Appendix K, Figure K6a). These increases indicate reduced effectiveness of coastal protective structures under SLR, meaning that upgrading of infrastructure may be required in the years to come. Groundwater changes were confined to a shallowing of the watertable adjacent to the coast.

For the City of Port Phillip, inundation hazard alone was found to be the most significant hazard (Figure 9.3). It showed a marked increase beyond 0.5 m SLR, increasing in area from 1.4 km^2 to 6.9 km^2 for 1.4 m SLR (Appendix K, Figure K7a). The groundwater hazard was found to be relatively minor under SLR change.

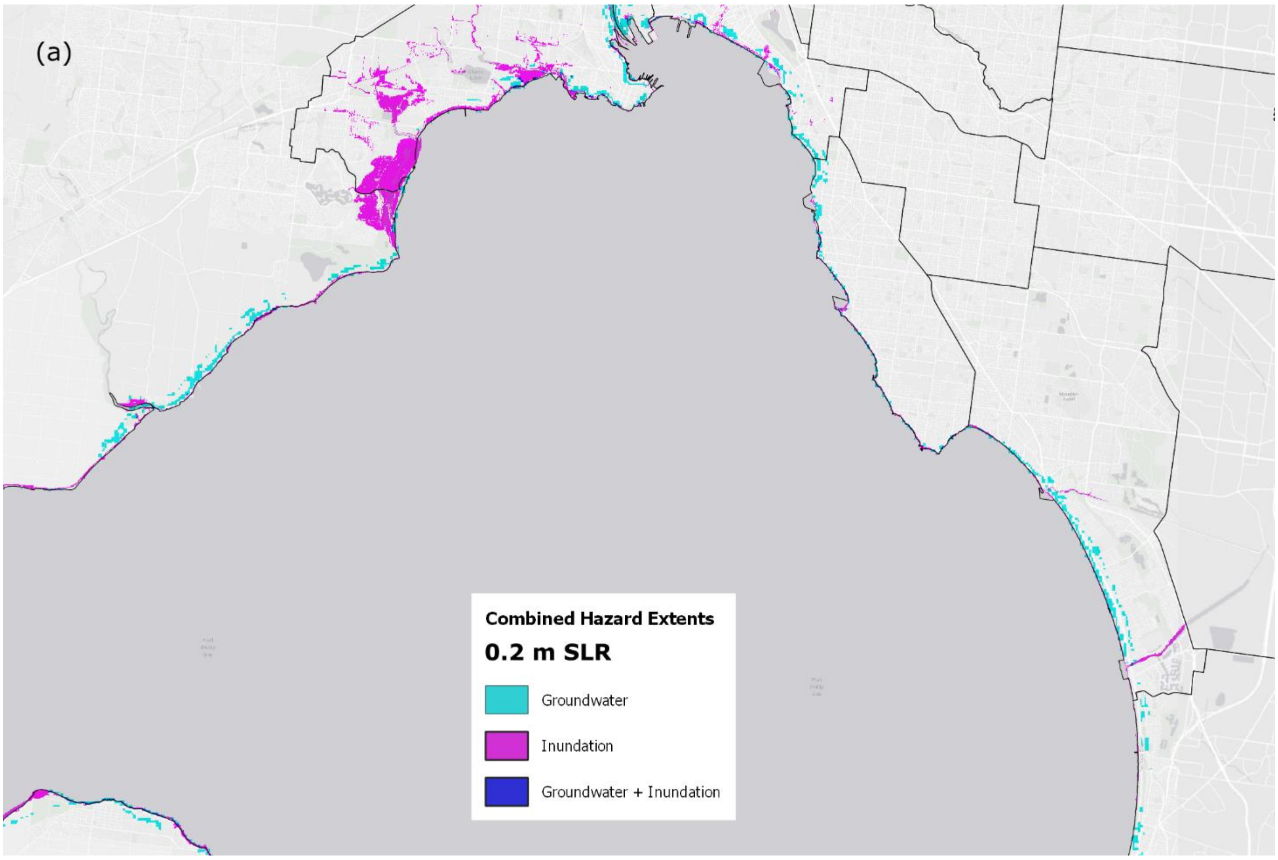

Figure 9.3: Overlay of hazard zones for inundation and groundwater for the north of the bay under (a) 0.2, (b) 0.8 and (c) 1.4 m SLR. The inundation zone is based on a 1% AEP storm tide.

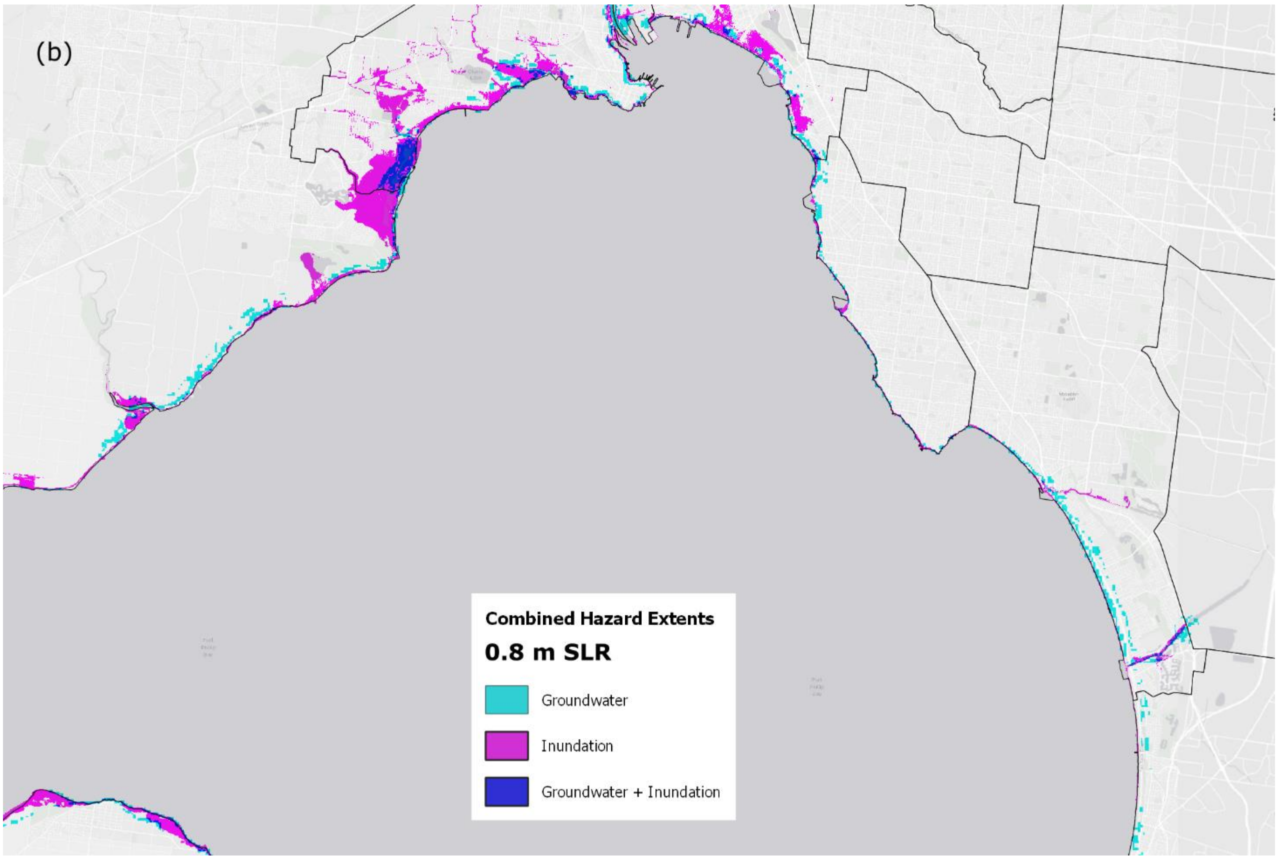

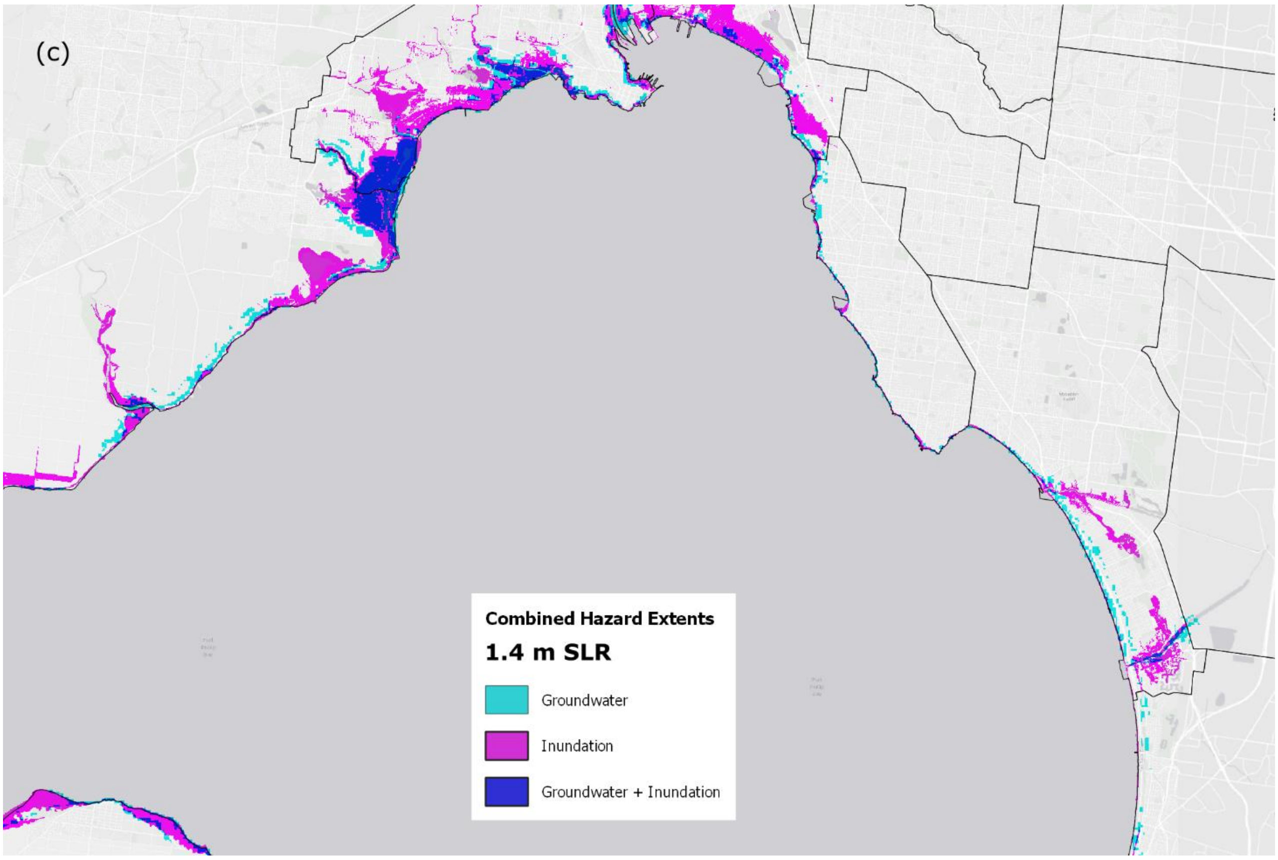

Figure 9.3: Continued.

Coastal hazards in Bayside City Council were found to be mainly confined to the beaches as protective structures such as seawalls and revetments prevent erosion from reaching most of the active cliff sectors. Inundation increased linearly from 0.34 km^2 under 0.0 m SLR to 0.74 km^2 under 1.4 m SLR (Appendix K, Figure K8a). Changes to groundwater were small for this council area.

City of Kingston inundation hazard increased tenfold from 0.4 km^2 under 0.0 m SLR to 4.4 km^2 under 1.4 m SLR, the significant increases occurring beyond 0.8 m SLR (Appendix K, Figure K9a). Much of this increase occurred in the Edithvale-Seaford Wetlands between Mordialloc Creek and Patterson River indicating that existing coastal protection structures would not be effective for 1.4 m SLR. There is an increase in the groundwater hazard along the coast (Figure 9.3) associated with the inland migration of the seawater-groundwater interface. This may have implications for below ground engineering infrastructure.

Coastal hazards in the Frankston City Council will occur along the bay coastline and inside Patterson Lakes. Inundation hazard increases from 0.1 km^2 under 0.0 m SLR to 0.3 km^2 under 1.4 m SLR (Appendix K, Figure K10a). Groundwater was found to undergo minimal change along this coastline (Appendix K, Figure K10d). Deeply weathered sedimentary, volcanic and granitic rocks comprise active cliffs exposed to storm waves from the long westerly and north-west fetch.

Mornington Peninsula Shire hazards are shown in Figure 9.4. Inundation hazard increases fourfold from 1.0 km^2 under 0.0 m SLR to 4.1 km^2 under 1.4 m SLR (Appendix K, Figure K11a) with the inundation occurring mainly around Martha Cove and the Balcombe Estuary Recreation reserve as well as along the foreshore from Rosebud to Dromana. Groundwater hazard is present along the coastline from Martha Cove to Point Nepean, mainly due to an increase in the presence of surface water (Appendix K, Figure K11d). The rising sea levels are predicted to have a greater impact especially on bores close to the coast. At Blairgowrie, it is estimated that the seawater-groundwater interface will migrate approximately 50 m inland at 20 metres depth for a 1.4 m rise in sea level (Figure 6.20) and will eventually require a revision of the management plan for the Nepean Groundwater Management Area.

In the low-lying Borough of Queenscliffe on the south of Swan Bay (Figure 9.4), the area affected by inundation and groundwater hazards are a significant proportion of the total land area of the Borough, particularly under the higher SLR scenarios. The inundation hazard increases from 3.6 km^2 under 0.0 m SLR to 5.7 km^2 under 1.4 m SLR (Appendix K, Figure K2a). Groundwater hazard also exhibits significant overlap (Appendix K, Figure K2c, d). While some coastal protection infrastructure is present, including a revetment and groynes facing the entrance to PPB, the township is also exposed on the southern side of Swan Bay and these protection structures likely will need extending and upgrading to minimise the hazards from SLR in the future.

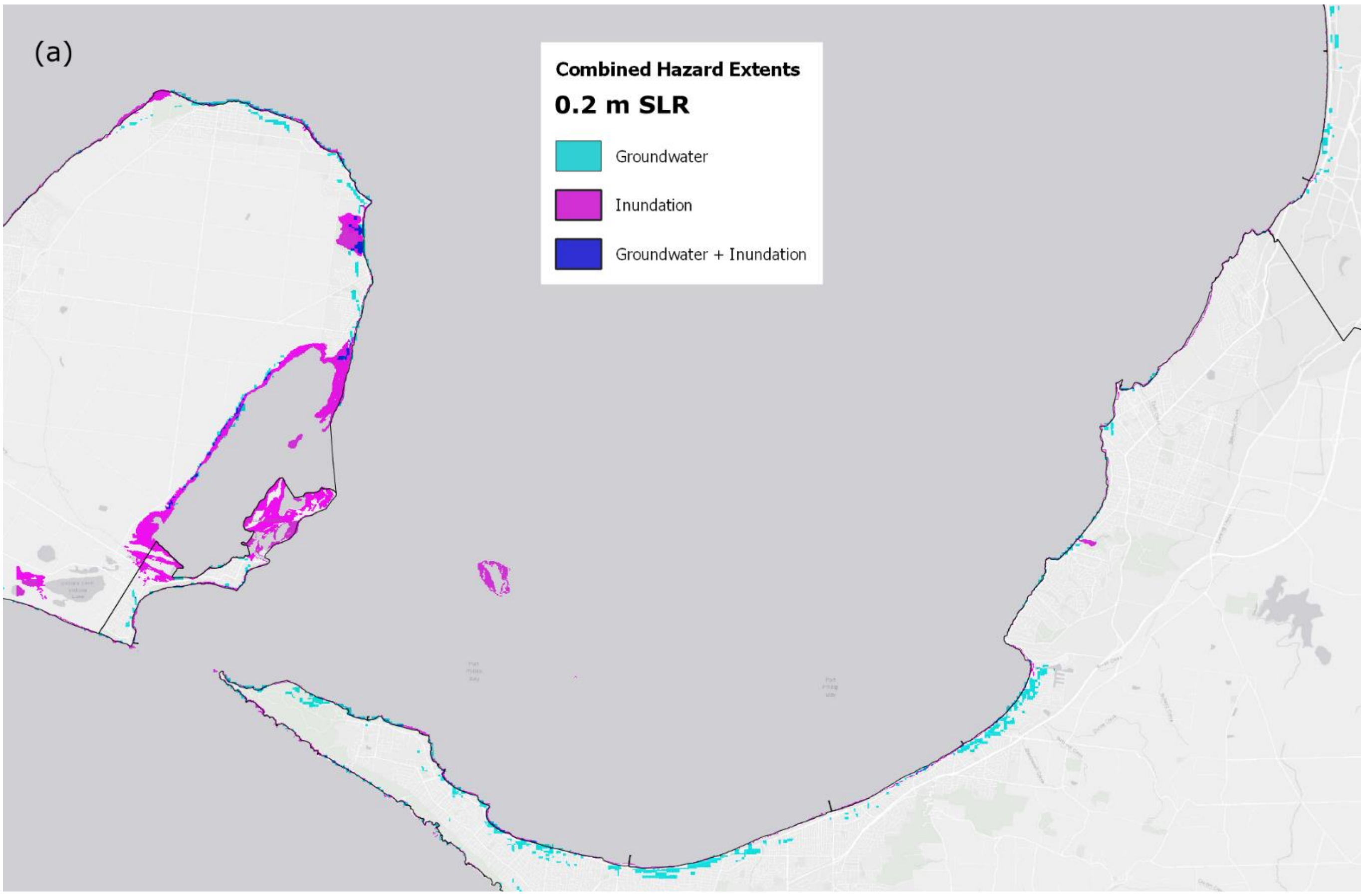

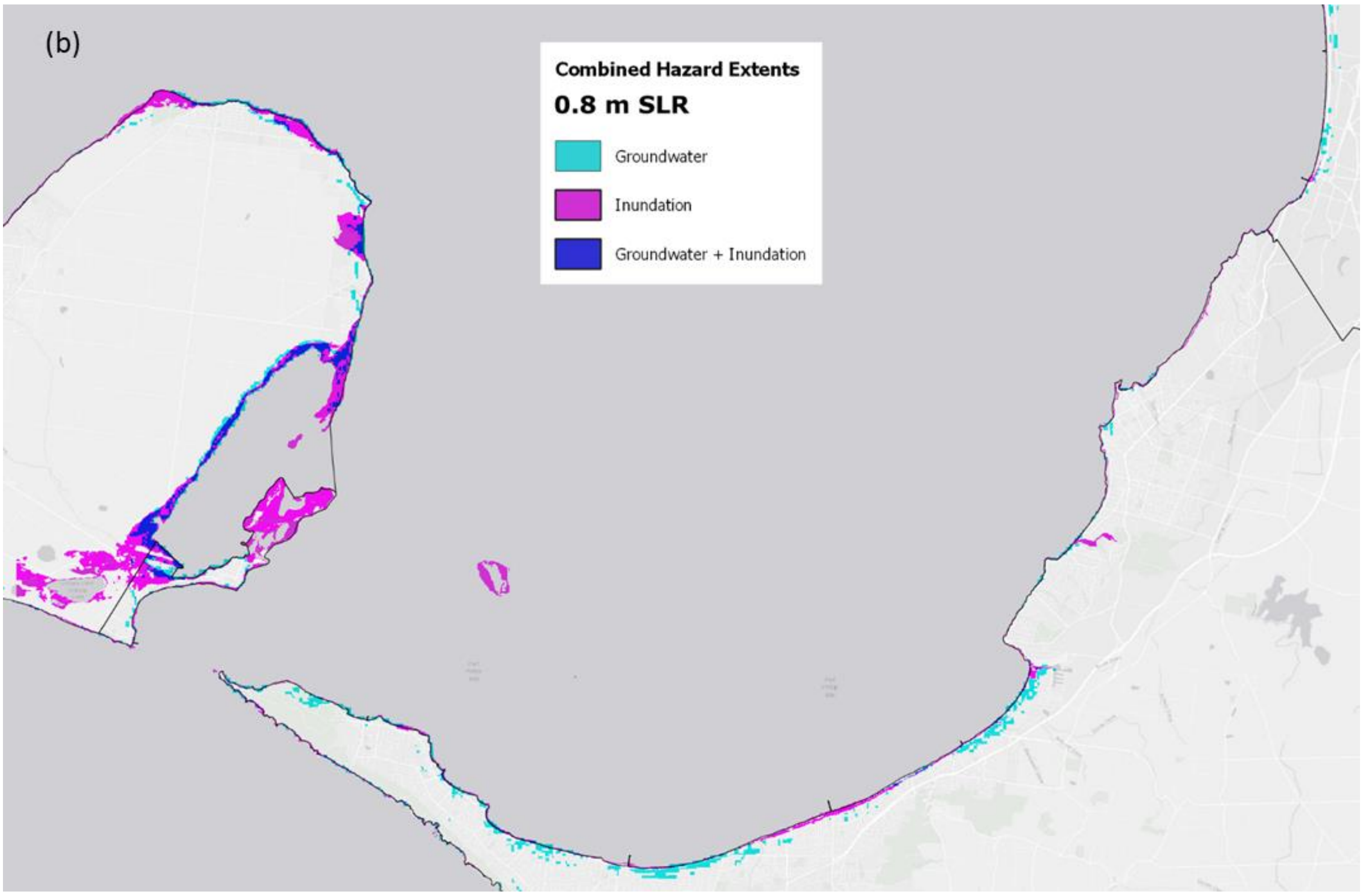

Figure 9.4: Overlay of hazard zones for inundation and groundwater for the south of the bay under (a) 0.2, (b) 0.8 and (c) 1.4 m SLR. The inundation zone is based on a 1% AEP storm tide.

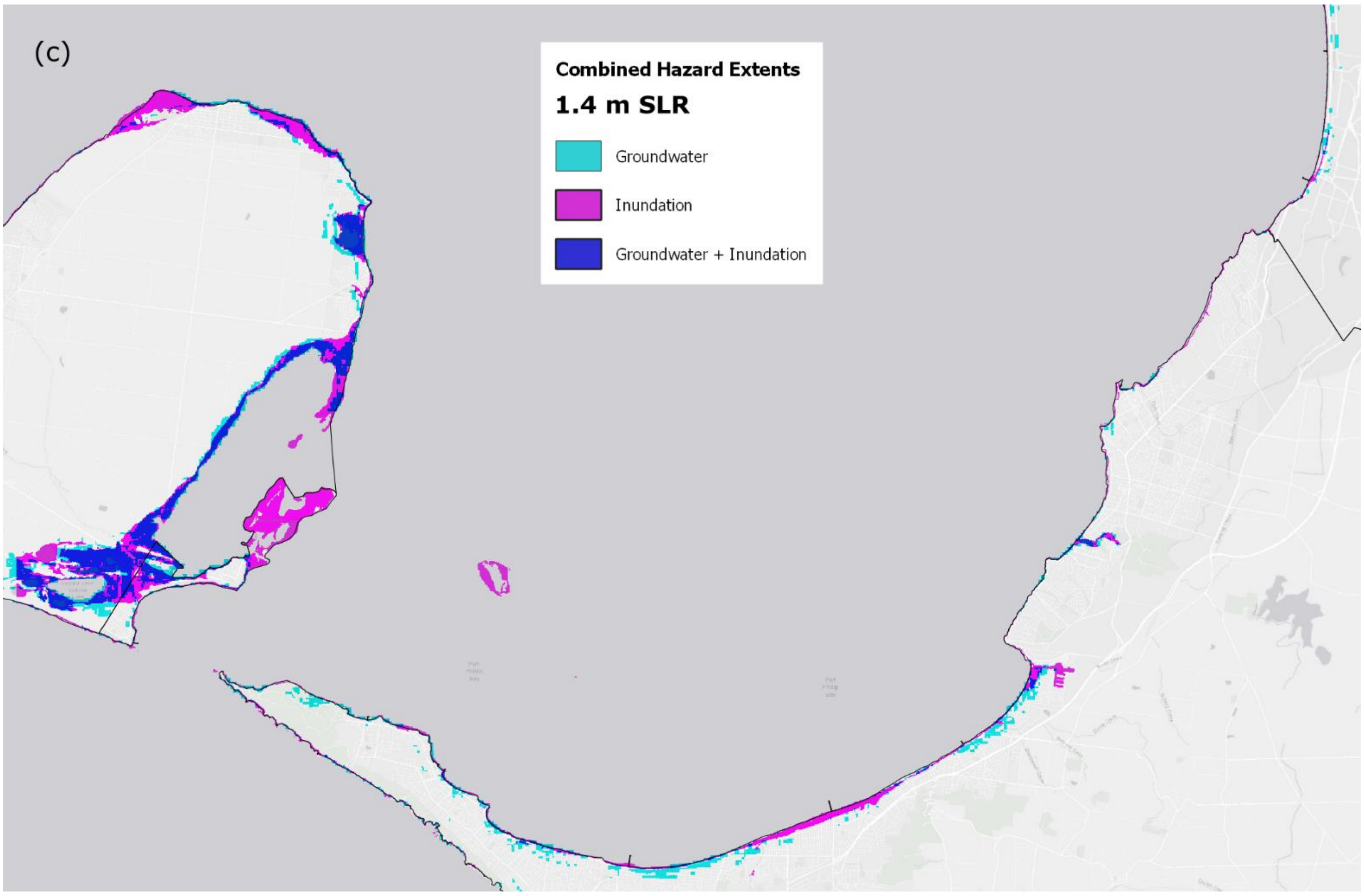

Figure 9.4: Continued.

9.3 Uncertainties and Recommendations for Future Work

The undertaking of the PBBCHA project has required bringing together a large range of data, information, and models to develop robust estimates of inundation and groundwater hazards under SLR around PPB. A key assumption in the development of the hazard layers was that existing coastal protection structures or coastal protection measures undertaken, such as periodic beach renourishment, would be maintained into the future, but would not be adapted for future sea levels. In recognition of the uncertainties in model results particularly in the context of sparse, limited or non-existent data or information available for validation of model results, the methodology for inundation hazard has been designed such that where a combination of models have been used to estimate the hazard zones, a probabilistic approach was implemented that both accounts for the uncertainties in model inputs and outputs and also recognises the different risk appetites of the users of the information. This section focuses on the key uncertainties identified within this study and recommendations for future work.

The whole-of-bay hydrodynamic and wave modelling was undertaken to provide consistent wave and sea level data inputs across the whole of the bay under present and future SLR scenarios for the hazard assessments. While the modelling addresses the limited data inputs, it was also identified that long term, readily available wave data within PPB (e.g. similar to the availability of tide gauge data), particularly in shallow coastal waters was a major gap and a priority for further investment. A limitation of all practical applications of hydrodynamically-coupled wave models in multidecadal hindcast simulations is the accurate representation of waves after breaking in very shallow water. This limitation has been considered for the wave height values extracted at the toe of the defence structures which were used in the overtopping estimates (see Section 5.3.4).

It is intuitive that the SLR simulations in this study, which indicate increased wave heights at the coast, will directly increase the relative estimates of longshore transport. Future wind changes are projected to be small and uncertain (VCP19) and therefore hydrodynamic and wave modelling under projected future weather conditions was not undertaken in the PPBCHA due to project constraints. However, a more detailed investigation into changes in wave climate would provide insight into changing patterns of longshore transport and sediment movement around the bay and their likely influence on shoreline change.

The relative increases in extreme water levels and waves within PPB under the modelled SLR scenarios are predicated on the assumption that the seabed remains static under SLR. While this simplifying assumption is not unfounded, since evidence suggests many shallow areas of the bay consist of relatively thin veneers of unconsolidated sediment over consolidated (lithified or partially lithified) substrates, particularly the Great Sands (see Section 2.1), it is an important caveat. In reality, some degree of morphological change under future SLR scenarios is almost certain, although how this may further affect the water level and wave dynamics remains unknown. Repeat bathymetric and beach surveys are required to monitor the changes in mobile sediments over the long term, and pre and post storm events. This is also a recommended area of future study.

This study has highlighted differences in inundation that arise from different modelling approaches. A number of possible contributing factors were identified such as subtle differences in input assumptions, and the differences in modelling approaches such as the temporally resolving hydrodynamic modelling approach undertaken in this study compared with the static and instantaneous bathtub infill approach used in a number of previous studies. However, other factors such as differences in urban landscape may also lead to differences between the results from the two modelling approaches. A more detailed and systematic investigation of the relative advantages and disadvantages of static and hydrodynamic modelling in different urban settings would lead to guidance on when bathtub fill is a sufficient approach or when detailed hydrodynamic modelling is required.

It is also noted that in this study, a design storm approach was taken to model catchment inputs and a 10% AEP rainfall event was considered. However, understanding the joint probability of storm tides and catchment inputs, both under present and future climate conditions was beyond the scope of this study and is recommended for future investigation.

As part of this study, a tertiary-scale geomorphic assessment of PPB was undertaken to identify the intertidal and backshore composition to provide foundation information for future erosion hazard assessments. However, a lack of continuous long-term shoreline profile monitoring in the specific environment of PPB remains a gap for future shoreline assessments. It is therefore recommended that co-ordinated and bay-wide monitoring of beach morphology using drone photogrammetry and simultaneous ground probing is undertaken to determine beach thickness and variations in beach stratigraphy to underpin future erosion hazard assessments. A priority location for such monitoring and subsequent modelling would be to understand the origin and regimes of beach and nearshore sediment movement on the northern and eastern Bellarine Peninsula—between Curlewis and Portarlington.

There are substantial challenges and limitations to the estimation of groundwater hazards related to SLR and climate change around PPB. These include availability, access and quality of data as well as the quality of whole-of-bay models of watertable depth and salinity that are used in this study. Watertables are dynamic, varying with changes in recharge, discharge, land-use, barometric pressure and transpiration by plants. However, the static maps produced in this project are aimed only at broad guidance and information rather than definitive input to decisions. Furthermore, while detailed conceptual cross-sections have been provided for three focus areas, these cross-sections should be seen as speculative in the context of changing climate and land management.

Amongst priorities for future research into groundwater are firstly; the establishment of a numerical model of the predicted response of groundwater to SLR that is at a suitable resolution and demonstrates credible performance. To achieve this will require working with data custodians in both the public and private sectors to liberate the required data, much of which is not currently in a suitable digital form (e.g. the substantial volume of potentially useful data in the grey literature). Data gaps will require filling through investigations that require remote sensing and/or geophysical surveys and/or drilling. A second priority for future work is to establish the evidence for the groundwater dependency of coastal ecologies, including terrestrial, aquatic, estuarine and marine ecologies. A final priority is to establish the evidence for understanding the dynamic response of the groundwater-seawater interface (the rate of change of both groundwater levels and chemistry). Based on the published literature, these are both poorly known at present.

Finally, with regards to the development and delivery of the hazards information in the PPBCHA, the modelling systems established during this project could, in the future, be applied to testing the effectiveness of a range of adaptation options. Additionally, the DSS developed to host the hazard layers and other relevant data in this project is scalable and could therefore be expanded to provide a single DSS for coastal hazards data in Victoria.

Acknowledgements

The authors of this report acknowledge the inputs from a number of people associated with this project. In particular, Dr Tamara van Polanen Petel from DELWP for her management of the project and useful discussions with the DELWP Technical Reference Group including Dr Chris Sharples, Richard Reinen-Hamill, Ralph Roob, Darren James, Keith Boniface and the peer reviewer, Associate Professor Ron Cox. The authors are also grateful for the constructive discussions with Ms Polly Matthews and Dr Jak McCarroll and for the careful review of the final document by Dr Brett Molony.

References

ABN (2015) Report 03 Port Phillip Bay Sea Level, report prepared by Cardno for Association of Bayside Municipalities.

Adams JR (1987) Tide Levels During November - December 1934 Flood and High Tide Frequency Analysis for Williamstown, Hydrology and Flood Warning Unit.

Advisian (2016) Portsea Front Beach Wave Modelling and Monitoring Investigation, report for the Department of Environment, Land, Water and Planning, Cornell University Press. doi:10.7591/9780801456329-006.

Allemand J, Keysers J, Quadros N and Deen R (2017) 2017 Victorian Coastal DEM report, Cooperative Research Centre for Spatial Information.

Ardhuin F, Rogers WE, Babanin AV, Filipot J-F, Magne R, Roland A, van der Westhuysen A, Queffeulou P, Lee B, Aouf L and Collard F (2010) Semiempirical Dissipation Source Functions for Ocean Waves. Part I: Definition, Calibration, and Validation. Journal of Physical Oceanography 40(9), 1917–1941. doi:10.1175/2010JPO4324.1

Atkinson AL, Power HE, Moura T, Hammond T, Callaghan DP and Baldock TE (2017) Assessment of runup predictions by empirical models on non-truncated beaches on the south-east Australian coast. Coastal Engineering 119, 15–31. doi:10.1016/j.coastaleng.2016.10.001.

Babister M and Barton C (2012) Two-dimensional modelling in urban and rural floodplains. Australian Rainfall and Runoff Revision Project 15, Engineers Australia.

Ball J, Babister M, Nathan R, Weeks W, Weinmann E, Retallick M and Testoni I (eds) (2016) Australian Rainfall and Runoff: A Guide to Flood Estimation, Commonwealth of Australia.

Bird ECF (2011) Changes on the Coastline of Port Phillip Bay. Office of the Environmental Monitor, East Melbourne, Victoria. 64 pages. http://www.oem.vic.gov.au/Assets/986/1/ChangesontheCoastlineofPPBBookforWeb2011.pdf

Black KP, Hatton DN and Coleman R (1990) Prediction of extreme sea levels in northern Port Phillip Bay and the possible effects of a rise in mean sea level. Board of Works, Melbourne by the Victorian Institute of Marine Sciences. 141 pages.

BMT WBM (2015) Southbank Stormwater Infrastructure Assessment: Final Report. 281 pages.

Brooke BF, Nichol SL, Huang Z and Beaman R (2017) Palaeoshorelines on the Australian continental shelf: Morphology, sea-level relationship and applications to environmental management and archaeology. Continental Shelf Research 134, 26–38.

Bruun P (1988) The Bruun Rule of Erosion by sea-level rise: a discussion on large- scale two- and three-dimensional usages. Journal of Coastal Research 4, 627–648.

Bucea L and Sirivivatnanon V (2003) Salinity hazard and deterioration mechanisms in the built environment. CMIT Document. Sydney, CSIRO Manufacturing and Infrastructure Technology Division. 2003-242: 29.

Buckland D and McGhie S (2005) Costs of Urban Salinity. NSW Department of Primary Industries and Department of Infrastructure, Planning and Natural Resources, Sydney.

Cardno (2007) Hydrodynamic and wave model calibration and validation. RM2127, Maunsell Australia on behalf of Port of Melbourne Corporation.

Cardno (2011) The Great Sands and Adjacent Coast and Beaches, RM2289_LJ5518 v1.0, Port of Melbourne Corporation.

Cardno (2015) Bellarine Peninsula - Corio Bay Local Coastal Hazard Assessment: Inundation. 179 pages.

Cardno (2017a) Hydrodynamics – Infrastructure Victoria Second Container Port Advice.

Cardno (2017b) Port Phillip Bay Beach Renourishment Strategy 2016-2036. Department of Environment, Land, Water and Planning.

Cardno (2018) Port Phillip Bay Storm Bite Analysis. Association of Bayside Municipalities Available at: https://abm.org.au/wp-content/uploads/2018/12/ABM0004_ReportSeries_report_5.pdf.

Cardno (2019) Port Phillip Bay Wave Climate. 59915505, Association of Bayside Municipalities. 51 pages.

Cayley RA, Taylor DH, VandenBerg AHM and Moore DH (2002) Proterozoic - Early Palaeozoic rocks and the Tyennan Orogeny in central Victoria: The Selwyn Block and its tectonic implications. Australian Journal of Earth Sciences 49(2), 225-254, doi:10.1046/j.1440-0952.2002.00921.x.

Cayley, R. A. (2011), Exotic crustal block accretion to the eastern Gondwanaland margin in the Late Cambrian–Tasmania, the Selwyn Block, and implications for the Cambrian–Silurian evolution of the Ross, Delamerian, and Lachlan orogens, Gondwana Research, 19(3), 628-649, doi:https://doi.org/10.1016/j.gr.2010.11.013.

CERC U.S. Army corps of Engineers (1984) SHORE PROTECTION MANUAL - Volume I. Coastal Engineering Research Center 1, 652. doi:10.5962/bhl.title.47830.

CeRDI (2018) Data Democracy FAQs. Centre for eResearch and Digital Innovation, Federation University Australia, Mt Helen, Ballarat, Victoria.

CeRDI (2020) VVG Visualising Victoria's Groundwater. Centre for eResearch and Digital Innovation, Federation University Australia Mt Helen, Victoria.Retrieved 13/4/2020 from http://www.vvg.org.au/.

Chambolle A (2004) An algorithm for total variation minimization and applications. Journal of Mathematical Imaging and Vision 20(1-2), 89-97.

Clarke JM, Grose M, Thatcher M, Hernaman V, Heady C, Round V, Rafter T, Trenham C and Wilson L (2019) Victorian Climate Projections 2019 Technical Report. CSIRO, Melbourne Australia. 96 pages.

Clunies GJ, Mulligan RP, Mallinson DJ and Walsh JP (2017) Modeling hydrodynamics of large lagoons: Insights from the Albemarle-Pamlico Estuarine System. Estuarine, Coastal and Shelf Science 189, 90-103.

Cohen RCZ, Hilton JE and Prakash M (2016b) Benchmark testing the Swift flood modelling solver: Version I. No. EP151977. CSIRO Data61.

Cohen RCZ, Hilton JE, Hasan Khan S, Wang Y and Prakash M (2015) Swift: A GPU based coupled hydrodynamic/hydraulic framework for urban flood prediction. Eleventh International Conference on CFD in the Minerals and Process Industries, Melbourne.

Cohen RCZ, Prakash M, O'Grady JG, McInnes KL and Hoeke RK (2019) C-FAST: Modelling and visualisation to improve flood adaptation planning processes in coastal cities. ResearchGate. Australasian Coasts & Ports Conference, Hobart.

Cohen RCZ, Wang Y, Woolard F and Prakash M (2016a) City of Greater Geelong & Borough of Queenscliffe Flood Adaptation Effectiveness Study. No. EP165982. CSIRO Data61.

Cohen RCZ, Wang Y, Woolard F, Stephenson A and Prakash M (2017) Integrated assessment of flood and stormwater management strategies Bunbury, WA. No. EP166941. CSIRO Data61.

Colberg F and McInnes KL (2012) The impact of storminess changes on extreme sea levels over southern Australia. Journal of Geophysical Research: Oceans, 117. DOI: 10.1029/2012JC007919.

Colberg F, McInnes KL, O'Grady JG and Hoeke RK (2019) Atmospheric Circulation Changes and their Impact on Extreme Sea Levels around Australia. Journal of Natural Hazards and Earth System Science 19, 1067-1086.

Coles SG (2001) An introduction to statistical modeling of extreme values. Springer, London.

CSIRO and BoM (2015) Climate Change in Australia Information for Australia's Natural Resource Management Regions: Technical Report, CSIRO and Bureau of Meteorology, Australia.

Currell, M., Gleeson, T., & Dahlhaus, P. (2016). A new assessment framework for transience in hydrogeological systems. Groundwater, 54(1), 4-14. doi: 10.1111/gwat.12300

Dahlhaus PG (2010) Salinity risk in the Corangamite Region, Australia, PhD thesis, Flinders University, Adelaide, Australia. 217 pages.

Dong J (2005) Splintering Urbanism and Sustainable Urban Water Management. Proceedings of the 2nd State of Australian Cities Conference, Brisbane, Australia.

DSE (2012) Victorian Coastal Hazard Guide. Department of Sustainability and Environment, Victoria, East Melbourne Victoria. 90 pages.

Dugor J, Rihouey D and Pierre L (2014) Flood modelling on Ile de Ré during Xynthia. 21st Telemac Mascaret User Conference, Grenoble, France, 15-17.

Durrant T, Greenslade D, Hemer M and Trenham C (2014) A Global Wave Hindcast focussed on the Central and South Pacific. CAWCR Technical Report 70. 54 pages.

Egbert GD and Erofeeva SY (2002) Efficient Inverse Modeling of Barotropic Ocean Tides. Journal of Atmospheric Oceanic Technology 19, 183–204.

Ekström M, Grose MR and Whetton PH (2015) An appraisal of downscaling methods used in climate change research. Wiley Interdisciplinary Reviews, Climate Change 2015, 6, 301–319.

Fan Y, Lin S, Griffies SM and Hemer MA (2014) Simulated Global Swell and Wind-Sea Climate and Their Responses to Anthropogenic Climate Change at the End of the Twenty-First Century. Journal of Climate 27, 3516–3536. https://doi.org/10.1175/JCLI-D-13-00198.1.

FedUniSpatial (2020a) Bore Details OGS2. FedUniSpatial Groundwater Monitoring Database Retrieved 14/05/2020, from https://www.vvg.org.au/view_bore.php?bore_id=917929.

FedUniSpatial (2020b) Bore Details OGS16. FedUniSpatial Groundwater Monitoring Database Retrieved 14/05/2020, from https://www.vvg.org.au/view_bore.php?bore_id=917930.

Fetter CW (2001) Applied hydrogeology, 4th edn. Prentice Hall, Englewood Cliffs, NJ, USA.

Flynn A, Edmunds M, Ierodiaconou D, Rattray A and Ferns L (2016) Cbics biotope classi1cation of port phillip bay habitat polygons, Unpublished Work by Fathom Paci1c, Australian Marine Ecology Pty Ltd, Melbourne. doi: DeakinUniversityandDepartmentofEnvironment,Land,WaterandPlanning.

Garzon JL and Ferreira CM (2016) Storm Surge Modeling in Large Estuaries: Sensitivity Analyses to Parameters and Physical Processes in the Chesapeake Bay. Journal of Marine Science and Engineering, 4, 45.

Geoscience Victoria (2011) Seamless Geology Project 2006-2011, Department of Primary Industries.

Gomes da Silva, P., G. Coco, R. Garnier, and A. H. F. Klein (2020), On the prediction of runup, setup and swash on beaches, Earth-Science Reviews, 204, 103148, doi:https://doi.org/10.1016/j.earscirev.2020.103148.

Goodfellow BW and Stephenson WJ (2005) Beach morphodynamics in a strong-wind bay: a low-energy environment? Marine Geology 214, 101–116. doi:10.1016/j.margeo.2004.10.022.

Greenslade D, Hemer M, Babanin A, Lowe R, Turner I, Power H, Young I, Ierodiaconou D, Hibbert G, Williams G, Aijaz S, Albuquerque J, Allen S, Banner M, Branson P, Buchan S, Burton A, Bye J, Cartwright N, Chabchoub A, Colberg F, Contardo S, Dufois F, Earl-Spurr C, Farr D, Goodwin I, Gunson J, Hansen J, Hanslow D, Harley M, Hetzel Y, Hoeke R, Jones N, Kinsela M, Liu Q, Makarynskyy O, Marcollo H, Mazaheri S, McConochie J, Millar G, Moltmann T, Moodie N, Morim J, Morison R, Orszaghova J, Pattiaratchi C, Pomeroy A, Proctor R, Provis D, Reef R, Rijnsdorp D, Rutherford M, Schulz E, Shayer J, Splinter K, Steinberg C, Strauss D, Stuart G, Symonds G, Tarbath K, Taylor D, Taylor J, Thotagamuwage D, Toffoli A, Valizadeh A, van Hazel J, Vieira da Silva G, Wandres M, Whittaker C, Williams D, Winter G, Xu J, Zhong A and Zieger S (2020) 15 Priorities for Wind-Waves Research: An Australian Perspective. Bulletin of the American Meteorological Society 101(4), E446-E461.

Haigh I, Wijeratne EMS, MacPherson LR, Pattiaratchi CB, Mason MS, Crompton RP and George S (2014) Estimating present day extreme water level exceedance probabilities around the coastline of Australia: tides, extra-tropical storm surges and mean sea level. Climate Dynamics 42, 121–138. doi: 10.1007/s00382-012-1652-1.

Harris IF (1976) Hydrogeology of the Rosebud area. Preliminary report in Geological Survey of Victoria Unpublished Report, edited Mines Department, Victoria. 4 pages.

Healy T (2006) Potential Channel Deepening-Induced Morphodynamic Changes on the Flood Tidal Delta ("The Great Sands") and Adjacent Coastal Areas of Port Phillip Bay. A Report to the Port of Melbourne Corporation November 2006. 30 pages.

Hemer MA, Fan Y, Mori N, Semedo A and Wang XL (2013) Projected changes in wave climate from a multi-model ensemble. Nature Climate Change 3, 471-476.

Holdgate GR (1976) Subsurface stratigraphy of the Nepean Peninsula, Mines Department, Victoria. 43 pages.

Holdgate G and Norvick M (2017) Geological evolution of the Holocene Yarra Delta and its relationship with Port Phillip Bay. Australian Journal of Earth Sciences 64(3), 301-318, doi:10.1080/08120099.2017.1297736.

Holdgate GR and Gallagher SJ (2003) Tertiary, Geology of Victoria. [Birch WD (ed)], Geological Society of Australia (Victoria Division), Melbourne, pages 289-335.

Holdgate GR, Geurin B, Wallace MW and Gallagher SJ (2001) Marine geology of Port Phillip. Australian Journal of Earth Sciences 48, 439-455. doi:10.1046/j.1440-0952.2001.00871.x.

Holdgate GR, Wagstaff B and Gallagher SJ (2011) Did Port Phillip Bay nearly dry up between ~2800 and 1000 cal. yr BP? Bay floor channelling evidence, seismic and core dating. Australian Journal of Earth Sciences 58(2), 157-175. doi:https://doi.org/10.1080/08120099.2011.546429.

Holdgate GR, Gallagher SJ and Wallace MW (2002) Tertiary coal geology and stratigraphy of the Port Phillip Basin, Victoria. Australian Journal of Earth Sciences 49(3), 437-453.

Hubbert GD and McInnes KL (1999) A storm surge inundation model for coastal planning and impact studies. Journal of Coastal Research 15, 168-185.

Keble RA (1946) The Sunklands of Port Phillip Bay and Bass Strait. Memoirs National Museum of Victoria 14, 69-122.

Kent DM, Kirono DGC, Timbal B and Chiew FHS (2013) Representation of the Australian sub-tropical ridge in the CMIP3 models. International Journal of Climatology 33(1), 48-57.

Kumbier K, Carvalho RC and Woodroffe CD (2018) Modelling Hydrodynamic Impacts of Sea-Level Rise on Wave-Dominated Australian Estuaries with Differing Geomorphology. Journal of Marine Science and Engineering 6, 66.

Lacey MJ and Mount RE (2011) Victorian Coastal LiDAR Inundation Modelling and Mapping, revised Version 2. Department of Sustainability and Environment, Victoria by the Blue Wren.

Lawson and Treloar (2004) POMC Channel Deepening, Hydrodynamics, Sediment Transport and Water Quality Modelling. Port of Melbourne Corporation, RM2054/J5372, Melbourne, Australia.

Leonard, J.G. (1979). Preliminary assessment of the groundwater resources in the Port Phillip Region, Geol. Surv. Victoria, Rept. no. 66.

Leonard JG (1992) Port Phillip Region Groundwater Resources - Future Use and Management. Department of Water Resources, Victoria, Melbourne. 297 pages.

Leonard JG (2003) Groundwater. Geology of Victoria. W.D. Birch, Geological Society of Australia, Victoria Division. Geological Society of Australia Special Publication 23, 519-531.

Leonard JG (2006) Hydrogeology of the Melbourne area. Australian Geomechanics 41(3), 14.

MAFRI (1996) Review of Data Collected by the Marine Models Laboratory, Port of Melbourne Authority. Marine and Freshwater Resources Institute to Coastal and Ports Policy Branch. Department of Natural Resources and Environment. 87 pages.

Mariani A, Shand TD, Carley JT, Goodwin ID, Splinter K, Davey EK, Flocard F and Turner IL (2012) Generic Design Coastal Erosion Volumes and Setbacks for Australia. Report 247. doi:10.4225/53/5786faf5b3c5c.

McGregor JL and Dix MR (2008) An updated description of the conformal-cubic atmospheric model, high resolution numerical modelling of the atmosphere and ocean. Springer, 51-75.

McInnes KL and Hubbert GD (1996) Extreme events and the impact of climate change on Victoria's coastline. Environment Protection Authority (Vic) and Melbourne Water. CSIRO Division of Atmospheric Research and Global Environmental Modelling Systems, EPAV Publication No. 488.

McInnes KL and Hubbert GD (2003) A numerical modeling study of storm surges in Bass Strait. Australian Meteorological Magazine 52, 143-156.

McInnes KL, White CJ, Haigh ID, Hemer MA, Hoeke RK, Holbrook NJ, Kiem AS, Oliver ECJ, Ranasinghe R, Walsh KJE, Westra S and Cox R (2016) Natural hazards in Australia: sea level and coastal extremes. Climatic Change, doi: 10.1007/s10584-016-1647-8.

McInnes KL, Macadam I and O'Grady J (2009a) The Effect of Climate Change on Extreme Sea Levels in Port Phillip Bay. Victorian Department of Sustainability and Environment.

McInnes KL, Macadam I and O'Grady J (2009b) The Effect of Climate Change on Extreme Sea Levels along Victoria's Coast. Victorian Department of Sustainability and Environment.

McInnes KL, Macadam I, Hubbert GD and O'Grady J (2013) An assessment of current and future vulnerability to coastal inundation due to sea level extremes in Victoria, southeast Australia. International Journal of Climate 33, 33-47. doi: 10.1002/joc.3405.

McInnes KL, Church JA, Monselesan D, Hunter JR, O'Grady J, Haigh ID and Zhang X (2015) Sea-level Rise Projections for Australia: Information for Impact and Adaptation Planning. Australian Meteorology and Oceanography Journal 65, 127–149.

McInnes KL, Macadam I, Hubbert GD and O'Grady JG (2009c) A Modelling Approach for Estimating the Frequency of Sea Level Extremes and the Impact of Climate Change in Southeast Australia. Natural Hazards 51, 115–137.

McPherson A, Hazelwood M, Moore D, Owen K, Nichol S and Howard F (2015) The Australian Coastal Sediment Compartments Project: Methodology and Product Development, 2015/25. Geoscience Australia, Canberra. http://dx.doi.org/10.11636/Record.2015.025.

Meucci A, Young IR, Hemer M, Kirezci E and Ranasinghe R (2020). Projected 21st century changes in extreme wind-wave events. Science Advances 6(24), eaaz7295.

Moftakhari HR, AghaKouchak A, Sanders BF, Allaire M and Matthew RA (2018). What Is Nuisance Flooding? Defining and Monitoring an Emerging Challenge. Water Resources Research 54(7), 4218-4227.

Morim J, Hemer M, Cartwright N, Strauss D and Andutta F (2018) On the concordance of 21st century wind-wave climate projections. Global and Planetary Change 167, 160-171.

Morim J, Hemer M, Wang XL, Cartwright N, Trenham C, Semedo A, Young I, Bricheno L, Camus P, Casas-Prat M, Erikson L, Mentaschi L, Mori N, Shimura T, Timmermans B, Aarnes O, Breivik Ø, Behrens A, Dobrynin M, Menendez M, Staneva J, Wehner M, Wolf J, Kamranzad B, Webb A, Stopa J and Andutta F (2019) Robustness and uncertainties in global multivariate wind-wave climate projections. Nature Climate Change 9(9), 711-718.

Mulligan RP, Gomes ER, Miselis JL and McNinch JE (2019) Non-hydrostatic numerical modelling of nearshore wave transformation over shore-oblique sandbars. Estuarine, Coastal and Shelf Science 219, 151-160.

Nicholson A, Wooldridge A and Muller R (2008) Urban salinity—a journey from discovery to change implementation. Salinity, Water and Society - Global Issues, Local Action, 2nd International Salinity Forum, Adelaide, South Australia. 5 pages.

Nolan ITU (2001) Deutgam GSPA Groundwater Technical Report – Final. Southern Rural Water, 38.

O'Grady JG, Cohen RCZ, Prakash M, McInnes KL and Hoeke RK (2019a) Wave Overtopping in the City Scale Coupled Hydrodynamic/Hydraulic Numerical Inundation Model: C-FAST. ResearchGate. Australasian Coasts & Ports Conference, Hobart.

O'Grady J, Babanin A and McInnes K (2019b) Downscaling future longshore sediment transport in south eastern Australia. Journal of Marine Science and Engineering 7, 1–17. doi:10.3390/jmse7090289.

Passeri D, Hagen SC, Smar D, Alimohammadi N, Risner A and White R (2012) Sensitivity of an adcirc tide and storm surge model to manning's n. Estuarine and Coastal Modeling, 457–475, doi:10.1061/9780784412411.00027.

Pattiaratchi C, Hetzel Y and Janekovic I (2018) Developing better predictions for extreme water levels. Final data report. Melbourne: Bushfire and Natural Hazards CRC. 36 pages.

Pelleg D and Moore A (1999) Accelerating exact k-means algorithms with geometric reasoning. Proceedings of the fifth ACM SIGKDD international conference on Knowledge discovery and data mining, 277-281.

Prakash M, Cohen RCZ, Hilton J and Khan SH (2019) An evidence based approach to evaluating flood adaptation effectiveness including climate change considerations for coastal cities: City of Port Phillip, Victoria, Australia. Journal of Flood Risk Management 13(S1). https://doi.org/10.1111/jfr3.12556

Prakash M, Hilton J and Ramachandran L (2015) Integrating Hydrodynamic and Hydraulic Modeling for Evaluating Future Flood Mitigation in Urban Environments. In ISESS 2015, IFIP AICT Denzer R et al., (eds). 282–292.

Pullen T, Allsop NWH, Bruce T, Kortenhaus A, Schüttrumpf H and Van der Meer JW (2007) Wave overtopping of sea defences and related structures: Assessment manual.

Rahmstorf S (2007) A semi-empirical approach to projecting future sea-level rise. Science 315(5810), 368–370.

Ranasinghe R, Callaghan DP and Stive MJF (2011) Estimating coastal recession due to sea level rise: beyond the Bruun rule. Climatic Change 110, 561–574. doi:10.1007/s10584-011-0107-8.

Rapizo H, Babanin AV, Provis D and Rogers WE (2017) Current-induced dissipation in spectral wave models. Journal of Geophysical Research: Oceans 122(3), 2205-2225.

Roelvink D, Huisman B, Elghandour A, Ghonim M and Reyns J (2020) Efficient Modeling of Complex Sandy Coastal Evolution at Monthly to Century Time Scales. Frontiers in Marine Science 7(535).

Rosengren N (2017) Infrastructure Victoria Second Container Port Advice Port Phillip and Western Port. Nearshore and Shoreline Geomorphology and Processes. Environmental GeoSurveys Pty Ltd, AECOM.

Saha S, Moorthi S, Pan H-L, Wu X, Wang J, Nadiga S, Tripp P, Kistler R, Woollen J, Behringer D, Liu H, Stokes D, Grumbine R, Gayno G, Wang J, Hou Y-T, Chuang H-Y, Juang H-MH, Sela J, Iredell M, Treadon R, Kleist D, Van Delst P, Keyser D, Derber J, Ek M, Meng J, Wei H, Yang R, Lord S, Van Den Dool H, Kumar A, Wang W, Long C, Chelliah M, Xue Y, Huang B, Schemm J-K, Ebisuzaki W, Lin R, Xie P, Chen M, Zhou S, Higgins W, Zou C-Z, Liu Q, Chen Y, Han Y, Cucurull L, Reynolds RW, Rutledge G and Goldberg M (2010) The NCEP Climate Forecast System Reanalysis. Bulletin of the American Meteorological Society 91, 1015–1057.

Salzman S (2010) The deltaic aquifer of the Werribee irrigation district (WID). Deakin University, Warrnambool. 7 pages.

Schwartz M (1979) Case history of a coastal investigation at the Cape Cod National Seashore.

Shand T, Shand R, Reinen-Hamill R, Carley J and Cox R (2013) A review of shoreline response models to changes in sea level. Coasts and Ports 2013: 21st Australasian Coastal and Ocean Engineering conference and the 14th Australasian Port and Harbour conference, Sydney, Australia, 676–684.

Short AD, Hogan CL and McLeod KA (2006) Beaches of the Victorian Coast & Port Phillip Bay: A guide to their nature, characteristics, surf and safety. Sydney University Press.

Shugg AJ (1985) Evaluation of nitrate content of groundwater on the Nepean Peninsula. Department of Industry, Technology and Resources, Victoria. 20 pages.

Sibson R (1981) A brief description of natural neighbour interpolation, Interpreting multivariate data. John Wiley & Sons, New York, 21-36.

Sinclair MJ, and Quadros N (2010) Airborne lidar bathytmetric survey for climate change. FIG 2010: Facing the Challenges - Building the Capacity, 11–16. http://www.fig.net/pub/fig2010/papers/ts02i%5Cts02i_sinclair_4083.pdf.

SKM (1997) Werribee Delta Groundwater Investigation-Monitoring Review. Southern Rural Water, Armadale, Victoria. 84 pages.

SKM (1998) Monitoring Bore Assessment Program - Frankston GMA. WC00759:RO3JMFRK, Sinclair Knight Merz, Southern Rural Water. 29 pages.

SKM (2005) Werribee Irrigation District Groundwater Investigations. WC02880\1, Sinclair Knight Merz, Aramadale, Victoria. 117 pages.

SKM (2007) Nepean Peninsular Groundwater Risk Assessment - Groundwater Flow and Transport Model. WC03748, Sinclair Knights Merz, St Leanards, New South Wales. 61 pages.

SKM (2011) Groundwater SAFE: Victorian Statewide Watertable Mapping. Department of Sustainability and Environment, Melbourne. 100 pages.

SKM (2012a) Groundwater SAFE: A review of the Victorian Aquifer Framework. Department of Sustainability and Environment, Melbourne. 28 pages.

SKM (2012b) Groundwater SAFE: Victorian Statewide Watertable Salinity Mapping. Department of Sustainability and Environment, Melbourne. 18 pages.

Southern Rural Water (2003) Seawater Intrusion Mitigation Strategy Deutgam Water Supply Protection Area FINAL. F. Terry. Maffra, Southern Rural Water, 13.

Southern Rural Water (2011) South West Victoria Groundwater Atlas. Maffra, Victoria, Southern Rural Water, 54.

Southern Rural Water (2014) Port Phillip and Western Port Groundwater Atlas. Maffra, Victoria, Southern Rural Water, 68.

Southern Rural Water (2015) Deutgam Local Management Plan. Maffra, Southern Rural Water, 6.

Southern Rural Water (2016) West Port Phillip Bay Groundwater Catchment Statement, Southern Rural Water, 32.

Standards Australia (2002) Risk Management Guidelines. AS ISO 31000:2018 https://www.iso.org/standard/65694.html

Stockdon HF, Holman RA, Howd PA and Sallenger AH (2006). Empirical parameterization of setup, swash, and runup. Coastal Engineering 53, 573–588. doi:10.1016/j.coastaleng.2005.12.005.

Suh S-W and Kim H-J (2018) Simulation of Wave Overtopping and Inundation over a Dike Caused by Typhoon Chaba at Marine City, Busan, Korea. Journal of Coastal Research 85, 711–715. doi:10.2112/si85-143.1

SWAN Team (2016) SWAN scientific and technical documentation. Delft University of Technology.

Thatcher M and McGregor JL (2009). Using a Scale-Selective Filter for Dynamical Downscaling with the Conformal Cubic Atmospheric Model. Monthly Weather Review 137(6), 1742-1752.

Thom BG (2015) Coastal Compartments Project: Summary for Policy Makers. http://www.environment.gov.au/system/files/resources/4f288459-423f-43bb-8c20-87f91adc3e8e/files/coastal-compartments-project.pdf.

Thom BG, Eliot I, Eliot M, Harvey N, Rissik D, Sharples C, Short AD and Woodroffe CD (2018) National sediment compartment framework for Australian coastal management. Ocean and Coastal Management 154, 103-120.

Tolman HL (1991) A Third-Generation Model for Wind Waves on Slowly Varying, Unsteady, and Inhomogeneous Depths and Currents. Journal of Physical Oceanography 21(6), 782–797. 10.1175/1520-0485(1991)021<0782:ATGMFW>2.0.CO;2.

Van der Meer JW, Allsop NWH, Bruce T, De Rouck J, Kortenhaus A, Pullen T, Schüttrumpf H, Troch P and Zanuttigh B (2016) EurOtop Manual II: Wave Overtopping of Sea Defences and Related Structures. Retrieved from www.overtopping-manual.com

Van der Meer JW, Allsop NWH, Bruce T, De Rouck J, Kortenhaus A, Pullen T, Schüttrumpf H, Troch P and Zanuttigh B (2018) EurOtop, 2018. Manual on wave overtopping of sea defences and related structures. An overtopping manual largely based on European research, but for worldwide application. Available at: http://www.overtopping-manual.com.

VandenBerg AHM, Willman CE, Maher S, Simons BA, Cayley RA, Taylor DH, Morand VJ, Moore DH and Radojkovic A (2000) The Tasman Fold Belt System in Victoria. Geological Survey of Victoria, East Melbourne. 462 pages.

Vellinga P (2008) Exploring high end climate change scenarios for flood protection of the Netherlands. International Scientific Assessment, 136 pages.

Victorian Government (2017a) Level Crossing Removal Project-Edithvale and Bonbeach Environment Effects Statement, Chapter 5, Modelling the Water Environment. Melbourne, Level Crosssing Removal Project 2019, 64.

Victorian Government (2017b) Level Crossing Removal Project-Edithvale and Bonbeach Environment Effects Statement Chapter 6 Edithvale-Seaford Wetlands and GDE ecosystems. Melbourne, Level Crosssing Removal Project 2019, 36.

Victorian Government (2018). Edithvale and Bonbeach level crossing removal projects environment effects statement - Technical Report B, Ecological Impact Assessment: Wetlands and Groundwater Dependent Ecosystems. Melbourne, Victoria: 311.

Vitousek S, Fletcher CH and Barbee MM (2008) A practical approach to mapping extreme wave inundation: Consequences of sea-level rise and coastal erosion. Solutions to Coastal Disasters 2008, 85–96. doi:10.1007/978-1-4614-7495-1_23.

Walker SJ and Sherwood CR (1997) A Transport Model of Port Phillip Bay. CSIRO Division of Oceanography Castray Esplanade, Hobart, Tasmania. Technical Report 39 Port Phillip Bay Environmental Study CSIRO Environmental Projects Office.

Water Research Laboratory (2013) Future Coasts – Port Fairy Coastal Hazard Assessment.

Water Technology (2010) Estimation of Design Wave Heights and Water Levels Portsea Front Beach

Water Technology (2014a) Mordialloc Lifesaving Clubhouse Coastal Hazard Vulnerability Assessment.

Water Technology (2014b) Report 2: Inundation Hazard Gippsland Lakes/90 Mile Beach Local Coastal Hazard Assessment Project.

Water Technology (2014c) Western Port Local Coastal Hazard Assessment Report 1 (R01) – Summary Report.

Water Technology (2014d) Western Port Local Coastal Hazard Assessment Report 4 (R04) –Inundation Hazards.

Water Technology (2014e) Western Port Local Coastal Hazard Assessment Report 5 (R05) – Erosion Hazards

Water Technology (2017a) Final Report Edithvale SLC Coastal Hazard Vulnerability Assessment.

Water Technology (2017b) Mount Martha Coastal Process Investigation and Future Management Recommendations, Final Report.

Water Technology (2017c) Port Phillip Flood Modelling, Report for Melbourne Water.

Water Technology (2018) Black Rock Seawall, Report for the Department of Environment, Land, Water and Planning.

Williams W (1992) Quaternary alluvial and swamp deposits, in Engineering Geology of Melbourne, [Peck N (ed.)], Olds, & Seddon, A A Balkema, Rotterdam. 271-280.

Wiltshire EHS, Harrison A, Bolger P, Foley G and Pratt M (2009) Hydrogeological Mapping of Southern Victoria, Southern Rural Water.

Wu W, McInnes KL, O'Grady J, Hoeke RK, Leonard M and Westra S (2018) Mapping dependence between extreme rainfall and storm surge. Journal of Geophysical Research: Oceans. doi:10.1002/2017JC013472.

Zheng F, Westra S and Sisson SA (2013) The dependence between extreme rainfall and storm surge in the coastal zone. Journal of Hydrology 505, 172-187.

Zhou L, Williams MA and Peterson JA (1994) Late Quaternary aeolianites, palaeosols and depositional environments on the Nepean Peninsula, Victoria, Australia. Quaternary Science Reviews 13(3), 225-239.

Zijlema M, Stelling G and Smit P (2011) SWASH: An operational public domain code for simulating wave fields and rapidly varied flows in coastal waters. Coastal Engineering 58, 992–1012. doi:10.1016/j.coastaleng.2011.05.015.

Appendix A. Geology of Port Phillip Bay

Figure A1 and summarises the main characteristics of the geological and landform regions surrounding Port Phillip. Table A1 and Figure A2 provides geological and landform regions of Port Phillip as a supplement to discussion in Section 2.1.1.

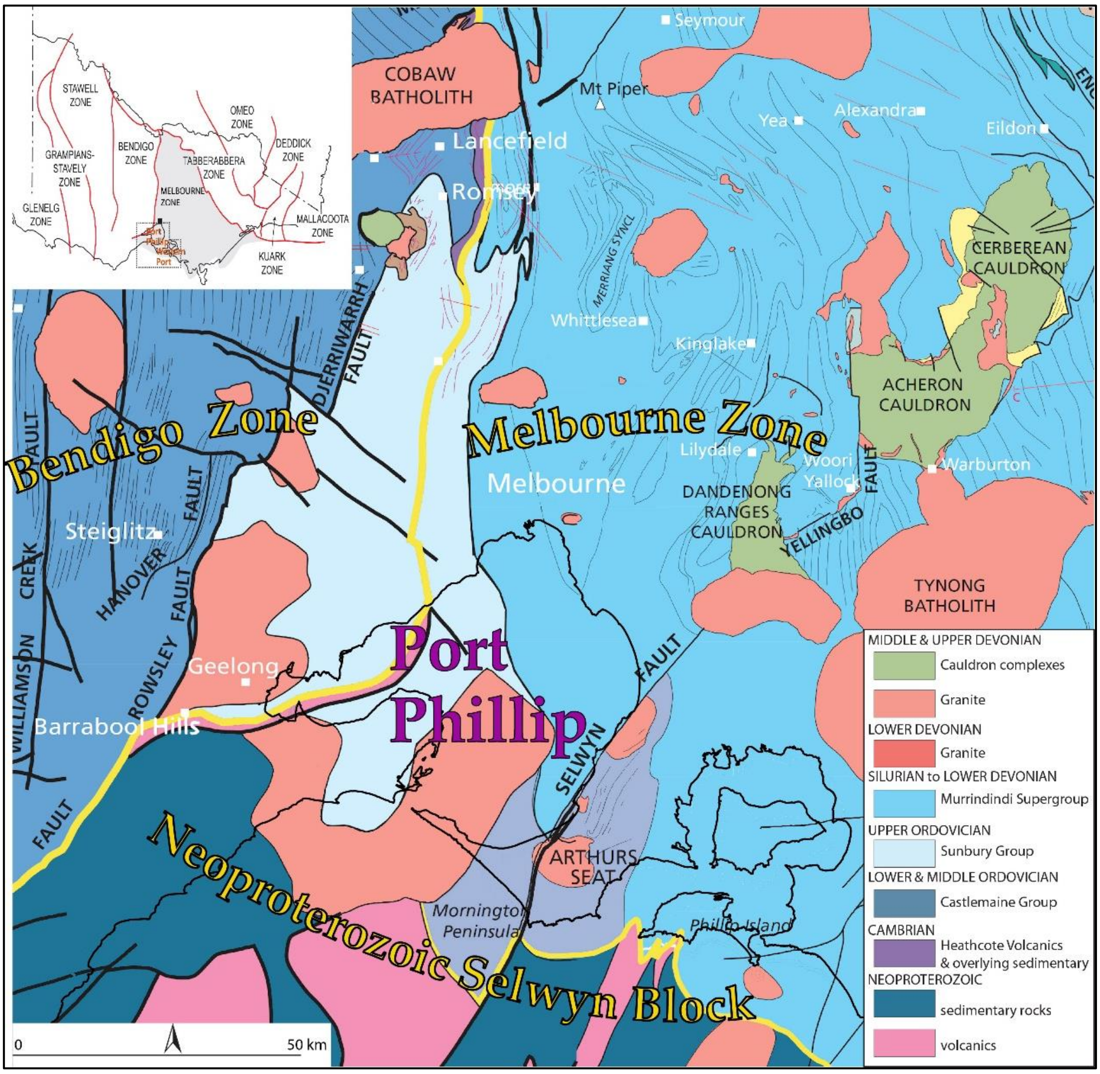

Figure A1: Port Phillip in relation to the Selwyn Block, Melbourne and Bendigo Zone bedrock geology (after VandenBerg et al., 2000).

Table A1: Geological and landform regions.

Number	Geomorphology	Geology
1	Downfaulted: Swan Bay, Swan Bay, eastern Bellarine Peninsula lowland.	Neogene. Sandringham Sandstone, Bridgewater Formation, Quaternary sediments.
2	Uplifted: Bellarine Peninsula plateau and ridges. Coastal cliffs, bluffs and terraces.	Mesozoic, Palaeogene, Neogene. Sediments overlain by Older Volcanics and Brighton Group sediments.
3	Downfaulted: Corio Bay, Lower Barwon-Connewarre wetlands.	Quaternary. Coastal and lagoon deposits, shell beds, minor limestone.
4	Uplifted: Brisbane Ranges, Pawan Valley, Lerderderg Ranges. Plateau and dissected ridge and valley terrain.	Ordovician. Metasedimentary sedimentary rocks. Cainozoic. Sediments and volcanics
5	Residual: Granite ridges surrounded by colluvium.	Devonian. You Yangs Granite batholith
6	Depositional: Werribee River alluvial and colluvial fans and floodplain.	Cainozoic. Sand, silt, mud, minor gravel
7	Volcanic Effusive: Werribee volcanic plains and hills.	Neogene. Newer Volcanics plains and valley basalt flows and eruption points.
8	Depositional: Point Cook sand ridges overlying basalt.	Cainozoic. Sand, silt, shell beds.
9	Depositional: lower Yarra floodplain and delta.	Cainozoic. Sand, silt, clay, lagoonal and swamp deposits, sand ridges.
10	Structural: Hills and valleys	Silurian and Devonian. Folded sedimentary rocks.
11	Depositional, uplifted: coastal plain and low parallel sand ridges.	Neogene: Brighton Group sedimentary rocks and Quaternary sand ridges.
12	Residual: Dandenong Ranges hills and ridges.	Devonian. Igneous complex - granites and associated volcanics.
13	Downfaulted: Carrum depression and associated wetlands, sand ridges.	Neogene. Terrestrial and coastal wetland deposits.
14	Uplifted: Mornington Peninsula hills and shallow valleys	Palaeozoic to Neogene. Sedimentary rocks, Older Volcanics, Sandringham Sandstone.
15	Downfaulted, depositional: Cardinia, Koo-wee-rup and Tobin Yaloak drained wetlands.	Late Quaternary swamp and coastal deposits.
16	Depositional, downfaulted: Nepean Peninsula low sand ridges, beaches, coastal cliffs and shore platforms.	Quaternary Bridgewater Formation and unconsolidated dune sands.
17	Depositional: Great Sands, submarine ridges and channels.	Quaternary sediments.
18	Downfaulted, depositional: Port Phillip embayment.	Quaternary sediments.

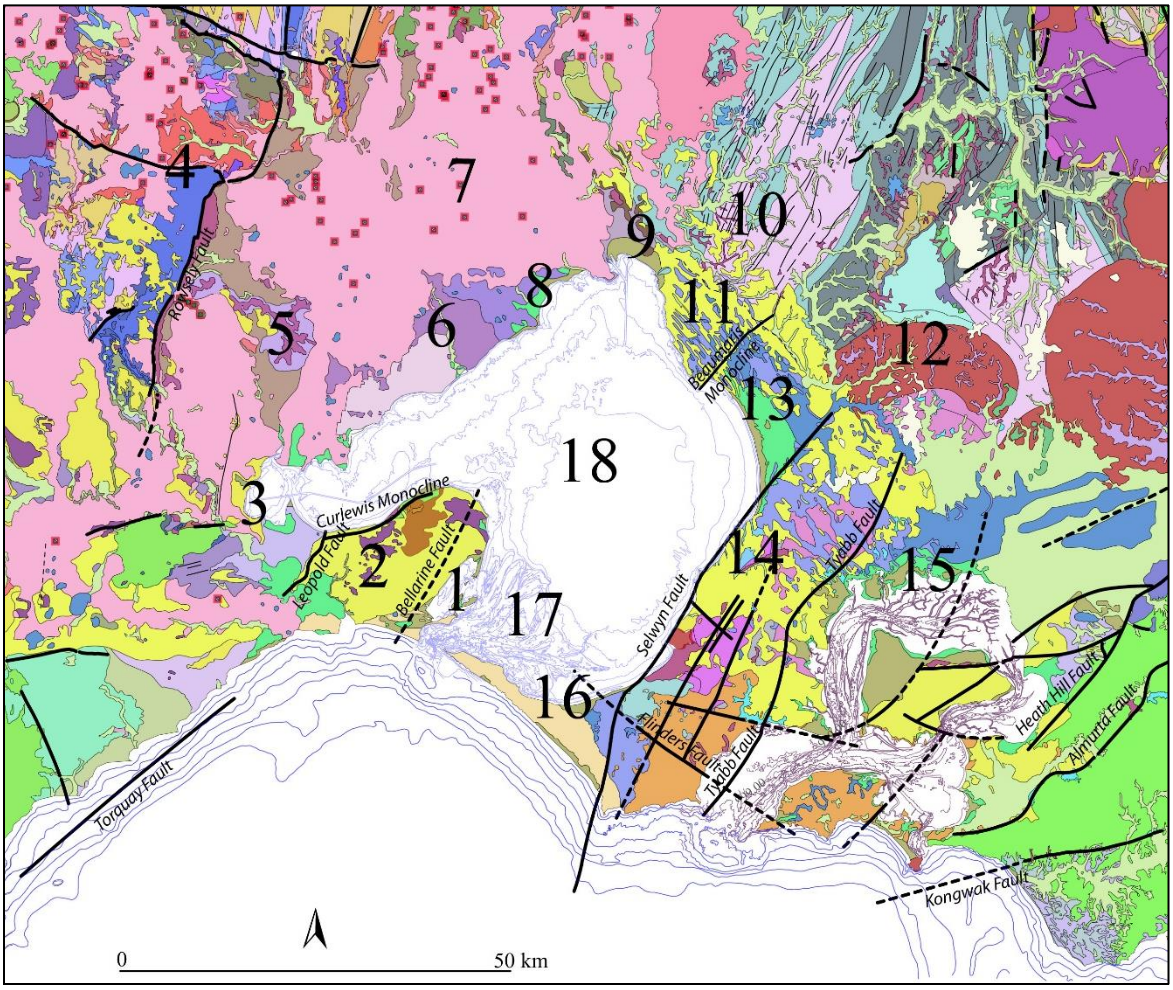

Figure A2: Geological and landform regions of Port Phillip and Western Port and submarine contours. For legend see Table A1 (Geology from Seamless Geology, Geoscience Victoria, 2011).

Appendix B. Additional Inputs for C-FAST

Rainfall data used in the C-FAST model are based on intensity-frequency-duration (IFD) data from the Bureau of Meteorology website (http://www.bom.gov.au/water/designRainfalls/revised-ifd/). Tables for the locations of the four high resolution C-FAST grids are reproduced in Figure B1 based on data for the City of Geelong, Wyndham City Council, Port Melbourne, and Kingston City Council.

Location

Label: Geelong

Latitude: -38.1481 [Nearest grid cell: 38.1375 (S)]

Longitude: 144.3541 [Nearest grid cell: 144.3625 (E)]

IFD Design Rainfall Intensity (mm/h)

Issued: 04 Febru

Rainfall intensity for Durations, Exceedance per Year (EY), and Annual Exceedance Probabilities

FAQ for New ARR probability terminology

Table | Chart

Unit:

	Annual Exceedance Probability (AEP)					
Duration	**63.2%**	**50%#**	**20%***	**10%**	**5%**	**2%**
1 min	65.9	76.5	112	137	164	201
2 min	54.0	62.6	91.0	111	131	156
3 min	49.0	56.7	82.2	100	118	142
4 min	45.2	52.3	75.8	92.6	110	133
5 min	42.1	48.7	70.6	86.4	103	125
10 min	31.4	36.5	53.2	65.6	78.4	96.8
15 min	25.4	29.5	43.2	53.3	63.9	79.1
20 min	21.5	24.9	36.6	45.2	54.2	67.1
25 min	18.7	21.8	32.0	39.5	47.2	58.4
30 min	16.7	19.4	28.5	35.1	42.0	51.8
45 min	12.9	14.9	21.8	26.8	31.9	39.1
1 hour	10.7	12.4	17.9	21.9	26.1	31.8
1.5 hour	8.25	9.49	13.6	16.5	19.5	23.6
2 hour	6.91	7.90	11.2	13.5	15.9	19.2
3 hour	5.42	6.14	8.52	10.2	12.0	14.4
4.5 hour	4.29	4.82	6.57	7.82	9.11	10.9
6 hour	3.64	4.07	5.49	6.51	7.56	9.06
9 hour	2.89	3.22	4.30	5.07	5.87	7.05
12 hour	2.45	2.72	3.62	4.27	4.94	5.94
18 hour	1.92	2.13	2.85	3.36	3.89	4.68
24 hour	1.59	1.78	2.39	2.83	3.28	3.95
30 hour	1.36	1.53	2.08	2.47	2.87	3.46
36 hour	1.20	1.35	1.85	2.20	2.56	3.09
48 hour	0.964	1.09	1.52	1.82	2.13	2.56
72 hour	0.696	0.798	1.13	1.36	1.60	1.91
96 hour	0.548	0.629	0.893	1.08	1.27	1.52
120 hour	0.455	0.521	0.735	0.890	1.05	1.25
144 hour	0.392	0.446	0.621	0.750	0.884	1.06
168 hour	0.348	0.392	0.535	0.643	0.758	0.908

Location

Label: Werribee South

Latitude: -37.9355 [Nearest grid cell: 37.9375 (S)]

Longitude: 144.665 [Nearest grid cell: 144.6625 (E)]

IFD Design Rainfall Intensity (mm/h)

Issued: 04 Febru

Rainfall intensity for Durations, Exceedance per Year (EY), and Annual Exceedance Probabilities

FAQ for New ARR probability terminology

Table | Chart

Unit:

	Annual Exceedance Probability (AEP)					
Duration	**63.2%**	**50%#**	**20%***	**10%**	**5%**	**2%**
1 min	80.1	91.7	131	160	191	236
2 min	68.3	77.9	110	134	158	192
3 min	61.4	70.0	99.1	121	143	174
4 min	56.0	63.9	90.7	110	131	160
5 min	51.7	59.1	83.9	102	122	149
10 min	38.2	43.7	62.6	76.7	91.6	113
15 min	30.9	35.4	50.8	62.3	74.6	92.3
20 min	26.2	30.1	43.2	53.0	63.4	78.5
25 min	23.0	26.3	37.8	46.4	55.5	68.6
30 min	20.6	23.6	33.8	41.4	49.5	61.1
45 min	16.0	18.3	26.0	31.9	38.0	46.7
1 hour	13.3	15.2	21.5	26.3	31.2	38.3
1.5 hour	10.2	11.6	16.4	19.9	23.6	28.9
2 hour	8.52	9.64	13.5	16.3	19.3	23.6
3 hour	6.56	7.40	10.2	12.3	14.5	17.7
4.5 hour	5.05	5.68	7.78	9.35	11.0	13.4
6 hour	4.19	4.70	6.42	7.70	9.06	11.0
9 hour	3.20	3.59	4.90	5.88	6.92	8.43
12 hour	2.63	2.95	4.04	4.86	5.73	6.97
18 hour	1.97	2.22	3.07	3.71	4.39	5.33
24 hour	1.59	1.81	2.52	3.05	3.62	4.39
30 hour	1.34	1.53	2.15	2.62	3.11	3.76
36 hour	1.16	1.33	1.89	2.30	2.74	3.31
48 hour	0.922	1.06	1.52	1.87	2.23	2.68
72 hour	0.657	0.757	1.10	1.36	1.63	1.95
96 hour	0.515	0.593	0.863	1.07	1.29	1.53
120 hour	0.427	0.490	0.708	0.874	1.05	1.25
144 hour	0.368	0.420	0.598	0.735	0.889	1.05
168 hour	0.326	0.369	0.516	0.631	0.764	0.903

Location

Label: Port Melbourne
Latitude: -37.8343 [Nearest grid cell: 37.8375 (S)]
Longitude: 144.9058 [Nearest grid cell: 144.9125 (E)]

IFD Design Rainfall Intensity (mm/h)

Issued: 04 February 202

Rainfall intensity for Durations, Exceedance per Year (EY), and Annual Exceedance Probabilities (AEP).
FAQ for New ARR probability terminology

Table | Chart   Unit: mm/h

	Annual Exceedance Probability (AEP)						
Duration	63.2%	50%#	20%*	10%	5%	2%	1%
1 min	92.4	104	144	174	206	253	293
2 min	79.1	88.4	120	144	170	207	237
3 min	70.9	79.3	108	130	153	186	214
4 min	64.6	72.5	99.2	119	141	172	198
5 min	59.6	67.0	92.1	111	131	160	185
10 min	44.1	49.8	69.2	83.9	99.4	122	141
15 min	35.8	40.5	56.4	68.4	81.1	99.8	116
20 min	30.5	34.4	48.0	58.2	69.1	85.0	98.5
25 min	26.8	30.2	42.0	50.9	60.5	74.4	86.2
30 min	24.0	27.0	37.5	45.5	54.0	66.4	76.9
45 min	18.6	20.9	28.9	34.9	41.4	50.8	58.8
1 hour	15.5	17.3	23.8	28.7	34.0	41.7	48.2
1.5 hour	11.9	13.2	18.0	21.7	25.6	31.4	36.2
2 hour	9.80	10.9	14.8	17.8	20.9	25.6	29.5
3 hour	7.48	8.32	11.2	13.4	15.7	19.2	22.1
4.5 hour	5.70	6.34	8.50	10.1	11.9	14.5	16.6
6 hour	4.70	5.23	7.02	8.37	9.79	11.9	13.7
9 hour	3.58	3.99	5.37	6.40	7.48	9.06	10.4
12 hour	2.94	3.29	4.46	5.31	6.20	7.50	8.58
18 hour	2.22	2.50	3.42	4.08	4.76	5.75	6.56
24 hour	1.81	2.05	2.83	3.38	3.95	4.76	5.41
30 hour	1.54	1.75	2.43	2.92	3.40	4.10	4.65
36 hour	1.34	1.53	2.15	2.58	3.01	3.61	4.09
48 hour	1.08	1.24	1.75	2.10	2.46	2.95	3.33
72 hour	0.783	0.901	1.28	1.55	1.82	2.17	2.43
96 hour	0.618	0.710	1.01	1.22	1.44	1.71	1.91
120 hour	0.511	0.585	0.828	1.00	1.18	1.40	1.57
144 hour	0.437	0.497	0.698	0.846	0.997	1.18	1.32
168 hour	0.382	0.431	0.600	0.727	0.857	1.01	1.13

Location

Label: Carrum
Latitude: -38.0771 [Nearest grid cell: 38.0875 (S)]
Longitude: 145.1192 [Nearest grid cell: 145.1125 (E)]

IFD Design Rainfall Intensity (mm/h)

Issued: 04 February 202

Rainfall intensity for Durations, Exceedance per Year (EY), and Annual Exceedance Probabilities (AEP).
FAQ for New ARR probability terminology

Table | Chart   Unit: mm/h

	Annual Exceedance Probability (AEP)						
Duration	63.2%	50%#	20%*	10%	5%	2%	1%
1 min	95.0	106	144	172	202	244	280
2 min	81.9	90.6	120	143	164	191	213
3 min	73.2	81.2	108	128	148	174	195
4 min	66.6	74.0	99.2	118	137	163	183
5 min	61.3	68.3	92.0	110	128	153	174
10 min	45.3	50.7	69.0	82.6	97.2	119	137
15 min	36.8	41.2	56.1	67.3	79.4	97.2	112
20 min	31.3	35.1	47.8	57.3	67.5	82.6	95.3
25 min	27.5	30.8	41.8	50.1	59.0	72.0	82.9
30 min	24.7	27.6	37.4	44.7	52.6	64.0	73.5
45 min	19.2	21.4	28.8	34.3	40.1	48.4	55.3
1 hour	16.0	17.8	23.7	28.2	32.8	39.3	44.7
1.5 hour	12.3	13.6	18.0	21.2	24.6	29.2	32.9
2 hour	10.1	11.2	14.7	17.3	20.0	23.6	26.5
3 hour	7.71	8.51	11.1	13.0	14.9	17.6	19.7
4.5 hour	5.85	6.45	8.41	9.79	11.2	13.2	14.7
6 hour	4.79	5.30	6.91	8.03	9.18	10.8	12.1
9 hour	3.61	4.00	5.25	6.10	6.99	8.26	9.28
12 hour	2.94	3.27	4.32	5.04	5.78	6.86	7.72
18 hour	2.20	2.45	3.27	3.85	4.43	5.29	5.98
24 hour	1.78	1.99	2.68	3.17	3.67	4.40	4.98
30 hour	1.50	1.69	2.29	2.73	3.16	3.80	4.31
36 hour	1.31	1.47	2.01	2.40	2.79	3.36	3.81
48 hour	1.05	1.18	1.63	1.95	2.28	2.74	3.11
72 hour	0.763	0.860	1.19	1.43	1.68	2.02	2.28
96 hour	0.608	0.683	0.938	1.13	1.33	1.59	1.79
120 hour	0.510	0.571	0.775	0.927	1.09	1.30	1.46
144 hour	0.442	0.492	0.659	0.780	0.922	1.10	1.23
168 hour	0.393	0.435	0.572	0.669	0.792	0.944	1.05

Figure B1: IFD data for (a) City of Geelong, (b) Wyndham City Council, (c) Port Melbourne, and (d) Kingston City Council.

C-FAST outputs and post-processing

The following data is recorded during each simulation run of C-FAST

- Instantaneous flood height rasters with data at 30-minute intervals
- Maps in raster format of
    - Maximum water height (m)
    - Maximum water speed (m/s)
    - Maximum hazard – water depth × speed (m^2/s)
    - Time above particular levels- 0.5, 1.0, 1.5, 2.0 and 2.5 m AHD
- Point gauge data
    - Time series of water levels at grid point locations through each region recorded in minute intervals

Further Postprocessing of the results is carried out to produce:

- Combined probabilistic flood maps which show the increase in flood extent with more extreme scenarios (Figure 5.9).

- Whole-of-bay inundation hazard assessment maps for each scenario by compositing together the finer results from regions A-D on top of results from coarser regions W, E and S.

Area of inundation, with line plots and contour maps summarising how these numbers change across the scenarios considered.

Computational Resources used by C-FAST

The final runs for this project were run on the CSIRO Bracewell cluster with 144 nodes, each of node having

- CPUs - Dual Intel Xeon 14-core E5-2690 v4
- GPUs - 4 × NVidia Tesla P100 (SXM2)

Each C-FAST simulation was run on a single CPU and a single GPU combination. The overall computational resources required for the final simulation runs are shown in Table B1. The significant compute and data requirements were supported by the CSIRO High Performance Computing infrastructure.

Table B1: Computational resources required for C-FAST simulations.

Resolution	Region	Grid size (approx)	Approx walltime (days)	Approx data storage per case (GB)	Cases	Total GPU days	Total data storage (TB)
5 m	A	2098 x 2830	0.5	2	120	60	0.240
5 m	B	4754 x 3706	3	2	120	360	0.240
5 m	C	4396 x 2454	3	2	120	360	0.240
5 m	D	2467 x 3643	1.0	2	120	120	0.240
25 m	Western	1540 x 1160	0.25	2	120	30	0.240
25 m	Eastern	644 x 2028	0.25	2	120	30	0.240
25 m	Southern	1520 x 940	0.25	2	120	30	0.240
						Total = 990	Total = 1.68

Example Overtopping Outputs

An example of the overtopping produced in the C-FAST EurOtop formulation is provided below. The time series of wave overtopping for each coastal protection structure for the baseline and 0.8 m SLR sensitivity simulations for Hobsons Bay City Council to City of Port Phillip region C domain is shown in Figures B2 and B3. The water levels (SWL), wave heights (Hs), wave periods (Tz and resulting overtopping discharge (Q) for all structures (Figure B4) are provided in Tables B2 and B3. Note, where the SWL is greater than the seawall crest, overtopping figures are not used, since C-FAST directly models the flow.

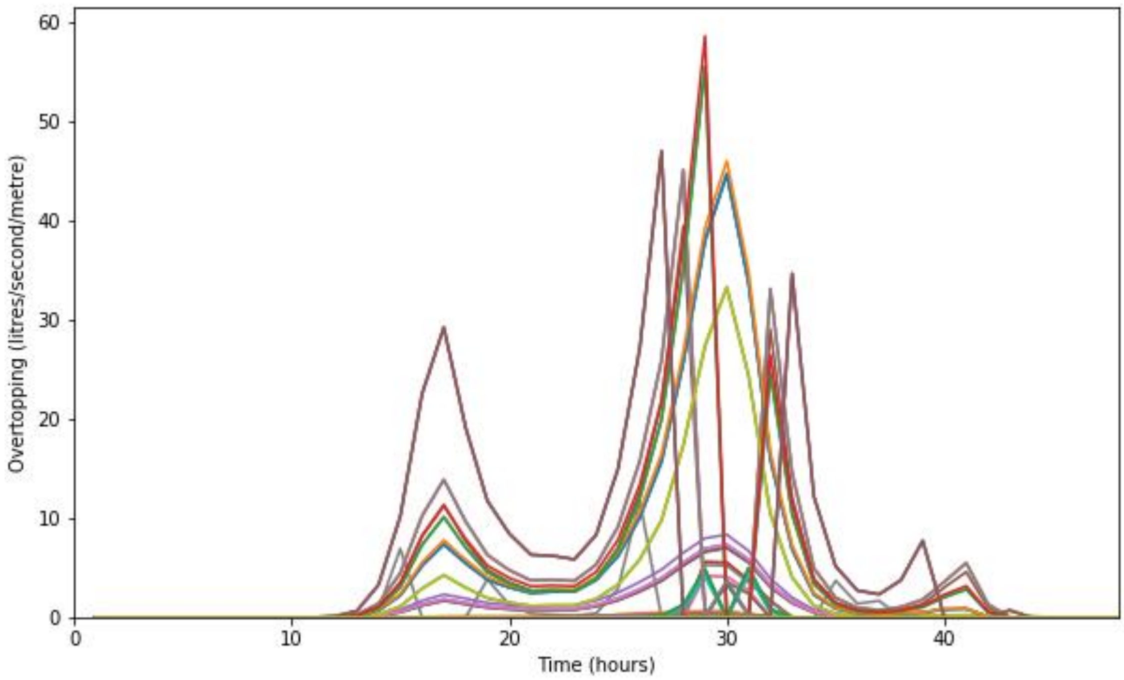

Figure B2: Time series of baseline SLR 1% AEP overtopping discharge for each structure in the Hobsons Bay City Council to City of Port Phillip region C domain.

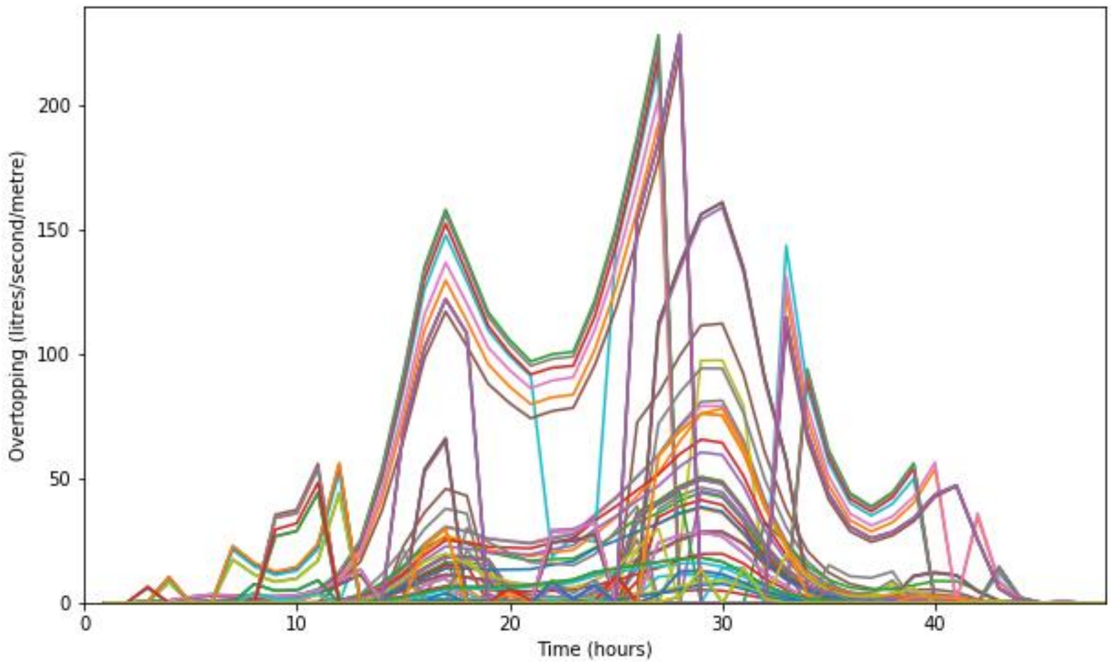

Figure B3: Time series of 0.8m SLR 1% AEP overtopping discharge for each structure in the Hobsons Bay City Council to City of Port Phillip region C domain.

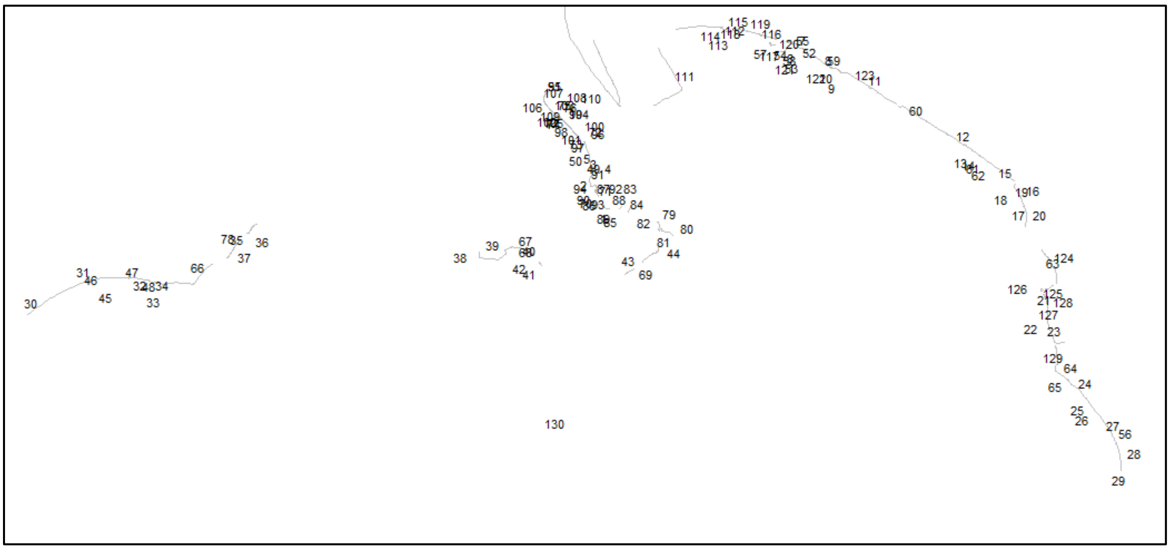

Figure B4 Structure ID for overtopping discharge for each structure in the Hobsons Bay City Council to City of Port Phillip region C domain.

Table B2: Coastal protection structure parameters for the overtopping discharge (Q) for the SCHISM input parameters (SWL, Hs, Tz) for baseline and 0.8m SLR simulations. Structure index shown in Figure B4.

Structure Parameters				**Baseline SWL = 1.1m, Tz = 4s**		**SLR = 0.8, SWL = 1.94m, Tz = 4.12s**	
Index	**Crest Height**	**Toe Height**	**Face Slope**	**Hs**	**Max Q**	**Hs**	**Max Q**
	[m] AHD	[m] AHD	deg	[m]	[L/s/m]	[m]	[L/s/m]
11	2.63	1.33	90	0.79	0.00	1.38	38.03
12	2.55	1.30	90	0.78	0.00	1.36	44.30
27	2.24	1.44	90	0.79	0.00	1.37	94.36
30	2.02	1.52	90	0.76	0.00	1.35	161.06
47	1.71	0.91	90	0.76	5.29	1.35	225.71
66	2.73	1.53	90	0.77	0.00	1.36	28.55
67	1.57	0.67	75	0.77	0.33	1.34	38.93

Table B3 ALL: Coastal protection structure parameters for the overtopping discharge (Q) for the SCHISM input parameters (SWL, Hs, Tz) for baseline and 0.8m SLR simulations. Structure index shown in Figure B4.

Structure Parameters				**Baseline SWL = 1.1m, Tz = 4s**		**SLR = 0.8, SWL = 1.94m, Tz = 4.12s**	
Index	**Crest Height**	**Toe Height**	**Face Slope**	**Hs**	**Max Q**	**Hs**	**Max Q**
	[m] AHD	[m] AHD	deg	[m]	[L/s/m]	[m]	[L/s/m]
0	1.26	0.16	85	0.46	7.35	0.73	32.44
1	1.42	-0.08	30	0.45	0.00	1.21	7.39
2	1.42	0.32	45	0.64	0.00	1.15	12.63
3	0.94	-0.06	30	0.67	0.02	1.00	0.00
4	1.24	0.34	20	0.58	0.00	1.01	5.94
5	3.06	1.56	90	0.00	0.00	0.00	0.00
6	3.06	1.56	90	0.78	0.00	1.37	13.13
7	2.53	1.55	90	0.78	0.00	1.36	46.40
8	2.72	2.06	90	0.78	0.00	1.36	0.00
9	3.12	1.42	90	0.79	0.00	1.37	11.33

10	2.95	0.59	90	0.78	0.03	1.39	18.23
11	2.63	1.33	90	0.79	0.00	1.38	38.03
12	2.55	1.30	90	0.78	0.00	1.36	44.30
13	2.76	0.88	80	0.79	0.00	1.40	5.27
14	2.55	1.75	90	0.79	0.00	1.37	45.08
15	2.18	1.38	90	0.79	0.00	1.38	112.34
16	2.26	0.96	90	0.79	0.61	1.30	79.19
17	2.23	0.93	90	0.79	0.70	1.27	81.41
18	2.23	1.73	90	0.79	0.00	1.37	97.56
19	2.36	1.86	90	0.79	0.00	1.37	14.13
20	1.11	-0.59	20	0.75	3.33	1.30	0.05
21	2.12	0.42	35	0.79	0.00	1.41	0.17
22	1.91	0.21	40	0.80	0.00	1.34	13.34
23	2.60	1.45	90	0.80	0.00	1.39	41.39
24	2.13	0.98	80	0.79	0.07	1.37	28.37
25	2.13	1.33	80	0.79	0.00	1.37	28.37
26	2.13	1.33	80	0.80	0.00	1.37	28.37
27	2.24	1.44	90	0.79	0.00	1.37	94.36
28	1.76	0.06	25	0.79	0.00	1.33	2.36
29	1.73	1.13	90	0.76	0.00	1.35	215.91
30	2.02	1.52	90	0.76	0.00	1.35	161.06
31	1.76	0.96	90	0.76	4.19	1.32	192.94
32	1.71	0.91	90	0.77	5.60	1.36	228.39
33	1.71	0.91	90	0.77	5.60	1.33	220.39
34	1.52	-0.38	40	0.63	0.00	1.14	6.23
35	1.52	-0.38	40	0.63	0.00	0.96	4.67
36	1.52	-0.38	40	0.63	0.00	0.96	4.67
37	1.57	0.67	60	0.77	0.00	1.40	25.53
38	1.57	-0.33	60	0.76	0.00	1.26	21.26
39	2.64	1.94	85	0.77	0.00	1.35	0.00
40	2.73	1.53	90	0.77	0.00	1.36	28.55
41	1.58	-0.32	25	0.77	0.00	1.28	5.61
42	1.83	1.03	80	0.78	0.43	1.37	44.48
43	2.25	0.55	80	0.77	0.02	1.32	19.78
44	2.02	1.52	90	0.76	0.00	1.34	159.03
45	2.02	1.52	90	0.76	0.00	1.35	161.06
46	1.76	0.96	90	0.76	4.19	1.36	203.11
47	1.71	0.91	90	0.76	5.29	1.35	225.71
48	0.94	-0.06	30	0.45	0.00	0.98	0.00
49	0.94	-0.06	30	0.58	0.01	1.09	0.00
50	1.26	-0.44	40	0.47	0.00	0.87	6.53
51	2.50	1.30	90	0.78	0.00	1.37	50.66
52	2.50	1.30	90	0.78	0.00	1.37	50.66
53	2.50	1.30	90	0.78	0.00	1.36	49.57
54	2.50	1.30	90	0.78	0.00	1.36	49.57
55	2.13	1.33	80	0.80	0.00	1.38	28.77
56	2.42	0.32	35	0.67	0.00	1.15	0.00
57	0.71	-0.79	65	0.72	11.82	1.28	0.00
58	2.32	1.52	90	0.78	0.00	1.36	76.26
59	2.99	0.99	90	0.78	0.03	1.38	16.11

60	2.60	0.50	90	0.79	0.15	1.36	38.62
61	2.16	0.36	90	0.75	0.67	1.14	78.22
62	1.81	1.41	90	0.79	0.00	1.37	228.53
63	2.38	0.08	90	0.79	0.37	1.36	65.71
64	2.38	0.08	90	0.79	0.37	1.32	60.60
65	1.80	1.00	90	0.77	3.60	1.33	221.26
66	2.73	1.53	90	0.77	0.00	1.36	28.55
67	1.57	0.67	75	0.77	0.33	1.34	38.93
68	1.74	0.04	75	0.70	0.02	1.25	29.85
69	1.08	-0.52	70	0.45	4.50	0.85	3.60
70	1.26	0.16	85	0.45	7.03	0.66	27.78
71	1.03	0.13	90	0.60	45.15	0.97	54.19
72	1.17	0.07	90	0.55	33.33	0.84	44.25
73	1.16	0.26	90	0.63	44.76	0.94	55.34
74	1.06	0.16	90	0.58	55.61	0.97	44.30
75	0.90	0.10	90	0.58	47.06	1.08	0.00
76	0.93	0.13	20	0.61	0.00	0.96	0.00
77	1.52	-0.38	40	0.64	0.00	0.99	4.92
78	2.25	0.55	80	0.49	0.00	0.96	8.89
79	1.42	-0.08	30	0.30	0.00	0.47	0.32
80	2.25	0.55	80	0.48	0.00	0.91	7.66
81	1.42	-0.08	30	0.30	0.00	0.54	0.59
82	1.42	-0.08	30	0.48	0.00	0.64	1.14
83	1.42	-0.08	30	0.46	0.00	0.51	0.47
84	1.26	0.16	85	0.49	8.36	0.74	33.13
85	1.26	0.16	85	0.45	7.03	0.66	27.78
86	1.26	0.16	85	0.46	7.35	0.73	32.44
87	1.08	-0.52	70	0.44	4.34	0.91	4.02
88	1.08	-0.52	70	0.45	4.50	0.85	3.60
89	1.08	-0.52	70	0.44	4.34	0.91	4.02
90	1.08	-0.52	70	0.48	4.99	1.36	9.07
91	1.42	-0.08	30	0.48	0.00	1.36	9.73
92	1.08	-0.52	70	0.48	4.99	1.36	9.07
93	1.42	0.32	45	0.54	0.00	1.06	10.73
94	1.26	-0.44	40	0.47	0.00	0.87	6.53
95	1.03	0.13	90	0.56	39.51	0.99	55.94
96	1.03	0.13	90	0.60	45.15	0.97	54.19
97	1.03	0.13	90	0.60	45.15	0.97	54.19
98	1.17	0.07	90	0.55	33.33	0.84	44.25
99	1.16	0.26	90	0.63	44.76	0.91	52.50
100	1.16	0.26	90	0.63	44.76	0.94	55.34
101	1.16	0.26	90	0.64	46.07	0.95	56.30
102	1.06	0.16	90	0.58	55.61	0.97	44.30
103	1.06	0.16	90	0.60	58.67	1.02	48.39
104	0.90	0.10	90	0.58	47.06	1.08	0.00
105	0.90	0.10	90	0.58	47.06	1.08	0.00
106	0.93	0.13	20	0.61	0.00	0.96	0.00
107	1.26	-0.44	40	0.51	0.00	1.03	9.32
108	0.93	0.13	20	0.57	0.00	0.99	0.00
109	1.26	-0.44	40	0.39	0.00	0.45	1.31

110	1.24	0.34	20	0.68	0.00	1.22	8.52
111	2.42	0.32	35	0.70	0.00	1.24	0.00
112	2.42	0.32	35	0.68	0.00	1.24	0.00
113	2.42	0.32	35	0.64	0.00	1.01	0.00
114	2.42	0.32	35	0.58	0.00	0.66	0.00
115	2.42	0.32	35	0.59	0.00	0.77	0.00
116	2.42	0.32	35	0.59	0.00	0.66	0.00
117	2.42	0.32	35	0.59	0.00	0.77	0.00
118	2.42	0.32	35	0.67	0.00	1.15	0.00
119	2.42	0.32	35	0.59	0.00	0.74	0.00
120	3.06	1.56	90	0.78	0.00	1.36	12.72
121	2.32	1.52	90	0.78	0.00	1.36	76.26
122	2.95	0.59	90	0.79	0.04	1.39	18.23
123	1.81	1.41	90	0.79	0.00	1.37	228.53
124	1.81	1.41	90	0.79	0.00	1.37	228.53
125	1.11	-0.59	20	0.79	3.65	1.31	0.06
126	2.12	0.42	35	0.79	0.00	1.41	0.17
127	1.11	-0.59	20	0.80	3.73	1.32	0.06
128	1.91	0.21	40	0.80	0.00	1.38	13.94

Appendix C. Storm Duration and Design Storms

Design storm time series have been studied for the east coast of Australia (Carley and Cox, 2003; Harrison et al., 2019). Typically, a triangular time series of wave height is used with a Total Water Level (TWL) time series including tide and non-tidal residual extremes (e.g. Cardno, 2018). The width of the triangular time series is defined by a storm duration based on known event and the vertical height is scaled by AEP wave height. A previous PPB study using the SBEACH model (Cardno, 2018) used a storm duration of 72 hr which is significantly less than guidance for the NSW coast (Carley and Cox, 2003) but on the order of the two to three day storm tracks which pass over PPB.

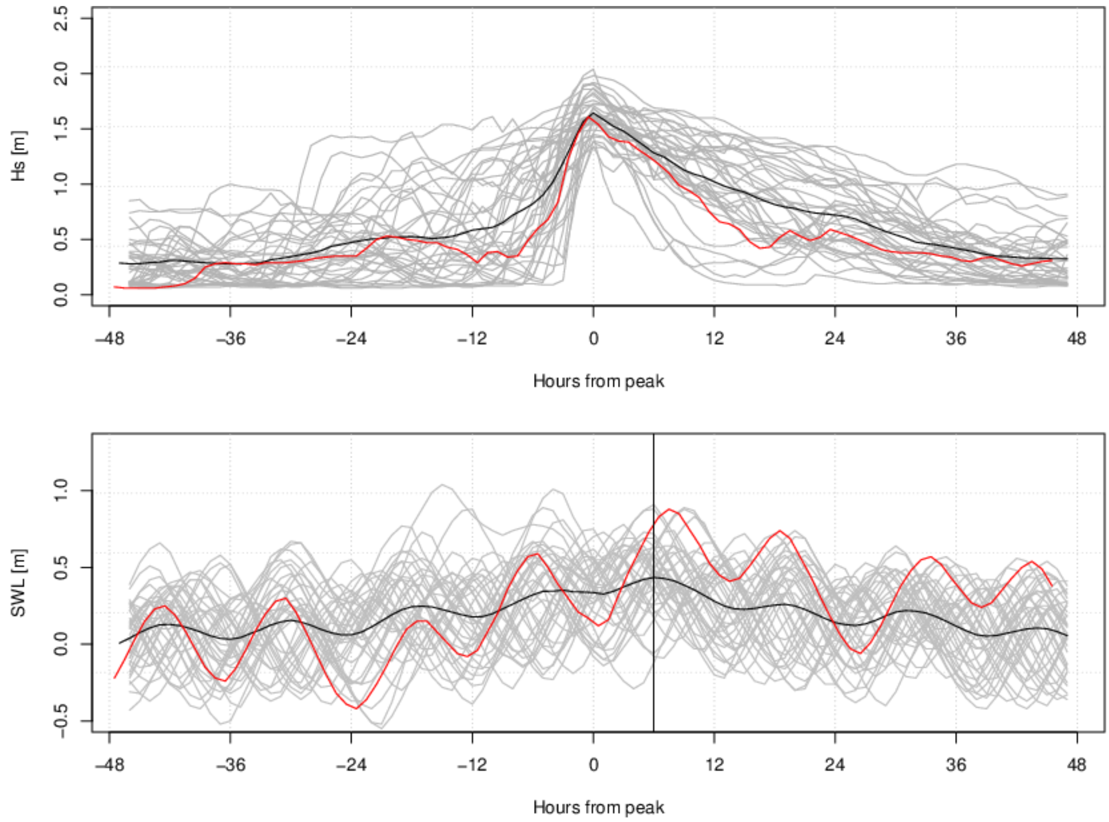

Figure C1: CoPP C-FAST boundary point time series around the annual maximum wave height time series (grey lines), mean of all time series (black line) and the 2014-06-23 event (red line). Top plot shows Hs and the bottom plot shows the corresponding SWL time series. Black vertical line is the peak of the mean of all the SWL time series.

Here, output from the SCHISM modelling is undertaken to assess the phasing of wave and extreme water level time series for the design storms used by C-FAST (Chapter 5) and for the application of storm tide and wave information in the short term (storm bite) component of the erosion hazard (Chapter 6). Figure C1 shows event time series, 48 hrs around each of the 34 annual maximum wave height events at the offshore boundary location of the City of Port Phillip (CoPP) grid of the C-FAST model. It shows the triangular form of the wave height time series, which typically peaks six hours before the peak of the mean of all of the TWL time series. Figure C2 is the same as Figure C1, but now shows the time series at the peak of the TWL. It shows that the TWL is always peaking at the high tide. All other locations also showed TWL peaking at high tide. Figure C3 shows similar time series at the Kingston offshore location to the CoPP, with the northerly winds during the 23 June 2014 event generating larger waves in the southern parts of the bay. Figure C4 shows on average a shorter period wave event at Geelong.

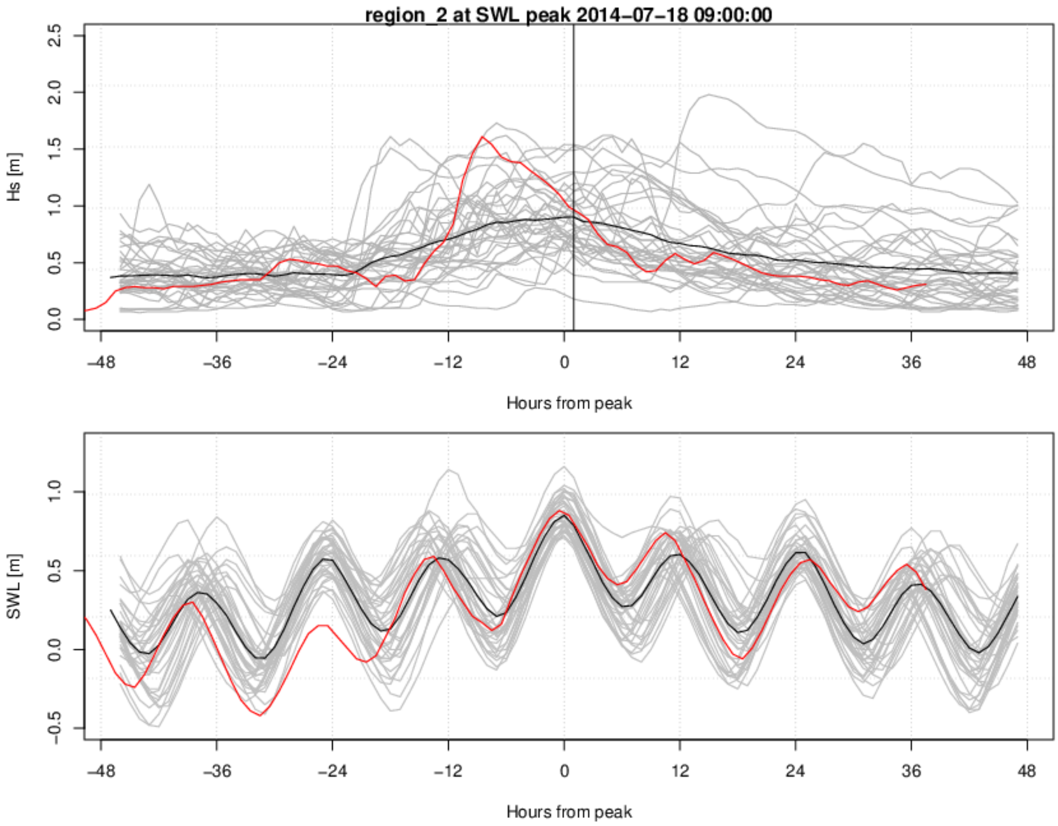

Figure C2: Same as Figure C1, but at the peak annual max SWL.

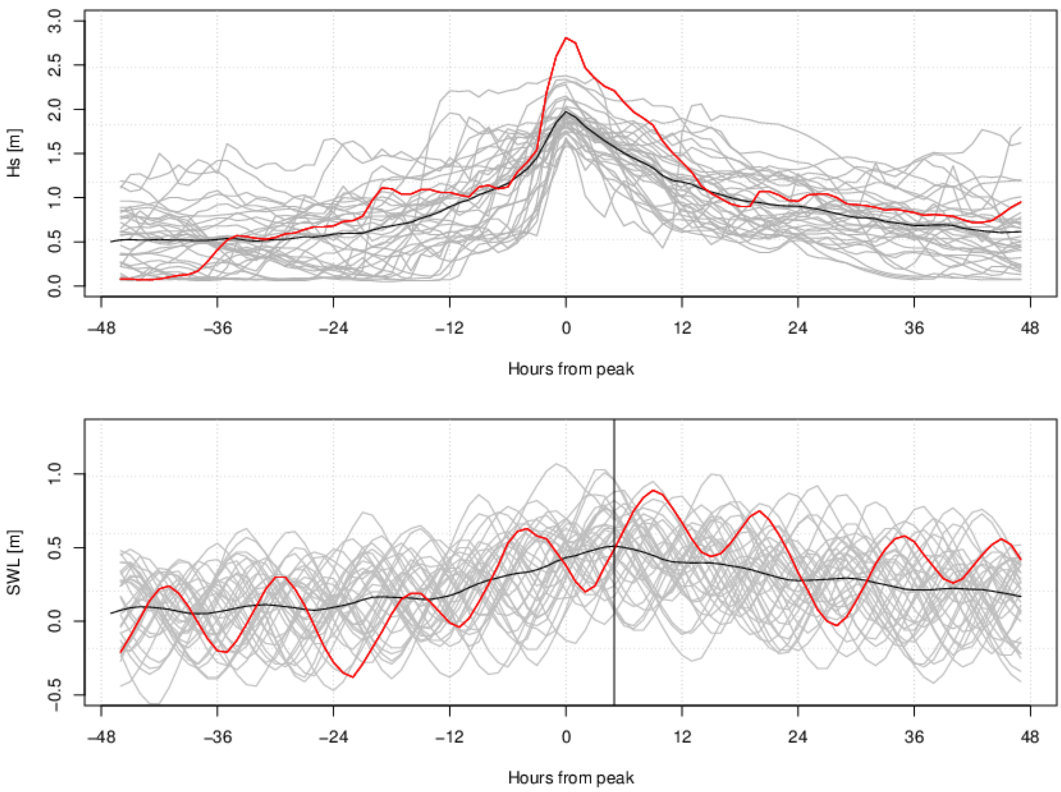

Figure C3: Same as Figure C1, but for the Kingston (Aspendale) C-FAST boundary point.

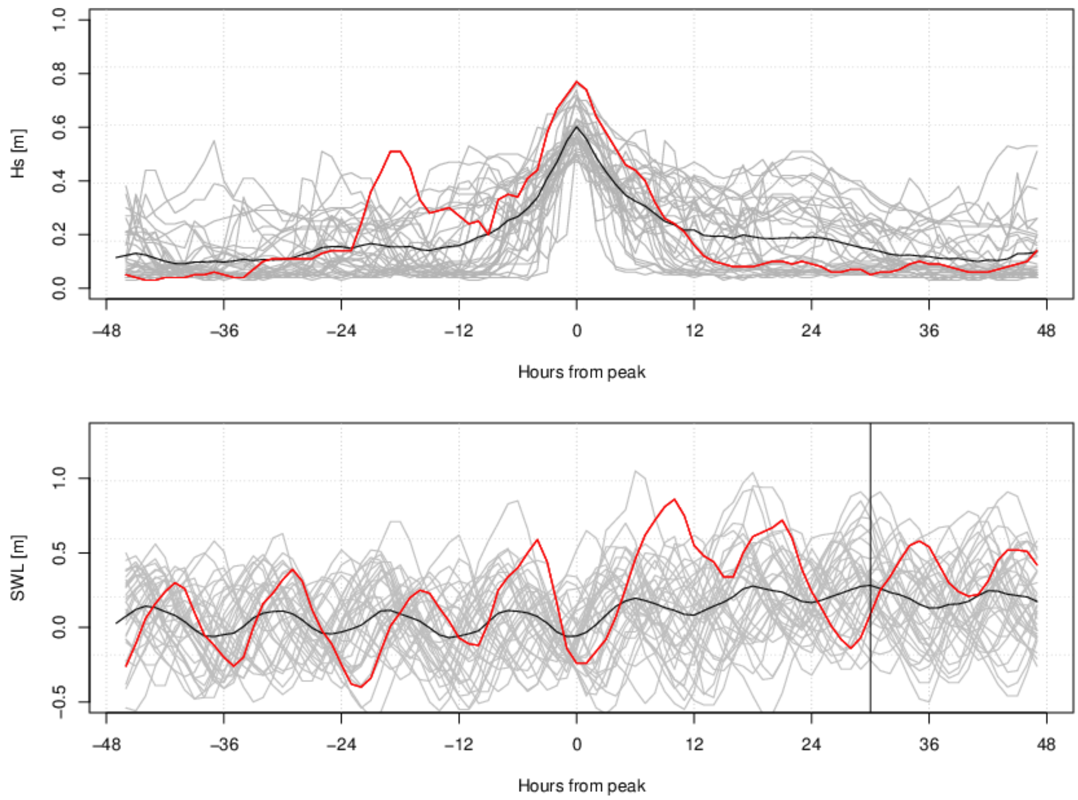

Figure C4: Same as Figure C1, but for the CoGG (Geelong) C-FAST boundary point.

In all plots the 23 June 2014 event captures the representative characteristics of a design storm and will be used to model the design storm for 48 hours. The June 2014 event also provides recent living memory of known locations of inundation to verify the analysis (e.g. overtopping of Beaconsfield parade and Altona). The triangular design wave height will peak 6hrs prior to the SWL peak for all C-FAST simulation and last the full 48, except at CoGG (Geelong) where the duration of the triangular wave time series will last for only 24 hours (Figure C5). In all simulations of the C-FAST model (table C1), the TWL will be raised so the time-series peak reaches the design AEP including SLR (Figure C5). The triangular wave time series will peak at the design AEP, six hours prior to the SWL peak.

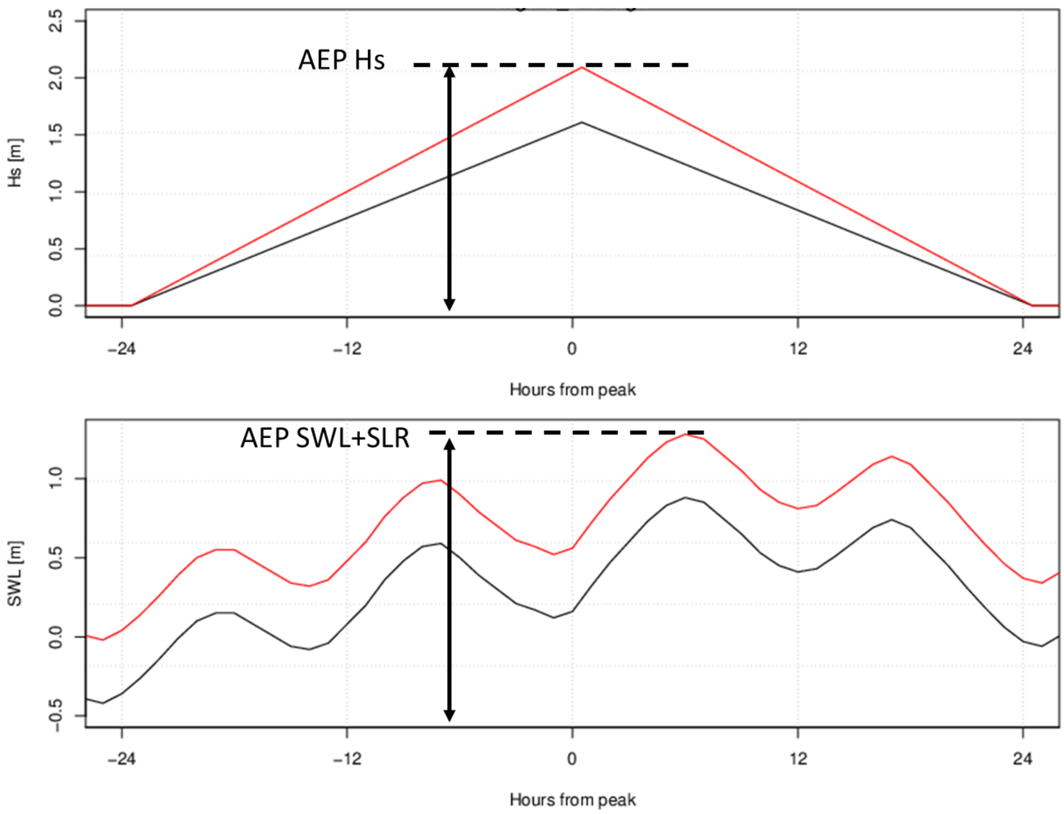

Figure C5: Design time series of Hs and TWL.

Based on AEP estimates calculated in Chapter 8, Table C1 presents the boundary condition levels that are used in the C-FAST model for the inundation hazard assessment.

References

Carley JT and Cox RJ (2003) A methodology for utilising time-dependent beach erosion models for design events. Coasts and Ports Australasian Conference 2003, 1–9.

Harrison AJ, Carley JT, Coghlan IR and Drummond CD (2019) Methodology for modelling dynamic coastal tailwater levels. Australasian Coasts and Ports 2019 Conference, 527–533.

Table C1: Boundary conditions for the C-FAST simulations.

Region		SLR	5% AEP			2% AEP			1% AEP		
			95th	50th	5th	95th	50th	5th	95th	50th	5th
0	A	0	0.96	1.02	1.08	1.02	1.09	1.16	1.05	1.13	1.21
0	A	0.2	1.11	1.17	1.23	1.16	1.23	1.30	1.18	1.26	1.34
0	A	0.5	1.42	1.48	1.54	1.47	1.54	1.61	1.49	1.57	1.65
0	A	0.8	1.73	1.79	1.85	1.78	1.85	1.92	1.80	1.88	1.96
0	A	1.1	2.04	2.10	2.16	2.09	2.16	2.23	2.11	2.19	2.27
0	A	1.4	2.35	2.41	2.47	2.40	2.47	2.54	2.42	2.50	2.58
1	B	0	0.97	1.03	1.09	1.02	1.10	1.18	1.07	1.16	1.25
1	B	0.2	1.12	1.18	1.24	1.15	1.24	1.33	1.19	1.29	1.39
1	B	0.5	1.43	1.49	1.55	1.46	1.55	1.64	1.50	1.60	1.70
1	B	0.8	1.74	1.80	1.86	1.77	1.86	1.95	1.81	1.91	2.01
1	B	1.1	2.05	2.11	2.17	2.08	2.17	2.26	2.12	2.22	2.32
1	B	1.4	2.36	2.42	2.48	2.39	2.48	2.57	2.42	2.52	2.62
2	C	0	1.00	1.07	1.14	1.06	1.14	1.22	1.10	1.20	1.30
2	C	0.2	1.15	1.23	1.31	1.20	1.28	1.36	1.22	1.33	1.44
2	C	0.5	1.46	1.54	1.61	1.51	1.59	1.67	1.53	1.64	1.75
2	C	0.8	1.77	1.84	1.91	1.82	1.90	1.98	1.83	1.94	2.05
2	C	1.1	2.08	2.15	2.22	2.13	2.21	2.29	2.14	2.25	2.36
2	C	1.4	2.39	2.46	2.53	2.43	2.51	2.59	2.45	2.56	2.67
3	D	0	1.00	1.07	1.14	1.06	1.15	1.24	1.11	1.21	1.31
3	D	0.2	1.14	1.22	1.30	1.19	1.29	1.39	1.23	1.34	1.45
3	D	0.5	1.45	1.53	1.61	1.50	1.60	1.69	1.54	1.65	1.76
3	D	0.8	1.76	1.84	1.92	1.81	1.90	1.99	1.84	1.95	2.06
3	D	1.1	2.07	2.15	2.23	2.12	2.21	2.30	2.15	2.26	2.37
3	D	1.4	2.37	2.45	2.53	2.43	2.52	2.61	2.46	2.57	2.68
4	E	0	0.95	1.01	1.07	1.00	1.07	1.14	1.04	1.12	1.20
4	E	0.2	1.16	1.21	1.26	1.21	1.28	1.35	1.25	1.33	1.41
4	E	0.5	1.47	1.52	1.57	1.52	1.59	1.66	1.56	1.64	1.72
4	E	0.8	1.78	1.83	1.88	1.83	1.90	1.97	1.87	1.95	2.03
4	E	1.1	2.09	2.14	2.19	2.14	2.21	2.28	2.18	2.26	2.34
4	E	1.4	2.40	2.45	2.50	2.45	2.52	2.59	2.49	2.57	2.65
5	F	0	1.01	1.08	1.15	1.07	1.16	1.25	1.12	1.22	1.32
5	F	0.2	1.21	1.28	1.35	1.27	1.36	1.45	1.32	1.42	1.52
5	F	0.5	1.52	1.59	1.66	1.58	1.67	1.76	1.63	1.73	1.83
5	F	0.8	1.83	1.90	1.97	1.88	1.97	2.06	1.93	2.03	2.13
5	F	1.1	2.14	2.21	2.28	2.19	2.28	2.37	2.24	2.34	2.44
5	F	1.4	2.44	2.51	2.58	2.50	2.59	2.68	2.55	2.65	2.75
6	G	0	0.92	0.98	1.04	0.98	1.05	1.12	1.02	1.10	1.18
6	G	0.2	1.13	1.19	1.25	1.17	1.25	1.33	1.23	1.31	1.39
6	G	0.5	1.44	1.50	1.56	1.48	1.56	1.64	1.54	1.62	1.70
6	G	0.8	1.74	1.80	1.86	1.79	1.87	1.95	1.84	1.92	2.00
6	G	1.1	2.05	2.11	2.16	2.10	2.18	2.26	2.15	2.23	2.31
6	G	1.4	2.36	2.41	2.46	2.40	2.48	2.56	2.45	2.53	2.61

Appendix D. Comparison with Melbourne Water Flood Extents

Here, inundation results are compared against Melbourne Water's coastal flood modelled outputs that are currently being used for planning purposes and are available for Region C. It is noted that Melbourne Water's current data uses a bathtub fill approach.

Figure D1 compares the results obtained from this study with Melbourne Water's bathtub fill-based model outputs for the 0.0 and 0.8 m SLR Scenarios. It is noted that bathtub fill-based flood models provide conservative flood predictions as they do not take into account the effect of protective measures such as seawalls in reducing inundation and because bathtub fill models are static models, they do not take account of the overland flow and retreat of flood water. Furthermore, the Melbourne Water data does not consider catchment input from rivers or local rainfall. Therefore, such comparisons are not "like-for-like", however understanding the differences is informative. In order to make the comparison more meaningful the flood height cut-off is set to 0.01 m and no duration cut-off has been imposed. Note that the Melbourne Water bath-tub fill outputs do not have a depth or duration cut-off. It is evident that for all cases presented below without rainfall input that the C-FAST results show reduced levels of flooding. From a flooded-area perspective the most comparable case is the one with storm surge, overtopping and a 2-hr rainfall input for both the 0.0 m and 0.8 m SLR except for some locations where the C-FAST model results show low levels of flooding due to rainfall that is not present in the Melbourne Water data.

Figures D2 and D3 show further comparisons at zoomed in locations around Elwood and Hobsons Bay. These outputs also show that the most comparable case from a flood inundation perspective is the one with storm surge, overtopping and 2-hr rainfall included, except for some locations where there are flooded areas in the C-FAST simulation at very low depths (less than 0.2 m) due to the effect of rainfall that are not present in the Melbourne Water data. These comparisons provide valuable insights into the relative importance of different flood-producing factors in the coastal urban landscape, which can complement other information sources to assist coastal managers and decision makers in their decision making.

SLR = 0.0 m	SLR = 0.8 m
Melbourne Water flood extents	
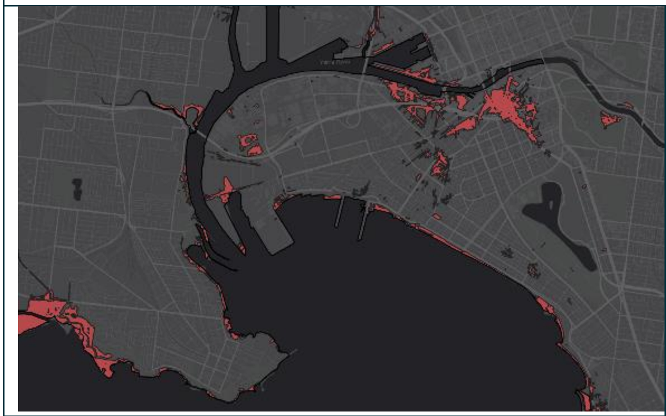	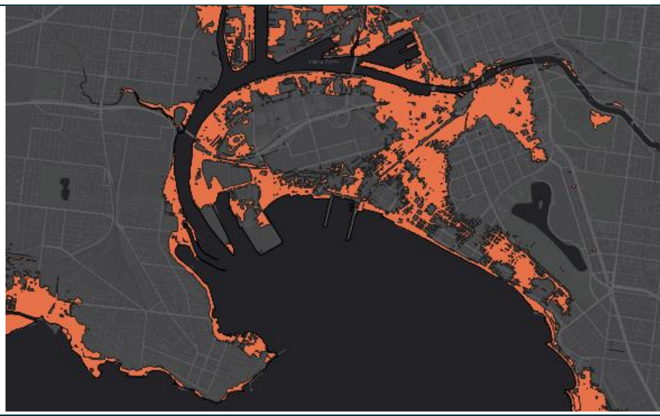
Storm surge – current study	
	
Storm surge + overtopping – current study	
	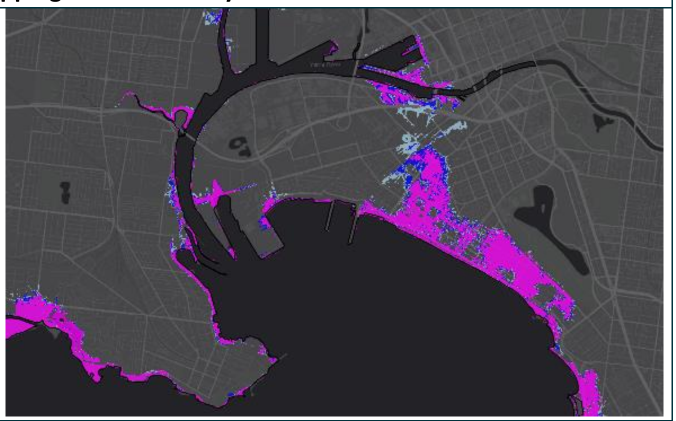

Figure D1: Comparison in Port Melbourne between Melbourne Water flood extents (top row) and sensitivity study simulations (5 m resolution) flood extent maps (maximum height exceeding 0.01 m) with each map showing three different 1% AEP storm surge likelihood results (magenta is 95% likelihood, dark blue is 50% likelihood and light blue is 5% likelihood).

SLR = 0.0 m	SLR = 0.8 m
Storm surge + overtopping + rainfall 24 hr – current study	
	
Storm surge + overtopping + rainfall 12 hr – current study	
	
Storm surge + overtopping + rainfall 2 hr – current study	
	

Figure D1: Continued.

SLR = 0.0 m	SLR = 0.8 m
Storm surge + overtopping + rainfall 2 hr + drainage – current study	
	

Figure D1: Continued.

SLR = 0.0 m	SLR = 0.8 m
Melbourne Water flood extents	
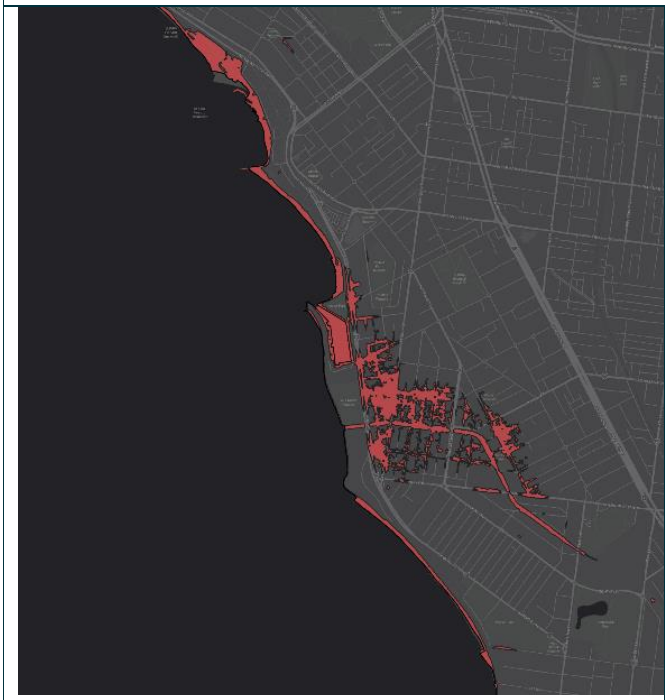	

Figure D2: Comparison in Elwood between Melbourne Water flood extents (top row) and sensitivity study simulations (5 m resolution) flood extent maps (maximum height exceeding 0.01 m) with each map showing three different 1% AEP storm surge likelihood results (magenta is 95% likelihood, dark blue is 50% likelihood and light blue is 5% likelihood).

SLR = 0.0 m	SLR = 0.8 m
Storm surge	
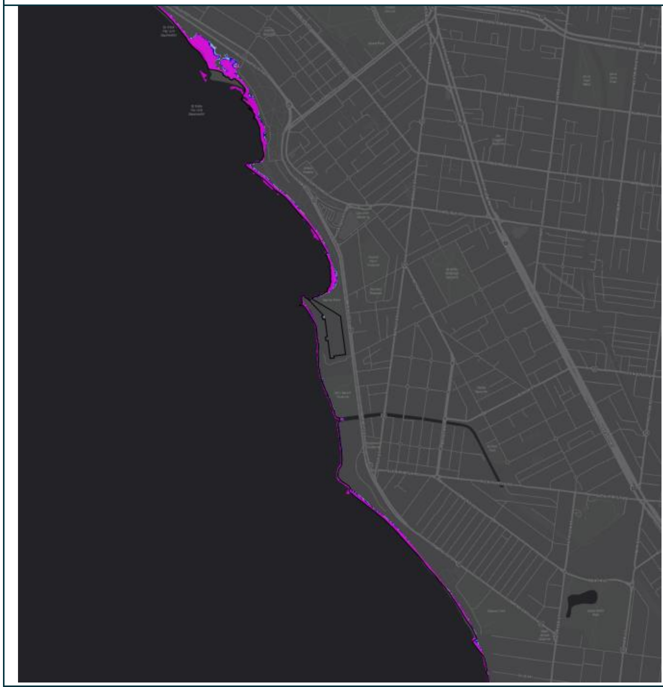	
Storm surge + overtopping	
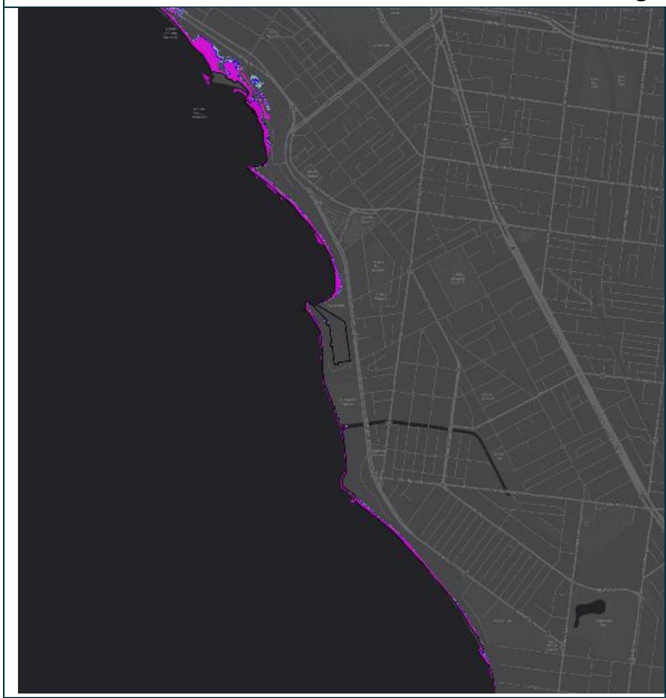	

Figure D2: Continued.

SLR = 0.0 m	SLR = 0.8 m
Storm surge + overtopping + rainfall 24 hr	
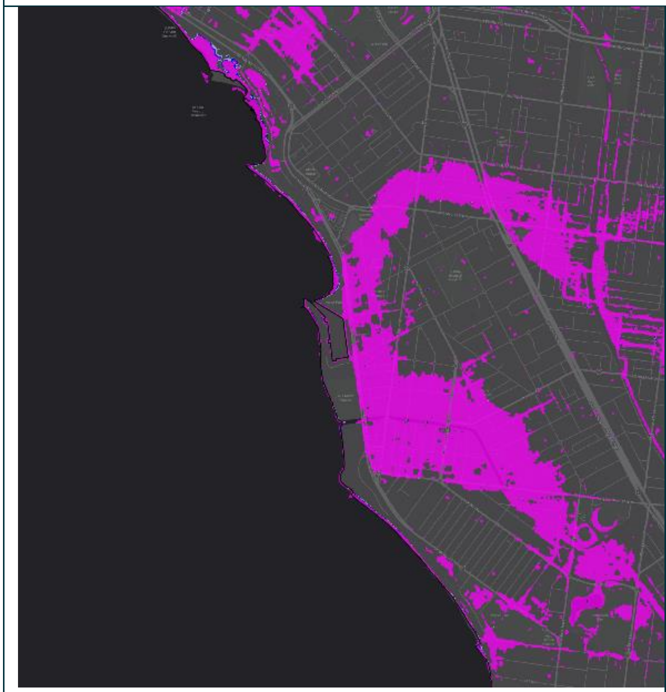	
Storm surge + overtopping + rainfall 12 hr	
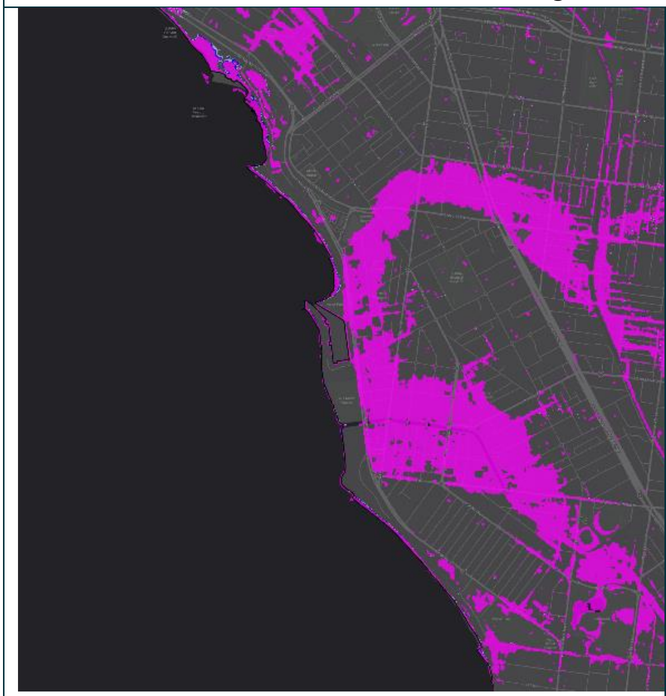	

Figure D2: Continued.

SLR = 0.0 m	SLR = 0.8 m
Storm surge + overtopping + rainfall 2 hr	
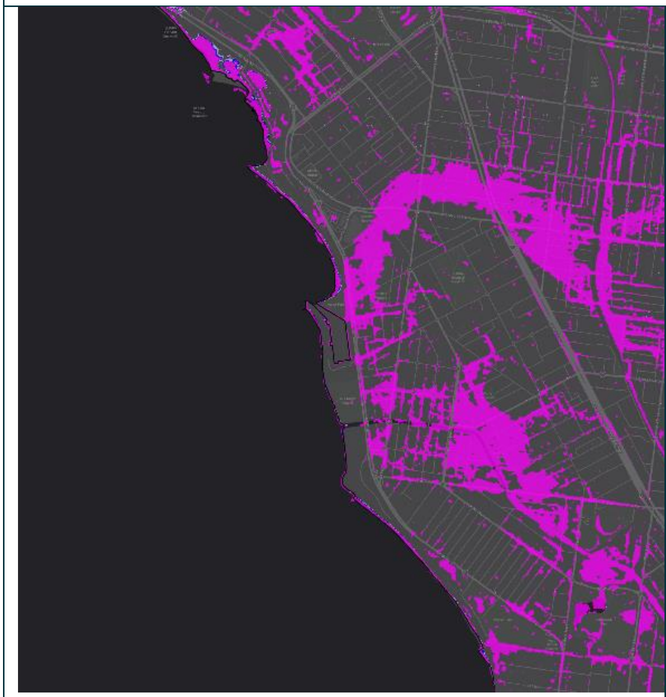	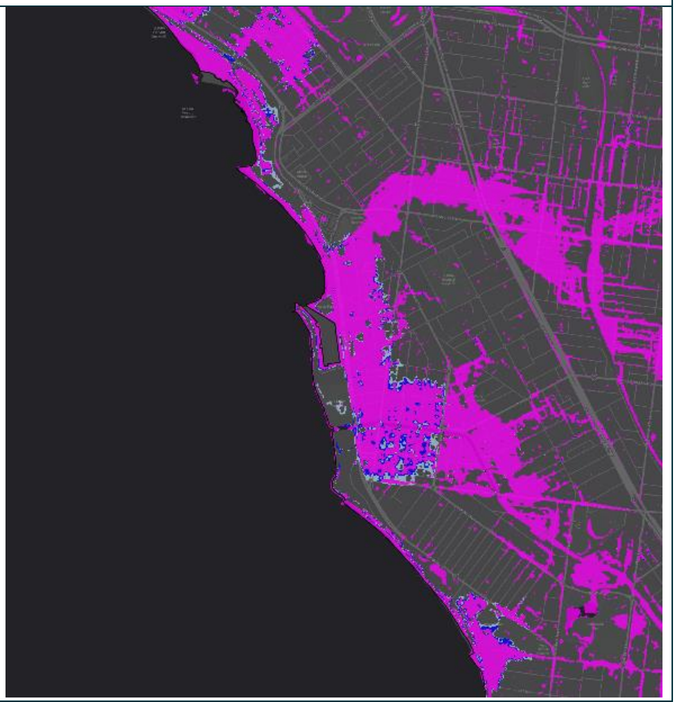
Storm surge + overtopping + rainfall 2 hr + drainage	
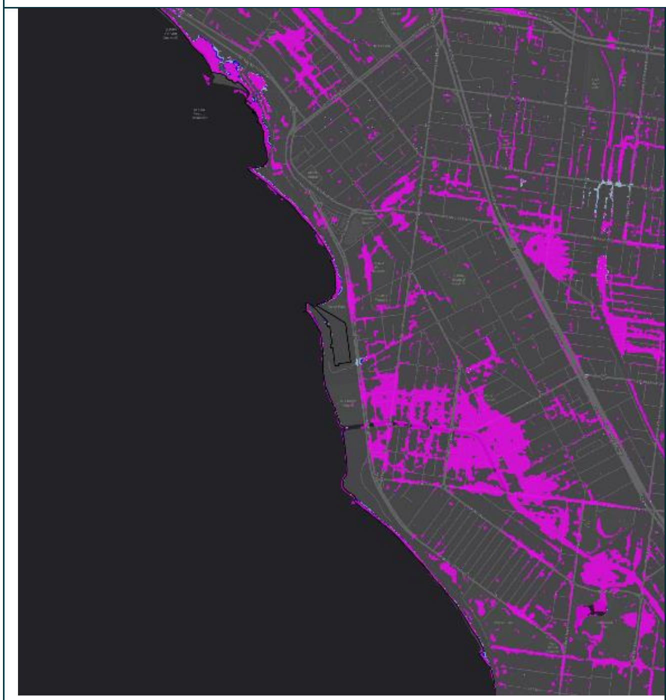	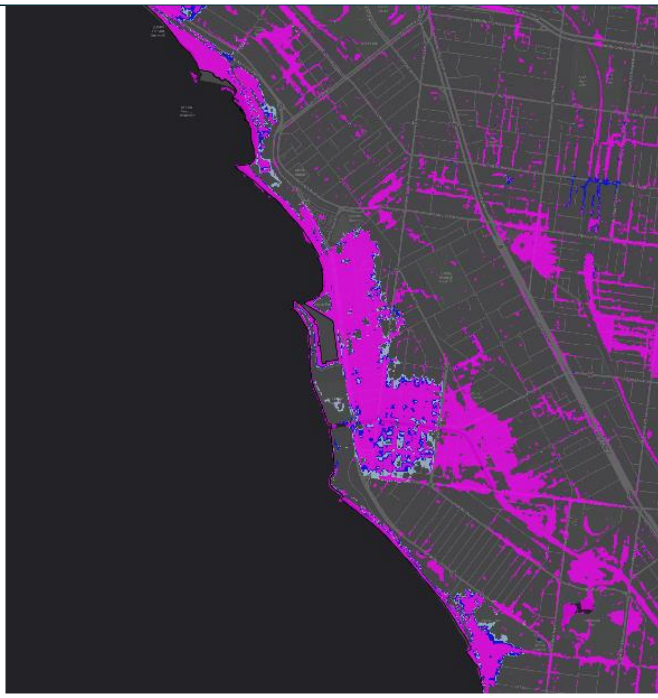

Figure D2: Continued.

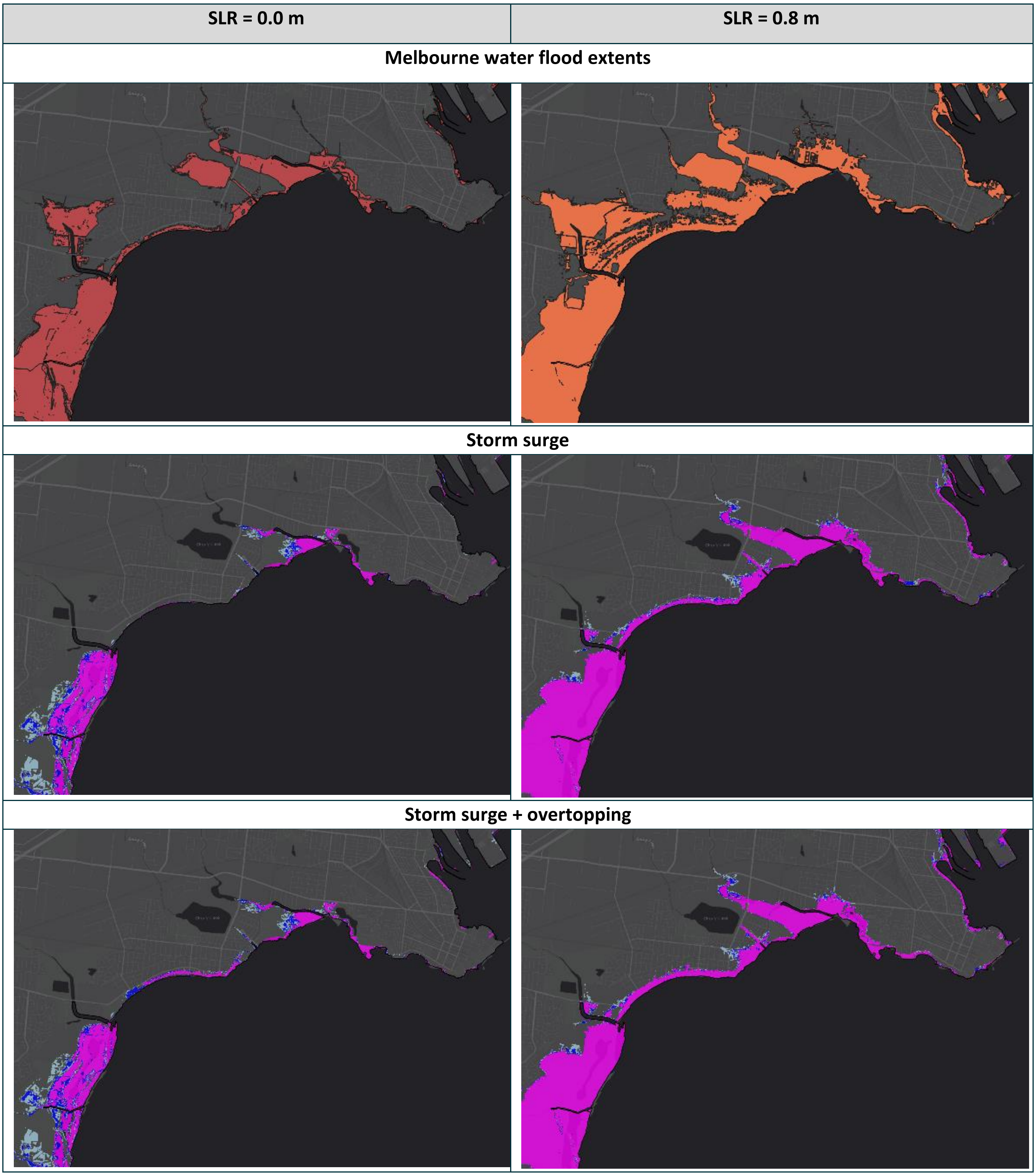

Figure D3: Comparison in Hobsons Bay between Melbourne Water flood extents (top row) and sensitivity study simulations (5 m resolution) flood extent maps (maximum height exceeding 0.01 m) with each map showing three different 1% AEP storm surge likelihood results (magenta is 95% likelihood, dark blue is 50% likelihood and light blue is 5% likelihood).

SLR = 0.0 m	SLR = 0.8 m
Storm surge + overtopping + rainfall 24 hr	
	
Storm surge + overtopping + rainfall 12 hr	
	
Storm surge + overtopping + rainfall 2 hr	
	

Figure D3: Continued.

SLR = 0.0 m	SLR = 0.8 m
Storm surge + overtopping + rainfall 24 hr + drainage	
	

Figure D3: Continued.

Appendix E. Geomorphological Definitions

Table E1: Geomorphological definitions used in this report

Shoreline (Instantaneous Shoreline)
The shoreline is the interface between ocean and land represented by an irregular line in planform and elevation. It is the seaward limit at which land at any moment is submerged by coherent wave swash (as distinct from wave splash). It is determined by two interactive components: (a) forcing factors—astronomical tidal wave, swell and wind waves—that propagate through the water column and transfer energy landward; (b) the three-dimensional form—elevation and slope—of the marine and landfall surface the water crosses. On a coherent rock shore platform substrate the shoreline position varies momentarily according only to the state of the tide and local wave and wind conditions and displays limited temporal variation. On beaches (unconsolidated substrate) where wave swash can mobilise the substrate, the shoreline can vary rapidly (between waves and between tides) responding to changes in substrate morphology, slope and elevation. The shoreline—as represented by a line on images (maps, photographs, 3-D representations)—is referred to an elevation such as “0” AHD. On sandy shorelines this line will be a generalisation, for as substrate elevation changes the fixed datum plane may be emerged or submerged according to sand accretion or depletion.
Swash Limit (Wave Runup)
This is the oscillating line marking the limit to which water from a progressive wave extends landward. It defines the wet-dry beach margin and is best recorded by video photography from aerial or fixed ground cameras. Swash motion is driven by wave height, wave length/period and intertidal slope while the runup distance is determined largely by infiltration, beach grain size, surface roughness and the wave turbulence and swash-backwash interaction (Erikson **et al.,** 2007).
Shore Zone (Intertidal Zone)
The shore zone or intertidal zone is the area between the upper subtidal zone (effectively the lowest low-water level) and the landward limit of swash. On intertidal areas of unconsolidated sediment (boulders, gravel, sand, mud), the shore zone is the beach face where sediment moves cross-shore and along-shore in response to wave-induced currents in the swash and backwash (below left). Wind also plays a significant role particularly during low tide exposure of fine-sand beaches and can deflate or aggrade beach elevations. Wind is the key driver of backshore sand accumulation along with less-frequent wave-driven chenier deposits. A sub-unit of the shore zone is the supratidal zone—an area landward of direct swash that is impacted by wave splash and occasionally washed by a storm surge. The supratidal zone is the seaward limit of the backshore. On rocky shores the shore zone is a shore platform (below right). The shore zone may be of composite morphology where the lower shore zone is a rock platform and the upper shore zone is a beach overlying the rock. The variable components of a shore zone are width, slope, substrate type, sediment type (composition, size, and thickness), organics (e.g. mangroves, reef organisms) and human-built structures (e.g. seawalls, groynes). By combining these variables multiple shore zone classes can be recognised. The major landforms of the shore zone are beaches and shore platforms.

Shore zone on a sandy intertidal coast, McCrae. (N. Rosengren June 2019).

Shore zone on a rocky intertidal coast, Ricketts Point Beaumaris. (N. Rosengren June 2019).

Coastal Geomorphic Sectors

A coastal geomorphic sector (CGS) is a discrete length of coast that comprises a mappable unit with significant differences to adjacent sectors. Lateral variation in one or more key characteristics defines the boundary between sectors. A differentiator between adjacent sectors is their reaction to coastal processes and in particular how they respond to changed water levels and wave energy. Shore sector mapping is a means of rapidly compiling information on shoreline form, substrate, and vegetation type and can be used as a method for assessing the response (sensitivity) of a coast to water level and other environmental changes. A CGS is therefore a distinctive reach of coast where the shore zone and backshore have a limited range of landform variation. The resolution of shore zone components and boundaries is determined by the scale—the length of coastline assessed and methodology of the study—desktop or field-based. This CGSs defined in this study are based on field inspections related to other research activities by the author over many years supplemented by the 95 sites visited for sediment sampling and a low-altitude aerial inspection and photography in June 2019.

The basis of CGS mapping is recognition of Coastal Landform Categories (CGC). A Coastal Geomorphic Sector is comprised of two or more Coastal Geomorphic Categories, for example a sandy beach in front of a low coastal bluff or a shore platform at the base of a hard rock active cliff. The landforms of the shore zone and backshore are the two key determinants of a CGS. The landforms of the shore zone are determined by the intrinsic geometry of the coast—in turn determined by the geological base, tectonic history and the overlap of subaerial and coastal/marine physical, chemical and biological processes that have shaped the coast over varied time periods. Superimposed to varying degrees—in places to be definitive of a CGS—is the direct and indirect effect of human activity. This is most evident as engineered structures such as seawalls, groynes and renourished beaches. The impact of changed coastal processes, e.g. changes in wave dynamics and water level, may initially be displayed in the shore zone before it is translated to the backshore.

COASTAL LANDFORM CATEGORIES

The key characteristics of the Coastal Landform Categories of the Shore Zone and Backshore used in defining the Coastal Geomorphic Sectors are described and illustrated below.

SHORE ZONE (INTERTIDAL TYPE)

Beach

The subaerial beach is the area exposed as the (intertidal) shore zone, while the subaqueous beach is subtidal sediment that is regularly moved by wave action. A beach thus extends from the landward limit of swash to a variable distance seaward. Beaches have a surface and variable thickness of unconsolidated sediment that may range in texture and composition from mud to sand, gravel, cobbles and boulders. Beaches attached along their entire length to a backshore are termed mainland beaches. Beaches that diverge seaward as elongate or lobate forms are spits while beaches partially or not attached to a different backshore landform are coastal barriers.

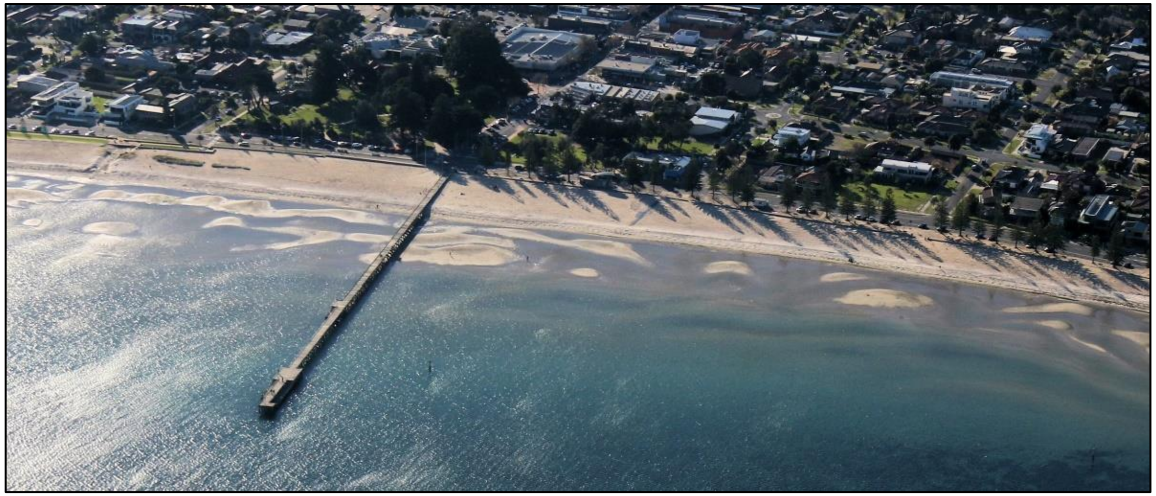

Sand (renourished) beach at Altona with seawall at swash limit and urban backshore.

Gravel and coarse sand beachface at Point Cook

Shore Platform

A shore platform is a shelf or bench of variable slope, width and micromorphology extending across all or part of the shore zone and with variable cover of surficial sediments. Most Port Phillip shore platforms are of consolidated hard rock—sandstone (Ricketts Point), limestone (Point Lonsdale), granite (Mount Martha) or basalt (Williamstown) — but also develop in resistant clays at Point Henry west.

Shore platform in consolidated clay, Point Henry west.

Shore platform in basalt with gravel, sand and seagrass cover, Point Cook

BACKSHORE

The backshore extends landward from the swash limit. It is initially higher than the limit of swash but may then slope inland and become lower than sea level (e.g. a lagoon). The backshore has two components (1) *Proximal* backshore—the first landform type immediately above swash limit, (2) *Distal* backshore—distinctive landform landward of proximal backshore. Where the proximal backshore landform extends inland for some distance e.g. over 500 metres, the distal backshore landform is taken to be similar. In the illustration (right), the proximal backshore is an established foredune. The distal backshore is a similar landform but highly modified by human activities and is classed as engineered backshore.

Coastal cliffs

Coastal cliffs are slopes in excess of 40^{o} exposing geological material that may be fresh or variably weathered but with minimal and discontinuous soil or vegetation cover. Cliffs in Port Phillip occur on a range of geological materials and terrain including crystalline igneous (Mount Martha) and cemented sedimentary rock (Beaumaris) to weakly consolidated and/or deeply weathered sediments such as at Red Bluff, Black Rock. Cliffs develop by marine truncation and partial submergence of hinterland slopes. The slope base is subject to frequent or continuous wave swash, turbulence or currents that preclude extensive or long-term accumulation of clastic materials by alluvial-colluvial or beach depositional processes. Rock material is episodically detached from the slope and removed by wave action, but the slopes are comprised of geological materials of sufficient cohesion, volume and backshore elevation to form a persistent steep profile.

Soft Rock Cliffs

On long sectors of Port Phillip cliffs are developed in “soft rocks” i.e. poorly consolidated and/or deeply weathered sedimentary, volcanic and granitic formations prone to rapid slope failure and particle and block detachment. The four principal areas are: Bellarine Peninsula northeast of Clifton Springs (geomorphic unit 13), the northeast coast from Green Point to Beaumaris (geomorphic units 34 and 35), Frankston to Balcombe Creek (geomorphic unit 38), and intermittent sites between Rye and Point Nepean (geomorphic units 45 to 48). Short sectors of hard rock active cliff and coastal bluffs occur inside and adjacent to these localities.

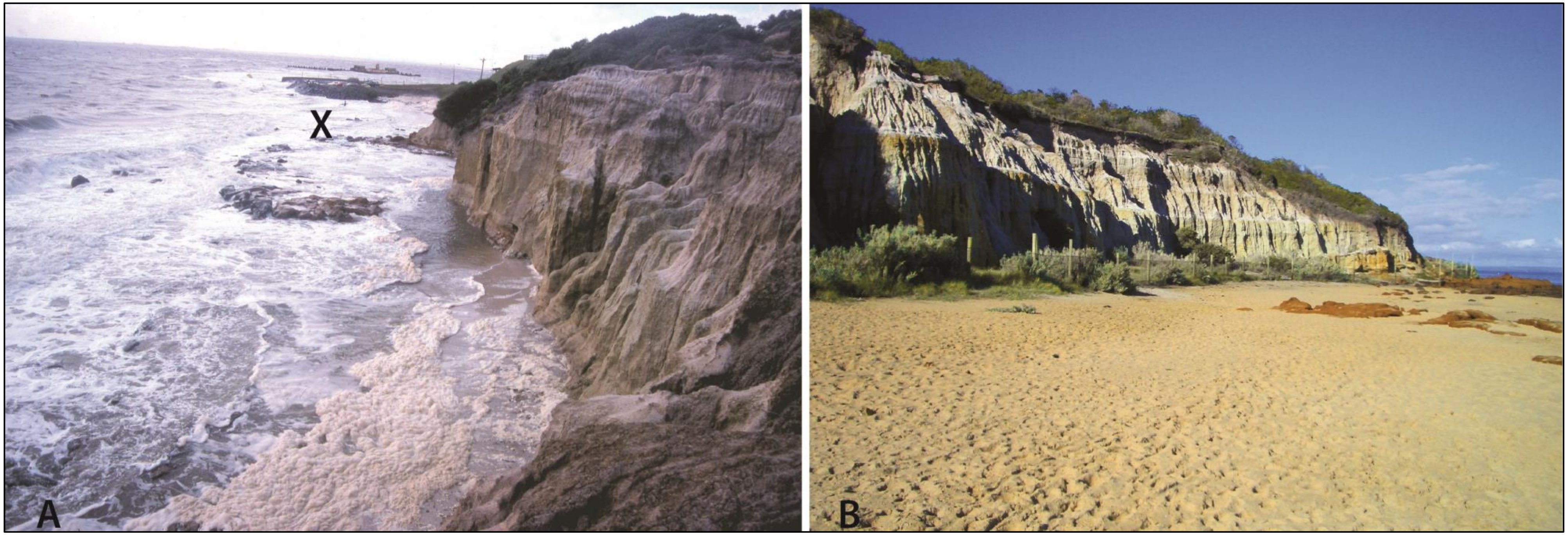

Soft rock cliffs with rills and gullies at Black Rock Point - awash at the base in a storm in 1998 (A) and with a wide beach in 2007 (B). X on photo A shows the photo point in photo B. (N. Rosengren, 1998 and 2007).

Hard Rock Cliffs

Hard rocks are subjectively defined as exposures that resist weathering and undergo only irregular detachment of fragments and larger blocks by waves and currents or by structural failure due to release of compressive stress in the rock mass. Hard rocks around Port Phillip are limited to the Mount Martha Granodiorite, short sectors of Mount Eliza Granodiorite, ferruginous beds of Beaumaris Sandstone, Older Volcanics basalt and Bridgewater Formation calcarenite. Comparison of shoreline and cliff crest positions from maps and aerial photographs show the five kilometres of high cliffs and bluffs formed on Mount Martha Granodiorite south of Balcombe Creek is the most stable cliff coast in Port Phillip.

Hard rock cliffs in Mt Martha Granodiorite. N. Rosengren June 2019).

Tectonics

Tectonics is a factor in the location of active soft rock cliffs around Port Phillip. On the Mornington Peninsula coast the highest and most active cliffs are along the trace of Selwyn Fault in fractured bedrock and displaced rock masses and debris flows from older large-scale landslides. Landslides are common in the cliffs that extend along the north side of the Bellarine Peninsula, between Curlewis in the west and Portarlington in the east. The landslides near Curlewis in the west have developed within the Gellibrand Marl and tuffaceous soils of the Older Volcanics, both of which are characterized by fissured clays of high plasticity and low residual angles of friction. As such these slides tend to be translational or shallow rotational and are capable of undergoing large displacements (Wilson and Miner, 2006). Extensive rills and close-spaced gullies are a major mechanism for slope retreat in addition to basal marine erosion.

Newly developed cliff in landslide basal debris, Daveys Bay, Mt Elisa. (N. Rosengren May 2016).

Multiple rotational slides and slope-face gullies, MacAdams Lane, Portarlington. (N. Rosengren, 2013).

Regolith Cliffs

Regolith cliffs are designated as a separate class of active cliffs in Port Phillip although could be incorporated into soft rock cliffs. The distinguishing feature selected is they are comprised of *transported*—as distinct from *in* situ— regolith of unconsolidated Late Pleistocene to Holocene sedimentary and partially organic alluvial, colluvial and coastal deposits. They may include a large or predominant fraction of coarse sediment. Parts of soft rock landslip cliffs and scarps developed in coastal dunes are regolith cliffs. The materials have sufficient cohesion, packing or clast size to maintain a steep face when exposed to wave action, but are susceptible to disaggregation and dispersal under some wave regimes. The distinctive delta-shaped sedimentary body, with the apex several kilometres upstream from Werribee and the distal ends on the coastline from south of Point Cook to the mouth of Little River, is the floodplain of the Werribee River. It is not a true sub-aqueous delta as it consists dominantly of a reddish-brown, poorly bedded silty and sandy clay with minor sand and gravel and lacks marine fossils. It originated as a floodplain crossed by distributary streams, traces of which can be seen at other localities. It has formal recognition as the Deutgam Silt. Outcrops along the coast are therefore classed as regolith cliffs. Coastal dunes in Port Phillip are dominantly low, narrow shore-parallel ridges or established foredunes developed as barriers, spits and forelands. Transgressive dunes and high dunes are of limited extent but locally form a distinctive class of class of regolith cliffs and bluffs. Cliffs develop in beaches and foredunes in direct response to storm waves, but rapidly degrade or backfill to lower angle stable slopes. On vegetated established dunes, beach depletion allows wave removal of basal support causing slumping and sliding of sand higher up the slope. This may be washed away, but if of sufficient volume and if the vegetation cover survives, will persist as a protective apron at the slope foot restricting further erosion. With further vegetation recovery, the slope will become quasi-stable as a grassy to scrubby bluff.

Regolith cliffs in Deutgam Silt north of mouth of Werribee River. (N. Rosengren, June 2019).

Sand cliff, Dog Beach, Point Lonsdale. (N. Rosengren, 2013).

Backshore Bluffs

Coastal bluffs are slopes with variable or continuous cover of regolith, soil and vegetation and limited exposure of basement or resistant rock. Some bluffs are former (stranded) or inactive sea cliffs relict from higher sea level, or more recently isolated from wave action due to tectonic uplift, by accumulation of slope debris, beach deposits, growth of organic materials (vegetation or reef), or by shoreline or offshore engineering structures that diminish the effectiveness of wave and current action. As with coastal cliffs, most bluffs are a continuation of the slopes and geomorphology of the hinterland topography, intersected as the shoreline recedes. The distinction between an active cliff and a coastal bluff may be temporal, as sectors of bluff may be or initiated as cliffs or reactivated due to changed marine or onshore conditions. A qualitative but relevant distinction in Port Phillip is between high bluffs and low bluffs. Low bluffs can be overtopped in a storm surge resulting in backshore inundation as well as creating or activating a cliff. High bluffs may be subject to major landslides that extend the toe seaward and initiate cliff development. This process is occurring along a number of cliff sectors on the tectonic coast of the Mornington Peninsula and northern Bellarine Peninsula. Bluffs form the backshore terrain of much of the Bellarine Peninsula where they alternate with sectors of active soft rock cliff. A five-kilometre long bluff behind the cuspate foreland complex of Point Richards links the two sectors of active cliff at Portarlington and Spray Farm Lane.

Backshore slopes at Portarlington: low bluff, high bluff, hard rock cliff, soft rock cliff. (N. Rosengren, June 2019).

Backshore ridges (beach ridges, foredunes)

Backshore sand ridges around Port Phillip are developed by wave and wind (aeolian) processes. Although a distinction is made between beach ridges—produced by wave swash—and ridges and mounds built up by wind, they are not mutually exclusive and many ridges are or composite origin. The terms incipient foredune and established foredune are most commonly used. Narrow zones of backshore ridges are widely distributed but persistent and multiple wide wave-built beach ridges are a feature of the Bellarine Peninsula, western coast from Altona to Point Wilson and at Observatory Point at the western end of Nepean Peninsula. The ridge complex forming the Point Richards foreland at Portarlington is composed of coarse sand, shell and minor gravel and has very limited aeolian component

Wide zone of stranded sand and shell ridges in front of high bluff, Point Richards. (N. Rosengren, June 2019).

Aeolian ridges

Aeolian ridges (foredunes) are significant features of the eastern and southern shores of Port Phillip, although they are most likely composite features building on an initial wave deposit. Transgressive dunes—sand bodies that have moved across the backshore region and overlie older terrain—are of very limited extent in Port Phillip. The long barrier beaches on eastern Port Phillip (Mordialloc to Frankston), Safety Beach, Dromana to Rye Beach) are backed by sandy terrain of variable width, origin and preservation. They are now substantially modified by backshore built structures and facilities, the impact of high number of beach users and beach management including mechanical cleaning and sand scraping. The 17 km continuous beach between Mordialloc Creek and Frankston was originally backed by elongate narrow ridges of stranded established foredunes that enclosed the former Carrum Swamp. Although fetch-limited, the beach experiences occasional high-energy wind and wave conditions. North of Paterson River backshore dunes are now largely covered by urban and recreational structure. The Seaford Foreshore Reserve has a dune zone averaging 100 metres wide with two to four parallel ridges generally less than two metres high and an outermost ridge three to six metres high. This dune ridge develops a high scarp during storms but appears to recover over a six-to-twelve month period.

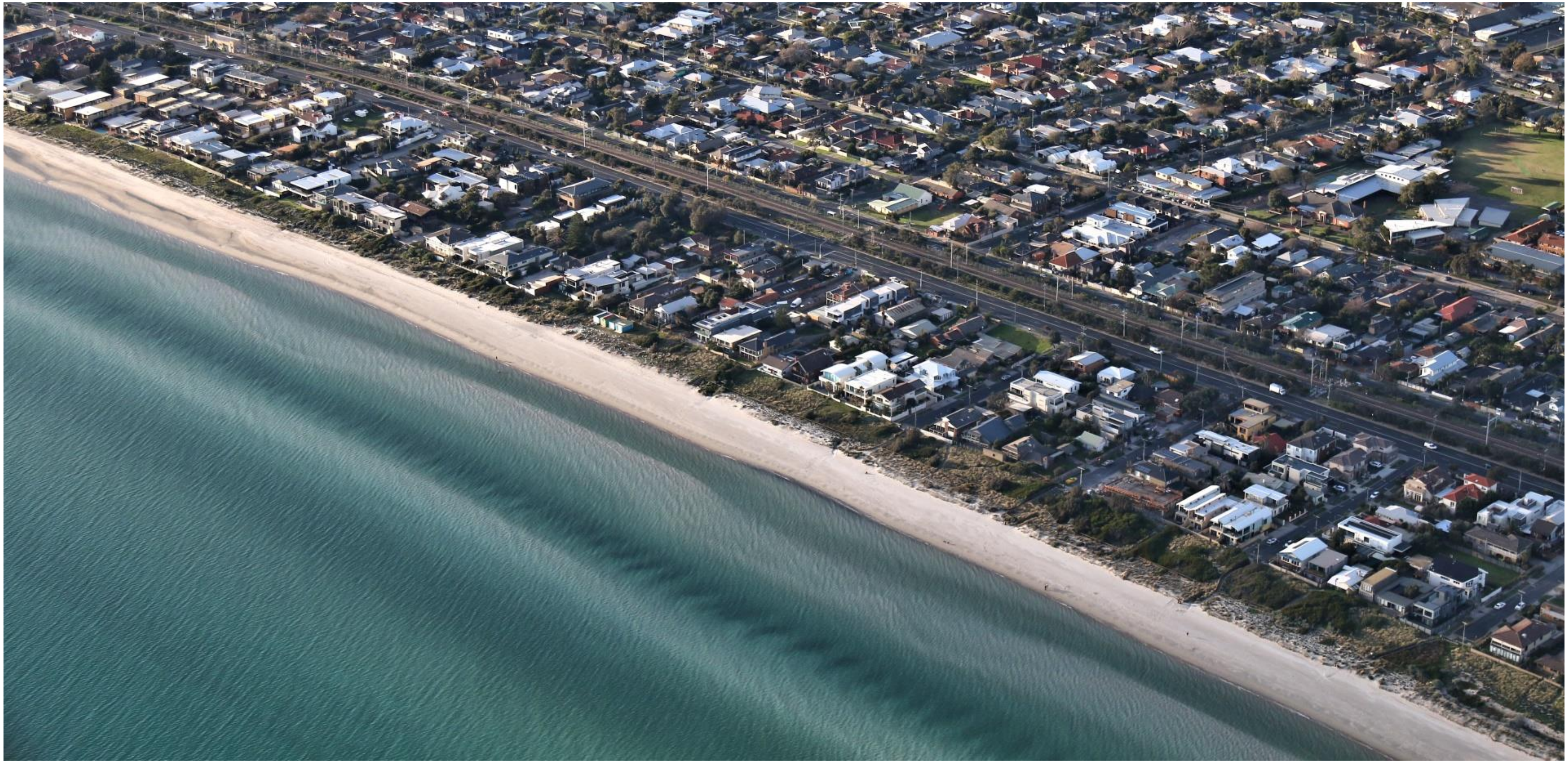

The barrier beach fringing the narrow unclaimed remnant of the multiple foredunes of the Carrum barrier. (N. Rosengren, June 2019).

Estuaries & stream mouths

Wetlands associated with estuaries and streams are either non-existent, vestigial or at best remnant around much of Port Phillip. Coastal wetland extent and diversity is limited by ambient factors such as backshore and intertidal slope, substrate type, water quality and turbulence as well as by past and ongoing disturbances. Limeburners Bay (Hovells Creek) retains fresh to brackish-saline flora and fauna communities including a substantial stand of mangroves along both shorelines in the upper estuary. The tidal entrance to Limeburners Bay, although restricted by a curving spit on the east, is always open. Balcombe Creek estuary is intermittently closed by a sand bar. Apart from the Yarra River and Werribee River, most streams are intermittent to ephemeral. Most waterways are modified and highly regulated by flow diversions, adjacent land use and channel engineering including dredging to maintain a marine connection for boat access. These works have substantially changed the natural estuarine character and processes of Mordialloc Creek, Patterson River (former Dandenong Creek), Little River and Brokil Creek (Martha Cove Marina). The least modified lower waterways are Balcombe Creek and the funnel-shaped estuary of Limeburners Bay at the mouth of Hovells Creek.

Relatively unmodified (physically) Balcombe Creek estuary compared with the obliterated former Brokil Creek now Martha Cove marina canal estate. (N. Rosengren, June 2019).

Coastal wetlands

Compared with the limited extent of estuarine wetlands there are large areas of other coastal wetland types including Ramsar sites at Mud Islands and four large sites along the western coast of Port Phillip: Skeleton Creek to Point Cook; Werribee River to Avalon Airfield; northern coastline of Corio Bay from Point Wilson to Limeburners Bay; Swan Bay. Much of these are derived wetlands utilising abandoned salt ponds or other excavations and the constructed Western Treatment Plant area. Mud Islands, Swan Bay, and The Inlets retain the greatest array of natural landform wetlands.

Natural saline wetlands associated with coastal barrier ridges at Avalon and derived wetlands from former salt ponds. (N. Rosengren, June 2019).

Engineered Coast

Much of the pre-1840's shoreline of Port Phillip is now obscured or extensively modified by engineering works dating from the 1840's. Parts of PPB and the lower Yarra River channel have been artificially deepened since the 1850's to facilitate berthing and to accommodate larger vessels. Deepening the bay entrance by blasting limestone rock began in 1864 and continued until the 1950's. Subsequently, shipping channels in the south of the bay were established and maintained by regular dredging (South Channel, the Corio Bay and Yarra entrance channels) and dredge material grounds established.

The initial structures to service passenger and cargo trade were concentrated at Portsea, Port Melbourne and near Geelong, but to meet increasing requirements of recreational boating, mooring and launching facilities including large breakwater-defended marinas and canal estates are now widespread around Port Phillip. Seawalls, revetments, groynes and landfill have been constructed to prevent or reduce coastal recession and secure built assets. Since the mid 1970's beach re-nourishment using sand from land sources, nearshore dredging or low tide scraping has been applied to at least 30 sites around the bay. Extensive areas of the immediate backshore are now fundamentally reshaped by industrial and service facilities including the former salt works at Altona, Western Treatment Plant at Werribee, aerodromes at Point Cook and Laverton, and widespread residential subdivisions including bay-linked canal estates at Point Cook, Paterson Lakes and Martha Cove. Two groups of engineering structures are recognised: A: Engineered Effective and B: Engineered Ineffective.

A. Engineered Effective

Professionally designed and built to engineering standard include breakwaters, revetments and renourished beaches.

Engineered effective Brighton Pier and breakwater. (N. Rosengren, June 2019).

B. Engineered Ineffective

Structures of sub-standard design and/or construction or in disrepair. These include structures emplaced by individuals with title to high water mark such as along the northern coast of the Bellarine Peninsula and at Campbells Cove north of the Werribee River.

Examples of backshores at Campbells Cove behind built structures that are not to professional engineering standard. (N. Rosengren, June 2019).

Table E2: Sediment compartment barriers, including engineered groynes, training walls and marinas.

Location	Barrier
Half Moon Bay (St Leonards)	Headland
Geelong Eastern Beach	Engineered
Wyndham Cove (Werribee Sth)	Engineered
Williamstown	Engineered
Port Melbourne	Engineered
Sandringham Harbour	Engineered
Half Moon Bay – (Black Rock)	Headland
Mothers Beach - Mornington	Headland
Coral Cove	Headland engineered
Martha Point Beach/ Tassels Cove	Headland and engineered

References

Erikson LH, Hanes DM, Barnard PL and Gibbs AE (2007) Swash Zone Characteristics at Ocean Beach, San Francisco, California. Proceedings of the 30th International Conference, San Diego, California, USA, 3 – 8 September 2006. Edited by McKee Smith J. Coastal Engineering 2006. 909-921.

Wilson R and Miner AS (2006) Landslides on the Bellarine and Nepean Peninsulas, Victoria. Australian Geomechanics Journal 41(3). 75-84

Appendix F. Sediment Surveys and longshore transport

Sediment Surveys

Cardno (2017b) provided an analysis of beach renourishment that has occurred in PPB. This is summarised in Table E1. To complement this existing data on sediment size around the bay, an additional survey of sediments on PPB beaches was conducted in this study and is described herein.

Table F1: Summary of Beach Nourishment in PPB (from Cardno, 2017b). Entries in bold represent update/corrected information provided by DELWP.

Location	Completion Date	Length (km)	Volume in tonnes or (m3)*	Source	Nourishment Sand Size (mm)
Altona	Jun-82	0.3	(11,4000)	-	1.3-1.95
Altona	1989	-	(16,000)	-	1.3-1.95
Altona South	1990	-	(4,500)	-	1.3-1.95
Altona	2010	1	41,000	Gippsland Premium Quarries	Coarse
Altona	**2018**	**0.94**	**17,300**	**Quarried sand**	**Coarse**
Aspendale	Aug-79	2.8	(150,000)	-	1.01
Aspendale North	**2009**	**0.35**	**16,000**	**Gippsland Quarries**	**Coarse**
Blairgowrie	Jun-84	0.9	(33,000)	-	0.42
Blairgowrie	**2013**	**0.35**	**5,000**	**Relocated from spit near harbour**	**Fine/medium**
Brighton	**2014**	**0.35**	**25,000**	**Sandbars off foreshore**	**Medium**
Brighton - New St	Aug-87	1.1	(115,000)	-	0.7-0.94
Brighton - Park St	Jun-84	0.5	(40,000)	-	0.8
Carrum	**2017**	**0.3**	**5,000**	**Mouth of Patterson River**	**Fine**
Clifton Springs	2010	0.3	15,000	Burdetts, Langwarrin	Coarse
Clifton Springs	2014	0.3	12,8000	Quarry	Coarse
Dromana	**Nov 2014**	**0.28km east of Anthony's Nose, 0.38km west of pier**	**15,000**	**Quarry**	**coarse**
Elwood	Aug-83	0.8	(34,000)	-	0.2-0.7
Elwood	2011	0.8	36,000	Gippsland Premium Quarries	Coarse
Frankston	2014	0.7	15,000	Burdetts, Langwarrin	Coarse

Geelong (Rippleside)	Jun-84	0.5	(4,000)	-	0.23
Geelong (St Helens)	Jun-84	-	(3,000)	-	0.23
Geelong (Eastern Beach)	1984	0.4	(3,000)	-	0.23-1.1
Geelong (Eastern Beach)	1990	0.4	(15,000)	-	0.23-1.1
Hampton	1997	0.9	(156,000)	-	0.8
Hampton	**2018**	**0.8**	**22,000**	**Birdons near Sandringham Harbour**	**Fine/medium**
Mentone	Aug-78	1.8	(127,000)	-	-
Mentone	2007	0.8	15,000	Relocated from Mordialloc	medium
Mentone	**Aug 2012**		**15,000**	**Relocated from Mordialloc**	**coarse**
Middle Park	Aug-76	0.9	(120,000+)	-	0.25-0.33
Middle Park	2009	0.7	80,000	Offshore, dredged	mixture
North Aspendale	2009	0.35	16,000	Gippsland Quarries	coarse
North Aspendale	Aug-2012	0.4	10,000	Quarry	coarse
Mount Martha North	**2010**	**0.5**			
Parkdale	Aug-81	1.1	(65,000)	-	1.4
Parkdale / Mentone	2012	-	(15,000)	Relocated	-
Parkdale	**June 2019**	**0.2**	**8,000**	**Trucking sand from Mordialloc Beach**	**Coarse**
Portarlington	Nov-86	1.4	(35,300)	-	0.7
Portarlington	2010	0.4	15,000	Burdetts, Langwarrin	Coarse
Portarlington	**2012**	**0.4**	**16,000**	**Quarried**	**coarse**
Rosebud (west)	Aug-82	1	(27,000)		-
Rosebud	Jun-85	1.5	-	-	-
Rosebud	2010	0.16	3,000	Gippsland Premium Quarries	Coarse
Rosebud†	2014	-	2,064	Relocated from Rosebud foreshore	Medium
Rosebud West	**Dec 2019**	**0.3**	**9,400**	**Sandbars off foreshore**	**Medium**
Rosebud East†	**Feb 2020**	**0.35**	**13,300**	**Sandbars off foreshore**	**Medium**
Rye	Jun-75	1.8	(15,000)	-	0.73
Rye	1999	0.3	(10,000)	-	0.3
Rye	2010	0.14	3,000	Gippsland Premium Quarries	Coarse
Rye	2014	0.2	3,000	Relocated from Rye foreshore	Medium
Sandridge	1999	0.545	(76,000)		0.88

Sandringham	Aug-86	0.4	-	-	
Sandringham (Edward St)	1993	0.6	(16,000)	-	1.0+
Sandringham	2009	0.5	-	-	-
Sandringham	**2018**	**0.2**	**1,000**	**Birdons near Sandringham Harbour**	**Fine/ medium**
Sorrento	Jun-80	0.8	(40,000)	-	0.2
Sorrento East	**2014**	**0.4**	**9,000**	**Sandbars off foreshore**	**Fine/ Medium**
Sorrento West	2016	0.22	7,000	Sandbars off foreshore	Fine/medium
St Kilda	Jun-82	0.7	(70,000)	-	0.16-1.6
St Kilda	1984	0.7	(2800)	-	0.16-1.6
St Leonards	**2014**	**0.3**	**4,250**	**Burdetts, Langwarrin**	**Coarse**
Watkins Bay	1986				
West Rosebud	Aug-82	1.4	-	-	-
Williamstown	Jun-82	0.6	(29,000)	-	1.25

* Volumes in m^3 from Cardno (2017b)

† May be erroneous

Samples were collected at the mean tide level (MTL) or mid-tide line on a low or falling tide when mid-tide line was sub-aerial. The sample point was defined by taking a clinometer slope reading from mean high tide mark—recognized by strand—to the probable low water line position (using tide tables corrected for each location) and approximating the mid-tide line. Beaches with a stepped profile—a break or marked change of slope at mean water level coinciding with a change in grain size—coarser sediment concentrated at or below MTL and finer sediment above MTL (Figure F1) were sampled above and below the slope break.

Figure F1: Stepped beach profile with change in grain size at mid water level (Point Cook).

Samples were taken by cleaning and levelling the beach surface and excavating a test pit 300 mm x 300 mm pit to 400 mm below the surface. Approximately 700 g sample was extracted with a hand trowel at 100 mm below the smoothed surface. Gravel, larger granules, whole shells and shell fragments were removed by hand and samples placed in snaplock plastic bags. The sample holes were backfilled. At 13 sites the variation in grain size across the intertidal range was such that an additional sample was collected at the high tide beach to provide a more representative spread. Some beaches have coarser, back-beach sediments (towards high tide level) resulting from stranded storm deposits.

Many beaches around Port Phillip have been artificially renourished by sand imported from terrestrial, alongshore and offshore sources. Much renourishment has been to provide recreation space and has been largely placed on the area between high and low tide lines, leading to marked discontinuities in grain size, beach gradient and often colour (Figure F2).

Non-cohesive particle size analysis was undertaken in the Environmental Geoscience Laboratory of the Department of Ecology, Environment and Evolution at La Trobe University using a Malvern Mastersizer 2000 particle size analyser. Laboratory procedures as specified by the operations manual for the Mastersizer 2000 (Malvern Instruments Ltd Mastersizer 2000 User Manual MAN0384 Issue 1.0 March 2007) for sample preparation, operation, output and interpretation of the results were undertaken by a post-graduate student experienced in the use of the machine. Where there was a sample collected but no sediment size information provided the location is defined as “no data”. In some locations where beach nourishment was undertaken, the sand size was categorised qualitatively as fine, medium or coarse sand rather and by D50. Results of the sediment sampling are shown in Figures F3 to F10.

Figure F2: Marked discontinuity with renourished beach sand overlying wrack (dark layer) and older beach deposit (Altona).

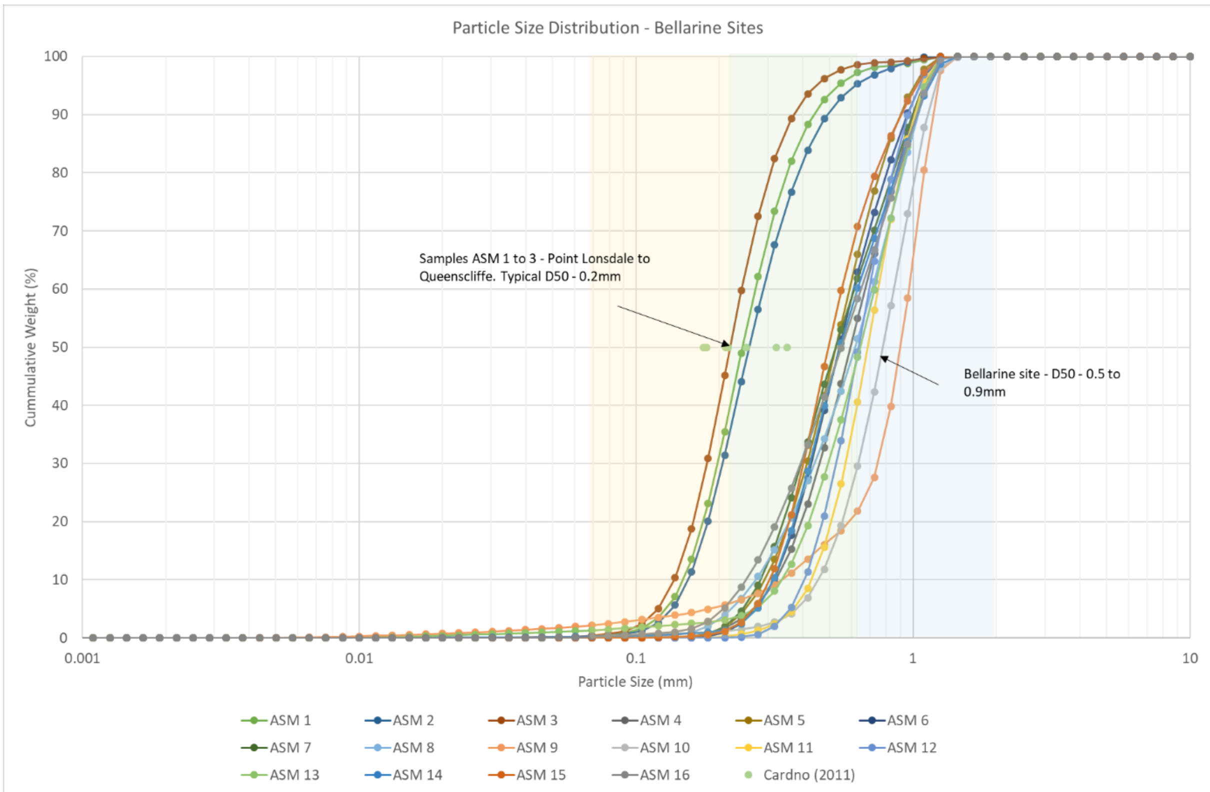

Figure F3: Particle size distribution for samples taken at Bellarine sites.

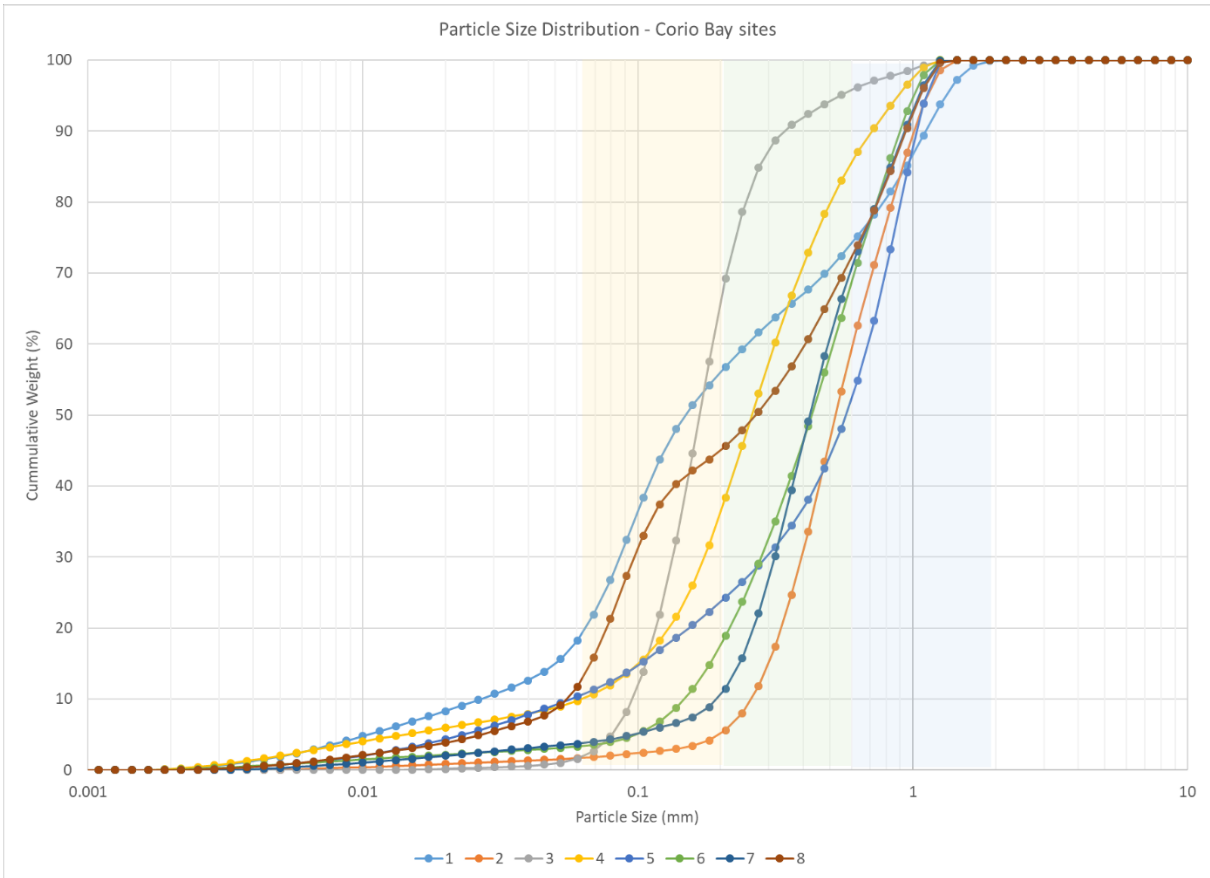

Figure F4: Particle size distribution for samples taken from Corio Bay sites.

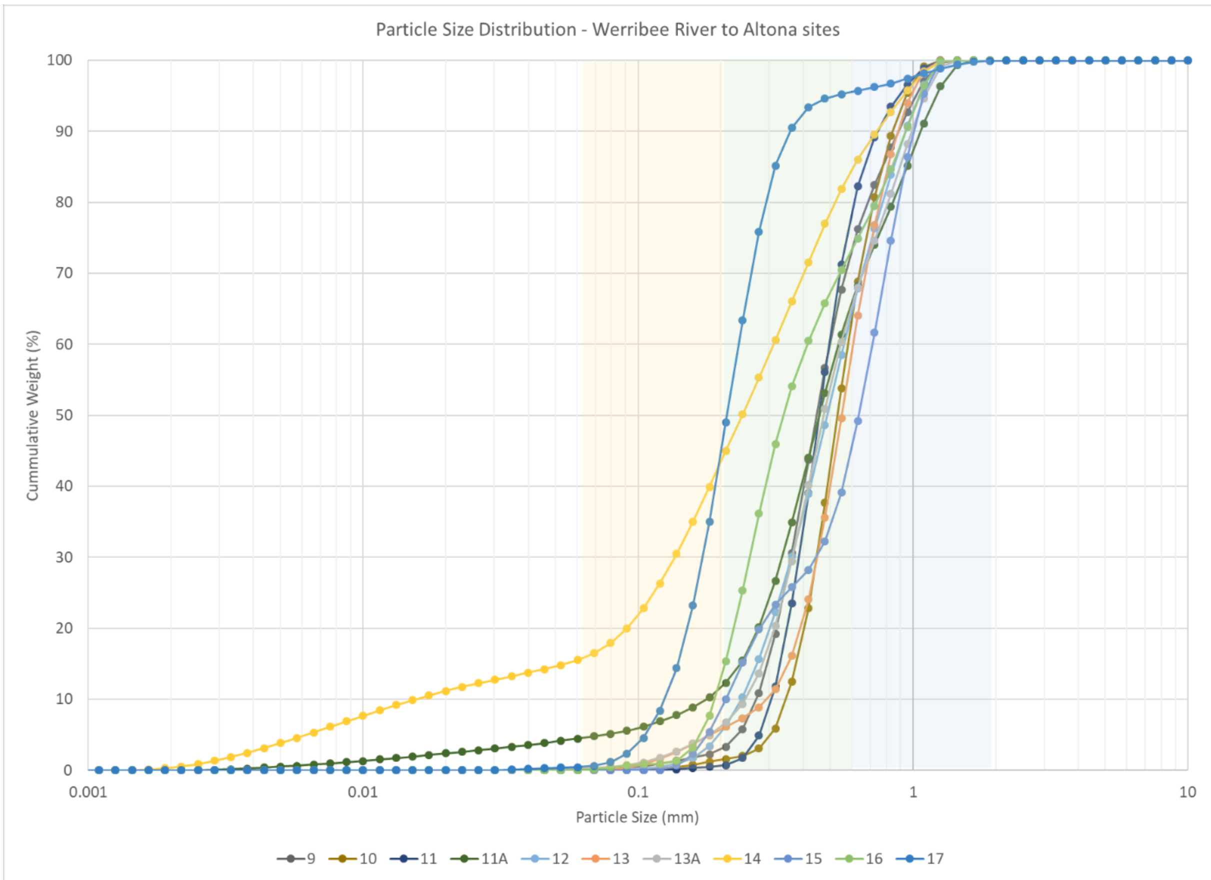

Figure F5: Particle size distribution samples taken from Werribee to Altona sites.

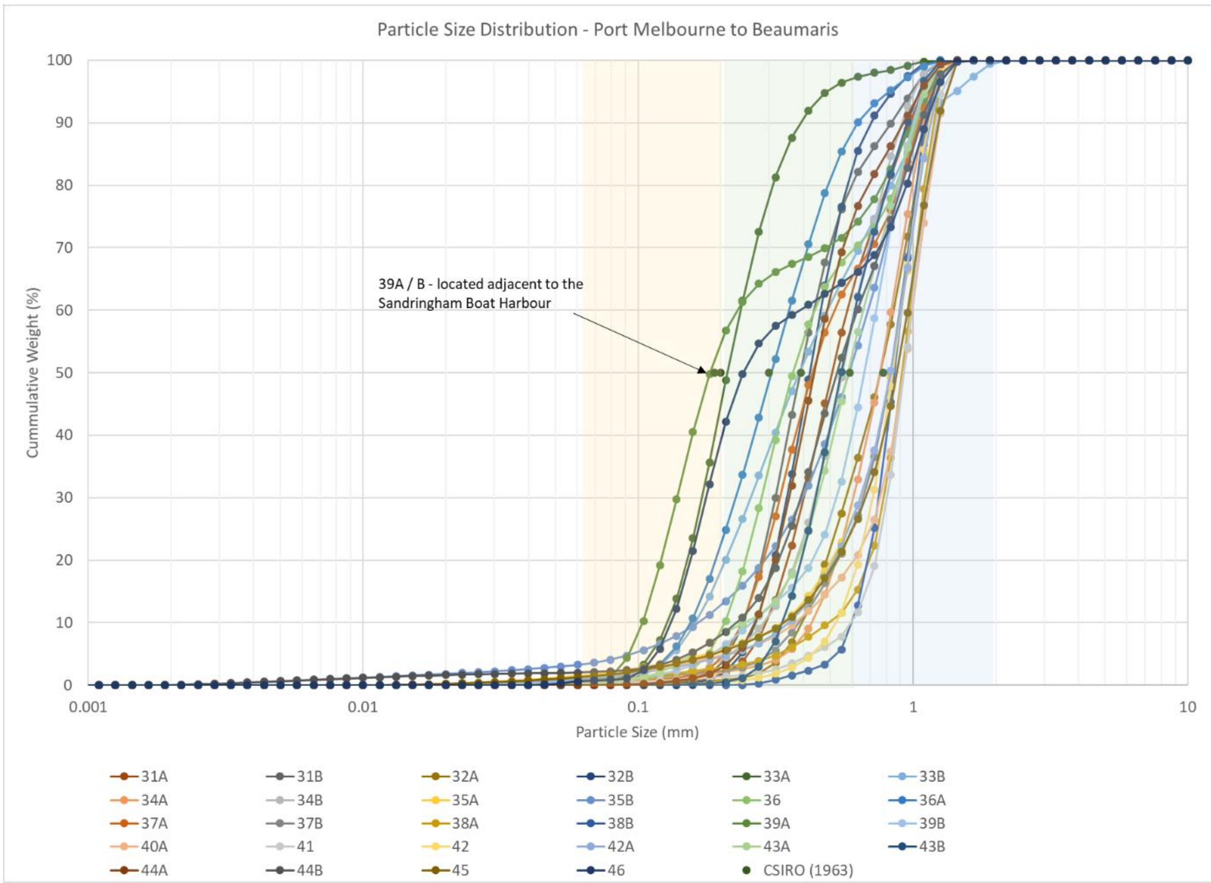

Figure F6: Particle size distribution for samples taken from Port Melbourne to Beaumaris sites.

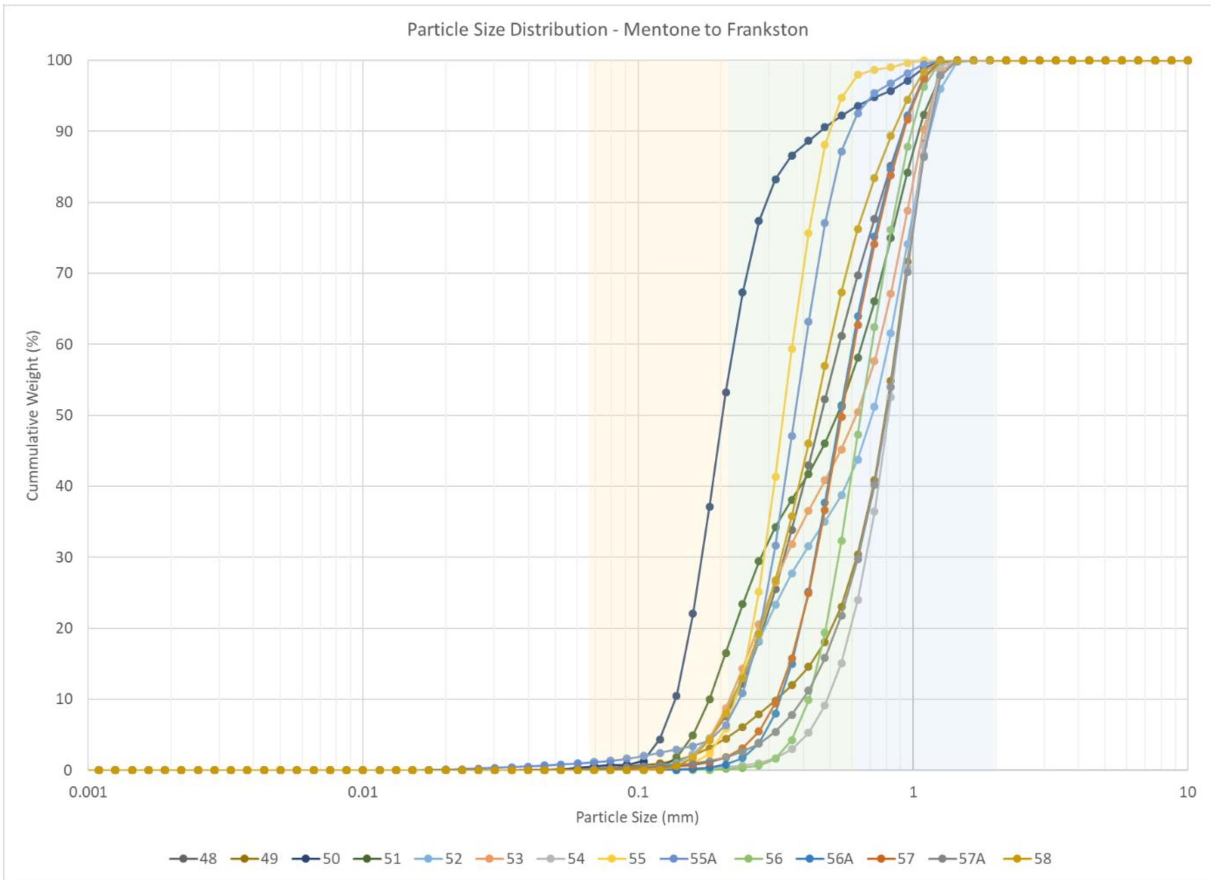

Figure F7: Particle size distribution for samples taken from Mentone to Frankston sites.

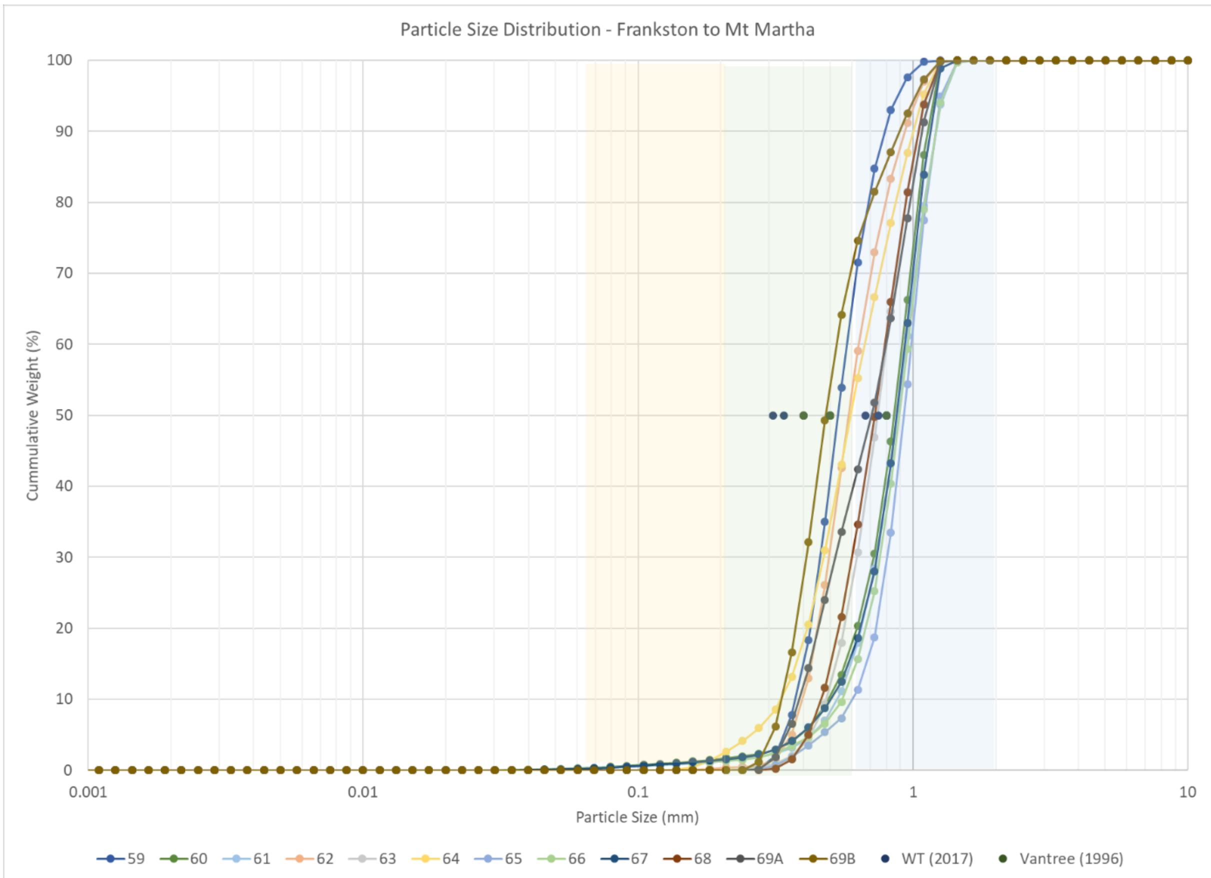

Figure F8: Particle size distribution for samples taken from Frankston to Mt Martha.

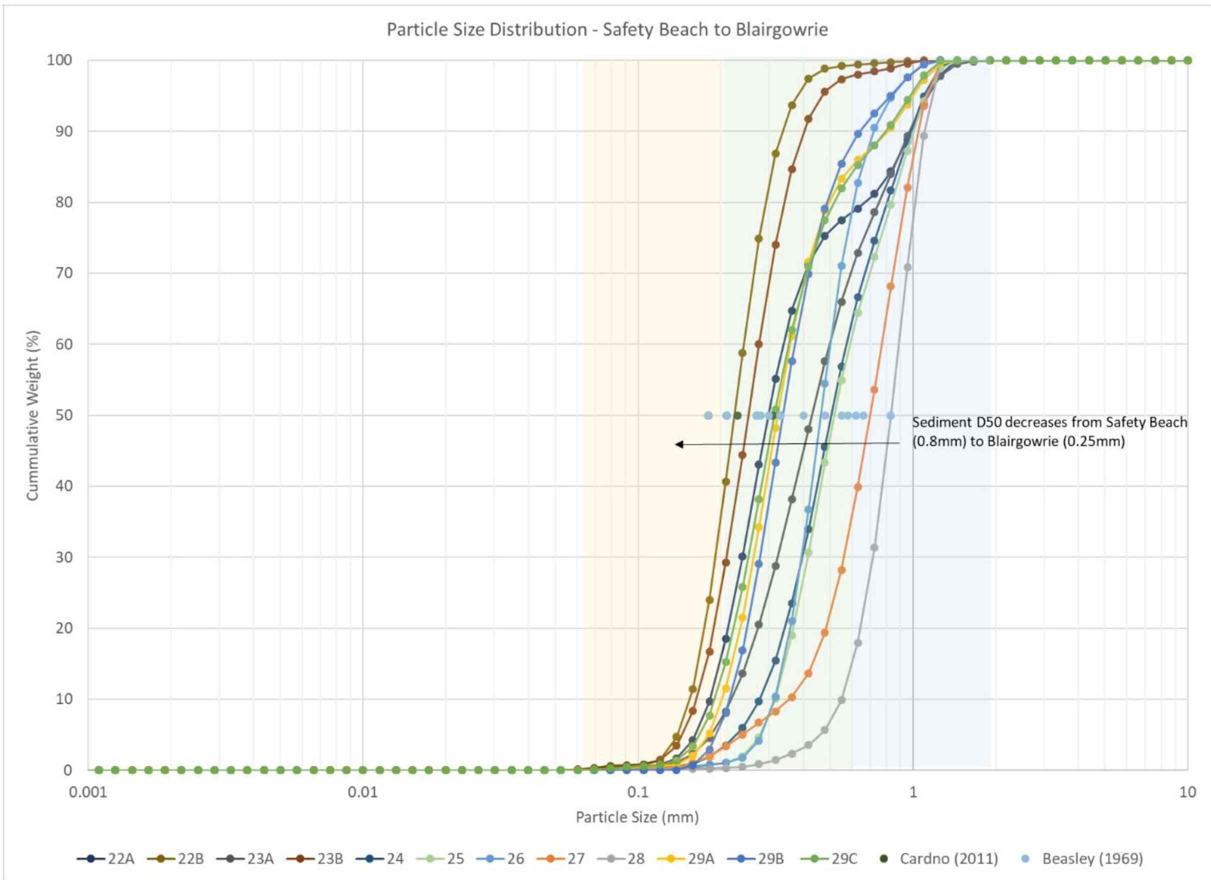

Figure F9: Particle size distribution for samples taken from Safety Beach to Blairgowrie.

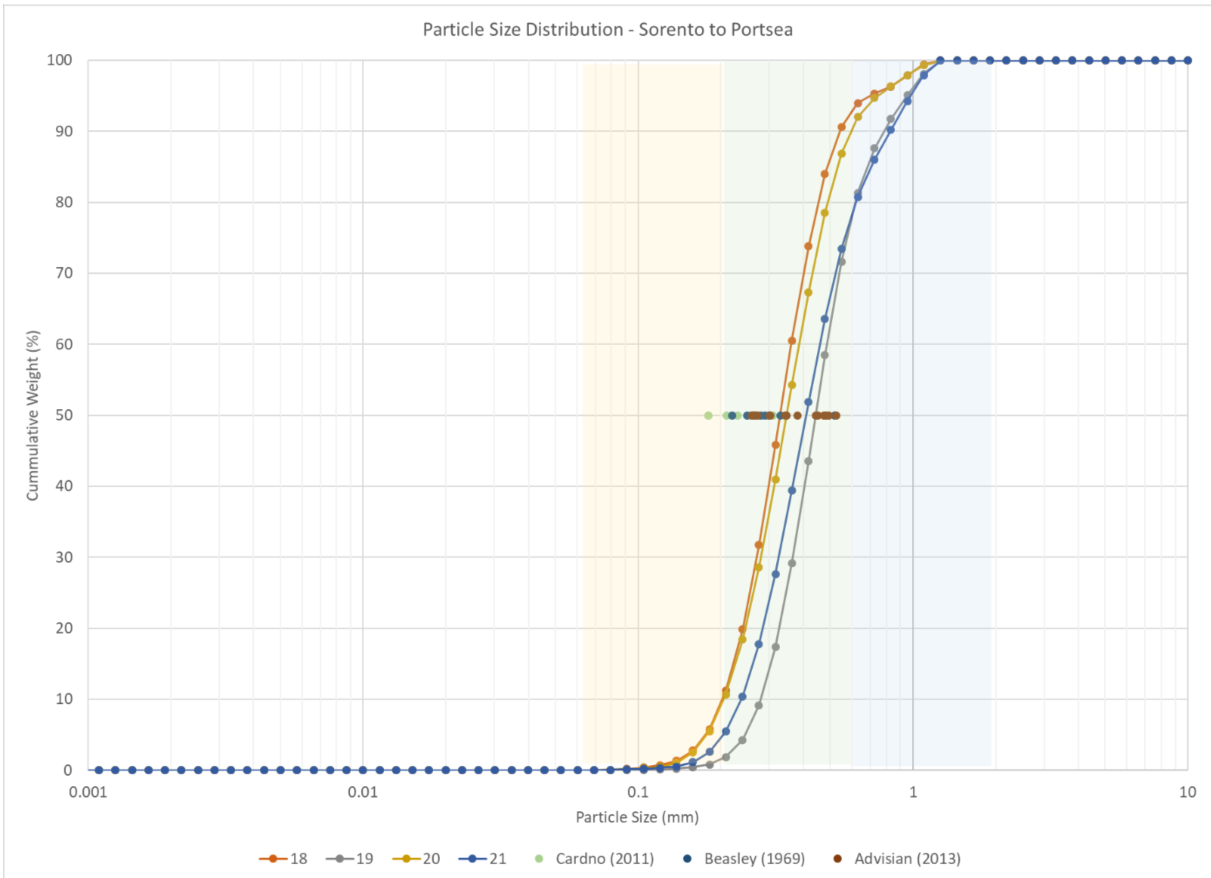

Figure F10: Particle size distribution for samples taken from Sorento to Portsea.

Historical sediment samples shown in Figure F11 have been collated from several sources (CSIRO, 1963; Beasley, 1969; Vantree, 1995; Cardno, 2011; Advisian, 2016; Water Technology, 2017b). The mean grain size (D50) for the historical and present surveys are presented in Figures F12 and F13. A sector scale comparison of mean grain size (D50) of the historic and the new PPBCHA 2019 survey is presented in Table F2. For each geomorphic consistent sector, all historic and new survey points within 120 m of the shoreline were compared (Figure F14) to investigate changes over time (Figure F15). Typically, only one (but up to three) historical sediment surveys were available per sector (Table F2). Historical reports of a range of D50 (Table F1) were not used in the comparison analysis (Table F2). Differences between the historic and 2019 grain sizes arise due to sample location and time of survey, where sediment size and composition varies across-shore, alongshore and vertically along a beach sector and also changes seasonally, annually or over the longer term. Considering a random sample of many locations, on average the sediment comparison should show no change. However, Table F2 shows that many beaches around the bay have increased in grain size. One possible cause for the increase in D50 is re-nourishment practices, where having larger grain sizes on a beach should stabilise it. Of the beaches where the data shows a decrease in D50, two are well nourished beaches (Aspendale and Middle Park beach), where the recorded historic D50 (Table F1) were likely the source material grain size D50 prior to laying the sand on the beach rather than a well-mixed beach sample. Martha Point beach stands out as a site with finer grain sizes in the 2019 survey, likely influenced by the Martha Cove development and Bluff stabilisation.

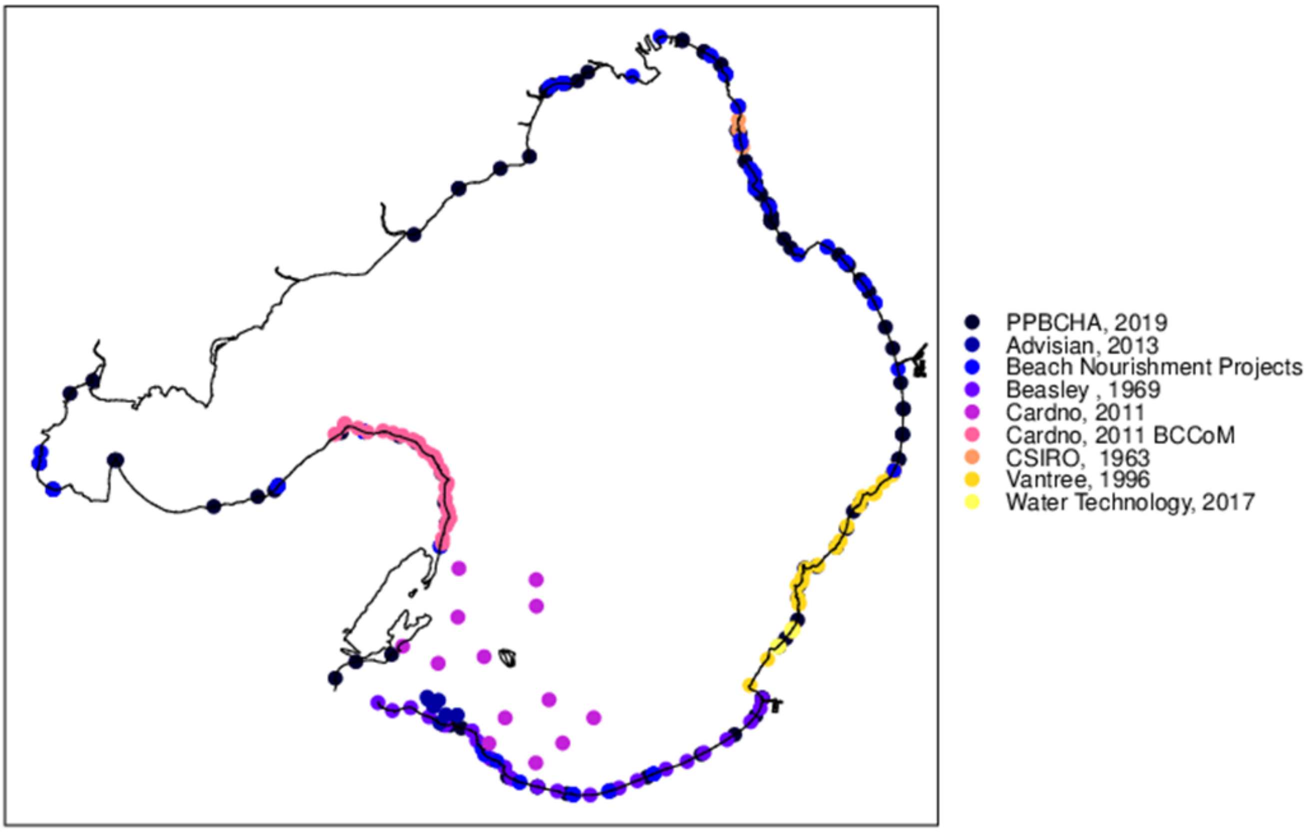

Figure F11: field studies of beach sediments.

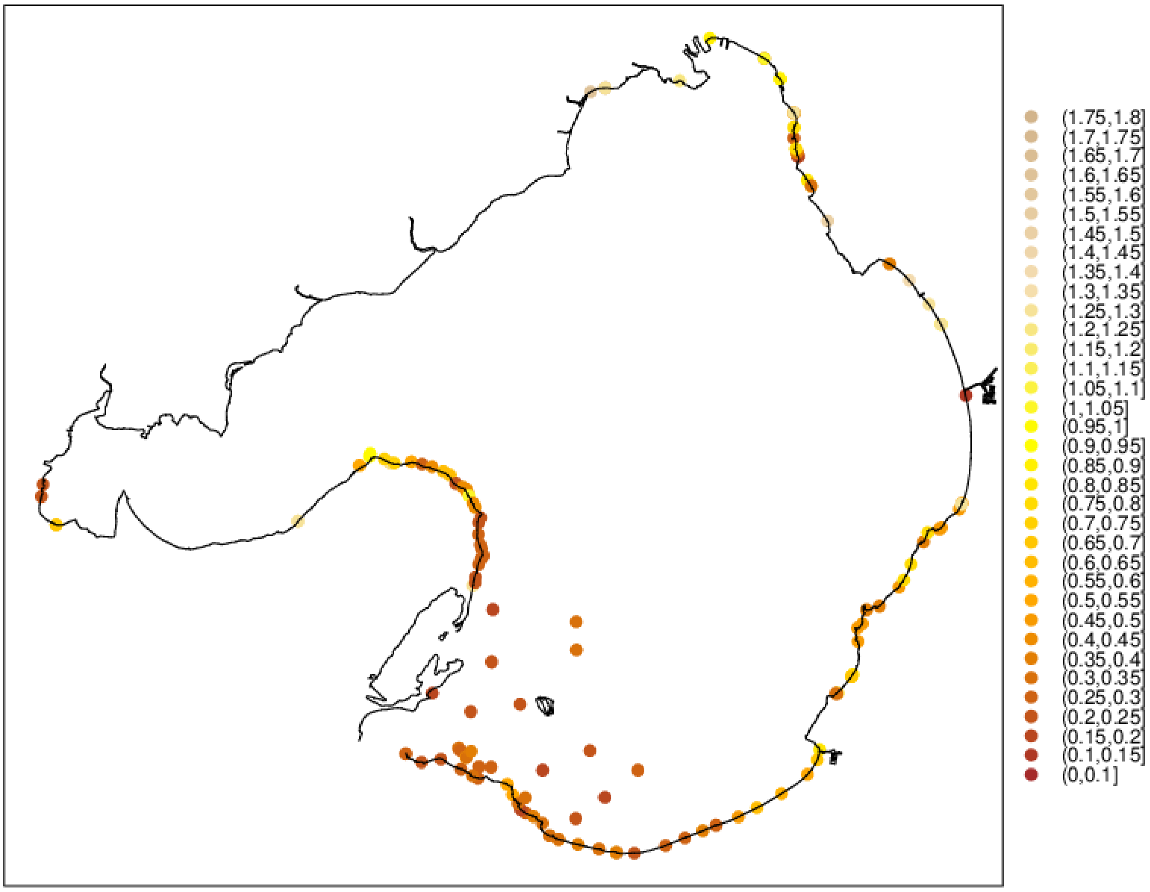

Figure F12: Historic sediment field surveys of mean grain size (D50) in mm.

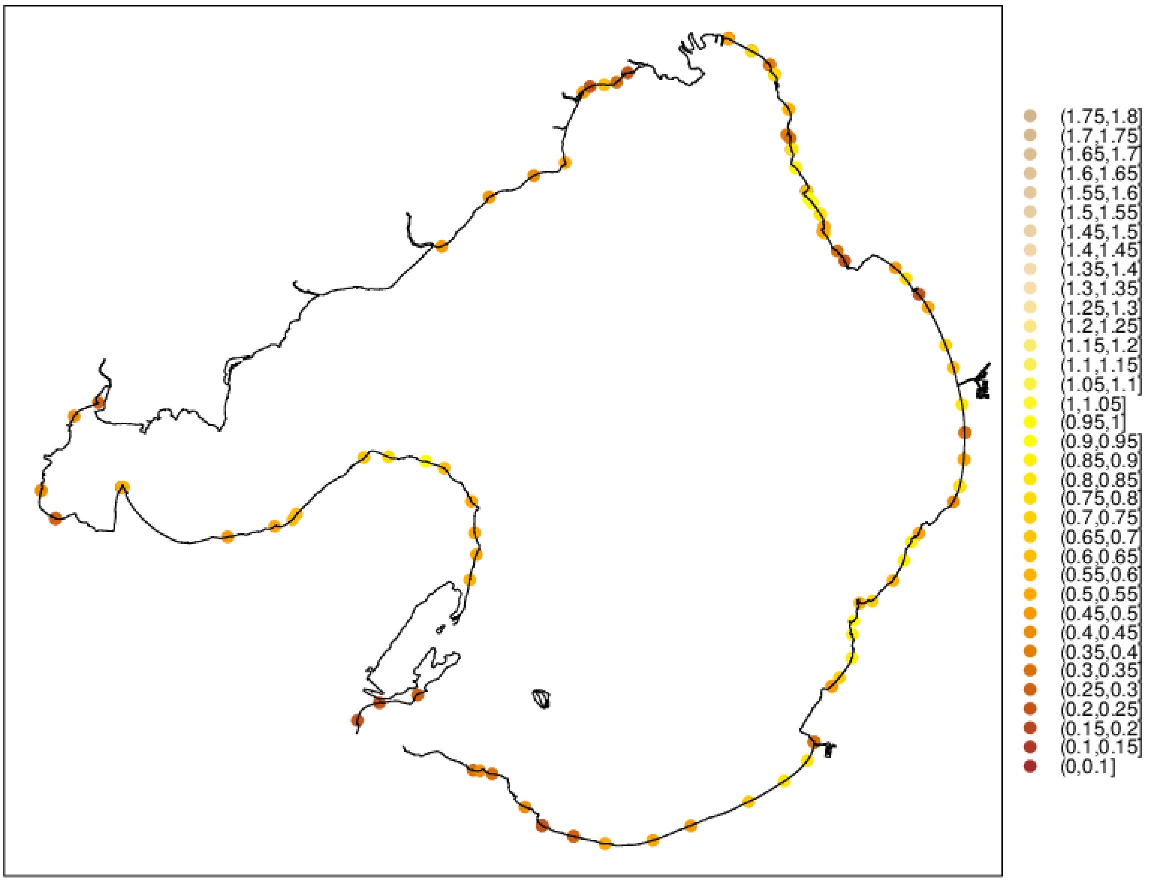

Figure F13: 2019 PPBCHA sediment field surveys of mean grain size (D50) in mm.

Table F2: Compartment comparison of past sediment sample mean grain size (D50) to presented PPBCHA samples. Location names include the intertidal composition. Values are means of all points within the compartment. All sediment diameters (D10, D50 and D90) have units in mm.

Location: Inertial composition	Sector	Past Sample Years D50 (mm)		PPBCHA D50 (mm)	Difference (mm)	PPBCHA D10 D90	
Bell Parade: sand and fine gravel	24	2011	0.24	0.59	0.35	0.32	1
St Leonards Boat Ramp: sand and fine gravel over rock	26	2011	0.28	0.53	0.25	0.29	0.9
St Leonards Esplanade: sand	29	2011	0.3	0.54	0.24	0.31	0.95
Salt Lagoon: sand	30	2011	0.26	0.54	0.28	0.31	0.95
Hood Bight: sand	32	2011	0.43	0.52	0.09	0.28	0.99
Coach Road: sand over rock	38	2011	0.44	0.62	0.18	0.27	1.04
Calhoun Road: gravel and sand over rock	39	2011	0.65	0.76	0.11	0.31	1.1
Bellarine Bayside Holiday Park: sand	44	1986, 2011	0.71	0.78	0.07	0.46	1.12
St Helens: sand	103	1984	0.23	0.5	0.27	0.1	0.56
Port Melbourne: sand	269	1999	0.88	0.52	-0.36	0.3	0.91
Point Ormond & Elsternwick: sand	275	1963	0.39	0.72	0.33	0.26	1.08
Middle Brighton foreland: sand	280	1963	0.3	0.37	0.07	0.21	1.04
Brighton Beach north: sand	283	1963, 1984	0.7	0.63	-0.07	0.32	1.08
Brighton Beach Bathing boxes: sand	284	1963	0.2	0.63	0.43	0.32	1.08
Green Point & Brighton beach: sand	285	1997	0.8	0.89	0.09	0.55	1.14
Mordialloc Bay St: sand over rock	312	1981	1.4	0.8	-0.6	0.32	1.11
Frankston south: sand	335	1996	0.5	0.44	-0.06	0.22	0.85
Canadian Bay north: sand over rock	343	1996	0.8	0.53	-0.27	0.38	0.78
Canadian Bay Beach: sand over rock	344	1996	0.4	0.53	0.13	0.38	0.78
Moondah Beach: sand over rock	350	1996	0.8	0.88	0.08	0.53	1.2
Sunnyside Beach: sand over rock	358	1996	0.5	0.58	0.08	0.4	0.93
Mothers beach: sand	373	1996	0.4	0.59	0.19	0.33	1
Fishermans Beach car park: sand	385	1996	0.5	0.93	0.43	0.61	1.19
Mount Martha Kilburn Gve: sand	413	1996, 2017	0.48	0.6	0.12	0.36	0.99
Mount Martha South: sand	414	1996, 2017	0.48	0.6	0.12	0.36	0.99
Martha Point beach: sand	420	1969	0.83	0.32	-0.51	0.2	0.75
Safety Beach central: sand	425	1969	0.66	0.82	0.16	0.58	1.08
Dromana Beach pier: sand	429	1969	0.58	0.83	0.25	0.55	1.1
Anthony's Nose: sand	431	1969	0.62	0.7	0.08	0.36	1.05
Rosebud beach north: sand	432	1969	0.38	0.7	0.32	0.36	1.05
Rosebud Beach south: sand	434	1969	0.29	0.46	0.17	0.31	0.72

Location: Inertial composition	Sector	Past Sample Years D50 (mm)		PPBCHA D50 (mm)	Difference (mm)	PPBCHA D10 D90	
Tootgarook: sand	436	1969, 1975, 1999	0.33	0.52	0.19	0.32	1
Blairgowrie north: sand	446	1969	0.4	0.34	-0.06	0.39	0.75
Blairgowrie Marina: sand	454	1969	0.33	0.18	-0.15	0.19	0.82
Sorrento Front Beach: sand	462	1969, 1980	0.24	0.41	0.17	0.24	0.83
Portsea Front Beach: sand over rock	479	1969	0.26	0.33	0.07	0.2	0.55

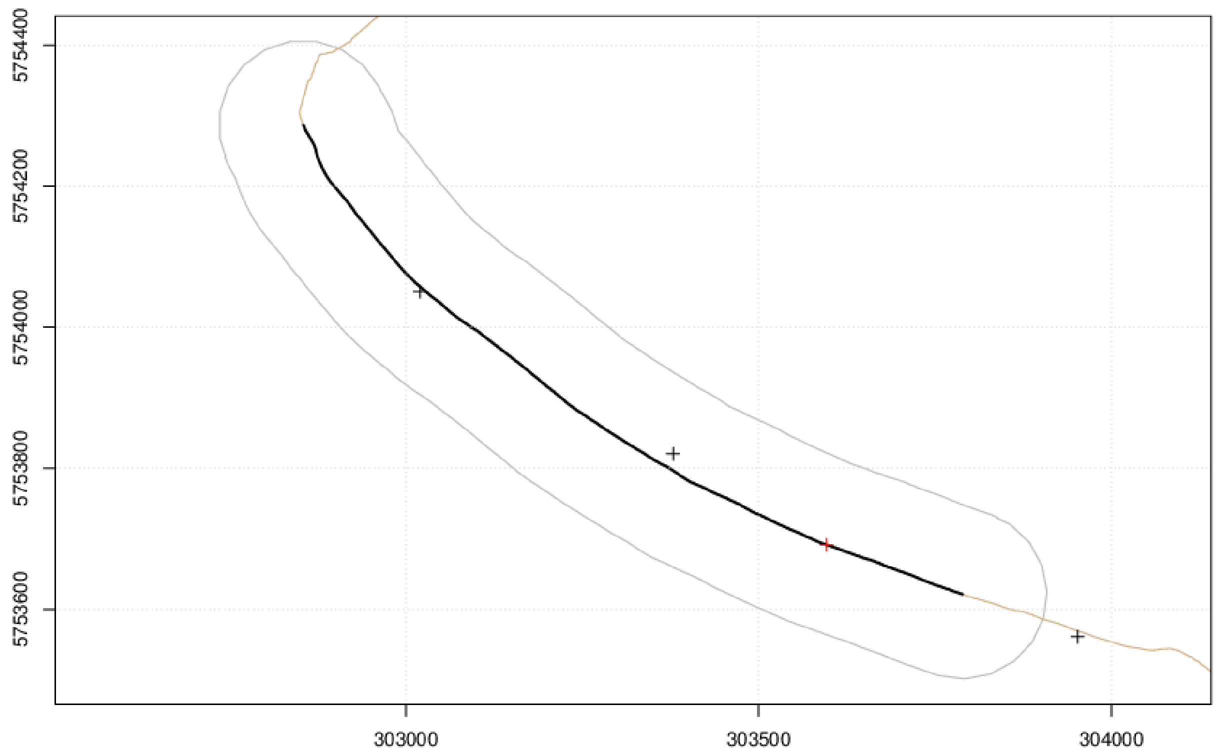

Figure F14: Example spatial comparison of surveys at Sorrento Front Beach (compartment sector 462). Grey line is the 120 m buffer search zone, tan line is the shoreline, black “+” are historic surveys, red “+” is the 2019 PPBCHA survey point.

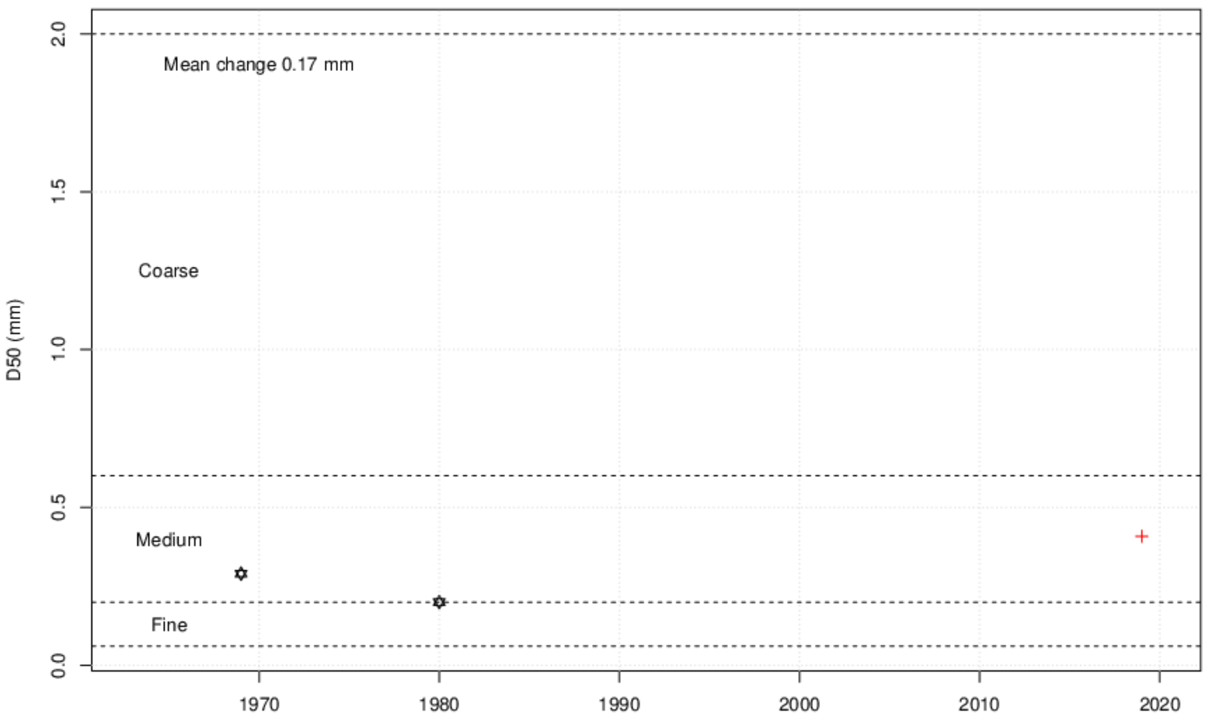

Figure F15: Example time series plot of mean grain size (D50) surveys at Sorrento Front Beach (compartment sector 462). black "*" are historic surveys, red "+" is the 2019 PPBCHA survey point.

Longshore Sediment Transport Analysis

The primary driver of beach morphology in PPB is storm waves but for much of the bay seasonal variability is determined by longshore sediment transport. Beaches adjust in profile and planform according to drift direction and volumes of sediment in transit. The timing and direction of these movements varies around the bay. The most marked and consistent changes occur between Rye and Brighton where summer southerly and south-westerly winds (November to April) produce northward drifting. From May to October a reversal of wind direction to north to northwest results in a winter southerly drift (Bird, 2011). Drift directions and timing are more complex for the Bellarine Peninsula and from Geelong to Altona-Williamstown.

Longshore transport pathways inform the identification of locations which could potentially gain sediments or be susceptible to erosion. A conceptual model of longshore transport around PPB (Bowler, 1966; Bird, 2010), informed by the wind regime and the locally observed seasonal rotation of the sand build-up along groynes, headlands and river entrances, provides insight into sediment movement around the bay (Figure F16).

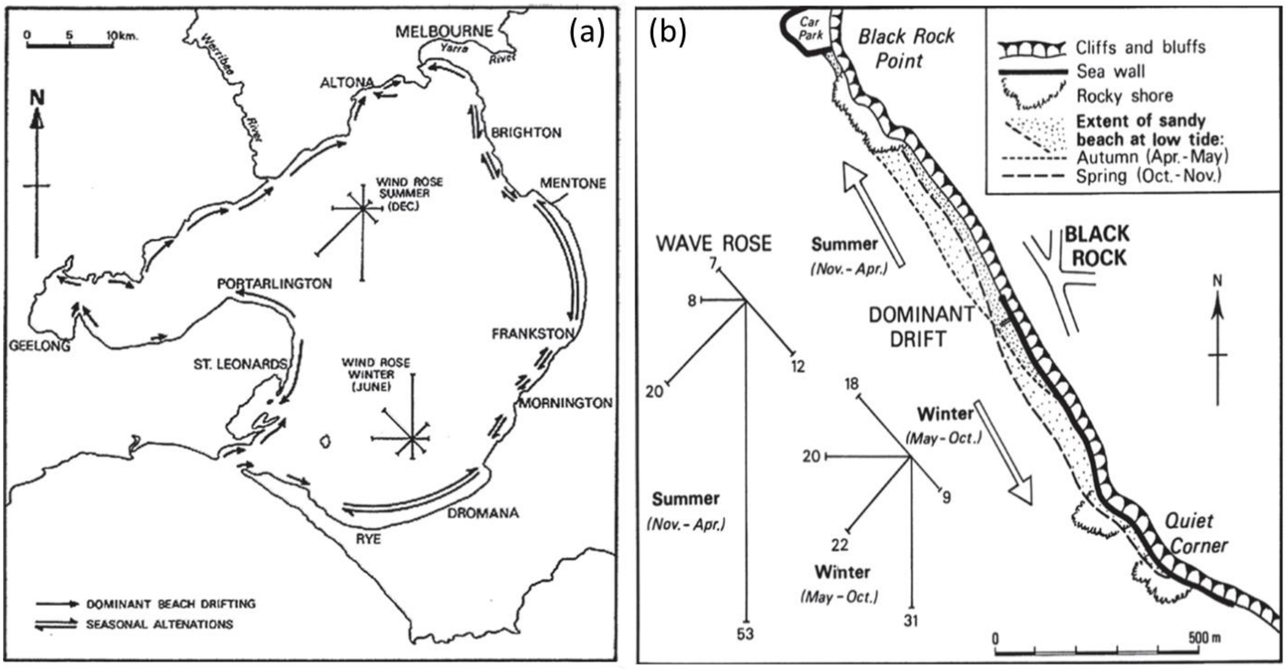

Figure F16: from Bird (2010) (a) Patterns of beach drifting on the shores of PPB, resulting from wave patterns determined by the summer and winter wind regimes (b) close up of Black Rock.

In recent studies, numerical modelling has been used to explore the seasonal transport reversal and interannual transport at specific locations on the eastern side of the bay (Water Technology, 2017, 2018) and the Bellarine (Cardno, 2015). Here, longshore transport potential is estimated for the entire bay from wave and current data from the SCHISM model (Chapter 8) in the CERC equation (CERC U. S. Army corps of Engineers, 1984) and the NMB-LM equation (O'Grady et al., 2019a). The significant wave height H_s and peak (dominant) wave direction were extracted at grid nodes along the 4 m depth contour (AHD) as input to the CERC Equation;

$$Q_w = K_s H_{sb}^{5/2} \, sin(2\theta_i)/2, \ -\frac{\pi}{4} \leq \ \theta_i \leq \frac{\pi}{4}$$

$$K_s = \frac{0.023 g^{1/2}}{(s-1)},$$

where g = 9.8 m/s^2 is acceleration due to gravity and s = 2.6 is the ratio of sediment and water. H_{sb} is assumed to have the value of the H_s at the 4 m depth contour and θ_i is the incident angle is calculated to the normal angle to the 4 m contour. The NMB-LM also used the longshore current data (U_l) from SCHISM,

$$Q_{wu} = D_1 K_s H_s^{D_2} \frac{sin(2\theta_i D_3)}{2} \ + D_4 U_l |U_l| \left| D_1 K_s H_s^{D_2} \frac{sin(2\theta_i D_3)}{2} \right|,$$

where U_l is the longshore current velocity, in the direction clockwise along the 4 m contour and $D_{i=1:4}$ = {0.30625, 5.65716, 0.07662, 2.77079}. The NMB-LM semi-empirical model is based on TELEMAC model simulations for Ninety Mile Beach in eastern Victoria. Both equations only consider the hydrodynamic transport, and do not consider the available sediment budgets.

Both equations consider only the hydrodynamic driven transport, and do not consider the available onshore/offshore sediment budgets or specific site sediment characteristics, which if available, would facilitate the direct prediction of shoreline movement.

Annual longshore transport estimates (m^3/day) for the CERC and NMB-LM models are shown in Figure F17 and F18, respectively. Both models predict a similar pattern of transport. The largest transport occurs at the high wave energy ocean entrance to PPB and along the east coast which are exposed to the largest waves. Along the low wave energy west coast of PPB, the NMB-LM model which includes the effects of longshore storm tide currents is in agreement with the CERC estimates, which only include wave effects, suggesting waves are the dominant driver of longshore transport in this region.

The seasonal alterations in longshore transport are shown in Figure F19 and are consistent with the conceptual models of transport for the eastern side of the bay from Bird (2010), (Figure F15) although model estimates indicate large anticlockwise transport near Frankston South. The modelling also indicates that there are sections of south-westerly transport along the Point Wilson-Point Cook coast, which are not evident in the conceptual model. At the very local scale, the model estimates of the seasonal reversal of sediments are asymmetric and are strongly influenced by local seabed undulations and embayment features (Figure F20).

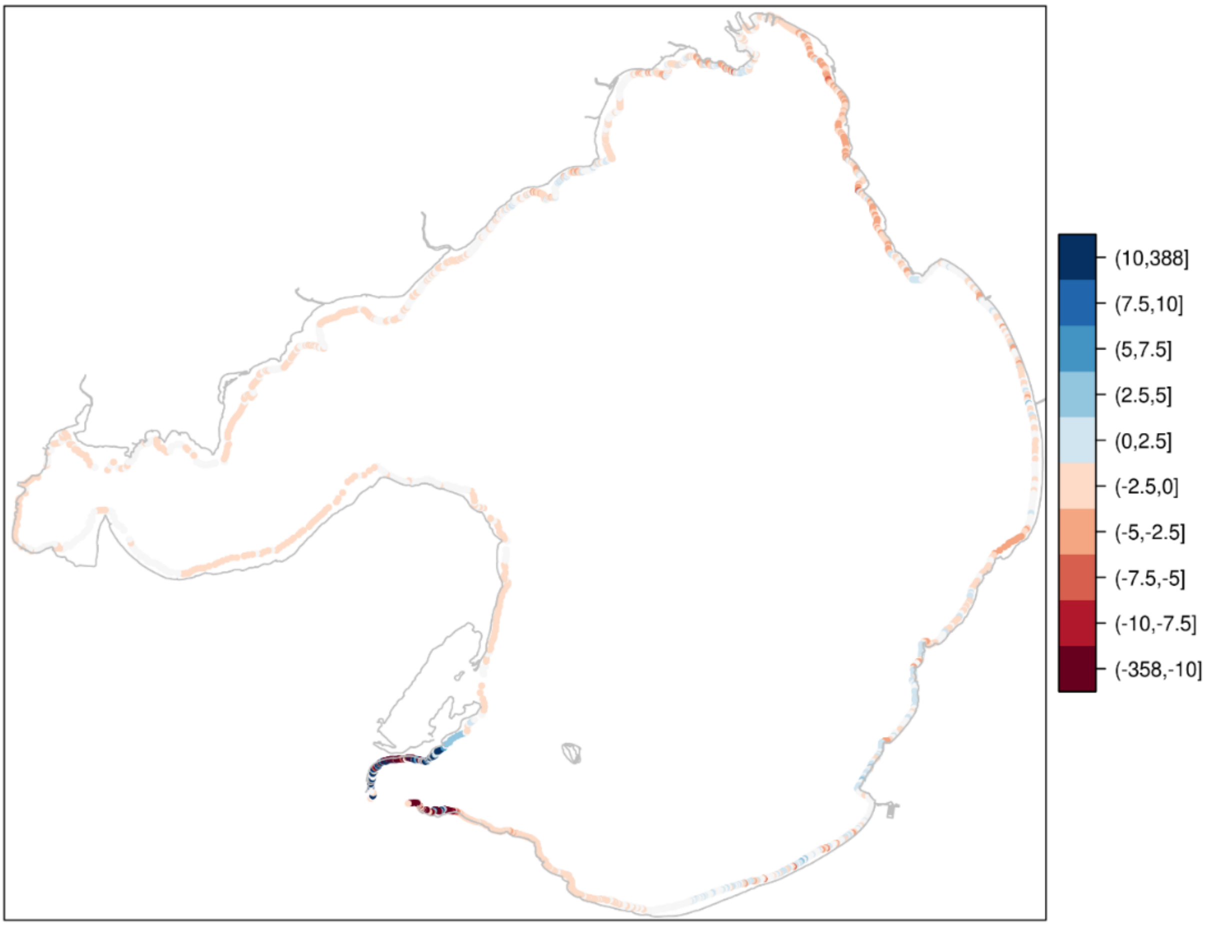

Figure F17: CERC annual net longshore transport potential (m^3/day). Blue values are clockwise net longshore transport and red values are anticlockwise net transport around the bay.

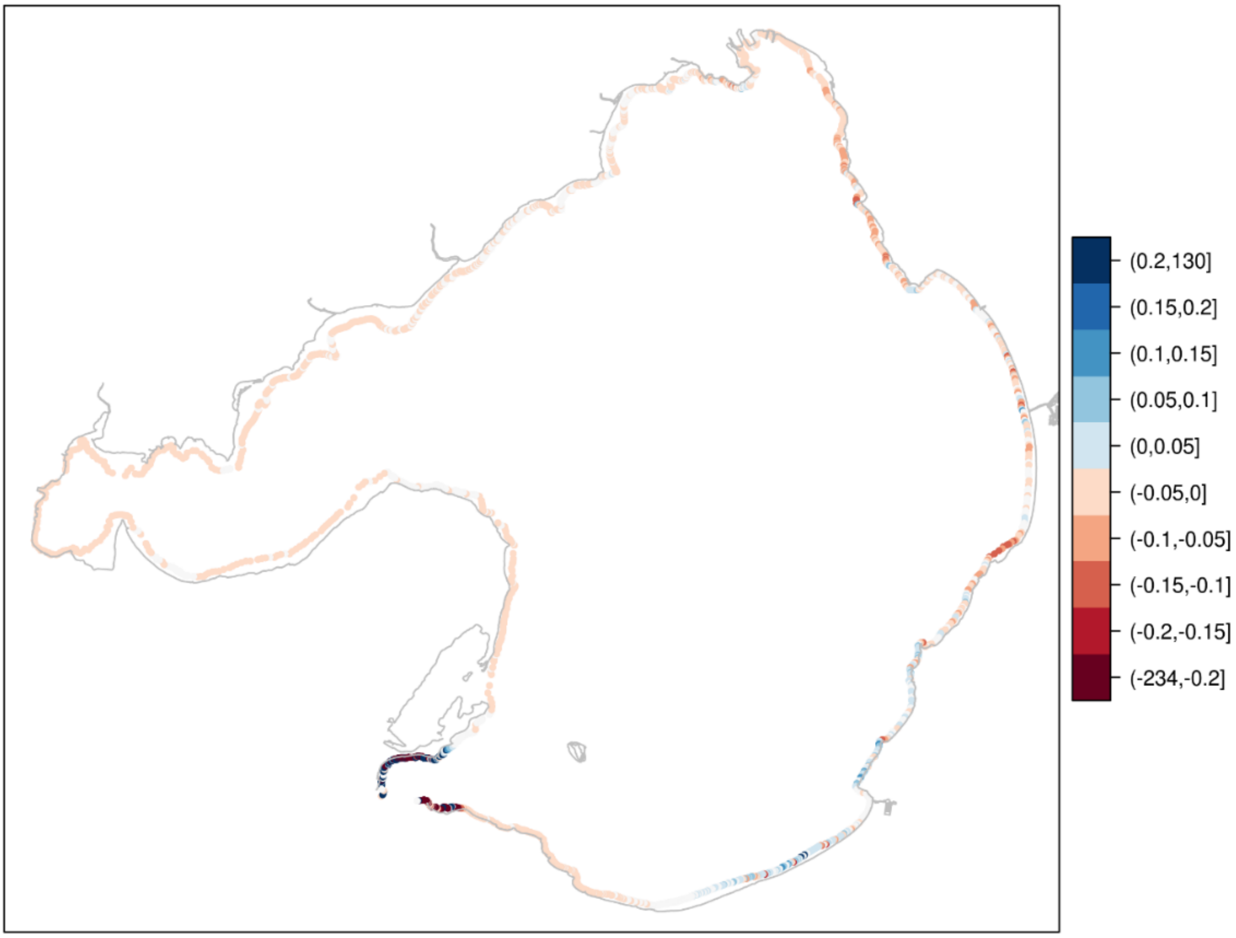

Figure F18: NMB-LM annual net longshore transport potential (m^3/day). Blue values are clockwise net longshore transport and red values are anticlockwise net transport in the direction from Point Lonsdale around the entire bay to Point Nepean.

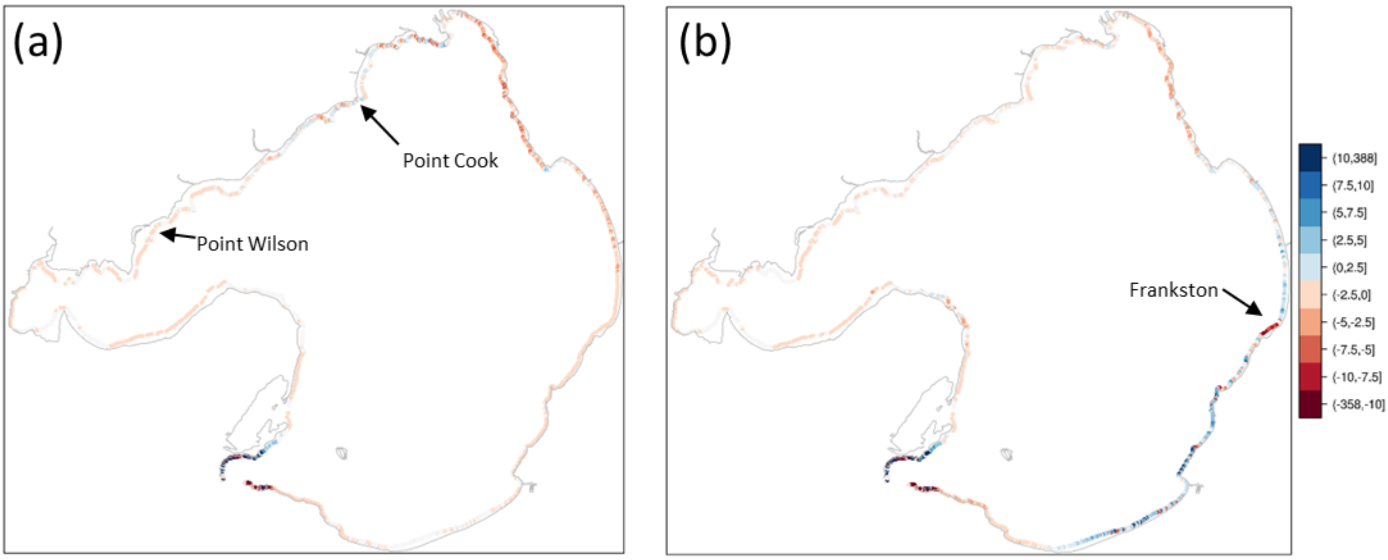

Figure F19: Seasonal longshore transport potential for the CERC equation (m^3/day). Left is summer (DJF) and right is winter (JJA). Blue values are clockwise net longshore transport and red values are anticlockwise net transport around the bay.

Figure F20: Modelled seasonal longshore transport vectors at Black Rock. (a) CERC model estimate, (b) NMB-LM. Blue arrows show the winter (JJA) longshore transport direction, red arrows indicate where the summer (DJF) transport is different to the winter transport direction. See Figure F15 for conceptual model comparison.

The convergence and divergence of longshore sediments are estimated by the amount of sediment leaving a model grid point and entering from the two neighbouring model grid points in the clockwise longshore direction. Here the closure depth of transport is uncertain, and sediment budgets are not conserved, therefore exact estimates of sediment accumulation cannot be determined, but the influence of waves convergence and divergence may indicate where coastlines are likely to undergo erosion or accretion (Hemer, 2009). The convergence and divergence estimates were found to be sensitive to small fluctuations in the coastal orientation in neighbouring coastal points, so a 21-point averaging filter was applied to consolidate a larger pattern of the convergence or divergence potential (Figure F21). Smoothing can lead to a reduced sediment flux where there are strong gradients in neighbouring model grid points (Roelvink et al., 2020). The model replicates known locations of sediment build up, e.g. at the entrances to Swan Bay and the Jawbone Marine Sanctuary shallows. The model also indicates locations of longshore sediment deficit along the Seaholme coast and sections of the Bayside (Sandringham and Brighton) and Mornington-Mount Martha coast. It is worth emphasising that the modelling only considers the hydrodynamic transport and that geomorphic interpretation is required to further consider the properties of the available onshore/offshore sediment budgets and the effectiveness of renourishment and engineered structures.

It is intuitive that the SLR simulations in this study, which indicate increased wave heights at the coast, will directly increase the relative estimates of longshore transport. While future projected wind changes are small and uncertain (VCP19), more detailed investigation into changes in wave directions would provide insight into changing patterns of longshore transport around the bay.

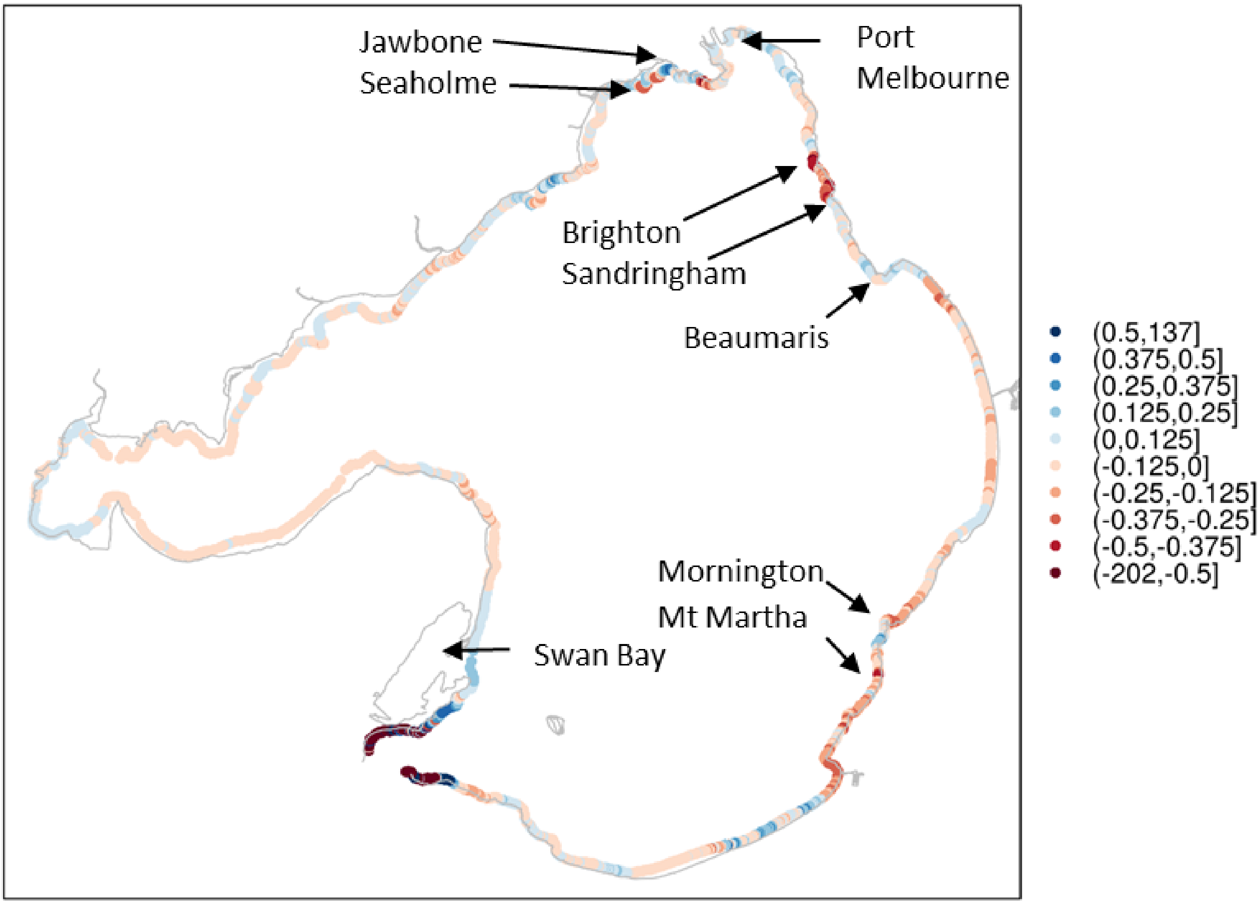

Figure F21: CERC annual net longshore convergence/divergence (m^3/day). Red points indicate potential divergence of sediments, blue points indicate convergence.

References

Advisian (2016) Portsea Front Beach Wave Modelling and Monitoring Investigation. Department of Environment, Land, Water and Planning, Cornell University Press. doi:10.7591/9780801456329-006.

Beasley AW (1969) Beach sands of the southern shore of Port Phillip Bay, Victoria, Australia. Memoirs of the National Museum of Victoria 29, 1–21. doi:10.24199/j.mmv.1969.29.01.

Bird ECF (2010) Victoria: Port Phillip Bay (Point Lonsdale to Point Nepean). In: Bird ECF (eds) Encyclopedia of the World's Coastal Landforms, Dordrecht: Springer Netherlands, 614–615. doi:10.1007/978-1-4020-8639-7.

Cardno (2011) The Great Sands and Adjacent Coast and Beaches.

Cardno (2017b) Port Phillip Bay Beach Renourishment Strategy 2016-2036.

CSIRO (1963) Mineragraphic investigations Report 875 Brighton foreshore reclamation plan, Port Phillip Bay, Victoria sand drift studies part I.

Vantree (1995) Frankston to Mt Martha: Coastal Processes and Strategic Coastal Plan.

Water Technology (2017b) Final Report Mount Martha Coastal Process Investigation and Future Management Recommendations.

Appendix G. Beach Profile Survey Digitisation

The digitisation of a series of shoreline surveys, carried out by Port of Melbourne Authority during the 1980's at 27 locations in PPB, is described herein. File folders for each survey assignment (Table 7.2) contained the elevations of each repeat transect survey (Figure G1a) and a text file describing the longshore survey-travel orientation (Figure G1b). To georeference the origin of the orienteering (Figure G2) to GDA94 MGA, survey drawings of the beach surveys along with AGD66 georeferenced markers were also provided in scanned maps for most locations, noting AGD66 can be 200 m off GDA94 MGA (https://www.icsm.gov.au/datum/australian-geodetic-datum-196684-agd) (Figure G3). Year 10 high school students seeking work experience were enlisted to read and digitise the marker coordinates displayed in these files to align the survey-travel with the AGD66 datum.

To account for errors in the compass bearing, the student-digitised survey marker locations at opposite ends of the survey travel were then used to adjust the values of the survey travel (Figure G3). The survey origin location was fixed at the digitised AGD66 marker, and then the bearing was adjusted by minimising the distance between the location of the final survey travel point to the final survey AGD66 marker (Figure G4) using least squares minimisation. The final processed files were stored in a georeferenced file format to be ingested into GIS software (Figure G5).

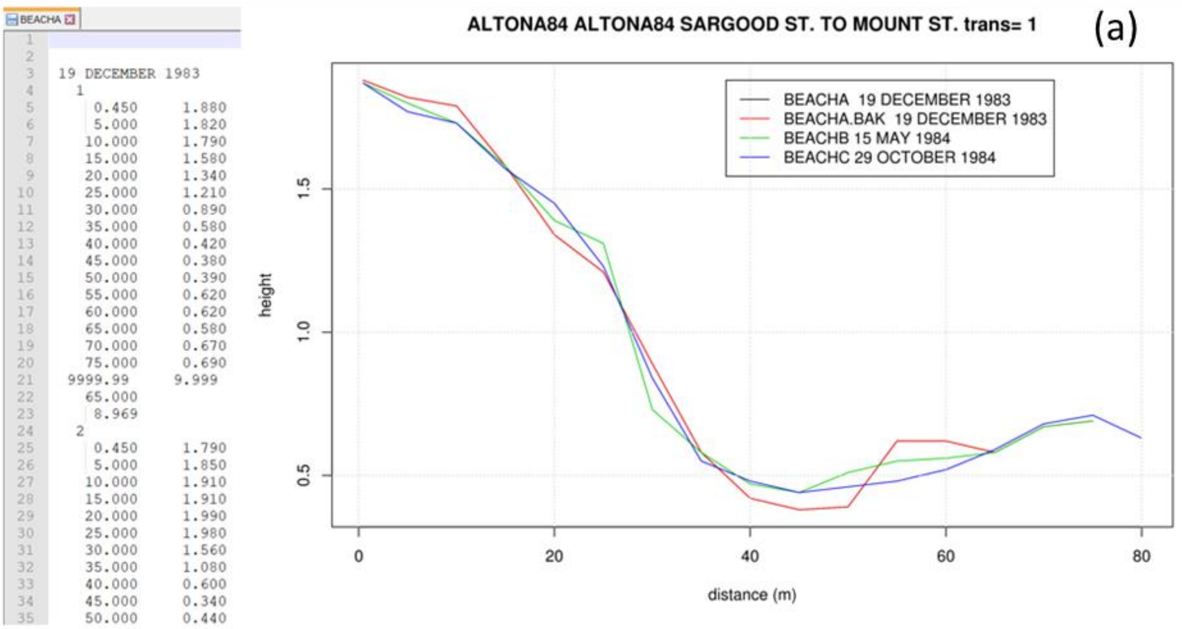

Figure G1: (a) Beach profile survey file (left) and plotted repeat survey values (right). Raw height values plotted (1 m above AHD), (b) Example orienteering file and resulting locations of the beach profiles referenced to origin (zero) of the survey.

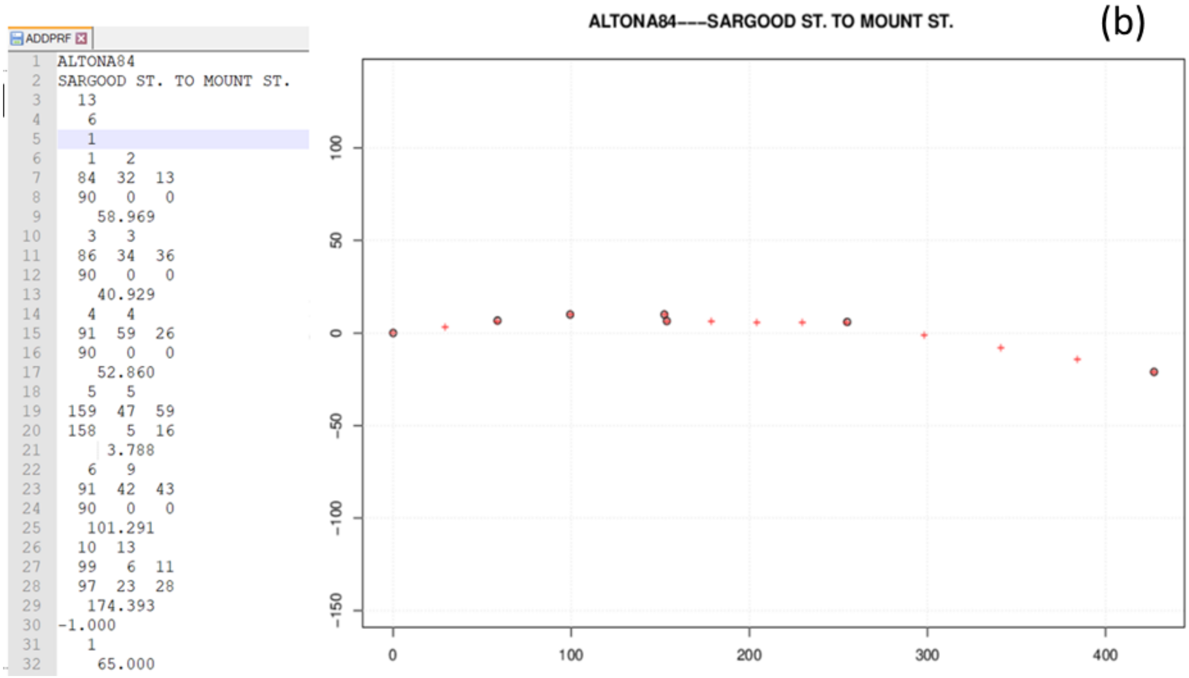

Figure G1: continued.

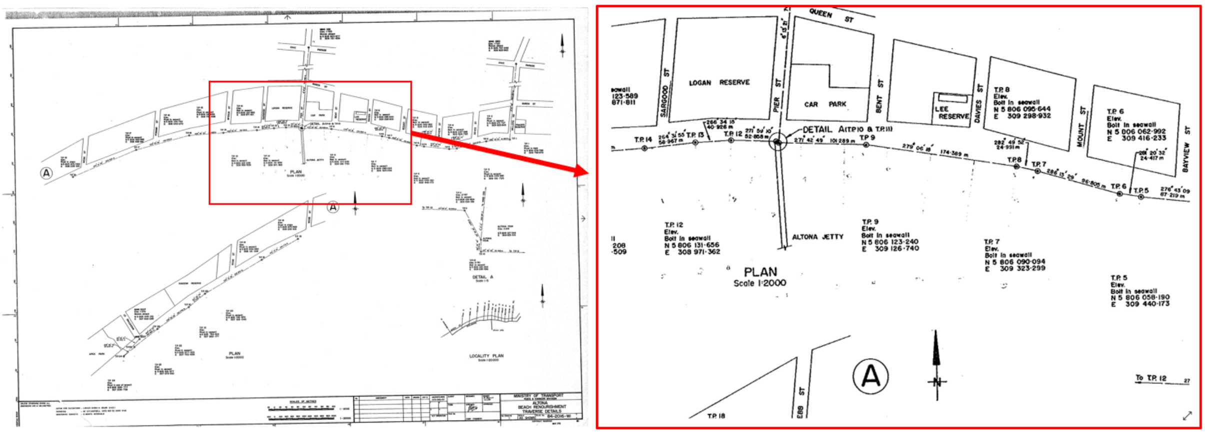

Figure G2: Survey drawing provided for georeferencing. Left is the full image and right is zoomed in section (red box) for the orienteering example shown in Figure G1.

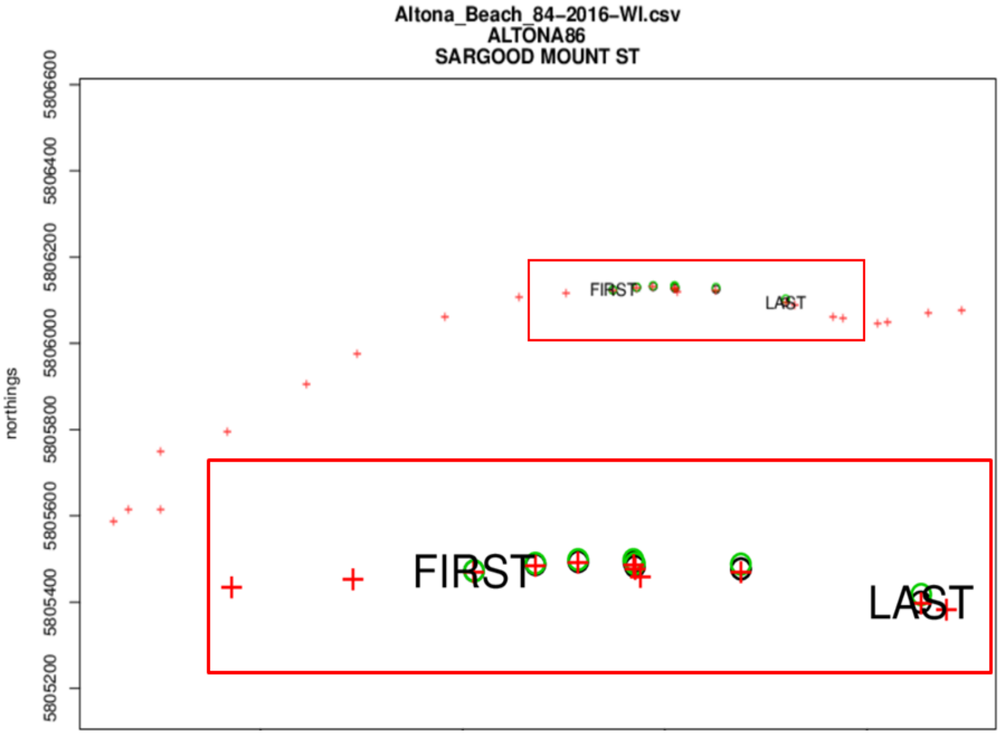

Figure G3: Example survey travel adjustment to the bearing. Student digitised markers (red crosses) unadjusted survey travel markers (green circles) and adjusted survey markers (black circles).

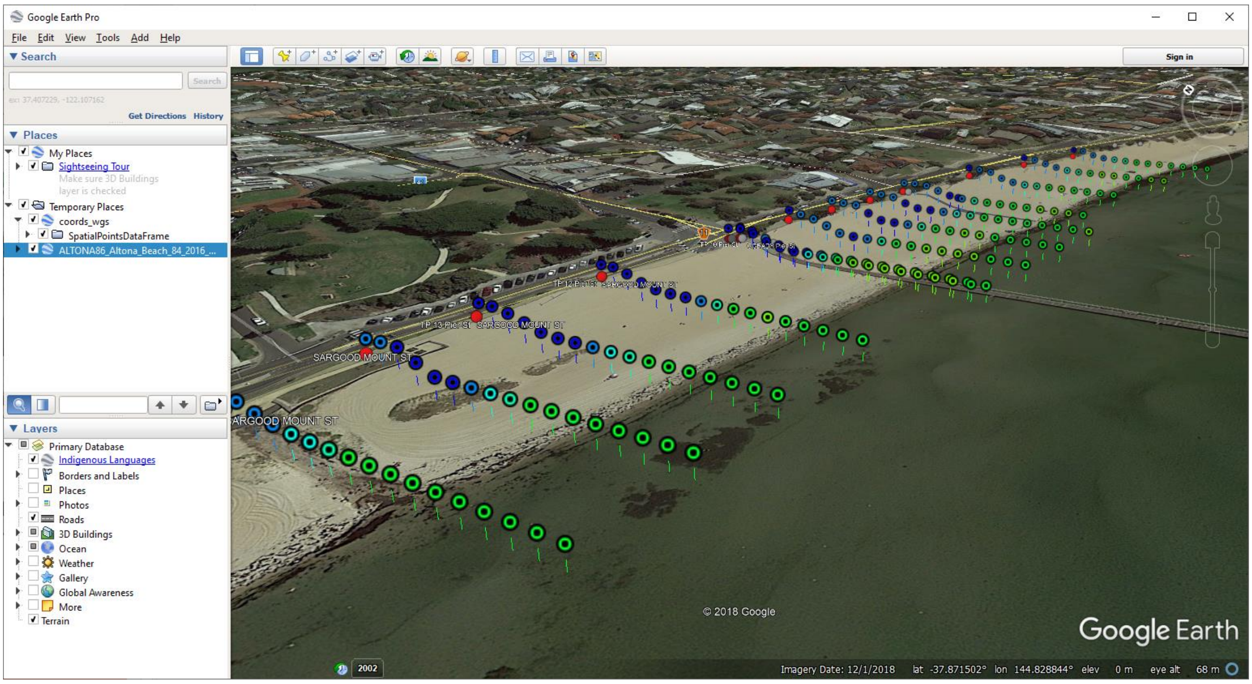

Figure G4: Google Earth 3D representation of the georeferenced beach profiles.

Appendix H. Unsupervised Shoreline Detection

An investigation was undertaken as to how well the unsupervised shoreline detection approach performed in identifying the shoreline across the mixed imagery that was available. In order to reduce the computational cost of the analysis, all the smoothed images were resampled at 50 cm spatial resolution. Finally, the marching squares algorithm (Lorensen and Cline, 1987) was used to delineate the boundary of each cluster.

For example, Seaford is a typical coastal landform consisting of a sandy beach. Figure H1 shows the application of the vegetation line detection using K Means and boundary detection algorithm for this area (1 km by 1 km). The black and white image (see Figure H1a) was collected in 1966 at spatial resolution of 15 cm; the RGB image (see Figure H1b) was captured in 1989 at 24 cm pixel sizes; the RGB+NIR image (see Figure H1c) with the pixel size of 10 cm was the observation available for 2018.

This coastal line detection algorithm works well for the dune-backed sandy beaches. It can successfully detect vegetation features (Figure H2a) as well as the seawalls (Figure H2b). Figure H2c) shows the two aerial observations between 1989 and 2018, indicating change of the coastal line during the past 3 decades due to human intervention.

However, the algorithm can struggle to consistently identify features across the wide range of the coastal geomorphic categories and the individual compartments when using a combination of single band (i.e., black and white images) and RGB images. For example, in the case of an active cliff combined with a sandy beach landform located in the Mornington area (Figure H3a), this algorithm was able to successfully detect the dry and wet line (Figure H3b) in this area, however some shallow water near the sandy beach (the bright yellow colour in Figure H3b) was misassigned.

Typical landcover types (e.g., vegetation, water, and soil) have their unique spectral signatures (Figure H4). Using visible bands to discriminate vegetation from water and soil can be difficult when the land cover types are non-uniform. In other words, the coastal geomorphic categories are complex. Figure G4 shows the most distinctive characteristic of water is the energy absorption at wavelength beyond visible depending on the turbidity of the water. The reflectance rate of bare soil increases steadily from visible band to near-infrared band (NIR), which can be affected by the soil moisture content, soil texture, and surface roughness. The chlorophyll in green vegetation absorbs energy in visible light and strongly reflects energy in NIR band. Therefore, the NIR band has been widely used with visible bands in land cover mapping and vegetation classification studies, because the main landcover types have the most distinctive signatures in the NIR band. In the future, RGB+NIR should be used for the coastal geomorphic classification. For the purposes of the classification undertaken in this study, it was decided that more uniform results were obtained from converting all imagery to black and white imagery.

References

Lorensen WE and Cline HE (1987) Marching cubes: A high resolution 3D surface construction algorithm. ACM siggraph computer graphics 21(4), 163-169.

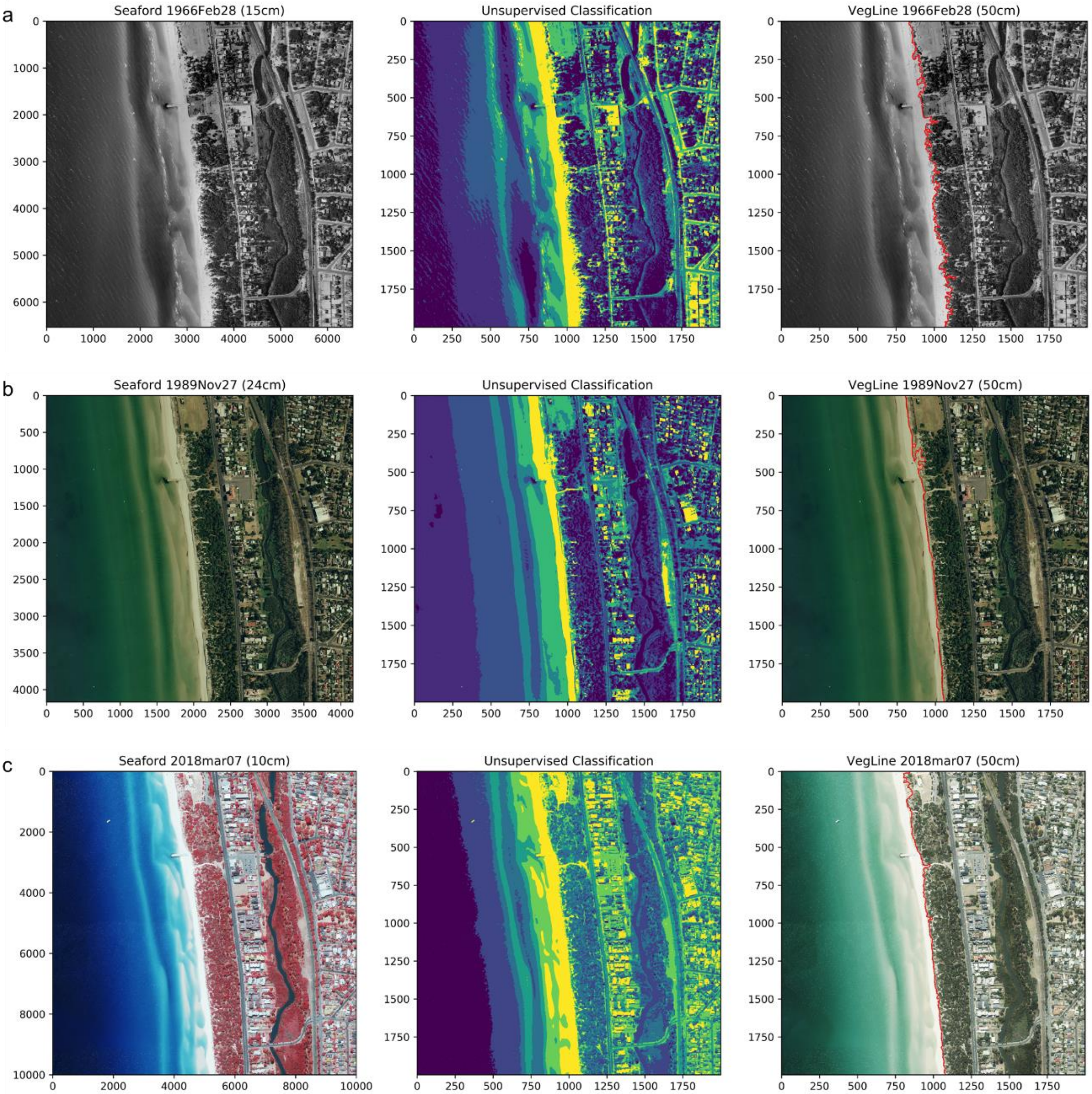

Figure H1: An example of vegetation line detection for Seaford using (a) a black and white image, (b) an RGB image, and (c) an RGB+NIR image captured in 1966, 1989, and 2018 respectively.

Figure H2: The delineation of vegetation line for Carrum using (a) the 1989 RGB image, and (b) the 2018 RGB image to show (c) the detected change in vegetation.

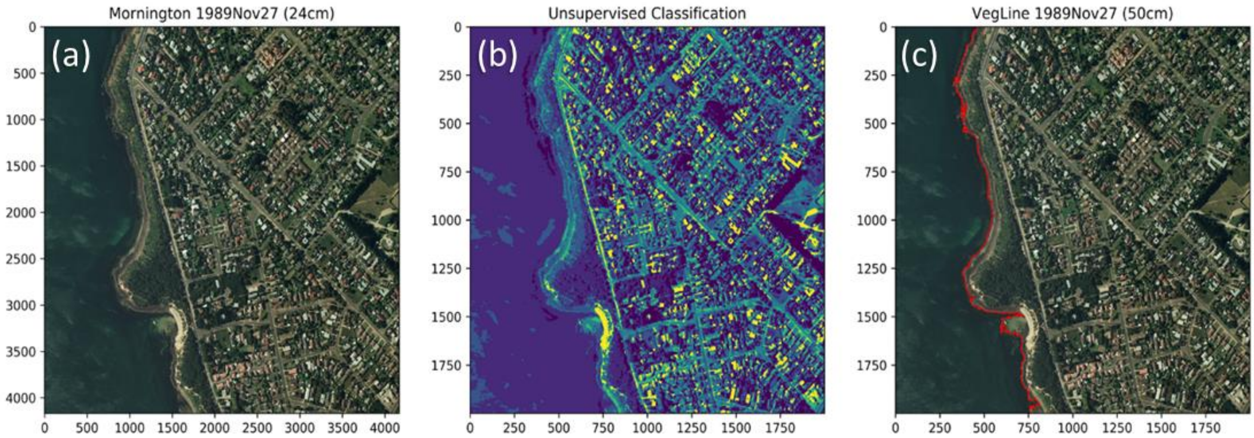

Figure H3: The delineation of the coastal line for Mornington area using (a) the 1989 RGB image, with (b) the unsupervised classification and (c) the boundary detection approach.

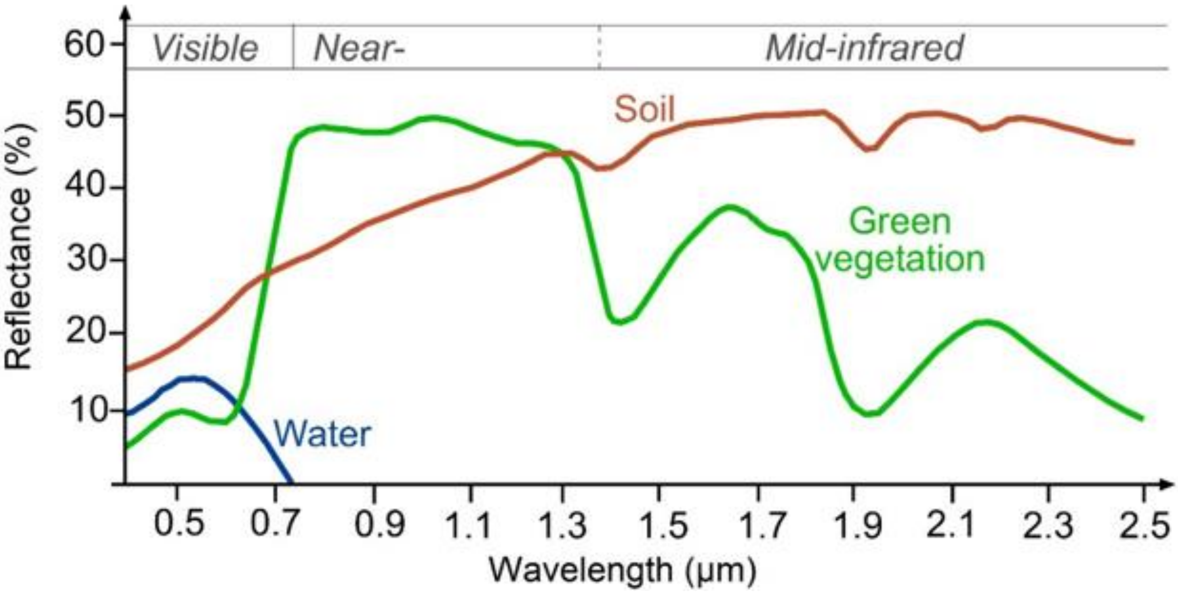

Figure H4. The spectral reflectance curves for healthy vegetation, soil, and water at visible, near-infrared and mid-infrared bands (Lillesand et al., 2015). The x-axis is the reflectance rate (%), and the y-axis is the wavelength (mm).

Table H1: Summary of shoreline change trends around the bay not provided in Table 7.3. Rate per year values give the mean, 5th and 95th percentile value in square brackets for each Sector and are positive for landward moving vegetation lines (erosion) and negative for seaward moving vegetation lines (accretion).

Location	Rate [m/yr]	Sector No.	Sector length	Description (Backshore with intertidal)
Dog Beach 2	-0.147 [-0.294 0.106]	4	1207	Dune with Beach
Queenscliff back beach	-0.112 [-0.260 0.016]	5	791	Dune with Beach
Queenscliff lighthouse	-0.046 [-0.161 0.044]	6	540	Hard Cliff with Beach
Queenscliff town beach	-0.714 [-2.006 0.206]	7	1508	Bluff with Beach
Bell Parade	-0.046 [-0.158 0.114]	24	276	Dune with Beach
St Leonards Red Bluff	-0.082 [-0.095 0.045]	25	156	Hard Cliff with Beach
Bluff Road	-0.193 [-0.278 -0.069]	27	133	Dune with Beach
St Leonards Breakwater	-0.320 [-0.522 0.098]	28	359	Dune with Beach
St Leonards Esplanade	-0.042 [-0.225 0.460]	29	920	Bluff with Beach
Dossetor Road	-0.080 [-0.313 0.064]	510	915	Wetlands with beach
Abalone Farm bluff	-0.067 [-0.174 -0.023]	31	216	Soft Cliff with Beach
Hood Bight	-0.176 [-0.375 -0.004]	32	972	Dune with Beach
Half Moon Bay south	-0.074 [-0.148 -0.025]	34	194	Bluff with Beach
Jubilee Avenue	0.048 [-0.002 0.086]	36	290	Dune with Beach
Beach Vista Drive	-0.137 [-0.285 0.311]	65	650	Soft Cliff with Beach
Point Wilson lagoons	-0.146 [-0.576 0.270]	151	1475	Dune with Beach
Werribee River O'Connors Road	-0.499 [-0.813 -0.103]	179	1080	Dune with Beach
Beach Rd 1	-0.302 [-0.417 -0.113]	181	143	Bluff with Beach
Point Cook Marine Sanctuary south	-0.331 [-0.373 -0.163]	202	315	Dune with Beach
Perc White Reserve	-0.375 [-0.773 -0.128]	268	340	Dune with Beach
Brighton Beach Bathing boxes	-0.150 [-0.354 -0.014]	284	375	Bluff with Beach
Gould Street bluff	-0.210 [-0.266 -0.126]	522	440	Bluff with Beach
Sandringham Harbour	-0.411 [-0.495 -0.352]	286	137	Bluff with Beach
Black Rock beach	-0.101 [-0.154 -0.016]	297	574	Bluff with Mixed
Ricketts Point CafÃ© beach	-0.233 [-0.426 -0.079]	300	409	Dune with Beach
Mordialloc Bowman St	-0.266 [-0.435 -0.059]	316	366	Engineering ineffective with beach
Aspendale Beach	-0.149 [-0.382 -0.036]	318	1615	Dune with Beach
Aspendale Alexandra St	-0.233 [-0.399 -0.127]	322	894	Dune with Beach
Chelsea Foreshore	-0.272 [-0.416 -0.092]	324	1166	Dune with Beach
Bonbeach	-0.237 [-0.378 -0.123]	326	1454	Dune with Beach
Bonbeach Lifesaving	-0.252 [-0.474 -0.128]	328	1032	Dune with Beach
Paterson River south	-0.348 [-0.760 -0.135]	330	304	Engineering effective with beach
Seaford	-0.185 [-0.418 0.013]	331	7837	Dune with Beach
Frankston south	-0.147 [-0.356 0.024]	335	702	Engineering ineffective with beach
Pelican Bay	-0.012 [-0.084 0.421]	342	495	Hard Cliff with Beach
Canadian Bay north	-0.039 [-0.100 0.019]	343	626	Bluff with Mixed
Canadian Bay Beach	-0.004 [-0.065 0.034]	344	422	Soft Cliff with Beach
Earimil Beach	-0.066 [-0.162 0.015]	348	282	Bluff with Beach
Moondah Beach	-0.034 [-0.165 0.027]	350	1664	Bluff with Mixed
Gunyong Creek	0.030 [-0.032 0.053]	351	68	River drain
Gunyang Creek beach	-0.012 [-0.138 0.052]	352	347	Bluff with Beach

Location	Rate [m/yr]	Sector No.	Sector length	Description (Backshore with intertidal)
Sunnyside Road	0.109 [-0.028 0.139]	356	157	Soft Cliff with Beach
Sunnyside car park	-0.072 [-0.158 0.111]	357	175	Engineering effective with beach
Manmangur Creek	0.031 [0.016 0.107]	359	70	Slope with Beach
Sunnyside gravel beach	0.106 [0.089 0.163]	360	91	Slope with Beach
Sunnyside North	0.018 [-0.042 0.041]	379	441	Bluff with Mixed
Royal beach	-0.058 [-0.079 -0.050]	381	170	Bluff with Beach
Fishermans Beach north	-0.019 [-0.141 0.006]	383	188	Engineering effective with beach
Fishermans Beach south	0.001 [-0.017 0.026]	384	289	Bluff with Beach
Dava Beach south	-0.027 [-0.047 0.013]	399	215	Bluff with Mixed
Birdrock Beach	-0.016 [-0.047 0.014]	400	393	Hard Cliff with Beach
Harmon Rocks	0.075 [0.026 0.121]	401	64	Hard Cliff with Platform
Harmon Rocks gravel	0.071 [-0.056 0.175]	402	153	Slope with Beach
Craigie Beach	-0.030 [-0.446 0.151]	404	460	Engineering effective with beach
Mount Martha Coolangatta Rd	0.011 [-0.027 0.036]	407	371	Soft Cliff with Beach
Mount Martha town beach	-0.126 [-0.217 -0.006]	412	325	Bluff with Beach
Mount Martha South	-0.012 [-0.144 0.065]	414	369	Bluff with Beach
Martha Point beach	-0.037 [-0.098 0.025]	420	141	Engineering effective with beach
Martha Point north groyne	-0.034 [-0.164 0.091]	421	54	Engineering ineffective with beach
Safety Beach south	-0.028 [-0.127 0.057]	426	458	Dune with Beach
Dromana Beach north	-0.062 [-0.171 0.003]	427	489	Engineering ineffective with beach
Dromana Beach central	-0.038 [-0.108 0.052]	428	1168	Bluff with Beach
Dromana Beach pier	0.022 [-0.056 0.164]	429	699	Engineering effective with beach
Dromana Beach south	-0.066 [-0.159 0.039]	430	819	Bluff with Beach
Dromana Beach huts	0.006 [-0.092 0.177]	526	670	Bluff with Beach
Anthony's Nose	-0.039 [-0.110 0.083]	431	805	Engineering effective with beach
Rosebud beach north	-0.099 [-0.422 0.147]	432	725	Dune with Beach
Rosebud Pier	-0.448 [-0.619 -0.032]	527	2129	Dune with Beach
Rosebud beach south	-0.338 [-0.772 0.014]	434	2413	Dune with Beach
Rye seawall	0.053 [-0.087 0.245]	435	129	Engineering effective with beach
Rye Pier north	0.077 [-0.400 0.349]	437	252	Engineering effective with beach
Rye Pier south	-0.041 [-0.442 0.113]	438	405	Engineering ineffective with beach
Rye beach	-0.693 [-0.831 -0.523]	439	564	Bluff with Beach
White Cliffs/Pt King	-0.461 [-0.740 0.007]	440	184	Engineering effective with beach
White Cliffs campground	-0.244 [-0.426 0.036]	441	789	Bluff with Beach
Blairgowrie Flinders St	-0.012 [-0.083 0.045]	442	56	Engineering ineffective with beach
Blairgowrie beach boxes	-0.285 [-0.354 -0.163]	443	155	Bluff with Beach
Tyrone Beach carpark	-0.116 [-0.272 0.031]	444	53	Engineering ineffective with beach
Tyrone Boat Ramp	-0.174 [-0.274 -0.096]	445	407	Bluff with Beach
Blairgowrie north	-0.116 [-0.139 -0.104]	446	160	Engineering effective with beach
Blairgowrie central	-0.123 [-0.225 -0.028]	447	415	Bluff with Beach
Blairgowrie seawall	-0.064 [-0.098 -0.008]	448	395	Engineering effective with beach
Blairgowrie south	-0.021 [-0.091 0.051]	449	582	Engineering ineffective with beach
Blairgowrie Inverness Ave	-0.087 [-0.102 -0.024]	450	68	Engineering effective with beach
Blairgowrie The Loop	-0.145 [-0.181 -0.092]	451	226	Bluff with Beach

Location	Rate [m/yr]	Sector No.	Sector length	Description (Backshore with intertidal)
Blairgowrie seawall	-0.035 [-0.058 0.046]	452	89	Engineering effective with beach
Blairgowrie groynes	0.018 [-0.030 0.167]	453	175	Engineering ineffective with beach
Blairgowrie revetment	-0.088 [-0.130 0.111]	455	70	Engineering effective with beach
Camerons Bight	-0.056 [-0.120 0.017]	456	251	Bluff with Beach
Sullivan Bay	-0.145 [-0.398 0.009]	458	417	Soft Cliff with Beach
Western Sister Beach	-0.064 [-0.144 -0.022]	460	167	Hard Cliff with Beach
Sorrento Front Beach	-0.119 [-0.229 -0.021]	462	1181	Soft Cliff with Beach
Point King Beach	-0.337 [-1.059 -0.021]	472	426	Bluff with Beach
Shelly Beach	-0.723 [-1.146 -0.266]	474	860	Bluff with Beach
Portsea Beach	-0.022 [-0.101 0.061]	477	266	Slope with Beach
Portsea Front Beach	0.000 [-0.032 0.035]	479	260	Bluff with Mixed
Weroona Bay	-0.005 [-0.062 0.048]	480	388	Engineering effective with beach
Quarantine station beach	-0.029 [-0.048 -0.004]	482	212	Bluff with Beach
Fort Nepean 2	0.215 [0.201 0.255]	497	19	Hard Cliff with Beach

Appendix J. SCHISM Model Comparisons

Meteorology and Sea Level Comparisons

The following sets of time series provide additional comparisons of the CCAM model and observations and the performance of SCHISM in simulating tides and storm surges at selected tide gauges within the model domain. Each of the time periods selected contain an extreme sea level event that contributes to the evaluation of AEPs for the hazard assessments.

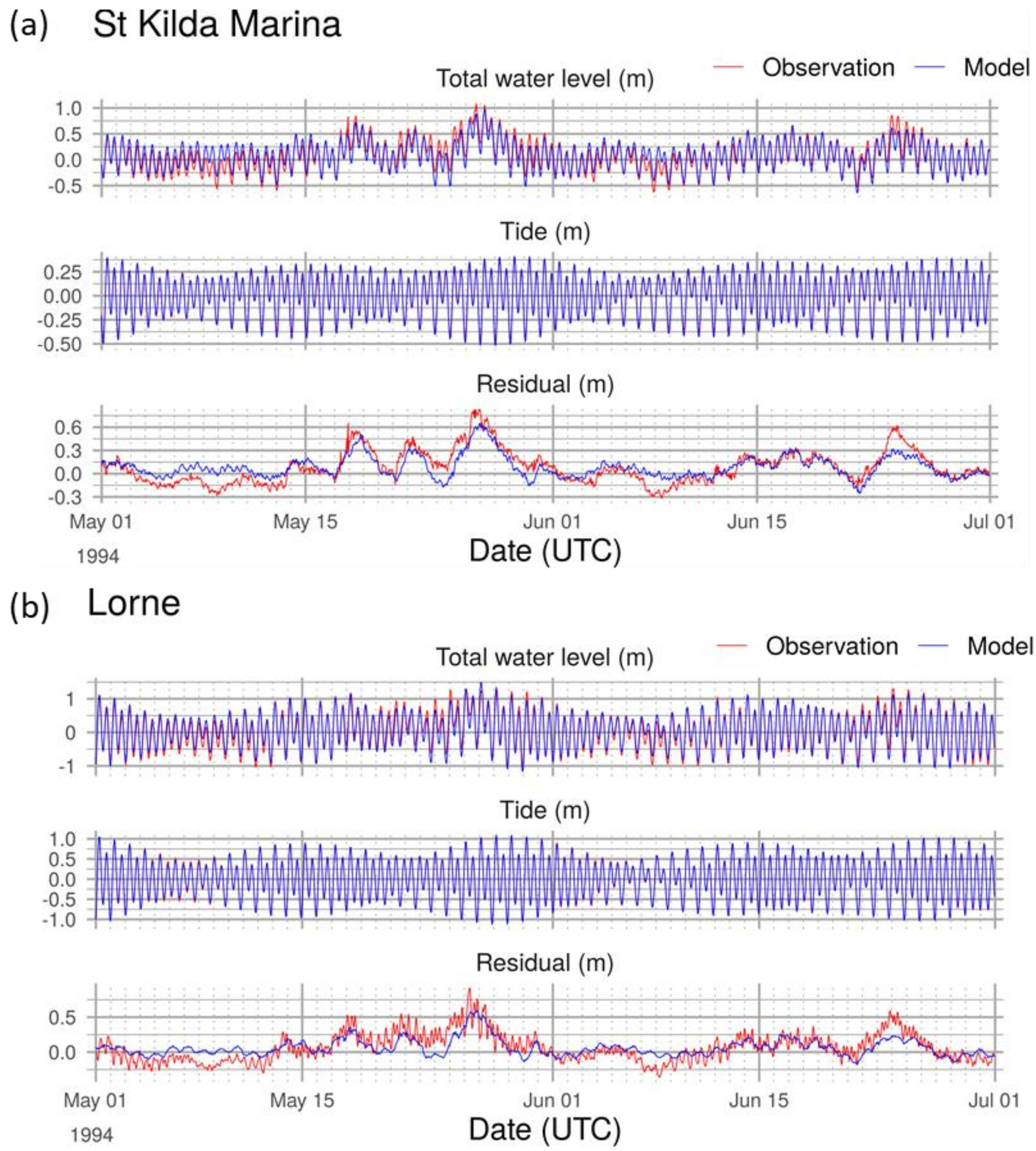

Figure J1: Additional comparison of SCHISM-simulated total water level, tidal and residual water levels with tide gauge measurements over May and June 1994 at (a) St Kilda Marina, and (b) Lorne.

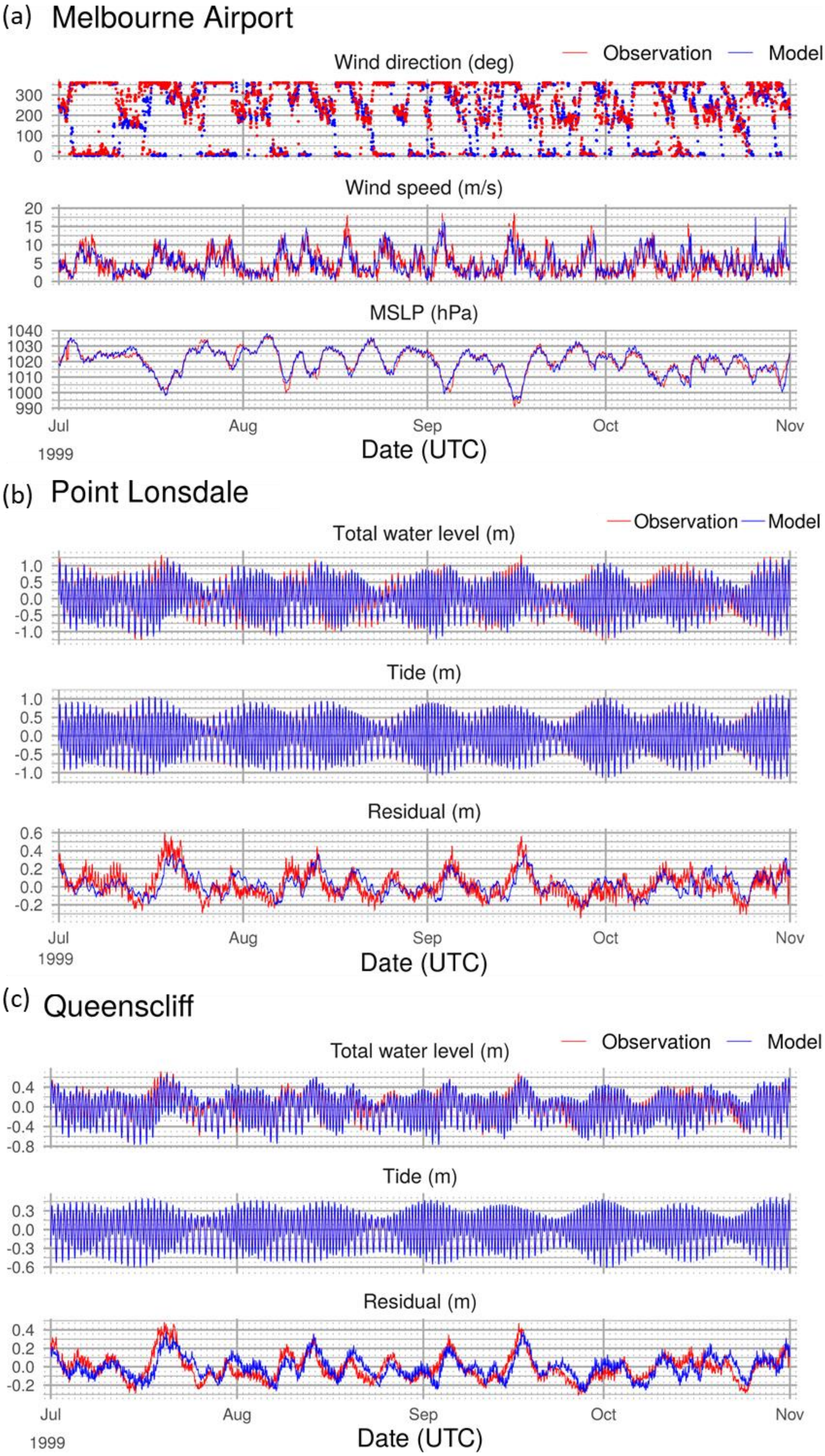

Figure J2: Comparison of CCAM-simulated wind direction, 10 m wind speed and MSLP with meteorological data at the location of Melbourne Airport over July to November 1999, (b-i) SCHISM-simulated total water level, tidal and residual water levels with tide gauge measurements at Point Lonsdale, Queenscliff, West Channel Pile, Geelong, Williamstown, St Kilda Marina, Hovell Pile and Lorne.

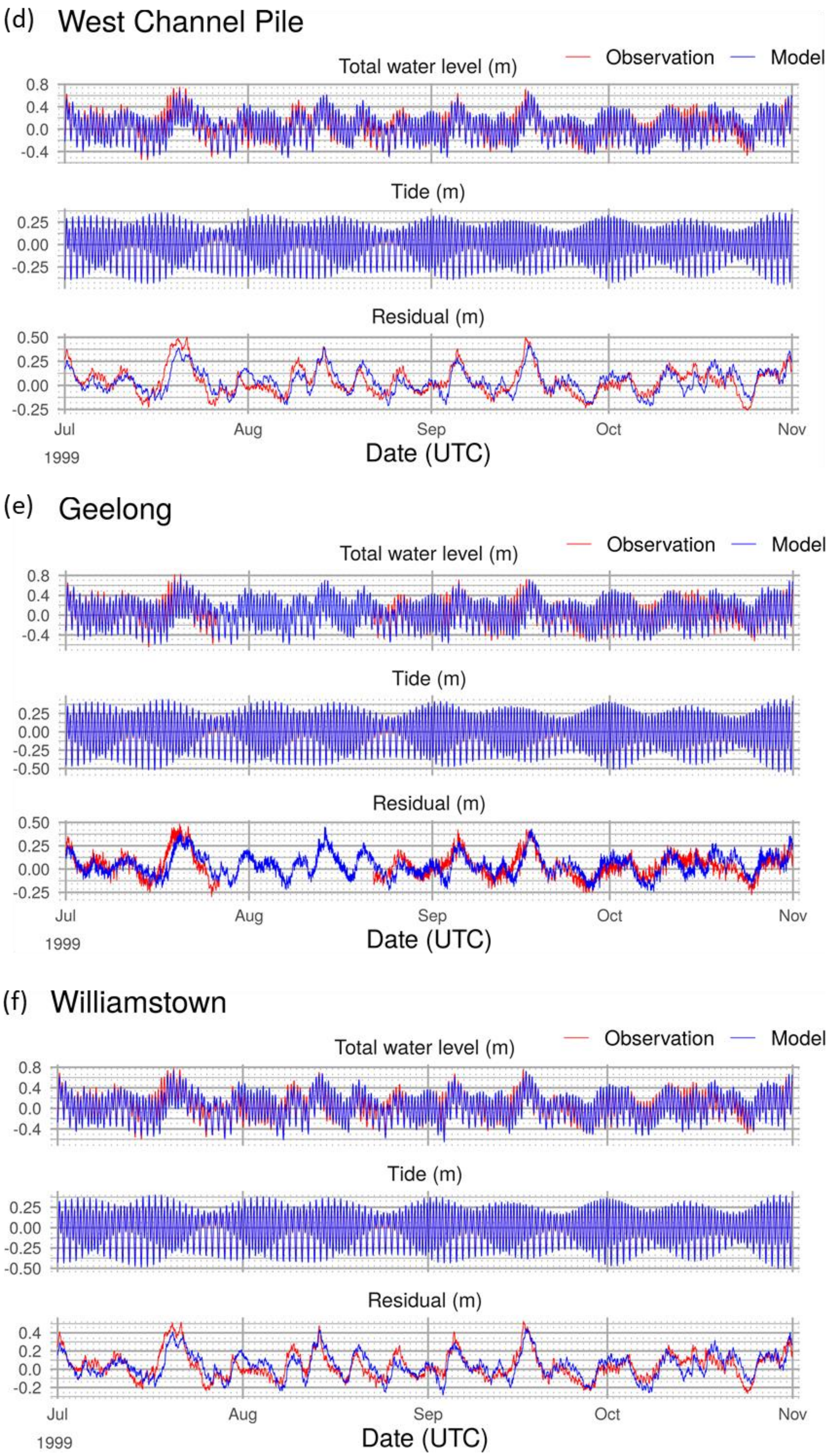

Figure J2: Continued.

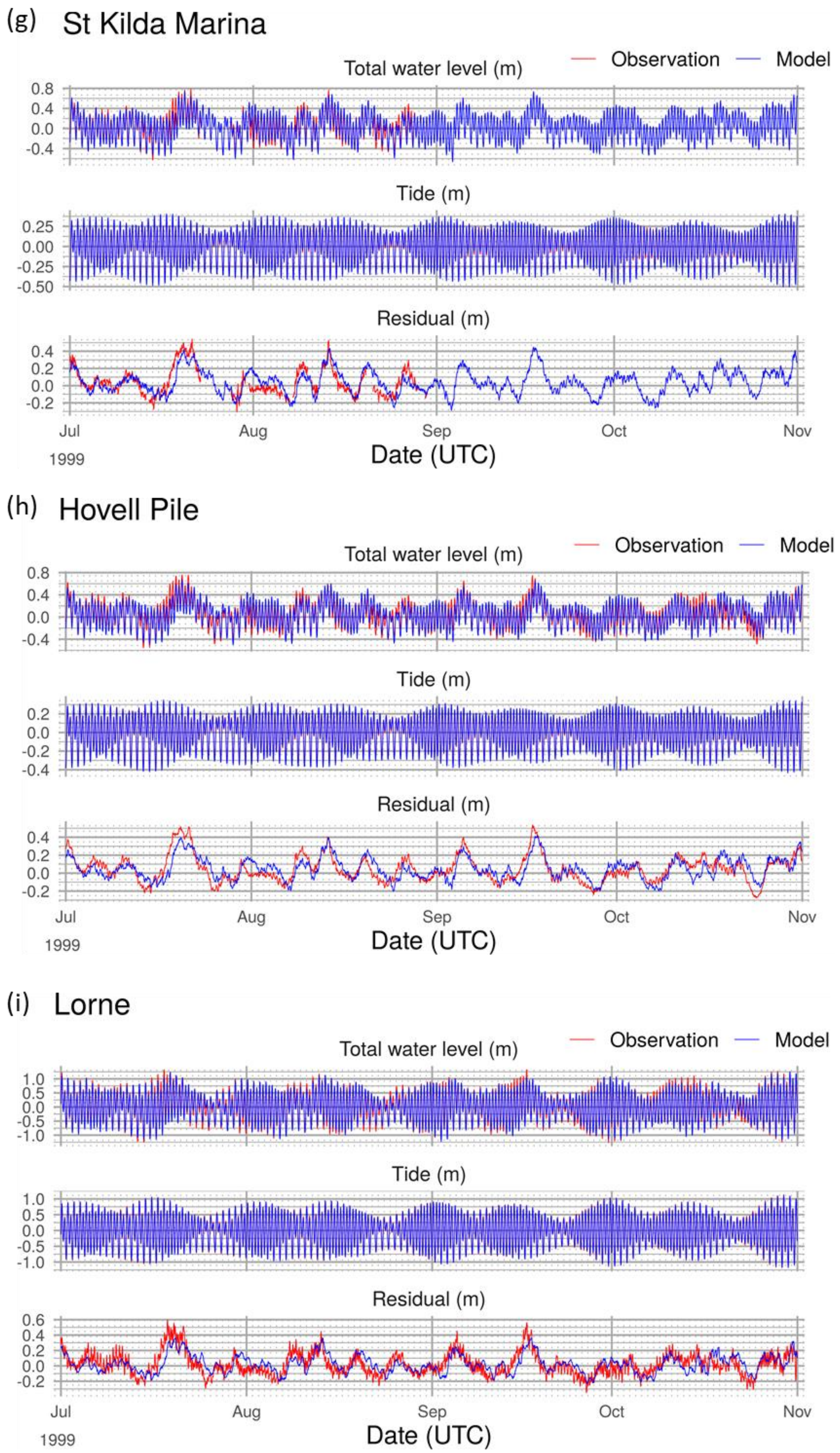

Figure J2: Continued.

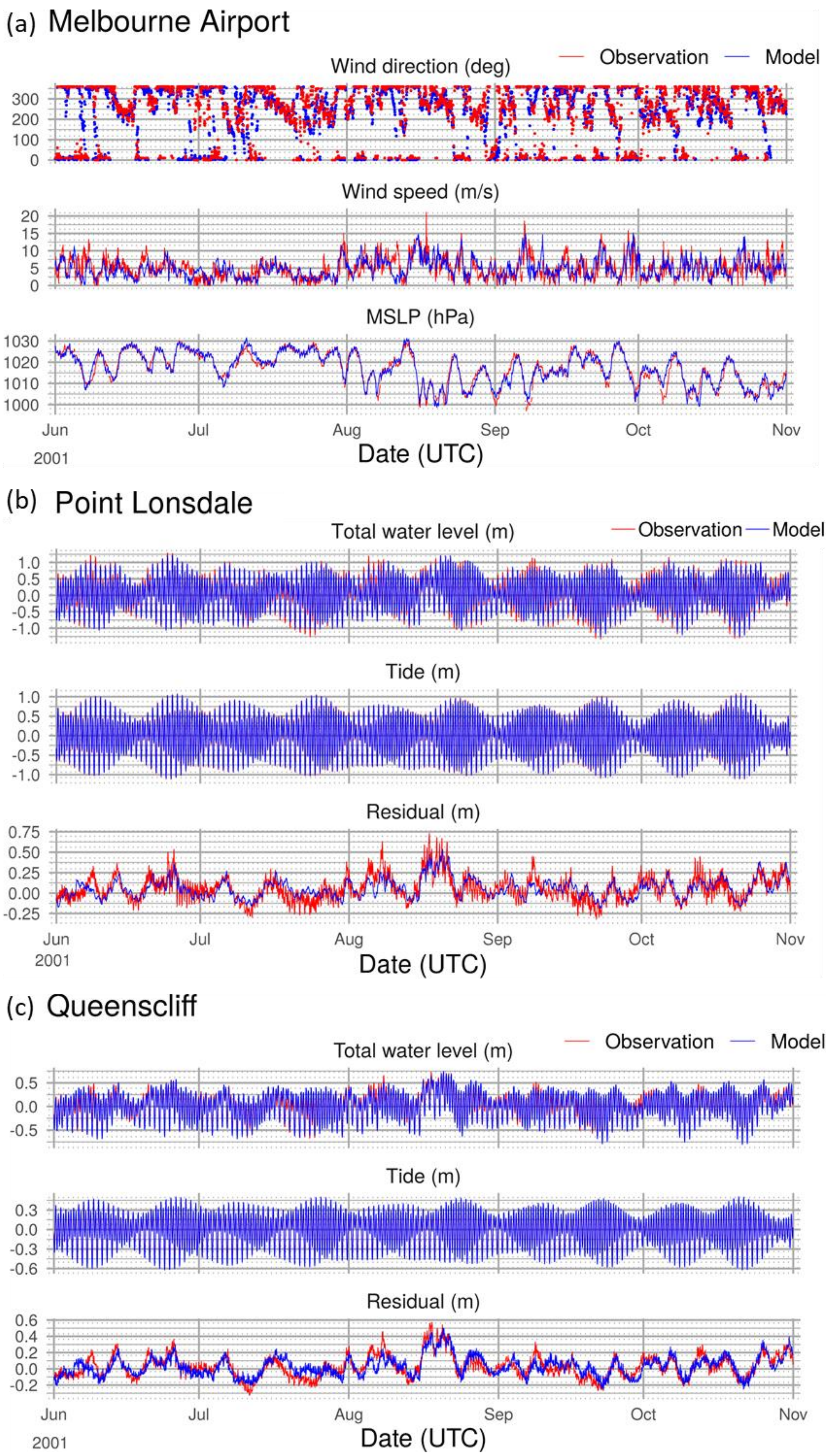

Figure J3: Comparison of CCAM-simulated wind direction, 10 m wind speed and MSLP with meteorological data at the location of Melbourne Airport from June to November 2001, (b-j) SCHISM-simulated total water level, tidal and residual water levels with tide gauge measurements at Point Lonsdale, Queenscliff, West Channel Pile, Point Richards, Geelong, Williamstown, St Kilda Marina, Hovell Pile and Lorne.

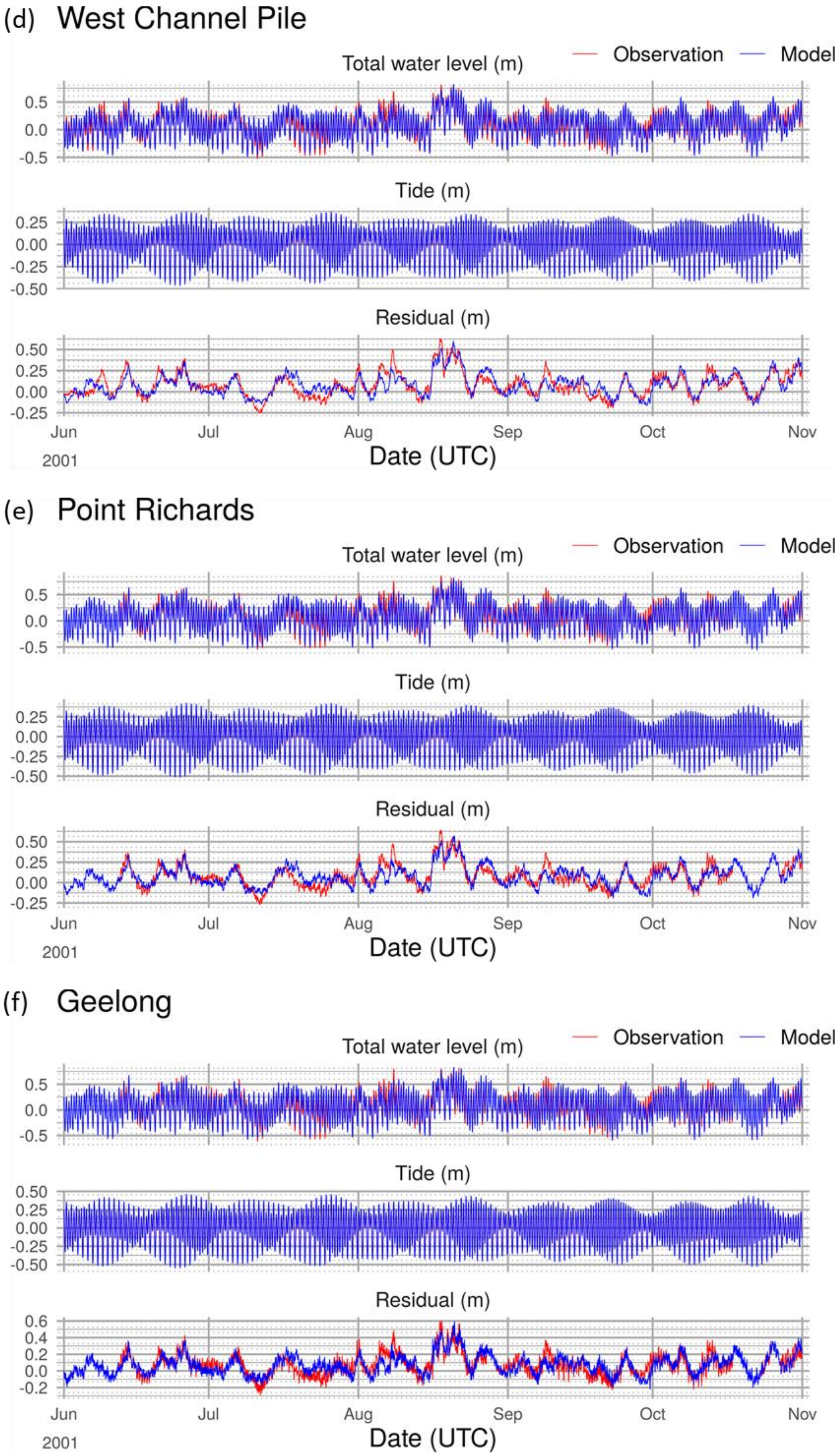

Figure J3: Continued.

(g) Williamstown

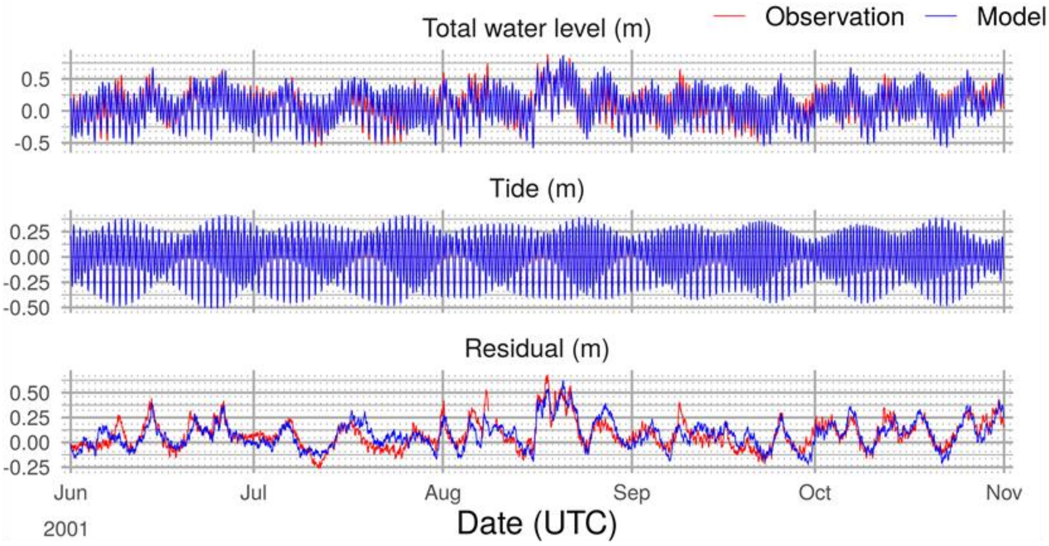

(h) St Kilda Marina

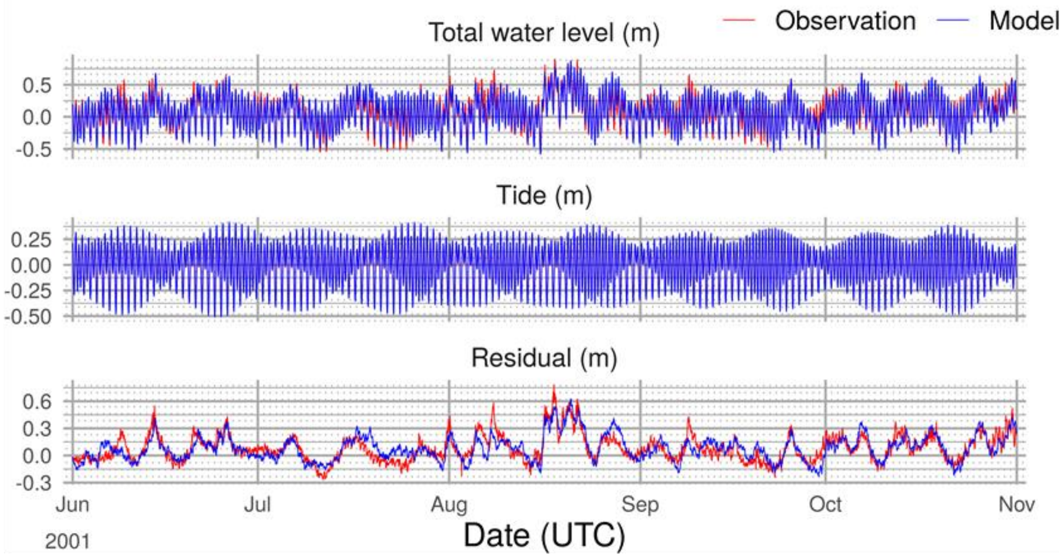

(i) Hovell Pile

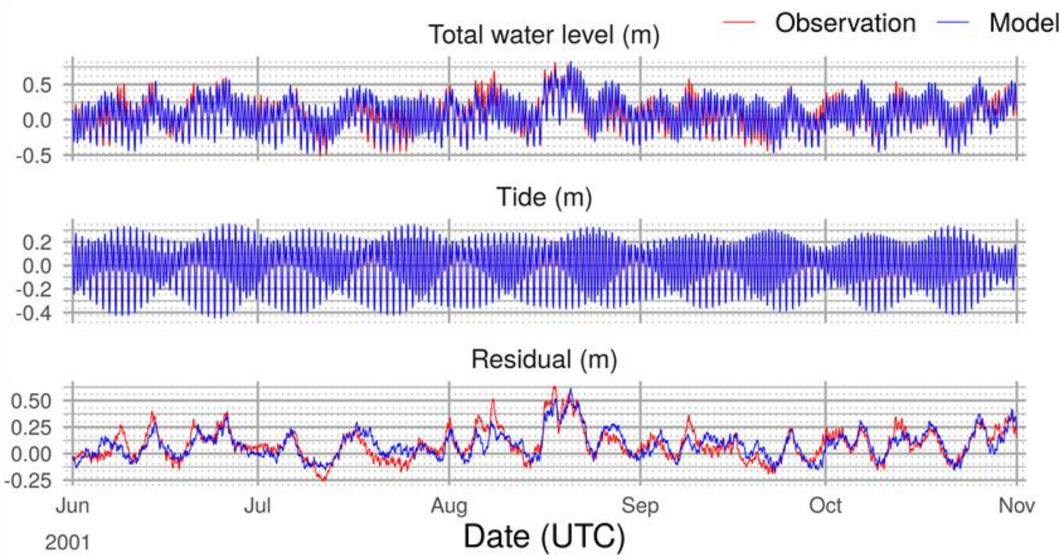

Figure J3: Continued.

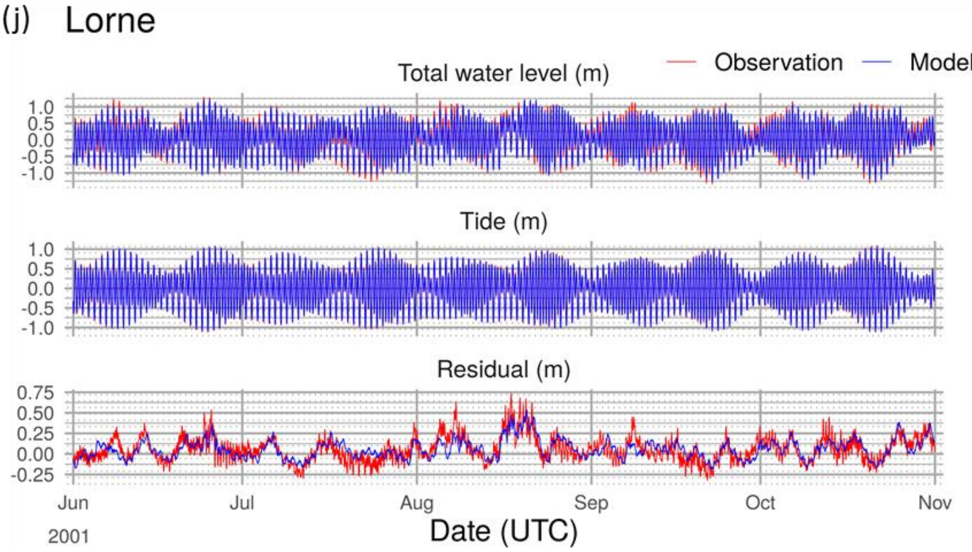

Figure K3: Continued.

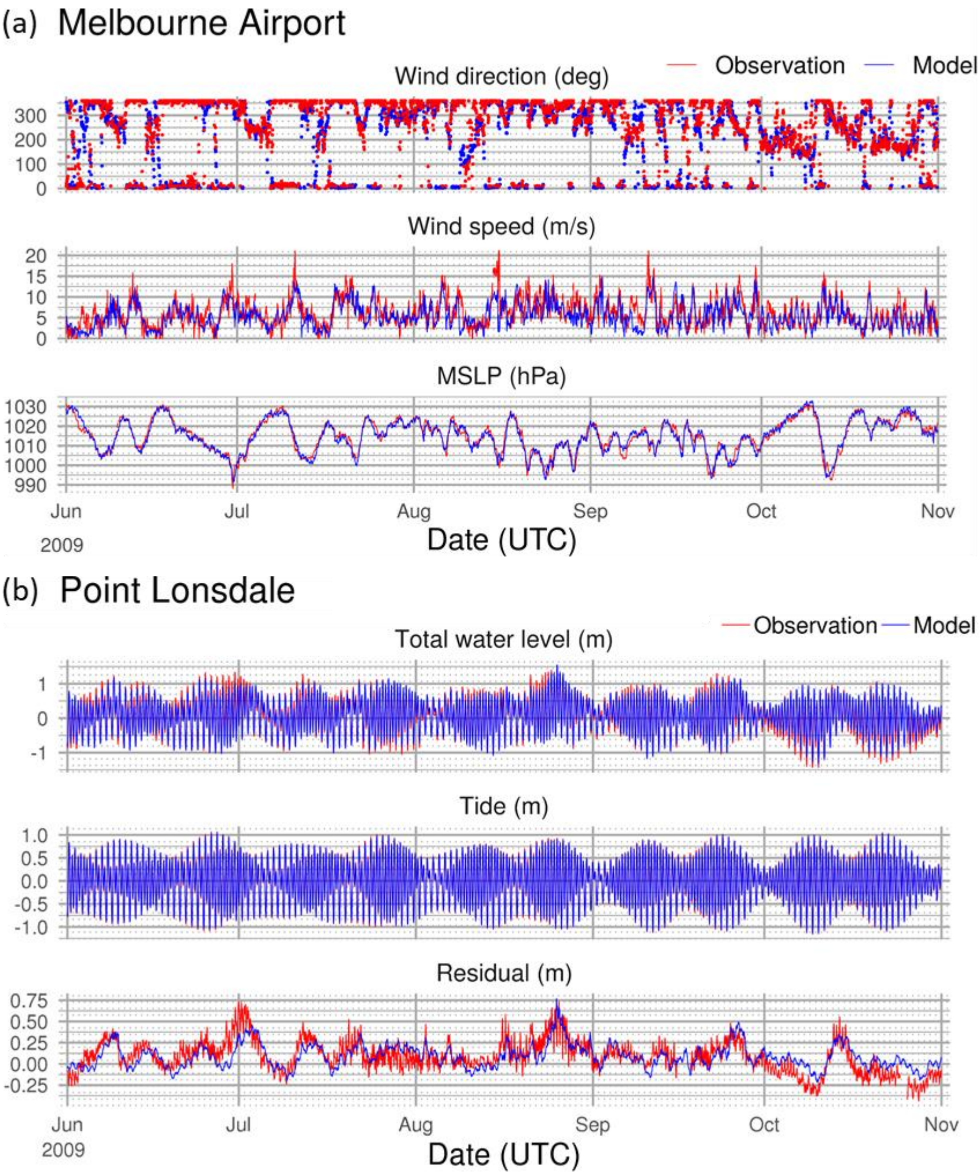

Figure J4: Comparison of CCAM-simulated wind direction, 10 m wind speed and MSLP with meteorological data at the location of Melbourne Airport from June to November 2009, (b-j) SCHISM-simulated total water level, tidal and residual water levels with tide gauge measurements at Point Lonsdale, Queenscliff, West Channel Pile, Point Richards, Geelong, Williamstown, St Kilda Marina, Hovell Pile and Lorne.

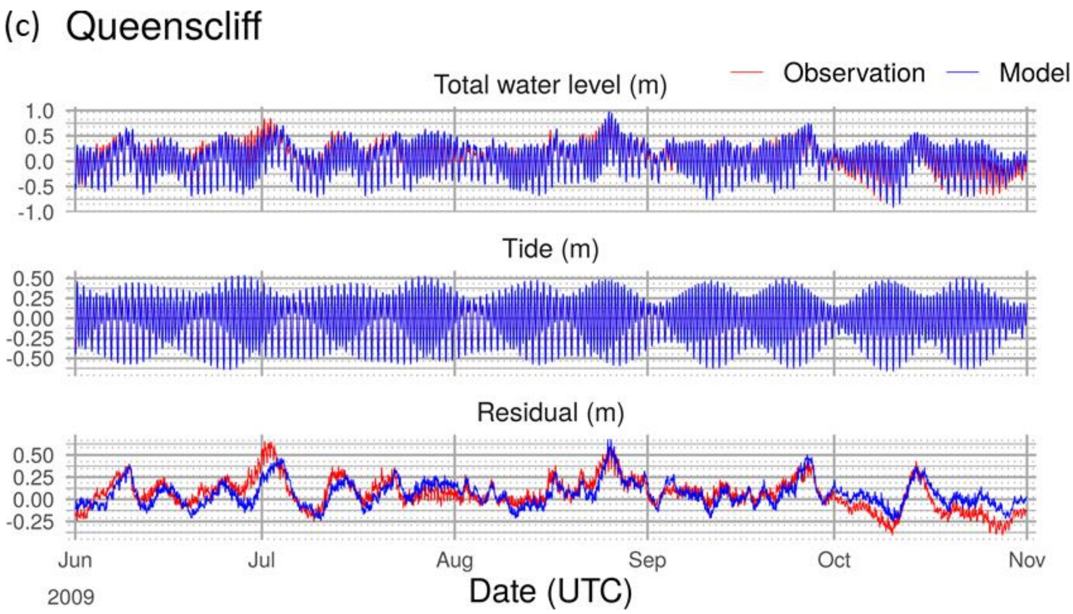

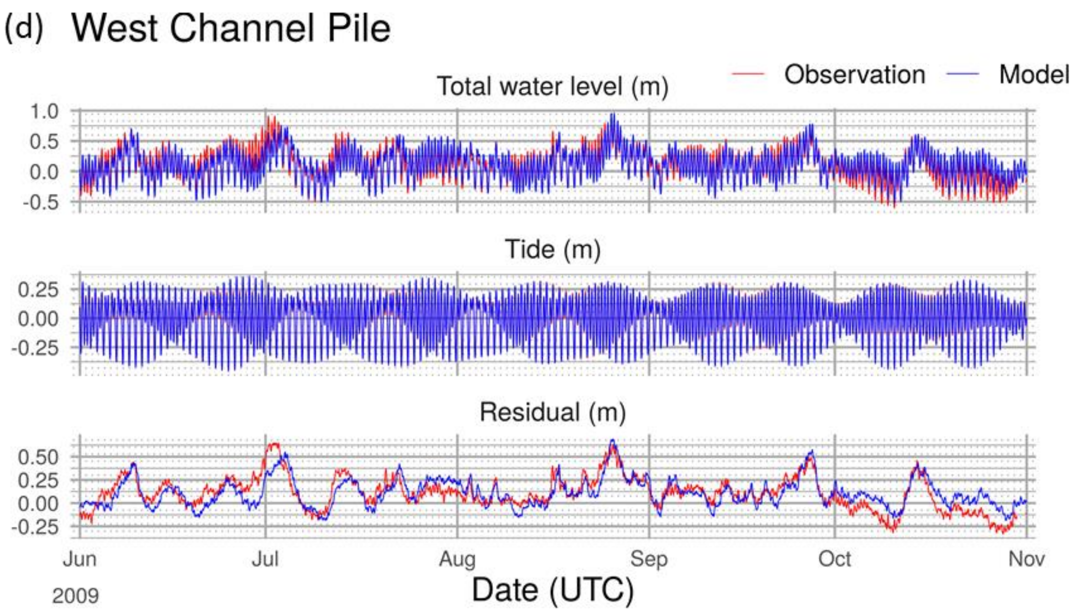

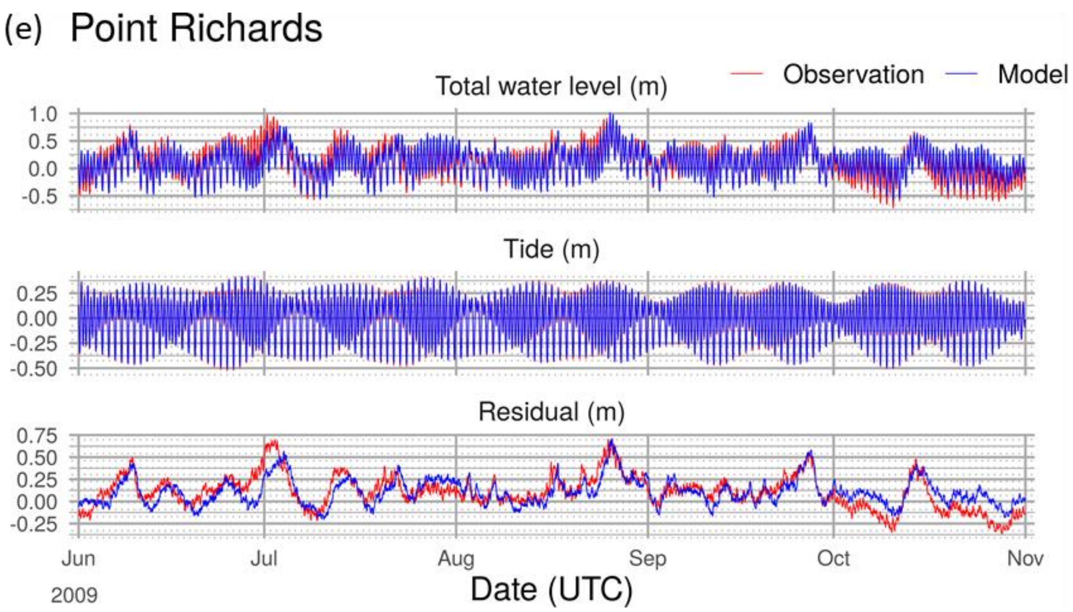

Figure J4: Continued.

(f) Geelong

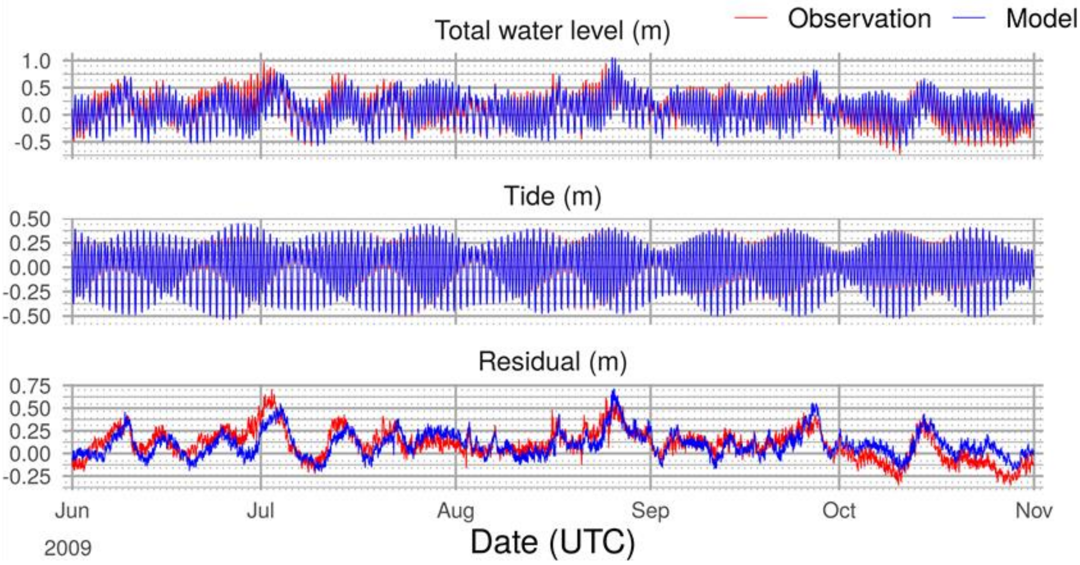

(g) Williamstown

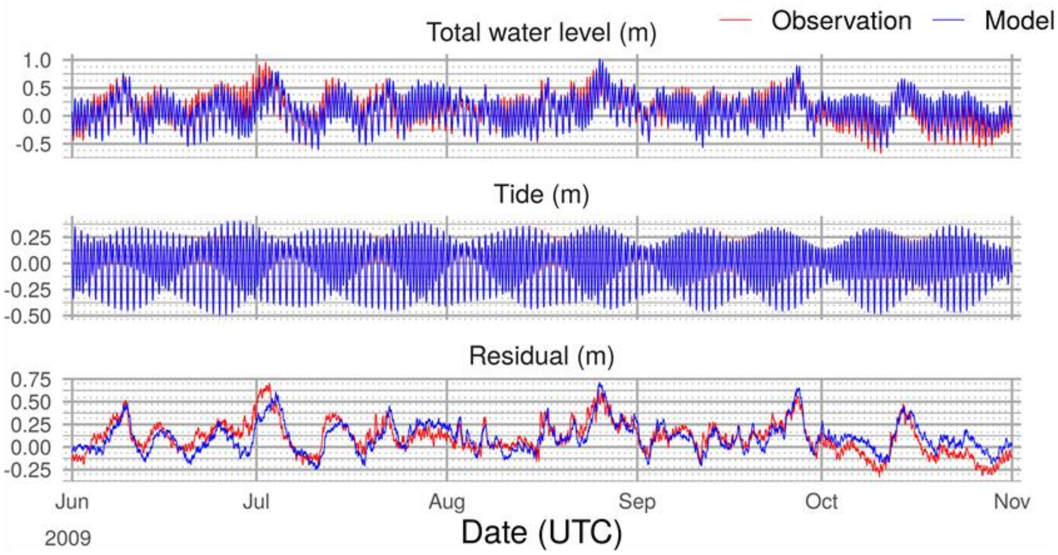

(h) St Kilda Marina

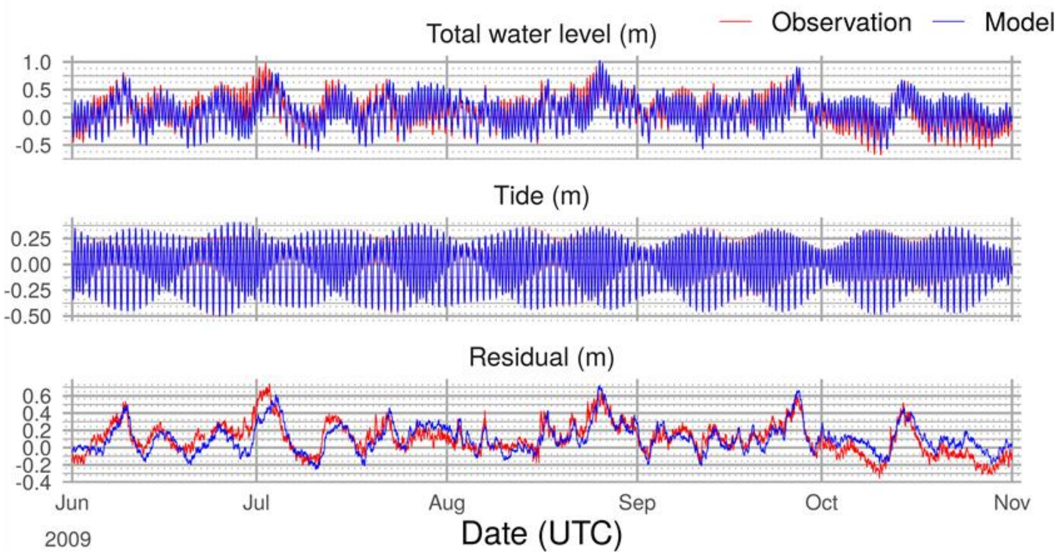

Figure J4: Continued.

(i) Hovell Pile

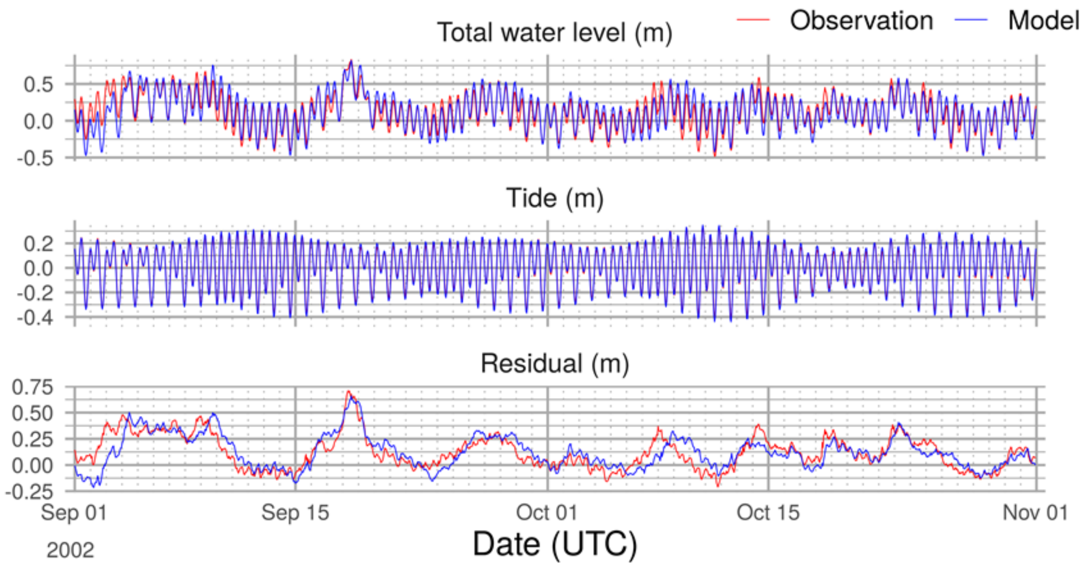

(j) Lorne

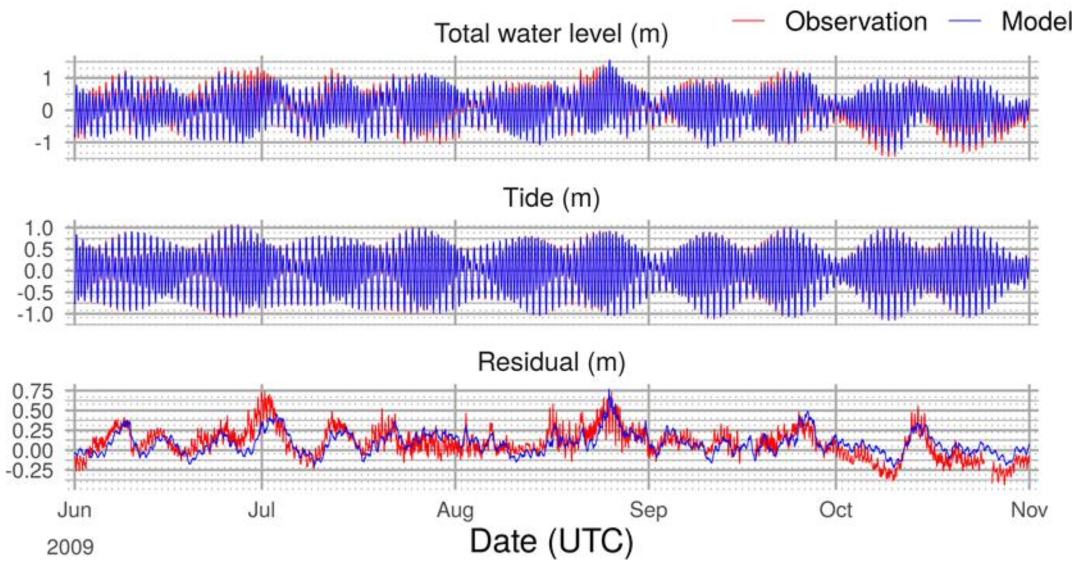

Figure J4: Continued.

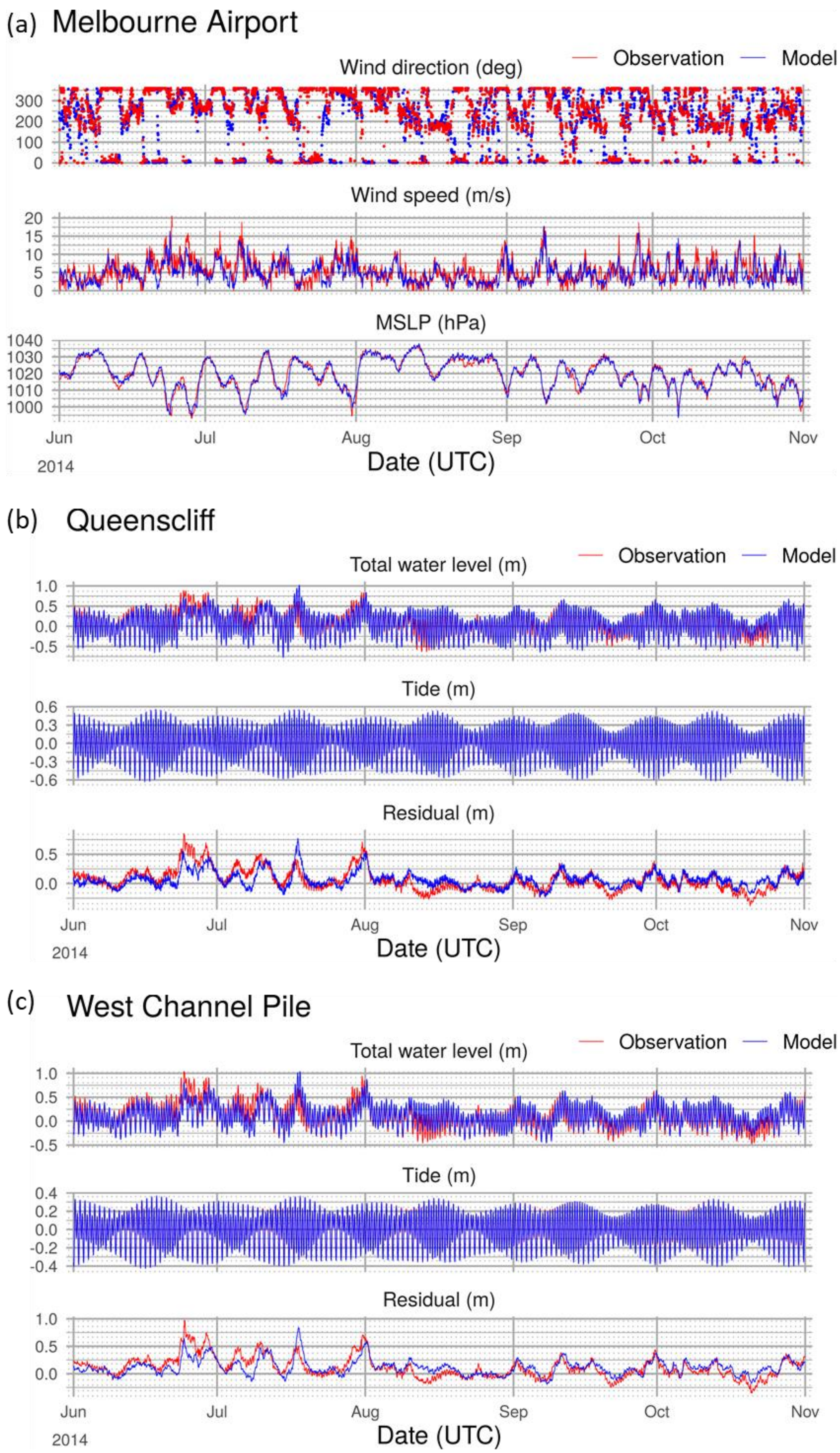

Figure J5: Comparison of CCAM-simulated wind direction, 10 m wind speed and MSLP with meteorological data at the location of Melbourne Airport from June to August 2014, (b-j) SCHISM-simulated total water level, tidal and residual water levels with tide gauge measurements at Point Lonsdale, Queenscliff, West Channel Pile, Point Richards, Geelong, Williamstown, St Kilda Marina, Hovell Pile and Lorne.

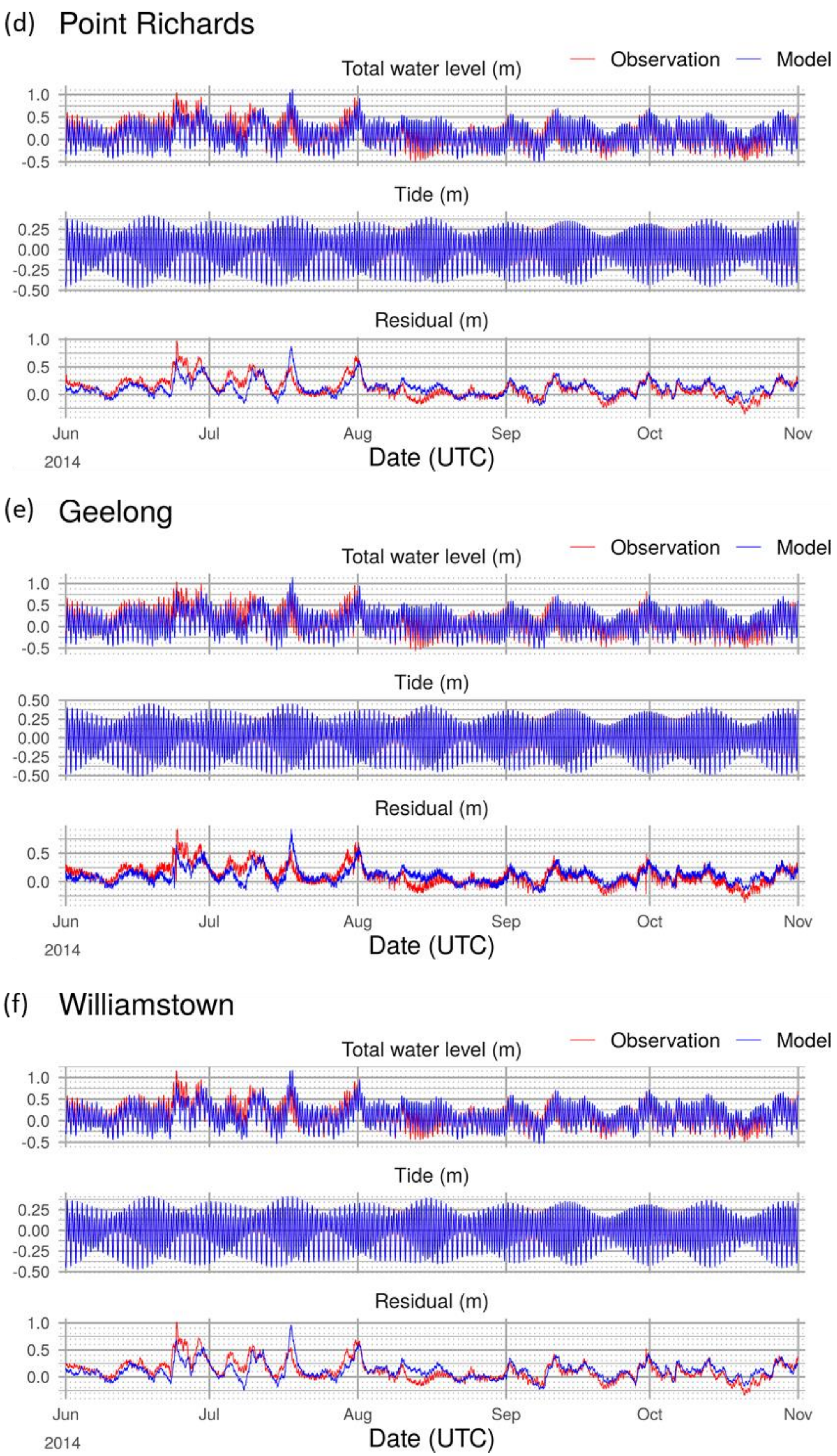

Figure J5: Continued.

(g) St Kilda Marina

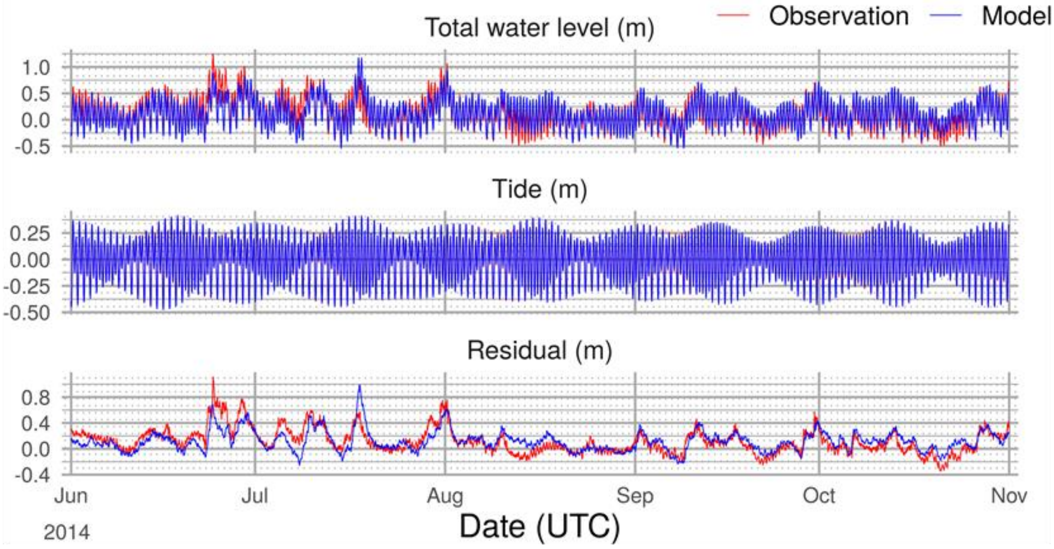

(h) Mornington Pier

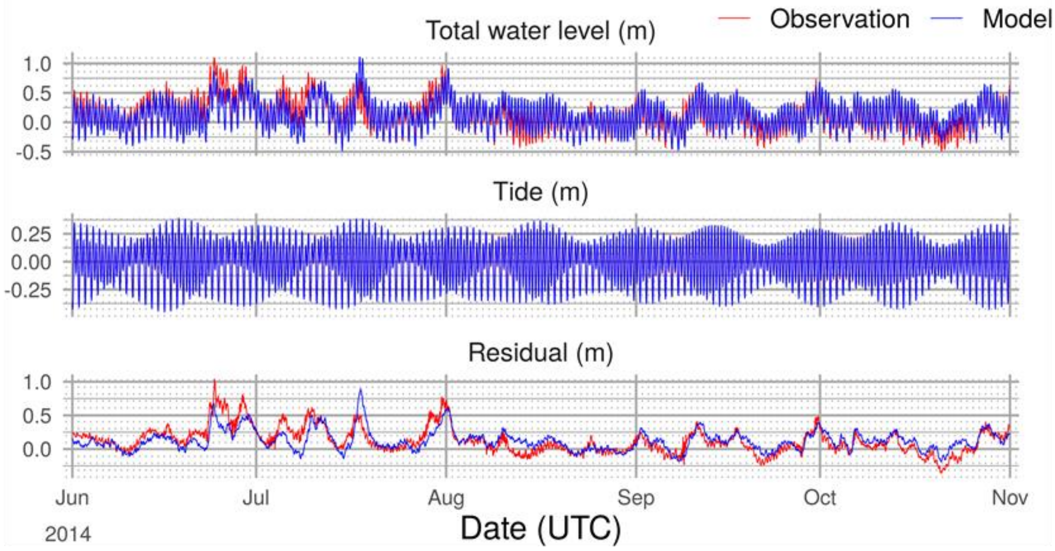

(i) Hovell Pile

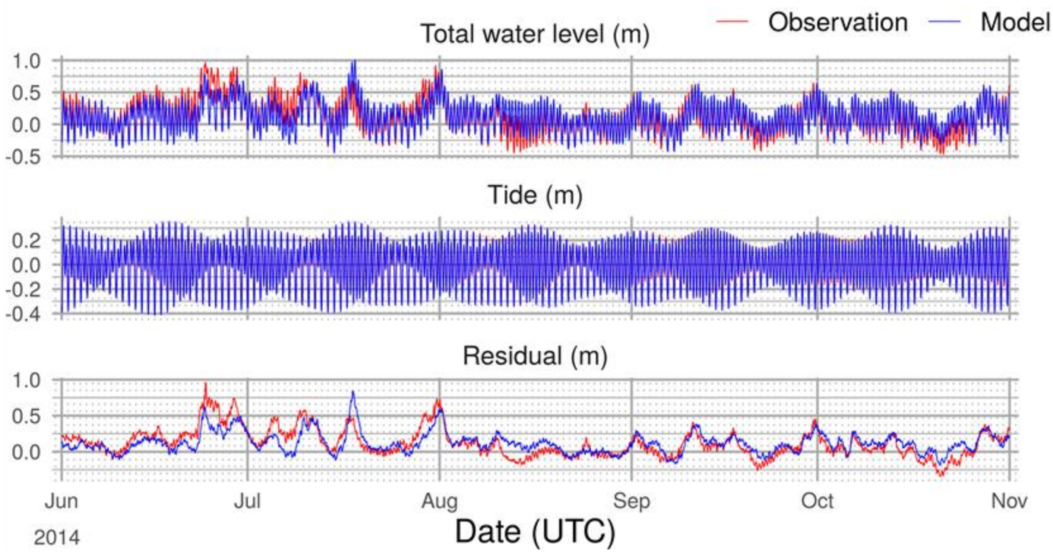

Figure J5: Continued.

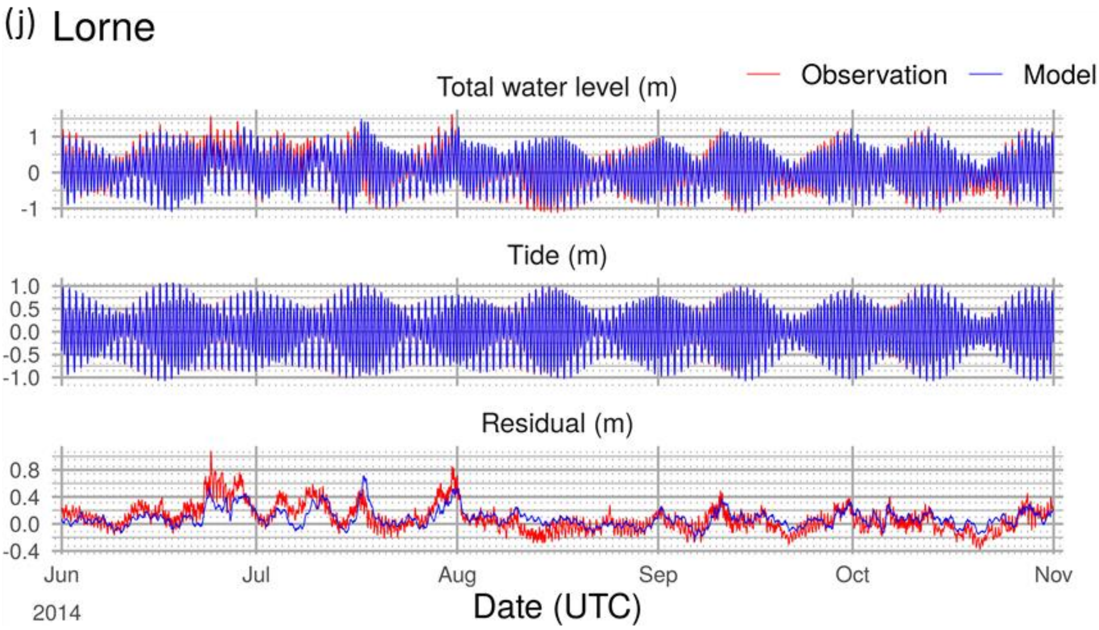

Figure J5: Continued.

Currents

Currents in the SCHISM model are compared with observations from current meters at the entrance to PPB over the time period October 2011. The locations of the gauges are shown in Figure K6. Results at RB are similar to ORB and so are not shown for brevity. An additional validation time for December 2011 was also carried out, but due to the similarity of the findings and in the interests of brevity, those comparisons are not shown here.

Site Name	Site ID
Offshore Sand Bar	OSB
Outer Rip Bank	ORB
Nepean Bank	NB
Rip Bank	RB

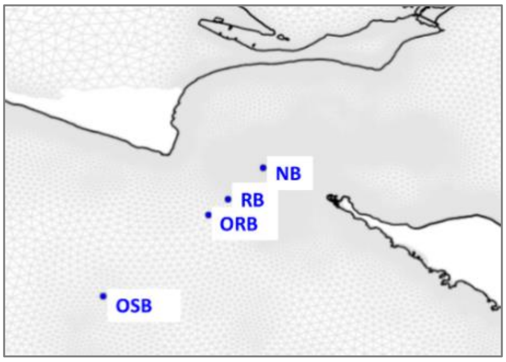

Figure J6: Location of current meters used for hydrodynamic validation.

Figure J7 shows time series of depth-averaged east-west, north-south component currents, total current speed and direction for Offshore Sand Bar. While there is a small phase error evident between the modelled and observed north-south component current (Figure J7-b), the current magnitudes in both the east-west and north-south direction are well captured (Figure J7a, b). The current speeds vary from about 0.1 to 0.9 ms^{-1} (Figure J7 c). The current directions (Figure J7d and K8) show that the model has a slight bias towards a more westward current during the ebb flow phase compared to observations, which indicates a more southwestward current.

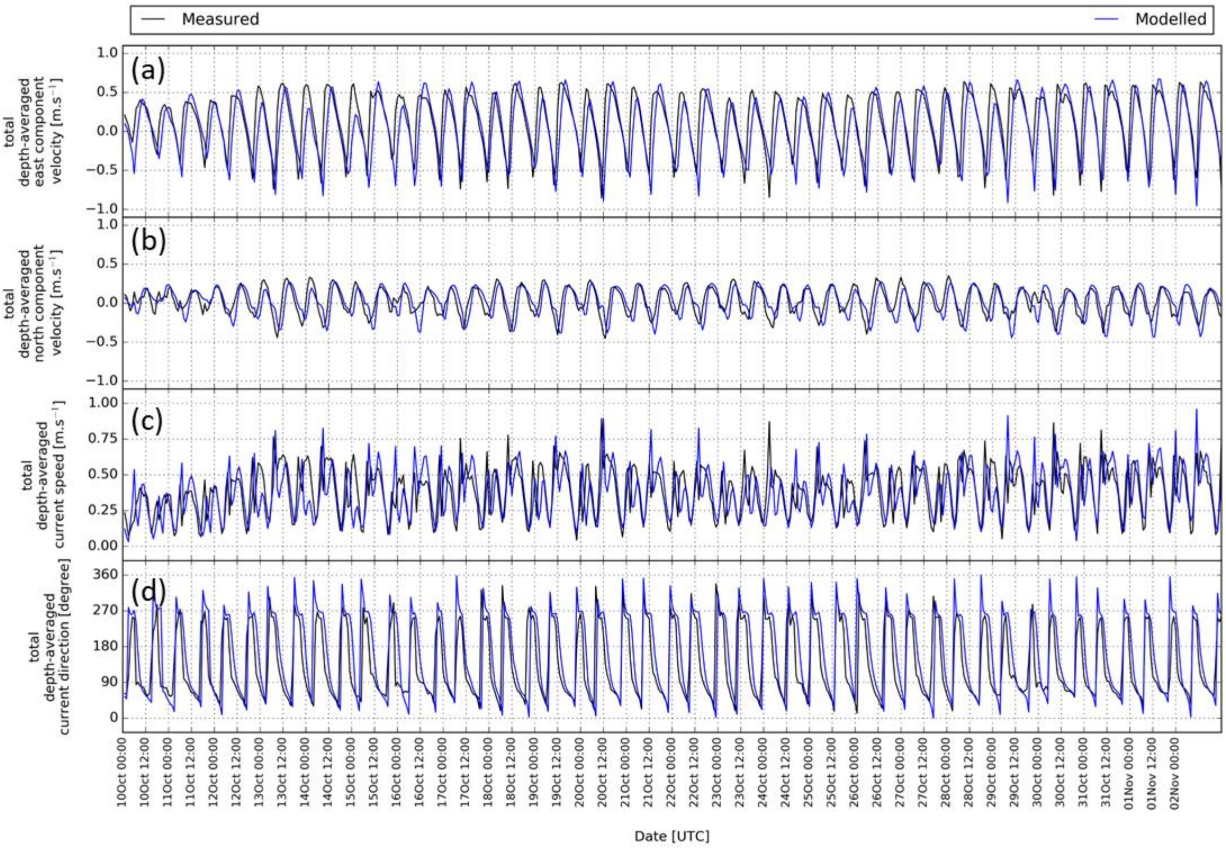

Figure J7: Measured (black) and modelled (blue) total depth-averaged current timeseries for October 2011 at Offshore Sand Bar. The panels show (a) east component velocity, (b) north component velocity, (c) total current speed and (d) depth-averaged current direction.

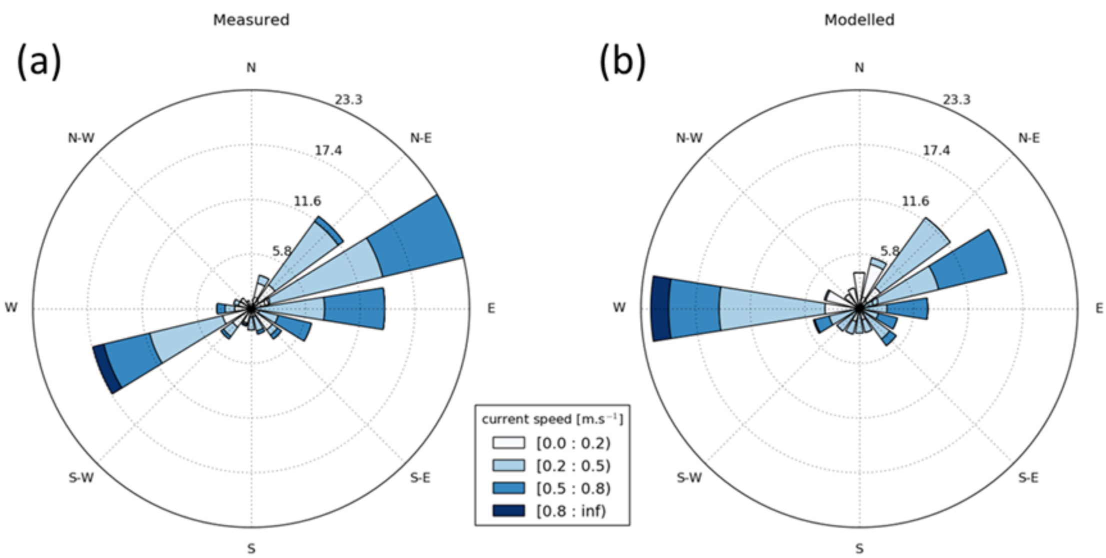

Figure J8: Measured (left) and modelled (right) total depth-averaged current roses for October 2011 at Offshore Sand Bar.

At Outer Rip Bank, the model slightly underestimates both the east and north component currents (Figures J9a, b) and a slight phase error is apparent in the modelled results resulting in an underestimation in the maximum current speed of up to 0.4 ms^{-1} (Figure J9c). The directions produced by the model show excellent agreement with observations (Figures J10).

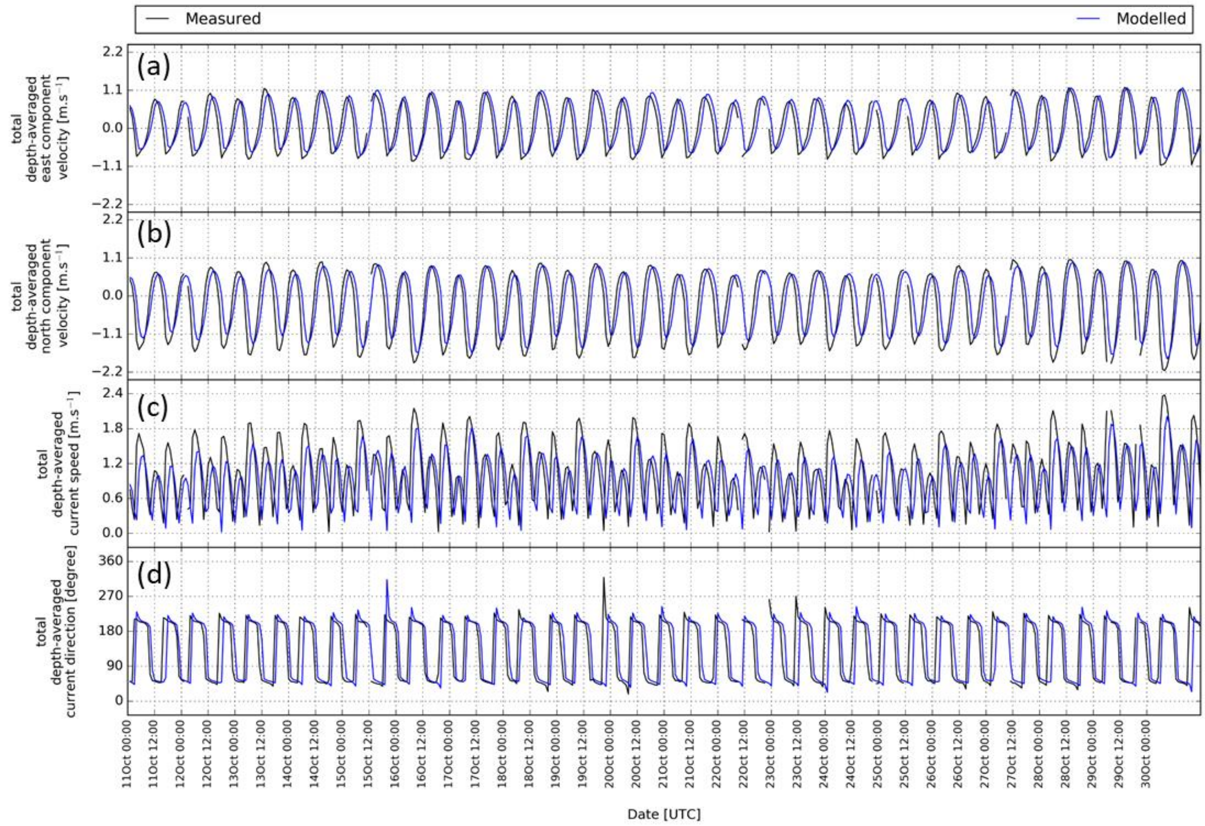

Figure J9: Measured (black) and modelled (blue) total depth-averaged current timeseries for October 2011 at Offshore Rip Bank. The panels show (a) east component velocity, (b) north component velocity, (c) total current speed and (d) depth-averaged current direction.

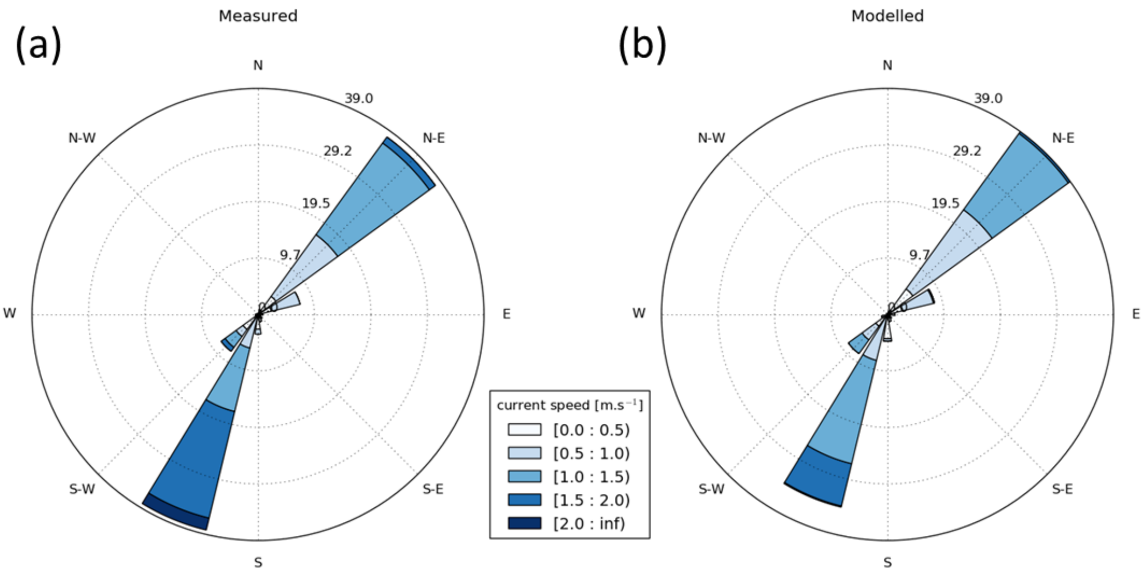

Figure J10: Measured (left) and modelled (right) total depth-averaged current roses for October 2011 at Offshore Rip Bank.

At Nepean Bank, the model shows an underestimation of the east-west component current and hence total current speed but shows close agreement with observations for the north-south component current (Figure J11a-c). Current directions in the model show a tendency to roses are also shown for the monthlong periods at Outer Rip Bank in Figure J12. There is a tendency for the model to produce currents with a stronger northward component compared to the more north-north-westward component in the observations.

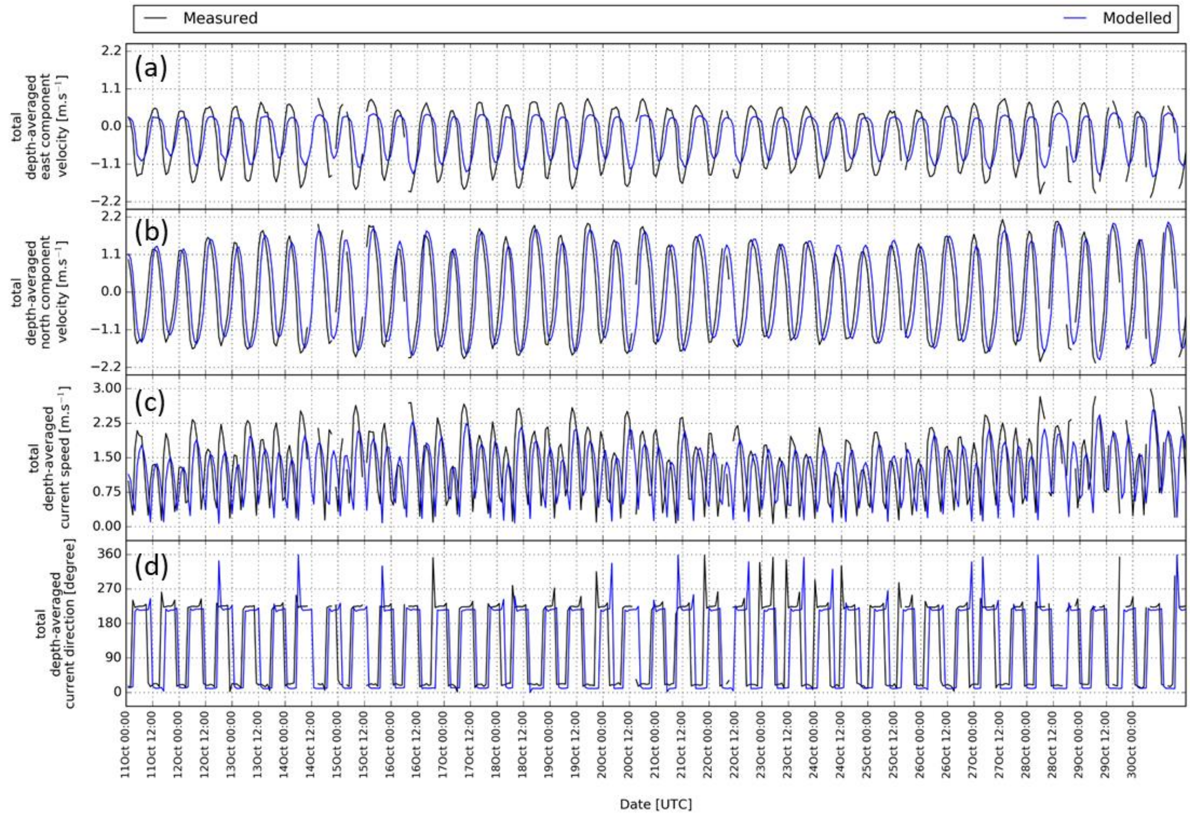

Figure J11: Measured (black) and modelled (blue) total depth-averaged current timeseries for October 2011 at Nepean Bank. The panels show (a) depth-averaged east component velocity, (b) from top to bottom show depth-averaged north component velocity, (c) total current speed and (d) depth-averaged current direction.

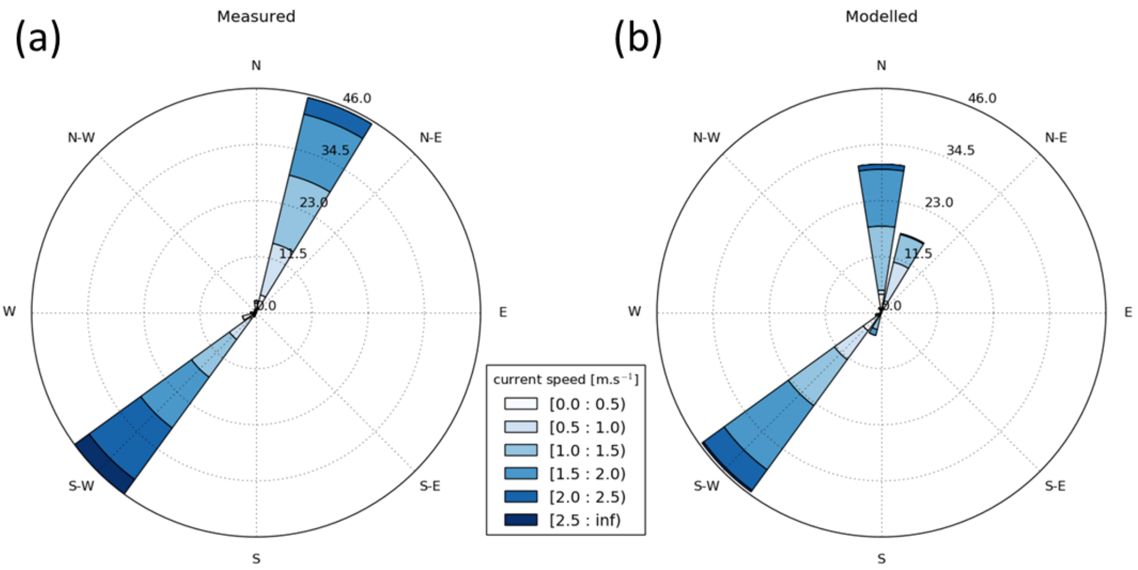

Figure J12: Measured (left) and modelled (right) total depth-averaged current roses for October 2011 at Nepean Bank.

Waves

Waves simulated by the SCHISM-WWMIII model were calibrated against wave observations from the Portsea wave buoy and two bottom-mounted acoustic wave and current profilers (AWACs) near the entrance to PPB (locations shown in Figure 8.11) during two simulation time periods between 1 October 2011 and 1 April 2012, and between June 2014 and August 2014 (when the AWACs were deployed). Figure J13 provides example time-series comparisons between measured and modelled wave heights (Hs) over two durations in October and December during the first (2011) time period. The influence of the semi-diurnal tides on significant wave height (Hs) at the two AWACs at the Entrance to PPB (Rip Bank and Outer Rip Bank) is well captured in the model, with the higher waves occurring during ebb tidal flow and lower waves occurring during the flood tide phase. The magnitudes of Hs are also well captured at these two AWACs for both time periods. The Portsea wave buoy data (in deeper water and away from the entrance channel) does not exhibit the semi-diurnal influence on wave height, which is also captured by the model. The wave heights are mostly well captured at the Portsea buoy although some events that occur during the time period are slightly under-estimated by the model.

Table J1 provides an extended summary of harmonic tidal analysis of major tidal constituents, phases and tidal summary statistics. These constituents and predictions are based on all inferred constituents (68) under both the baseline and the 0.2 m, 0.8 m and 1.4 m SLR scenario between 1980-1999 (chosen as a full tidal epoch and for consistency in comparison). Note that while tidal amplitudes are significantly different (within the bay) between the baseline and 1.4 m SLR scenarios, tidal phases (or timing) was not significantly different.

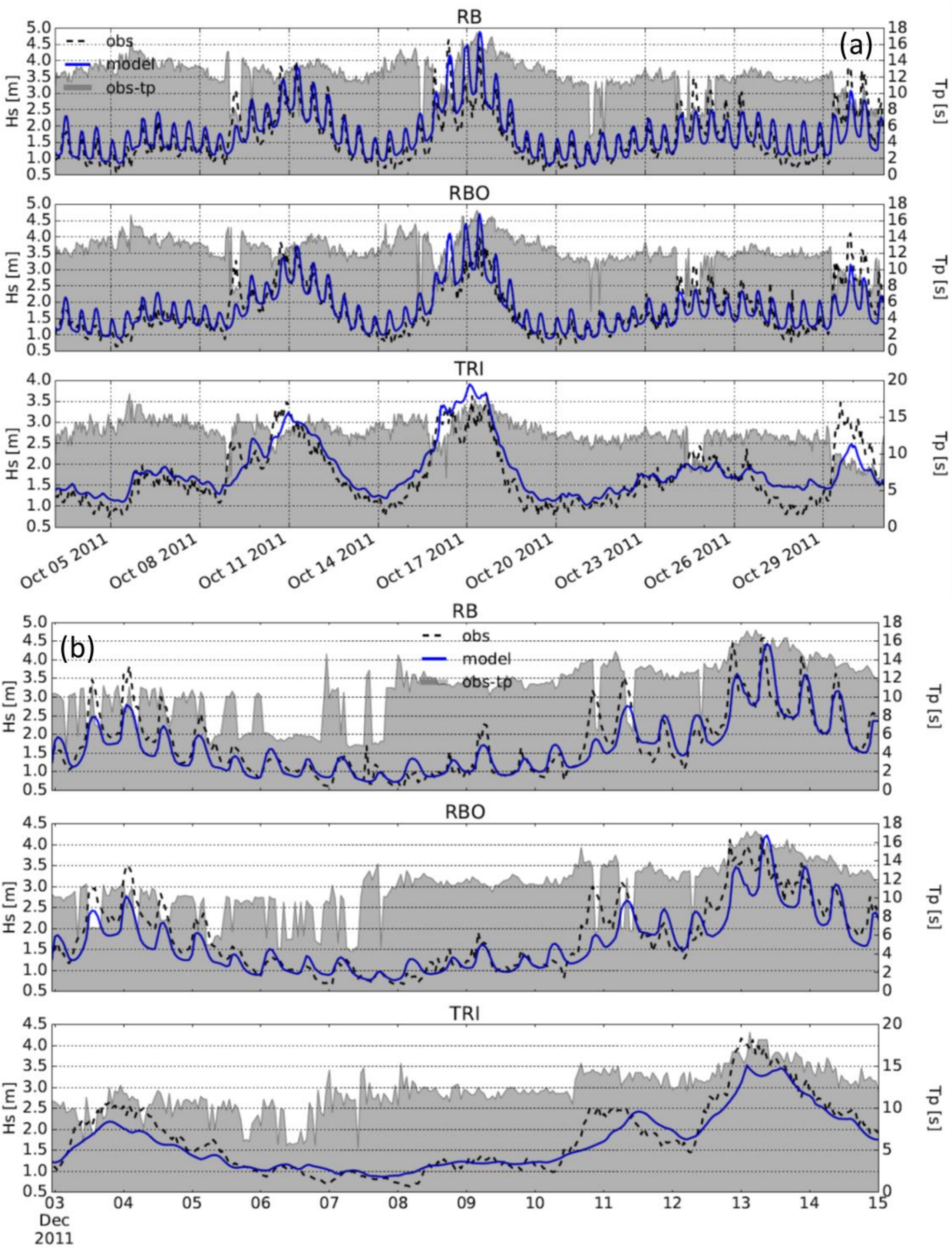

Figure J13: Measured (black line) and modelled (blue line) timeseries of significant wave height (Hs) at the three observation locations shown in Figure 8.11 during (a) October 2011 and (b) December 2011. Observed peak period (Tp) is plotted in grey to assist in interpretation.

Table J1: Modelled changes in amplitude and phase of major tidal constituents and summary tidal statistics between baseline sea level the 0.2 m, 0.8 m and 1.4m SLR scenarios at PPB tide gauge locations.

	Williamstown				St Kilda				Geelong				Mornington				Hovell Pile				Lorne			
Const.	Base-line	slr02	slr08	slr14	Base-line	slr02	slr08	slr14	Base-line	slr02	slr08	slr14	Base-line	slr02	slr08	slr14	Base-line	slr02	slr08	slr14	Base-line	slr02	slr08	slr14
M2 amp.	0.25	0.26	0.27	0.29	0.25	0.26	0.27	0.29	0.28	0.29	0.31	0.32	0.24	0.24	0.26	0.27	0.21	0.22	0.23	0.25	0.60	0.60	0.60	0.60
M2 phase	243.2	242.7	240.9	239.6	243.4	242.9	241.2	239.8	244.5	243.7	241.6	240.0	244.3	243.7	241.9	240.5	234.3	234.9	235.8	236.2	140.9	141.0	141.0	141.1
S2 amp.	0.06	0.06	0.07	0.07	0.06	0.06	0.07	0.07	0.07	0.07	0.07	0.08	0.06	0.06	0.06	0.07	0.05	0.05	0.06	0.06	0.20	0.20	0.20	0.20
S2 phase	254.5	254.0	252.7	251.7	254.5	254.1	252.8	251.8	258.0	257.2	255.2	253.7	256.6	256.1	254.5	253.3	245.1	246.0	247.6	248.6	148.4	148.4	148.4	148.5
N2 amp.	0.04	0.04	0.04	0.04	0.04	0.04	0.04	0.04	0.04	0.04	0.05	0.05	0.04	0.04	0.04	0.04	0.03	0.03	0.04	0.04	0.11	0.11	0.11	0.11
N2 phase	57.2	56.7	55.3	54.1	57.4	56.9	55.5	54.3	59.2	58.5	56.6	55.1	58.2	57.8	56.3	55.1	46.6	47.4	48.9	49.7	315.9	315.9	316.0	316.0
K1 amp.	0.11	0.11	0.12	0.12	0.11	0.11	0.12	0.12	0.11	0.11	0.12	0.12	0.11	0.11	0.11	0.12	0.10	0.11	0.11	0.12	0.21	0.21	0.21	0.21
K1 phase	341.9	341.2	339.2	337.6	342.1	341.4	339.3	337.8	342.5	341.6	339.4	337.7	342.1	341.4	339.4	337.9	336.2	336.1	335.5	334.9	267.5	267.5	267.5	267.5
O1 amp.	0.07	0.08	0.08	0.08	0.07	0.08	0.08	0.08	0.08	0.08	0.08	0.08	0.07	0.07	0.08	0.08	0.07	0.07	0.08	0.08	0.14	0.14	0.14	0.14
O1 phase	67.0	66.4	64.5	63.1	67.1	66.5	64.6	63.2	67.7	67.0	64.9	63.3	67.6	66.9	65.1	63.6	62.4	62.3	61.7	61.1	358.3	358.3	358.4	358.4
SA amp.	0.02	0.02	0.02	0.02	0.02	0.02	0.02	0.02	0.02	0.02	0.02	0.02	0.03	0.03	0.03	0.03	0.03	0.03	0.03	0.03	0.03	0.03	0.03	0.03
SA phase	280.6	280.7	279.6	278.5	281.0	281.0	279.5	278.5	268.0	268.0	267.2	266.5	260.3	260.5	260.3	260.1	255.9	256.0	255.9	255.9	252.0	252.3	252.2	252.1
SSA amp.	0.01	0.01	0.01	0.01	0.01	0.01	0.01	0.01	0.01	0.01	0.01	0.01	0.01	0.01	0.01	0.01	0.01	0.01	0.01	0.01	0.00	0.00	0.00	0.00
SSA phase	292.9	291.7	292.2	292.9	292.9	291.6	292.0	292.8	283.3	282.8	283.7	284.7	279.1	278.5	279.5	280.4	276.2	275.8	276.7	277.8	247.3	246.6	247.0	247.2
HAT	0.44	0.44	0.46	0.48	0.44	0.44	0.46	0.48	0.51	0.52	0.54	0.56	0.42	0.43	0.45	0.47	0.39	0.39	0.41	0.43	1.14	1.15	1.14	1.14
LAT	-0.52	-0.53	-0.56	-0.58	-0.52	-0.53	-0.56	-0.58	-0.57	-0.58	-0.61	-0.64	-0.49	-0.50	-0.53	-0.56	-0.47	-0.48	-0.50	-0.53	-1.27	-1.27	-1.27	-1.27
MHHW	0.31	0.32	0.34	0.35	0.31	0.32	0.34	0.35	0.36	0.36	0.38	0.40	0.29	0.30	0.32	0.34	0.27	0.27	0.29	0.30	0.74	0.74	0.74	0.74
MLLW	-0.37	-0.38	-0.40	-0.42	-0.37	-0.38	-0.40	-0.42	-0.42	-0.43	-0.45	-0.47	-0.35	-0.36	-0.38	-0.40	-0.33	-0.33	-0.35	-0.37	-0.82	-0.82	-0.82	-0.82
total range	0.90	0.92	0.98	1.03	0.90	0.92	0.98	1.03	1.04	1.06	1.11	1.16	0.85	0.87	0.93	0.97	0.79	0.80	0.85	0.90	2.40	2.40	2.40	2.40

Appendix K. Coastal Hazards by LGA

Additional bar charts summarising the hazard zones for the different SLR scenarios are provided for each of the ten Local Government Areas around PPB. Note that areas of inundation are calculated based on C-FAST modelling and do not include the slightly amended inundation areas that arise when the modelled wave setup is included.

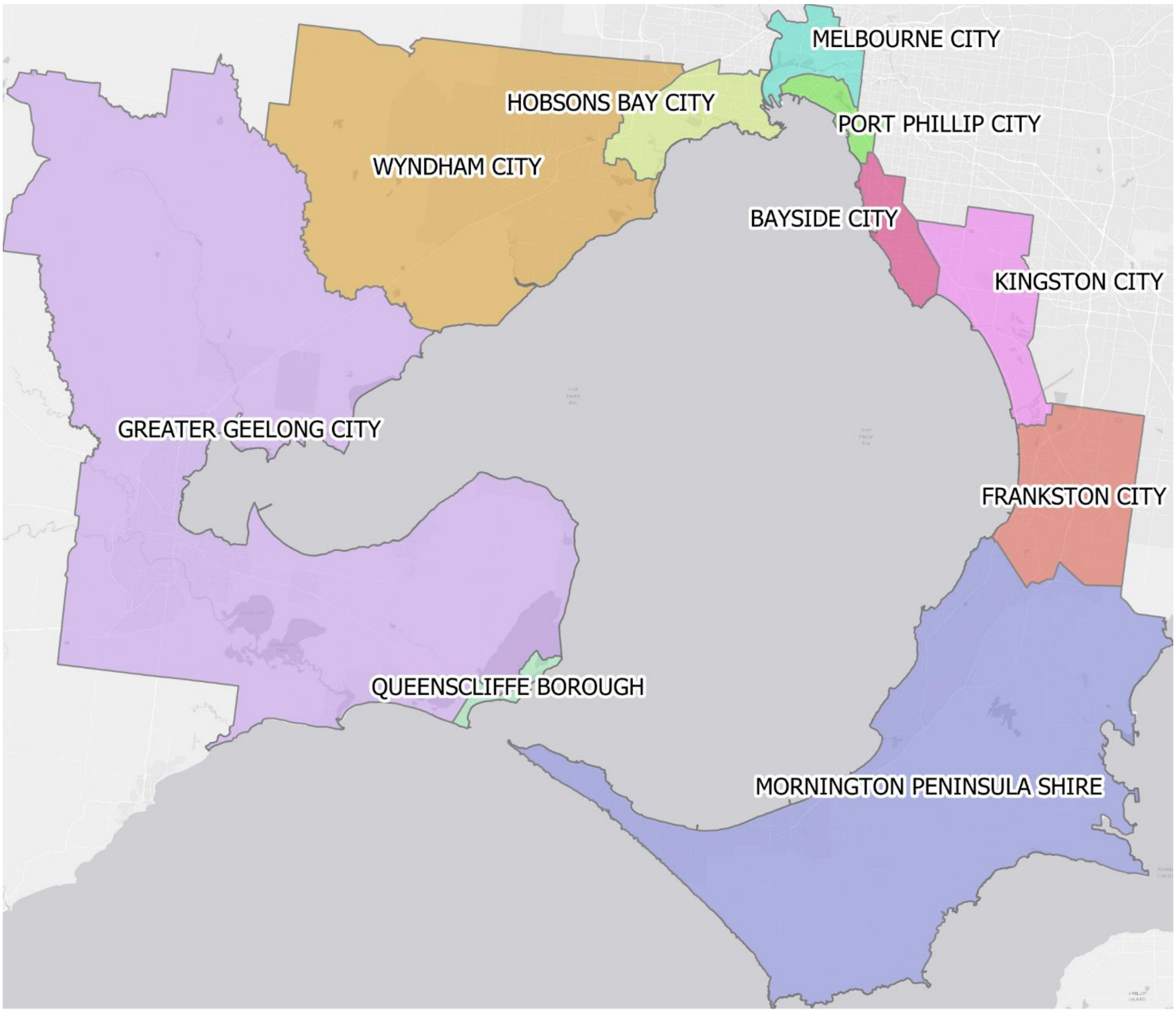

Figure K1: Map showing the LGA boundaries around PPB.

Borough of Queenscliffe

(a)

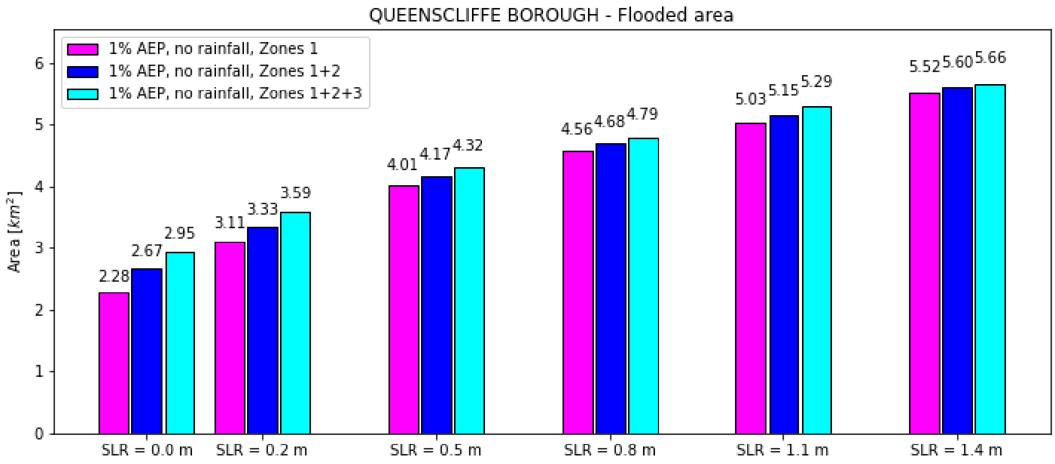

(b)

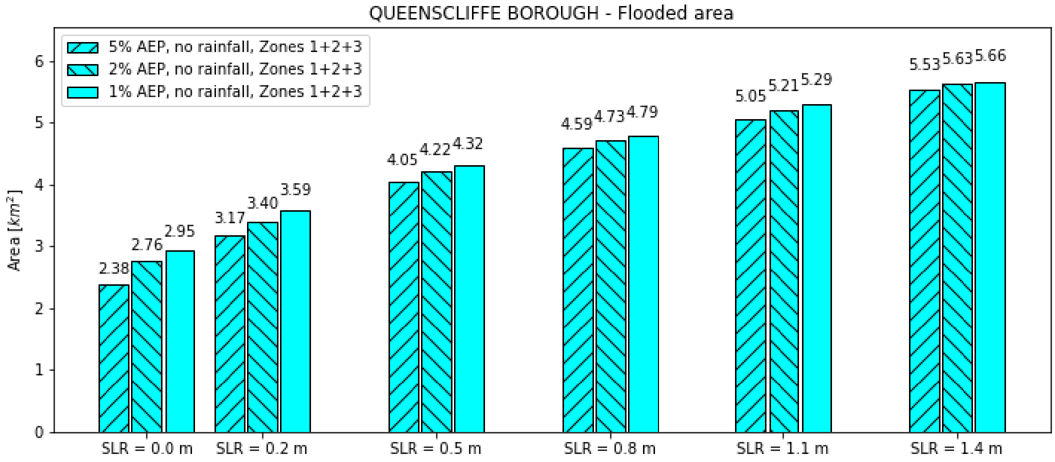

Figure K2: (a) Change in inundation area with SLR for a 1% AEP storm surge and no rainfall with 95% (zone 1), 50% (zone 2) and 95 % (zone 3) likelihood scenarios, (b) Change in inundation area with SLR for a 1%, 2% and 5% AEP storm surge, no rainfall and for zone 3 (i.e. 5% likelihood) scenario, (c) Total area of surface water, shallow, intermediate and deep ground water and (d) change to the total area of the layers under the different SLR scenarios. (c)

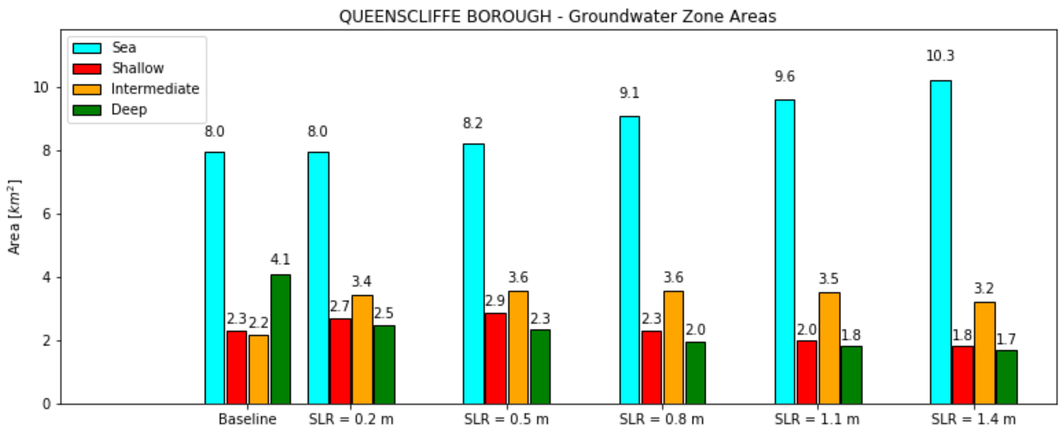

(d)

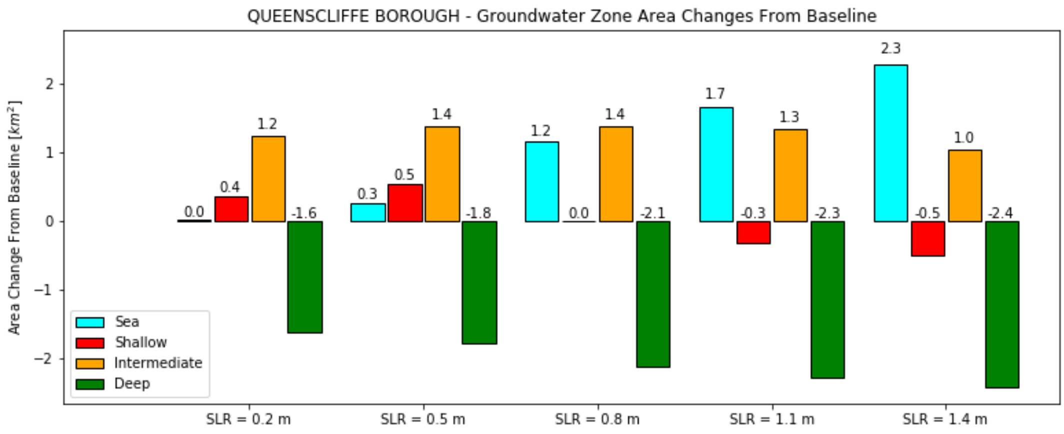

Figure K2: Continued.

Greater Geelong City

(a)

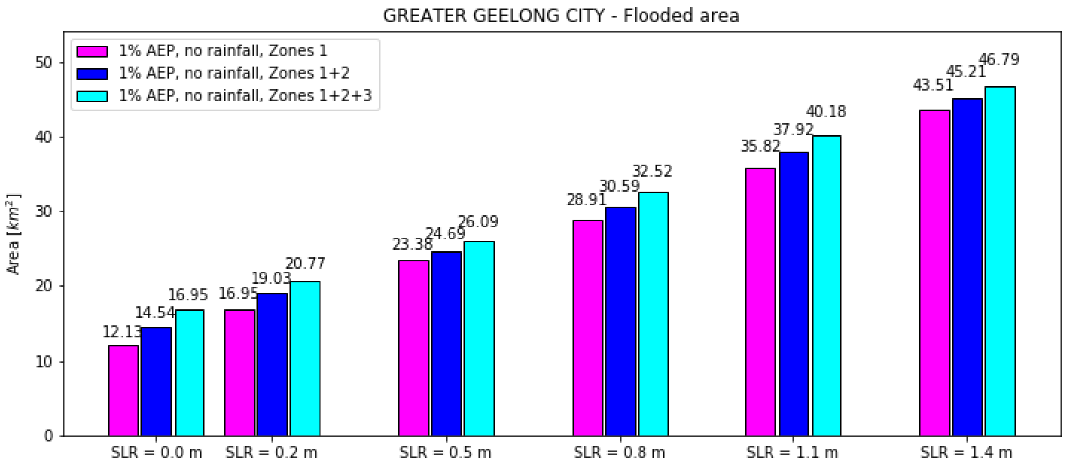

(b)

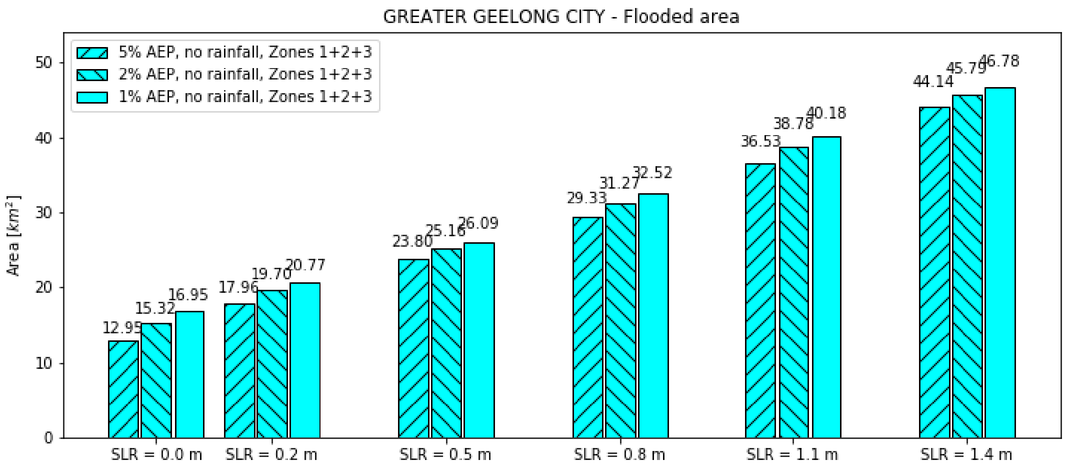

Figure K3: (a) Change in inundation area with SLR for a 1% AEP storm surge and no rainfall with 95% (zone 1), 50% (zone 2) and 95 % (zone 3) likelihood scenarios, (b) Change in inundation area with SLR for a 1%, 2% and 5% AEP storm surge, no rainfall and for zone 3 (i.e. 5% likelihood) scenario, (c) Total area of surface water, shallow, intermediate and deep ground water and (d) change to the total area of the layers under the different SLR scenarios.

(c)

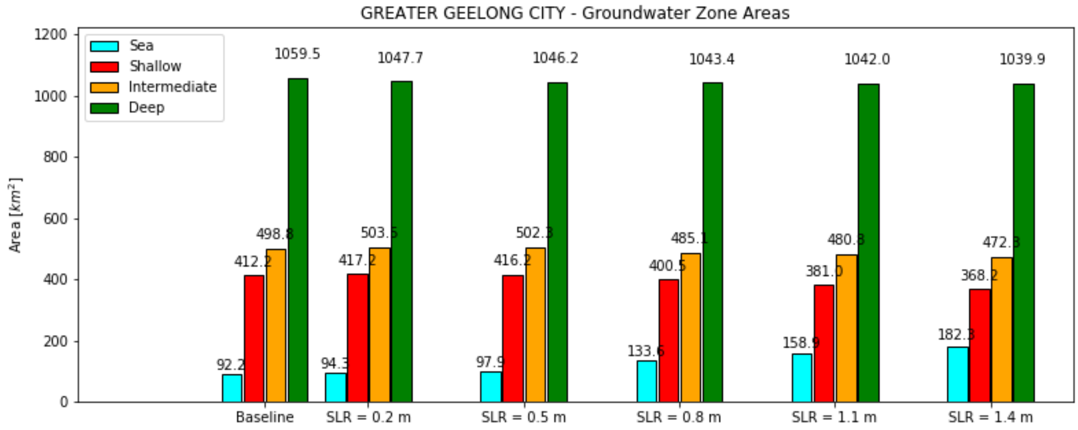

(d)

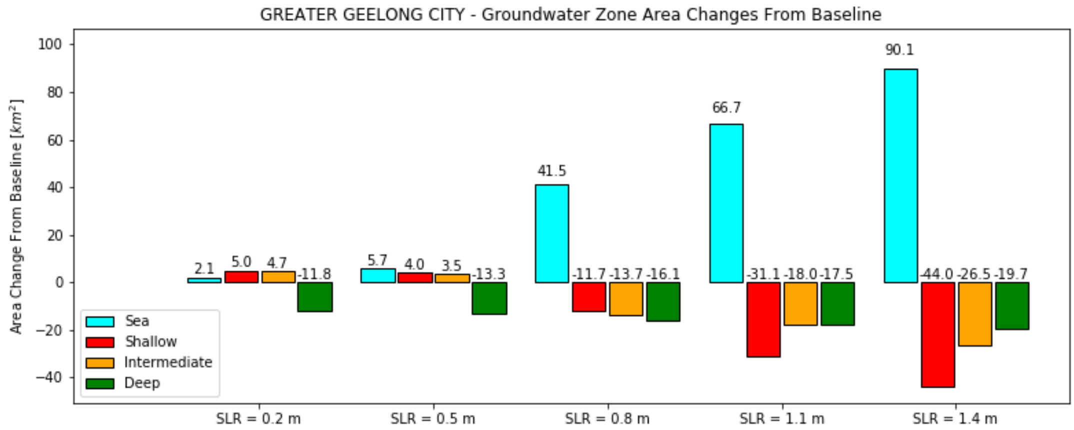

Figure K3: Continued.

Wyndham City

(a)

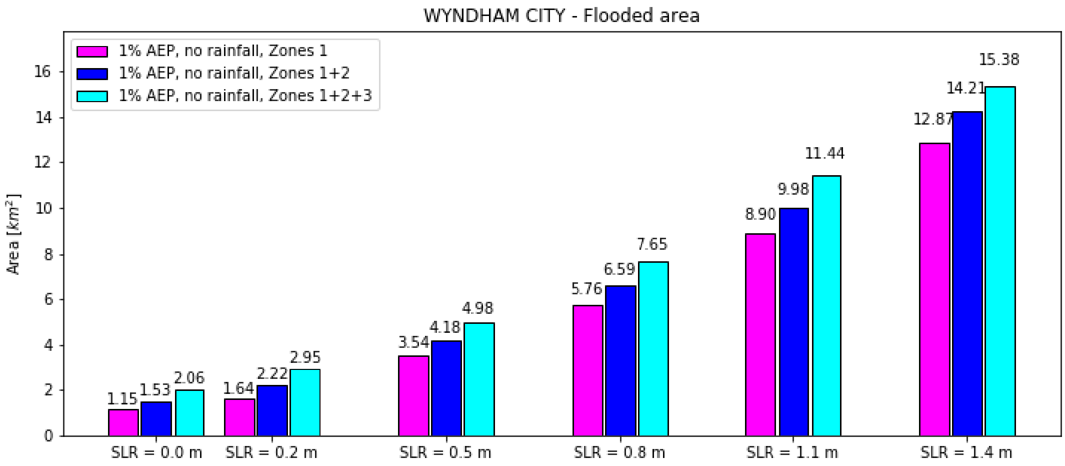

(b)

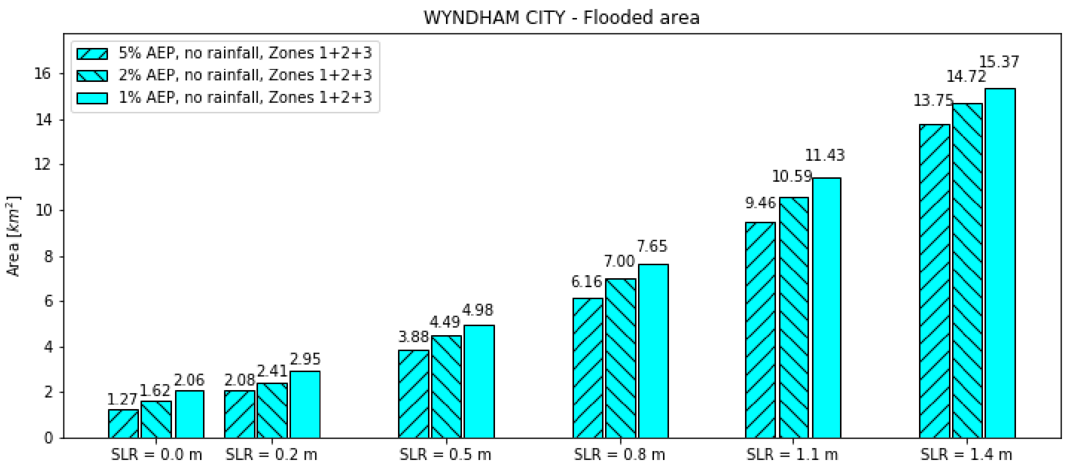

Figure K4: (a) Change in inundation area with SLR for a 1% AEP storm surge and no rainfall with 95% (zone 1), 50% (zone 2) and 95 % (zone 3) likelihood scenarios, (b) Change in inundation area with SLR for a 1%, 2% and 5% AEP storm surge, no rainfall and for zone 3 (i.e. 5% likelihood) scenario, (c) Total area of surface water, shallow, intermediate and deep ground water and (d) change to the total area of the layers under the different SLR scenarios.

(c)

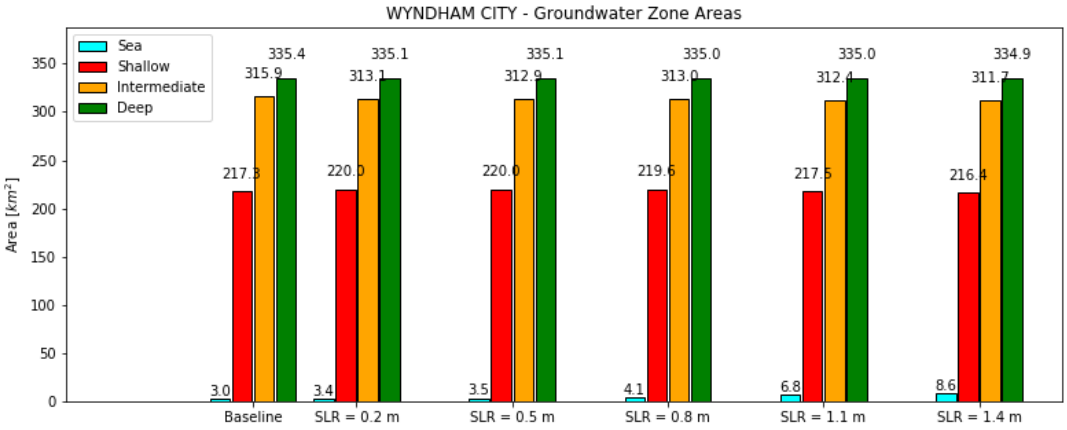

(d)

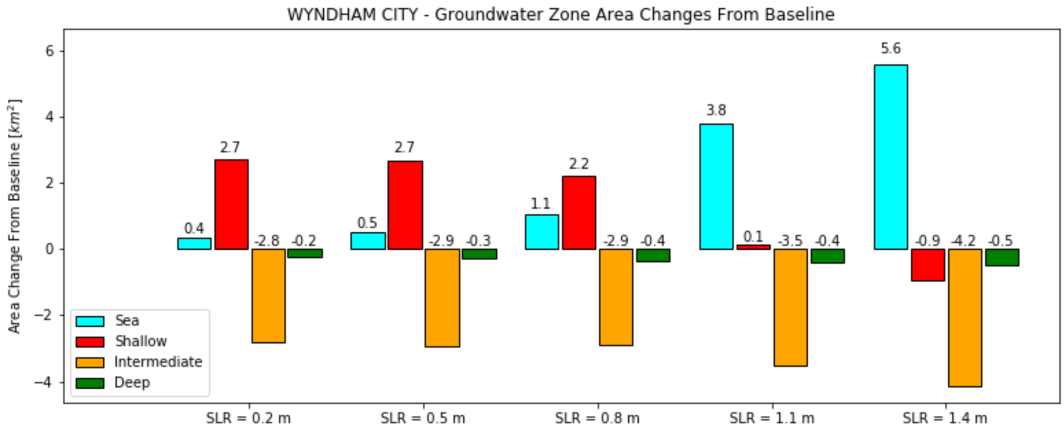

Figure K4: Continued.

Hobsons Bay City

(a)

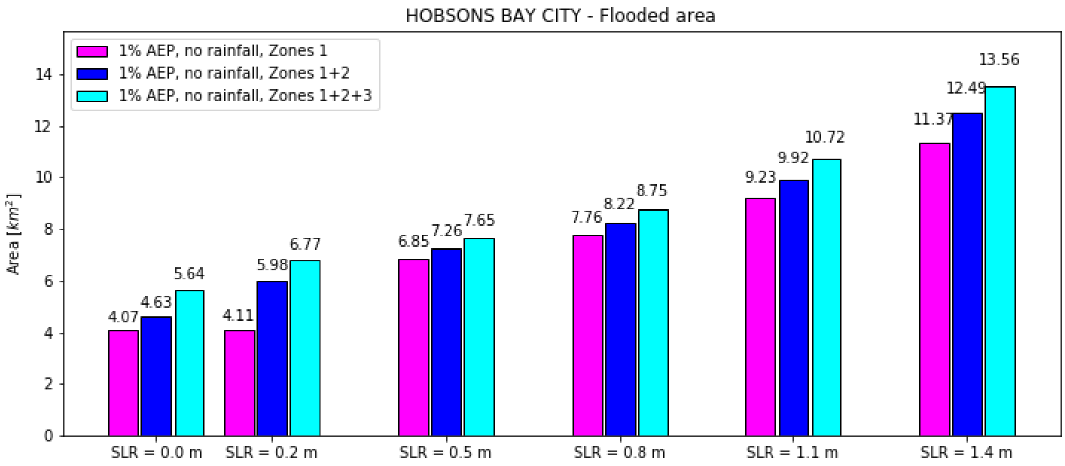

(b)

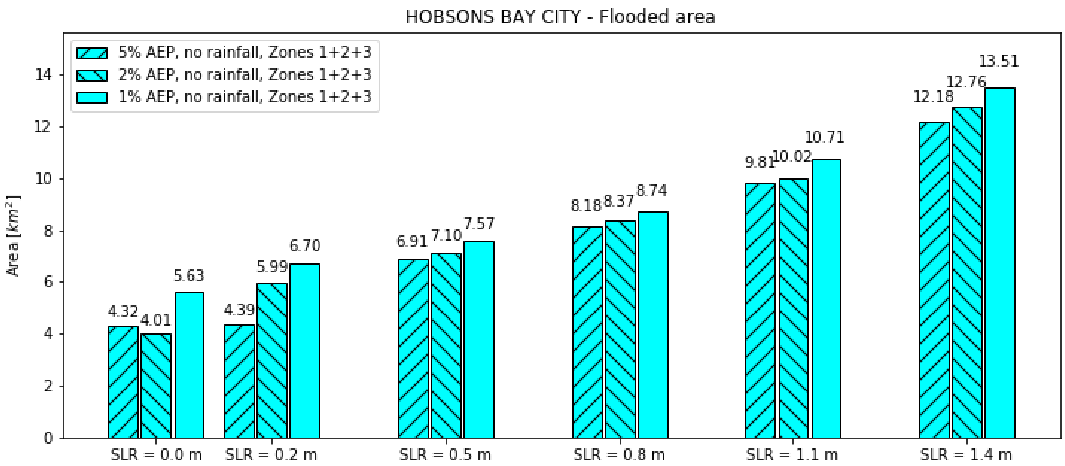

Figure K5: (a) Change in inundation area with SLR for a 1% AEP storm surge and no rainfall with 95% (zone 1), 50% (zone 2) and 95 % (zone 3) likelihood scenarios, (b) Change in inundation area with SLR for a 1%, 2% and 5% AEP storm surge, no rainfall and for zone 3 (i.e. 5% likelihood) scenario, (c) Total area of surface water, shallow, intermediate and deep ground water and (d) change to the total area of the layers under the different SLR scenarios.

(c)

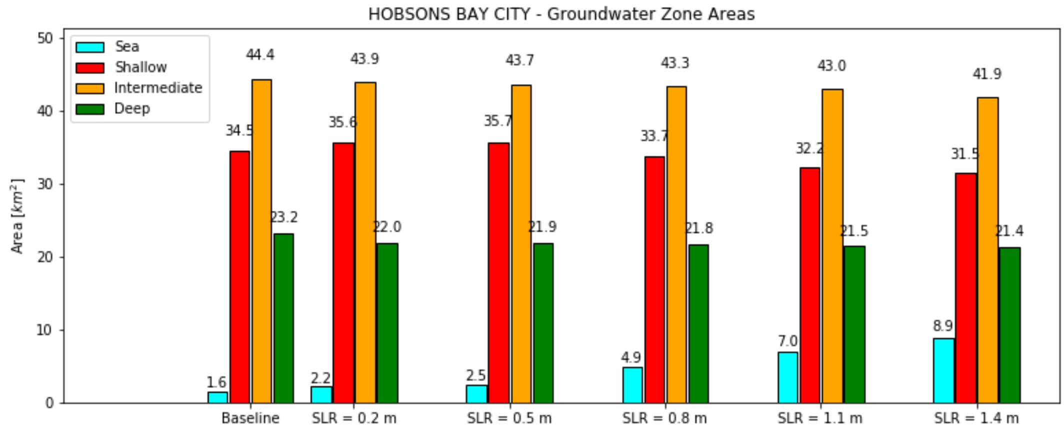

(d)

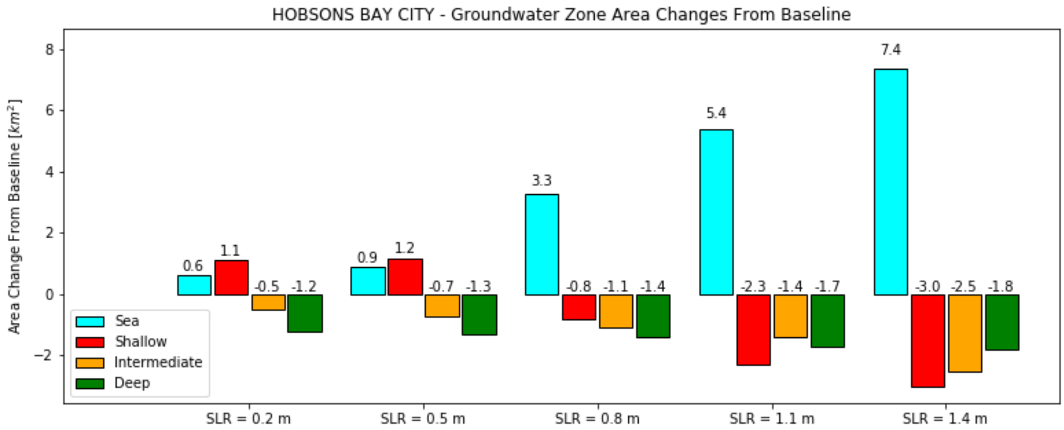

Figure K5: Continued.

Melbourne City

(a)

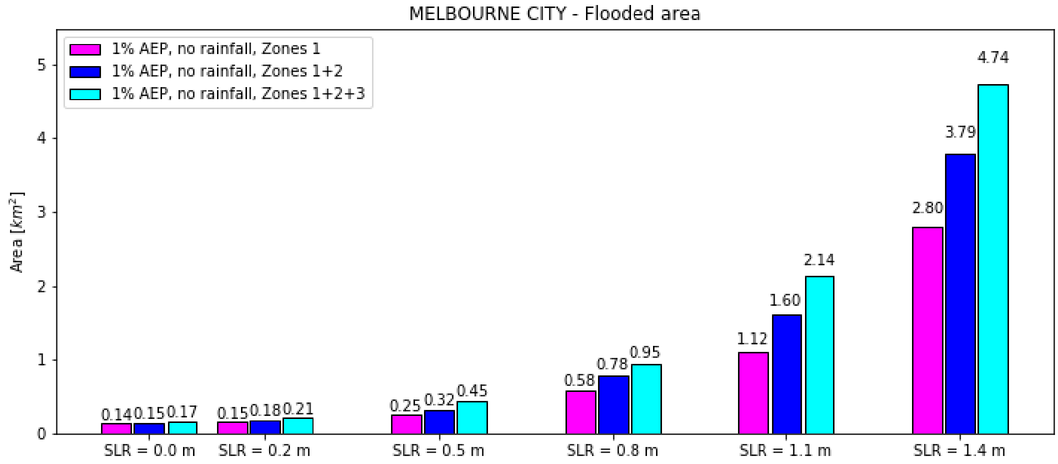

(b)

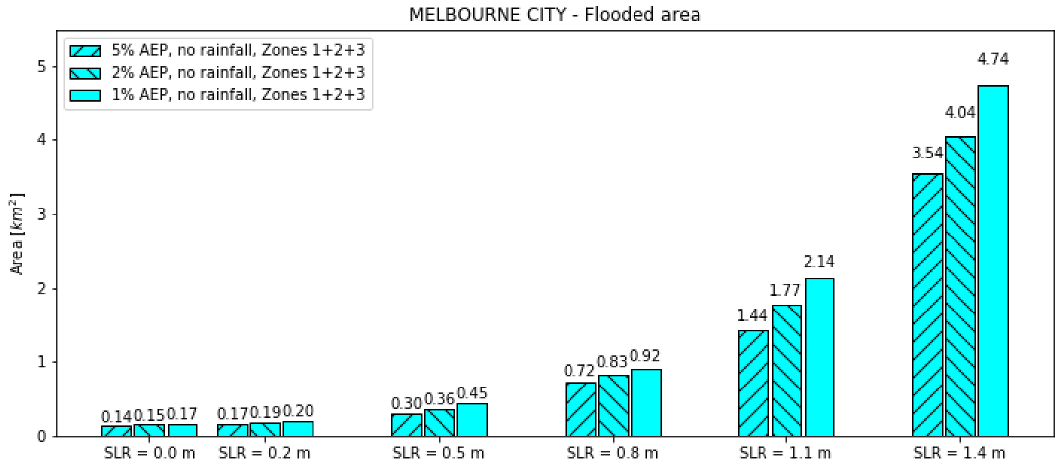

Figure K6: (a) Change in inundation area with SLR for a 1% AEP storm surge and no rainfall with 95% (zone 1), 50% (zone 2) and 95 % (zone 3) likelihood scenarios, (b) Change in inundation area with SLR for a 1%, 2% and 5% AEP storm surge, no rainfall and for zone 3 (i.e. 5% likelihood) scenario, (c) Total area of surface water, shallow, intermediate and deep ground water and (d) change to the total area of the layers under the different SLR scenarios.

(c)

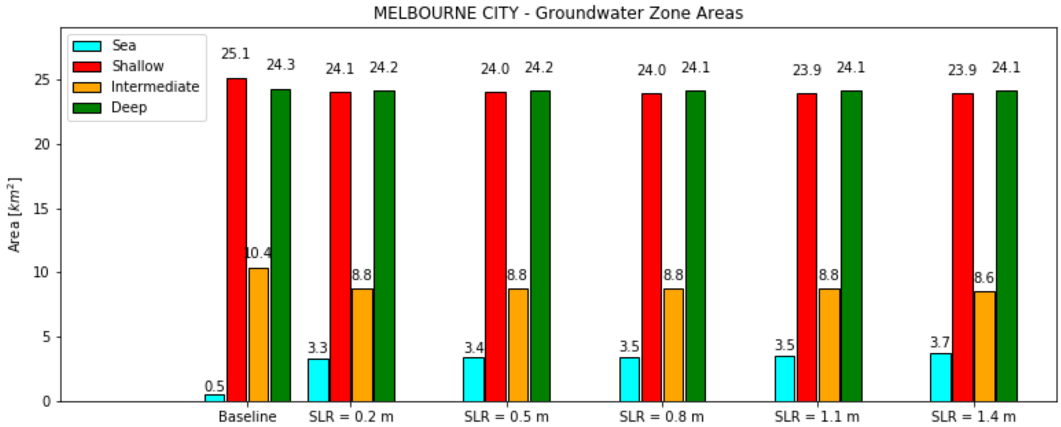

(d)

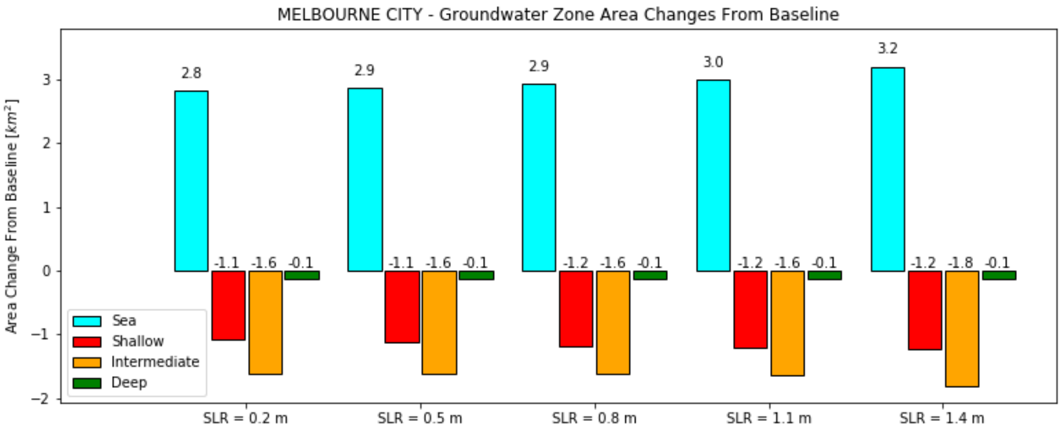

Figure K6: Continued.

Port Phillip City

(a)

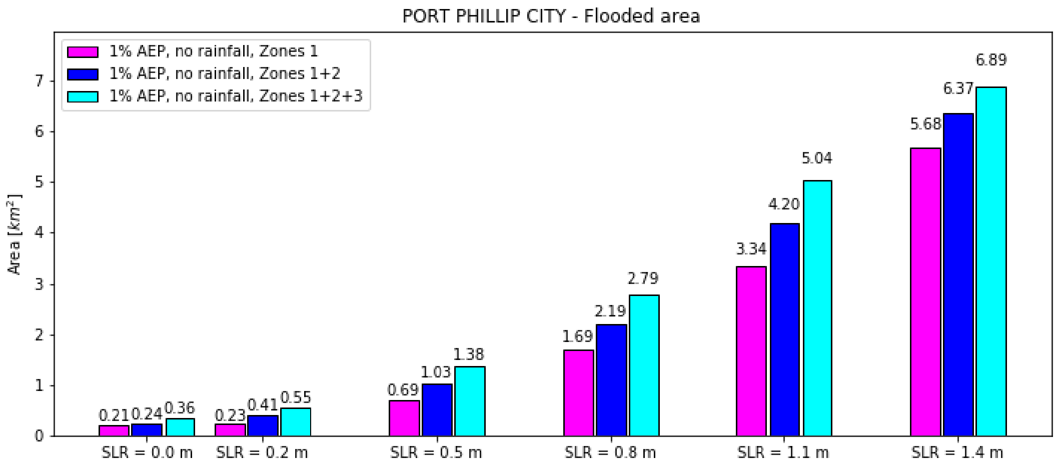

(b)

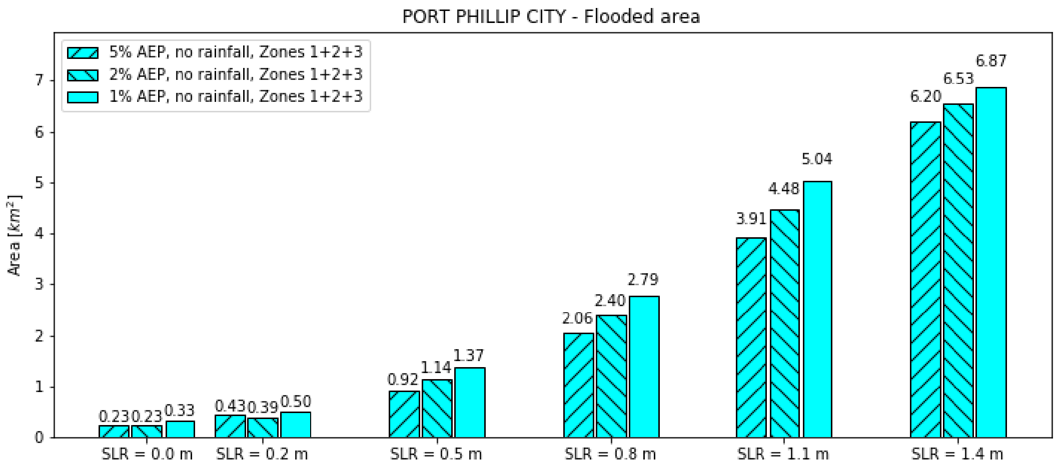

Figure K7: (a) Change in inundation area with SLR for a 1% AEP storm surge and no rainfall with 95% (zone 1), 50% (zone 2) and 95 % (zone 3) likelihood scenarios, (b) Change in inundation area with SLR for a 1%, 2% and 5% AEP storm surge, no rainfall and for zone 3 (i.e. 5% likelihood) scenario, (c) Total area of surface water, shallow, intermediate and deep ground water and (d) change to the total area of the layers under the different SLR scenarios.

(c)

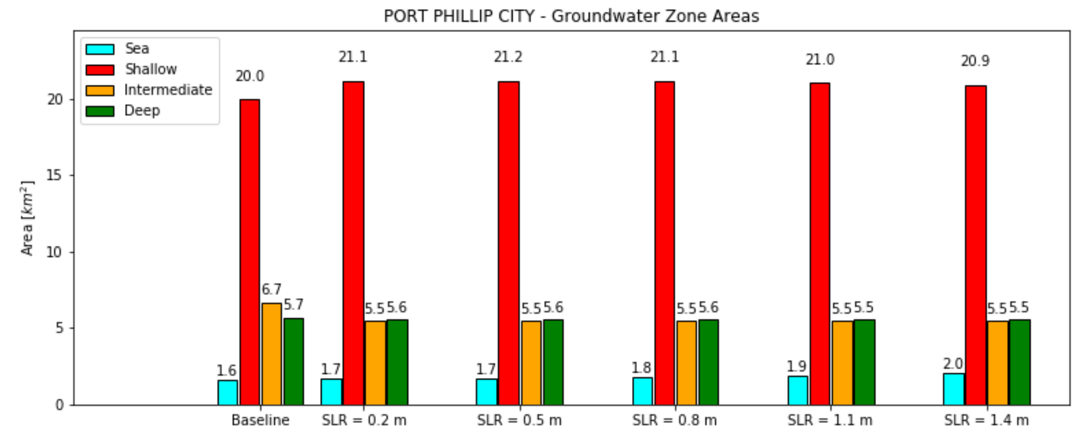

(d)

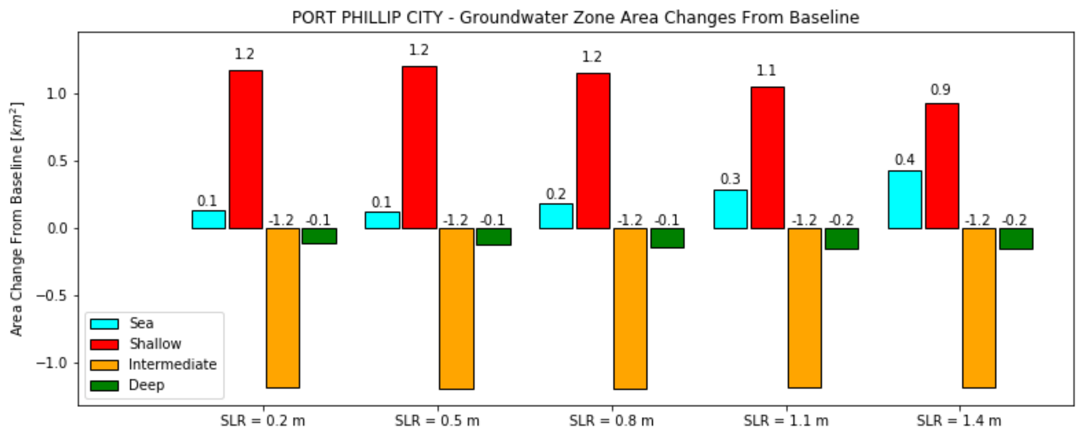

Figure K7: Continued.

Bayside City

(a)

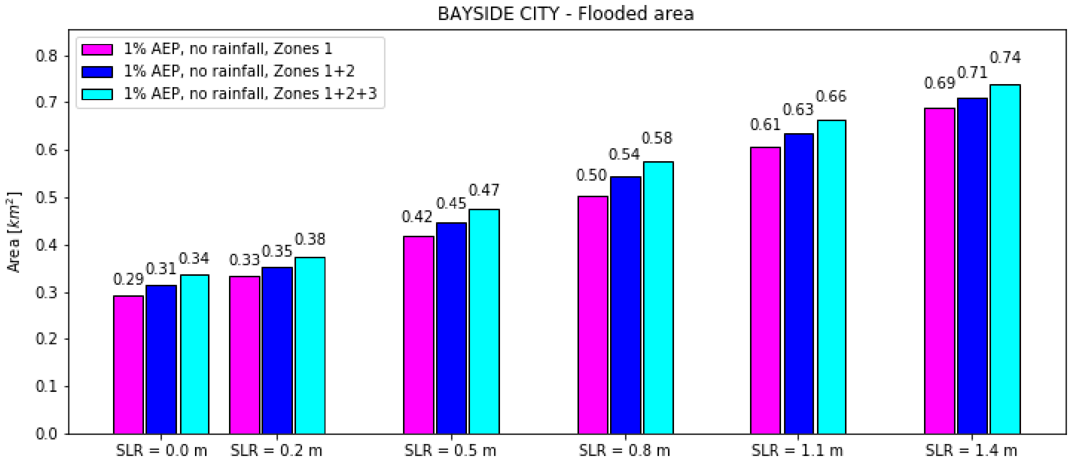

(b)

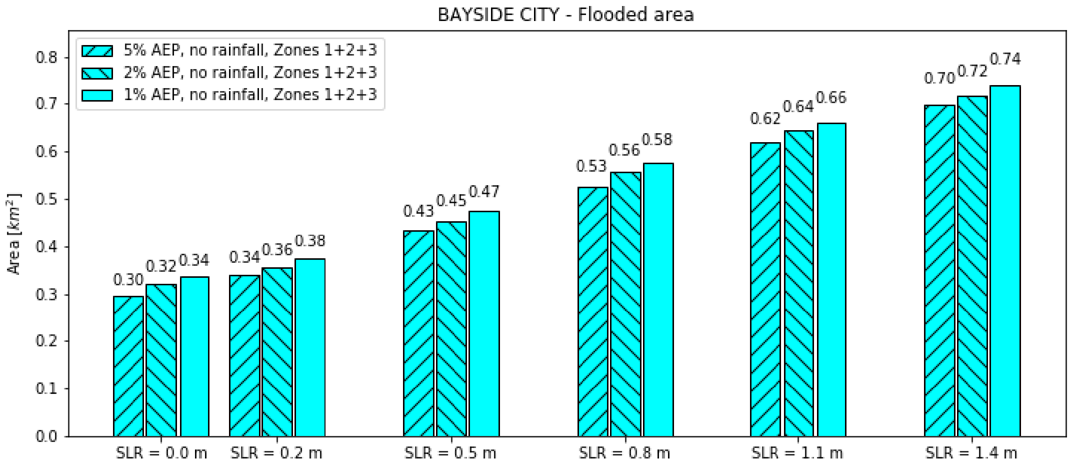

Figure K8: (a) Change in inundation area with SLR for a 1% AEP storm surge and no rainfall with 95% (zone 1), 50% (zone 2) and 95 % (zone 3) likelihood scenarios, (b) Change in inundation area with SLR for a 1%, 2% and 5% AEP storm surge, no rainfall and for zone 3 (i.e. 5% likelihood) scenario, (c) Total area of surface water, shallow, intermediate and deep ground water and (d) change to the total area of the layers under the different SLR scenarios.

(c)

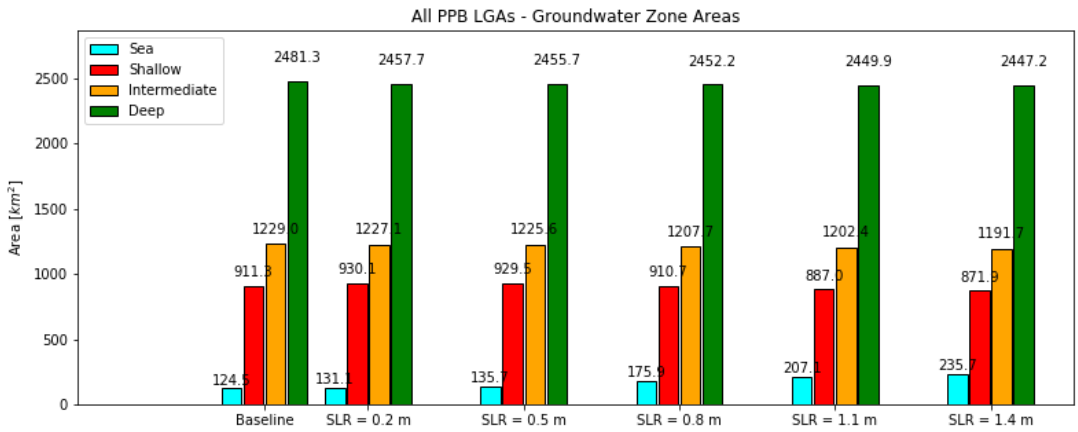

(d)

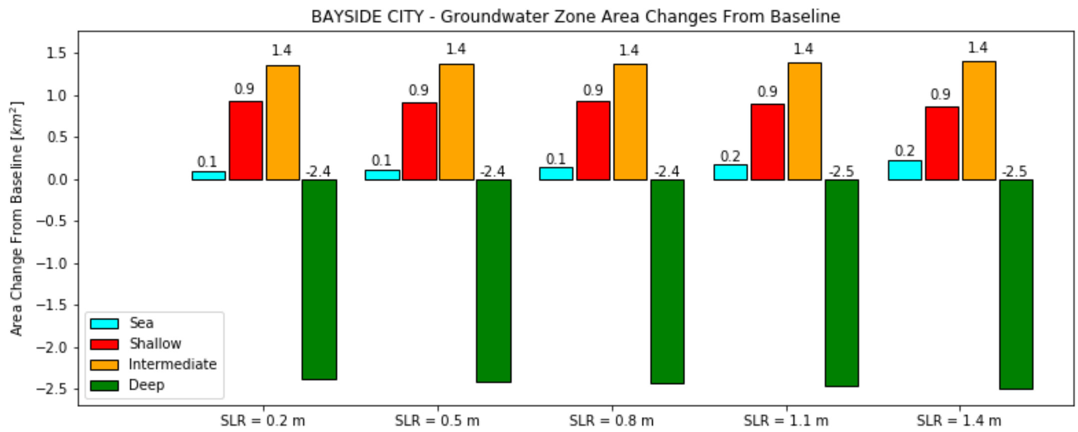

Figure K8: Continued.

Kingston City

(a)

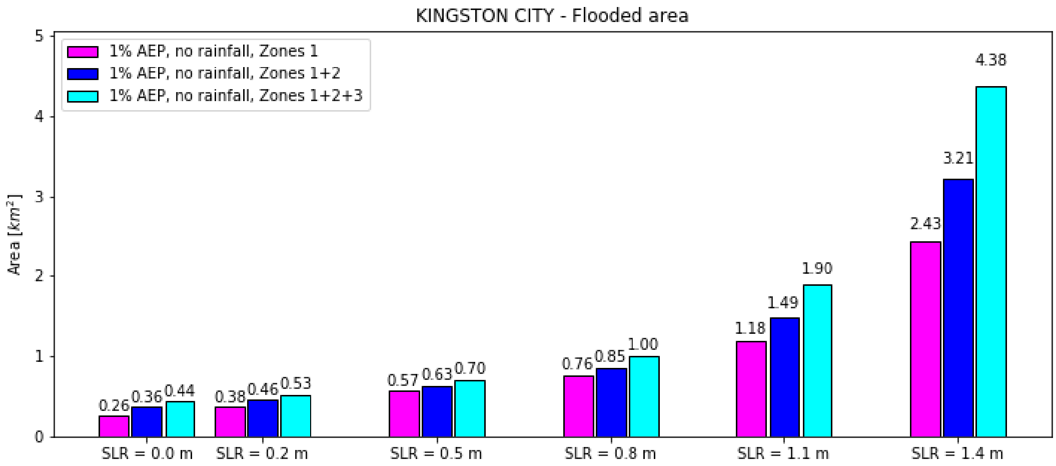

(b)

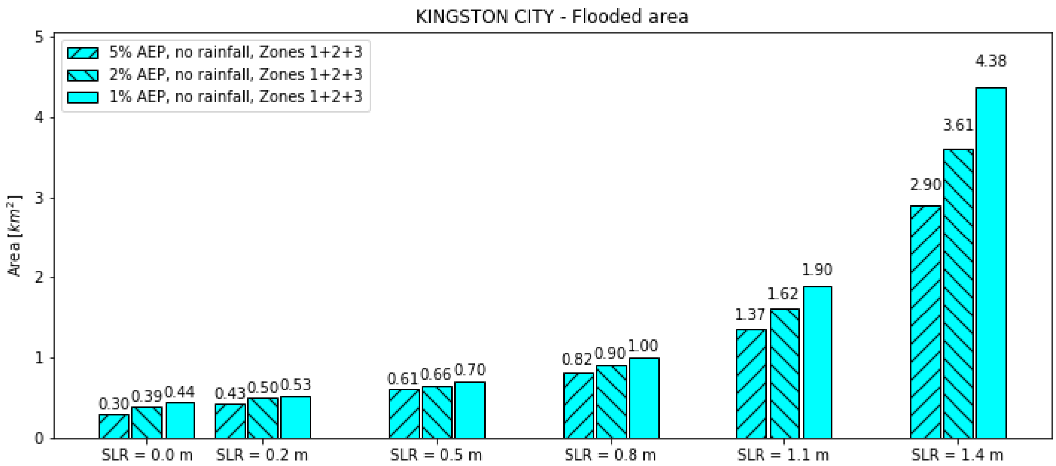

Figure K9: (a) Change in inundation area with SLR for a 1% AEP storm surge and no rainfall with 95% (zone 1), 50% (zone 2) and 95 % (zone 3) likelihood scenarios, (b) Change in inundation area with SLR for a 1%, 2% and 5% AEP storm surge, no rainfall and for zone 3 (i.e. 5% likelihood) scenario, (c) Total area of surface water, shallow, intermediate and deep ground water and (d) change to the total area of the layers under the different SLR scenarios.

(c)

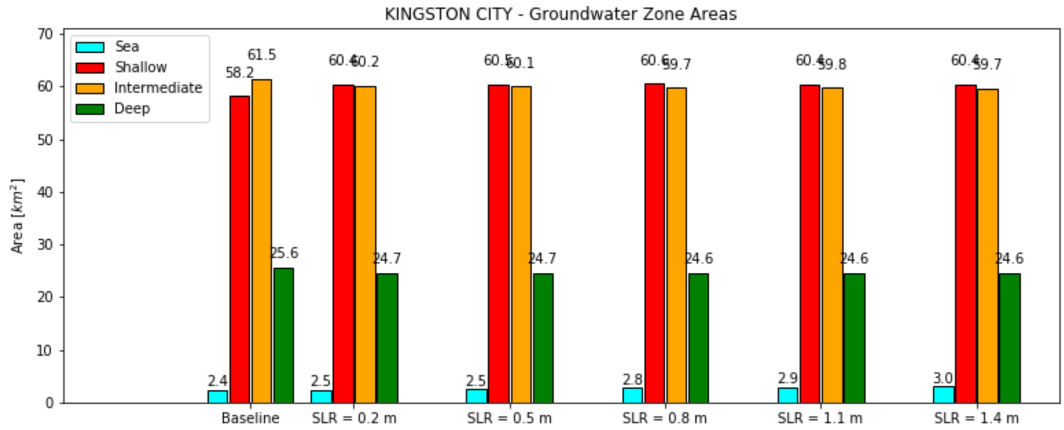

(d)

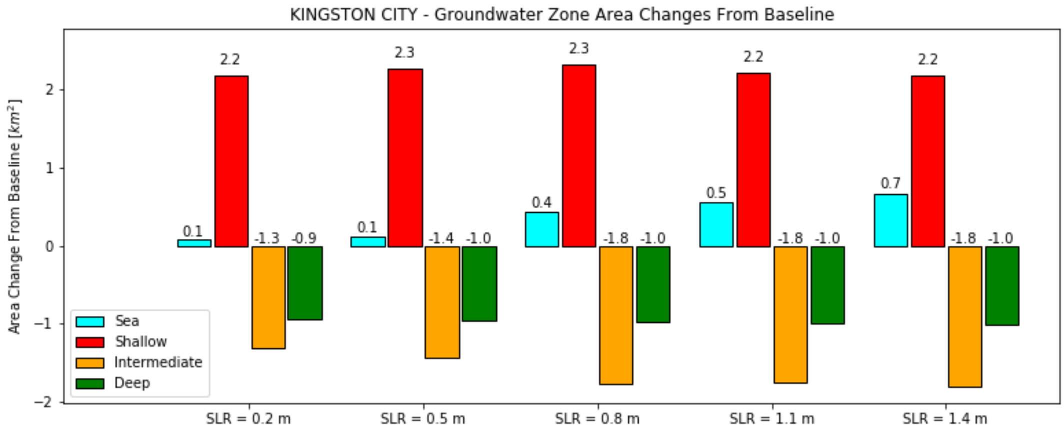

Figure K9: Continued.

Frankston City

(a)

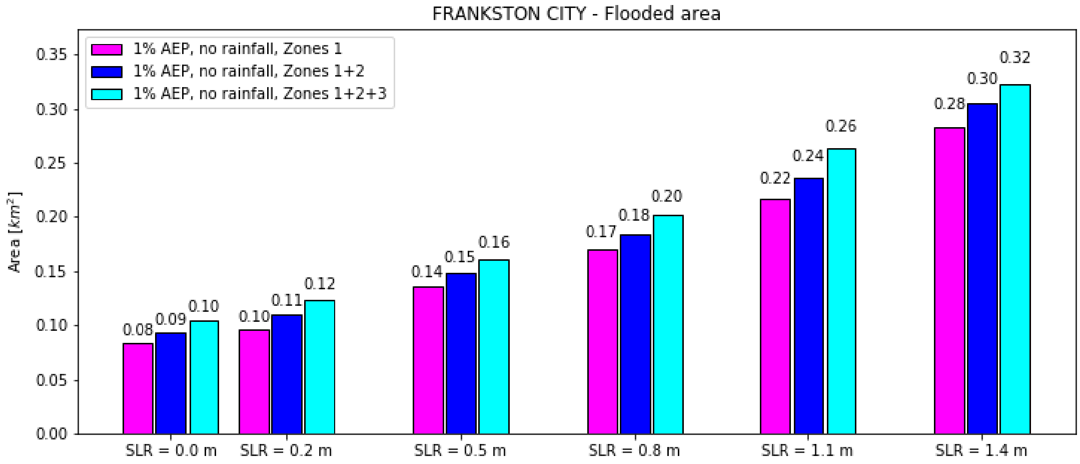

(b)

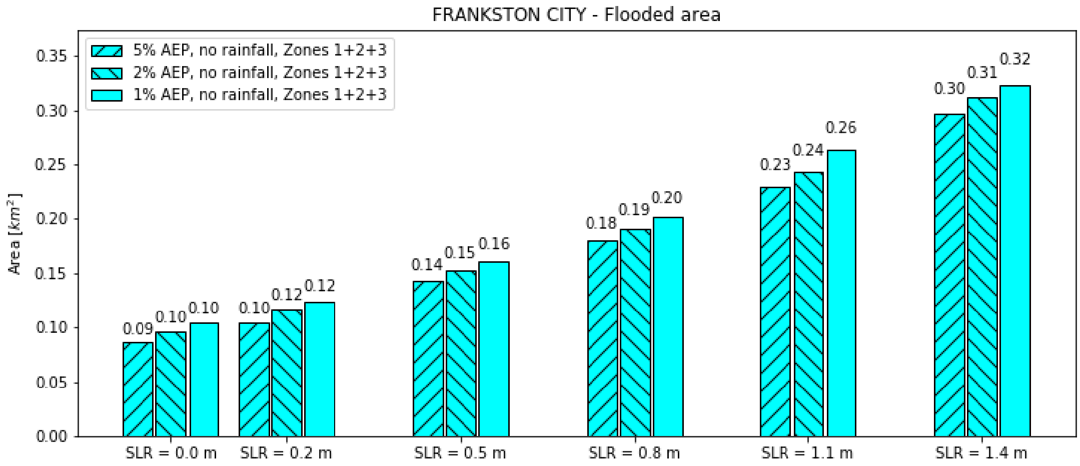

Figure K10: (a) Change in inundation area with SLR for a 1% AEP storm surge and no rainfall with 95% (zone 1), 50% (zone 2) and 95 % (zone 3) likelihood scenarios, (b) Change in inundation area with SLR for a 1%, 2% and 5% AEP storm surge, no rainfall and for zone 3 (i.e. 5% likelihood) scenario, (c) Total area of surface water, shallow, intermediate and deep ground water and (d) change to the total area of the layers under the different SLR scenarios.

(c)

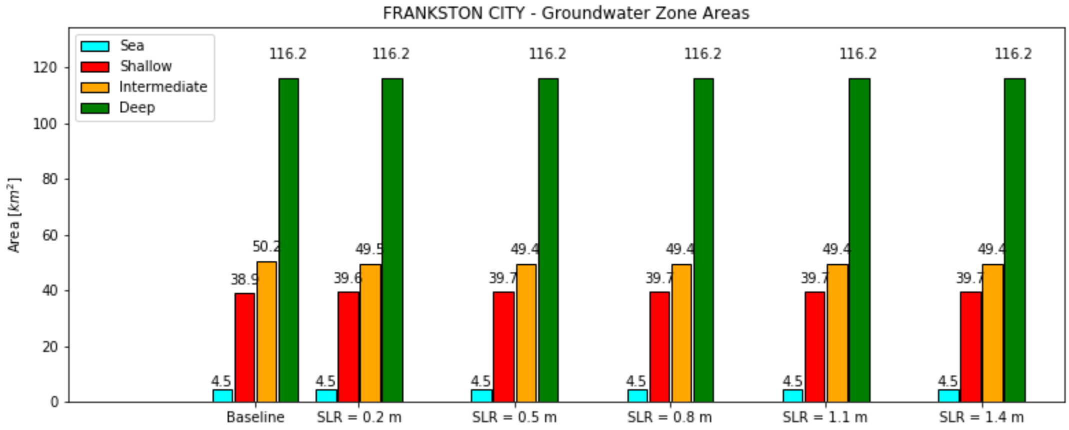

(d)

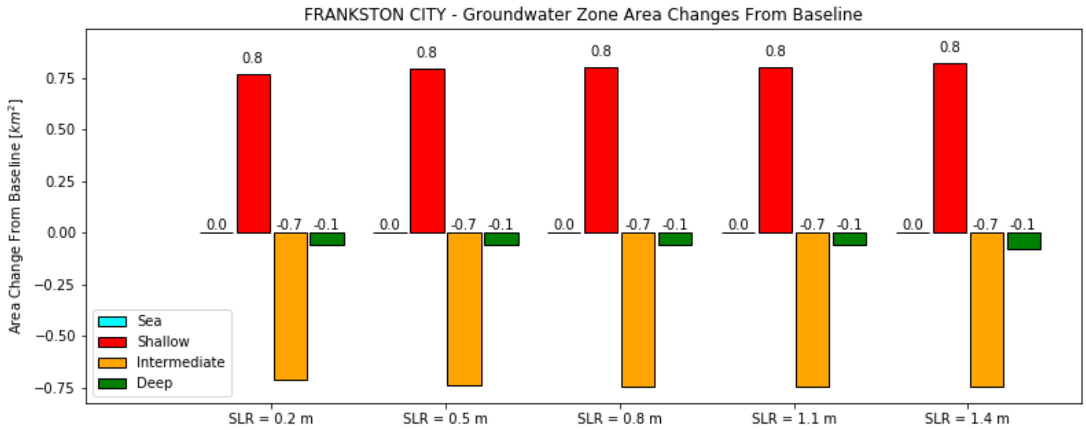

Figure K10: Continued.

Mornington Peninsula Shire

(a)

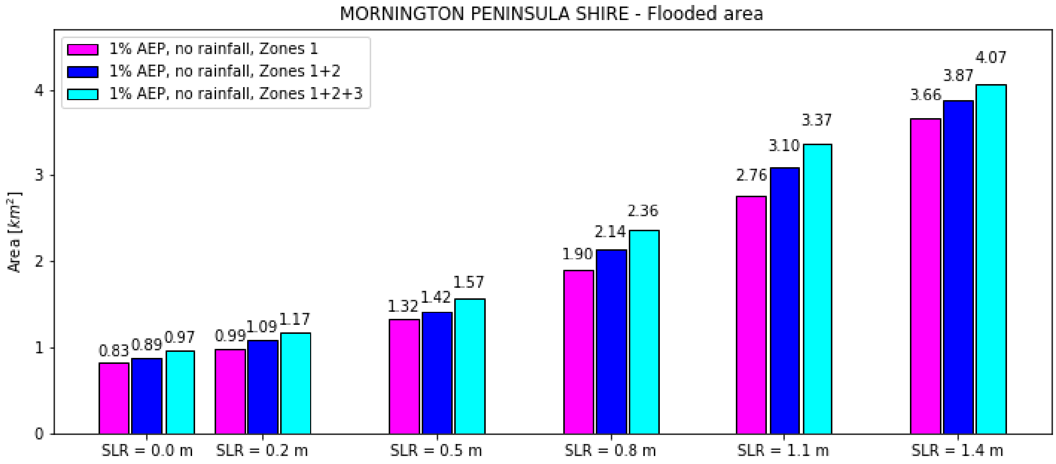

(b)

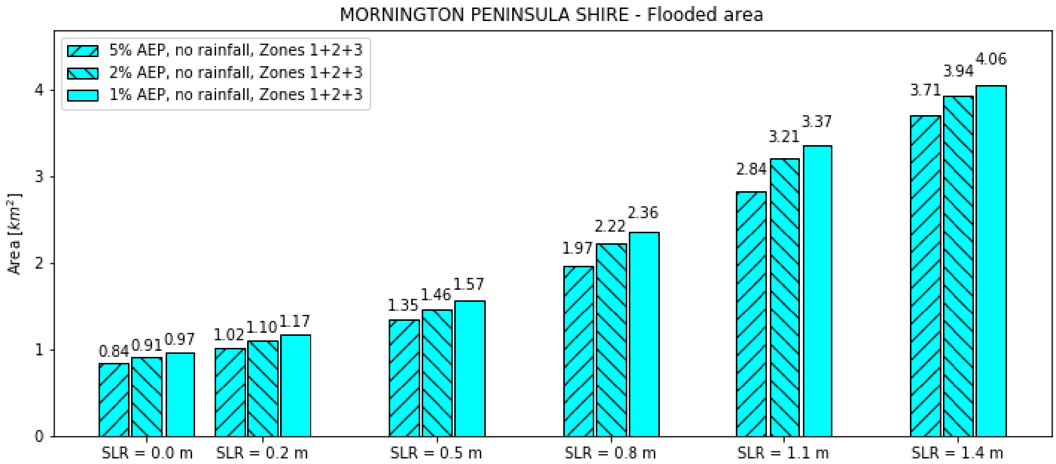

Figure K11: (a) Change in inundation area with SLR for a 1% AEP storm surge and no rainfall with 95% (zone 1), 50% (zone 2) and 95 % (zone 3) likelihood scenarios, (b) Change in inundation area with SLR for a 1%, 2% and 5% AEP storm surge, no rainfall and for zone 3 (i.e. 5% likelihood) scenario, (c) Total area of surface water, shallow, intermediate and deep ground water and (d) change to the total area of the layers under the different SLR scenarios.

(c)

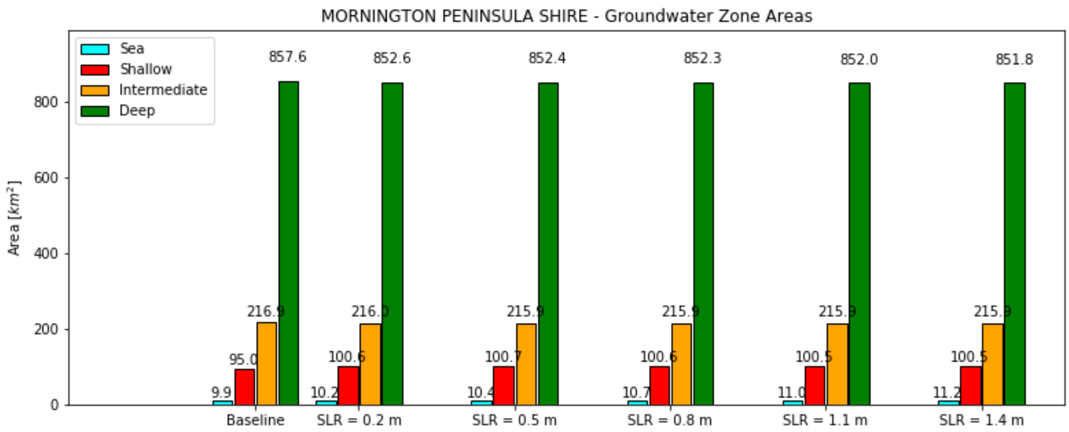

(d)

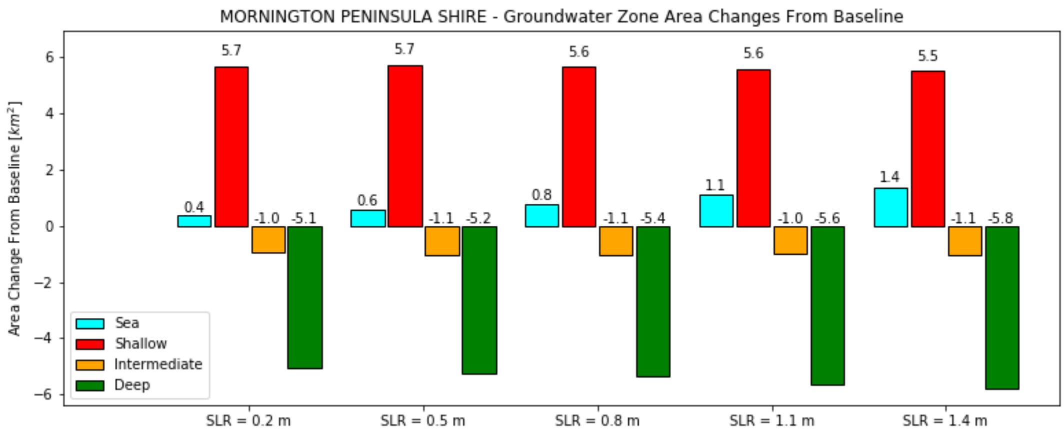

Figure K11: Continued.

Appendix L. Hazard Maps for Western, Northern and Southeastern PPB

Additional maps are provided in this appendix that focus on the western, northern and southeastern areas of PPB. The western region includes the Bellarine, Geelong and Werribee regions, the northern region takes in Melbourne and the adjacent suburbs while the southeastern regions focus on Dromana to Point Nepean and Queenscliff.

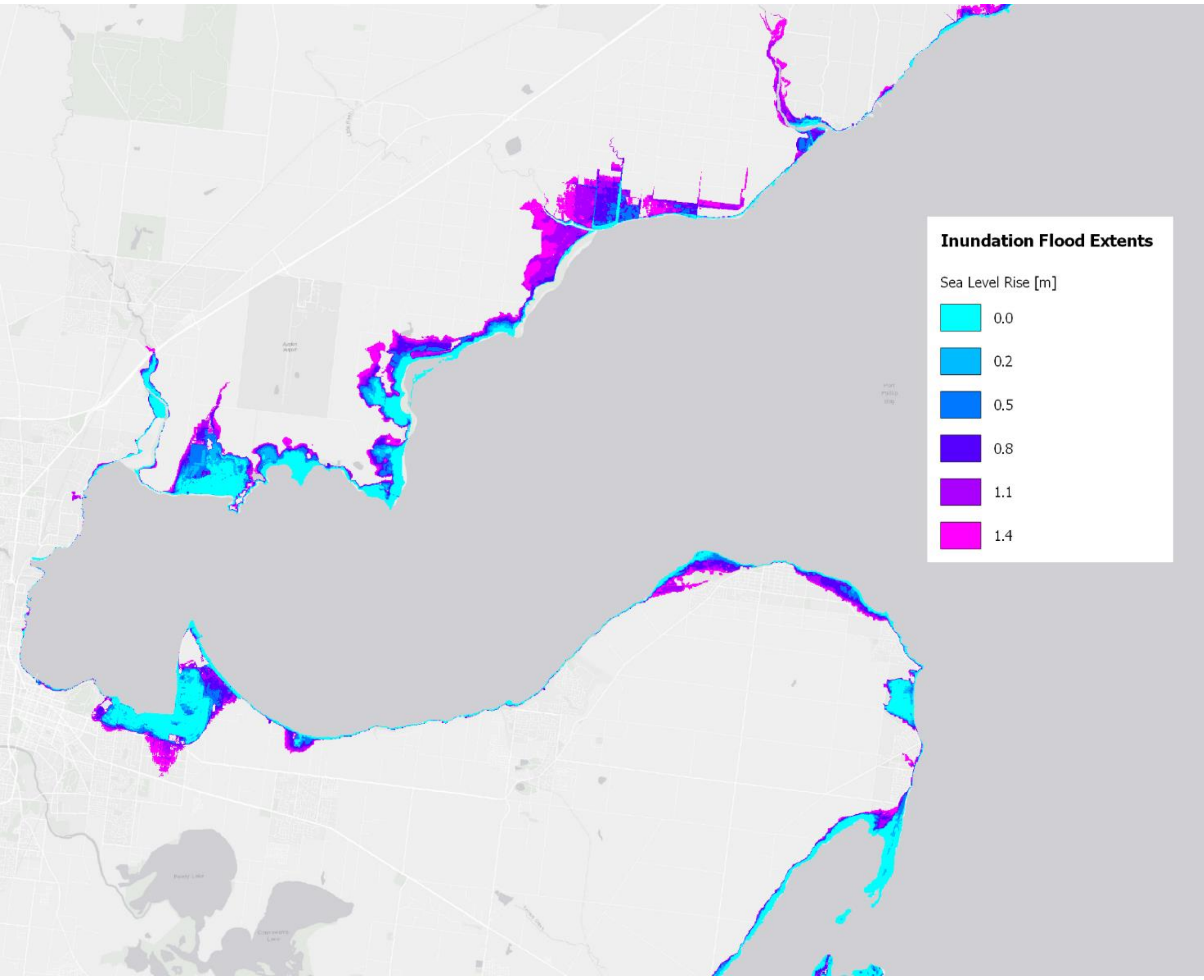

Figure L1: Inundation hazard for the 1% AEP storm tide (zone 3) and no rainfall for the different SLR scenarios for western PPB.

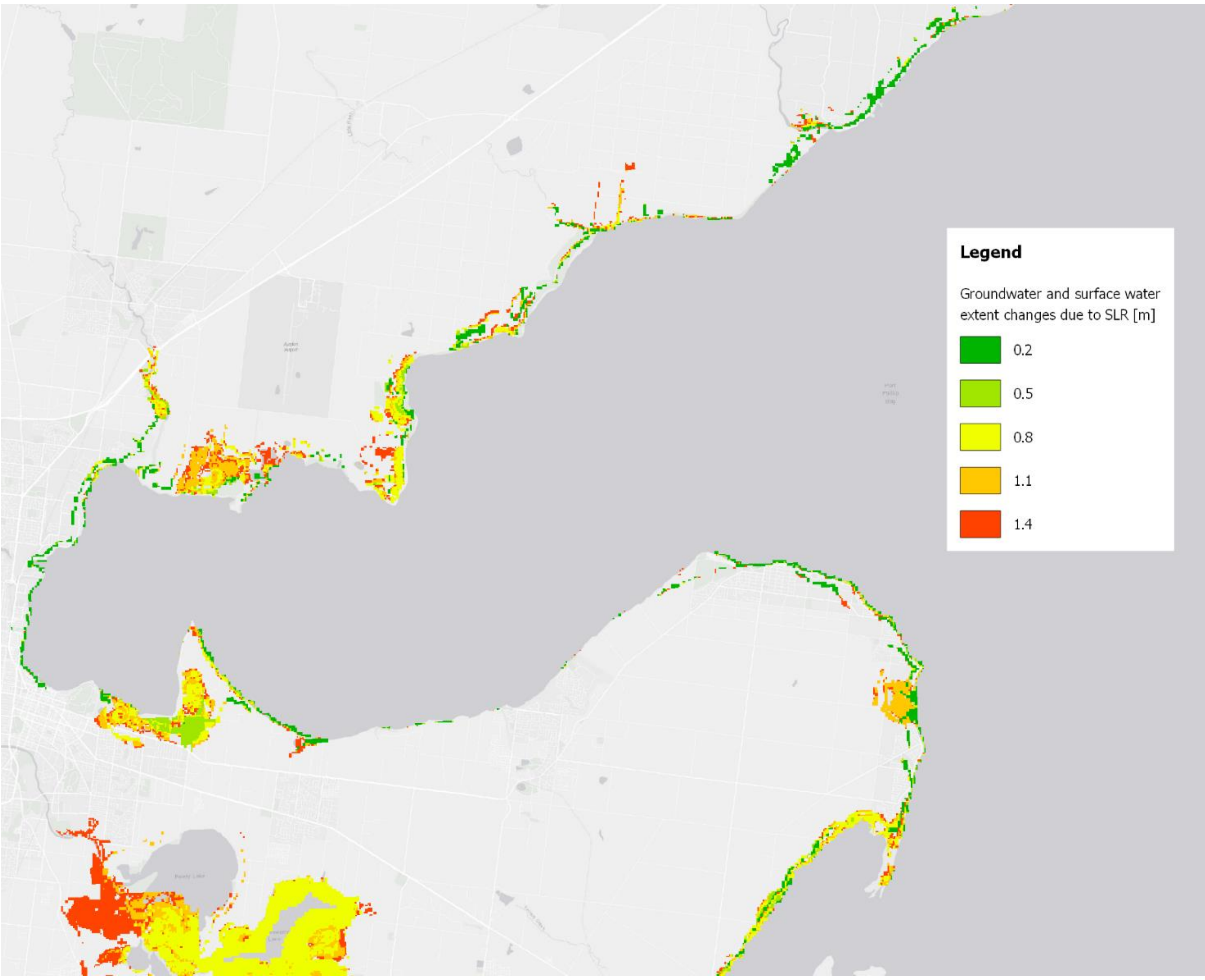

Figure L2: Change in groundwater hazard under the different SLR scenarios where hazard is the combination of the shallow groundwater and surface water changes for western PPB.

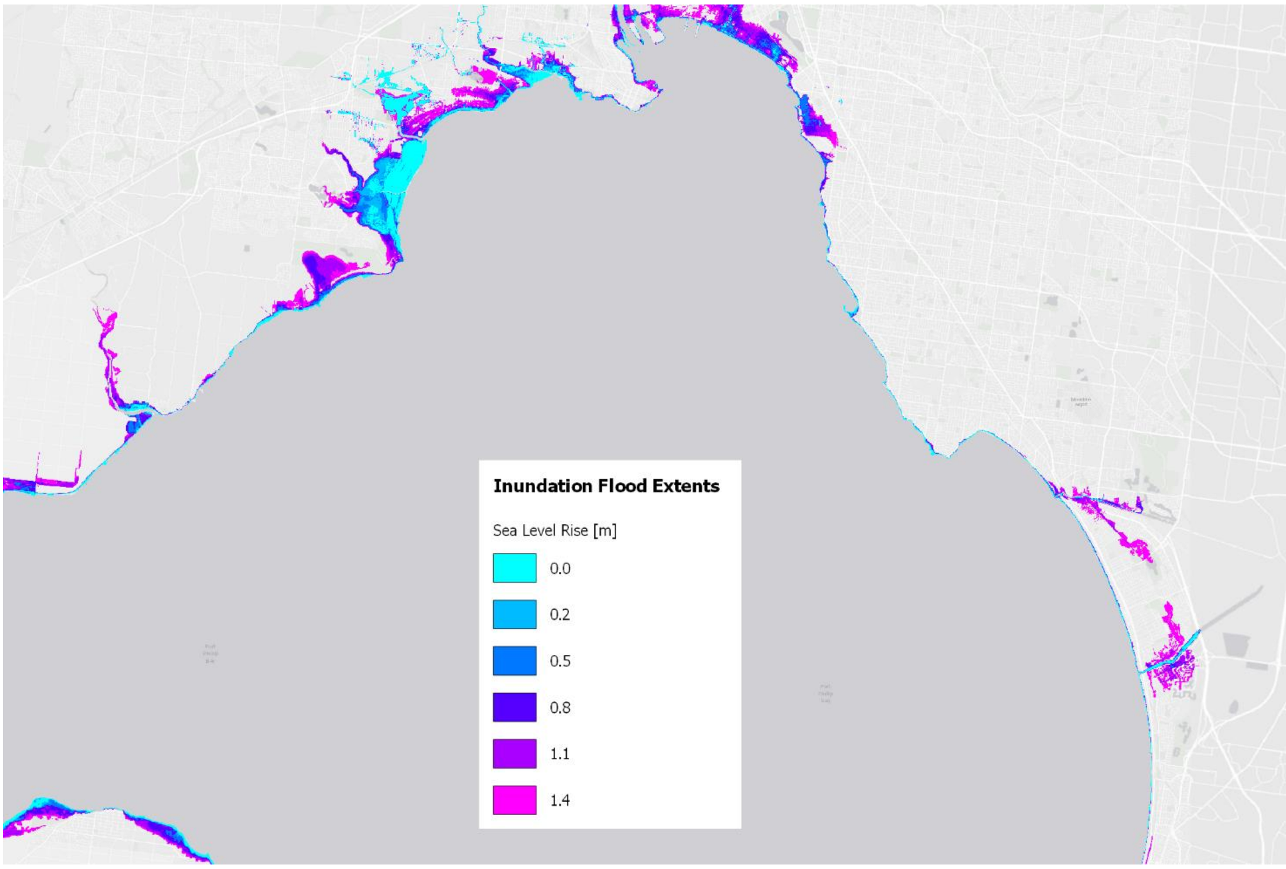

Figure L3: Inundation hazard for the 1% AEP storm tide (zone 3) and no rainfall for the different SLR scenarios for northern PPB.

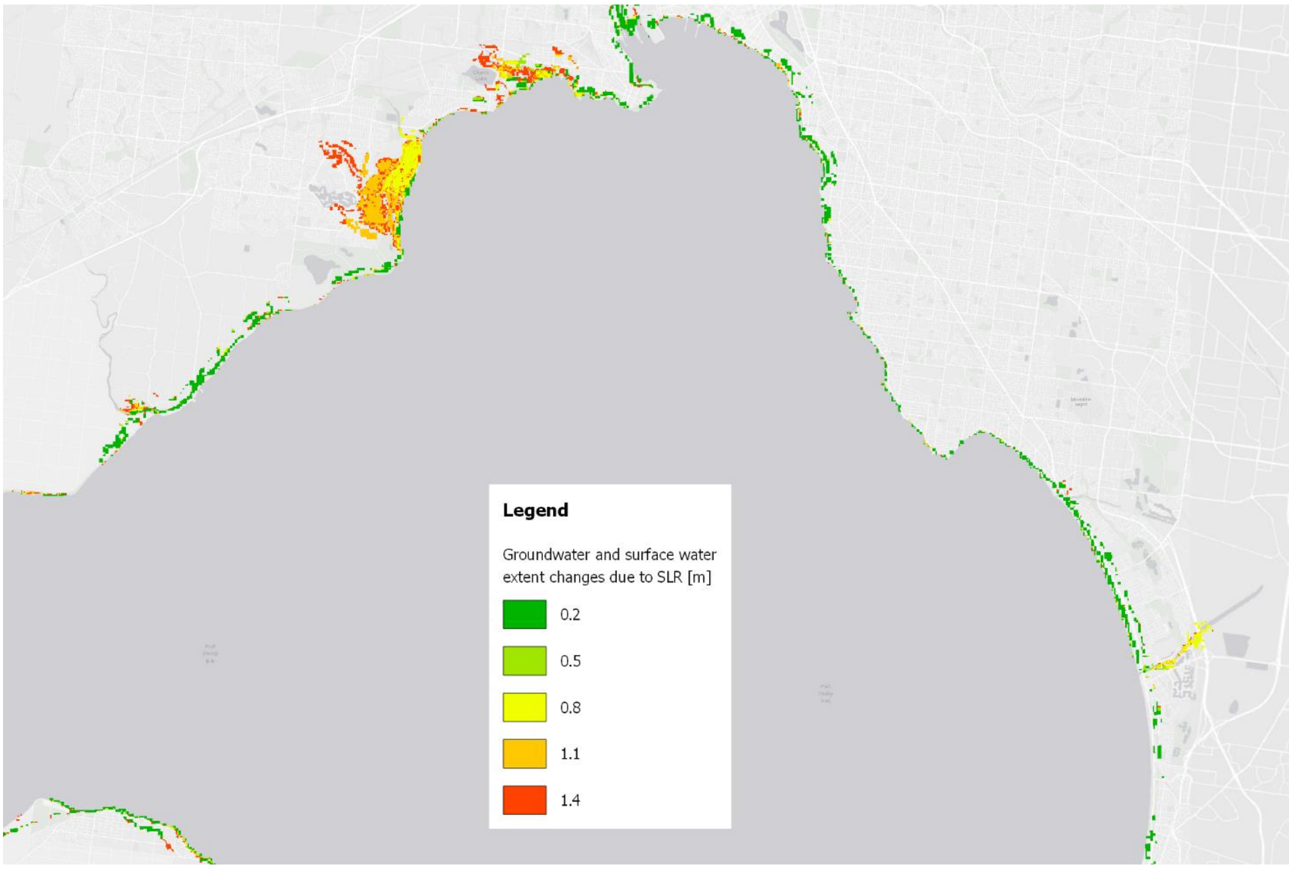

Figure L4: Change in groundwater hazard under the different SLR scenarios where hazard is the combination of the shallow groundwater and surface water changes for northern PPB.

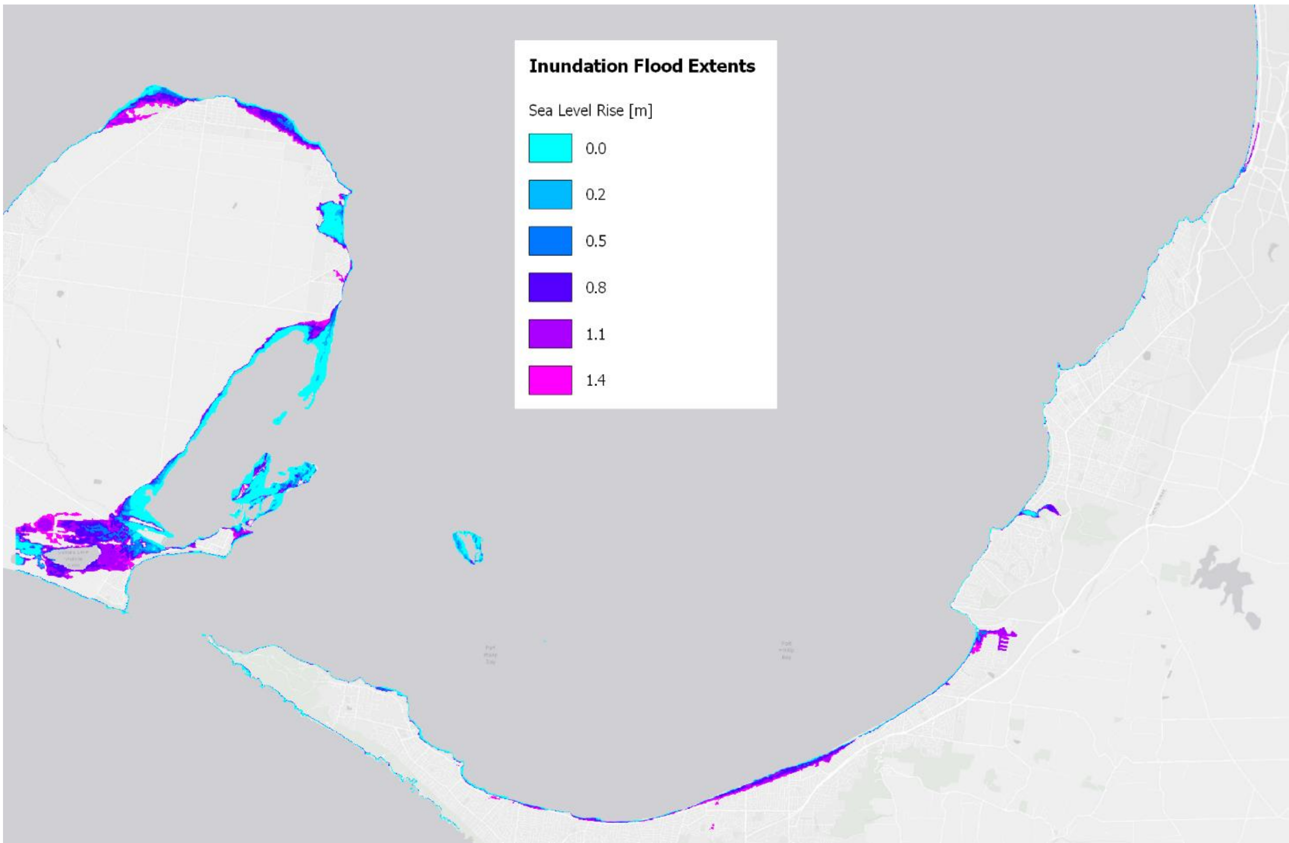

Figure L5: Inundation hazard for the 1% AEP storm tide (zone 3) and no rainfall for the different SLR scenarios for southeastern PPB.

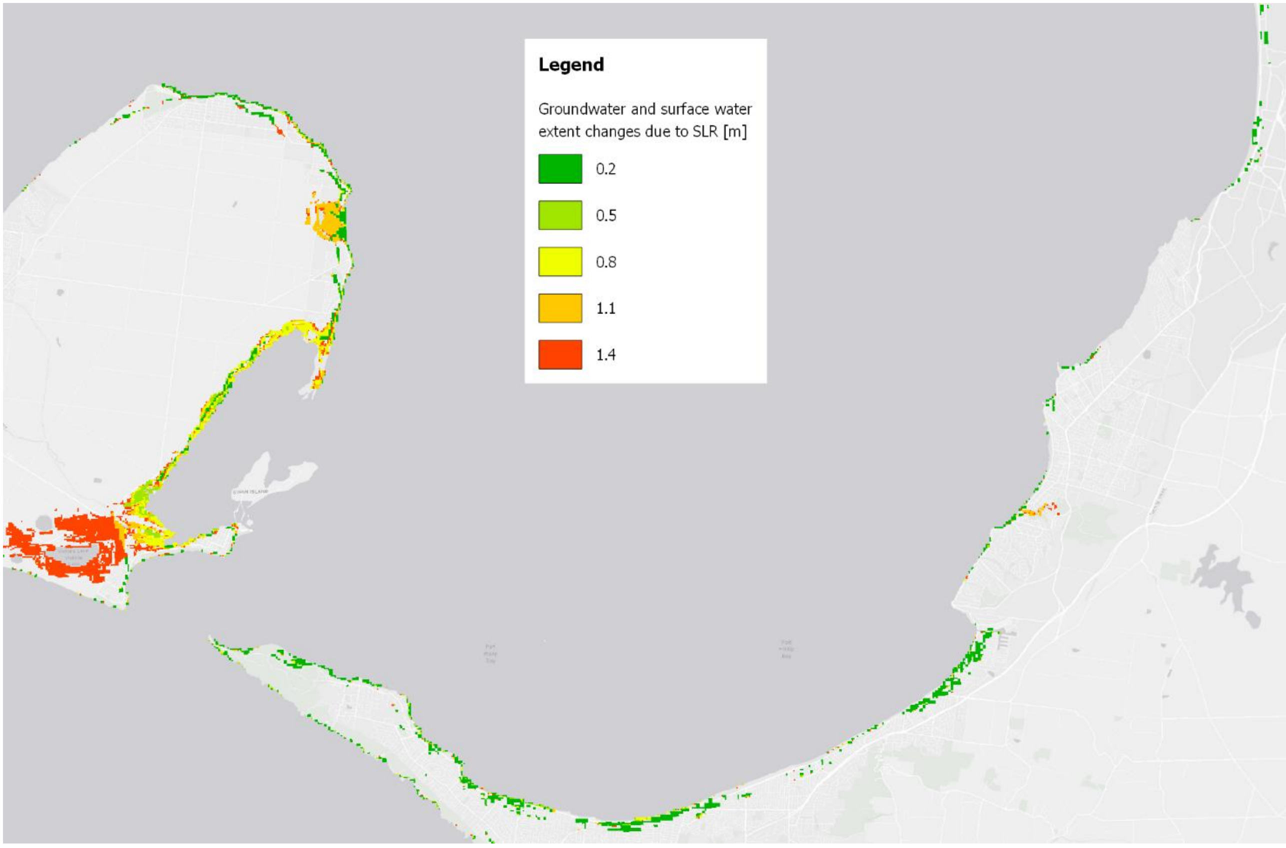

Figure L6: Change in groundwater hazard under the different SLR scenarios where hazard is the combination of the shallow groundwater and surface water changes for southeastern PPB.

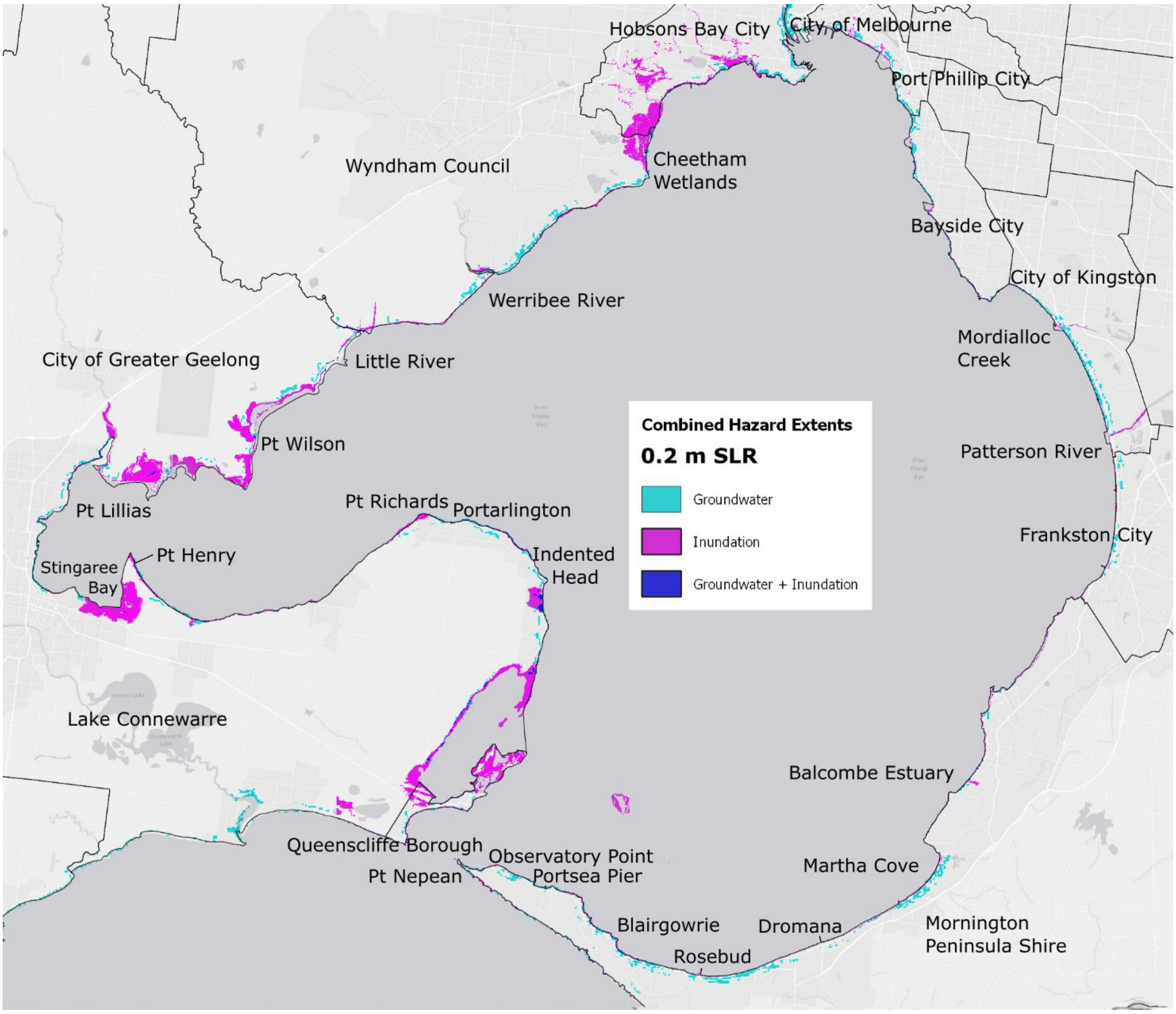

Figure L7: Overlay of hazard zones for inundation and groundwater under 0.2 m SLR where the inundation zone is based on a 1% AEP storm tide with no rainfall.

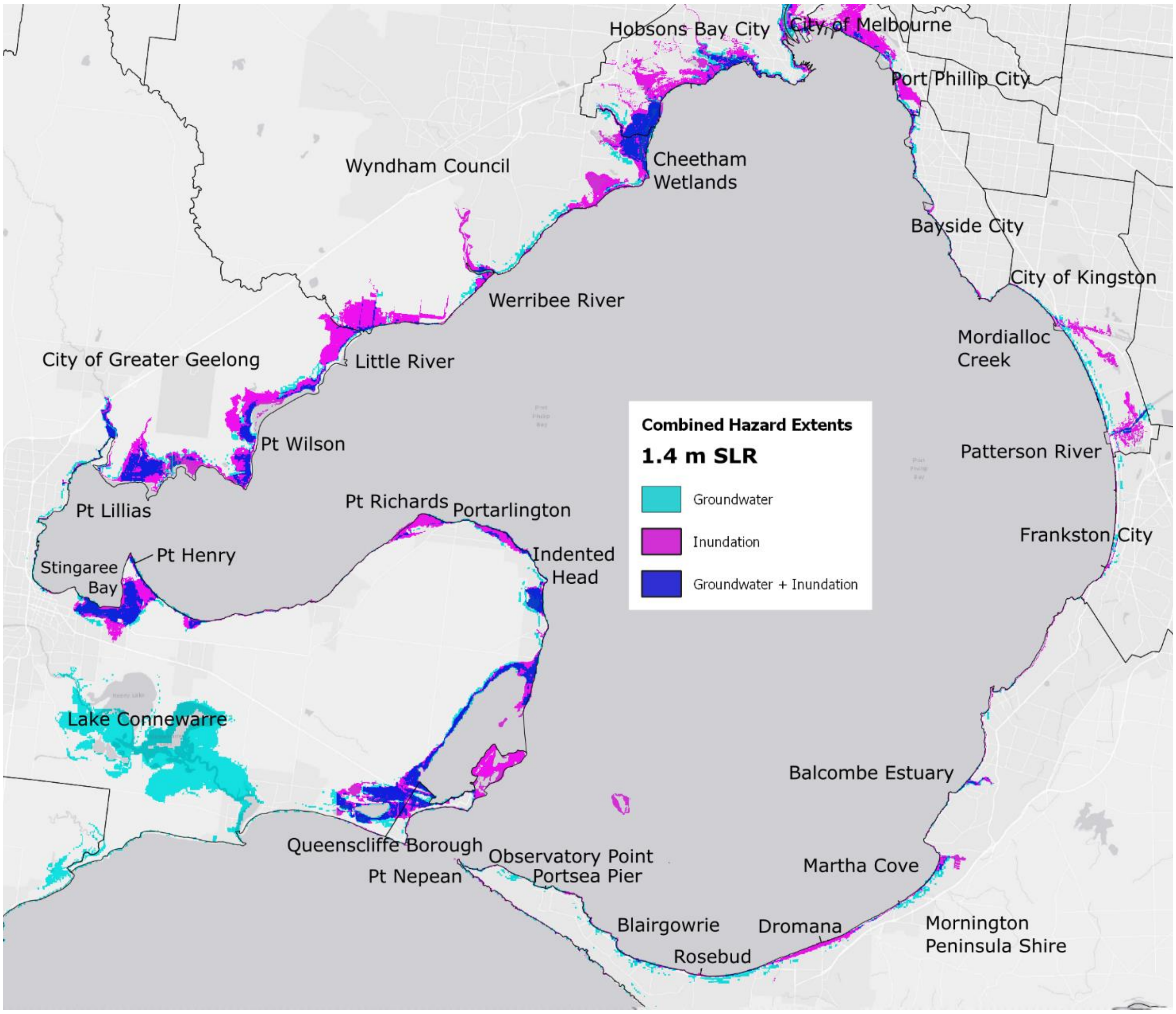

Figure L8: Overlay of hazard zones for inundation and groundwater under 0.2 m SLR where the inundation zone is based on a 1% AEP storm tide with no rainfall.

CONTACT US

t 1300 363 400
+61 3 9545 2176
e enquiries@csiro.au
w www.csiro.au

FOR FURTHER INFORMATION

Oceans and Atmosphere
Kathleen McInnes
t +61 03 9239 4569
e Kathleen.McInnes@csiro.au
w http://www.cmar.csiro.au/sealevel/